INTERPRETATION OF REGIONAL GEOCHEMICAL DATA AS AN AID TO EXPLORATION TARGET GENERATION IN THE NORTH WEST PROVINCE, SOUTH AFRICA

By

LIVHUWANI ERNEST MAPUKULE

A dissertation submitted in fulfillment of the requirements for the degree

of

MASTER OF SCIENCE IN GEOLOGY

In the
Department of Geology
Faculty of Science and Agriculture
University of Fort Hare, Alice, 5700, Eastern Cape

2009

ACKNOWLEDGEMENTS

I would like to express my sincere appreciation to Professor Baojin Zhao my supervisor for making this project a reality and to his colleagues (Mr. Gordon Koll and C.J Gunter) in the Department of Geology, University of Fort Hare, for supervising and giving guidance with constructive reviews and comments on my project. Special thanks to my family for the support and encouragement during my study and to God for being there for me all the time.
I gratefully acknowledge the generosity cooperation of the South African Council for Geoscience in assisting with financial support and resources (geological maps and the geochemical data set of the study area) towards making this project a success. I would particularly like to thank Mr. Kobus Elesnbroek and Mrs. Doreen van der Walt for assistance with the geochemical data analysis and GIS map production.

Thanks to Ms. Wendy Koll for English editing. I would also like to thank Mineral Resources and Evaluation Department (Anglo American), Dr. Christina E. Dhom, Dr. Michael Harley and Mrs. Samantha Reid for their help with the statistical aspects of this project.
Thanks are extended to the examiners Professor Christoph Gauert and Professor Richard Viljoen for their thorough comments, criticisms, recommendations and guidance.

DECLARATION

I, Livhuwani Ernest Mapukule declare this dissertation to be my own unaided work. It is submitted in fulfillment of the Degree of Master of Science at the University of Fort Hare, Alice. It has not been submitted before for any degree or examination in any other University.

---------- 15/02/2010

Signature of Candidate Date

ABSTRACT

This study involves the application, interpretation and utilization of regional geochemical data for target generation in the North West Province, South Africa. A regional soil geochemical survey programme has been carried out by the Council of Geoscience South Africa since 1973. A number of 1:250 000 sheet areas have been completed, but there are no interpretative maps which could aid in mineral exploration and other purposes. In order to utilize the valuable and expensive data, the project was motivated through data acquisition and interpretation to generate exploration targets.

The study area is confined to Mafikeng, Vryburg, Kuruman and Christiana in the Northwest Province, where potential exploration and mining opportunities exist in areas of great geological interest. These include geological events such as the Bushveld Complex, the Kalahari manganese field and the Kraaipan greenstone belts.

The aim of this project was to utilize geochemical data together with geophysical and geological information to verify and identification of possible obscured ore bodies or zones of mineralization, and to generate targets. Another objective was the author to be trained in the techniques of geochemical data processing, interpretation and integration of techniques such as geophysics, in the understanding of the geology and economic geology of the areas.

Approximately 5 kg of surface soil was collected per 1 km^2 by CGS from foot traversing. Pellets of the samples were prepared and analyzed for TiO_2, MnO and Fe_2O_3, Sc, V, Cr, Ni, Co, Cu, Zn, As, Y, Ba, Nb, Rb, Th, W, Zr, Pb, Sr and U using the simultaneous wavelength-dispersive X-ray fluorescence spectrometer technique at the Council for Geoscience, South Africa. For each element the mean +2 standard deviations were used as a threshold value to separate the negative from the positive anomalies. The integration of geological, geophysical and geochemical information was used to analyze and understand the areas of interest. A number of computer programmes were extensively used for data processing, manipulation, and presentation. These include Golden Software Surfer 8®, Arc-View 3.2a®, TNT-Mips®, JMP 8 ®, and Microsoft Excel®.

Through geochemical data processing and interpretation, together with the low resolution aeromagnetic data, gravity data and geological data, seven (7) exploration target areas have been generated: These have been numbered A to G. It is concluded that there is good potential for Cr, PGMs, vanadium, nickel, iron, copper, manganese, uranium and niobium in the targets generated. The results provide some indication and guide for exploration in the target areas.

In Target A, Cu, Cr, Fe, Ni and V anomalies from the lower chromitite zone of far western zone of the Bushveld Complex, which has be overlain buy the thick surface sand of the Gordonia Formation.

Target B occurs over the diabase, norite, andesitic lava and andalusite muscovite hornfels of the Magaliesberg Formation. This target has the potential for Cu, Fe and Ni mineralization.

The felsic rocks of the Kanye Formation and the Gaborone Granite in target C have shown some positive anomalies of niobium, uranium, yttrium and rubidium which give the area potential for Nb, REE and U exploration.

Target D is located on the Allanridge Formation, and has significant potential for Ni-Cu mineralization, and is associated with the komatiitic lava at the base of the Allanridge Formation in the Christiana Area.

The light green tholeiitic, calc-alkali basalt and andesitic rocks of the Rietgat Formation are characterized by a north-south trending yttrium anomaly with supporting Ba and Y anomalies (Target E). This makes the area a potential target for rare earth elements.

Calcrete on the west of the Kuruman has a low b potential target for vanadium. It is believed that the area might be potential for potassium-uranium vanadate minerals, carnotite which is mostly found in calcrete deposits.

This study has proved to be a useful and approach in utilizing the valuable geochemical data for exploration and future mining, generated by Council for Geoscience Science.

It is recommended that further detailed soil, rock and geochemical surveys and ultimately diamond drilling be carried out in the exploration target areas generated by this study.

TABLE OF CONTENTS

LIST OF TABLES

LIST OF FIGURES

LIST OF ELEMENTS

As	: Arsenic
Au	: Gold
Ba	: Barium
Co	: Cobalt
Cr	: Chromium
Cu	: Copper
Fe	: Iron
Fe_2O_3	: Iron Oxide
K	: Potassium
Mn	: Manganese
MnO	: Manganese Oxide
Nb	: Niobium
Ni	: Nickel
Pb	: Lead
Rb	: Rubidium
Sc	: Scandium
Sr	: Strontium
Th	: Thorium
Ti	: Titanium
TiO_2	: Titanium Oxide
U	: Uranium
V	: Vanadium
W	: Tungsten
Y	: Yttrium
Zn	: Zinc
Zr	: Zirconium

LIST OF ABBREVIATIONS

ANRT	: Association Nationale de la Recherche technique, Paris
BIF	: Banded Iron Formation
Canmet	: Canada Centre for Mineral and Energy technology
CCRMP	: Canadian Certified Reference Materials Project
CGS	: Council for Geoscience South Africa
CRPG	: Centre de Recherches Pétrographiques et Géochimiques
DL	: Detection limit
GIS	: Geographic Information System
GSJ	: Geological Survey of Japan
IGEM	: Institute of Geology of Ore Deposits, Petrology, Mineralogy and Geochemistry, Moscow
IGGE	: Institute of Geophysical and Geochemical Prospecting, People's Republic of China
Km	: Kilometer
LLD	: Lower limit of detection
M	: Meter
Max	: Maximum
Min	: Minimum
MINTEK	: Council for Mineral Technology, South Africa
PGE's	: Platinum group elements
PGM's	: Platinum group metals
Ppm	: Part per million
SACS	: South African Committee Stratigraphy
Sed	: Sediment and Cody shale, Fine grained offshore shale
Std. Dev	: Standard Deviation
Str. Sed	: Stream sediment
SWDXRF	: Simultaneous Wavelength-Dispersive X-ray Fluorescence Spectrometer
TH	: Threshold value
USGS	: United State Geological Survey
XRF	: X-Ray Fluorescence Spectrometer

SIMPLIFIED GEOLOGY AND SELECTED MINERAL DEPOSITS - SOUTH AFRICA, LESOTHO AND SWAZILAND

Mineral Data extracted from SAMINDABA

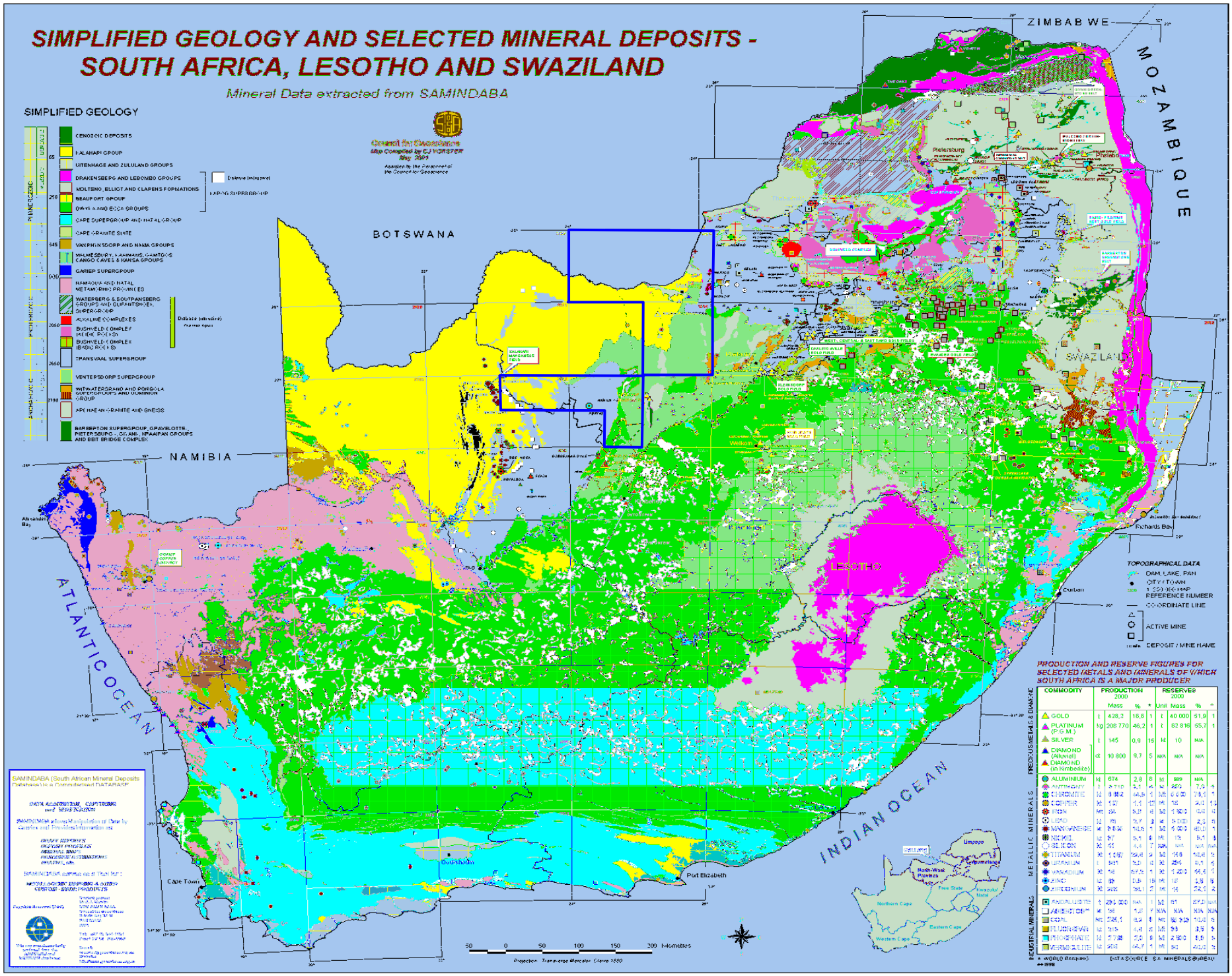

PRODUCTION AND RESERVE FIGURES FOR SELECTED METALS AND MINERALS OF WHICH SOUTH AFRICA IS A MAJOR PRODUCER

	COMMODITY	PRODUCTION 2000				RESERVES 2000		
		Unit	Mass	%	*	Unit	Mass	%
PRECIOUS METALS & DIAMOND	GOLD	t	428,2	16,6	1	t	40 000	61,9
	PLATINUM (P.G.M.)	kg	208 770	46,2	1	t	62 816	55,7
	SILVER	t	145	0,9	15	kt	10	N/A
	DIAMOND (Alluvial)	ct	10 800	9,7	5	N/A	N/A	N/A
	DIAMOND (in Kimberlite)							
METALLIC MINERALS	ALUMINIUM	kt	674	2,8	6	kt	889	N/A
	ANTIMONY	t	3 710	9,1	4	kt	220	7,9
	CHROMITE	kt	5 982	44,5	1	Mt	3 000	78,1
	COPPER	kt	197	1,1	12	Mt	13	1,2
	IRON ORE	Mt	29	3,7	8	Mt	1 800	12,5
	LEAD	kt	70	0,7	8	kt	3 000	2,3
	MANGANESE	kt	3 650	40,5	1	kt	4 000	40,0
	NICKEL	kt	37	0,5	8	Mt	1,0	0,7
	SELENIUM	kg	61	4,4	7	N/A	N/A	N/A
	TITANIUM	kt	1 087	50,8	2	kt	149	10,4
	URANIUM	t	843	5,0	6	kt	295	6,1
	VANADIUM	kt	14	11,5	1	kt	1 200	44,4
	ZINC	kt	99	0,6	14	Mt	1,0	1,9
	ZIRCONIUM	kt	260	56,1	2	Mt	14	72,1
INDUSTRIAL MINERALS	FLUORSPAR	t	295 000	N/A	1	kt	61	27,0
	ASBESTOS	kt	70	1,0	7	N/A	N/A	N/A
	COAL	Mt	224,1	5,4	6	Mt	55 325	13,0
	PHOSPHATE ROCK	kt	2 615	4,4	8	kt	1 500	2,5
	PHOSPHATE	kt	2 000	2,0	6	kt	2 500	6,5
	VERMICULITE	kt	260	44,7	1	Mt	540	40,0

* WORLD RANKING
** 1998

DATA SOURCE: SA MINERALS BUREAU

CHAPTER ONE

1 INTRODUCTION

1.1 BACKGROUND

The South African Council for Geoscience has been carrying out a regional geochemical soil sampling programme on a scale 1:250 000 since 1973. This survey will eventually cover the entire country (Fig. 1.1-1). The prime objective of the programme is to locate mineralized bodies or provinces that may be of economic importance, to create geochemical infrastructure and for environmental impact monitoring (Elsenbroek, 1994).

At present, the only analytical technique used for a variety of elements is quantitative X-Ray fluorescence spectrometry (XRF). Regional geochemical soil samples were analyzed on a 26 fixed and 2 scanner channel simultaneous XRF.In this method twenty four elements are analyzed simultaneously per sample: TiO_2 (%), MnO (%), Fe_2O_3 (%) Sc (ppm), V (ppm), Cr (ppm), Co (ppm), Ni (ppm), Cu (ppm), Zn (ppm), As (ppm), Rb(ppm), Sr (ppm), Y (ppm), Nb (ppm), Zr (ppm), Ba (ppm), W (ppm), Pb (ppm), Th (ppm) and U (ppm) (Elsenbroek, 1994).

This study deals with the interpretation and the application of the geochemical data collected by the Council for Geosciences for target generation in the following 1:250 000 Sheets of the North West Province of South Africa:

a) Christiana;
b) Kuruman;
c) Mafikeng; and
d) Vryburg.

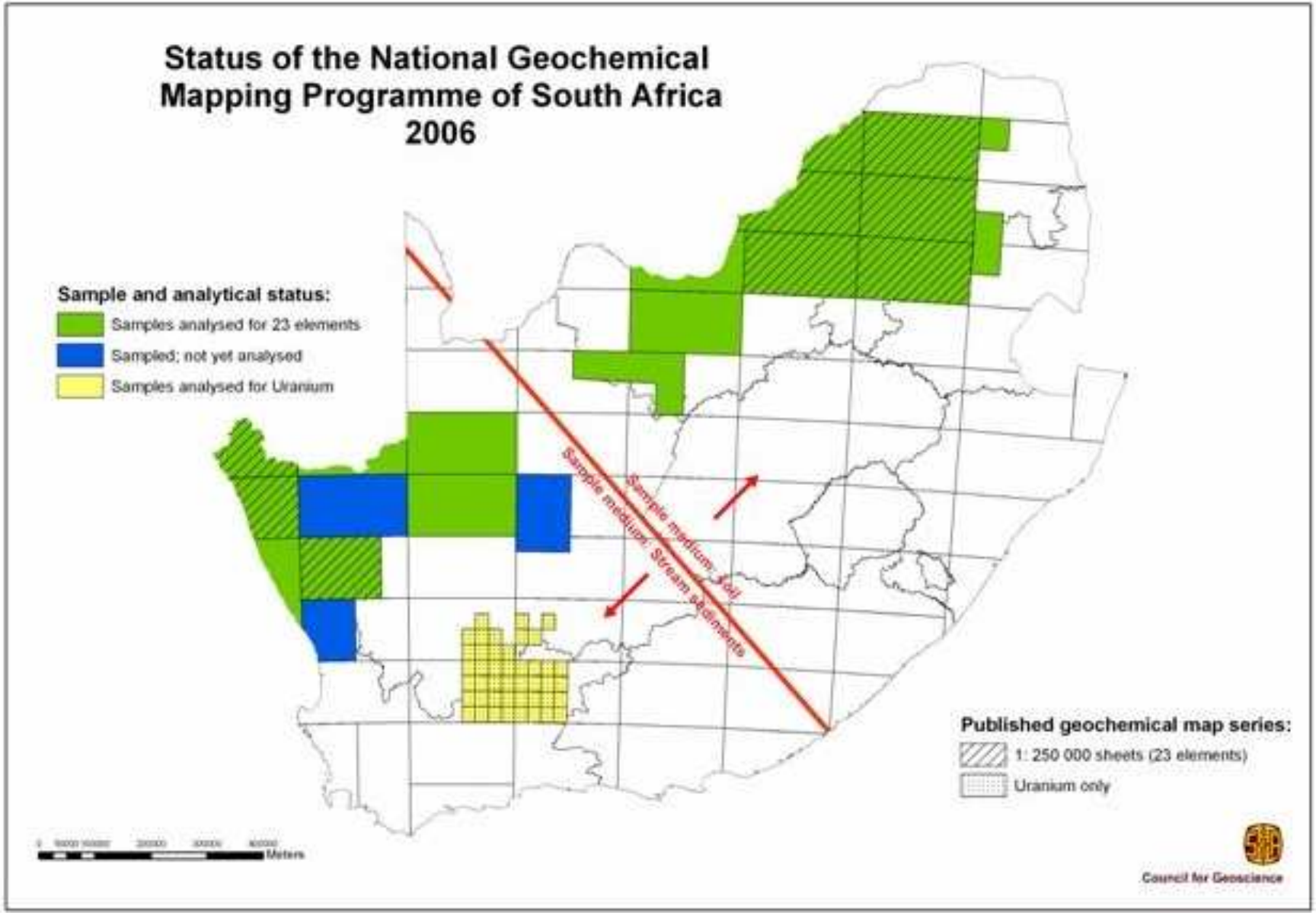

Figure 1.1-1: Current status of the national geochemical mapping programme of South Africa (Council for Geoscience, 2006).

1.2 AIMS AND OBJECTIVES

1.2.1 Overall objective

The overall objective includes: Data acquisition, interpretation and utilization of regional geochemical data acquired from the Council for Geoscience South Africa for target generation for mineral exploration within the North West Province, South Africa. The MSc candidate will be trained in field sampling, data collection, geochemical data interpretation and spatial analysis, and integration methodologies for target generation.

1.2.2 Specific objectives

The specific objectives are as follows:

- Carry out a comprehensive literature review of the study area in terms of geology, mineralization and relevant published information available;
- Obtain and review the regional geochemical data to identify some potential areas for carrying out more detailed geochemical data interpretation;
- Carry out spatial analysis (to carry out statistical analysis of geochemical data and overlay the geochemical, geophysics and geological data in order to understand the distribution and the nature of the geochemical anomalies resulted from each element outlined in the scope of this study) by using Surfer and Arc-View computer software techniques.
- Identify anomalies and relate to the geology and possible ore deposits;
- Utilize other available information, e.g. geophysical data and existing information to refine the interpretation; and
- Generate exploration targets.

1.3 RESULTS EXPECTED

- Geochemical classed post maps to show the distribution of all the major elements/trace elements in a geographic information system (GIS);
- Target generation maps indicate potential areas where there could be possibilities of obscured ore deposits; and
- Identification of areas of interest based on the location, geochemistry and all geophysical characteristics for possible detection of new ore deposits in the North West Province.

1.4 LOCATION OF THE STUDY AREA

The study area is located in North West Province which covers a total area of 116 320 km^2 (9.5% of the total of South Africa), which is the sixth largest of the nine provinces. Geographically it is situated between latitudes 25 and 28 degrees south equator and between longitudes 23 and 28 degrees east (Fig. 1.4-1). The North West Province is bordered by the provinces of the Northern Cape in the west, the Free State in the south, Gauteng in the east and Limpopo (formerly Northern Province) in the north-east. It shares an international border with the Republic of Botswana in the north.

1.4.1 Topography

The North West Province is purported to have the most uniform terrain of all the provinces with an altitude ranging between 920 and 1782 meters above sea level. The central and western regions are characterized by flat or gently undulating plains. Dunes associated with the arid environment of the Kalahari desert occur in the far western region. The eastern region (east and north-east of Zeerust) is of a more variable topography, giving rise to the Magaliesberg mountain range, formed of the Transvaal Sequence's Magaliesberg Quartzite Formation. Another prominent feature in the east is the Pilanesberg which consists of a formation of concentric hills or ring- dykes that

constitute the eroded remnants of an ancient volcano (the Pilanesberg alkaline Volacanic complex).

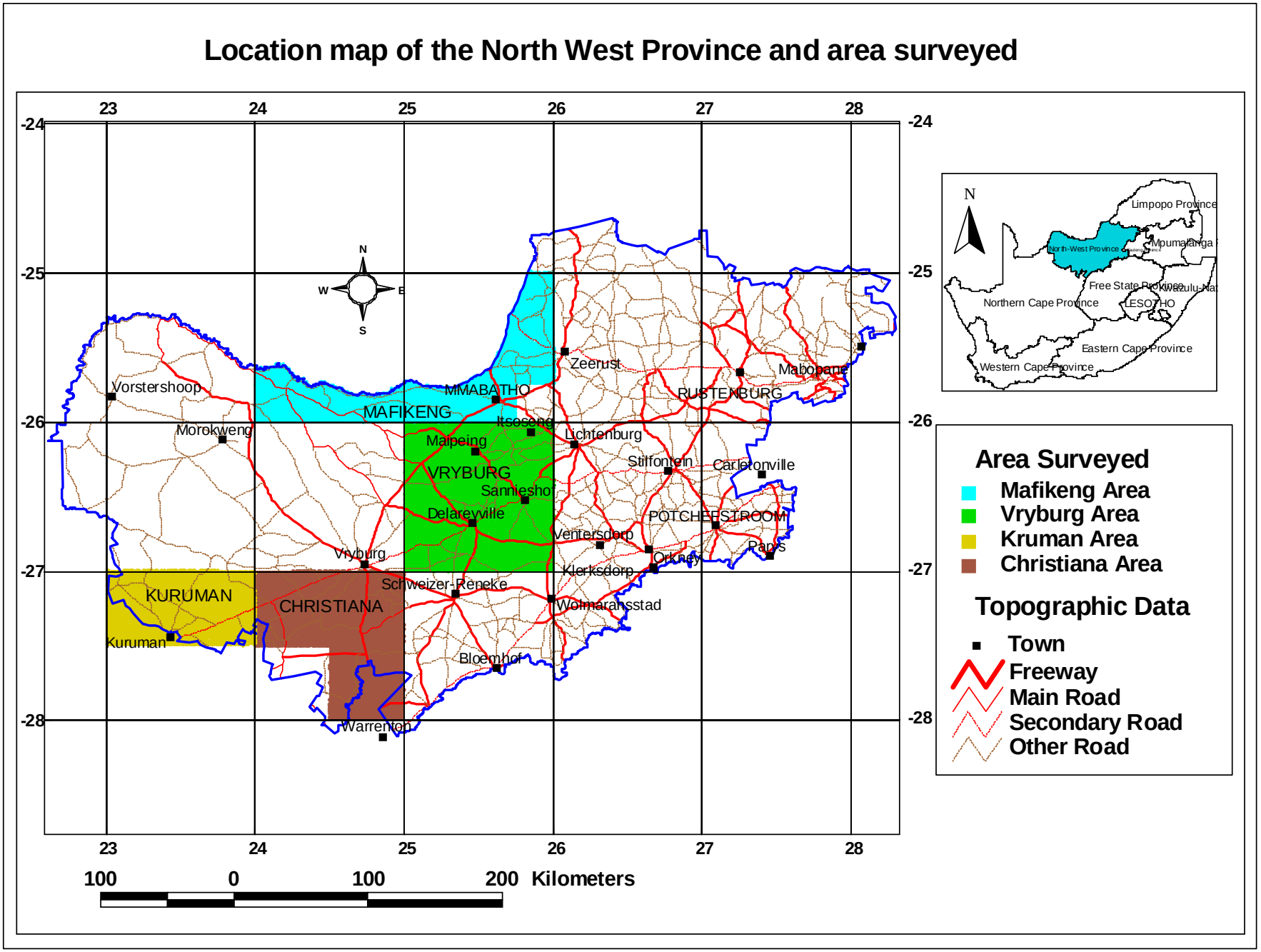

Figure 1.4-1: Locality map of the North West Province study area and sampling sites.

1.4.2 Climate and rainfall

Climatic conditions in the study area vary significantly from west to east. The far western region is arid (receiving less than 300 mm of rainfall per annum), and encompasses the eastern reaches of the Kalahari desert. The central region of the province is dominated by typically semi-arid conditions, with the eastern region being predominantly temperate. The rainfall pattern is highly variable both spatially and temporally and largely mirrors the prevailing climatic conditions of the province. On average, the western region receives less than 300mm per annum, the central region around 550 mm per annum, while in the eastern and south-eastern regions receive over 600 mm per annum. The dominant rainfall season in the central region is middle summer (peaking in January). The western parts of the province typically receive rain in the late summer (peaking in February), while the eastern parts, rainfall typically peaks in early summer (NWPSoER, 2002).

The province is also characterized by great seasonal and daily variations in temperature, being very hot in summer (daily average high temperatures of 32ºC in January) and mild to cold in winter (average daily minimum of 0.9ºC in July). Seasonal fluctuations in mean temperatures between the warmest and the coldest months exceed 15ºC in the western region, while the central and eastern regions experience a range between 12ºC and 15ºC. De Villers et al. (1994) noted that relative humidity is also typically low throughout the Province, being below 28% in the northern part of the Province in July and between 28-30% for the central and eastern regions. In February, the month with the highest relative humidity, the eastern and northern parts range between 66 and 68 % and the rest of the province ranges between 64-66%. This gives rise to high potential evapo-transpiration rates, affecting the flora of the region (NWPSoER, 2002).

1.4.3 Hydrology of the study area

Water is one of the North West Province's most critical and limiting natural resources. The sources of water available in the Province are surface water and groundwater. The North West Province's surface water comprises rivers, dams, pans, wetlands and dolomite eyes fed by underground springs. Apart from highly variable precipitation from year to year, one of the most important factors affecting surface water in the Province is the highly variable but low actual runoff. Runoff as a percentage of the precipitation ranges from less than 1% in the west to approximately 7% in the eastern region. The average runoff for the Province is 6%, which is below the average of 9% for Southern Africa (Schulze, 1997).

1.4.3.1 Drainage pattern

Being predominantly a dry province, the North West Province has very few perennial rivers. Of the six major drainage basins in South Africa, the Orange and the Vaal River basin partly fall within the boundaries of the province. With the exception of the Vaal River, the highly variable runoff from the non-perennial water sources prohibits direct utilization by runoff-river abstraction on a large scale from major rivers in the Province.

The Vaal River which forms the southern boundary of the Province with the Free State originates on the western slopes of the northern sector of the Drakensberg-range in Mpumalanga, flows for about 900 km westwards across the interior plateau, through Gauteng and North West Province and joins the Orange River near Douglas in the Northern Cape. Apart from the Molopo River, it is the only west flowing river system in the North West Province and is known for its exceptional flood plains, wetland systems, dolomite eyes and natural riverine vegetation in the lower reaches. Major tributaries of the Vaal River which have entire catchments within the North West Province are the Harts, Dry Harts, Schoonspruit, Makwassiespruit and Bamboesspruit Rivers. The Mooi River, another major Vaal River system tributary has its headwaters in the North West Province, but is joined by a number of tributaries flowing from Gauteng.

The Molopo River, which rises from the Molopo Eye near Mafikeng, flows westwards to form the northern border of the North West Province with Botswana. The Molopo River was once a tributary of the Orange (NWPSoER, 2002).

1.4.3.2 Groundwater

Although the North West Province has few surface water resources it has a large reservoir of subterranean water in the form of fractured aquifers and dolomitic compartments. According to Nel et al. (1995), groundwater regions in the North West Province can be divided into the following areas:

- Ghaap Plateau dolomites;
- Coetzersdam-Louwna Granite-Gneiss region;
- Vryburg Basin;
- Kalahari Basin:
- Western Transvaal dolomite; and
- Other groundwater reserves.

The Province's groundwater storage occurs in a number of ways. Most of the Province's aquifers comprise secondary fractured aquifers in South Africa. Storage and flow in these aquifers occur in the permeable transition zone between weathered soil and hard rock, fracture and fissure zones in hard rock, and contact zones between intrusions and country rock. Yields from secondary aquifers are usually far below those found in dolomite. Usually these aquifers are semi-confined, which means that the pressure in the aquifer exceeds the general air pressure causing groundwater to rise in a borehole. Excessive dewatering of the fracture zones that yield the water of a well might cause the fracture zone to be compressed due to the high pressure. Therefore the yield of the well might decrease if it is pumped above its sustainable yield (NWPSoER, 2002).

The groundwater from the basic igneous rocks is also liable to contain a certain amount of dissolved materials. NWPSoER, (2002) noted that in very highly weathered zones within the Ventersdorp rocks, a high degree of weathering produces a large amount of

clay, with the consequent impeding of the underground water seepage. Water from areas underlain by granites is usually very good, although water may be slightly acidic. Water in the Bankeveld is strongly controlled by the degree of metamorphism. The higher degree of metamorphism in the west has as a consequence that shale are better aquifers than quartzite, while the picture reverses in the east. The quality of the quartzite water is very pure, while that of the shale tends to vary.

The water from the Bushveld basin tends to vary in quantity and quality in accordance with the rock type as well as the degree of weathering. Noritic aquifers tend to display fairly high silica content. Water derived from underground sources in the Pilanesberg Complex has unusually high fluoride content due to its alkaline nature (NWPSoER, 2002).

Underground water seems to be limited in the areas covered by the Kalahari Group. Water is frequently brackish and the general yields are small. The depth of the water table is often in excess of 130 meters.

Groundwater in the Province is also stored in caverns and dissolution chambers in dolomitic rock and karstic formations that have extremely high transmissivity values. The yield of an aquifer is determined by its storativity and transmissivity. When a borehole is pumped, the groundwater level is drawn down in a cone around it. The depth of draw down and radius of the cone are determined by the physical properties of the aquifer. In dolomite the draw down is usually very small because water flows quickly towards the well due to the large transmissivity values. The water quality from dolomite sources is usually good (except where polluted by mining and other industries), although this water usually has high carbonate content (NWPSoER, 2002).

CHAPTER TWO

2 METHODOLOGY

2.1 GEOCHEMICAL SOIL SAMPLING AND SAMPLE PREPARATION

Soil samples were collected by Council for Geoscience (CGS) at a density (scale) of a sample km^2. Although the author was not involved in the sampling and laboratory data analysis for the data sets used in this study, he did undertake a similar excise of data collection (Benoni Project, November 2005- January 2006), laboratory preparation and X-ray analysis. The objective of this study was to familiarize and give the author an understanding of the processes of geochemical data analysis.

Approximately 3 kg of surface soil samples were collected by the CGS at each locality. Sampling was initially carried out by foot traversing, but this method proved to be tedious, time consuming and unreliable. Helicopter supported transport was introduced, which speeded up the operation considerably. Samples were dried at ±75 ºC and then sieved to the <75µm fraction. Only the fine fractions (<75µm fraction) were analyzed. A few drops of poly-vinyl-alcohol (PVA) is mixed with 20-25grams of the sieved powder sample and placed in an aluminum cup from which a pellet is pressed at 30 tons $inch^{-2}$. The pellets are then analyzed for 24 elements using a Simultaneous Wavelength-Dispersive X-ray Fluorescence Spectrometer (SWDXRF). The original sample and the remaining <75µm fraction were stored for future use (Elsenbroek, 1994).

2.2 GEOCHEMICAL ANALYSIS

2.2.1 Instrumentation

Only the trace elements were analyzed and the analysis was performed on a Philips PW1606 SWDXRF with 28 channels. Of these 28 channels, 24 are used for the element

concentration determination, and three are for measuring the RhKβ Compton peak for mass absorption coefficient determination. A 3 kW Rh-target end-window tube is used, which is operated at 60 kV and 40 mA. An Ag mask (shielding plate) spectral lines, crystal, detector, 2θ angle and counting times used are summarized in Table 2.2-1.

Table 2.2-1: Instrumental setting on the SWDXRF (Elsenbroek, 1994).

Element	Line	Crystal	Detector	Count time/s	Angle 2θ
Sc	Kα	LiF200	Krypton, sealed	100	97.7
Ti	Kα	LiF200	Krypton, sealed	100	86.14
V	Kα	LiF200	Krypton, sealed	100	76.94
Cr	Kα	LiF200	Krypton, sealed	100	69.36
Mn	Kα	LiF200	Krypton, sealed	100	62.98
Fe	Kα	LiF200	Krypton, sealed	100	57.52
Cu	Kα	LiF200	Krypton, sealed	100	52.8
Ni	Kα	LiF200	Krypton, sealed	100	48.66
Cu	Kα	LiF200	Krypton, sealed	100	45.03
Zn	Kα	LiF200	Xenon, sealed	100	41.8
As	Kα	LiF200	Xenon, sealed	100	30.44
Rb	Kα	LiF200	Xenon, sealed	100	26.62
Sr	Kα	LiF200	Xenon, sealed	100	25.16
Y	Kα	LiF200	Xenon, sealed	100	23.8
Zr	Kα	LiF200	Scintillation	100	22.56
Nb	Kα	LiF200	Scintillation	100	21.4
Mo	Kα	LiF200	Scintillation	100	20.33
Sn	Kα	LiF200	Scintillation	100	14.04
Sb	Kα	LiF200	Scintillation	100	19.07
Ba	Kα	LiF200	Krypton, sealed	100	87.18
W	Kα	LiF200	Xenon, sealed	100	43.02
Pb	Kα	LiF200	Xenon, sealed	100	28.24
Th	Kα	LiF200	Xenon, sealed	100	27.48
U	Kα	LiF200	Xenon, sealed	100	26.14
Bg1	--	LiF200	Xenon, sealed	100	39.5
Bg2	--	LiF200	Xenon, sealed	100	33.2
Bg3	--	LiF200	Scintillation	100	15
Rh comp	--	LiF200	Scintillation	100	16.365

2.2.2 SWDXRF calibration procedures

The SWDXRF was calibrated by using the following steps:

- Pure chemical standards were used for background determination;
- Interference standards were used for determining interference correction factors; and
- International reference materials listed in table 3 were used for the calibration of the peak intensity (kcounts s-1) to concentration (% or ppm) (Elsenbroek, 1994).

2.2.3 SWDXRF correction procedures

Although SWDXF is a very stable instrument for analyzing the samples, it is subject to a definite, though minimal degree, of drift. Compensation for this drift is made on the basis of corrections to quantitative measurement using an internal monitor. The in-house internal monitor was prepared as a lithium tetraborate glass disc containing detectable concentrations of the analyzed elements. Measurements of the internal monitor were carried out prior to the measurement of calibration reference materials and corrections for drift were applied to the calibration reference materials. Internal monitor sample measurement made during the analysis of geochemical stream sediment samples are compared with the original results. Any drift can thus be quantified and calibration of the instrument can be maintained relative to its initial condition. The internal monitor standard can be measured regularly (approximately every 10th sample), and the appropriate corrections are made (Elsenbroek, 1994).

Background calibration graphs were set up by using blank samples where background below the spectral peaks related to a nearby interference-free background. Using this relationship, the background below the spectral peaks in both reference material and unknown material was determined and the net spectral peaks intensities were calculated. With the exception of the elements Ti, V and Fe, background determinations were made by using the three interference free background channels. Interference standard of Hoechst Wax with 0.2% of the pure element were used to determine the degree of

spectral line overlap and for the calculation of the spectral line overlap correction factors, as described by Nisbet et al, 1979.

Matrix correlation was carried out by using mass absorption coefficients to correct for absorption effects. The mass absorption coefficients were calculated from known international reference material of major element composition using the following formula:

$$\mu_{\lambda} = \sum_{i} c_i \mu_i$$

Where μλ, is the mass absorption coefficient at wavelength (λ); í, the individual element; cí the mass fraction of element (í); and μí the mass absorption coefficient of element (í).

The values for μí were obtained from the table of Heinrich. The linear dependence of 1/RhKβ Compton intensity on the mass absorption coefficient of CuKα wavelength (μCu) (Elsenbroek, 1994).

International reference material was found by regressing the calculated μCu on the measured 1/RhKβ Compton. The regression equation was used to estimate μCu for unknowns. The μCu value was multiplied by the geometric factor and the net peak intensities of the entire elements on the short wavelength side of the FeKα absorption edge. The element Co, Fe, Cr, Mn, V, Ti and Sc the mass absorption coefficients of the CrK wavelength (μCr) -were determined by using the FeKα net peak intensity in the following linear equation of the form y = mx +c

$$\frac{\mu_{cu}}{\mu_{cr}} = mI_{Fe} + c$$

Where y = μCu /μCr; x is IFe (kcounts s-1); m is the slope; and c is the intercept. For all the 24 chemical elements the calibrations are simple linear fits between the net peak intensity (in kcounts s-1) and the concentration (in % or ppm). The net peak intensity is the result of the following corrections: internal monitor drift, background, interference and mass absorption (Elsenbroek, 1994). A wide variety of geochemical reference samples that cover most typical rock, soil and steam sediments composition was used for the calibration Table 2.2-2 (Elsenbroek, 1994).

2.2.4 Lower limit of detection and determination limit

The lower limit of detection is generally defined as that concentration equivalent to a certain number of standard deviations of the equivalent background count rate. According to Jenkins (1988) three major factors will affect the detection limit for a given element; (i) the sensitivity of the spectrometer for that element in terms of the counting rate per unit concentration of the analyte element; (ii) background (blank) counting rate and (iii) the available time for counting peak and background photons (Elsenbroek, 1994).

The actual detection limit measurable also depends upon the characteristics of the specimen itself. The detection limits vary not only with the atomic number of measured element but also with the sample matrix. This is because both slope and background intensity is affected by changes in the matrix. In general, the background intensity increases with a decrease in average atomic number of the measured wavelength. According to Potts (1987) lower limits of detection and determination limits are defined by the following equation. The lower limit of detection (LLD) is the smallest signal that can be measured:

$$3Sp = 3\sqrt{2N_b} = 3/m\sqrt{N_b}$$

The determination limit is the smallest signal that can be quantitatively measured.

$$6Sp = 6\sqrt{2N_b} = 6/m\sqrt{\frac{R_b}{T}}$$

Where Sp is the standard deviation of the net analyte peak: Nb is the background counts; m is the slope of the calibration graph; Rb is the background count rate under the peak; and T is the total counting on peak and background (Elsenbroek, 1994). In this work the formula for calculating the determination limit was used at (99% confidence). The 1σ counting error (CE3) was calculated from the following equation:

$$1\sigma(CE) = \sqrt{\frac{R_p / T_p + R_b + R_b / T_p \times c}{R_p}}$$

Where Rp is the net peak in counts s-1; Rb is the net background in counts s-1; Tp is the peak counting time; and Tb is the background counting time. The average determination limit (DL) of all 24 elements is summarized in Table 2.2-3, together with their calibration concentration (c) ranges. The determination limit was calculated for calibration reference material together with 1σ counting error for the calibration of the elements (Elsenbroek, 1994).

Table 2.2-2: International reference material used for instrument calibration (Elsenbroek, 1994).

No.	Reference Material	Origin	Description
1	ABV-1	USGS*	Andesite
2	BCR-1	USGS*	Basalt
3	G-2	USGS*	Granite
4	GSP-1	USGS*	Granodiorite
5	PCC-1	USGS*	Peridotite
6	BHVO-1	USGS*	Basalt
7	MAG-1	USGS*	Marine mud
8	QLO-1	USGS*	Quartzite
9	SCo-1	USGS*	Cody shale
10	SDC-1	USGS*	Mica schist
11	STM-1	USGS*	Syenite
12	BIR-1	USGS*	Basalt
13	DNC-1	USGS*	Diabase
14	W-2	USGS*	Diabase
15	SY-2	Canmet*	Syenite
16	SY-3	Canmet*	Syenite
17	MGR-1	Canmet*	Gabbro
18	GR	CRPG *	Granite
19	GA	CRPG *	Granite
20	GS-N	ANRT*	Glass
21	FK-N	ANRT*	Granite
22	MW-1	IGME*	Maiskite
23	JB-1	GSJ*	Basalt
24	NIM-D	MINTEK*	Dunite
25	NIM-G	MINTEK*	Granite
26	NIM-L	MINTEK*	Lujavrite
27	NIM-N	MINTEK*	Norite
28	NIM-P	MINTEK*	Pyroxenite
29	NIM-S	MINTEK*	Syenite
30	Fer-1	Canmet*	Fe formation
31	GSD-1	IGGE*	Str Sed*
32	GSD-2	IGGE*	Str Sed*
33	GSD-3	IGGE*	Str Sed*
34	GSD-4	IGGE*	Str Sed*
35	GSD-5	IGGE*	Str Sed*
36	GSD-6	IGGE*	Str Sed*
37	GSD-7	IGGE*	Str Sed*
38	GSD-8	IGGE*	Str Sed*
39	GSD-9	IGGE*	Sed*
40	GSD-10	IGGE*	Sed*
41	GSD-11	IGGE*	Sed*
42	GSD-12	IGGE*	Sed*
43	GSR-1	IGGE*	Granite
44	GSR-2	IGGE*	Andesite
45	GSR-3	IGGE*	Basalt
46	GSR-4	IGGE*	Sandstone
47	GSR-5	IGGE*	Shale
48	GSR-6	IGGE*	Limestone
49	GSS-1	IGGE*	Soil
50	GSS-2	IGGE*	Soil
51	GSS-3	IGGE*	Soil
52	GSS-4	IGGE*	Soil
53	GSS-5	IGGE*	Soil
54	GSS-6	IGGE*	Soil
55	GSS-7	IGGE*	Soil
56	GSS-8	IGGE*	Soil
57	Fer-2	IGGE*	Fe formation
58	Fer-3	Canmet*	Fe formation
59	Fer-3	Canmet*	Fe formation

*USGS, United State Geological Survey; CCRMP, Canadian Certified Reference Materials Project; Canmet, Canada Centre for Mineral and Energy technology; CRPG, Centre de Recherches Petrographiques et Geochimiques; ANRT, Association Nationale de la Recherche technique, Paris; IGEM, Institute of Geology of Ore Deposits, Petrology, Mineralogy and Geochemistry, Moscow; MINTEK, Council for Mineral Technology, South Africa; IGGE, Institute of Geophysical and Geochemical Prospecting, People's Republic of China and GSJ, Geological Survey of Japan. Str Sed; Stream sediment, Sed; sediment and Cody Shale; Fine grained offshore shale.

Table 2.2-3: Calibration concentration range of various elements and their determination limits (Elsenbroek, 1994).

Elements	Range	DL
Sc	1-55 (ppm)	1 (ppm)
TiO_2	0.20-3.77 (%)	100 (ppm)
V	9-526 (ppm)	5 (ppm)
Cr	10-2900 ppm	4 (ppm)
MnO	0.01-0.32 (%)	100 (ppm)
Fe_2O_3	1.40-18.76 (%)	100 (ppm)
Co	11-210 (ppm)	10 (ppm)
Ni	10-2380 (ppm)	10 (ppm)
Cu	19-1230 (ppm)	9 (ppm)
Zn	10-680 (ppm)	3 (ppm)
As	18-412 (ppm)	10 (ppm)
Rb	9-860 (ppm)	1 (ppm)
Sr	25-1100 (ppm)	1 (ppm)
Y	5-718 (ppm)	1 (ppm)
Zr	22-1210 (ppm)	1 (ppm)
Nb	10-960 (ppm)	5 (ppm)
Mo	10-960 (ppm)	0.2 (ppm)
Sn	3-370 (ppm)	2(ppm)
Sb	10-2000 (ppm)	5 (ppm)
Ba	114-2400(ppm)	10 (ppm)
W	24-490 (ppm)	4 (ppm)
Pb	11-636 (ppm)	4 (ppm)
Th	17-1000 (ppm)	4 (ppm)
U	9-650 (ppm)	2 (ppm)

2.3 SPATIAL DATA ANALYSIS TECHNIQUES

Spatial data analysis was carried out using the following software: Arc-View 3.2a©, Surfer 8.0©, and Statistica© for manipulating the data from various study areas (see detail in Chapter 4) and intergrated data interpretation.

A range of statistical functionality is provided for working with high volume geochemical data, including histograms, scatter plots, box plots and probability analysis functions. The histogram analyses provide visual presentation, with distribution patterns identifying outlier samples and describing the variability frequency of the element. A box plot function is used to plot three channels and interactively interrogate data and information visually and numerically. Scatter plots and correlation matrixes enable one to plot one element against another and are dynamically linked to the database and maps.

The integrated data interpretation (geochemical, geology and geophysical data for interpretation) was used in producing a map and to provide the spatial distribution of the geochemical element within the identified study area, it provides the detailed relationship between the geology of the overlain area by the identified geochemical anomalies whether they are related to the parent bedrock and to existing mineralization. This was done by superimposing the geology, geophysical and geochemical data. The geochemical data which were equal or higher than the threshold values were demarcated by the polygon to separate them from the values below the threshold values. This technique provides relationship among the geology and geochemical data for the interpretation purposes and the exact location of the geochemical anomalies in relation to geology.

CHAPTER THREE

3 GEOLOGY OF THE AREA

3.1 GEOLOGICAL SETTING OF THE STUDY AREA

The Northwest Province is situated in the western terrane of Kaapvaal Craton, west of the Colesberg magnetic anomaly. This anomaly is considered by Corner *et al*. (1990) to represent a mid-crustal layer up warped along the western edge of the Kaapvaal Craton. The region also incorporates three of the twelve sub domains demarcated by de Wit *et al*. (1992) in their evolutionary model of the Kaapvaal Craton and it includes the Colesberg, Amalia and Kraaipan subdomains. Metamorphosed Archaean mafic volcanic rocks and interlayed ferruginous and siliceous metasediments, together with a variety of granitoid rocks, including tonalitic and trondhjemitic gneisses, granodiorites and adamellites.

The regional trend of greenstone belts in this part of the Craton is generally north-south, virtually at right angle to the east northeast trends displayed by greenstone belts in the Northern and Eastern part of the Kaapvaal Craton. Information on these western belts and surrounding granitoids is limited due to their poor exposures beneath Neo-Archaean- to late-Palaeozoic Ventersdorp-Karoo cover sequences and Cenozoic Kalahari sands. In addition, this terrane is further obscured by exposures of the Gaborone Granite Complex, consisting of rhyolitic, granophyric and granitic rocks which occur to the north of Mafikeng and in southeast Botswana.

The oldest basement rocks in the Western Terrain occur in mine exposures and borehole intersections in the Kimberley region, and consist mainly of gneissic-to migmatitic, heterogeneous, tonalitic-to-granodioritic rocks,. Several hundred kilometers north of Kimberley, but still part of the Western Terrane, are the Amalia and Kraaipan granite-greenstone terranes, which extend northwards to the Botswana border and beyond. The

northernmost Kraaipan terrane can be subdivided into three, norths-northwest-trending belts, spaced at 30-40 km intervals, namely the western, eastern and Madibe belts.

The Madibe Greenstone Belt represents the easternmost belt in the Kraaipan terrane. The strata strike in a north-south direction and represent an assemblage of metamorphosed and strongly deformed volcanic and minor sedimentary rocks, now represented by phyllites, quartz-sericite and quartz-chlorite schists, amphibolites, talc-carbonate schists and banded iron formation. The succession, which is poorly exposed, has been interpreted as a mid-Mesoarchaean volcanic island arc that was welded onto the western margin of the Kaapvaal Craton. The Amalia granite-greenstone terrane further to the south is dominated by a narrow, north-northwest trending linear belt consisting mainly of mafic metavolcanic rocks, banded iron formation and various mafic schists (Van Eeden *et al*., 1963; Anhaeusser, 1991). An accretionary lapilli tuff unit, described by Jones and Anhaeusser,1993), has been dated at 2754 ± 5 Ma, while a quartz-chlorite-sericite schist in the same vicinity was dated at 2740 ± 13 Ma (Poujol *et al*., 2001).

The youngest granitoid recorded in the Western Terrane consists of a biotite-muscovite granite (Skalkseput pluton) in the Marydale granitoid-greenstone terrane on the extreme southwestern flank of the Kaapvaal Craton, which was dated at 2718 ± 8 Ma (McCourt, 2000).

3.2 STRATIGRAPHY

North West Province has an ancient geological heritage, rich in minerals and paleontological artifacts. The north-eastern and north-central regions of the province are largely dominated by igneous rock formations, as a result of the intrusion of the Bushveld Complex. Ancient igneous volcanic rocks dating back to Ventersdorp age (more than 2 000 Ma) appear to be the dominant formations in the western, eastern and southern regions of the area. Sedimentary rocks dating back to the Quaternary period (65 Ma) occur in the north-western corner of the Province.

The oldest rock formations in the study area are the basement Archaean Granites (3 204 ± 65 Ma) as out lined in table 3.2-1, which mostly form flat to slightly undulating landscapes. Outcrops of these granites occur in the south-eastern portion of the Province (in the Potchefstroom district) and further west as far as the north-central portion of the Vryburg and Ganyesa districts (de Villiers *et al*., 2002).

The Kraaipan Group, which can not be less than 3048 m thick, makes three important but narrow belts through the Mafikeng district trending almost north-south, flanked on either side by granite and gneiss; the formations have been heavily folded and considerably faulted. (Du Toit, 1926).

The Kraaipan Succession consists mainly of mafic volcanic rocks with subordinate iron formation and schist and a small proportion of dolomite (SACS, 1980). This formation forms a series of narrow, more or less parallel, discontinuous ridges approximately 60 km south-west of Mafikeng running north to north-north-west. Another series of parallel, discontinuous outcrops occur near Stella approximately 50 km further west.

The Dominium Group, dated at 2 800 Ma, is predominantly volcanic in origin and lies on top of a basement of granite. It spreads over an area bounded by Ventersdorp in the north, a point west of Klerksdorp in the south and a point south west of Hartebeesfontein. It is comprised of erinaceous sediments, conglomerates, grits, basic volcanics, tuffs, coarse pyroclastic rocks and quartzite. It is predominantly volcanic in origin, forming a

series of hills to the west of Klerksdorp (in the vicinity of the old gold-mining town of Dominium Reefs). The thickness of the Group is 2 250 m in this area. A second important outcrop occurs at Ottosdal. The third outcrop (maximum thickness of 240 m) occurs as a narrow band of the rocks on the fringe of the younger Witwatersrand outcrops in the southern portion of the Potchefstroom district (SACS, 1980).

The Witwatersrand Supergroup is dated between 2 800 and 2 300 Ma and extends into the North West Province from the east and south. It is comprised of a thick sequence (more than 5 km) of shale, quartzite and conglomerates. The quartz-pebble conglomerate has the gold bearing reefs and uranium mineralisation (SACS, 1980).

Ventersdorp volcanic rocks also comprise an important geological formation in the area. This covers an extensive area both within and around the Witwatersrand basin, ranging in thickness from around 50 m to 300 m. It is especially prevalent near Ventersdorp, Vryburg, Klerksdorp and Mafikeng where it extends into south eastern Botswana. Other outcrops occur near the Vredefort Dome. The Ventersdorp Supergroup is composed largely of volcanic andesitic lavas and related pyroclastics (metamorphic rocks formed by the extremely hot temperatures associated with volcanic activity). Various conglomerates, tuffaceous and calcareous shales and porphyries are also constituents of this formation (van der Westhuizen *el al.*, 2006).

Transvaal Supergroup represents a large component of the Province's geology and consists of two main sedimentary groups: the Pretoria-Griquatown group and the Olifants River-Campbell Rand Groups. Both groups occur discontinuously in the North West Province. The western section occurs in an area bounded by Vryburg, Kuruman and Douglas known as the Ghaap Plateau. The eastern section extends from the south to the north of Ventersdorp, west of Mafikeng and to the Rustenburg section.
Lower strata of the Transvaal Supergroup comprise mostly of dolomite with some chert and shales interspersed in places while the upper strata appear to be more varied in constituents. Dolomite consists largely of calcium carbonate and is hence vulnerable to solution, especially by the carbonic acid found in rainwater percolating downwards. The

dissolution of dolomite can lead to the formation of underground caverns and horizontal chambers often filled with large volumes of groundwater. The Malmani Dolomite Subgroup appears to be one of the lithostratigraphic units of the Transvaal Supergroup. It contains abundant algal stromatolites which presents evidence of an aquatic environment in ancient times. The algal stromatolites have a number of distinctive shapes such as domes, columns and spheres, their shape being governed by the environment in which they were formed (Eriksson *et al*., 2006).

Near Zeerust is an overlying banded iron layer known as the Penge Formation as well as a mixed zone containing chert breccia, carbonaceous shale or mudstone and limestone. The basal sequence of the Malmani Dolomite Subgroup is underlain by the Black Reef Formation which consists of a very thin sequence of quartzite, conglomerates and shales. In the western region of the province is the dolomitic Ghaap Plateau that includes the Campbell Rand, Kuruman and Griquatown Formations. The former consists of limestone, dolomite, chert, shale siltstone and quartzite. The Kuruman Formation consists of banded iron formation deposits, not unlike the Penge Formation. The latter formation, which overlies the other two, contains jasper in abundance as well as layers of iron (Eriksson *et al.*, 2006).

The Pretoria Group is sequence running westward from Lobatsi past Rustenburg and Pretoria almost reaching Witbank in the east (Eriksson *et al*. (2006). This formation occurs in a thick layer ranging from 4000m to 7000m, consisting of chert, conglomerates and quartzite. Between the Magaliesberg and Daspoort Formations, there is a thick volcanic sequence as well as shales and other pyroclastic materials. The shales often contain metamorphic minerals such as cordierite, staurolite, garnet, andalusite and sillimanite. Slate is also prevalent in this area (Eriksson *et al.*, 2006).

The western portion of North West Province is dominated by rocks of the Griqualand West Sequence (similar in age to that of the Transvaal Supergroup) (SACS, 1980). Quartzite, shale, siltstone and lava of the Vryburg Formation (approximately 75-100 m

thick) are the oldest rocks in the sequence and outcrop to the east of Vryburg (Eriksson *et al.*, 2006).

Dolomite of the Campbell Rand Group, consisting of the Schmidtsdrif (3 - 275 m thick) and Ghaap Plateau Formations (alternating in thickness between 900 and 1600 m) are made up of alternate intercalated layers of dolomite, shale, limestone, calcareous sandstone, siltstone and chert. The main outcrop of this group occurs in the area to the south west of Vryburg and stretches down to the border of the Province near Kudumane.

The Bushveld Complex occurs in the north-eastern region of the area, from Brits and Rustenburg in the east to north of Zeerust and Swartruggens into Botswana. Of the three suites making up the Complex, only the peripheral mafic intrusive phase occurs in the North West Province. This consists of four main layers: Upper Zone of gabbro, olivine, diorite to granodiorite with some anorthosites and magnetites. The Main Zone of 5 200m which consists mostly of gabbros, and gives rise to topographic features such as hills. Below this is the critical zone consisting of norites, anorthosites, pyroxenites and chromites, below which is the Basal Zone mostly of pyroxenite and peridotite. Platinum and chromite from this zone are mined extensively in Rustenburg (Cawthorn *et al.*, 2006).

The isolated ring of alkaline rocks at Pilanesberg, called the Pilanesberg Complex, is basically a series of concentric hills covering over 500 km^2. It consists of an overlying layer of alkaline volcanic and pyroclastic rocks, the latter consisting of fragmental volcanic material that was blown into the atmosphere by explosive activity. The top layers have largely been eroded away. The intrusive base is composed of foyaite and syenite. It also consists of small outcrops of quartz-rich rocks. The complex was formed by the coalescence of a number of small volcanoes and the welling up of successive ring-dykes around the collapsed crown (Verwoed, 2006).

Outcrops of the Karoo sediments occur between Lichtenberg and Mafikeng as well as to the south of Vryburg. Another small outcrop occurs to the east-north-east of Schweizer-

Reneke and near Bloemhof (SACS, 1980). Another outcrop of these rocks covers a portion of the Bushveld Complex rocks north of Brits. Karoo sediments are also known within sinkholes in the dolomite in the vicinity of Stilfontein.

Kimberlites are diamond bearing vertical "pipes" or "fissures" which have intruded to the surface. They contain a number of minerals including mica, olivine, augite, red garnet and pyrite to name a few. Several kimberlite fissures occur in North West Province the most notable being around the Harts River 100km north west of Kimberley (Shee *et al*., 1989).

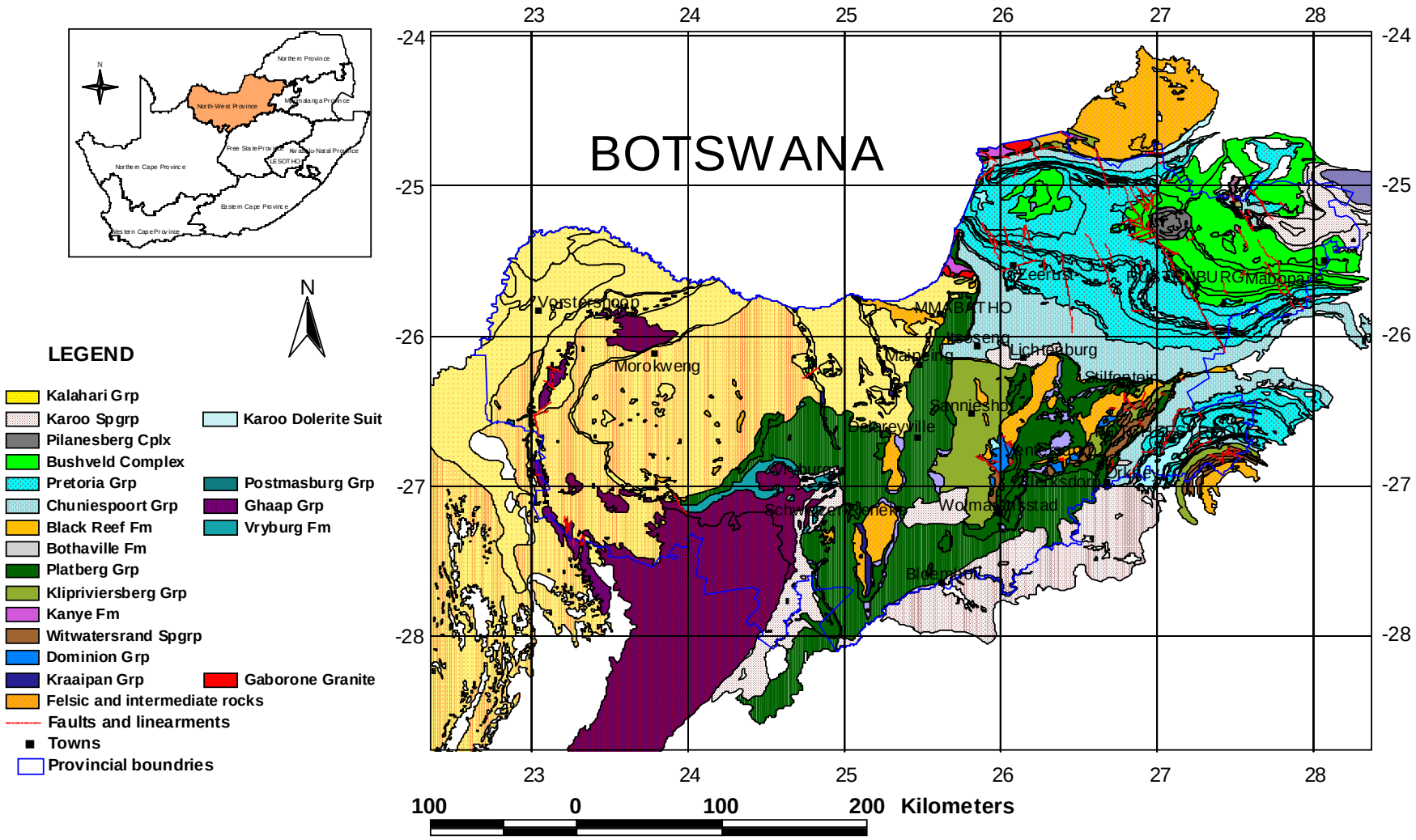

Figure 3.2-1: Simplified geological map of North west Province, South Africa (source from Metallogenic map of the Republic of South Africa; Vorster, 2001).

Table 3.2-1: Generalized lithostratigraphic column of the North West Province (from SACS, 1980).

Eon	Sedimentary and volcanic accumulation	Lithological discription	Major igneous rocks	Mineralization
PHANEROZOIC	**KALAHARI GROUP** (±45 Ma)	Surface deposits, calcrete		
	KAROO SUPERGROUP (±250Ma)	Kimberlite Karoo sediments including shale, mudstone limestone , calcrete and dolerite	Kimberlite Karoo dolerite Karoo dolerite	Diamond (alluvial deposits), dolerite and uranium
PROTEROZOIC	**OLIFANTSHOEK SUPERGROUP** (±1800 Ma)	Quartzite, interlayed tuff, conglomerate, mudstone and agglomerate	Pilanesberg Complex and similar rocks	Fluorite, thorium Uranium Platinum group elements, crocidolite, iron, manganese, limestone, dolomite vanadium, nickel, chromite, salt, clay, zinc, lead, gold and copper
	TRANSVAAL SUPERGROUP (±2000 Ma)	Quartzite, conglomerates, siltstones, metamorphosed shale, slates and hornfelses, dolomite, diabase and amygdaloidal andesitic lavas	Bushveld Complex	
ARCHAEAN	**VENTERSDORP SUPERGROUP** (2714Ma)	Andesitic lavas and related pyroclastics, conglomerates, tuffaceous and calcareous shale and porphyries	Basaltic andesitic lava	VCR Gold on the bottom
	WITWATERSRAND SUPERGROUP (±2714 -3070 Ma)	Quartzite, shale, and conglomerates	Brown Lava	Gold and Uranium
	DOMINION GROUP (±2900 -3086Ma)	Pyroclastic rocks, tuffs, quartzite conglomerates, grits, volcanic rocks, arenaceous sediments,	Interbeded lavas.	Uranium
	KRAAIPAN GROUP (±3500 Ma)	Schist, amphibolite, jaspilite, lava, banded ironstone and dolomite and granites	Granites and diorites associated with greenstone belts	Gold and iron

3.3 GEOLOGY OF THE MAFIKENG AREA

The Northwestern part of the area is almost completely covered by recently windblown reddish-brown sand of the Cenozoic of the Kalahari Group. More than 30% of the central part of the area is covered by calcrete of Tertiary age (Pliocene or younger) and recent orange-brown poorly sorted, terraced river gravels (Kalahari age) which lie to the south and west of Mafikeng along the old course of the paleo-Molopo river and its tributaries. Some of the gravels are diamondiferous and have been irregularly excavated over the last hundred years. Active, white calcrete pans, which give rise to a fine, black soil that are frequently filled up with standing water in the rainy season, occur around Mmabatho, Signal Hill and Lonely Park (Michaluk and Moen, 1991). Refer to Fig. 3.3-1.

To the east of the area the calcrete usually lies unconformably on blue-green amygdaloidal a basaltic to andesitic lava belonging to the Allanridge Formation (Ventersdorp Supergroup). The calcrete is conspicuous as hard caps on raised areas of lava in the Mafikeng Game Park. The Ventersdorp Supergroup was intruded by porphyritic graphic granophyres, microgranite and luecogranite of the Gabrone Granite. Vent agglomerate, belonging to the Kameeldoorns Formation crops out over the greater part of Mafikeng area. It consists mainly of angular fragments of granite (basement rocks) and mafic lava in a fine grained dark grey matrix. The size of the blocks ranges from large to small, which indicates poor sorting (Michaluk and Moen, 1991).

To the west of the Mafikeng area, the surface deposits consist of unconsolidated, dune-free, and orange-yellow aeolian sand belonging to the Gordonia Formation (Fig 3.3-1). These beds range up to 3 meters in thickness and make excellent building sand due to the low clay content (<10%). The sand lies on Archaean gneiss with the best example being at the wall of Modimola dam. The granite-gneiss shows alternating bands of grey and white and dark green amphibole rich layers and pale pink granite (consisting mainly of pink orthoclase feldspar and quartz) (Michaluk and Moen, 1991).

In the northeast the rocks are also not well exposed and are overlain by a thin layer of calcrete which is sometimes overlain by lenses of ferricrete underlying the topsoil. The calcrete overlies fine grained slates, shales and mudstones belonging to the Rietgat Formation. The shales are frequently quarried for brick making and at the bottom of the quarries in the vicinity of Molelwane micaceous granite is exposed. Elsewhere this weathered granite is quarried for sand. Outcrops of blue green amygdaloidal lavas interlayered with weathered tuffs and shales may belong to the younger Allanridge Formation but a contact was not observed. The rounding of the clasts indicates that the rock must have originated as a mud slide down the flanks of a volcanic cone or fault scarp (Michaluk and Moen, 1991).

Diabase and norite dykes of Tertiary age are common in this area, especially in the north-eastern (Mokgwapane) part (Fig. 3.3-1). Major and minor faults occur in an area striking north-west to south-east in the eastern part of the area (Michaluk and Moen, 1991).

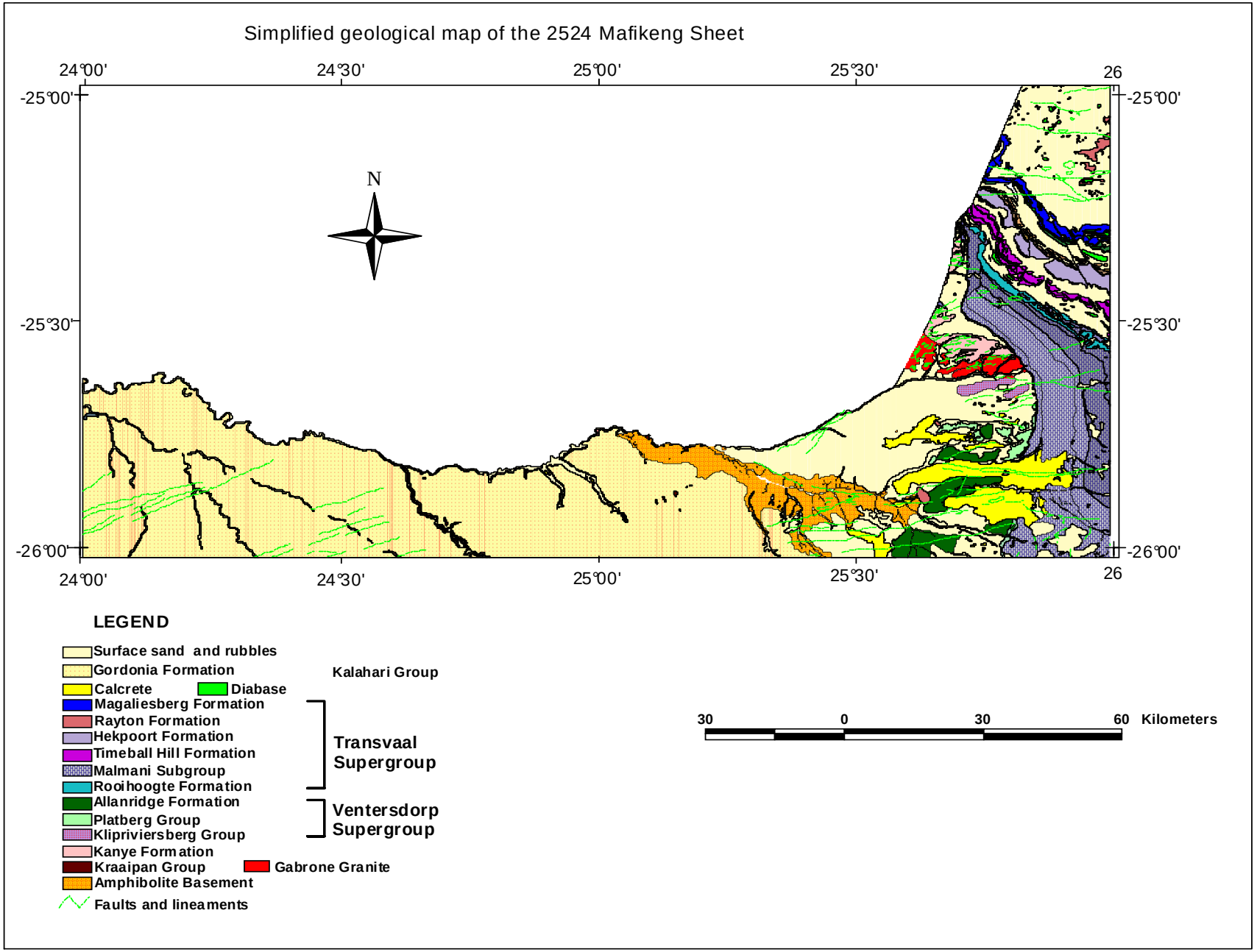

Figure 3.3-1: Simplified geological map of the Mafikeng Area (after Michaluk and Moen, 1992).

Table 3.3-1: Lithostratigraphic column of the Mafikeng Area (Fm- Formation) summarized from SACS, 1980.

STRATIGRAPHY				DESCRIPTION	MAGMATIC EVENT	AGE(Ma)
				River sand alluvium		1.6 -2.5
				Superficial deposits		
				Wind-blown, partially reworked sand, colluvial.		
KALAHARI GROUP		Gordonia Fm		Wind-blown sand		
				Siliceous sandstone, pebble conglomerate, gritstone, silcrete		
				River terrace gravel		
				Calcrete	Diabase and Norite	±190-240
TRANSVAAL SUPERGROUP (± 6km)	PRETORIA GROUP	Rayton Fm		Hornfels and quartzite.		2060-2500
		Magaliesberg Fm		Orthoquartzite, limestone and hornfels.		
		Silverton Fm		Hornfels, slate and minor dolomite.	Bushveld Complex (±2095-1670 Ma)	
		Daspoort Fm		Quartzite.		
		Strubenkop Fm		Slate, shale, quartzite.		
		Dwaalheuwel Fm		Magnetic quartzite, hornfels.		
		Hekpoort Fm		Andesitic lava and muscovite hornfels.		
		Boshoek Fm		Conglomerate, quartzite.		
		Timeball Hill Fm		Carbonaceous slate, quartzite, slate, ferruginised quartzite hornfels and slate.		
		Rooihoogte Fm		Orthoquartzite, conglomerate; minor slate and limestone, Banded iron formation, basal breccia.		
	CHUNIESPOORT GROUP	Penge Fm		Banded Iron formation chert and breccia.		
		Malmani Subgroup	Frisco Fm	Undifferentiated dolomite and chert and shale.		
			Eccles Fm			
			Lyttelton Fm			
			Monte Christo Fm			
			Oaktree Fm			
	Black Reef Fm			Quartzite, shale basal conglomerate		
	Skilpadhek Group			Conglomerate, basic, acidic lava, tuff, quartzite, shale and schist.		
VENTERSDORP SUPERGROUP (± 2km)	Allanrigde Fm			Andesitic to basic lava and minor tuff.	Basaltic–andesitic lavas	2714
	PLATBERG GROUP	Rietgat Fm		Volcanic gritstone, sandstone and, tuff and conglomerate		
		Makwassie Fm		Silicified tuff, tuffaceous sediment, felsic lava, chert, conglomerate, schist sandstone, felsic lava, and breccias.		
		Kameeldoorns Fm		Volcanic breccias, basic lava, tuff, conglomerate, schist, sandstone, felsic lava and breccias.		
	KLIPRIVIERSBERG GROUP			Amygdaloidal lava, and homogeneous lava, porphyritic lava.	Gaborone Granite	
Kanye Fm				Felsic lava, Breccias.		2830-2770
KRAAIPAN GROUP (1100m)		Khunwana Fm		Banded chert, Jaspilite.	Undifferentiated granitoids	±3640
		Ferndale Fm		Variegated jaspilite interbanded iron formation, pillow lava, rhyolite		
		Gold Ridge Fm		Banded iron formation, mica, pyrophyllite, and chlorite schist.		
Amphibolite basement						

3.3.1 Geological Structure of the Mafikeng Area

The structure of the Mafikeng area is the result of several phases of deformation. The oldest structures are found in the banded gneisses, west of Mafikeng in the form of tight isoclinal, intrafoliaged folds. Morphologically similar folds also occur in banded rocks of the Kraaipan Group, but it is not certain whether they are of the same age, as those gneisses appear to be related to higher grade of metamorphism than those in the Kraaipan. The general trend of the foliation and banding in the gneisses as well as the megastructures in the Kraaipan, is due north, in contrast to structures associated with the Transvaal Supergroup which trends northwest. Northeast trending kink bands, minor folds and shears have been recognized in the Kraaipan rocks and indicate a dextral shear event, possibly of early Bushveld age. For the deformational history of the area west of Mafikeng Du Toit (1905) proposed an initial north-south compressional phase during which east-west-trend in isoclinal folds and quartz veins developed. These were followed by a period of east-west compression which led to tightening of existing folds, as well as thrust faulting. A final episode of brecciation, quartz veining and minor faults could be related to the emplacement of the Bushveld complex (Michaluk and Moen, 1991).

Work done by the Geological Survey of South Africa towards the south on the Vryburg sheet led to the alternative view that the initial compression acted from east to west, resulting in various fold styles with north-trending axes. Later north-south compression superimposed broad, open folds on the existing fabric, followed by intense localized shearing (Michaluk and Moen, 1991).

Post Ventersdorp, pre-Transvaal folding and faulting are evident from the relationship between the Ventersdorp lava and the Black Reef Formation, and can be seen on Klippan 81, where a northwest –trending, open syncline is developed in silicified tuff of the Makwassie formation. Numerous northeast-eastwest-trending shear zones cut the tuff, some showing displacement, with none extending into the Black Reef Formation. In the Skilpadhek area, folding in the Skilpadhek Group is parallel to that in the Black Reef Formation (Michaluk and Moen, 1991).

Two periods of faulting, expressed as the pre-and post-Bushveld faults, have been recognized in the Gopane area. The first is a dominant northwest-trending set of steeply dipping faults which forms a series of horst and graben structures. The second trends east-west and is prominent in the Black Reef Formation and the Chuniespoort Group. These are particularly well displayed in the Gaborone Granite and elsewhere, particularly in the Rooigrond area. Both sets are regarded as having formed under tensional conditions (Klop, 1978).

North of the Skilpadhek, the complex structural pattern exhibited in the Transvaal Supergroup is attributed to a series of gravitational slides that occurred before the Bushveld Complex was emplaced. The boundary of this tectonic regime roughly coincides with the international border. The Woodlands Fault displaces the Timeball Hill Formation a vertical distance of 70 m. To the north the Boshoek Formation displaced some 90 m along the trace slip of a fault which is the extension of a fault in the Strubenkop Shale Formation in Botswana (Klop, 1978).

3.3.2 Commodities

Andalusite is developed in slate of the Timeball Formation of the Pretoria Group particularly in the upper portion and is a result of thermal metamorphism associated with the emplacement of the Bushveld complex. Because of the westward-decreasing metamorphic grade, deposits at Gopane are characterized by incipient andalusite formation and are therefore of economic interest (Michaluk and Moen, 1991).

Diamonds occur in some of the Quaternary gravels, which are present in the southern part of the area. In south of Mafikeng, the gravel deposits have been worked for diamonds, while the associated gravels are used in the construction industry (Michaluk and Moen, 1991).

Gold was found in the northwest trending, near vertical quartz reef which dip to the west and southwest. The gold occurred as nuggets, scale and specks and was accompanied by

some copper, pyrite, galena and sphalerite. In the north of Madibeng, gold was mined from quartz vein in quartz-sericite-chlorite schist and banded iron formation (BIF) of the Kraaipan Group (Michaluk and Moen, 1991).

Iron as magnetite lenses of up to 30 cm thick have been found in a weathered magnetite-rich norite on Rietgat 91-JP and further to west.

Limestone. Major limestone deposits are found in the Slurry-Rooigrond area, where large quarries have been opened in the calcrete. Calcrete deposits cover approximately 220 km^2, of which 200 km^2 is sufficiently thick economically recoverable limestone with a potential of ±1 400 million tons (Michaluk and Moen, 1991).

Lead occurs as galena associated with sphalerite. The mineral is hosted almost exclusively in laterally extensive, stratabound bodies in the stromatolitic dolostones of the Frisco Formation of the Malmani Subgroup of the Transvaal Supergroup (Pöetter, 2001).

Manganese occurs in the limestone beds of the Bevets Conglomerate Member (Rooihoogte Formation) and was the result of supergene enrichment of the limestone host rock. Elsewhere small diggings have been opened in Malmani dolomite, of the Lyttelton Formation. The ore is composed of crystalline lumps and concentrations from a few millimeters to several centimeters in diameters or of a soft mixture of silica, manganese and iron oxide called wad or manganiferous earth (Michaluk and Moen, 1991).

A **sericite** deposit occurs as a white powdery bed in the Makwassie Formation.

3.3.3 Geophysical Interpretations

The gravity map (Fig 3.3-3) shows the low Bouger anomaly in the east and south east which are related to a Malmani Dolomites and Archaean granites and gneisses. On the northeast of the map, higher Bouger values coincide with higher magnetic values and are correspond to a various diabase outcrops in that area. To the west of the low, Bouguer anomalies north south trends of higher bouguer values is clearly visible and could be related to the northern extension of the Colesberg-Mafikeng trend. West of this anomaly, a low gravity coinciding with the negative magnetic anomaly is correlated with the archaeangranites-gneiss and the kraaipan granites (Kotzé, 1996b).

Two parallel north-south striking trend of high Bouguer and magnetic anomalies coincide with the ultramafic and mafic and banded iron formation of the Kraaipan Group.
In the eastern part of the magnetic map (Fig. 3.3-2), a wedge shaped area of slightly higher magnetic anomalies outlined by low magnetic anomalies is associated with Gaborone Granite and Kanye Formations.
Higher magnetic anomaly extending from east to west across the eastern part of the magnetic map coincides with the Ventersdorp Supergroup (southeast of the Gaborone Granite) (Kotzé, 1996b).
In thw northeast of the Kanye Formation in the eastern part of the magnetic map, a prominent linear negative anomaly trending southwest to southeast can be seem this anomaly is related with the banded iron formation of the Penge Formation. South of this anomaly the outcrops of Malmani dolomites are present on geology map (Fig. 2.3-1) and they are not distinctive on aeromagnetic map.

The positive magnetic anomaly tends to be high in the northern part of the eastern sector and coincides with diabase outcrops. This higher value could result from the combination of the Pretoria Group and diabase sill covering the area (Kotzé, 1996b).

The eastern sector and the dolomites in the southern-most mart of the map are underlain by the Kraaipan Greenstone terrain, which is consists of Kraaipan greenstone.

The western sector of the aeromagnetic map has both higher Bouguer and magnetic anomalies which coincide with the lithologies of the Kuruman Formation of the Asbestos Hill Subgroup and the area are covered by Kalahari sand.

Several linear features in magnetic map of the Mafikeng are attributed to the diabase dykes.

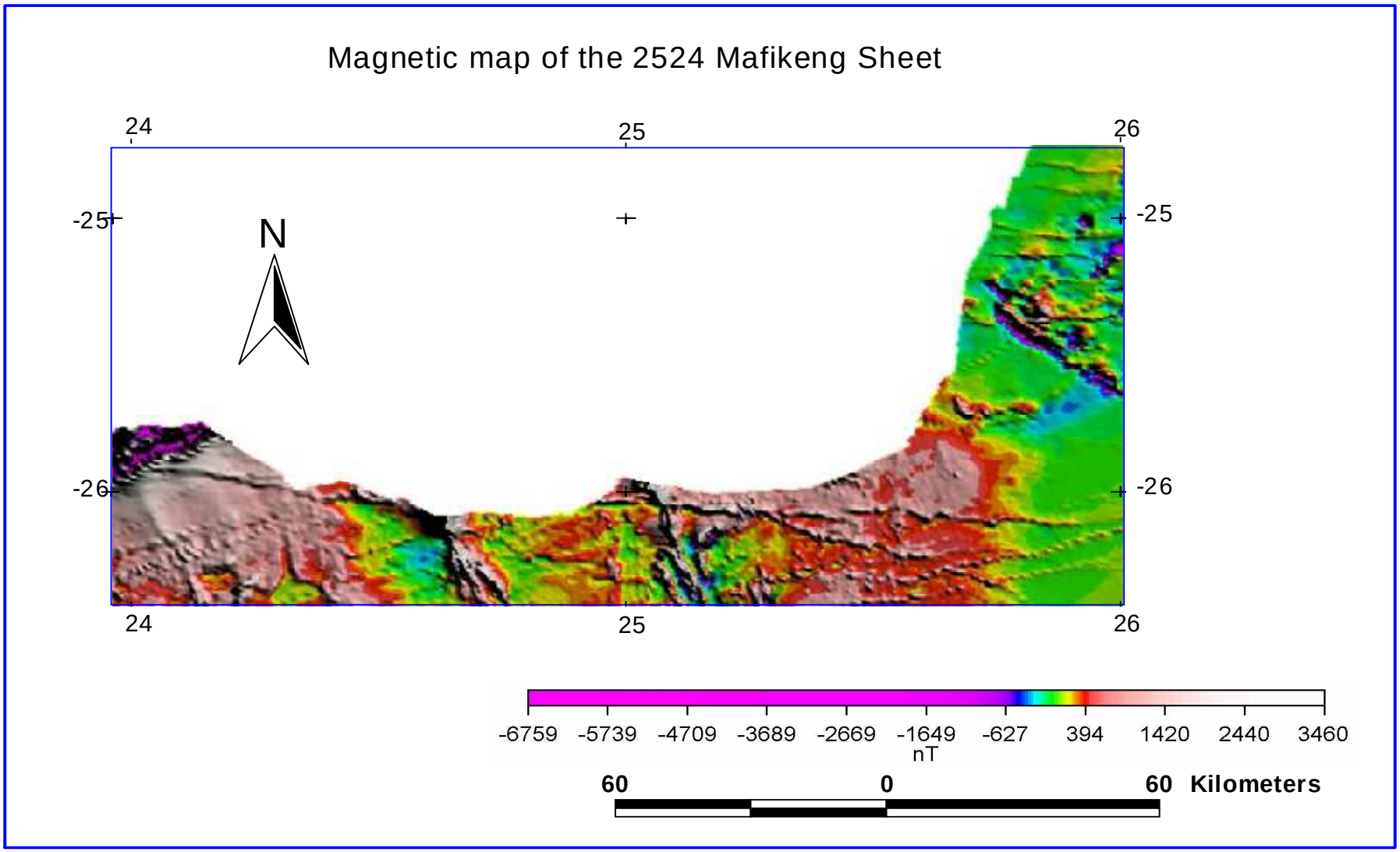

Figure 3.3-2: Magnetic map of 2524 Mafikeng Sheet (Council for Geoscience, 2000).

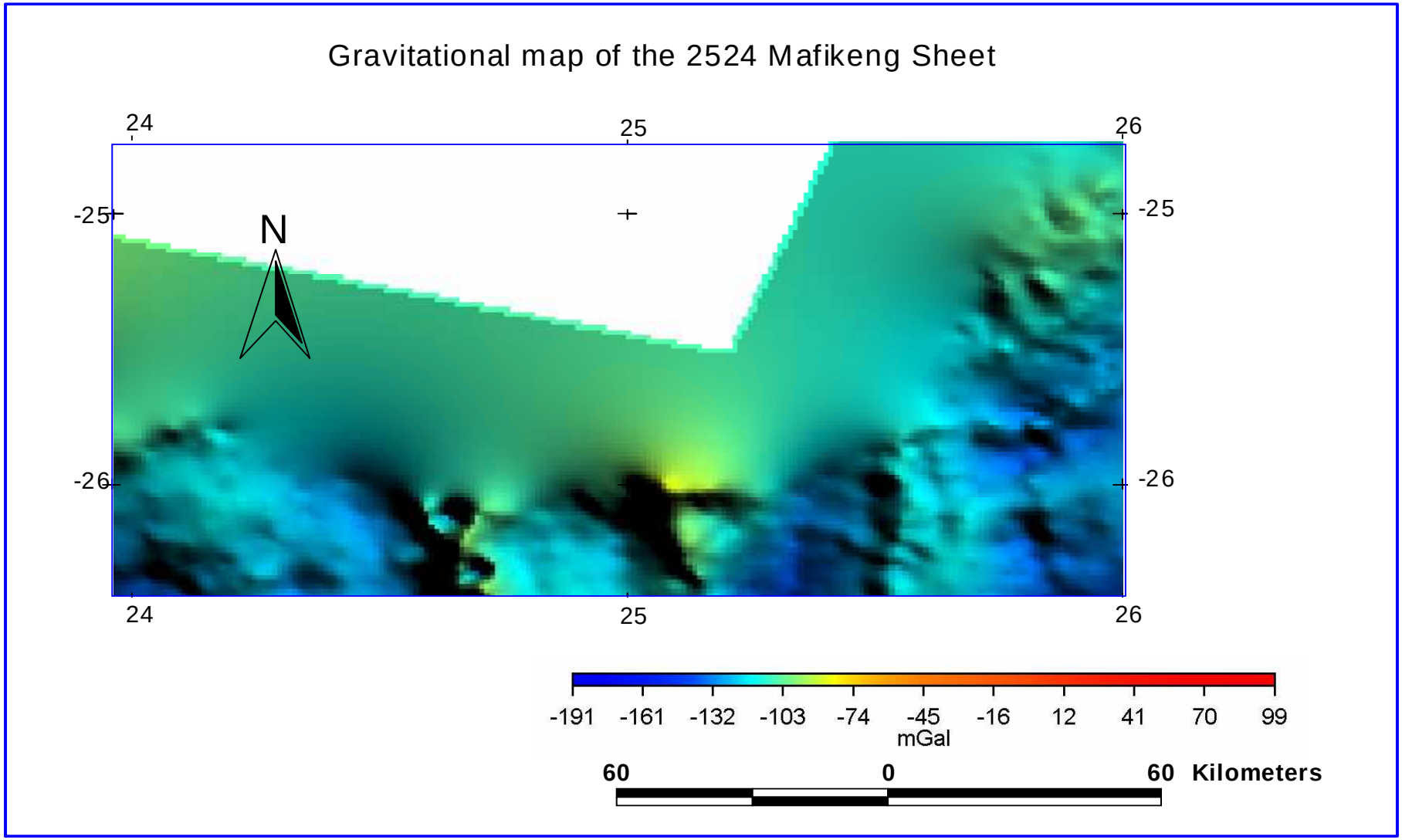

Figure 3.3-3: Gravity map of 2524 Mafikeng Sheet (Council for Geoscience, 2000).

3.4 GEOLOGY OF THE KURUMAN AREA

Rocks of the area are composed of pink white and grey fined-grained porphyritic granitic types which are the oldest rocks of the Swazian Erathem in the area Fig.3.4-1. A few pegmatite veins cut the granite. The Vryburg Formation lies unconformably on granite and Ventersdorp rocks and has a maximum thickness of 50 m. The lowest 8 m consist of arkoses, in places rich in mica, followed by whitish quartzite in which cross bedding is common. A thin band of conglomerate is present at the base and thin lenses of shale occur in the lower portion.

The Schmidtsdrif Subgroup forms the lower part of the Ghaap Group and is divided into two formations (Boomplaas and Clearwater Formations) of approximately 100m thick. In the middle of the formation shale becomes more predominant and ferruginised shale grey with siltstone and interbanded thin dolomite. Chert and chert conglomerate are present at the base. The upper formation consists of calcretic dolomite with few stromatolites and thin banded shale and siltstones (Beukes, 1987).

The Ghaap Plateau Formation can be distinguished from the underlying formation only where the quartzite is present on the latter. Elsewhere the rocks consist of dark blue fine-grained dolomite. A few stromatolite-bearing zones, small lenses of black chert locally developed in thin shale and siltstone are present. Brown ferruginous jasper layers up to 12 m thick, separate the lower part of the formation from the overlying grey course-grained dolomite. A Breccia of black chert and a few stromatolites occur in the dolomite. A third zone can be distinguished in the upper part of the formation. It contains lenses of limestone and a prominent layer of chert forms the top of the succession. The layer of chert occurs sporadically on the Maremane anticline where it is brecciated in places to form the silica breccia (Moen *et al*., 1977).

Asbestos Hills Subgroup is the sole representative of the Ghaap Group in this area and follows conformably on the underlying rocks. The formation is divided into the Kuruman

and Danielskuil Formations. The uppermost chert of the Ghaap Group grades into banded iron formation of the Kuruman Formation which varies in thickness from 180 m to 240 m. It consistes of a succession of thin alternating layers of light coloured chert and jasper and dark coloured ferruginous jaspilite. The jaspilite contains mainly magnetite, haematite and limonite. A few thin layers of riebeckite-amphibolite and shale occur in places. The rock has well developed bedding plane cleavage and contains several crocidolite bearing zones. The basal layer of the banded iron formation lies on the dolomite of the Ghaap Plateau Formation in the Maremane anticline, is brecciated and ferruginised in places and constituts the Blinkklip Breccia (Moen *et al*., 1977).

The "Main Marker" with a thickness of approximately 10m, lies conformably on the banded iron formation (BIF) and forms the base of the overlying jaspilite. It is characterized by an undulating structure and consists of brown jaspilite with thin magnetite layer and chert nodules. The overlying jaspilite attains a thickness of 150 m and contains several marker layers. Several "speckled markers" are present in the lower 40 m of the succession, of which only the upper one is indicated on the map. In the south a layer of oolitic chert with the appearance of quartzite is associated with the upper speckled marker. The two together are known as the quartzite marker. The intermediate quartzite maker occurs between lower speckled markers (Moen, 1977).

The Gamagara Formation was deposited on the Maremane anticline and rests unconformably on dolomite and the BIF of the underlying strata Ghaap Plateau Formation. The succession consists of a basal conglomerate with pebbles of jasper and banded iron formation, shale and white to brown quartzite.

The Makganyene Formation lies unconformably on the Gamagara Formation and has a maximum thickness of less than 480 m. Tillite occurs at the base of formation and contains fragments of black, white and red chert in a reddish brown sandy ground mass. Higher up in the succession, alternating layers of grit, tillite, and silicified mudstone and feldspathic quartzite occur. Dolomite or limestone occur interbanded in mudstone (Moen *et al*., 1977).

The Ongeluk Formation forms the lower part of the Olifantshoek Group. The formation consists of greyish-green andesitic lava with amygdales and lenses of red jasper. The Voëlwater Formation overlies the Ongeluk Formation and has a thickness of 450 m. The lower beds are banded iron stone and banded red jaspilite with chert, dolomite and lava. The upper portion of the succession consists predominantly of dolomite with chert, banded jasper and lava (Moen *et al*., 1977).

The Lucknow Formation occurs east of the Olifantshoek Group in the Korannaberg where the strata are disturbed by a number of faults Fig 3.4-1. It lies unconformably on the Voëlwater Formation and is absent in places in the north. The formation has a maximum thickness of 1500 m. The lower portion consists mainly of shale with subordinate layers of quartzite and lava and an upper portion of whitish quartzite with lenses of flagstone and dolomitic limestone. The Hartley Formation, the upper part of Olifantshoek Group, follows conformably on the Lucknow Formation with a basal conglomerate containing pebbles of quartzite, jaspilite and lava. It is overlain by andesitic lava which contains amygdales, tuff, breccia and pebbles of quartzite (Moen *et al*., 1977).

The Matsap Subgroup lie conformably on the Hartley Formation but in places is found unconformably on the Voëlwater Formation in the Korannaberg. Three members were recognized. They consist predominantly of sub-greywacke and purple, grey and brown quartzite with thin pebble beds and a layer of conglomerate in which quartz, banded iron formation and red jasper pebbles are abundant. The Brulsand Formation consists mainly of quartzite with subordinate shale and sub-greywacke. Together with the Matsap Subgroup they form the Volop Group with a thickness of 500m (Moen *et al*., 1977).

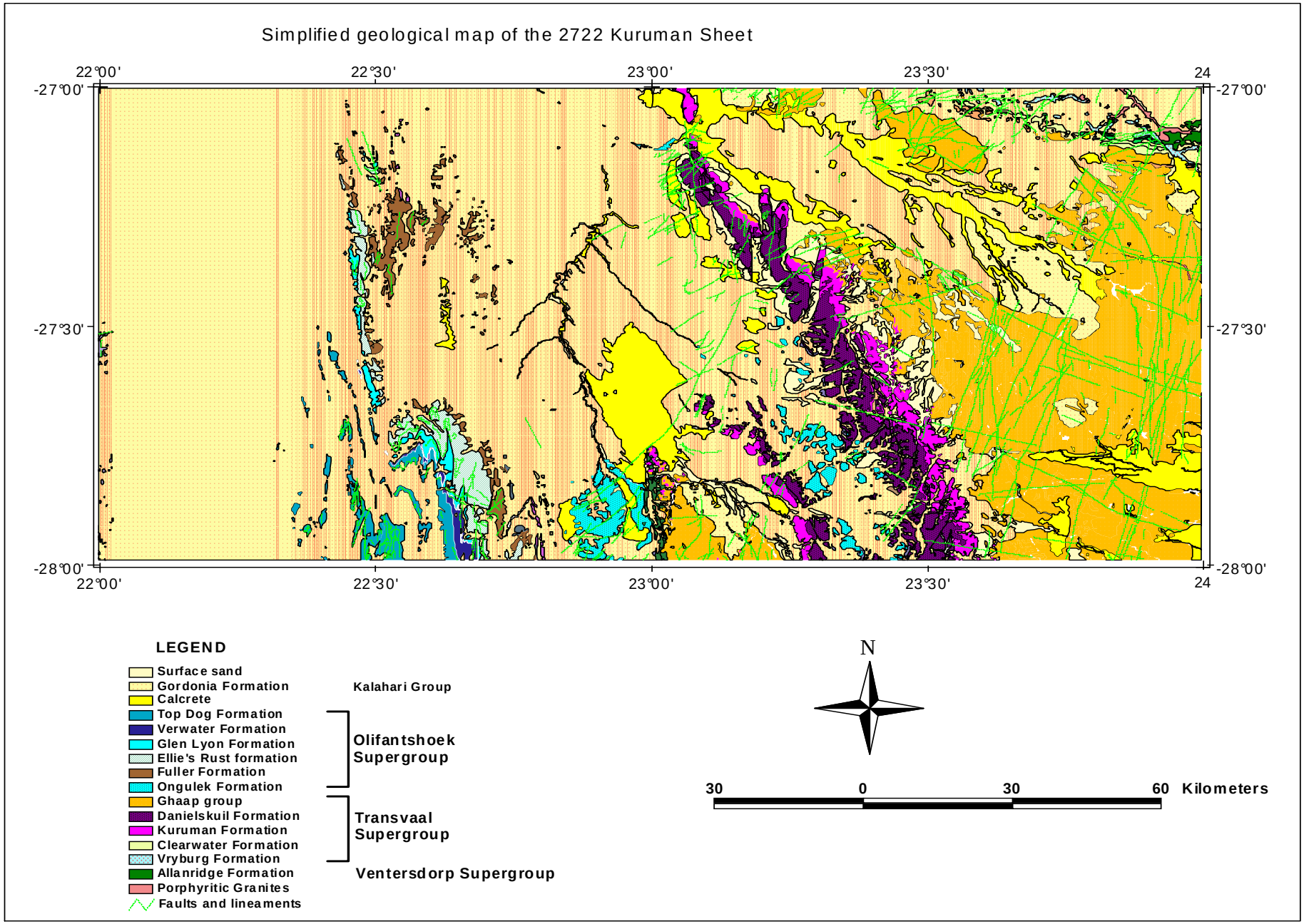

Figure 3.4-1: Simplified geological map of the Kuruman Area (after Moen, 1979).

The Groblershoop Formation is largely covered by sand and crops out along the western boundary of the area. Rocks encountered are grey glassy quartzite, light-coloured vitreous sandstone and quartz-sericite schist. Calcrete has a wide distribution, mainly on the Ghaap plateau and to the north on the Maremane anticline, where its thickness exceeds 20m. Lime-rich kieselguhr is present at few places in pans and along the valley. A large number of dolerite dykes of both Vaalian and Jurassic age occur in area. In general the dykes are approximately 6 m wide. Some of the faults in the Kuruman hills are intruded by dykes. Diabase sills are present in the Asbestos Hills Formation and also in the Olifantshoek succession. Kimberlite pipes and fissures are known, especially southeast of Sishen and north of Kuruman (Moen *et al*., 1977).

Dolomite strata on the Ghaap Plateau are very gently folded and have a small regional dip to the west and south west. The Asbestos Hills Formation has a regional dip of less than 10°. Folds increase sharply west of the Maremane anticline and at least part of Groblershoop Formation is folded. A number of north-south striking faults traverse the Asbestos Hills Formation and most of them have vertical displacement. Grabens are fairly common (the graben west of Kuruman has a vertical displacement of ~350 m) and where the faults bifurcate, block faults are found (Moen *et al*., 1977).

3.4.1 Commodties

Barite is present as an impurity in the manganese ore of the Maremane Anticline but is not of economic importance.

Crocidolite occurs in a number of zones in the Asbestos Hills Formation. The basal zone occurs approximately 25 m above the base of the formation. The important main zone occurs in the 120 m immediately below the main marker. Four to five subordinate zones are present in the main maker. The ore above the main marker is of little economic importance. Asbestos occurs in lenticular bodies which are elongated north–south (Moen *et al*., 1977).

Diaspore occurs in the lower shale of the Gamagara Formation.

Iron is mined at Sishen. The ore occurs in the Blinkklip Breccia, and also in the lower shale and conglomerate of the Gamagara Formation where the latter lies on the BIF (banded Iron Formation) and became ferruginised to a high grade ore in place. Large reserve is available (Moen *et al*., 1977).

Limestone occurs as lenses in the upper portion of the Ghaap Plateau Formation; Flagstone suitable as paving floor, is obtained from banded iron formation.

Manganese occurs in large quantities in the Voëlwater Formation and is mined at the Black Rock and Hotazel. A manganised silica breccia (The Manganese Marker) at the top of Ghaap Plateau Formation and especially the lower Gamagara shale, which is manganised where it rests on the dolomite, are the main ore carriers in the Maremane Anticline (Moen *et al*., 1977).

Table 3.4-1: Lithostratigraphic column of the Kuruman Area (summary from SACS, 1980, Eriksson *et al.*, 2006) (SBGRP: subgroup; Fm: Formation).

STRATIGRAPHY				DESCRIPTION	MAGMATIC EVENT
				Red to flesh-coloured wind blown sand	
				Rubble	
				River-sand and gravel	
				Surface limestone	
OLIFANTSHOEK SUPERGROUP (±2223-2216 MA)	BRULPAN GROUP		Groblershoop Fm	Quartzite, quartz-sericite schist	Dolerite dykes
	VOLOP GROUP	Brulsand SBGRP	Top dog Fm	White, grey and pink quartzite with subordinate brown subgreywacke	
			Verwater Fm	Grey quartzite with nodule of and lenses of haematite	
		Matsap SBGRP	Glen Lyon Fm	Brown subgreywacke and conglomerate	
			Ellie's Rust Fm	Quartzite and subgreywacke	
			Fuller Fm	Quartzite, subgreywacke and conglomerate	
		Hartley Fm		Andesitic lava with interbedded tuff, agglomerate, quartzite and conglomerate	
		Lucknow Fm		Quartzite, dolomitic limestone; shale and lava	
TRANSVAAL SUPERGROUP (±2224-2219 MA)	POSTMASBURG GROUP	Voëlwater SBGRP		Red jasper, dolomite, chert and lava	Basic lava
		Ongeluk Fm		Amygdaloidal andesitic lava with interbedded tuff, agglomerate, chert, red jasper	
		Makganyene Fm		Diamicite, banded jasper, siltstone, mudstone, sandstone grit and dolomite	
	GHAAP GROUP	Campbell Rand SBGRP	Monteville Fm	Dolomite; quartzite	
		Asbestos Hills SBGRP	Danielskuil Fm	Yellow-brown jaspilite with crocidolite; conglomerate	
			Kuruman Fm	Banded iron formation, subordinate amphibolite, crocidolite, jaspilite and, chert	
		Schmidtsdrif SBGRP	Clearwater Fm	Conglomerate, chert and dolomite, shale	
			Boomplaas Fm	Oolitic and stromatic dolomite and dolomite with chert and quartzite lenses	
	Vryburg Fm		Quartzite, grit, conglomerate, shale amygdaloidal lava		
VENTERSDORP SUPERGROUP (±2714 MA)			Allanrigde Fm	Andesitic lava, amygdales and agglomerate	Andesitic lava
Porphyritic granite (basement)					

3.4.2 Geophysical Interpretation

In Figure 3.4-3 the low bouguer anomaly are obtained in the east, coinciding with the Ghaap Group dolomite of the Campbell Rand Group this indicates that the dolomite have no great depth. On the total aeromagnetic map the dolomite are characterized by the featureless background with the random high anomalies due to dykes and deeper seated plug-like bodies.

The BIF and jaspilite of the Asbestos Hill Subgroup together with the andesitic lava of the Ongeluk Formation has a high magnetic anomaly cutting through the central part of the map (Fig. 3.4-2). This anomaly correlates with the gradient between low and high except in the north where the banded iron formation and jaspilite are not thick (Prinsloo, 1998).

The quartzitic composition of the Olifantshoek Supergroup is thought to be responsible for a low gravity anomaly in the west. The north-south striking linear features, which are characterized by high magnetic anomalies in this area, represent the dykes and faults in the area (Prinsloo, 1998).

The high magnetic anomalies are represented by the elliptical shaped anomalies (A, B, C, D and E in Fig. 3.4-2) which are on both sides of the Asbestos Hill Group. These anomalies have resulted from the unknown geology in the area and therefore are assumed that they are from the deep seated structures.

The L (F) shaped high magnetic anomaly in the north (approximately 22°45’E -27°15’S) corresponds with the negative bouguer anomaly. These anomalies have resulted from the presence of the Ongeluck lava (Prinsloo, 1998).

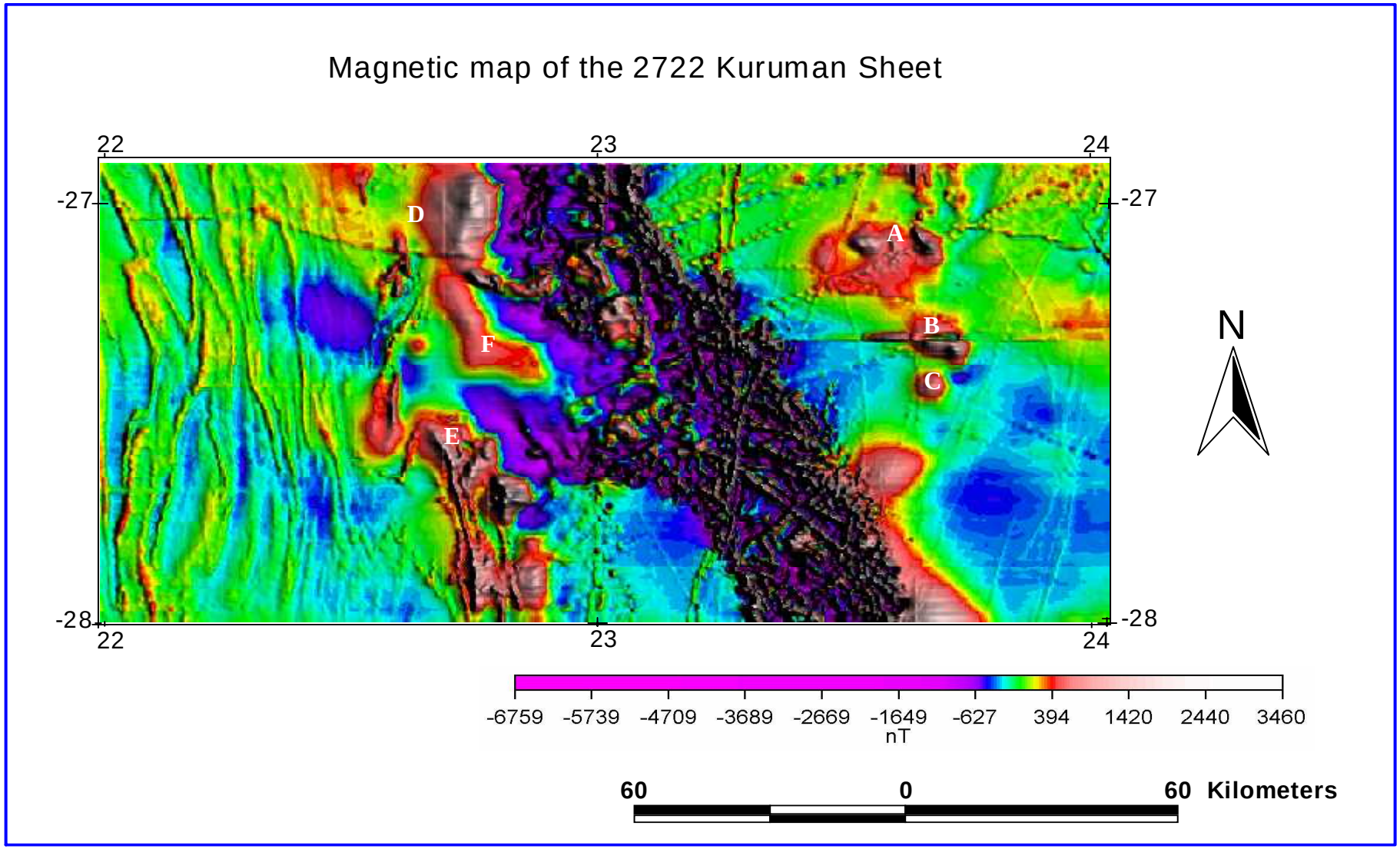

Figure 3.4-2: Magnetic map of 2722 Kuruman Sheet (Council for Geoscience, 2000).

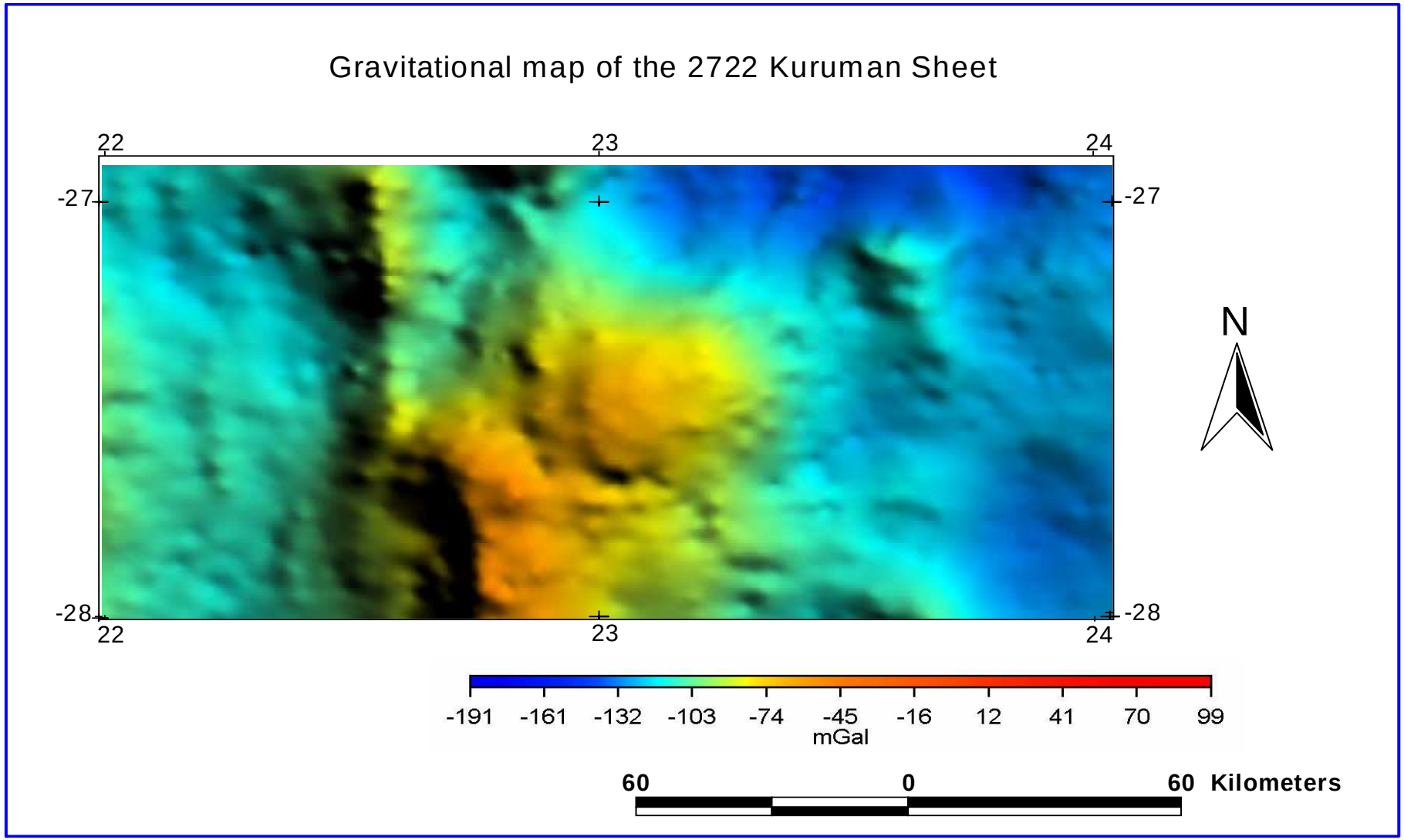

Figure 3.4-3: Gravity map of 2724 Kuruman Sheet (Council for Geoscience, 2000).

3.5 GEOLOGY OF THE VRYBURG AREA

The northern and western parts of the area are completely covered by aeolian sand of the Kalahari Group which overlies the undifferentiated granite gneiss of Swazian age. The oldest rocks or the basement complex comprise mainly low grade metamorphic rocks which also form part of the Kraaipan Group (Keyser and Du Plessis, 1993) Fig. 3.5-1. Granite and gneiss cover a substantial part of the area. It is, however, rarely exposed due to a thick cover of Kalahari sand (Gordonia Formation) in the western and north western part of the area and a thick soil cover. The basement granite-gneiss comprises migmatite, gneiss, granite, amphibolite and schist.

The Dominion Group overlies the Archaean granite and gneiss (Table 3.5-1), and forms prominent outcrops in the vicinity of Ottosdal Town. The area is situated about 35km east of Ottosdal in the Vicinity of Dominion Reef Mine (SACS, 1980).

The Witwatersrand Supergroup is represented by rocks of the Hospital Hill Subgroup of the West Rand Group, and it occurs in two synclinal structures, the one of which lies to the north of the Doornkuil-Klipfontein fault and strikes southwest-northwest, while the other lies to the south of the fault and strikes north-northwest-south-southwest (Keyser and Du Plessis, 1993).

The eastern part of the area is mainly dominated by the basaltic lava of the Klipriviersberg Group which outcrops in the extensive eastern area and overlies the Central Rand Group of the Witwatersrand Supergroup. It extends into the southeastern part in the area between Ottosdal and Migdol, and northwards to the Sannieshof-Biesiesvlei area and further north to the area of Isotseng where it is overlain by the Transvaal Supergroup.

The central and south western parts of the area are mainly composed of Ventersdorp Supergroup rocks which include breccias, conglomerate greywacke and feldspar porphyry. The basaltic amygdaloidal lava and tuff of the Allanridge Formation cover a

large part of the area especially in the north and north-east. It occurs in a more or less continuous belt from Lotlhakane in the north to Migdol in the south, and in the area between Broedespruit, Vryburg, Zoetlief and Stella (Fig.3.5-1).

The Allanridge Formation conformably overlies the Bothaville Formation but where the latter pinches out the Allanridge Formation oversteps onto diverse older lithologies. The formation consists of two types of lava: dark-green and light green-grey amygdaloidal lava. In the central part of the area the rocks are not well exposed as they are covered by sand of the Kalahari Group (Keyser and Du Plessies, 1993).
The dark-green lava, which is by far the most prominent unit in the Allanridge Formation, also constitutes the greater part of the Ventersdorp Supergroup in the area.

The Dwyka Group of the Karoo Supergroup occurs in the vicinity of Vryburg but is seldom exposed in outcrop. Large erratic boulders, which lie strewn all over the country-side, are the only indication of the presence of the Dwyka Group in the area. It can be seen in road quarries along the main road between Vryburg and O'Reilly's Pan and it also is exposed in the area surrounding O'Reilly's Pan (Keyser and Du Plessis, 1993).

Calcrete covers large areas, especially in the dolomitic terrain and to a lesser degree in areas underlain by Ventersdorp lava. The calcrete which overlies dolomite of the Transvaal Supergroup probably formed by evaporation of water charged with carbonate derived from underlying rocks (Keyser and Du Plessies, 1993).

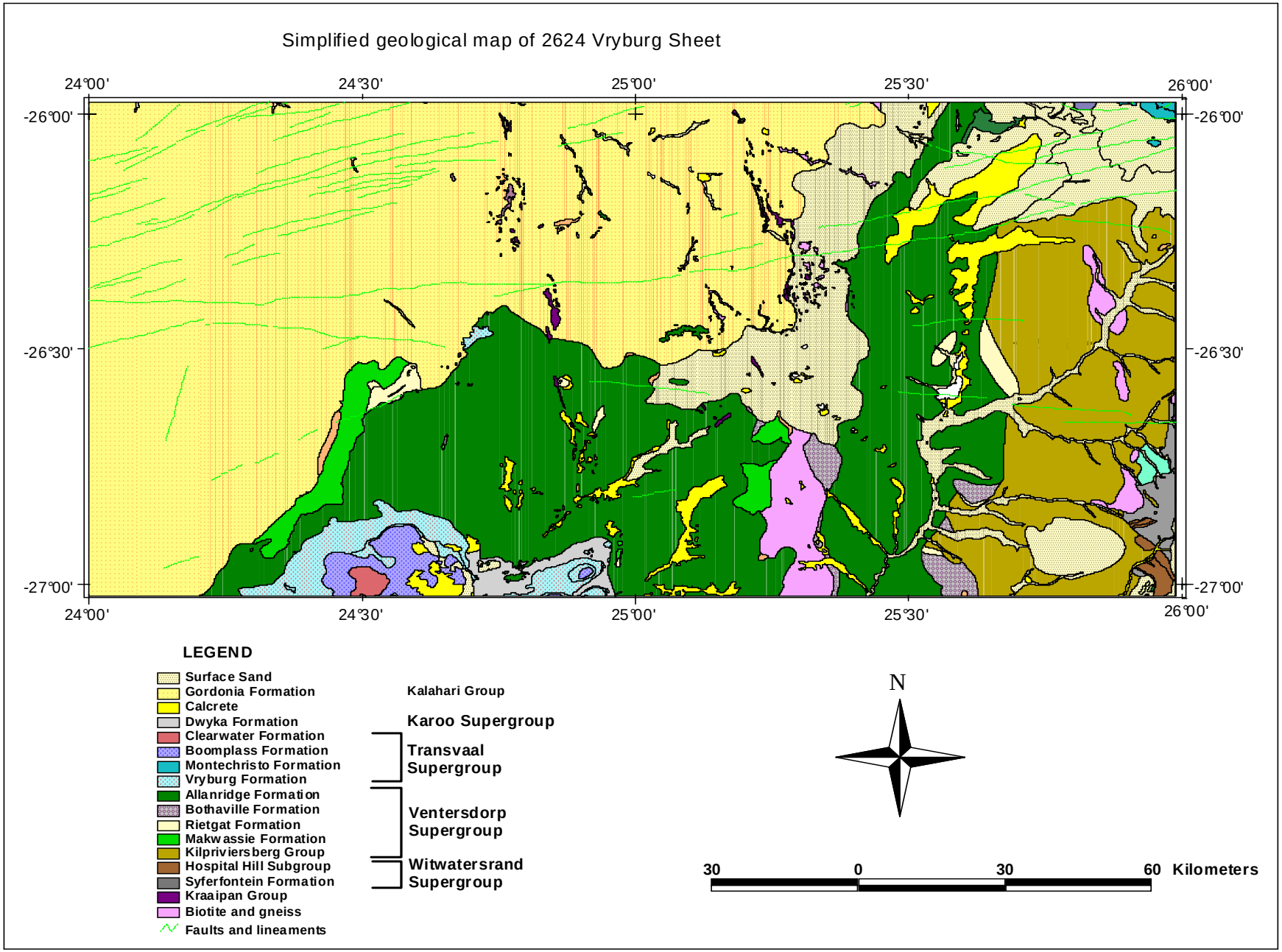

Figure 3.5-1: Simplified geological map of the Vryburg Area (after Keyser and Du Plessies, 1993).

3.5.1 Intrusives

The Mosita granite dated at 2710 ± 65 Ma. (Burger *et al.*, 1979, cited in Keyser and Du Plessis, 1993) differs considerably from older granite-gneiss in appearance and outcrop. It is intrusive in the Archaean granite-gneiss and the Kraaipan Group.

To the North of Ottosdal and Humanskraal gabbro occurs in rocks of the Syferfontein Formation of the Dominion Group. The gabbro consists of a coarse-grained, light coloured type and a fine-grained dark coloured type (Keyser and Du Plessis, 1993).

There are few pre-Karoo dykes in the Vryburg area. Two diabase dykes occur on Humanskraal 346 IQ. Numerous dolerite dykes traverse the map area. They are mostly covered with sand, but can be traced out on aerial photographs because of vegetation they support. In general two groups of dykes can be distinguished. One group strikes east-west and the other strikes about north-south and mostly occurs in the area to the west of Vryburg and to the south of Ganyesa. (Keyser and Du Plessies, 1993)

3.5.2 Commodities

Diamonds occuring in river terraces have been reported on the western section of Kunana Location N.4 and in the Vryburg district. The occurrence at Kunana is related to the Lichtenburg diamond field.

Gold was reported from the Madibi belt of the Kraaipan Group where it occurs in weathered brecciated schist cut by lenticular quartz veins with a width of approximately 1-2 m that stand almost vertically, (Du Toit, 1906).
In the Khunwana location, gold was also found in a body of schist following the edge of the banded iron formation. The reef was subsequently worked at Muir's Mine where the gold content was 17 g/t (Coetzee, 1976, cited in Keyser and Du Plessis, 1993). A similar occurrence has been described west of Grysdorp on Lynplaats 8IO. The lode was 0.75 meters wide and was traced for over 2.5 km. A gold content of 20g/t was reported (Schanzlin, 1928).

Brick Clay- At Stella building bricks are manufactured from clay derived from the Kraaipan rocks. The bricks are exclusively used by the local community.

Iron: The only comparatively important iron occurrences are in the banded iron formation of the Kraaipan Group and in the magnetic shale of the Park Town Formation.

- Kraaipan ore. The siliceous iron formation near Kraaipan Station has a reserve of ore containing 37-42% iron and 35-42 % silica estimated at about 200 million tons.
- Hospital Hill ore. The Park Town Formation contains ferruginous shale that has excited some interest in the past. The deposit consists of lenticular bodies of haematite with some magnetite, bounded by limonitic shale and interbedded with softer shale (Coetzee, 1976, cited in Keyser and Du Plessis, 1993). Drilling has shown that the secondary enriched zone extended to a depth of only 10-15 m. The haematite contains 50-60 % iron and soft limonite ore contains 40-54 % iron.

Limestone in the form of calcrete was quarried on Dutfield 35IP and Springbok 61 IQ. The limestone was used in the manufacture of cement.

Salt occurs in nearly all the pans in the Vryburg area with only two pans being in production at present. The pans occur in the areas underlain by the Dwyka Group or the lower Ecca Group.

Table 3.5-1: Lithostratigraphic column of the Vryburg Area (summarized from SACS, 1980). Fm: formation; SBGRP: subgroup.

STRATIGRAPHY				DESCRIPTION		MAGMATIC EVENT	AGE(MA)
				Alluvium			2.5-1.6
				Soil cover			
				Undifferentiated aeolian sand			
KALAHARI GROUP			Gordonia Fm	Aeolian sand			
				Gravel diamondiferous in place and silcrete			
				Calcrete			
KAROO SUPERGROUP			DWYKA GROUP	Diamictite, shale		Dolerite dyke	±180
TRANSVAAL SUPERGROUP (± 6km)	CAMPBELL RAND GROUP		Monteville Fm	Dolomite; quartzite		Diabase dyke	±240-190
	GHAAP GROUP		Schmidtsdrif SBGRP	Clearwater Fm	Conglomerate, chert and dolomite, shale		25571-2224
				Boomplaas Fm	Oolitic and stromatic dolomite and dolomite with chert and thin quartzite lenses		
	Vryburg Fm			Quartzite, siltstone, flagstone, conglomerate			
	CHUNIESPOORT GROUP	Malmani Subgroup	Monte Christo Fm	Undifferentiated dolomite and chert, shale			
			Oaktree Fm				
	Black Reef Fm			Quartzite, shale, conglomerate		Mosita Granite(2710 ± 62 Ma	2714
VENTERSDORP SUPERGROUP (± 2km)	Allanridge Fm			Andesitic to basic lava, minor tuff			
	PLATBERG GROUP	Bothaville Fm		Quartzite, greywacke, conglomerate			
		Rietgat Fm		Amygdaloidal lava, quartzite, tuffaceous sediments			
		Makwassie Fm		Quartz feldspar porphyry , feldspar porphyry lava			
		Goedgenoeg Fm		Basaltic amygdaloidal and porphyritic lava			
		Kameeldoorns Fm		Breccias, conglomerate, greywacke, shale tuff			
	KLIPRIVIERSBERG GROUP			Basaltic lava			
WITWATERSRAND SUPERGROUP			WEST RAND GROUP	Hospital Hill SBGRP	Quartzite, ferruginous shale		± 9370-2914
DOMINION GROUP			Syferfontein Fm	Quartz feldspar porphyry, andesite, tuff,		Gabbro	± 3086-3074
			Rhenosterhoek Fm	Andesitic lava			
			Rhenosterspruit Fm	Quartzite, conglomerate, lava			
KRAAIPAN GROUP (1100m)			Khunwana Fm	Banded chert, Jaspilite, amphibolite, lava, schist		Mosita Granite(2710 ± 62 ma)	±3640
			Ferndale Fm	Variegated banded jaspilite			
			Gold Ridge Fm	Banded iron formation, mica, pyrophyllite, and chlorite schist			

3.5.3 Geophysical interpretations.

The high magnetic anomalies and low Bouguer anomalies in the eastern part of the map (Fig. 3.5-2 and Fig. 3.5-3) are related to the gneiss, schist and amphibolites. The higher Bouguer and magnetic anomalies over the center of the map are due to the basaltic lava of the Ventresdorp Supergroup that is partially coved by the surface sand of the Kalahari Group.

On the Magnetic map in Fig. 3.5-2, the horse shoe shaped set of high amplitude anomalies in the center of the map indicates the outcrops position of the of the BIF of the Kraaipan Greenstone Belt. On the bouguer gravity map (Fig. 3.5-3) the response of the Kraaipan Group is only vaguely discernible indicating that the rock units are not very thick. The Kraaipan Greenstone Belt is flanked on its eastern and western part by the granitic intrusion (Kotzé, 1996a).

In the south-eastern corner high magnetic anomaly is caused by the ferruginous shale from the Hospitals Hill Subgroup.
In the north east, high magnetic anomalies are associated with the dolerite sills, which are coved by the surface sand. On west, the vertical north-south strips of low magnetic and high Bouguer anomalies are associated with the Colesberg in the north-eastern Cape to Botswana. From the aeromagnetic map, east-west trends of high magnetic lineaments, which are caused by the intrusion of the magnetic dykes, are clearly visible. The two parallel linear features cutting across the map horizontally represent the normal faults which are intruded by the dolerite dykes.

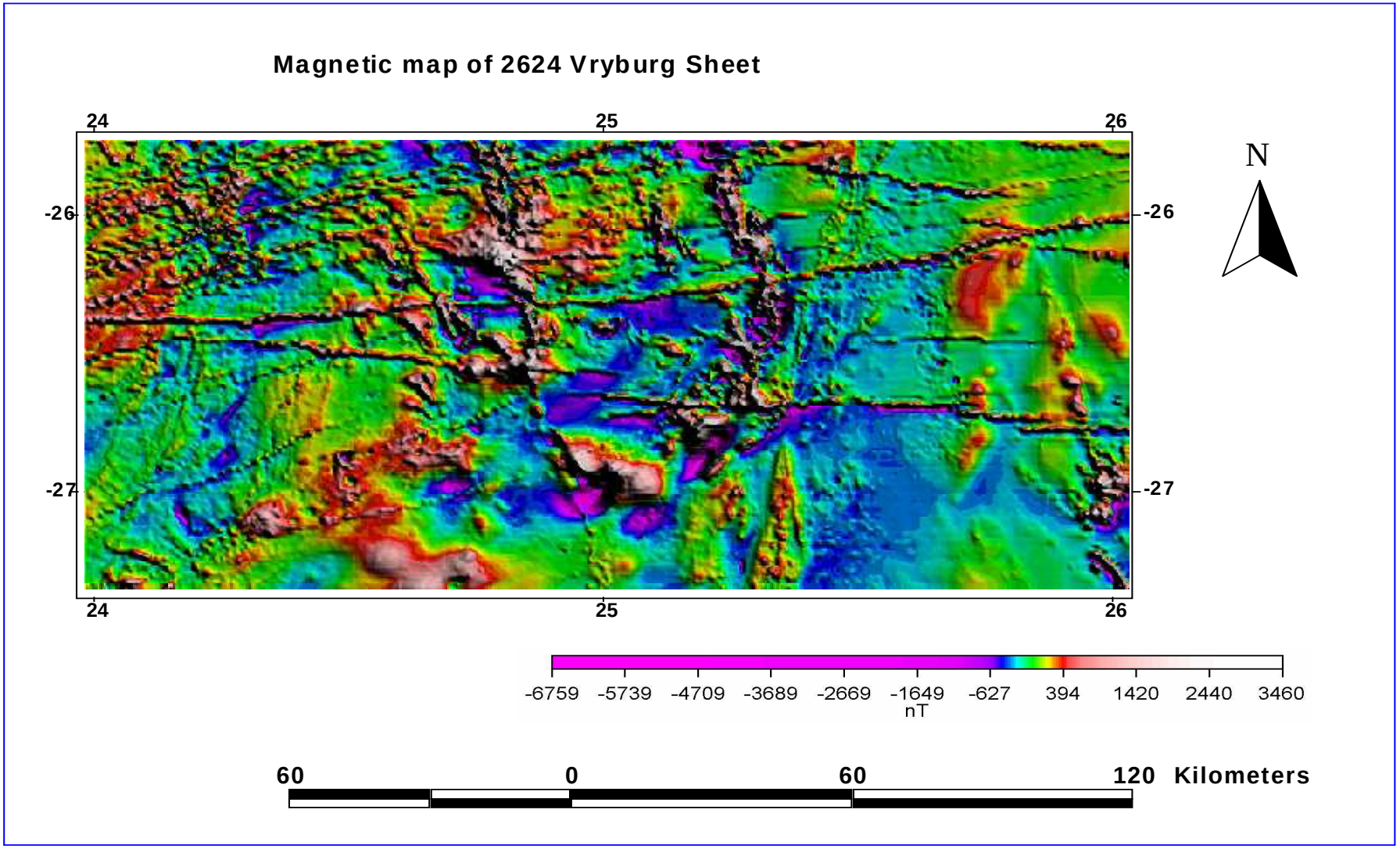

Figure 3.5-2: Magnetic map of the 2624 Vryburg Sheet (Council for Geoscience, 2000).

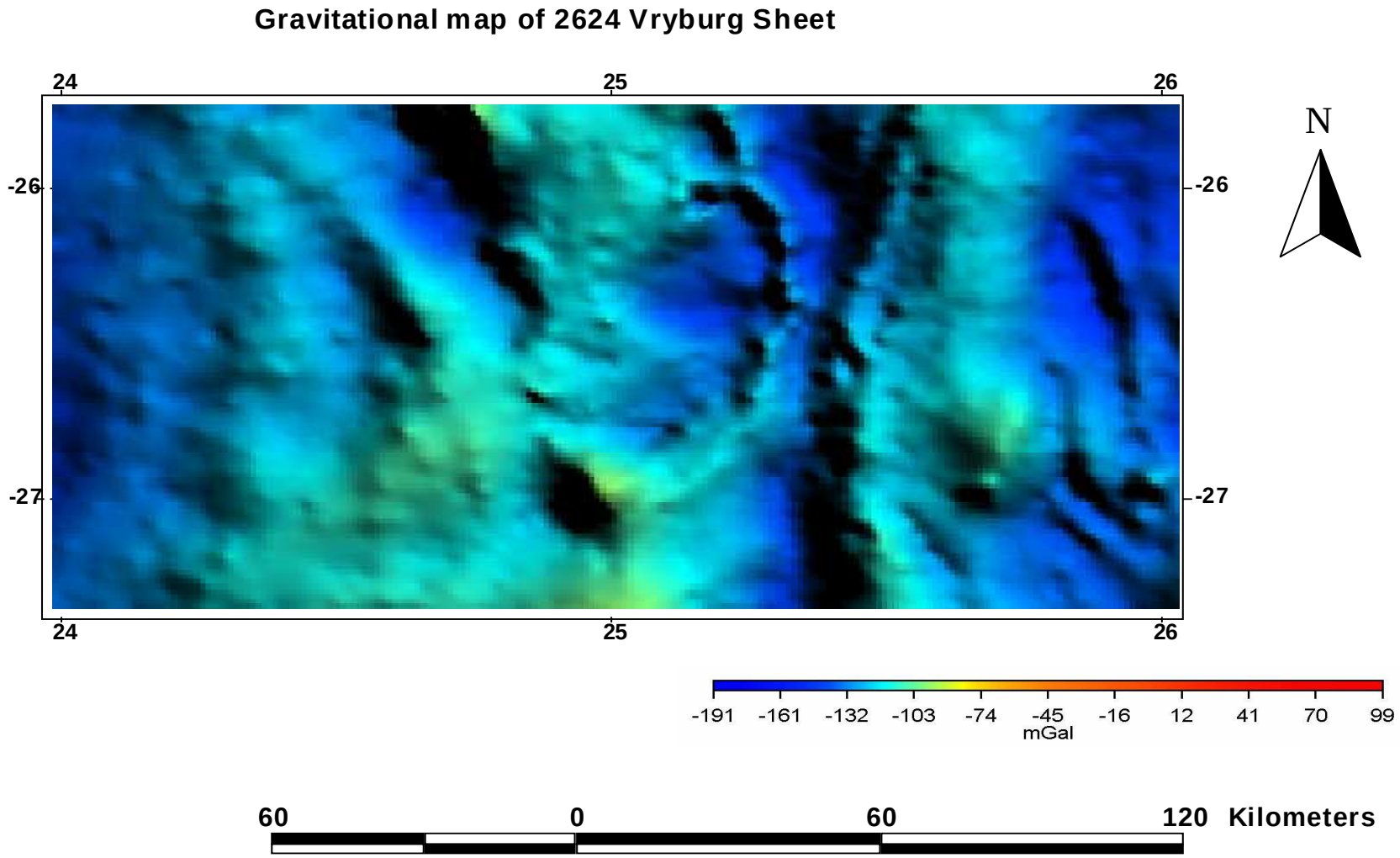

Figure 3.5-3: Gravity map of 2624 Vryburg Sheet (Council for Geoscience, 2000).

3.6 GEOLOGY OF THE CHRISTIANA AREA

The rocks of the Kraaipan Group are the oldest rocks in the Christiana area and they outcrop in the vicinity of the Amalia, where they are represented by the lithologies of the Goldrige Formation which mainly consists of amphibolites, BIF and schist.

The Witwatersrand Supergroup is represented by the Hospital Hill Formation of the West Rand Group which outcrops on the northern part of the Wolmarransstad and rests discordant on the Dominion Group (Hugo, 1948). The formation consists of red iron rich shale. The quartzite has a thickness of 30 mm and extends over an area about 100 m wide (Schutte, 1994) refer to Fig 3.6-1.

The Ventersdorp Supergroup covers most of the central to the eastern part of the area and has the dominant lithologies of the area. Other outcrops occur near the Vredefort Dome near Parys. The Ventersdorp Supergroup is composed largely of andesitic lavas and related pyroclastics that are formed by, or involve the fragmentation as a results of volcanic or other igneous activity. Various conglomerates, tuffaceous and calcareous shales and porphyries are also constituents of this formation.

The Ventersdorp Supergroup is divided into Klipriviersberg Group and the Platberg Group. The Witwatersrand Supergroup is conformably overlain by the Klipriviersberg group which is mainly composed of light green amygdaloidal and non-amygdaloidal lava and outcrops in the western part of the Wolmaransstad district (Schutte, 1994).

The Platberg Group in this area is represented by the Kameeldoorns Formation which is composed of conglomerate, greywacke, shale, limestone and chert. The Makwassie Formation is well exposed in the southern part of Wolmaransstad district and in the Makwassie area the formation has maximum thickness of 200 m and is composed of quartz porphyry, feldspar porphyry and rhyolite with the Rietgat Formation being exposed in the central part of the area over a distance of few km only. Lava, tuff,

pyroclastic breccia, chert and sandstone outcrop north of Wolmaransstad and Christiana and in the Amalia area. The formation outcrops with good exposures from Doringlaagte extending up to Hartswater. The formation rests conformably on the Archaean granite and gneiss and on shale of the Witwatersrand Supergroup, conglomerate of the Kameeldoorns Formation and quartz porphyry of the Makwassie Formation.
The Allanridge Formation occupies a large area at Christiana, from Schweizer-Reineke to Marokwane and in the Taung area and overlies the Bothaville Formation. It consists of basaltic lava and andesite. At Taung the formation has a maximum thickness of 300 m (Schutte, 1994).

The Vryburg Formation is comprised mainly of siltstone with subordinate shale, quartzite and andesitic lava and shows good outcrops northwest of Christiana.
The Schmidtsdrif Subgroup represents a transition between the underlying Vryburg Formation and the overlying Ghaap group. Its lower part (the Boomplaas Formation) consists of interlayered dolomite, shale and limestone, while its upper part (the Clearwater Formation) consists of dolomite, shale and sandstone layers.
The Campbell Rand Group in this area is represented by the Monteville Formation which consists of dolomite with stromatolitic limestone and shale, and outcrops in the western part near Taung. The Reivilo Formation which mainly consists of dolomite, limestone and chert covers a wide area in the western part of the Christiana area (SACS, 1980).

The Fairfield Formation has good exposures to the west of Reivilo and is composed of coarse-crystalline recrystallyzed dolomite with interbedded chert.
The Karoo Supergroup is represented by the Dwyka and Ecca Groups. The Dwyka Group is composed of tillite, mudstone, shale, and sandstone. It is well exposed on Venter Dwaal 881 and Lefton 827 farms.
The Ecca Group in this area is represented by the Vryheid and Volkrust Formations which are well exposed west of Schweizer-Reineke. The Formations are composed mainly of sandstone and shale (Schutte, 1994).
The south western part of the map is mainly covered by surface sand of the Gordonia Formation and calcrete.

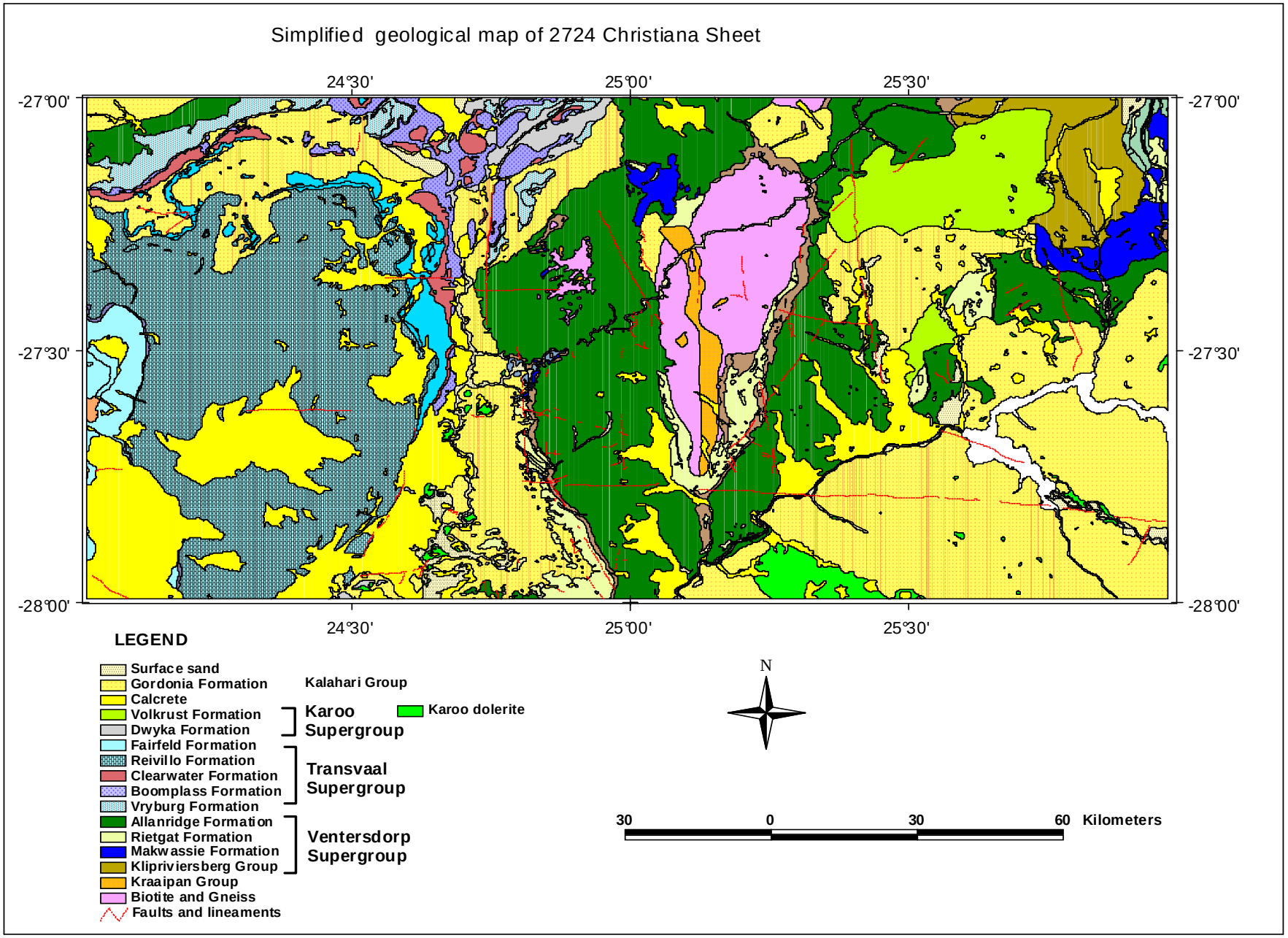

Figure 3.6-1: Simplified Geological map of the Christiana Area (after Schutte, 1991).

3.6.1 Igneous intrusive

Diabases

The diabase dykes that occur on Zwartkrans 132 are probably associated with the emplacement of the Bushveld Complex.

Post Karoo Dolerite

The intrusive dolerite suite represents the shallow feeder system to the flood basalt eruption. The dykes are generally are 2 m-50 m wide and less than 5 km long. Dolerite dykes and sills intruded in the rocks of the Griqualand West Supergroup which are exposed in the western part of the area covered by the map. Dolerite sills can be found west of Pudimoe in the dolomite and in the Dwyka Group west of Jan Kempdorp. The thickness of the dolerite dykes ranges between 4.5-10 m thick (Schutte, 1994).

3.6.2 Commodities

Diamonds occur in the Schweizer Reneke area, are deposited on rock (principally lavas) of the Ventersdorp Supergroup and have been described by Marshall (1987) who recognised three distinct gravel types:

Oldest Rooikoppie gravel, which occurs as chemically mature 1-2 m thick unsorted, lateritised coluvial gravel. Young terrance type gravel, occurring on the lower slope of the present drainage valley and averaging 1-4 m thick. The youngest spruit-type gravel occurs on the modern valley floor and texturally and compositionally similar to terrace-type gravel.

Iron. Algoma type ore is found in the Kraaipan Group. The siliceous iron formation of the Goldridge Formation occurs near Kraaipan Station, at Khunwana location and in the Ditsobotla district and Familyplaats 8 Io and Mooiplaats. In the Delareyville District six boreholes were drilled by the SAMCOR who estimated the reserves of ore containing 37-

42 % Fe and 35-42 % Fe SiO_2 to be about 200mt. Some 44000t of detrital ore were mined during 1969 and 1970 for New Castle Steel works (Schutte, 1994).

Limestone and Dolomite were deposited in a number of pans in North West Province. The deposits are generally low grade although they occasionally reach 85% carbonate on the Farm Witpan 126 IO north-northeast of Delareyville. In Delareyville-Schweizer Reneke area and Barberspan, limestone has accumulated in dunes on the southern margin of several pans.

Zink and Lead. Mineralization of zinc and lead occurs in dolomite of the Reivilo Formation of the Campbell Rand Group. The dolomite is characterised by columnar stromatolites and thin carbonaceous shale interbeds. The deposit has two principal and intimately associated types of zinc-lead mineralization. These include broadly sub-horizontal stratabound layers and sub-vertical breccia zones. Zinc/lead ratios range from 5:1 to 2:1 with higher ratios in stratabound layers. Sphalerite and Galena, with minor pyrite and traces of chalcopyrite are the ore minerals. Sphalerite hosts approximately 0.55 % of the iron and up to 0.28 % cadmium in the lattice.

Salt. The majority of salt in South Africa especially in the western areas, occurs in a curved belt of 50-60 km wide mostly underlain by the Karoo Supergroup. A salt pan occurs on the basalt of the Lebombo Group here several pans occur on the Pretorozoic granite gneiss south of Pafadder and also west of Vryburg town. Most of the pans in the vicinity of Dalareyville are underlain by lava of the Ventersdorp Supergroup (Schutte, 1994).

Table 3.6-1: Lithostratigraphic column of the Christina Area (summarized from SACS, 1980,). Fm: Formation; SBGRP: Subgroup; GRP: Group.

STRATIGRAPHY					DESCRIPTION	MAGMATIC EVENT	AGE (MA)
					Wind-blown, partially reworked sand, colluvial		2.5-1.6
KALAHARI GROUP			Gordonia Fm		Siliceous sandstone, pebble conglomerate, gritstone, silcrete		
					River terrace gravel		
					Tertiary Calcrete		
KAROO SUPERGROUP		ECCA GROUP	Volkrust Fm		Mudstone and sand stone		±180
			Vryheid Fm		Fine grained sand stone		
		DWYKA GROUP			Diamictite, shale and tilites	Karoo Dolerite	
TRANSVAAL SUPERGROUP	GHAAP GROUP	Campbell Rand SBGRP	Fairfield Fm		Dolomite and chert	Diabase	2500 -2224
			Reivilo Fm		Dolomite with stromatolites and carbonaceous shale		
			Monteville Fm		Dolomite; quartzite		
		Schimdtsdrift SBGRP	Clearwater Fm		Conglomerate, chert and dolomite, shale		
			Boomplaas Fm		Stromatic dolomite and dolomite with chert and quartzite lenses		
Vryburg Fm					Quartzite, grit, conglomerate, shale amygdaloidal lava		
VENTERSDORP SUPERGROUP	Allanrigde FM				Basaltic amygdaloidal lava, agglomerate, tuff		2714
	Platberg GRP		Rietgat Fm		Amygdaloidal lava, tuff, quartzite,		
			Bothaville Fm		Tuffaceous sediments		
			Makwassie Fm		Quartz-feldspar porphyry, feldspar porphyry		
			Kameeldoorns Fm		Breccias, conglomerate, shale greywacke, tuff		
	KLIPRIVIERSBERG GROUP				Light green amygdaloidal, and non-amygdaloidal lava		
WITWATERSRAND SUPERGROUP		WEST RAND GROUP		Hospital Hill SBGRP	Red iron-rich shale; magnetic shale, quartzite		2970 ± 8
DOMINION GROUP			Rhenosterhoek Fm		Andesitic lava, tuff and shale		3074 ± 6
			Rhenosterspruit Fm		Quartzite, conglomerate, shale and interbanded lava		
KRAAIPAN GROUP					Banded iron formation, chert, quartzite, greywacke, grit and schist, amphibole andesitic and rhyolitic lava, tuff and pyroclastic breccia, light-coloured fine to medium – grained granite, gneiss		±3640
Biotite and gneiss							±3640

3.6.3 Geophysical Interpretation

The high magnetic anomalies which are found on the central part of the aeromagnetic map (Fig. 3.6-2) coincide with the BIF of the greenstone belts. These magnetic units are highly block faulted and have probably been subjected to the block faulting that took place after the deposition of the Klipriviersberg Group.

A spectacular sill anomaly is situated near the north-western corner of the map and even flow fronts in the sill are clearly visible. The highly magnetic anomaly in the western part of the map is associated with the deep-seated geological units (sills). These magnetic units have associated gravity high (Fig. 3.6-3) and are extensively block faulted (Kotzé, 1997).

A major east west trend of high magnetic anomaly on aeromagnetic map reflect the major fault in the area which is fill up by the ultramafic dyke, other dykes and lineaments are coinciding with the north-south striking high magnetic band. The eastern part of the aeromagnetic map is characterized by high magnetic anomalies which are believed to be coinciding with the mafic lava of the Allanridge Formation which is covered by the surface sand of the Gordonia Formation.

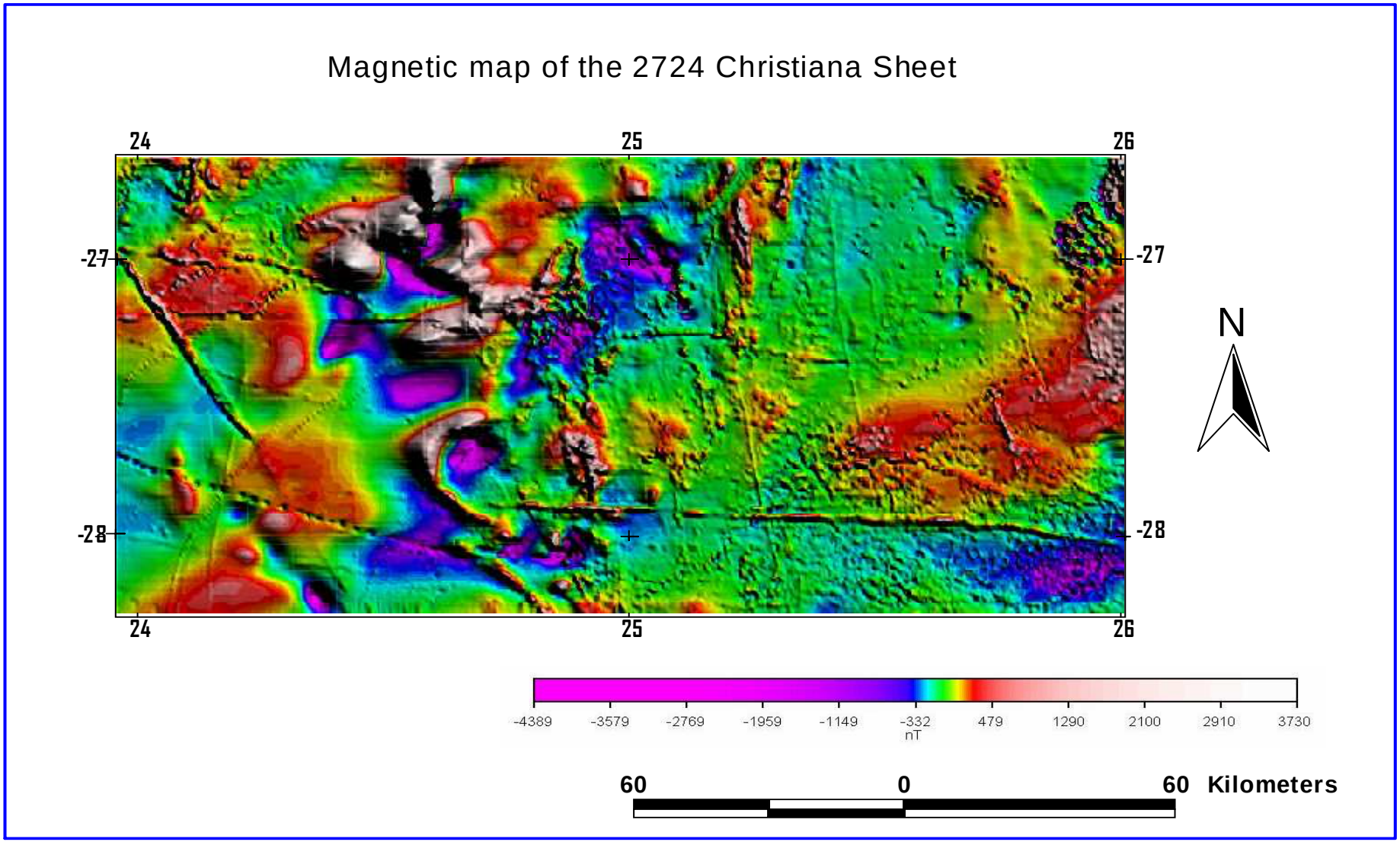

Figure 3.6-2: Magnetic map of 2724 Christiana Sheet (Council for Geoscience, 2000).

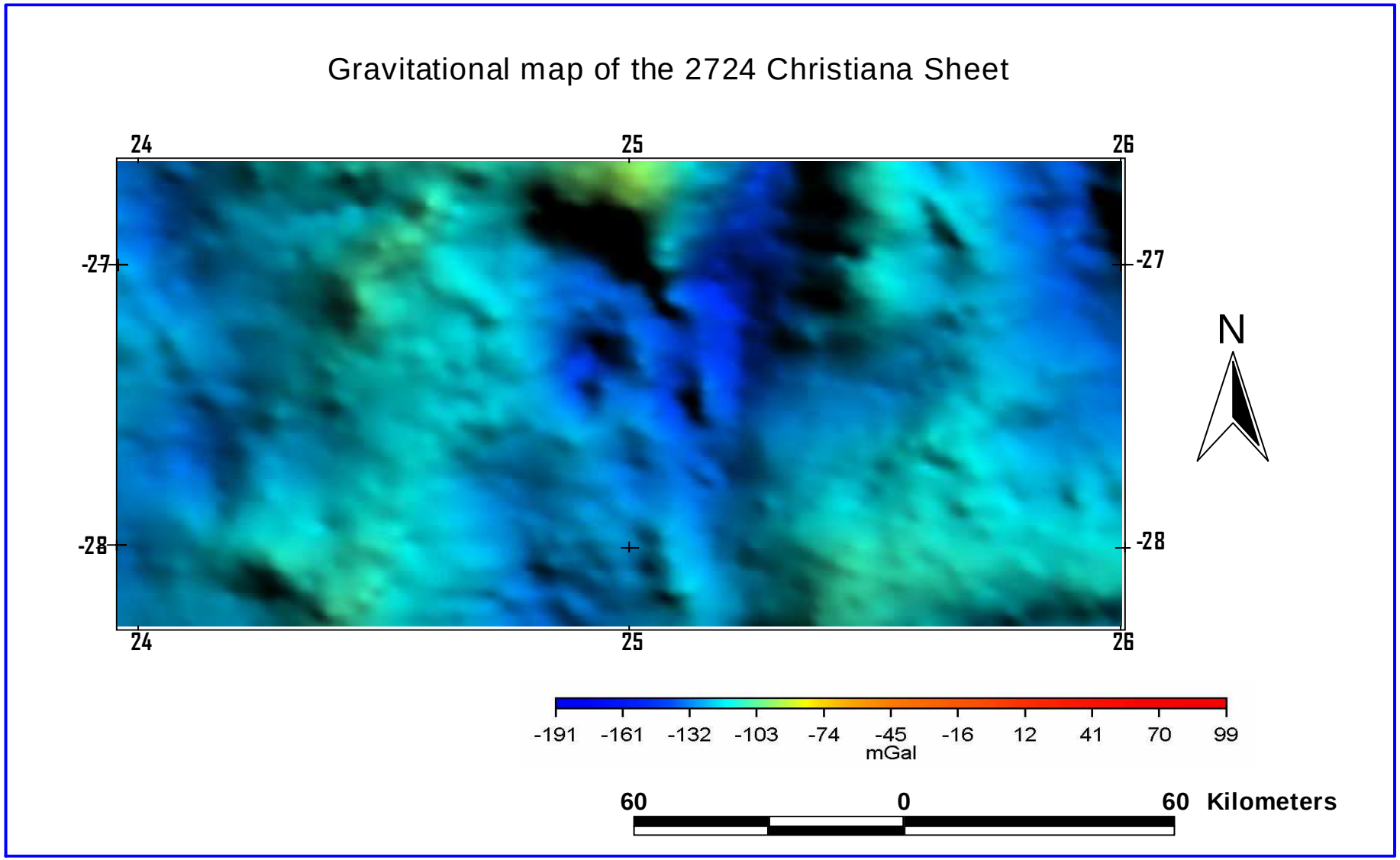

Figure 3.6-3: Gravity map of 2724 Christiana Sheet (Council for Geoscience, 200).

CHAPTER FOUR

4 DATA PRESENTATION AND INTERPRETATION

4.1 GRIDDING AND MAPPING METHODS

Geochemical sampling points were extracted, using TNTMips® and Arc-View® GIS Software (version 3.2a), based on their host formation.

Samples of the same lithological descriptions/ polygon were grouped together (Table 4.1-1) and were plotted on as value classed data points using Surfer 8® in order to assist in the identification of positive anomalies.

Table 4.1-1: Lithological groups derived from the similar lithological polygons and geological units.

LITHOLOGICAL GROUPING	SUCCESSIONS	LITHOLOGICAL DESCRIPTIONS
Surface sand		Wind-blown, partially reworked sand, colluvial, and river sand alluvium
Gordonia Formation		Siliceous sandstone, pebble conglomerate, gritstone, silcrete and sand
Calcrete		Calcrete and surface lime stone
Hekpoort Formation		Andesitic lava and muscovite hornfels
Pretoria Group shale and slate	Rooihoogte, Timeball Hill, Strubenkop and Silverton Formations	Carbonaceous slate, ferruginised quartzite hornfels and slate
Pretoria Group quartzite	Boshoek, Dwaalheuwel, Daspoort, Magaliesberg and Rayton Formations	Conglomerate, quartzite and hornfels.
Asbestos Hill Subroup	Kuruman and Danielskuil Formation	jaspilite with crocidolite; conglomerate and banded iron formation
Ghaap Group dolomite	Boomplaas, Clearwater, Monteville, Reivillo, and Fairfield Formations	Undifferentiated dolomite,chert , conglomerate and shale.
Malmani Subgroup dolomite	Oaktree, Monte Christo, Lyttelton, Eccles and Frisco Formations	Undifferentiated dolomite and chert and shale
Vryburg Formation		Quartzite, grit, conglomerate, shale amygdaloidal lava
Black Reef Formation		Quartzite, shale basal conglomerate
Allanridge Formation		Andesitic to basic lava and minor tuff.
Platiberg Group	Kameeldoorns, Goedgenoeg , Makwassie Bothaville and Rietgat Formations	Silicified tuff, tuffaceous sediment, felsic lava, chert, conglomerate, schist sandstone, felsic lava, and breccias
Klipriviersberg Group		Basaltic lava
Hospital Hill Subgroup		Quartzite, ferruginous shale
Dominion Group	Rhenosterspruit and Syferfontein Formations	Pyroclastic rocks, tuffs, quartzite conglomerates, grits, volcanic rock
Gaborone Granite		Granite
Kanye Formation		Felsic lava, breccias.
Kraaipan Group	Goldridge, Ferndale and Khunwana Fomartions	Schist, amphibolites, jaspilite, lava, banded ironstone and dolomite
Amphibolites basemet		Amphibolites

Geochemical data were interpolated into a regular grid using the Golden Software SURFER® Package. A kriging interpolation method was used to generate the grid, which was then converted into an 8-bit raster image, each element producing a "geochemical image", in which the intensity of each pixel (colour level) was proportional to the content of the respective element. Point Kriging was used as a gridding method for 2D contour generation. The spatial resolution of the geochemical images was defined according to its level of concentration. Contour intervals were set at various levels depending on the data distribution pattern of each element.

Due to noisy geochemical results from the contouring method and limited software availability, the classed post map method was used for geochemical presentation because:

- It is able to plot the actual true sample positions.
- It does not interpolate the non-sampled areas.

4.2 DETERMINATION OF THE THRESHOLD VALUES

Defining background and anomalous values is a fundamental issue in exploration geochemistry. In the past, the traditional statistical methods assumed that the concentration of chemical elements in the crust follow a normal or log-normal distribution (Rose *et al*., 1979; Chork and Mazzuchelli, 1989; Stanley, 2003; Nezampour and Mosazadeh, 2006). A geochemical anomaly is defined as a region where the concentration of the element of interest is greater than a certain threshold value, and the latter is determined based on statistical parameters, such as mean, median, and standard deviation. In general, a geochemical threshold value is defined as 1.5 to 3 standard deviations (σ) above the mean ($\bar{x}$) value (Rose *et al*., 1979; Li, *et al*., 2003); Çiftçi *et al*., 2005). In this study the geochemical threshold of the raw data is defined as:

$$Th = \bar{x} + 2\sigma$$

These threshold values were calculated for each of the variables within each of the major lithological units (Table 4.1-1).

In this study the geochemical data are characterized by their spatial position, which means that the element concentration varies spatially. However, the traditional methods

emphasize the frequency distribution of the element concentration. The normal (Gaussian) distribution is not a commonly identified geochemical distribution. It was found that most of elements, especially some trace elements, do not obey the normal distribution, but show a right or left skew or a power-law tail and multi-modal distribution. As a result, it was considered best to transform the geochemical data to enhance its characteristics before numerically or graphically evaluating them.
A variety of transformation functions have been employed in geochemical applications. In this paper a simple transformation of data to a logarithmic function was used (Stanley, 2003; Stanley, 2006*a*, 2006*b*; Stanley and Ryan, 2008).

$$y = \ln(x)$$

Data quality and validation was carried out using JMP 8® in order to identify the duplicate, missing values and zero values. Samples which have zero values are below the detections limit and are mostly found on uranium, lead and thorium.

Histogram and box plots were computed for each lithological group as well as the map sheet in order to observe the distribution of the data. Most of the elements in each lithological group are characterized by the distribution which departure from normality towards highest values (Zhang *et al*., 2005). The results are referred to as the positively skewed featured of the distribution for most elements shown on the histogram (Appendix 2). It should be noted that the slopes of the plots cannot be directly compared, as axial scales vary to encompass the wide disparity in concentrations. Most of the trace elements do demonstrate some form of convex shapes and some show that they are composed of multiple phases and have closer overall similarities to lognormal distributions.
The plots provide useful information for outlier detection. For example, single samples of Zn, Fe and Cr (Fig 4.2-4 and fig. 4.2-3) are separated from the distribution curve. Similar outliers can be identified for other elements.

All samples which have zero and outlying values were omitted for the following reasons: (a) They cause the frequency distribution to be excessively skewed; (b) There is no logarithmic transformation of the zero value; (c) They give a bias of higher variance. If

the values are not omitted it will gives rise to the over estimation of threshold values (refer to table 4.2-1 to 4 and Fig. 4.2-41 to 7).

Table 4.2-1: Summary statistics of Fe, Cr and Zn raw data in Gordonia Formation.

Element	N	Min	Max	Mean	Median	St. Dev	Var	CV	Skew	Kurt	Threshold
Fe_2O_3	3514	0.77	74.83	**3.17**	3.10	1.43	2.06	0.45	35.68	1773.02	6
Cr	3510	2.00	7677.00	**70.50**	66.00	131.65	17331.57	1.87	55.06	3178.62	334
Zn	3514	2.00	85015.00	45.81	20.00	1433.82	2055853.00	31.30	59.27	3513.62	2913

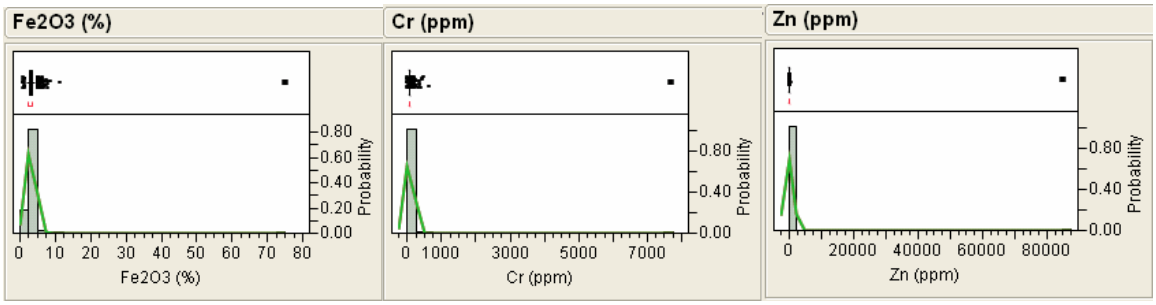

Figure 4.2-1: Histogram and box plot of Fe, Cr and zinc distribution raw data in Gordonia Formation.

Table 4.2-2: Summary statistics of Fe, Cr and Zn log-transform data in the Gordonia Formation.

Element	N	Min	Max	Mean	Median	St. Dev	Var	CV	Skew	Kurt	Log Threshold
Fe_2O_3	3514	-0.26	4.32	1.12	1.13	0.25	0.06	0.22	0.25	9.51	**6.5**
Cr	3510	0.69	8.95	4.16	4.19	0.37	0.14	0.09	-0.11	15.08	**194.6**
Zn	3514	0.69	11.35	3.00	3.00	0.40	0.16	0.13	2.87	58.06	**66.0**

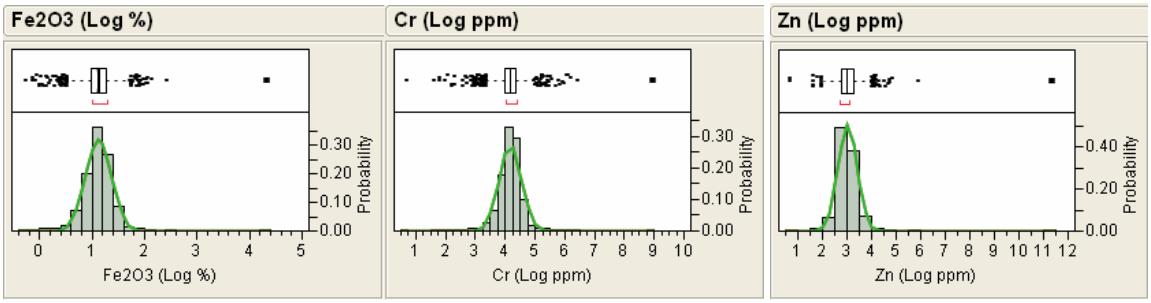

Figure 4.2-2: Histogram and box plot of Fe, Cr and zinc log-transform data in Gordonia Formation.

Table 4.2-3: Summary statistics of Fe, Cr and Zn raw data with outliers excluded, in the Gordonia Formation.

Element	N	Min	Max	Mean	Median	St. Dev	Var	CV	Skew	Kurt	Threshold
Fe_2O_3	3513	0.77	11.25	3.15	3.10	0.77	0.60	0.25	1.24	6.77	**5**
Cr	3509	2.00	610.00	70.50	66.00	28.95	17331.57	0.41	6.00	3178.62	**128**
Zn	3513	2.00	354.00	21.63	20.00	10.58	112.04	0.49	10.49	285.35	**43**

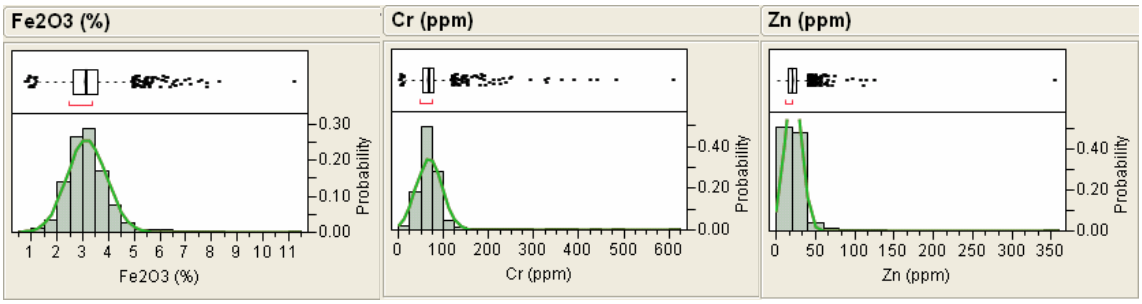

Figure 4.2-3: Histogram and box plot of Fe of Fe, Cr and zinc raw data with outliers excluded in Gordonia formation.

Table 4.2-4: Summary statistics of Fe, Cr and Zn log-transform data outliers excluded in Gordonia Formation.

Element	N	Min	Max	Mean	Median	St. Dev	Var	CV	Skew	Kurt	Log Threshold
Fe_2O_3	3513	-0.26	2.42	1.12	1.13	0.24	0.06	0.22	-0.36	2.31	**6.3**
Cr	3509	0.69	6.41	4.16	4.19	0.36	0.13	0.09	-0.77	8.11	**189.3**
Zn	3513	0.69	5.87	3.00	3.00	0.37	0.14	0.12	0.25	2.96	**60.9**

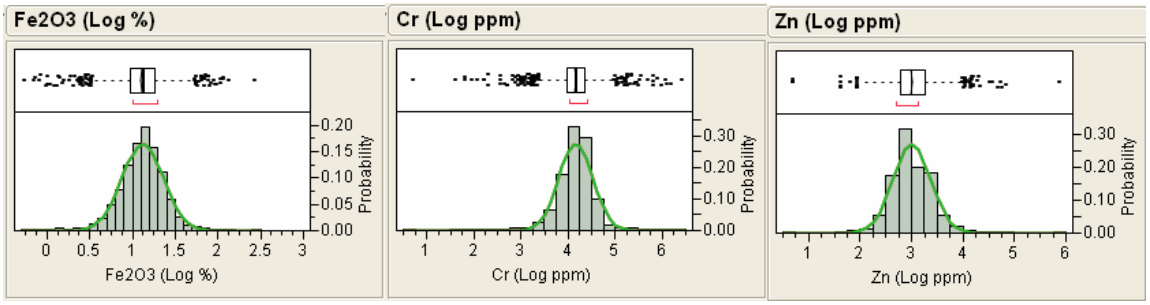

Figure 4.2-4: Histogram and box plot Fe, Cr and zinc log-transform data outliers excluded in Gordonia formation.

The Normal model was use to define the threshold of the log-transformed data (see tables in appendix 1).

$$Log\ Th = exp\left[\left(x + \frac{(\sigma)^2}{2}\right) + 2\sigma\right]$$

Where x; log mean; σ, log stand derivation

The *error variance stabilization* is defined as: $\frac{(\sigma)^2}{2}$ in the above equation.

The error variance stabilization is added to the log mean when doing the back transformation of the log transform data into original data in order to minimize the error that arises during the process of log transformation.

In most cases the threshold values calculated from all data on the map sheet (regardless of lithology) and the threshold value calculated for each lithological unit were not dissimilar from each other. Therefore crustal abundance of each element (Clarke values, table A-41) was introduced in order to compare the local threshold values of each element as well as to delineate the background and anomalous values.

In this study the threshold values (raw data) were used in conjunction with the map sheet areas (Mafikeng, Vryburg, Christiana and Kuruman). The plotting of geochemical anomalies on the lithological grouping by filtering the geochemical data using the threshold values of each lithological groups. This was done by the overlaying of the geochemical data sets and Geological maps on GIS (Arc-View 3.2a programme).

The reason why the geochemical anomalies were not plotted for each of the litho groups are as follows.

- Most of the litho groups are characterized by small dataset this includes Kraaipan Group, Kanye Formation, Gaborone Granite, Hospital hill Subgroup, Black Reef Formation, Pretoria Quartzite, Pretoria shale, Hekpoort Formation. The above lithological groups are characterized by fewer extremely high values which over estimate the threshold values. Consider nickel distribution over the Kraaipan

Group (fig. 4.2-5 and fig. 4.2-6) and chromium distribution over Pretoria Quartzite Groups (fig. 4.2-7 and fig. 4.2-8).

- Plotting the geochemical anomalies based on the litho grouping does not define the spatial continuity (size and shape) of the anomalies. With the neighboring lithological groups it clearly shows the shape, size and continuity of the anomalies. If these neighboring values were omitted, the anomaly would not be clear.
- To eliminate underestimation or over estimation of threshold values. Too low threshold, time and money will be wasted on the following up non-significant anomalies. Too high threshold values will mean that some portions of the anomalies will be missed (example Fig. 4.2-7 and fig. 4.2-8).
- Although the geochemical maps were plotted from the Map Sheet, the geochemical anomalies were filtered the Arc-view 3.2a based on the Litho groups threshold values and it was found that it produce similar results as the Map Sheet results (see fig.4. 2 -9 to fig. 4.2-12).
- Threshold values were considered approximately twice the concentration of the crustal abundance. Therefore because a global threshold for each map is used, the threshold will cover all values within individual lithological units where their thresholds are below the crustal abundance concentration.

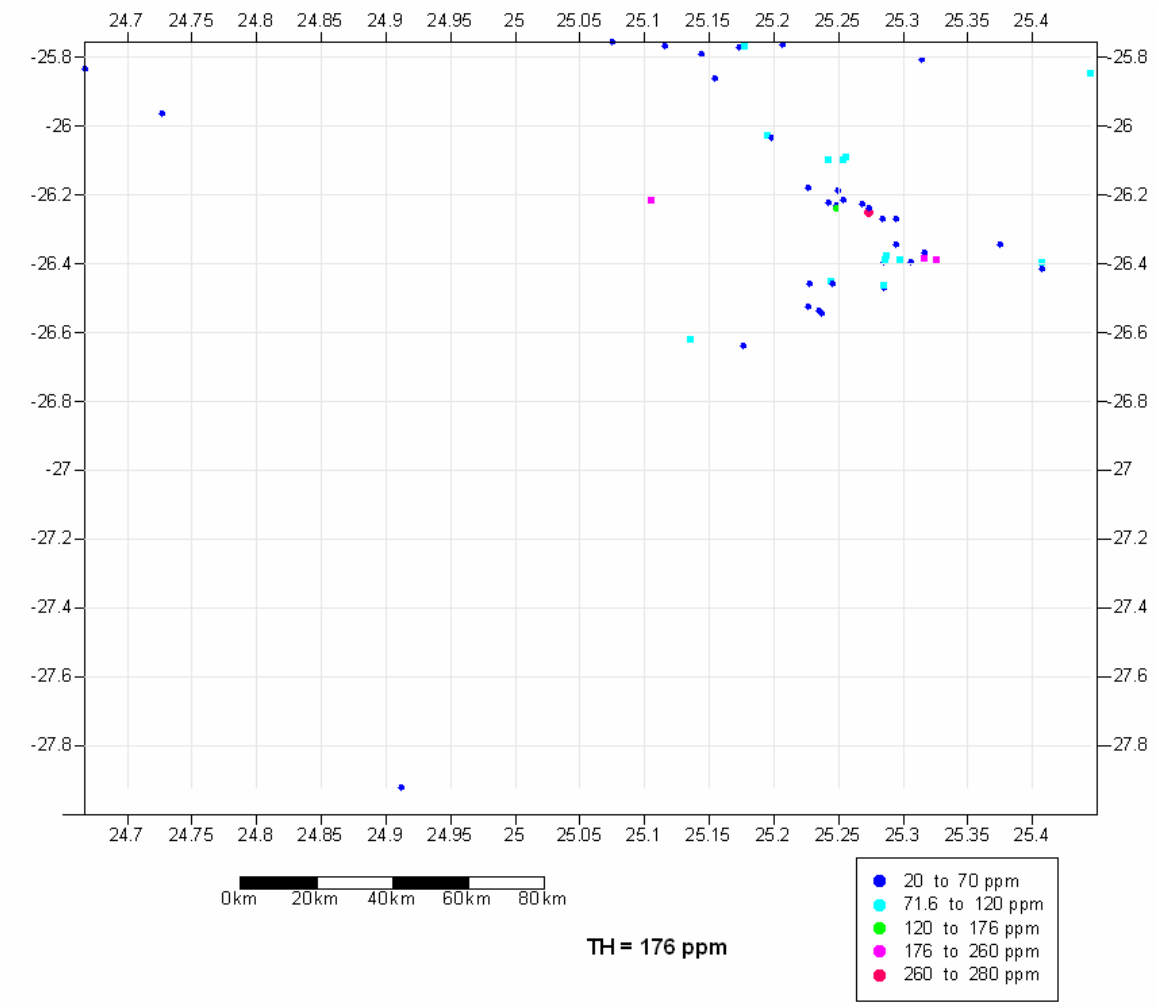

Figure 4.2-5: **Classed post map of Nickel distribution on Kraaipan group, TH = 176ppm (lithology group threshold value).**

In fig. 4.2-5 some of the data are omitted due to over estimation of the threshold values as a result of one of the outlier values (278ppm). The special continuity and shape is not clearly defined on this single lithological group. Fig.4.2-6 is the map sheet of the entire data set of the Vryburg Area, where the continuity of the anomaly is visible as they are connected with adjacent anomalies of the lithological groups.

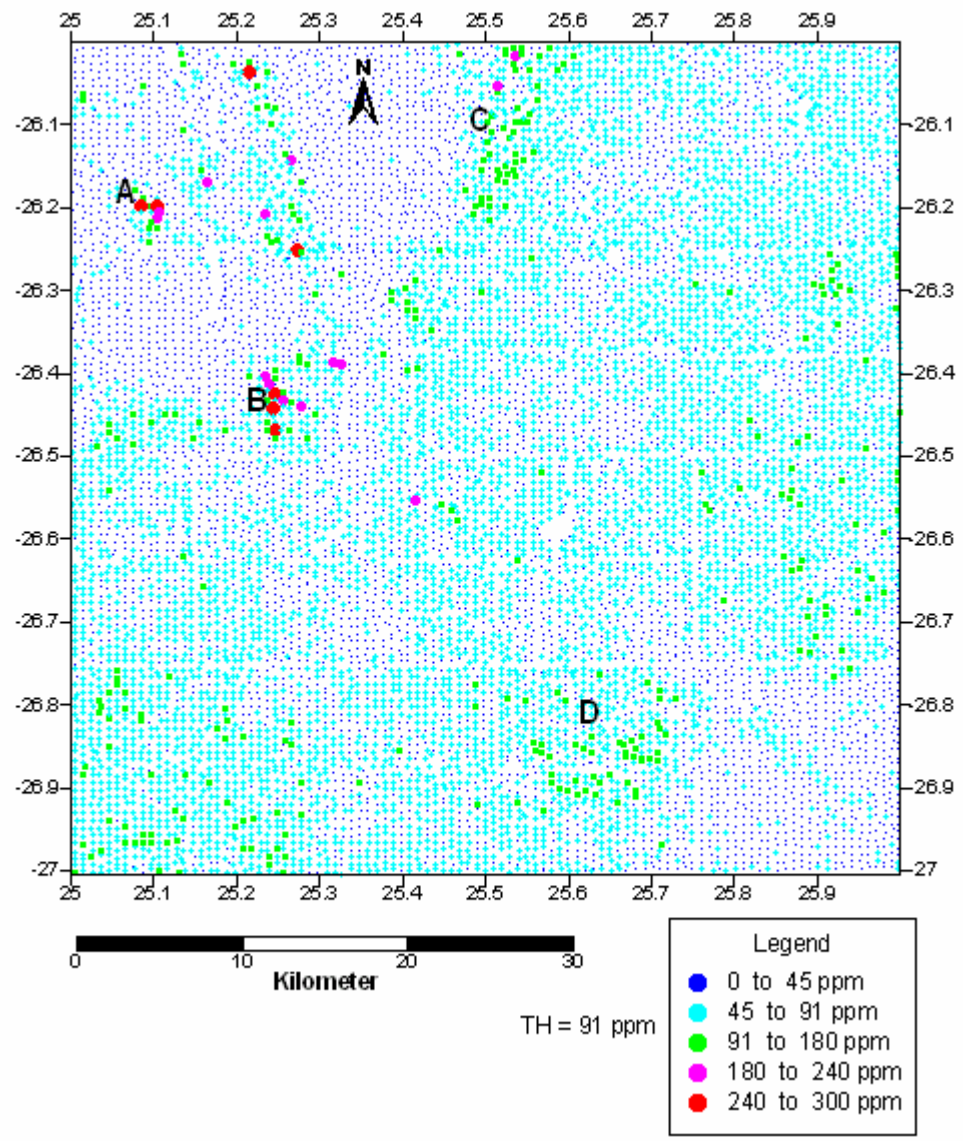

Figure 4.2-6: Classed post map of Nickel distribution on Kraaipan group, TH = 91ppm (Vryburg Geological Map Sheet threshold value).

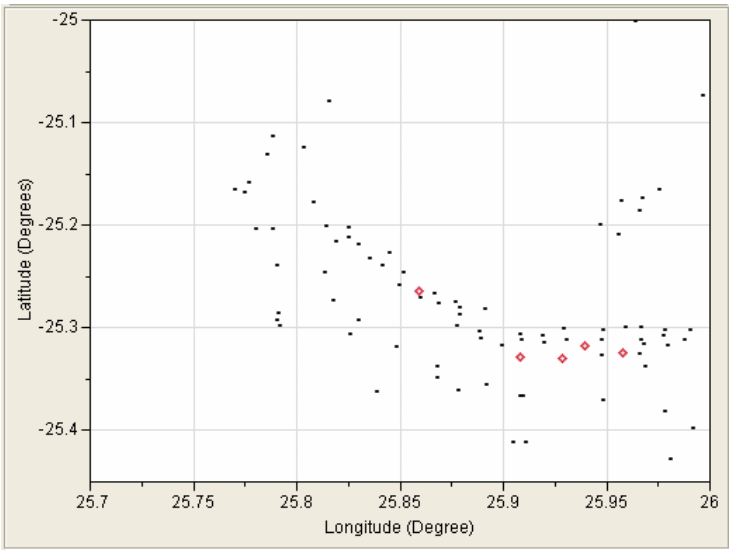

Figure 4.2-7: Classed post map of Chromium anomaly in Pretoria Quartzite grouping where threshold of 1328 ppm.

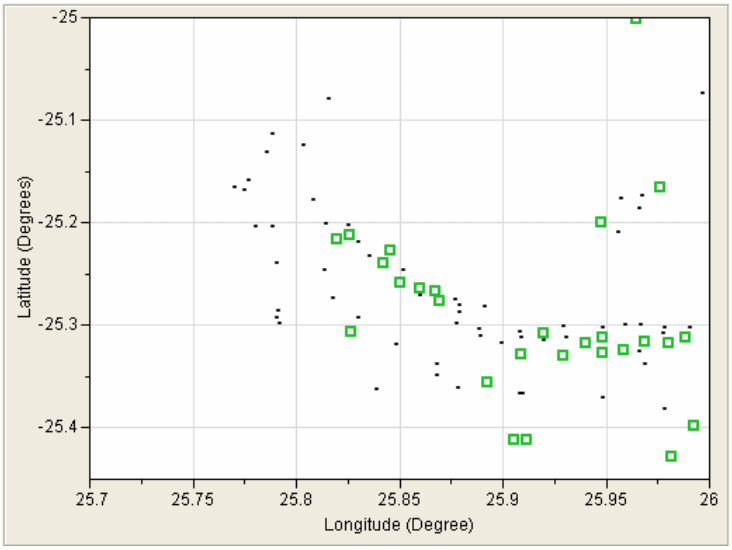

Figure 4.2-8: Classed post map of Chromium anomaly in Pretoria Quartzite grouping where threshold of 485 ppm (Mafikeng Sheet- threshold values).

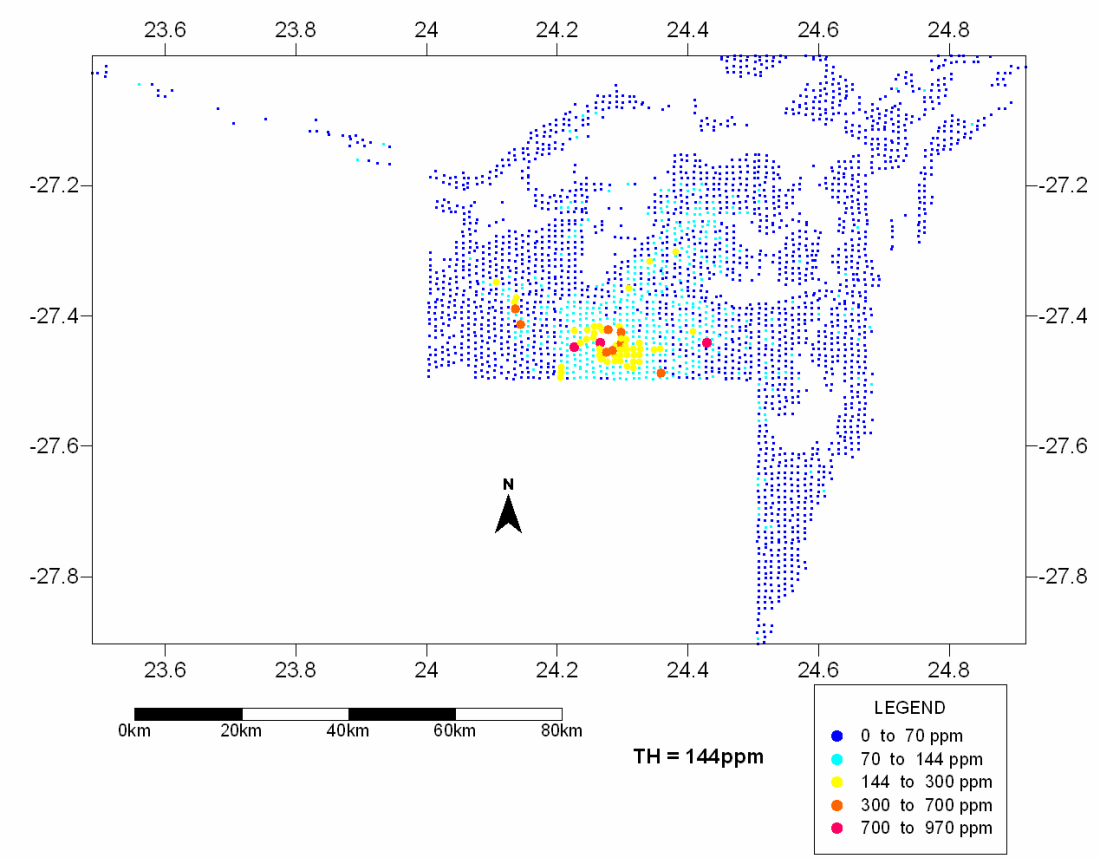

Figure 4.2-9: Classed post map of zinc distribution on Ghaap group dolomite.

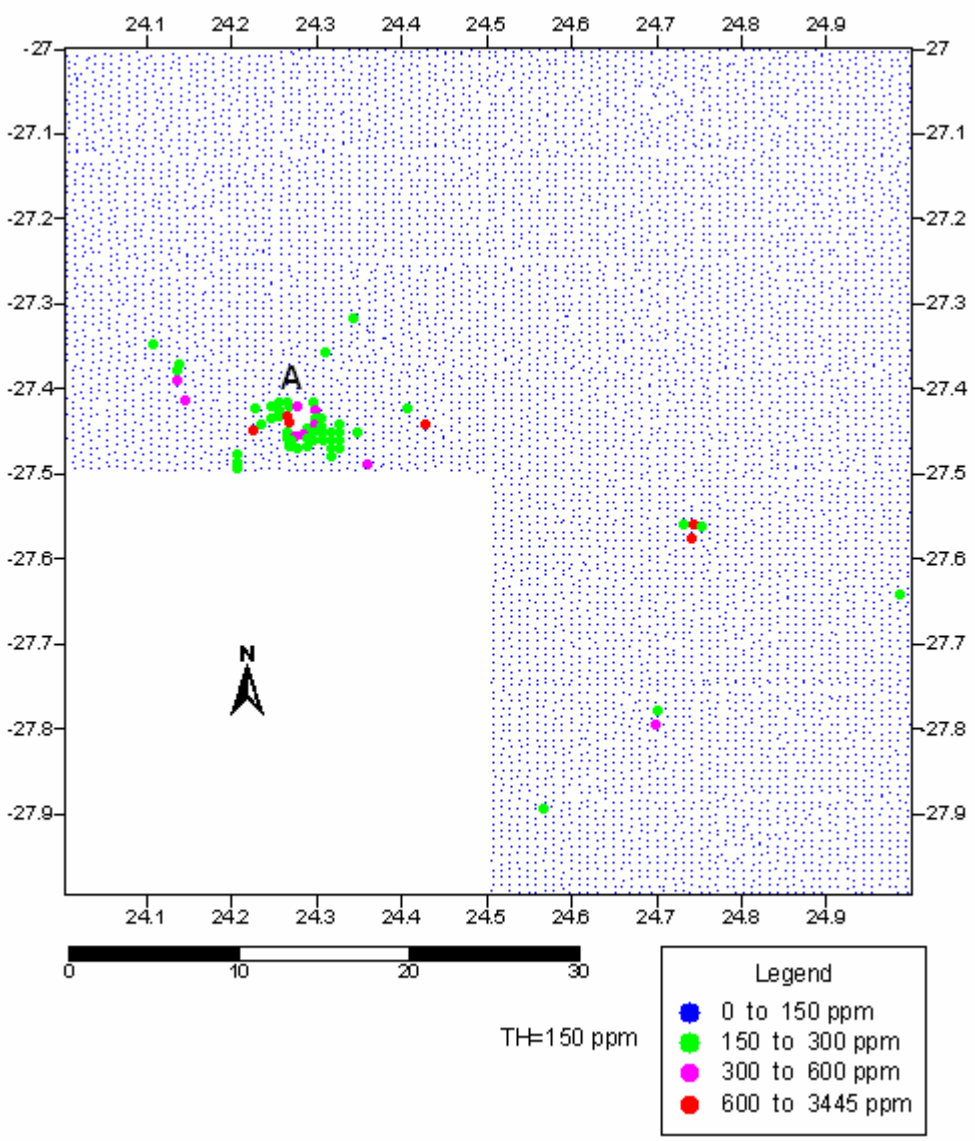

Figure 4.2-10: Classed post map of zinc distribution zinc anomaly in the 2724 Christiana Sheet.

Figure 4.2-9 and fig.4.2-10 shows the geochemical anomaly of the zinc on the Reivilo Formations of the Campbell Rand Subgroup. The anomaly reflects the Pering Zn-Pb mineralization which is circular in shape, where the inner part of the anomalies has a gap as no sample could be collected from the abandoned open cast mine. The deposit was mined from 1984 to the end of November, 2002 (Southwood, 1986).

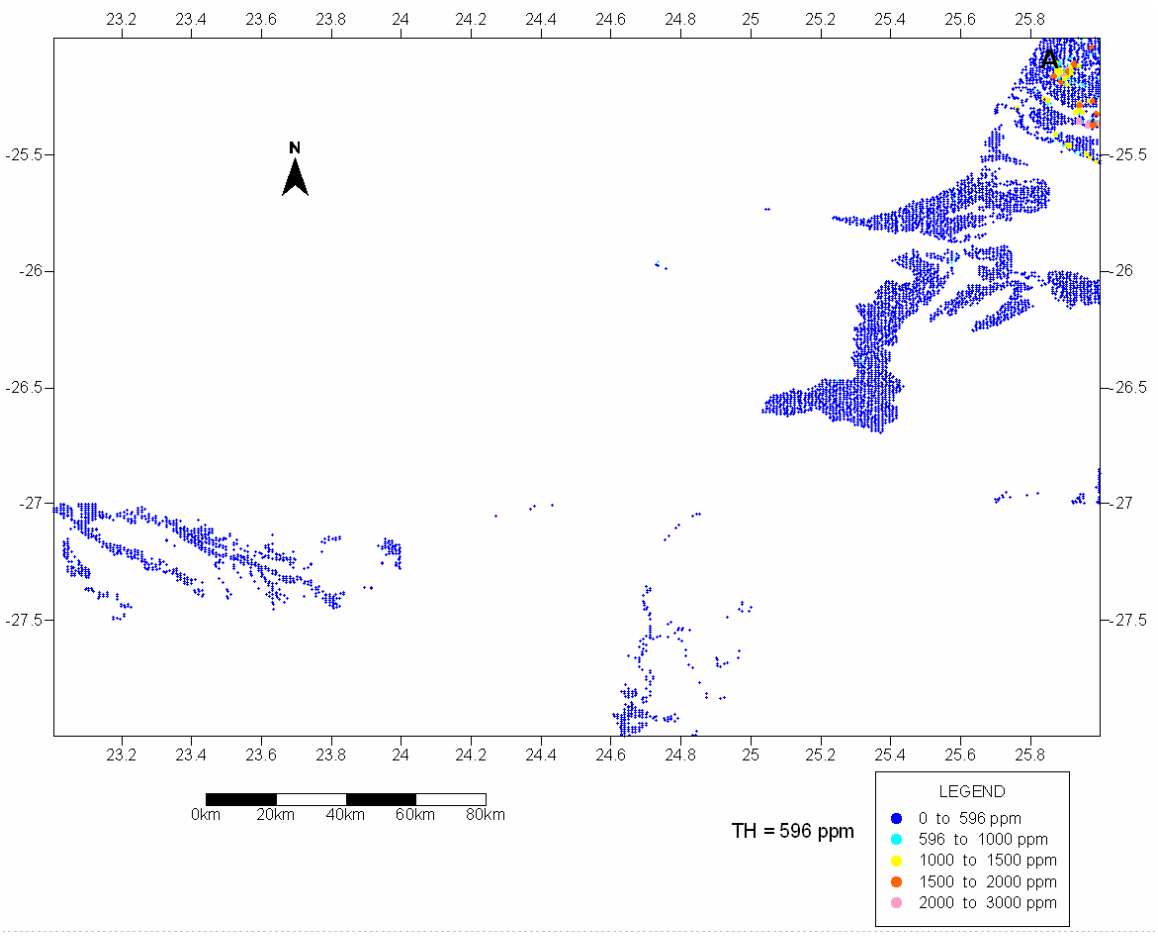

Figure 4.2-11: Classed post map of chromium anomalies on surface sand.

Both fig.4.2-11 and fig. 4.2-12 they represent similar geochemical distribution (Anomaly A) over the surface sand. Fig. 4.2-11 is not clear visible; the data covers wide areas. There are no clear trends of anomaly B and C as the data was modeled on the surface sand litho group. In fig. 4.2-12 it shows three trends where all the higher values of different anomalies from various litho groups are connected together to clearly defined shape and extent of the anomaly.

Although the geochemical maps were created from the global threshold, (map sheets) the lithological units threshold were also applied, to the identified anomalies to justify the anomalies associated with that particular lithological group based on lithological threshold value. This was done by overlaying the geology and geochemical data set and filtering the data in that particular lithological group based on lithological units.

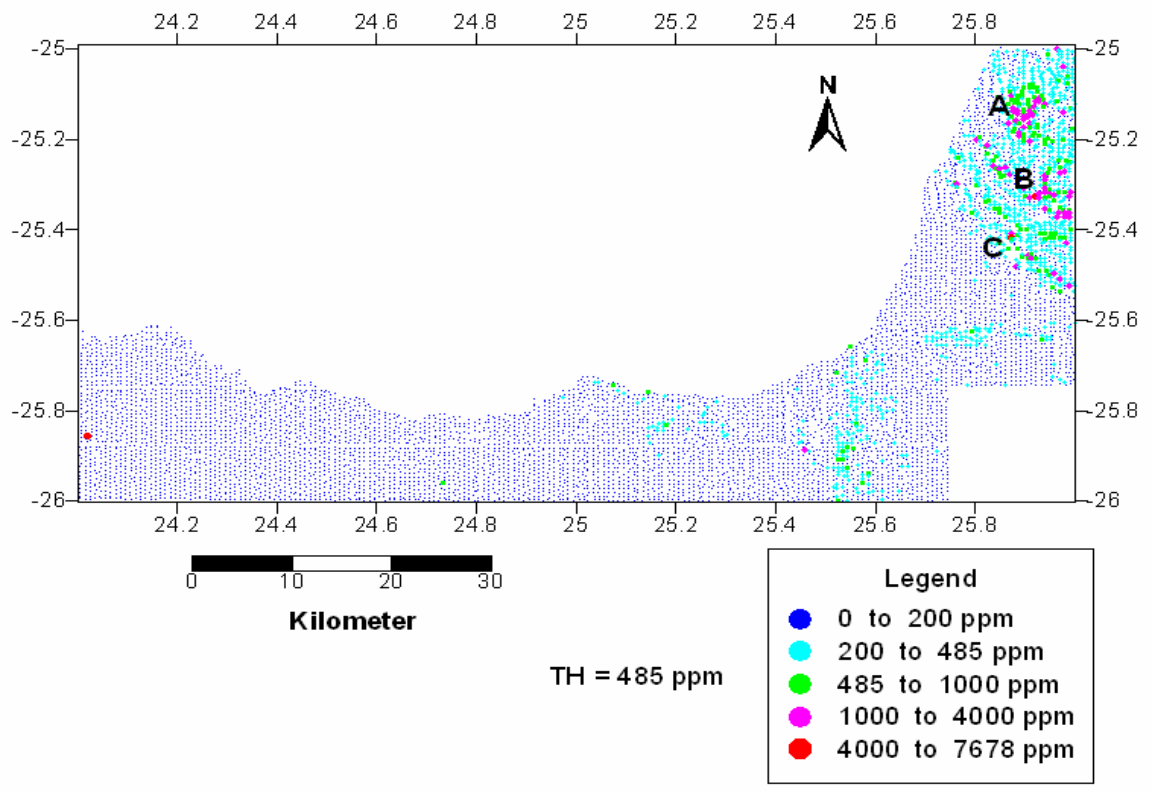

Figure 4.2-12: Classed post map of chromium anomalies on Mafikeng area.

4.3 DATA PROCESSING

Published geological and geophysical maps (Mafikeng, Vryburg, Christiana and Kuruman) at scale of 1:250 000 were used to evaluate the spatial association between bedrock lithologies and soil geochemistry. The geological maps are in hard copy and vector format, geophysical maps were in Tiff-format whereas geochemistry data were in point data. This was done by a spatial overlaying (labeling) of the sample concentrations of 21 analyzed elements over the geological and geophysical maps (magnetic and gravity) using Arc-View 3.2a, which was reclassified into lithotypes (metasediments, granitic rocks, carbonates, volcanics and to Quaternary sediments), representative for the internal lithological variation.

4.4 DISTRIBUTION OF ELEMENTS ON THE 2524 MAFIKENG SHEET

4.4.1 Statistical analysis

Summary on the statistics on the complete validated data set (7690 samples) covering sheet 2524 Mafikeng are presented in Table 4.4-1, with the values for minimum (Min), maximum (Max), standard deviation (Std. Dev), mean, range, variance, kurtosis and skewness. The mean plus two times standard deviations of each element are displaced in the last column to show the general threshold of the complete data set across various lithological units. For example, contouring intervals for the map were based on a 95% confidence interval (mean + two std. dev) to show chemical variation in the different lithological units. In general the values with concentrations higher than the average plus two times standard deviation were considered as anomalous. Sample B12, MAP No 2UM was not considered when computing the statistical analysis of this area because the sample was characterized by higher values e.g. 85015ppm in Zn, 7677ppm in Cr and 74 wt% in Fe_2O_3 and other elements. As the values of the above mentioned elements were extremely high and this would have a higher impact on the mean of higher values which would result in biased estimation (mean) of the threshold values. As the data set containing different lithological units, threshold values were calculated separately each lithological units and map on each element.

4.4.2 Correlation of elements

All 21 elements in Mafikeng 2524 Sheets were correlated to one another and in the correlation results only 11 correlations were identified. Out of the 11 correlations five were found to be positively correlated (Ti-Zr, Cu-Zn, Co-Cu, Co-Zn, Cu-W, and Zn-W) where their correlation coefficients were ranging between 80-95 %.

These correlations are tabulated in Table 4.4-2, while seven correlations were found weakly positively correlated which include the correlation among the following elements: Fe-V, Co-W, Cr-Ni, Co-Zn, Ti-Nb, Zn-Pb, Y-Th, Co-Cu and Y-Nb all this elements their coefficient of correlation were ranging between 59-68% .Cobalt, tungsten, yttrium and

niobium show poor correlations as they have no correlation coefficients (Co-W; 55% and Y-Nb, 52%, Fig. 4.4-2. None of the outlined elements have perfect correlation as the coefficient of perfect correlation is 1 (R^2=1).

Table 4.4-1: Summary statistics on the complete geochemical data set for the 2524 Mafikeng Sheet.

Element	N	Min	Max	Mean	Median	St. Dev	Var	CV	Skew	Kurt	Threshold
TiO_2	7691	0.10	3.52	1.01	0.99	0.28	0.08	0.28	0.67	2.75	**1.6**
MnO	7691	0.01	5.35	0.13	0.06	0.28	0.08	2.11	6.54	61.11	**0.7**
Fe_2O_3	7690	0.50	25.41	4.29	3.68	2.02	4.07	0.47	2.11	8.42	**8**
Sc	7686	1.00	92.00	11.99	12.00	4.13	17.04	0.34	3.66	53.14	**20**
V	7688	1.00	382.00	60.60	54.00	28.80	829.51	0.48	1.82	7.31	**118**
Cr	7684	2.00	4253.00	133.24	89.00	175.99	30973.69	1.32	8.45	117.23	**485**
Co	7667	1.00	654.00	14.01	12.00	15.46	238.90	1.10	32.28	1265.27	**45**
Ni	7689	5.00	706.00	46.26	34.00	41.22	1699.34	0.89	41.22	49.50	**129**
Cu	7688	4.00	234.00	24.83	21.00	13.86	191.97	0.56	2.55	15.08	**53**
Zn	7690	2.00	1288.00	33.51	29.00	23.58	555.87	0.70	21.16	1053.39	**81**
As	6725	1.00	164.00	13.17	12.00	9.56	91.43	0.73	3.57	32.67	**32**
Rb	7690	10.00	196.00	75.63	73.00	21.23	450.75	0.28	0.73	1.51	**118**
Sr	7686	7.00	555.00	50.97	44.00	29.23	854.39	0.57	3.90	33.65	**109**
Y	7686	1.00	102.00	28.09	27.00	7.70	59.28	0.27	1.09	4.48	**43**
Zr	7691	45.00	4196.00	957.78	933.00	444.80	197845.22	0.46	0.62	0.88	**1847**
Nb	7689	1.00	47.00	21.02	21.00	3.72	13.85	0.18	-0.01	1.27	**28**
Ba	7687	10.00	1819.00	311.64	302.00	92.32	8522.85	0.30	2.41	23.56	**496**
W	7685	1.00	20.00	9.77	9.00	2.59	6.73	0.27	0.03	-0.87	**15**
Pb	4326	1.00	177.00	4.82	4.00	5.92	35.08	1.23	12.39	260.28	**17**
Th	7652	1.00	27.00	14.83	15.00	2.30	5.27	0.15	-1.00	4.70	**19**
U	1603	1.00	12.00	1.72	1.00	1.05	1.09	0.61	2.80	15.53	**4**

Table 4.4-2: Correlation matrix of the elements in 2524 Mafikeng Sheet.

	TiO_2	MnO	Fe_2O_3	Sc	V	Cr	Co	Ni	Cu	Zn	As	Rb	Sr	Y	Zr	Nb	Ba	W	Pb	Th	U
TiO_2	1.00																				
MnO	-0.31	1.00																			
Fe_2O_3	-0.29	0.32	1.00																		
Sc	0.12	0.13	**0.69**	1.00																	
V	-0.24	0.22	**0.79**	**0.69**	1.00																
Cr	-0.24	0.09	**0.58**	0.44	**0.53**	1.00															
Co	-0.07	0.06	0.47	**0.60**	0.41	**0.56**	1.00														
Ni	-0.29	0.08	**0.55**	**0.50**	**0.57**	**0.78**	0.21	1.00													
Cu	-0.09	0.06	**0.50**	**0.57**	0.33	**0.50**	**0.82**	0.11	1.00												
Zn	-0.04	0.04	0.38	0.27	0.20	0.44	**0.81**	0.00	**0.98**	1.00											
As	-0.55	0.18	0.34	0.22	0.27	0.18	0.10	0.21	0.34	0.27	1.00										
Rb	-0.06	-0.17	0.09	0.04	0.07	-0.04	0.00	0.04	0.18	0.24	-0.03	1.00									
Sr	-0.03	-0.16	0.00	0.11	0.07	-0.08	0.02	0.06	0.03	-0.01	-0.02	0.15	1.00								
Y	0.49	-0.25	-0.15	0.01	-0.15	-0.16	-0.04	-0.17	-0.02	0.00	-0.31	0.56	-0.07	1.00							
Zr	**0.86**	-0.30	-0.57	-0.19	-0.56	-0.36	-0.15	-0.45	-0.14	-0.03	-0.61	-0.12	-0.04	0.42	1.00						
Nb	**0.81**	-0.34	-0.43	-0.14	-0.46	-0.26	-0.04	-0.38	-0.01	0.07	-0.57	0.22	-0.11	**0.72**	**0.83**	1.00					
Ba	0.01	0.35	0.23	0.26	0.25	0.00	0.21	0.06	0.19	0.15	-0.04	0.37	0.34	0.14	-0.07	-0.05	1.00				
W	0.12	-0.01	0.25	-0.24	0.08	0.35	**0.75**	-0.12	**0.93**	**0.97**	-0.40	-0.22	-0.07	0.07	0.14	0.22	-0.18	1.00			
Pb	-0.23	0.10	0.34	-0.01	0.17	0.39	0.49	0.03	**0.55**	**0.55**	0.13	0.09	0.06	-0.10	-0.19	-0.18	0.11	**0.50**	1.00		
Th	0.31	-0.33	-0.26	-0.08	-0.22	-0.07	0.05	-0.13	0.07	0.10	-0.28	0.36	0.08	**0.50**	0.33	**0.54**	0.04	0.11	0.07	1.00	
U	-0.18	0.07	0.03	-0.09	-0.13	0.17	0.22	-0.21	0.24	0.24	0.10	0.19	0.13	0.17	0.01	0.21	0.05	0.26	0.31	0.38	1.00

4.4.3 Statistical distribution

In the Mafikeng sheet, titanium, zirconium, niobium and tungsten show an asymmetrical, bimodal distribution (Fig. 4.4-1). All these elements show that they have a higher concentration dominated over the western part of the map on the surface sand of the Gordonia Formation and they have a poor concentration on the eastern side of the map, over the mafic and intermediate rock, (Transvaal Supergroup, biotite gneiss and Allanridge Formation lithologies.

Manganese, scandium, iron, vanadium, chromium, cobalt, nickel, copper, zinc, arsenic, strontium, lead, and uranium show asymmetrical, positively skewed distributions with occasional outliers and lower concentrations or are characterized by lower values in the felsic rocks (surface sand of the Gordonia Formation, biotite and gneiss, Gaborone Granite and Kanye Formation). The eastern part of the area is predominantly occupied by higher values of those elements on top of the mafic and ultramafic rocks.

Yttrium, thorium, rubidium and barium shows symmetrical, leptokurtic distribution with occasional outliers, vanadium has a fairly symmetrical distribution which is positively skewed in Fig. 4.4-1.

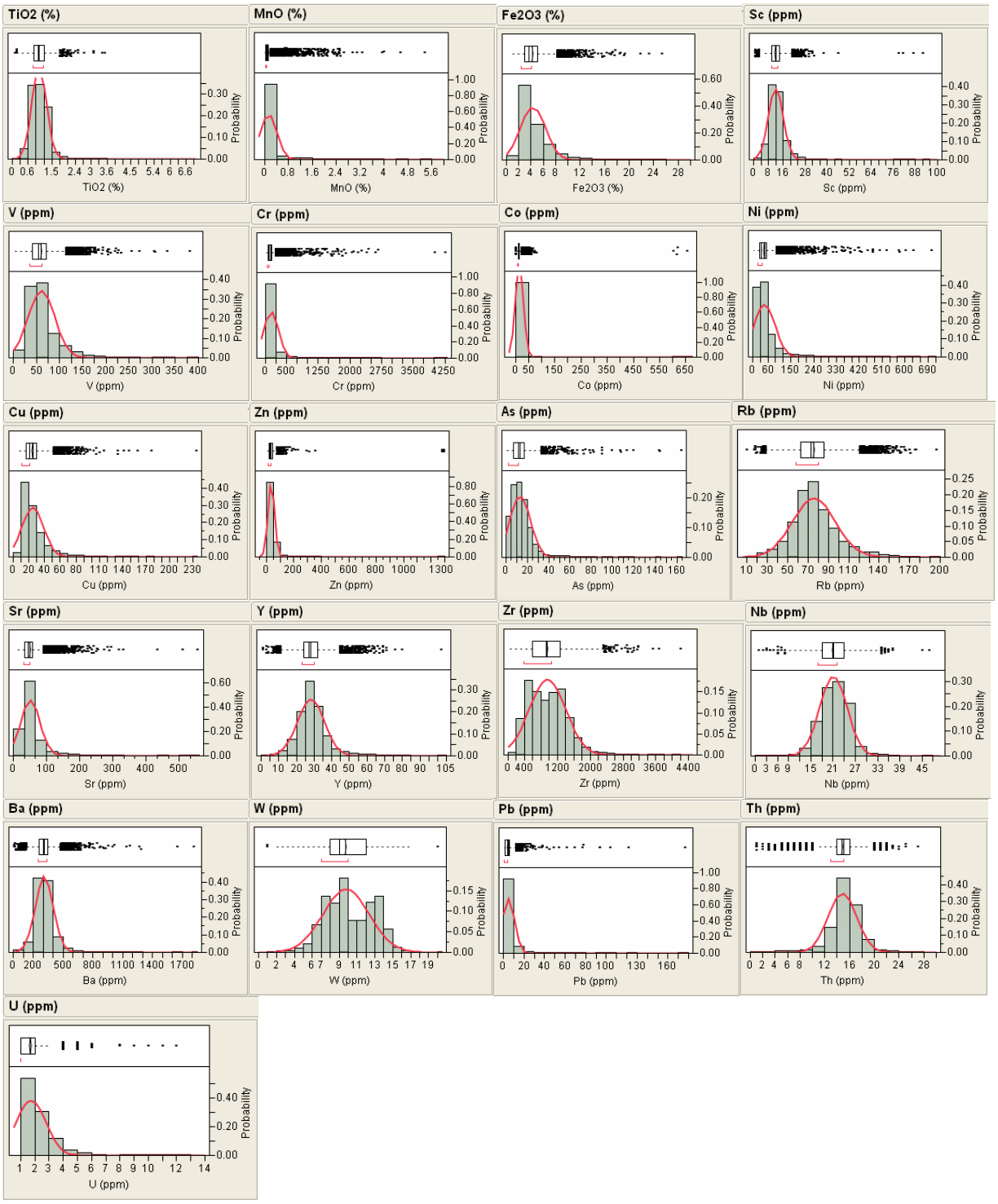

Figure 4.4-1: Histograms and box plots of the elements on the Mafikeng Area.

4.4.4 Geochemical distribution

Chromium (Cr) Distribution

The Fig 4.4-2 shows chromium anomalies in the Mafikeng area. Towards the north margin of the sheet, anomalous values are occasionally encountered in the centre. Anomaly A is located in surface sand, river sand and alluvium of Quaternary age, which the author believes is from the Lower Chromitite zone of the Bushveld Complex. The highest values occur in the middle of the anomaly, where the chromium content reaches 2202 ppm. The second anomaly B occurs to the south of anomaly A and extends toward the Botswana and South Africa border. It consists of three separate peaks, with the highest having a concentration of 4017 ppm.

This anomaly (trend B) resulted from andesitic lava and pyroclastic rock of the Hekpoort Formation. The third anomaly (trend C) lies southwest of the anomaly B, and occurs on the surface deposit, river sand and alluvium of Quaternary in age. The anomalies trend in a NW-SE and cover a wide area in terms of kilometers and have an irregular shape.

Nickel (Ni) Distribution

Nickel shows two major anomalous areas (A and B) which cover a large portion of the eastern part of the Mafikeng Sheet as shown in (Fig 4.4-3). In the north-east part of the map, nickel shows similar trends as chromium over the same lithological units (probably mafic sills).

Anomaly A has a peak concentration of 706 ppm and is located in surface sand, river sand and alluvium of Quaternary age.

Anomaly B occurs over quartzite, minor shale, limestone, and minor hornfels of the Magaliesberg Formation and andulusite muscovite hornfels, tuff, conglomerate, andesitic lava and pyroclastic rocks of the Hekpoort Formation. This anomaly has a peak value of 1009 ppm on diabase. This trend extends over a large distance.

Anomaly (C) is located south of the Mafikeng area. It reflects the andesitic lavas of the Allanridge Formation to the southeast of Mafikeng Town. It could also reflect surface sand of the Gordonia Formation as it extends north of Mafikeng. It has a maximum value of 385 ppm in biotite gneiss and amphibolites of the basement complex.

Copper (Cu) Distribution

Figure 4.4-4 depicts the distribution of copper anomalies in Mafikeng area. Anomaly A which covers an area of a few square kilometers is located in the Mafikeng area. It trends northeast-southwest of Mafikeng town, towards the southern map margin, occurs on andesitic lava and tuff of the Allanridge Formation. The anomaly has a maximum peak value of 148 ppm over the tholeiitic basalt of the Klipriviersberg Formation of the Ventersdorp Supergroup. The upper two anomalies found over the Magaliesberg Formation (C, north-south trend) and far right towards the end of sheet which appears in the point form B on the surface sand of the Gordonia Formation (Fig 4.4-4). Anomaly D extends over a few kilometers (±12.8 km) and it is likely that it is caused by andalusite muscovite hornfels, tuff conglomerate, andesitic lava and pyroclastic rock of the Hekpoort Formation.

Zinc (Zn) and Lead (Pb) Distributions

Fig 4.4-5 and Fig 4.4-6 show anomalies of zinc and lead, both of which are similar in shape and closely associated. Lead however gives rise to anomaly A and B, while zinc gives rise to anomalies A, B and C. The anomalies for zinc and lead differ in their concentrations and threshold values. Anomaly A is associated mainly with the greywacke and shale of the Kameeldoorns Formation and also in tertiary calcrete.
Anomaly B (both zinc and lead) is associated with the cherty dolomite of the Eccles Formation while an anomaly C is hosted by the Frisco Formation.

The mineralogy of lead-zinc ore from the dolomite consists of sphalerite, galena and minor chalcopyrite as ore minerals, with diagenetic pyrite, hydrothermal dolomite, quartz and calcite as gangue minerals. Sphalerite predominates over galena.
Anomalies of zinc and lead at point B are hosted by weakly metamorphosed and virtually underformed stromatolitic carbonates of the Middle and Upper Frisco formations (2520 Ma) of the Malmani Subgroup of the Transvaal Supergroup. The fact that both carbonaceous host rock and hydrothermal mineralization have experienced a mild contact metamorphic overprint due to the intrusion of the Paleoproterozoic (2065 Ma) Bushveld Igneous Complex, is strong evidence for a Paleoproterozoic age for these anomalies. Anomalies B and C lie on known occurrences mineralization which is generally regarded as being the oldest examples of carbonate-hosted Mississippi Valley-Type mineralization (Pöetter, 2001).

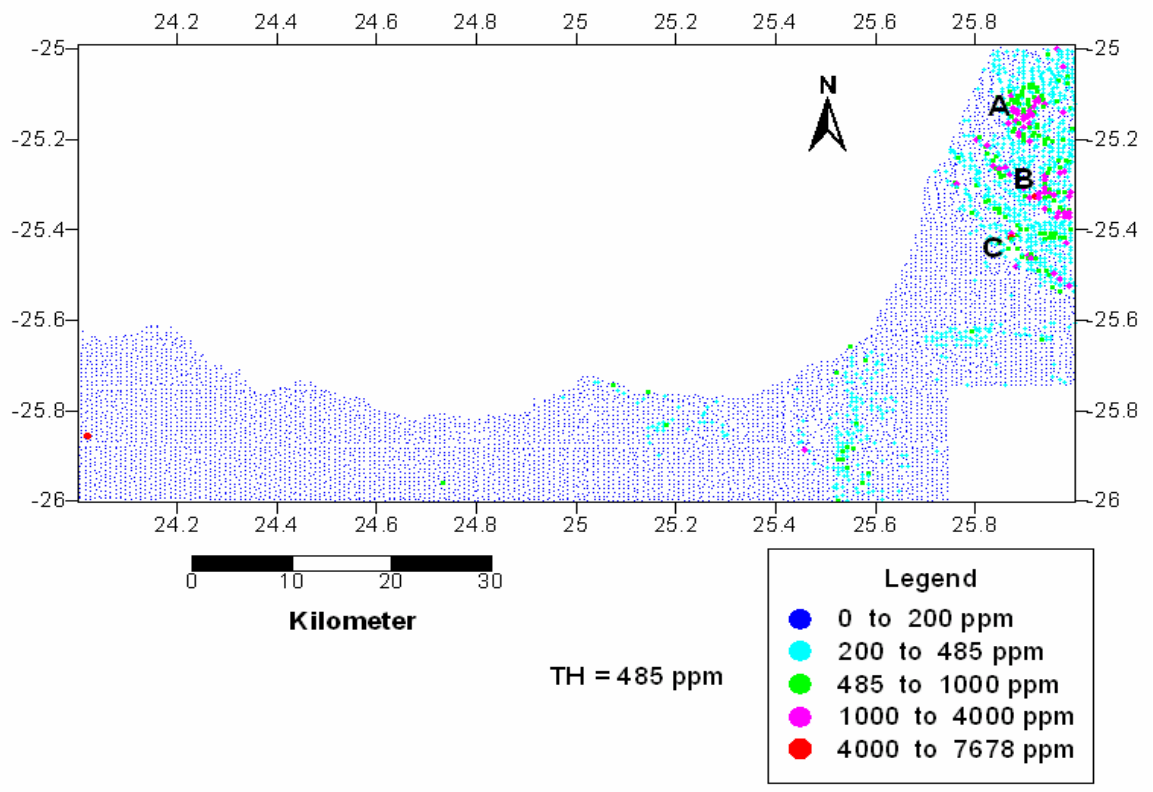

Figure 4.4-2: Distribution of chromium anomalies on the Mafikeng Area.

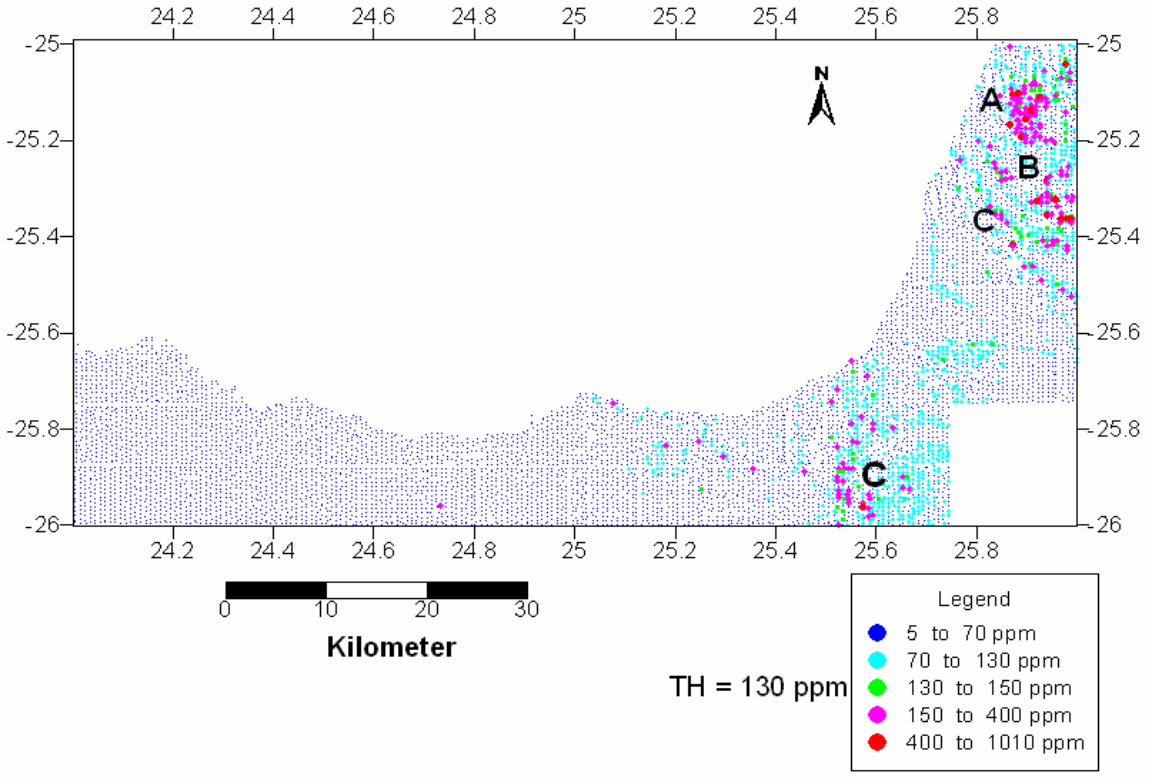

Figure 4.4-3: Nickel distribution concentration on the Mafikeng Area.

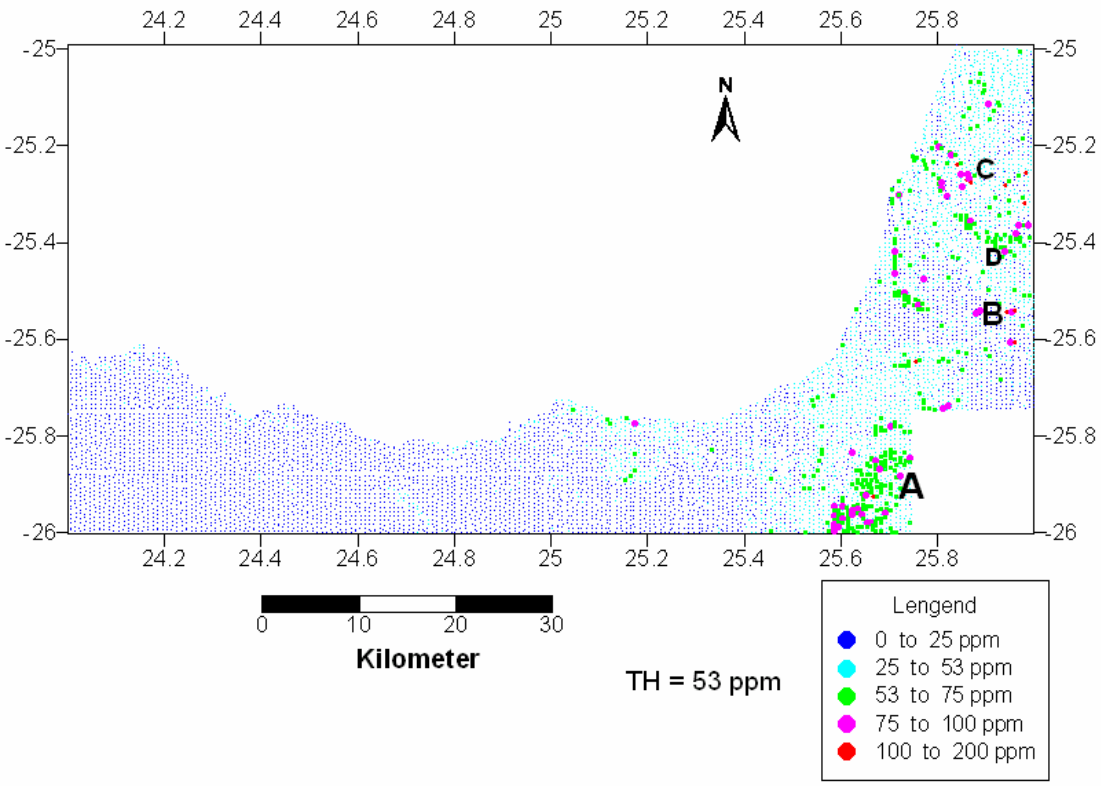

Figure 4.4-4: Classed post map of copper anomalies on the Mafikeng Area.

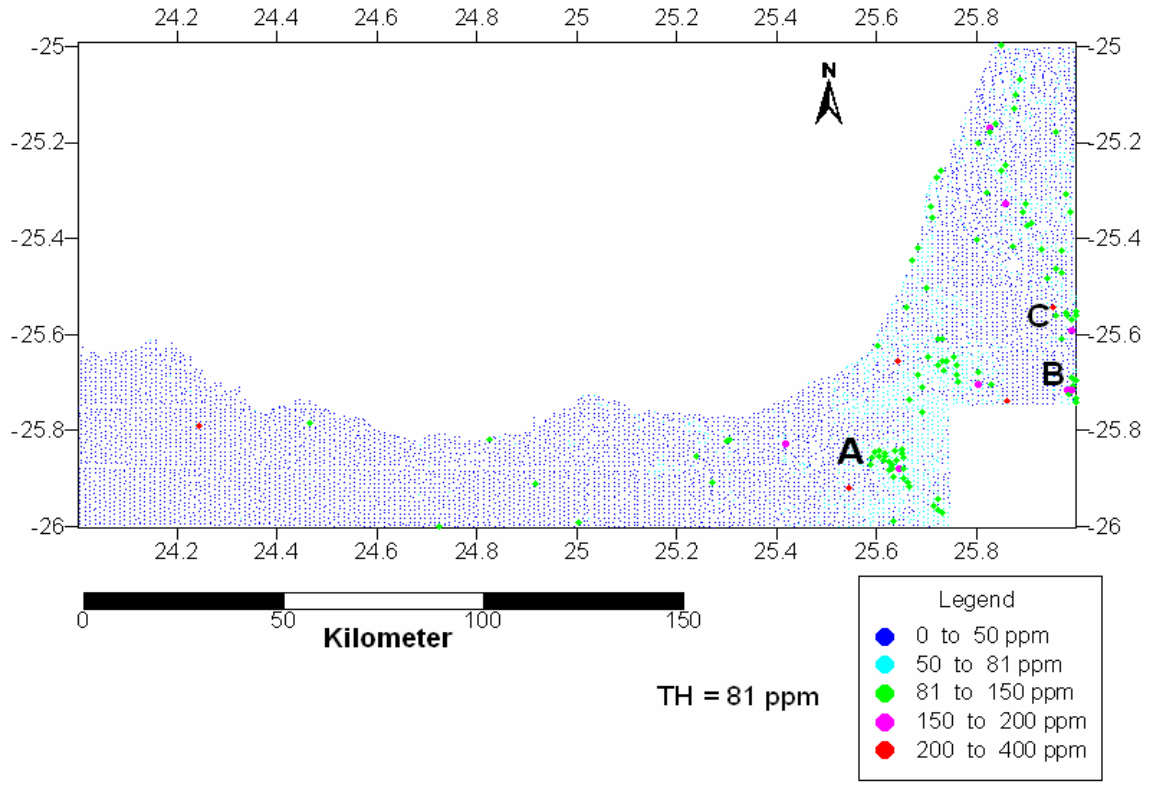

Figure 4.4-5: Classes post map of zinc anomalies on the Mafikeng Area.

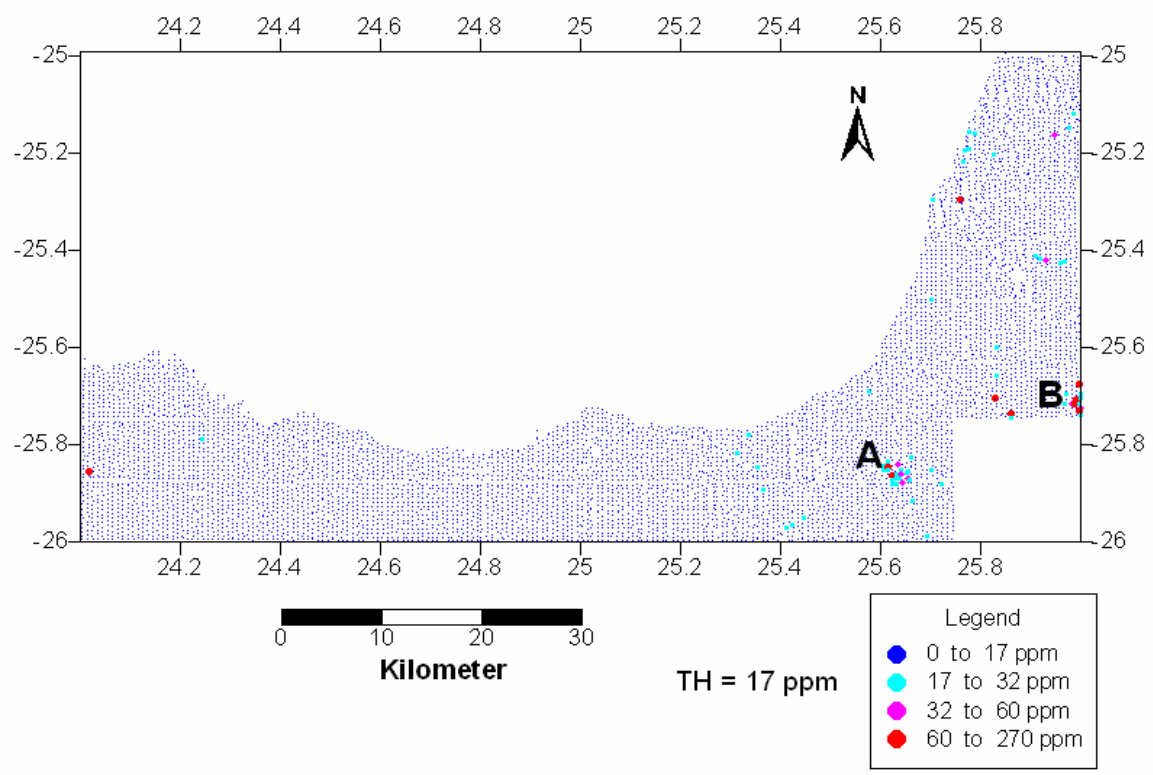

Figure 4.4-6: Classed post map of lead distribution in the Mafikeng Area.

Arsenic (As) distribution

Arsenic shows clear anomalous trends to the south and northeast of Mafikeng. The southern anomaly A (Fig. 4.4-7) trends in a north south direction and has the maximum value of 164 ppm Arsenic. It lies on colluvial sand which extends northwards into amphibolite, biotite gneiss of Archean age and calcrete. This anomaly might be associated with the known gold mineralization which occurs in this area. The extension of the anomaly north might be due to the weathering and transportation of the material from the mineralization source, through river channels, as they drain northwards to the Molopo River.

The second anomaly (B) is situated on the chert rich dolomite of the Eccles Formation. This anomaly is also located around an old gold mine (mineralization) which is no longer operating. The anomaly has a maximum value of 108 ppm Arsenic. The upper anomaly

(B) trends northwest to southeast, towards Botswana border. This anomaly is mostly dominated by the threshold concentrations. It has the maximum value of 144 ppm Arsenic on ferruginous quartzite, siltstone and shale of the Timeball Hill and Klapperkop Quartzite Formations. Towards the South Africa-Botswana border, the highest anomaly occurs on dolomitic rocks of the Malmani Subgroup.

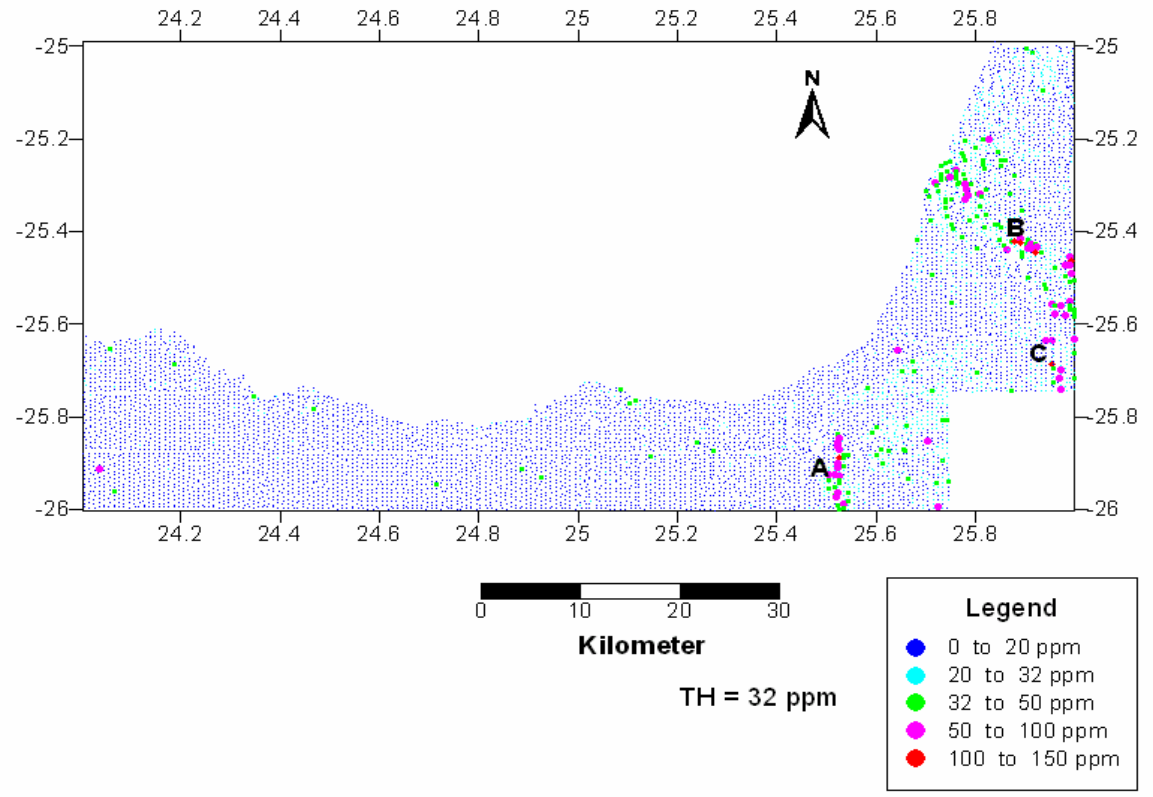

Figure 4.4-7: Classed post map of arsenic distributions in the Mafikeng Area.

Iron (Fe) distribution

Iron shows two parallel anomalies A and B in the eastern part of the Mafikeng sheet (Fig. 4.4-8). The strike northwest –southeast and extend along strike for over 10kilometer. Anomaly A has three separate peaks; upper (23 wt %), middle (19 wt %) and lower (14 wt %). These geochemical anomalies reflect exactly the same pattern as the higher magnetic anomalies. This trend occurs over the Rooihoogte and Penge Formations. Anomaly B has a peak value of 25.4 wt % and occurs over diabase and norite, andesitic

lava and andalusite muscovite hornfels of the Magaliesberg Formation. The anomaly highlights a known iron deposit that is situated on the diabase and noritic rocks.

The anomaly C is situated south of the Mafikeng Town. It trends north north east to south south west and reflects dark minerals of the intermediate to mafic volcanic rocks of the Allanridge Formation.

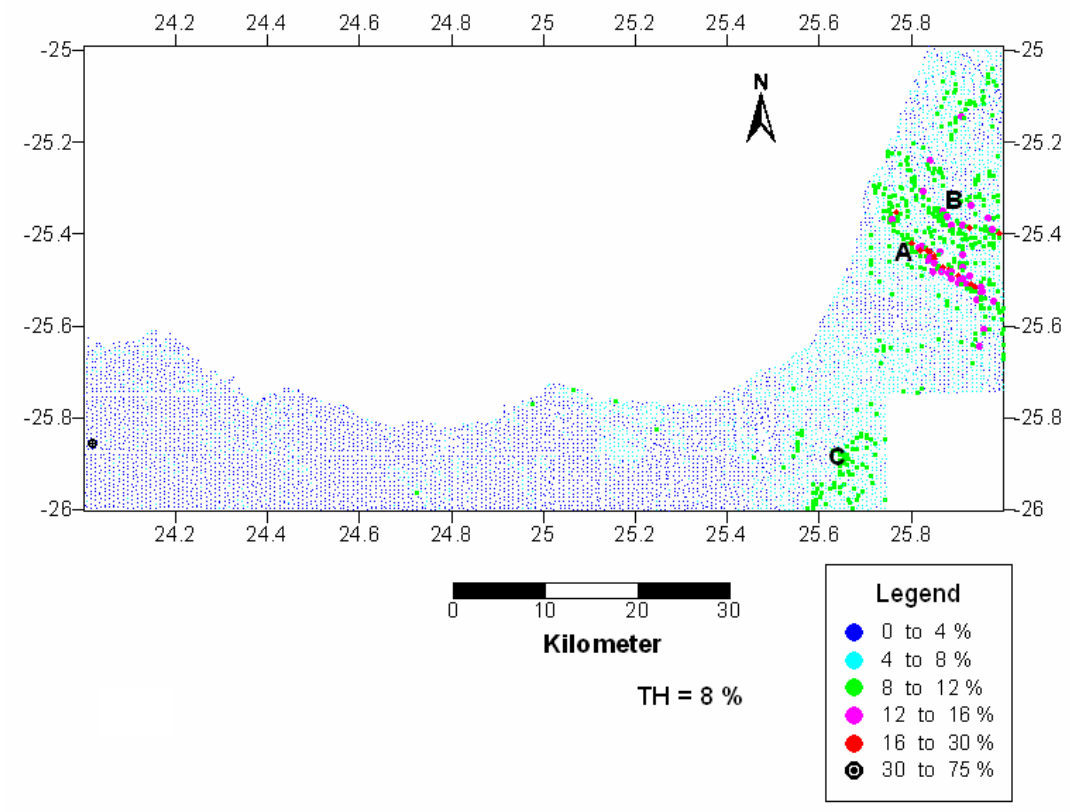

Figure 4.4-8: Distribution of iron concentration in the Mafikeng Area.

Rubidium (Rb) and Yttrium (Y) Distribution

Figure 4.4-9 shows the close spatial correlation of rubidium and yttrium with the lithological units of the Gabrone Granite and the Kanye Formation. Gabrone Granites have the highest rubidium contents of up to 196 ppm with maximum yttrium values of 80 ppm. In contrast, much lower concentrations of rubidium are found over of the Gordonia Formation in the western part of the map area and over Formations of the Transvaal Supergroup in the eastern part of the map area. These distribution patterns suggest that the host rock mineralogy of rubidium and yttrium may, to a large extent have been derived from feldspar in granite. The felsic rocks of the Kanye Formation show that the rubidium concentration mainly reflects the regional threshold values. The area is also characterized by high magnetic anomalies ranging between 340-1420 nT extending to the east of the Botswana -South Africa border.

It is assumed that the rubidium and yttrium anomaly in this area is hosted by the red Gabrone Granite. Yttrium shows or reflects background concentration on the Monte Christo, Lyttelton and Eccles Formations. It seems as though an increase in the chert concentration in the dolomite, decreases the concentration of yttrium.

Niobium (Nb) distributions

Like rubidium and yttrium, niobium shows similar anomalous trends to rubidium and yttrium in the Gabrone Granite. The only difference is that the rubidium and yttrium anomaly extends to the Kanye Formation but the niobium anomaly is found only on the Gabrone Granite (Fig 4.4-10). These two elements show a close relationship with yttrium as they have similar chemical behavior.

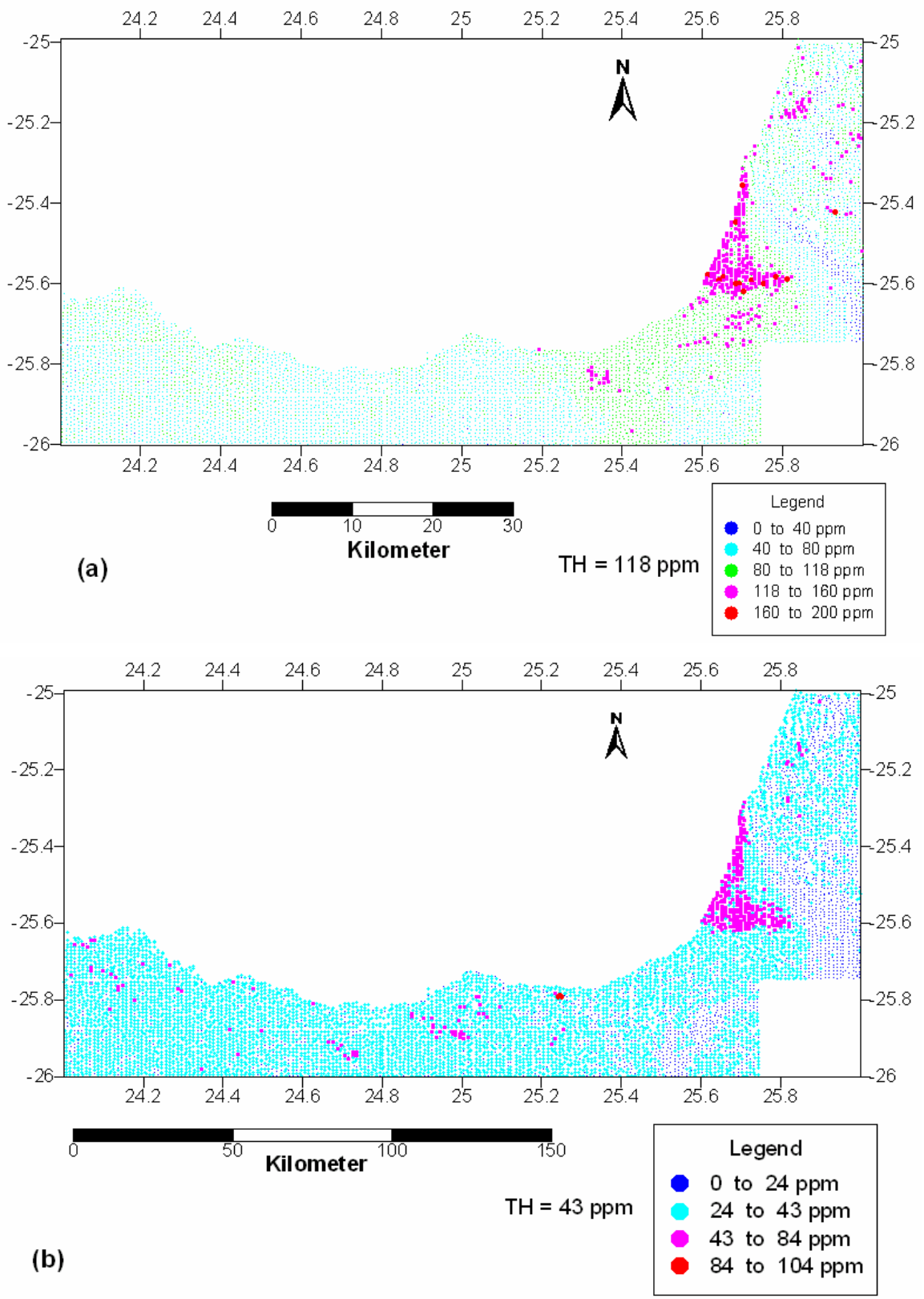

Figure 4.4-9: Classed post map of rubidium and yttrium in the Mafikeng Area; (a) Distribution of rubidium and (b) yttrium distribution.

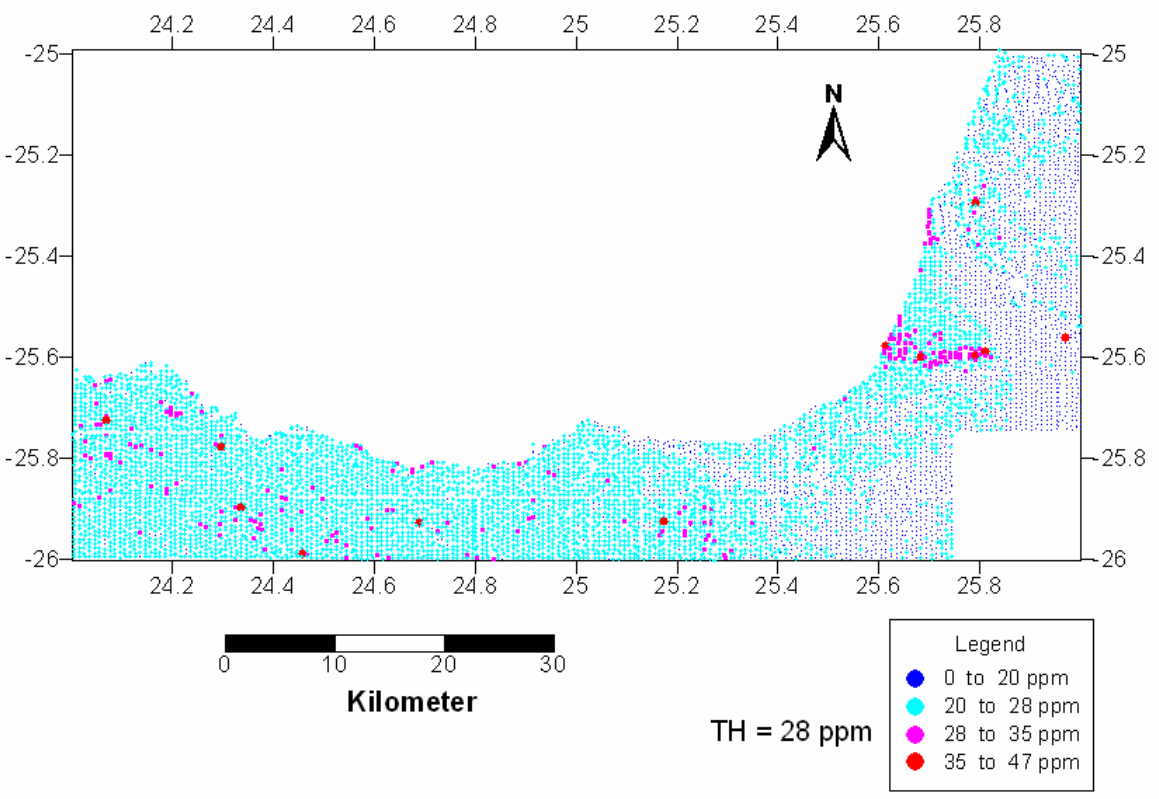

Figure 4.4-10: Classed post map of niobium concentration in the Mafikeng Area.

Vanadium (V) Distribution

Fig 4.4-11 shows a vanadium distribution pattern which has similar patterns to iron. Anomaly A occurs almost in the same area as that of iron, and it is assumed that the anomaly resulted from the lower volcanic units of the Hekpoort Formation. This formation consists of andesitic lava which has been metamorphosed to the upper green schist facies and consists of altered plagioclase, green hornblende and quartz with accessory biotite, cummingtonite, chlorite and epidote. It is assumed that vanadium is hosted as a minor or accessory mineral within these lithological units. Vanadium concentration decreases towards the Botswana border; which might indicate thermal effects of the Bushveld Complex, decreasing towards the west and increasing towards the east.

The second anomaly B, lies on the Magaliesberg Formation and diabase. The presence of vanadium in the area might be the result of the diabase intrusion in the Magaliesberg and Silverton Formations.

The third anomaly (C) of the vanadium situated south of Mmabatho, has a concentration ranging between 118 to 220 ppm, and is hosted by the andesitic lava of the Allanridge Formation.

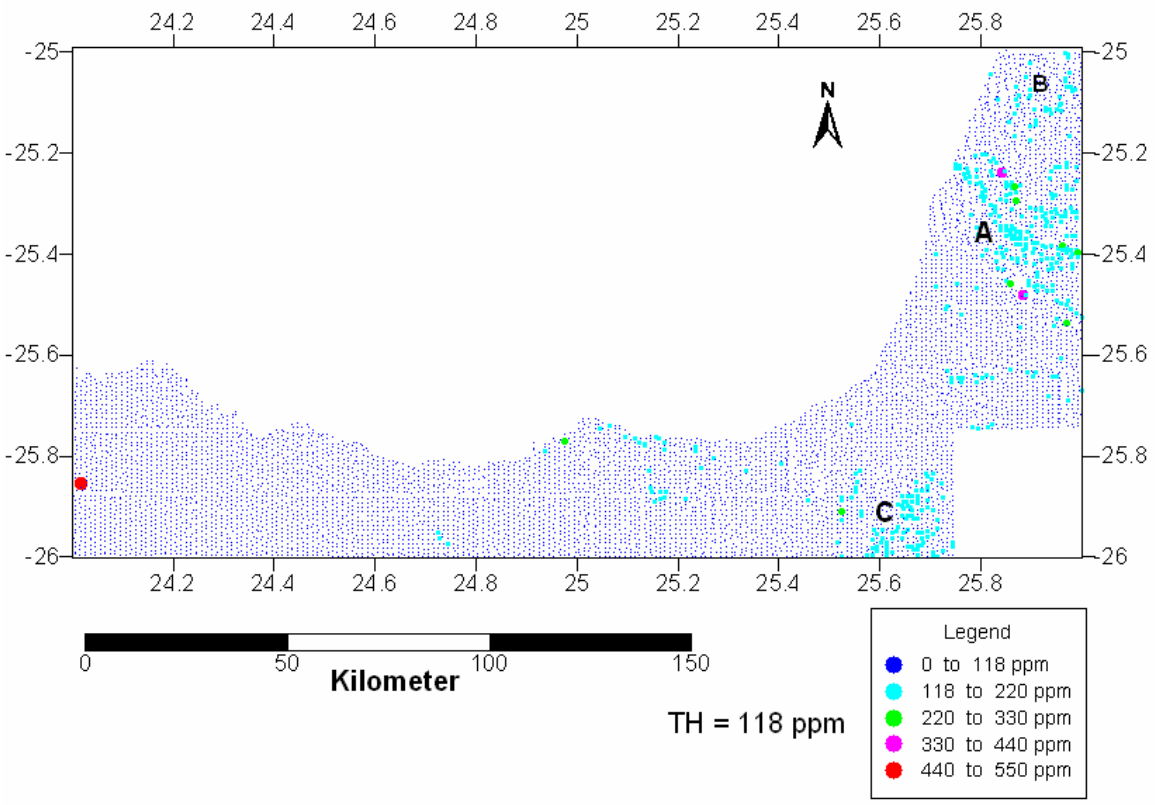

Figure 4.4-11: Classed post map of vanadium distributions in the Mafikeng Area.

Barium (Ba) Distributions

Barium anomalies are subdued and dispersed (Fig. 4.4-12). The element shows borderline cluster distribution on the dolomite and chert of the Malmani Subgroup of the Chuniespoort Group. The element has a maximum concentration of 1819ppm along the fault zone in the chert rich dolomite zone of the Monte Christo Formation.

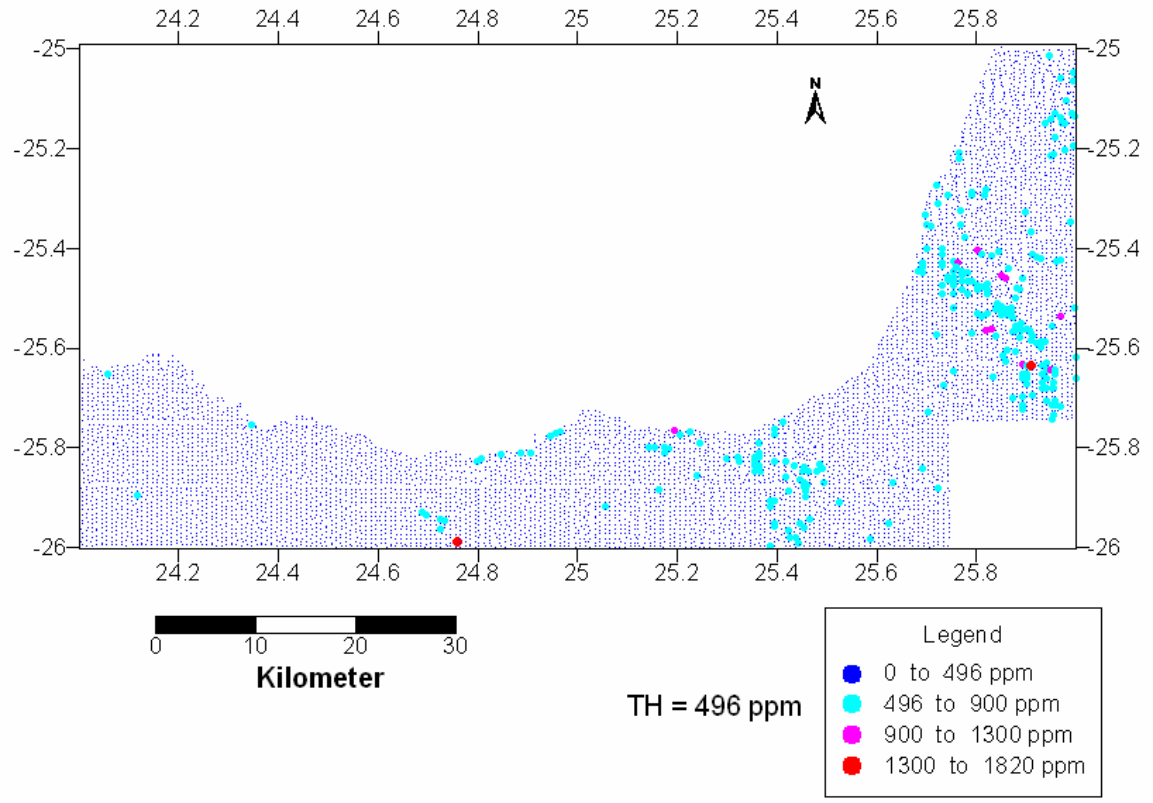

Figure 4.4-12: Classed post map of barium distribution in the Mafikeng Area.

Manganese (Mn) Distribution

Manganese show similar distribution to barium on the undifferentiated dolomite and chert-rich dolomite of the Lyttelton Formation. Manganese anomalies follow a distinct northwest-southeast stratigraphic trend with only two single point anomalies occurring in the southern part of the map, a further anomaly occurs towards Botswana's border (Fig. 4.4-13). The lithologies of the formations which give rise to manganese anomaly are mainly carbonaceous rocks.

Uranium (U) distribution

Uranium distribution pattern shown in Fig 4.4-14 indicates the granitophile association of this element. Elevated uranium values from 0ppm and up to a maximum of 10 ppm occur on the Gaborone Granite (area A Fig 4.4-14). The anomalies do not show a clear trend in the northern part of the sheet but rather spherical cluster in the case of anomaly A and a

wide cluster in the case of the anomaly B area. The uranium distribution in area A, is dominated by the regional threshold concentrations ranging between 4ppm -10ppm and it shows a close relationship to the Gaborone Granite. The anomalous area B, also represented by dispersed concentrations of uranium occurs on amphibolite and gneiss of Archean age. The higher concentration anomalies are represented by single points as indicated on the map.

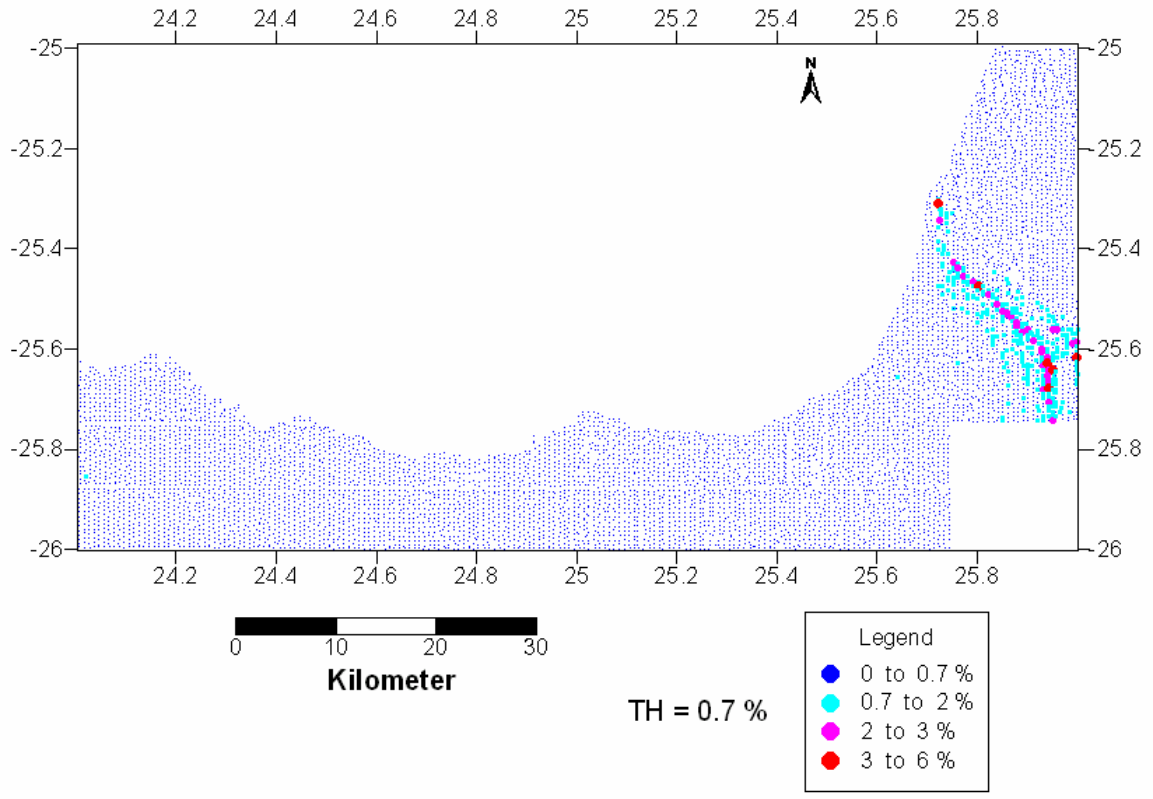

Figure 4.4-13: Classed post map of manganese distribution in the Mafikeng Area.

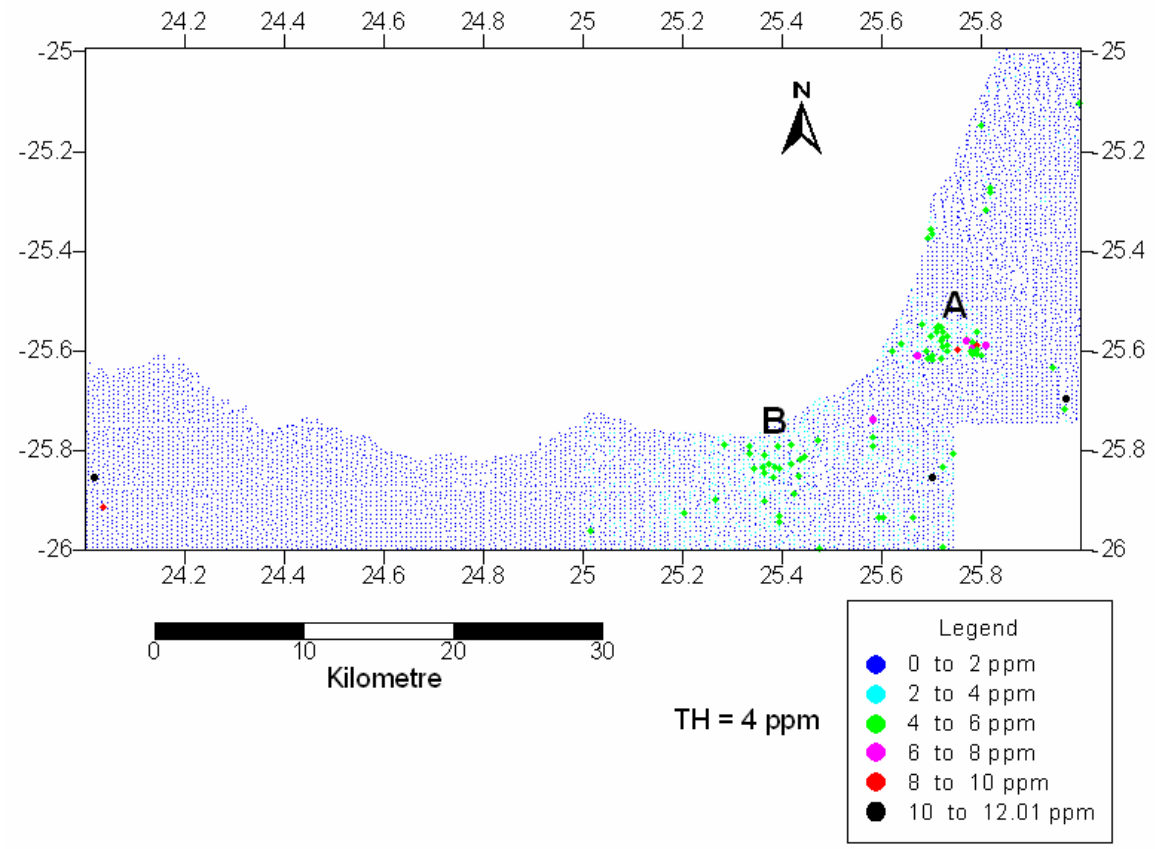

Figure 4.4-14: Classed post map of uranium concentration in the Mafikeng Area.

Distribution of other elements

Titanium does not show any positive anomalies an area of low or negative anomalies occurs in the Mafikeng area. Single point positive anomalies of titanium are found over various lithological units of the map area, with the concentration of between 2-3 wt%. The lithologies in the eastern part of the map area have low titanium concentration as compared to the lithologies of the western part of the map (Fig. 4.4-15). The aeolian sand of the Gordonia Formation is characterized by background titanium concentration in the western part of the Mafikeng area.

The BIF of the Penge Formation is characterized by the 4 single point cobalt anomalies with concentrations of between 600 ppm to 655 ppm (Fig. 4.4-16) reflects mainly regional threshold values which are located on the surface deposits of Quaternary age.

Cobalt does not give rise to any continuous geochemical anomalies in Mafikeng map accept for three anomalies which appear to be associated with a lithological units of the Transvaal Supergroup.

Tungsten has the same concentrations level as titanium being below the threshold values of 21 ppm, there are no obvious anomalous tungsten trends in the map area.

Scandium anomalies are scattered (Fig. 4.4-17) over surface deposit and represent mainly regional threshold concentrations (A). Over the andesitic lava, subordinate pyroclastic rocks and quartzite of the Hekpoort Formation, scandium is characterized by clusters of elevated values (around anomaly B area). The anomalies trend in the same direction as the Hekpoort Formation (northwest to south east). Over the chert breccia and conglomerate of the Rooihoogte Formation scandium shows a scattered distribution pattern and trends in the same direction as the underlying lithologic units. The anomaly over the Rooihoogte Formation has a maximum value of 93 ppm. Around Mafikeng Town (Area C) scandium shows scattered distribution pattern of regional threshold values. It is assumed that scandium anomalies result from intermediate volcanics of the Allanridge Formation.

The andesitic lavas and tuffs of the Allanridge Formation are characterized by elevated values of zirconium which shows scattered distribution patterns south of the Mafikeng area (Fig. 4.4-18). The west to east trend of zirconium anomalies results from biotite gneiss, homogeneous granite and micro granite of the Basement Complex. Strong zirconium anomalies are represented by single point's over surface deposits.

Thorium in the Mafikeng area shows two positive anomalies consisting of a few clustered points of the regional threshold concentration (Fig. 4.4-19). Anomaly A occurs over shale of the Strubenkop Formation while anomaly B lies over porphyrytic graphic granite and micro granite of the Gaborone Granite. Anomaly (B) shows positive correlation with a magnetic anomaly over this lithological unit.

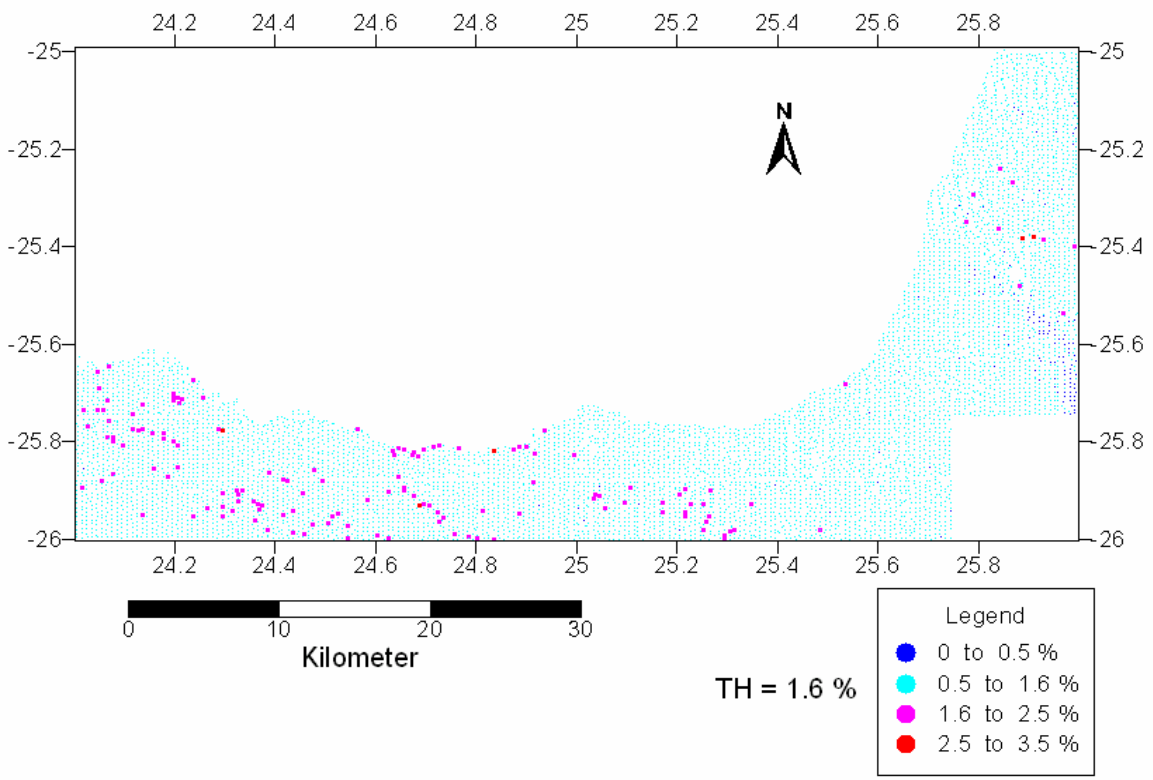

Figure 4.4-15: Classed post map of titanium distribution in the Mafikeng Area.

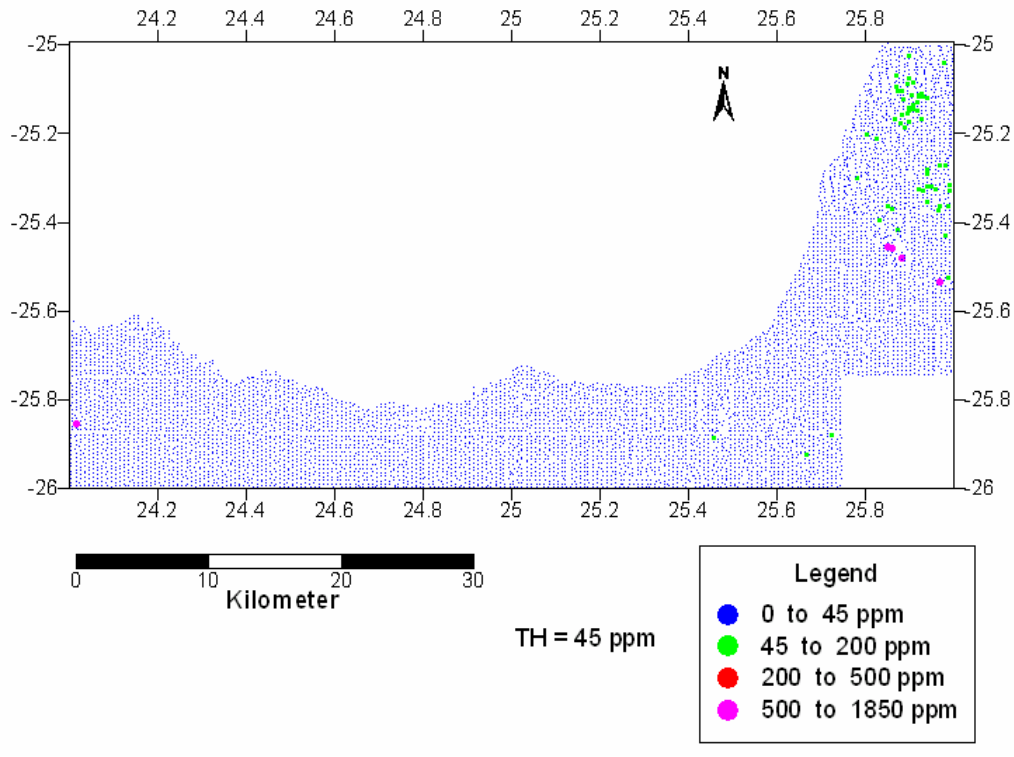

Figure 4.4-16: Classed post map showing cobalt anomalies in the Mafikeng Area.

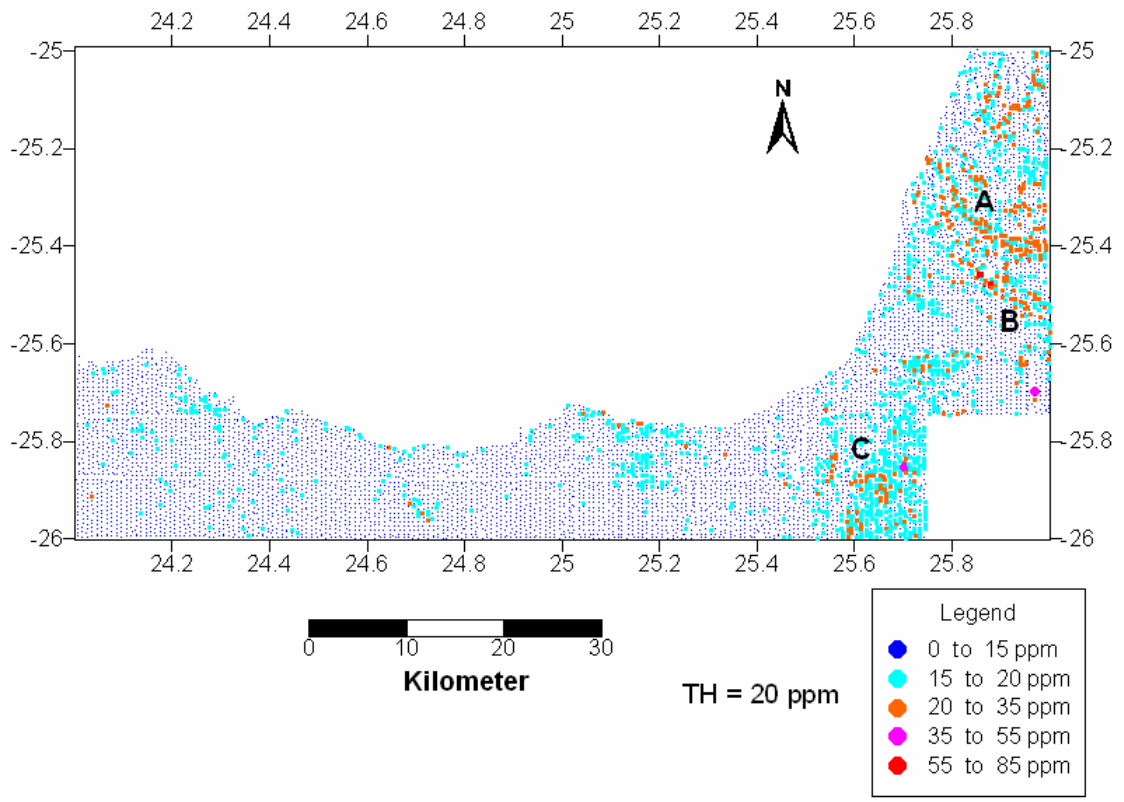

Figure 4.4-17: Classed post map of scandium anomaly in the Mafikeng Area.

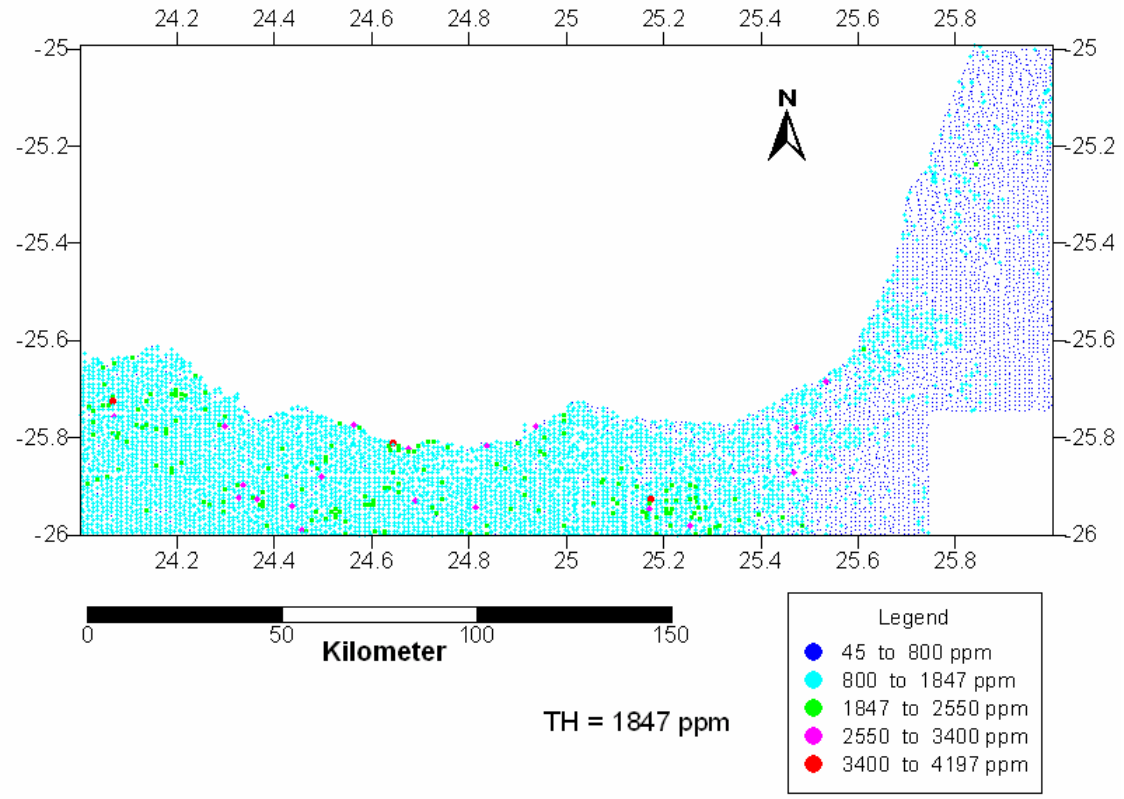

Figure 4.4-18: Classed post map of zirconium concentration in the Mafikeng Area.

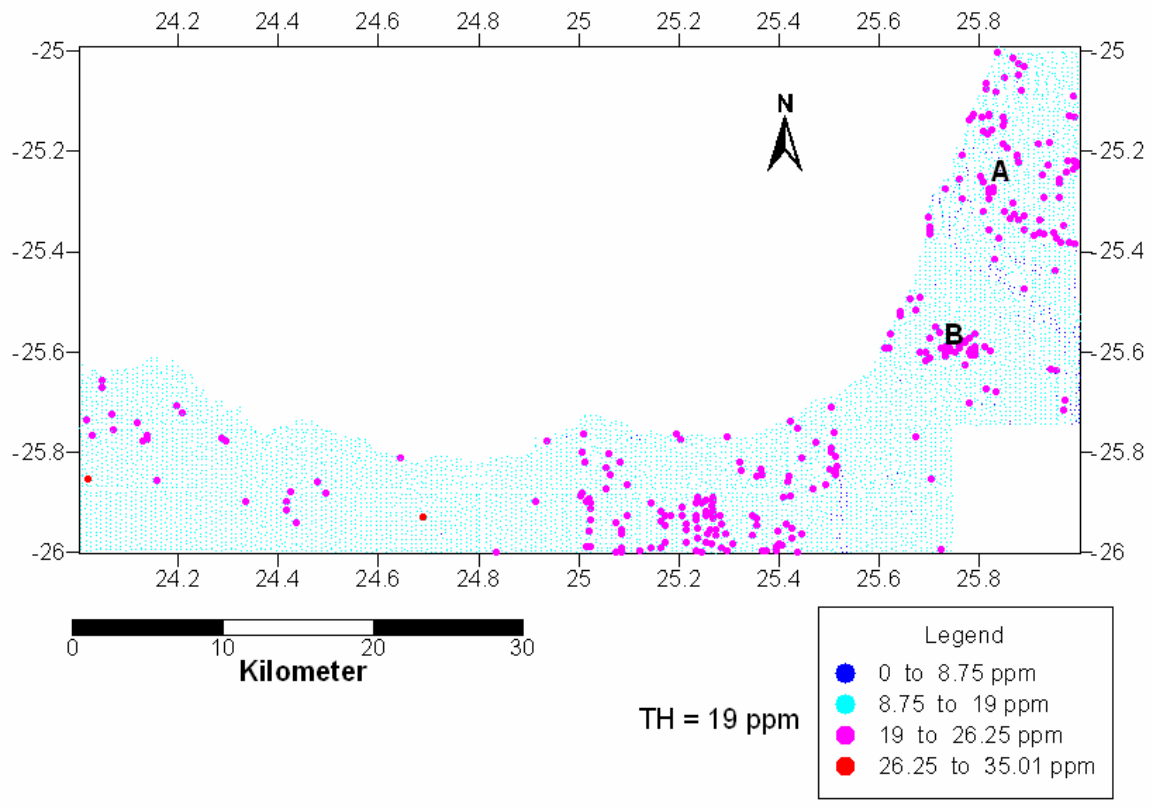

Figure 4.4-19: Classed post map of thorium distribution in the Mafikeng Area.

4.5 DISTRIBUTION OF ELEMENTS IN THE EASTERN PART OF 2625 VRYBURG SHEET

4.5.1 Statistical analysis

A summary of the statistics on obtained from the Vryburg 2625 Sheet, data set (11088 samples) is presented in Table 4.5-1. Threshold, minimum, maximum, standard deviation (Std. Dev.), mean, range, variance kurtosis and skewness values are shown. The mean plus two standard deviations is displayed in the second column to show the general background of the complete data set across various lithological units. Contouring intervals for the map were based on a 95% confidence interval (mean + 2(std. dev.)) to show chemical variation in the different lithological nits. In general, the values with a concentration higher than the average plus two times standard deviation (Threshold values) were considered positive anomalies. On a data set containing different lithological units, anomalous values were calculated separately for each element.

4.5.2 Correlation of elements

All 21 elements in the 2625 Vryburg Sheets were not well correlated with each other. From the results, only 11 correlations were identified in Table 4.5-2. Out of the 11 five were found to be positively correlated (Fe-Cu, Fe-V, Fe- Ni, Fe-Sc and V-Cu with correlation coefficients ranging from 0.80-0.95 (80-95%). The correlation coeficients are tabulated in table 4.5.2. Seven weak correlations were obtained by Cr-Ni, Sc-V, Sc-Ni, Sc-Cu, V-Ni, Ni-Cu, Ti-Nb, Ti-Zr and Zr-Nb the coefficients of correlation ranged between (0.75-68%). Cobalt, tungsten, yttrium and niobium show poor correlations with very low correlation coefficients (Co-W; 0.17% and Y-Nb, 0.48%).

Table 4.5-1: Summary statistics on the complete geochemical data set for the Eastern part of 2625 Vryburg Sheet.

Element	N	Min	Max	Mean	Median	St. Dev	Var	CV	Skew	Kurt	Threshold
TiO_2	11088	0.21	2.70	0.97	0.97	0.15	0.02	0.16	0.36	4.43	**1.3**
MnO	11088	0.02	1.04	0.09	0.08	0.04	0.00	0.51	6.74	95.75	**0.2**
Fe_2O_3	11088	0.92	16.50	4.53	4.52	1.37	1.88	0.30	0.47	1.28	**7**
Sc	11088	1.00	43.00	13.06	13.00	3.14	9.88	0.24	0.27	2.23	**19**
V	11088	1.00	291.00	69.74	70.00	22.78	518.70	0.33	0.49	1.86	**115**
Cr	11087	5.00	1156.00	116.23	106.00	58.38	3408.03	0.50	3.58	29.26	**233**
Co	11088	2.00	803.00	16.77	16.00	8.75	76.60	0.52	65.49	5873.61	**34**
Ni	11088	9.00	298.00	49.76	48.00	20.55	422.49	0.41	20.55	16.47	**91**
Cu	11082	1.00	160.00	29.52	28.00	11.16	124.58	0.38	1.18	3.90	**52**
Zn	11088	16.00	894.00	48.35	47.00	17.95	322.05	0.37	19.01	712.73	**84**
As	10944	1.00	125.00	13.47	13.00	6.15	37.84	0.46	2.27	22.87	**26**
Rb	11088	25.00	157.00	73.00	72.00	12.66	160.22	0.17	0.45	1.82	**98**
Sr	11088	20.00	1115.00	70.23	60.00	38.76	1502.23	0.55	5.21	76.09	**148**
Y	11088	7.00	67.00	24.36	24.00	4.09	16.76	0.17	0.42	2.03	**33**
Zr	11088	104.00	3695.00	812.73	797.00	231.06	53387.51	0.28	1.25	7.46	**1275**
Nb	11088	4.00	101.00	19.66	20.00	1.93	3.73	0.10	6.67	286.13	**24**
Ba	11088	35.00	1134.00	313.11	309.00	77.66	6031.21	0.25	0.95	4.39	**468**
W	11087	1.00	56.00	11.66	12.00	2.41	5.83	0.21	1.52	20.24	**16**
Pb	8951	1.00	161.00	4.60	4.00	3.70	13.71	0.80	11.82	406.17	**12**
Th	11080	1.00	30.00	13.59	14.00	1.52	2.30	0.11	-0.23	8.04	**17**
U	82	1.00	13.00	2.23	1.00	2.29	5.24	1.03	2.65	7.56	**7**

Table 4.5-2: Correlation matrix of 21 elements on the 2624 Vryburg Sheet.

	TiO_2	MnO	Fe_2O_3	Sc	V	Cr	Co	Ni	Cu	Zn	As	Rb	Sr	Y	Zr	Nb	Ba	W	Pb	Th	U
TiO_2	1.00																				
MnO	-0.08	1.00																			
Fe_2O_3	0.16	0.46	1.00																		
Sc	0.22	0.42	**0.83**	1.00																	
V	0.09	0.47	**0.88**	**0.75**	1.00																
Cr	-0.14	0.33	**0.51**	0.47	0.46	1.00															
Co	0.12	0.20	0.36	0.34	0.35	0.18	1.00														
Ni	0.04	0.36	**0.81**	**0.70**	**0.71**	**0.72**	0.36	1.00													
Cu	0.12	0.33	**0.90**	**0.75**	**0.82**	0.35	0.37	**0.74**	1.00												
Zn	-0.07	0.32	0.40	0.35	0.35	0.25	0.12	0.31	0.37	1.00											
As	-0.52	0.21	0.18	0.30	0.20	0.21	0.02	0.21	0.20	0.26	1.00										
Rb	0.11	0.01	0.21	0.10	0.14	-0.02	0.03	0.10	0.16	0.13	-0.04	1.00									
Sr	0.06	-0.14	0.14	0.13	0.07	-0.16	0.11	0.15	0.26	0.01	-0.01	0.00	1.00								
Y	**0.51**	0.32	0.44	0.43	0.40	0.07	0.22	0.27	0.36	0.16	-0.13	0.41	-0.07	1.00							
Zr	**0.66**	-0.26	-0.48	-0.30	-0.47	-0.29	-0.16	-0.44	-0.52	-0.29	-0.58	-0.14	-0.15	0.13	1.00						
Nb	**0.72**	-0.15	-0.17	-0.01	-0.20	-0.21	-0.05	-0.24	-0.22	-0.17	-0.47	0.09	-0.10	0.48	0.72	1.00					
Ba	0.33	-0.02	0.14	0.04	0.07	-0.20	0.10	0.08	0.18	-0.02	-0.24	**0.51**	0.47	0.23	0.02	0.11	1.00				
W	0.18	-0.20	-0.45	-0.38	-0.36	-0.18	-0.17	-0.35	-0.46	-0.31	-0.17	-0.15	-0.31	-0.10	0.48	0.27	-0.10	1.00			
Pb	-0.09	0.07	-0.02	0.03	-0.02	-0.09	0.01	-0.04	-0.01	0.35	0.16	0.31	0.11	0.05	-0.13	-0.13	0.29	-0.09	1.00		
Th	0.28	-0.09	-0.16	0.05	-0.16	-0.18	-0.03	-0.19	-0.17	-0.19	-0.07	0.20	-0.05	0.32	0.29	0.50	0.13	0.12	0.15	1.00	
U	-0.38	-0.08	-0.34	0.31	-0.09	-0.22	0.12	-0.01	-0.16	0.06	0.65	-0.36	0.73	-0.20	-0.27	0.11	0.02	-0.55	0.40	0.06	1.00

4.5.3 Statistical distribution

On the histogram plots titanium, iron, scandium, vanadium, barium, tungsten, rubidium, yttrium, thorium and zirconium show symmetrical distribution patterns with occasional outliers. Titanium, tungsten zirconium and thorium distributions are leptokurtic (highest pick) when compared to the other elements. Manganese, chromium, cobalt, nickel copper, zinc, arsenic, strontium, niobium and lead, show asymmetrical distribution patterns and positively skewed (Fig. 4.5-1). Manganese has higher values over the Monte Christo Formation, and nickel, strontium, copper and iron are positively skewed due to high concentrations over the Allanridge Formation. Chromium shows high values over the Kilpriviersberg Group. The rest of the elements are fairly evenly distributed over various lithological units or areas. Uranium distribution patterns are not obviously due to low concentrations.

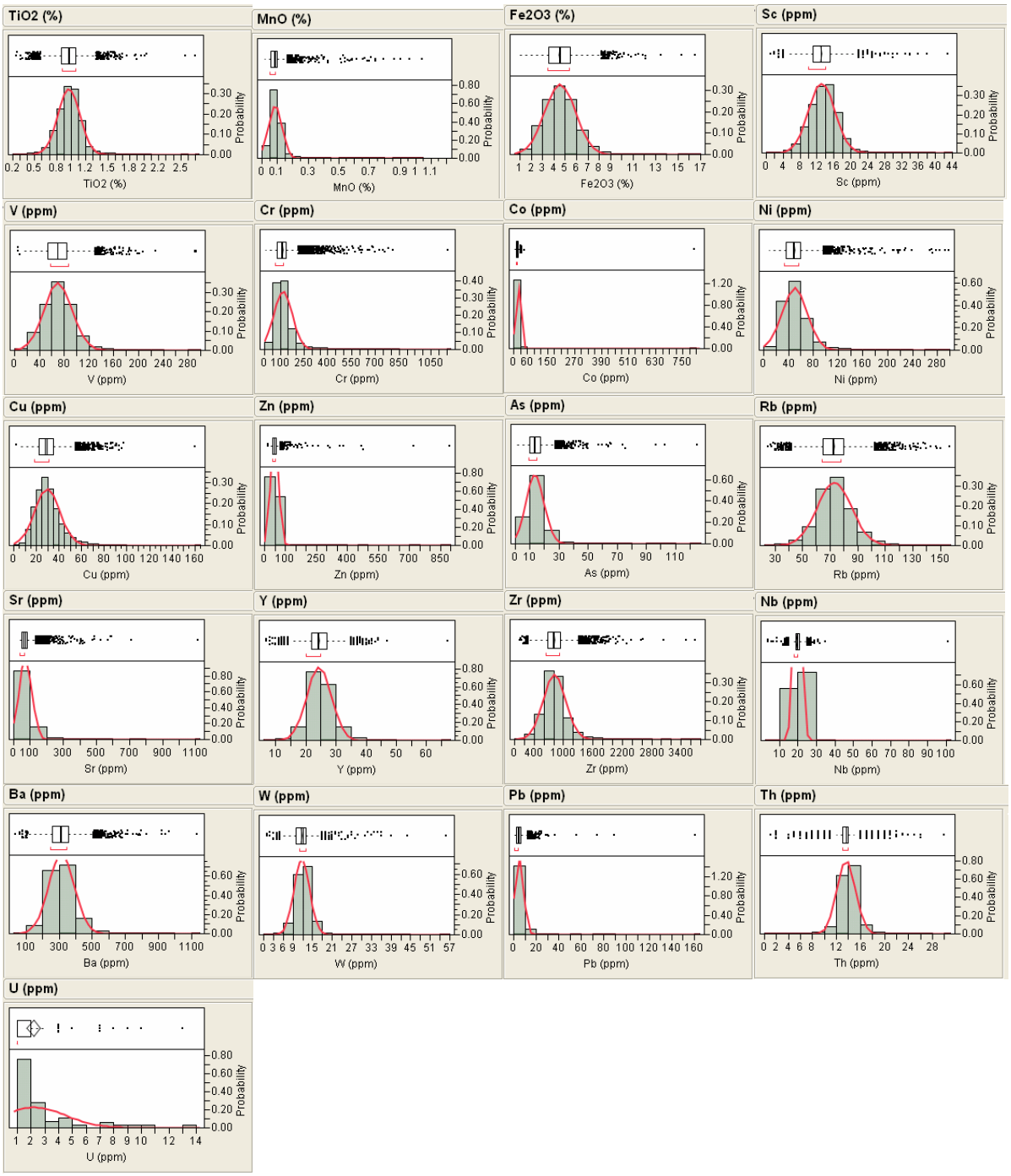

Figure 4.5-1: Histograms and box plots of the elements in the 2625 Vryburg Sheet.

4.5.4 Geochemical distribution

Chromium (Cr) Distribution

Chromium and nickel show very good correlation, especially anomalies in the case of A and B (Fig. 4.5-2 and 4.5-3). In both cases the anomalies occurs on the Goldridge Formation of the Kraaipan Greenstone Belt. Nickel has a lower concentration than chromium. A third anomalous area of chromium (C) lies on the East of the Migdol area where it occurs on basaltic lava of the Klipriviersberg Group. The maximum value of Cr is 1156 ppm and is represented by single sample over the Goldridge Formation. Extending further North-east of anomaly C, chromium distribution appears to be more scattered on the same lithologies as anomaly C.

Nickel (Ni) Distribution

Fig 4.5-3 shows the distribution of nickel anomalies in the Vryburg area, with two major anomalies (A and B) having high concentrations over Gold ridge Formation of the Kraaipan Greenstone Belt. Both anomaly A and B have maximum concentrations of up to 298 ppm. It is assumed that the nickel concentration or the anomalies in area A and B result from weathering of mafic rocks. The Basement complex lithologies of the Goldridge Formation show a poorly developed north-south trend (anomalous zone C) with values up to 200 ppm, and with a scattered distribution pattern.

Anomaly D located in the Maipeng area trends north-south and occurs on amygdaloidal lava of the Kliprieversberg Group. This trend is made up mainly of regional threshold values. This anomaly lies over basaltic amygdaloidal lava of the Allanridge Formation.

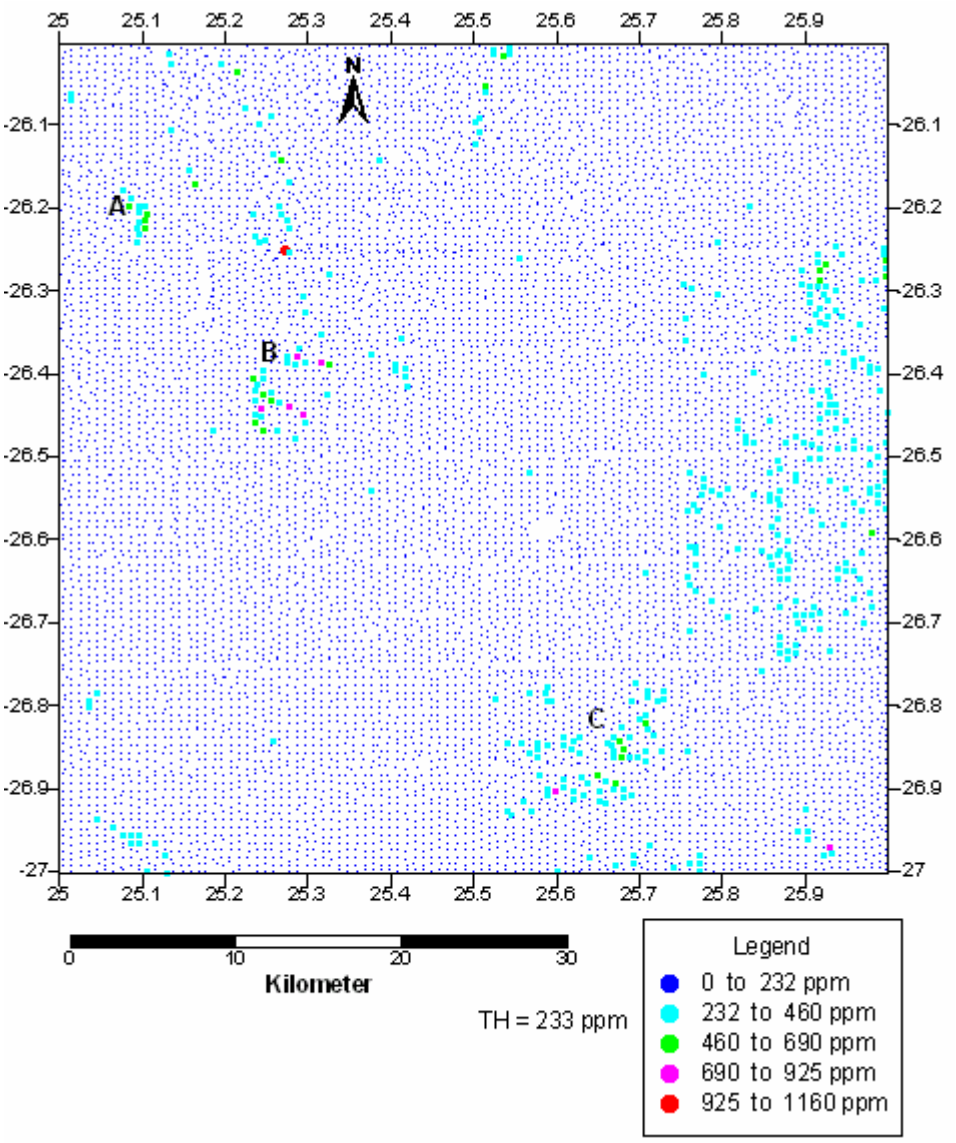

Figure 4.5-2: Distribution of chromium concentration in the 2625 Vryburg Sheet.

Copper (Cu) Distributions

The well developed copper anomaly A lies over the intermediate lithologies of the Allanridge Formation (Fig. 4.5-4). The Anomaly trending NNE-SSW and is dominated by the values of greater than 50 ppm. In the central part of the map area, low copper concentrations occur. Anomaly C has scattered distribution pattern made up of background values lies on the intermediate rocks of the Allanridge Formation.

Anomaly B, lies on the felsic and intermediate rocks of the Goldridge Formation. The anomaly has a scattered distribution pattern of elevated values, forming a poorly developed north-south trend. High copper values with concentrations of 160 ppm represented by a single point.

Arsenic (As) Distribution

Arsenic has a scattered distribution pattern with concentrations ranging between 21-50 ppm, representing the regional threshold values. Very scattered threshold arsenic values are found in the southern part of the map area see Fig. 4.5-5.

A well- developed clustered of arsenic anomalies (A) lies on calcrete, river sand and alluvium of Quaternary age. This anomalous cluster has a maximum value of 76 ppm. Anomaly B, lies over andesitic lava and tuff of the Allanridge formation.

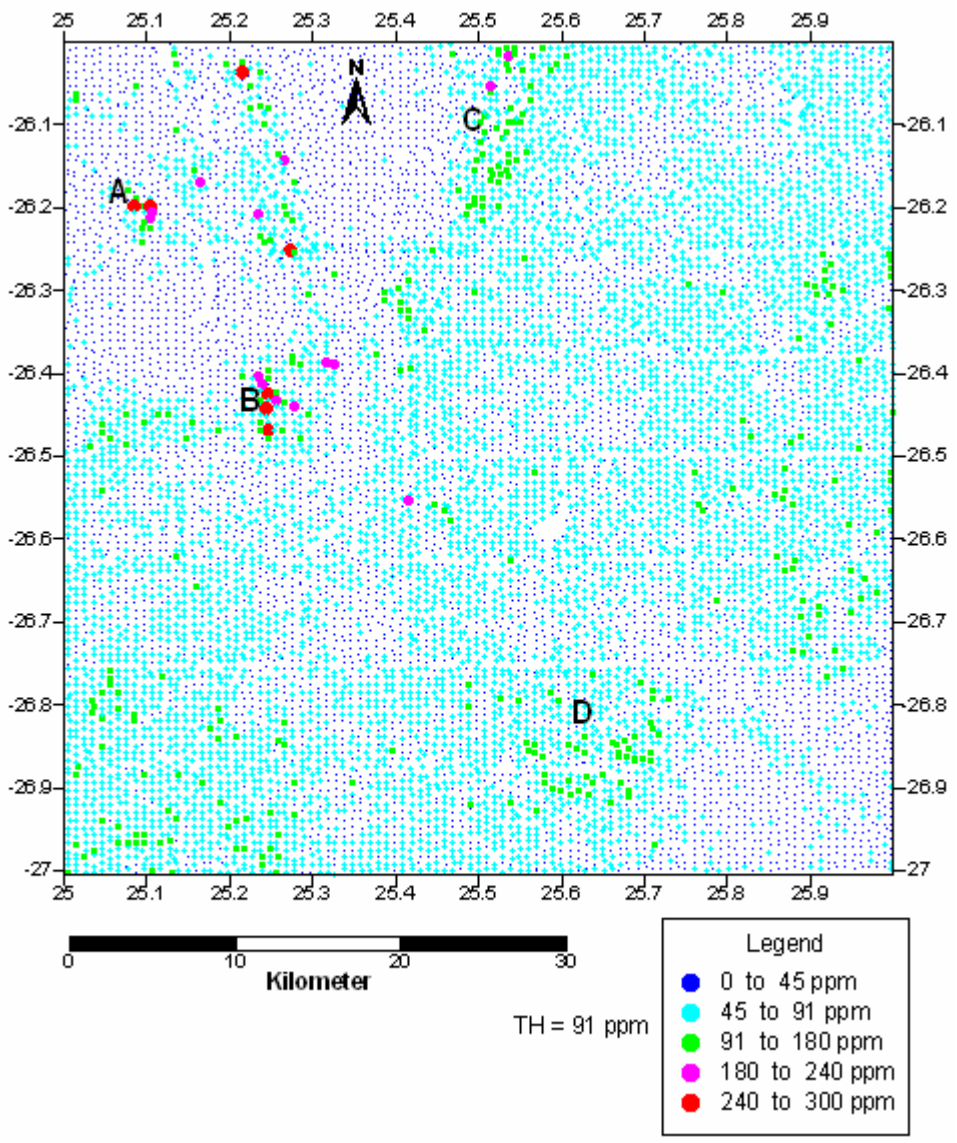

Figure 4.5-3: Distribution of nickel concentration in the 2625 Vryburg Sheet.

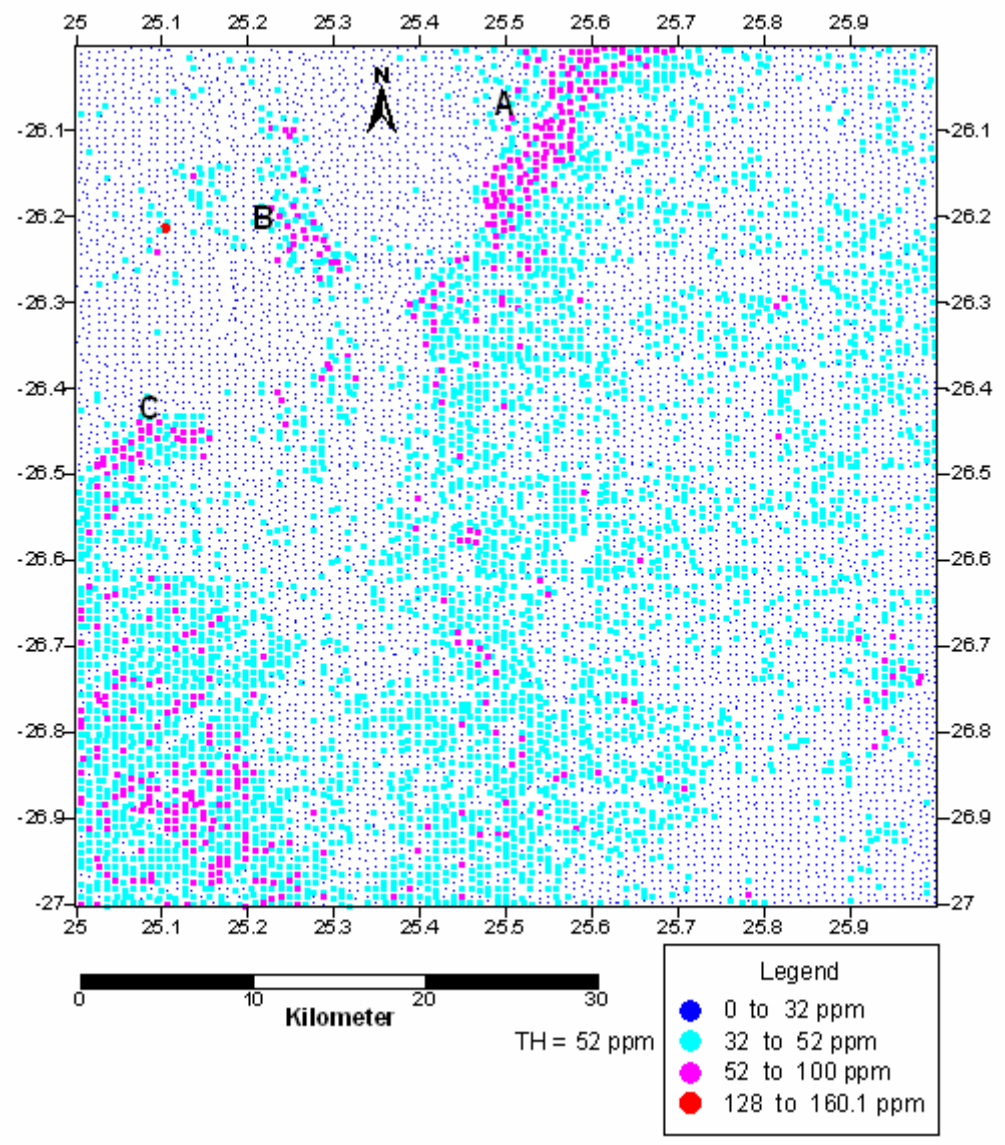

Figure 4.5-4: Distribution of copper concentration in the 2625 Vryburg Sheet.

Iron (Fe) Distribution

Iron occurs in three anomalous areas viz: A B and C in Fig. 4.5-6. A and B lie on the eastern belt of the Kraaipan Group. The highest iron values occur to the south on the Goldridge Formation (anomaly A) and represent known bended iron formation in the area. The other lithologies of the Goldridge Formation are characterized by medium to high iron values. Anomaly C trending NNE-SSW is associated with mafic rocks of the Allanridge Formation. In contrast, much of the lower iron values are found over the extensive Klipriviersberg Group and other lithological units in this area. There are some dispersed iron anomalies in the southern portion of the map area.

Rubidium (Rb) Distribution

Rubidium anomalies form a north-south trend through out the map area and characterized by two main anomalous clusters (A and B). It shows a clustered pattern and a dispersed pattern of elevated values (regional threshold concentration). These clusters occur over undifferentiated granite and gneiss, migmatite, schist and amphibolite of the Basement Complex and undifferentiated Aeolian sand of Quaternary age sediments in the case of cluster A (Fig. 4.5-7). The distribution of Rb in area A resembles the shape, size and extent of the Basement formations. Cluster B occurs on aeolian sand and the granitic rocks.

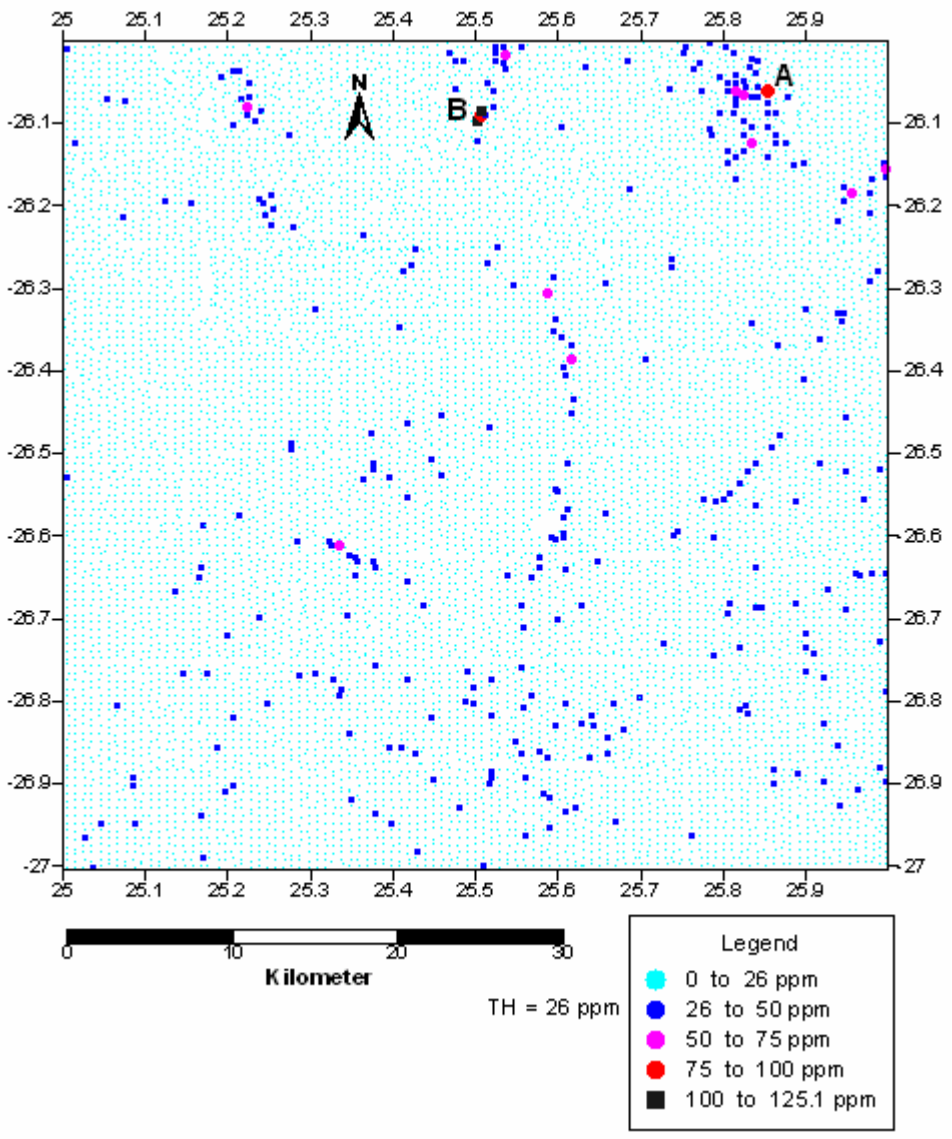

Figure 4.5-5: Distribution of arsenic concentration in the 2625Vryburg Sheet.

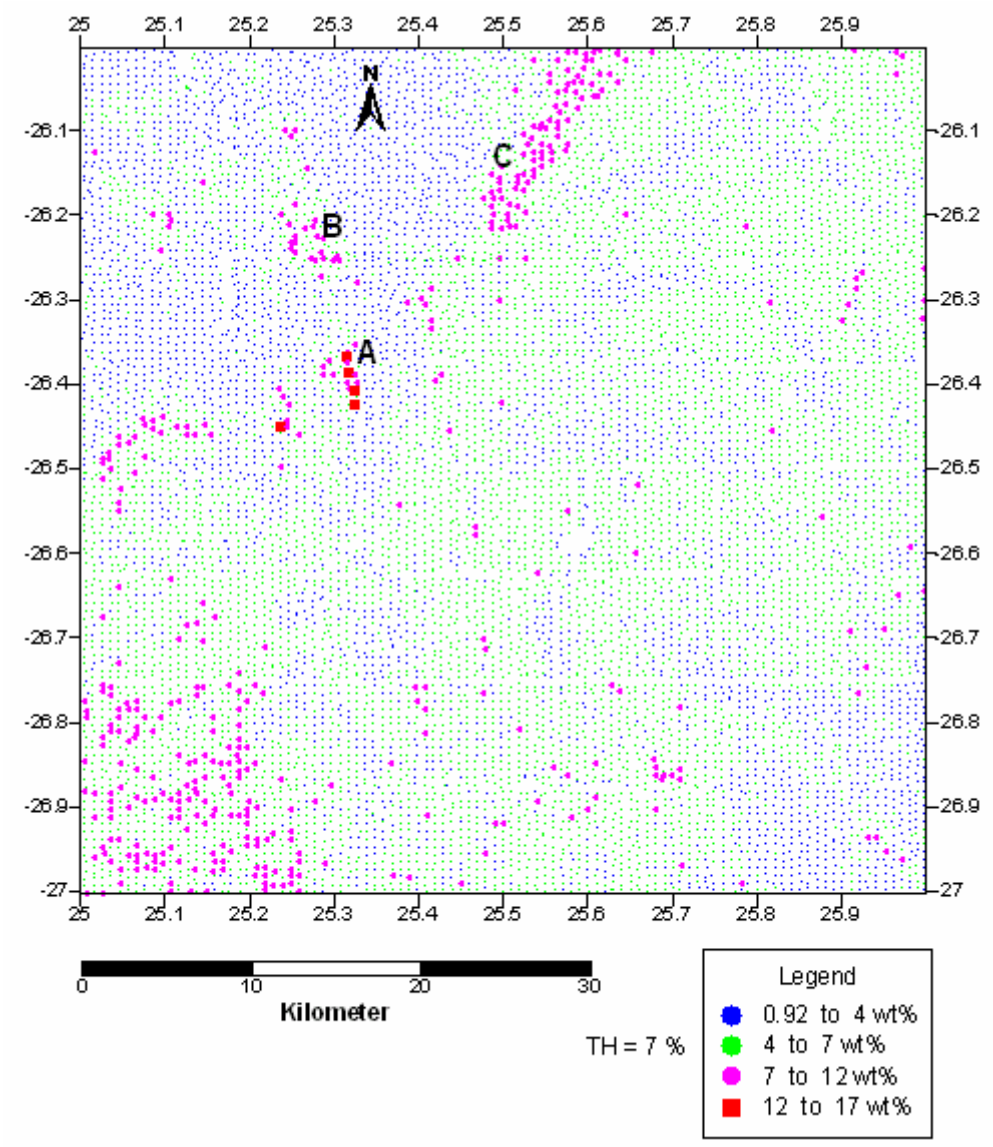

Figure 4.5-6: Distribution of iron concentration in the 2625 Vryburg Sheet.

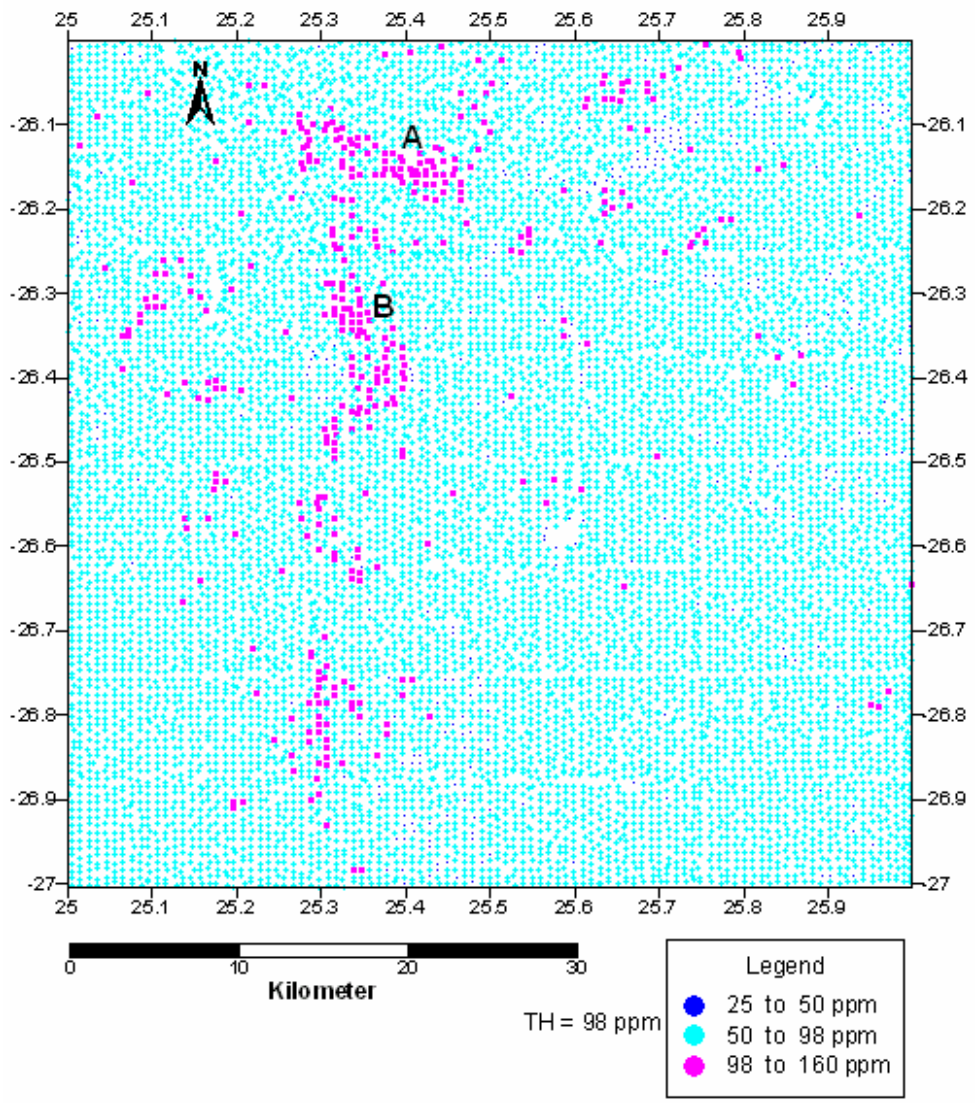

Figure 4.5-7: Distribution of rubidium concentration in the 2625 Vryburg Sheet.

Vanadium (V) Distribution

Fig. 4.5-8 shows the distribution pattern of vanadium in this area. Vanadium anomalies at cluster A are attributed to the basaltic amygdaloidal lava and amphibolites of the Goldridge Formation. The anomalous clusters B and C are located on basaltic lava of the Allanridge Formation. They are mainly defined by the regional threshold values. In the south eastern part map area, anomaly D is characterized by few points close to each other with values ranging between 130-200 ppm. This anomaly has a similar distribution pattern to that of chromium.

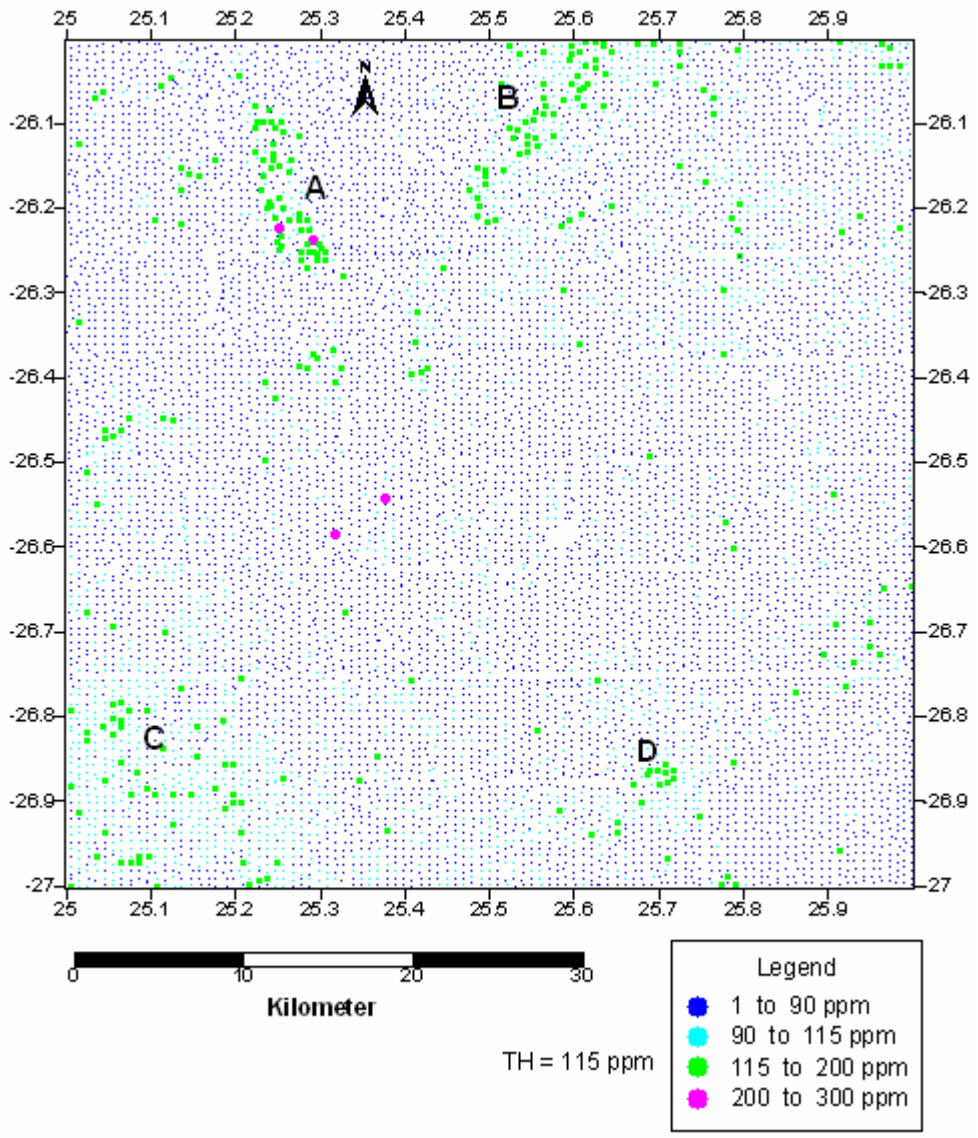

Figure 4.5-8: Distribution of vanadium concentration in the 2625 Vryburg Sheet.

Barium (Ba) distribution

Barium occurs in three anomalous clusters in the Vryburg map area (Fig 4.5-9). Both Anomalies B and C are elongated in shape and both trend almost in the same direction i.e. north to south. Anomaly A has a maximum value of 945ppm and the trend is dominated by concentrations ranging between 470 ppm-695 ppm. Trend C is defined mainly by regional threshold concentrations of barium. Barium anomalies in the area appear to be mainly related to biotite gneiss, augen gneiss, porphyritic and homogeneous granite and pegmatite of the basement rock of Swazian age. It is possible that the presence of the barium concentration in sand or surface deposits result from the basement rocks, due to weathering and mobilization of the element. No barium anomalies occur in the southern part of the area accepts for a few single point anomalies with background values.

Scandium (Sc) Distribution

Fig. 4.5-10 shows three areas of anomalous scandium concentration in the Vryburg map area. A Sc anomaly appears to be mainly related to the river sand and alluvium of Quaternary age, Area A. Is comprised of elevated Sc values of up to 45 ppm, also accompanied by thorium concentration. Anomalous areas B and C are found over jaspilite, lava and amphibole of the Ferndale and Khunwana Formations and mainly represent regional threshold values.

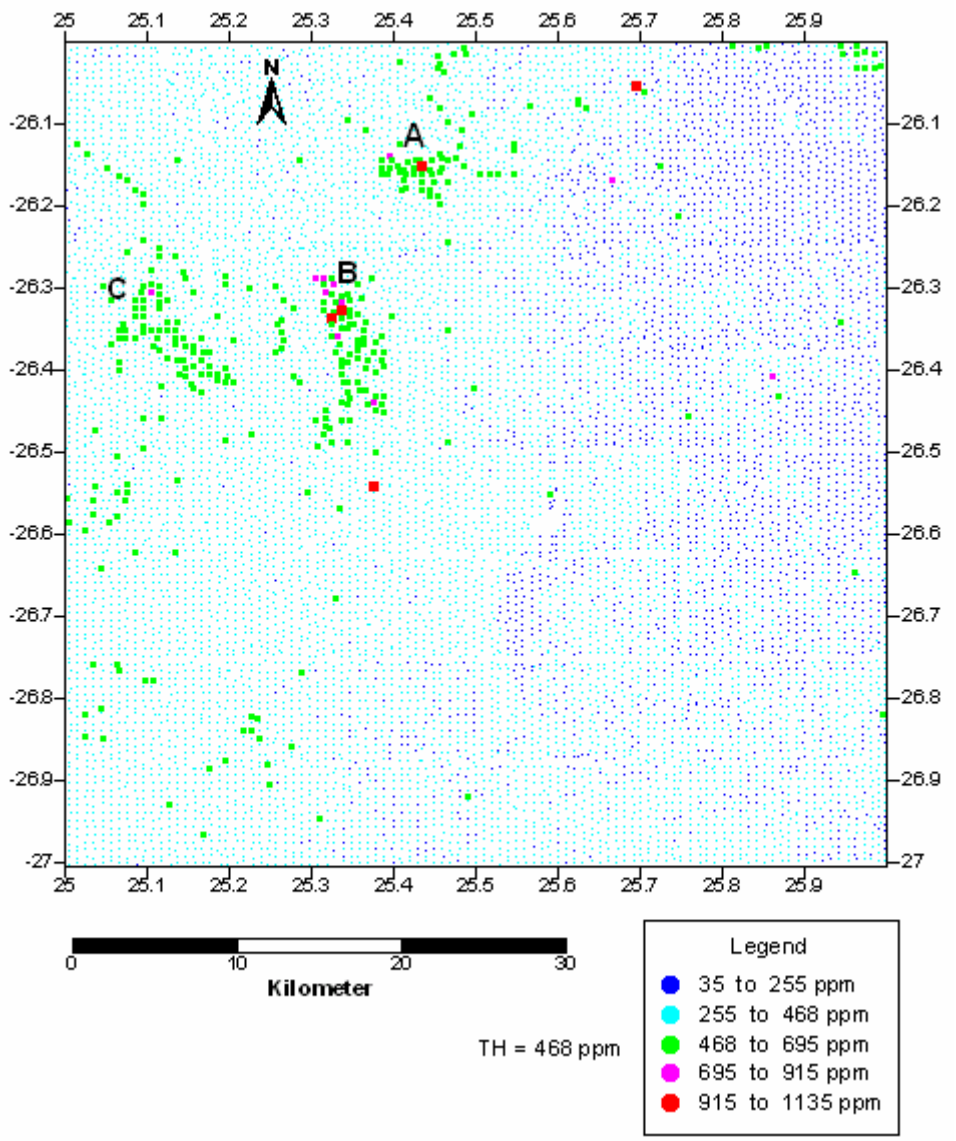

Figure 4.5-9: Distribution of barium concentration in 2625 Vryburg Sheet.

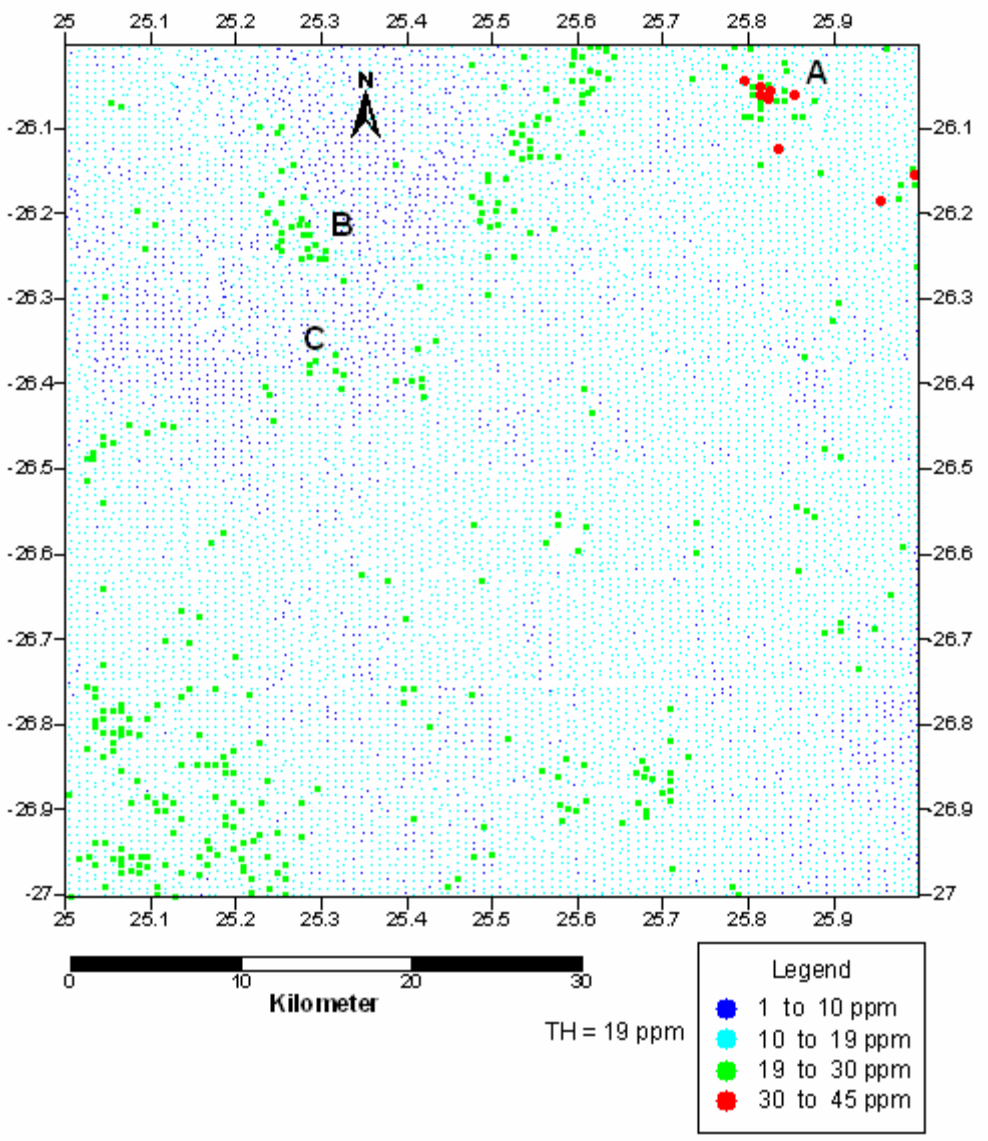

Figure 4.5-10: Distribution of scandium concentration in the 2625 Vryburg Sheet.

Thorium (Th) Distribution

Fig. 4.5-11 shows two major clusters of thorium anomalies in the northern part of the map area. Anomaly A has values of up to 30 ppm, over the Goldridge Formation. A cluster also occurs just a few km south of anomaly A (Area B, Fig. 4.5-11). The anomaly has highest value of 30 ppm, which is found over the Goldridge Formation. The third anomaly is mainly represented by the regional background concentration over surface

sand deposits. This thorium anomaly is also accompanied by high scandium concentrations.

Zirconium (Zr) Distribution

Zirconium distribution patterns shows a major, well defined cluster of anomalies (area A, Fig. 4.5-12) with values of up to 2975 ppm in the north-west portion of the area and extending over a distance excess of 50km in the aeolian sand of the Gordonia Formation.

Distribution of other Elements

Single point anomalies are associated with zinc, lead, cobalt, yttrium, uranium, manganese, titanium, tungsten and niobium in the Vryburg map area. Zinc has a highest value of 894 ppm while the highest anomalous lead value is 161 ppm. Both lead and zinc anomalies are found in the same area over surface Quaternary deposit. It is clear that the anomalies originated from underlying dolomitic and associated rocks

Manganese has a negative anomaly over the chert-rich dolomite of the Monte Christo Formation and the anomaly is mainly composed of values between 0.428wt%-1.041wt%.

Titanium shows a clustered distribution patterns in the northwestern part of the map over the Gordonia Formation. This is similar to the pattern for manganese with the concentrations ranging between 1.2wt%-2.2wt%.

Cobalt and niobium show single point anomalies (Fig. 4.5-13). Cobalt has a maximum concentration of 803ppm over the Acidic lava (mainly quartz porphyry) of the Makwassie Formation. Niobium shows a well developed anomaly in the northwestern part of the map. It covers an extensive area similar in extent to the titanium anomaly and lying over undifferentiated aeolian sand. The trend is mainly composed of regional threshold values with single point anomalies of 101.1ppm in the eastern part of the map area.

Banded jaspilite and acidic lava of the Khunwana Formation on the Madiba belt is characterized by a poorly developed north-south tungsten trend. Maximum values of 20 ppm of tungsten are correlated with the Acidic lava of the Kraaipan Group. Tungsten in this area shows a scattered distribution pattern. Anomaly B in Fig. 4.5-18 has a definite north-south trend and lies on river sand and Aeolian sand of the Gordonia Formation. This anomaly has a maximum concentration of 39ppm.

Uranium is characterized by single point anomalies which are widely scattered in the area. High uranium value is found on undifferentiated aeolian sand.

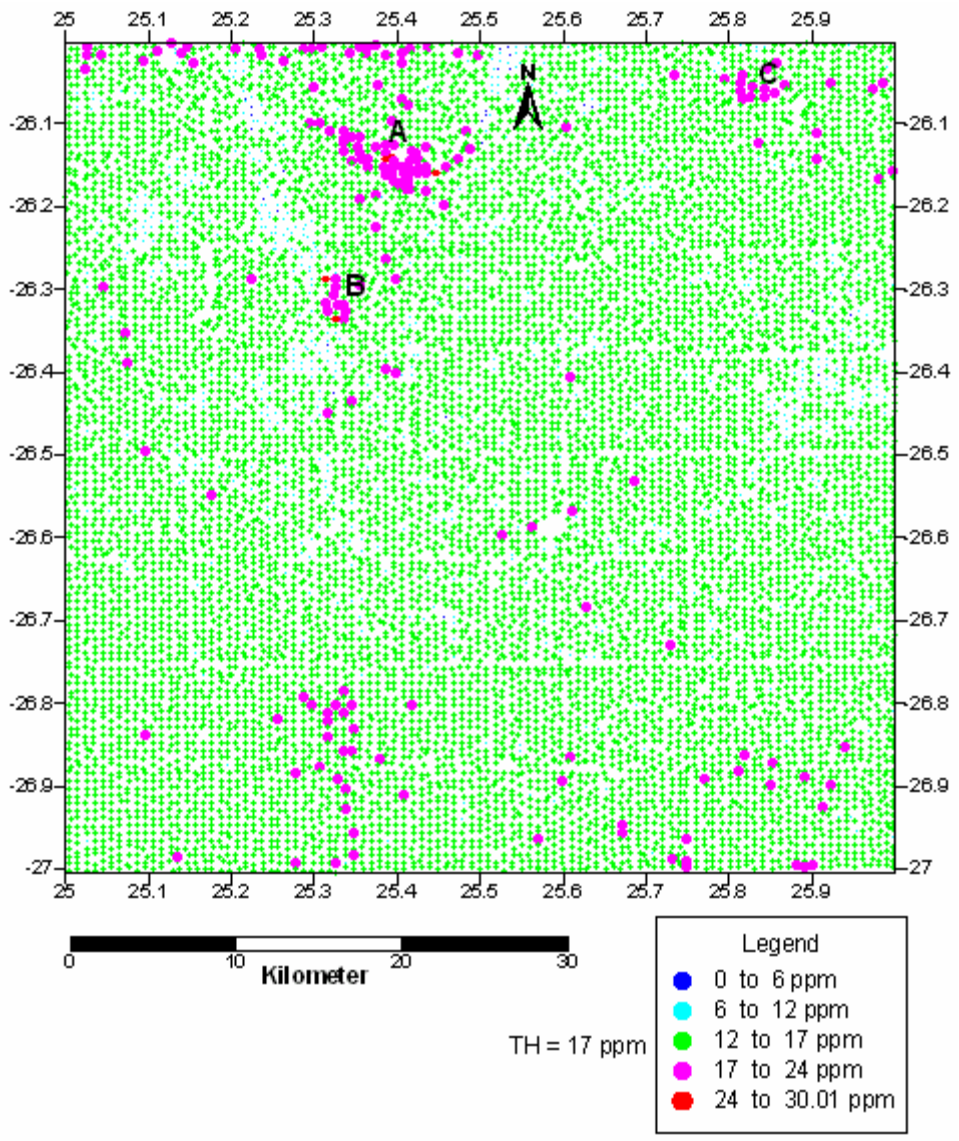

Figure 4.5-11: Distribution thorium concentration in the 2625 Vryburg Sheet.

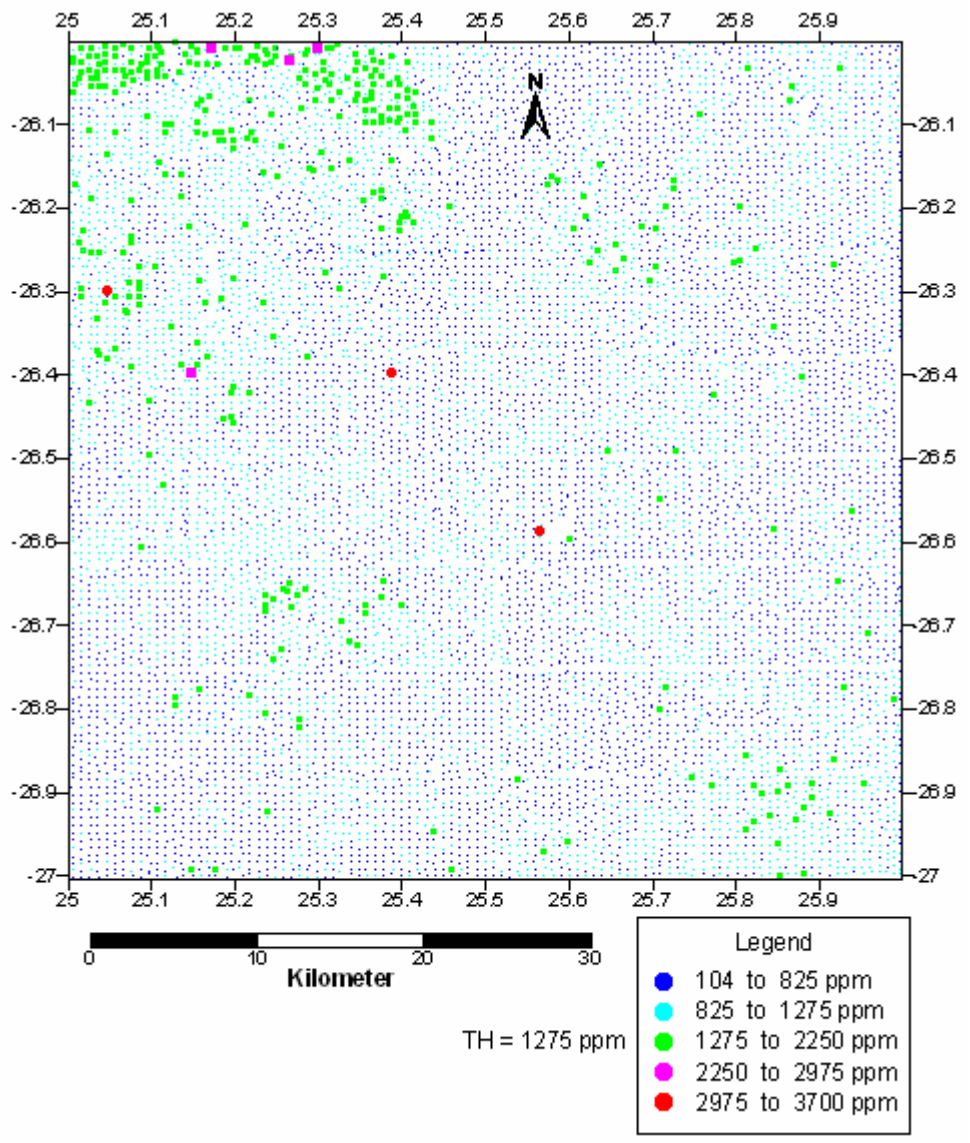

Figure 4.5-12: Distribution of zirconium concentration in the 2625 Vryburg Sheet.

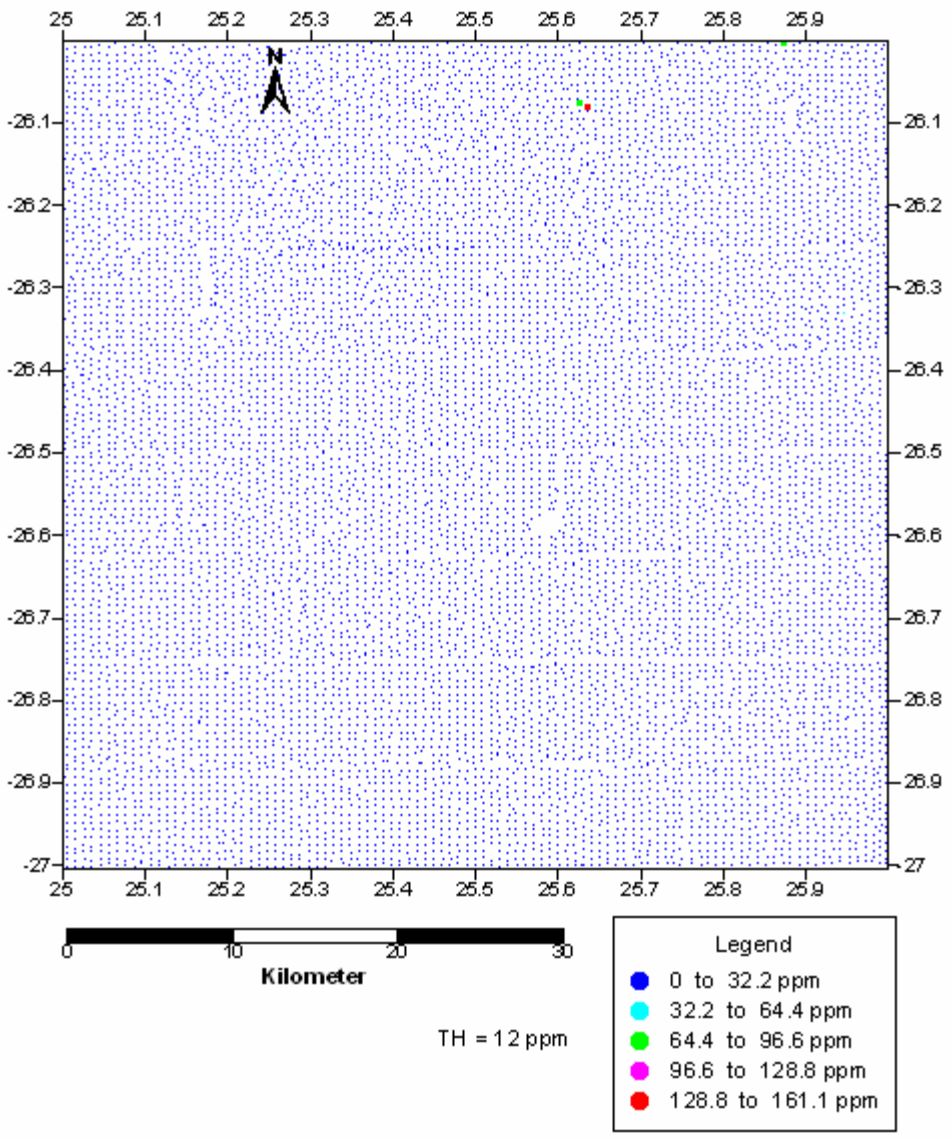

Figure 4.5-13: Distribution of lead concentration in the 2526 Vryburg Sheet.

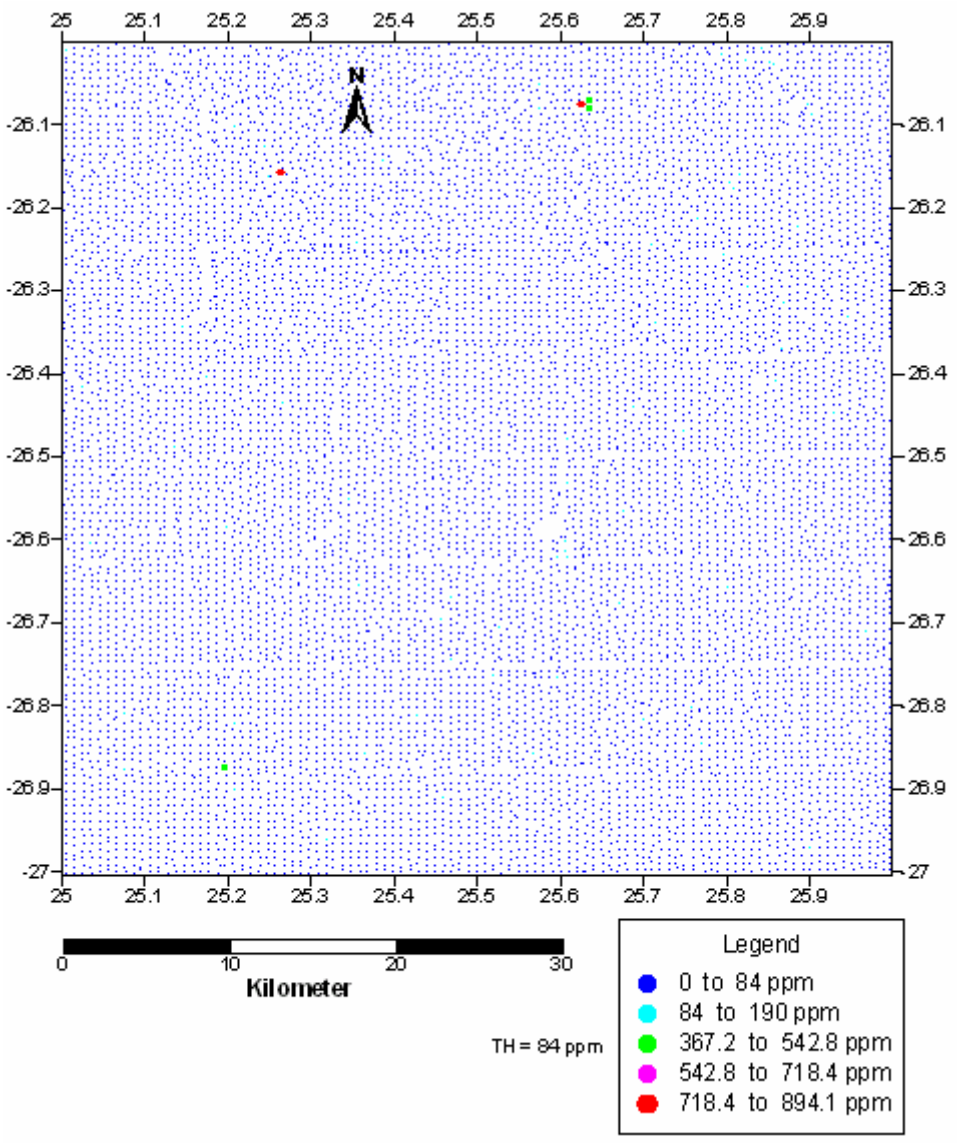

Figure 4.5-14: Distribution of zinc concentration in the 2526 Vryburg Sheet.

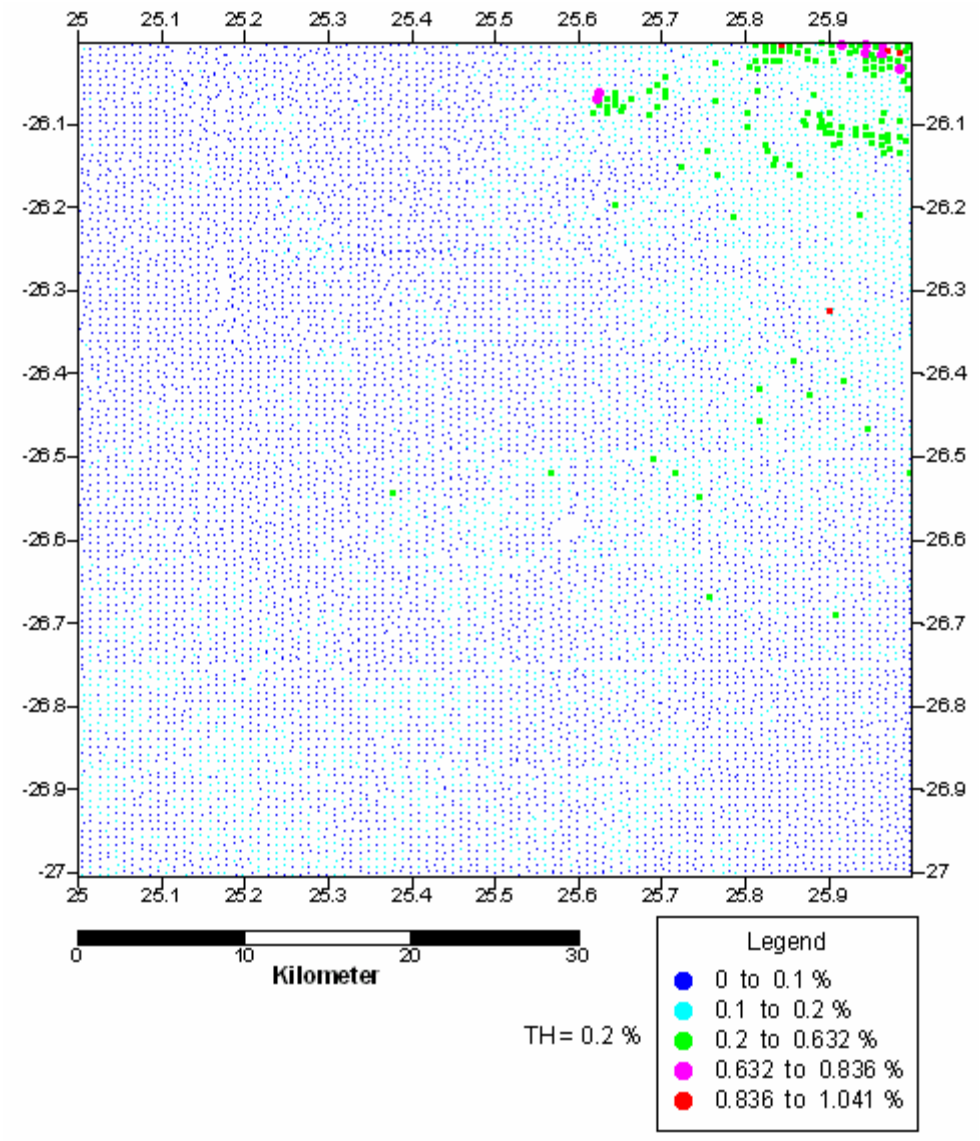

Figure 4.5-15: Distribution of manganese concentration in the 2625 Vryburg Sheet.

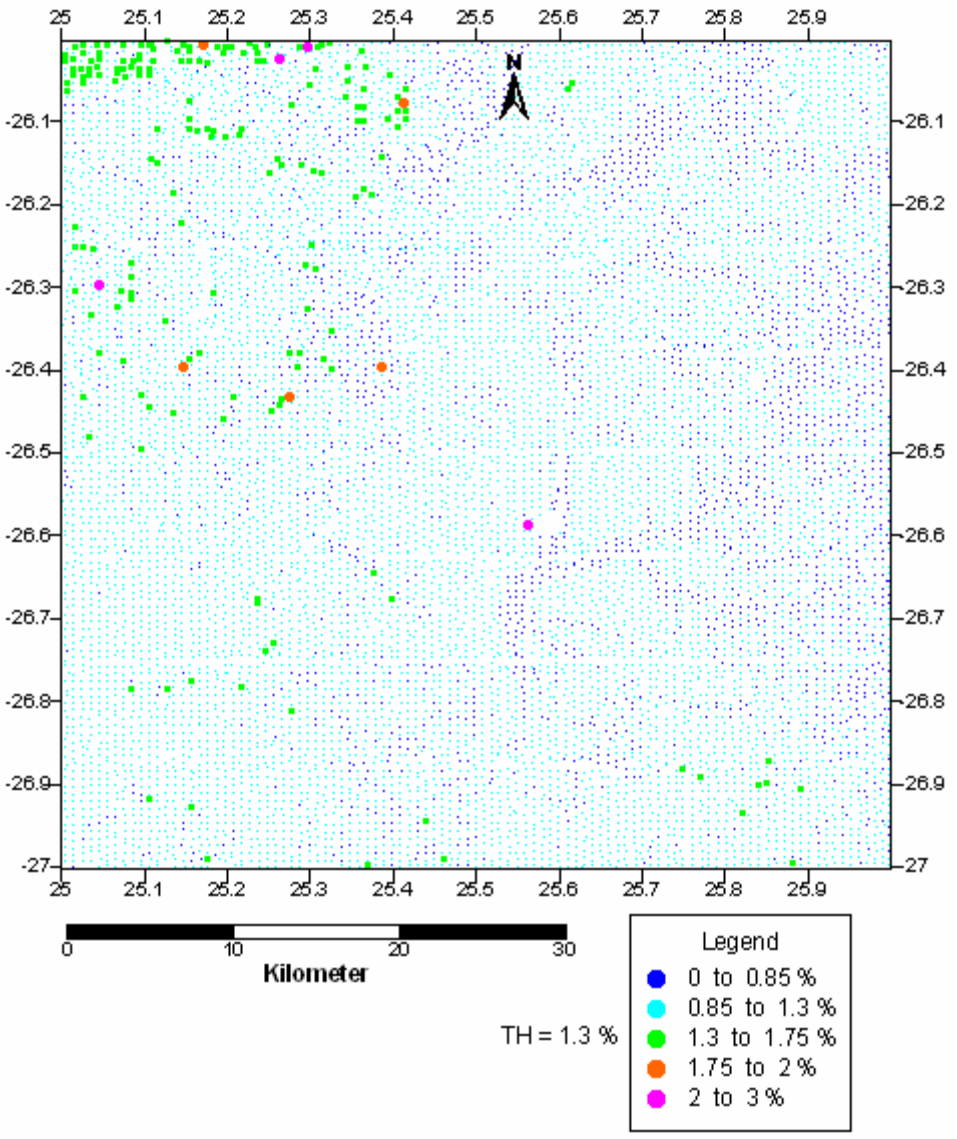

Figure 4.5-16: Distributions of titanium concentration in the 2625 Vryburg Sheet.

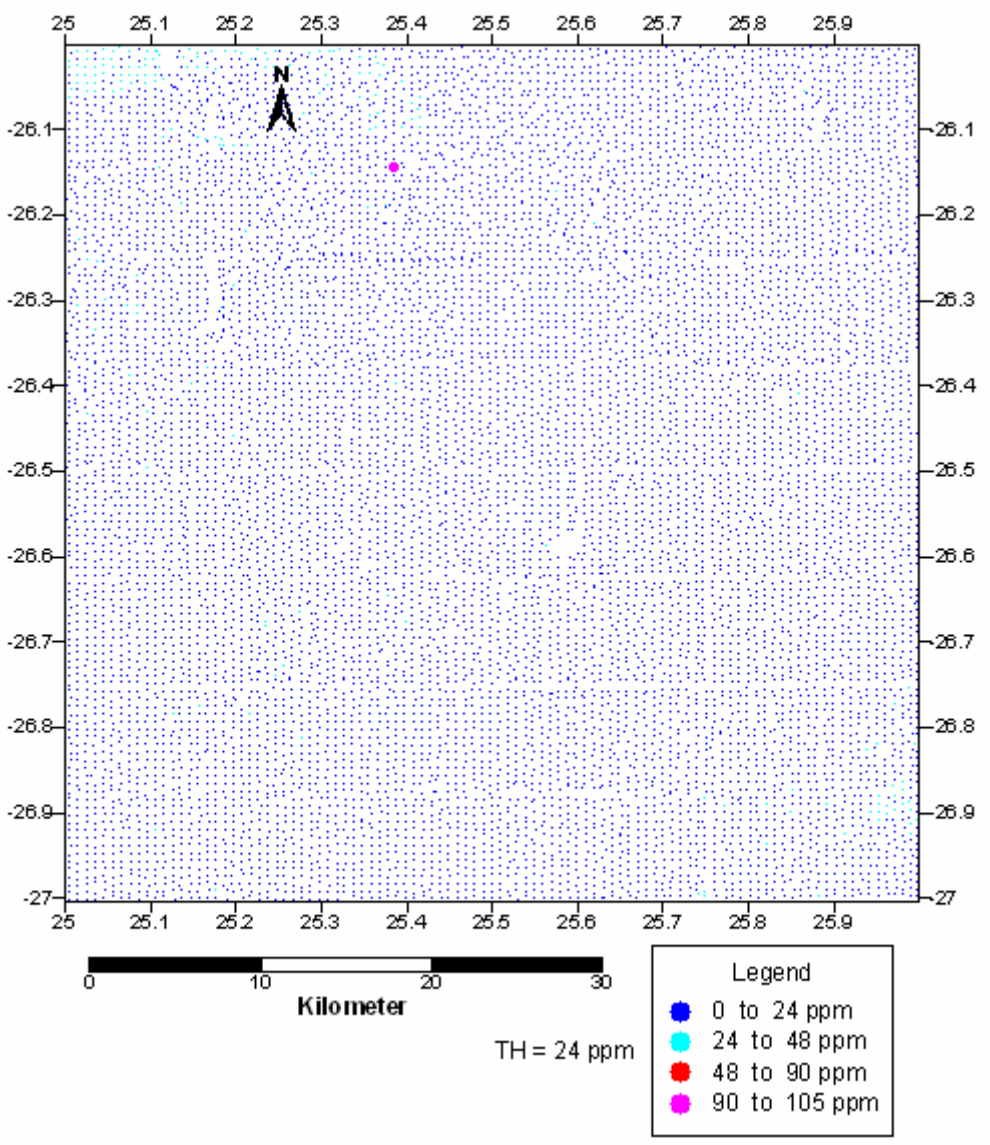

Figure 4.5-17: Distribution of niobium concentration in the 2625 Vryburg Sheet.

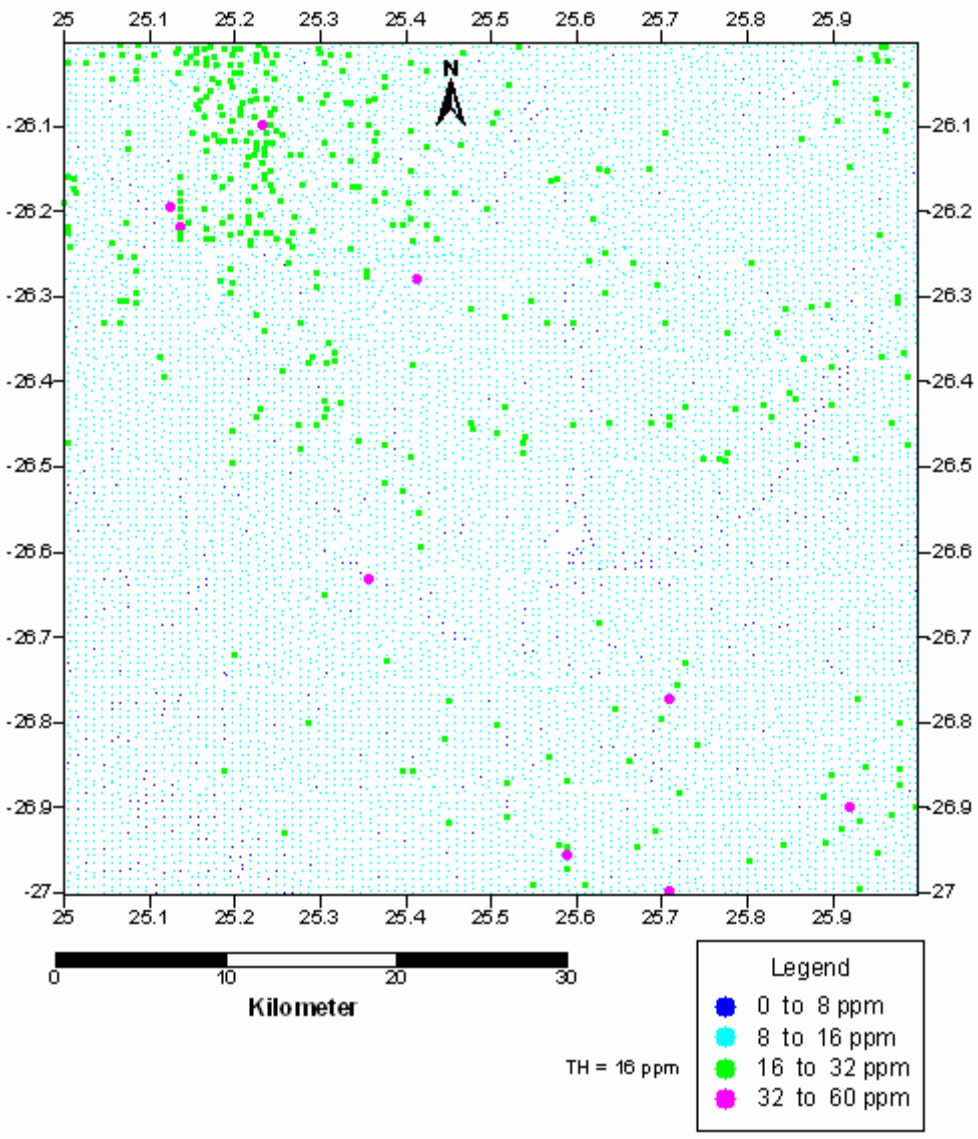

Figure 4.5-18: Distribution of tungsten concentration in the 2625 Vryburg Sheet.

4.6 DISRIBUTION OF THE ELEMENTS ON THE 2723 KURUMAN SHEET

4.6.1 Statistical analysis

A summary of the statistics of the Kuruman Sheet (2723) data set (5517 samples) is presented in Table 4.6-1. Threshold values, minimum (Min), maximum (Max), standard deviation (std. dev), mean, range, variance, kurtosis and skewness are given in the table. The mean plus two standards deviation is displaced in the last column to show the general background of the complete data set across various lithological units. Contour intervals for the map were based on 95% confidence interval (mean + 2(std. dev)) to show chemical variation in the different lithological units. In general the values with concentrations higher than the average plus two times standard deviation (Threshold values) were considered anomalous. On a data set containing different lithological units, anomalous values were calculated separately for each element.

4.6.2 Correlation of elements

None of the above 21 elements in Kuruman Sheets (2723) were well correlated each other. Only 6 correlations are apparent from table 4.5-2 include; Ti-Zr and Nb, Rb-Sr and Zr-Nb. Their correlation coefficients range from 0.82-0.95 (80-95% correlation).

Table 4.6.2, a weakly correlation was found with Cr-Ni and Cu-V. All these elements have correlation coefficients ranging between (0.62-0.73) 62-73%. Other elements are not correlated with each other and some of them show negative correlations.

Table 4.6-1: Summary statistics on the complete data set for the 2723 Kuruman Sheet.

Element	N	Min	Max	Mean	Median	St. Dev	Var	CV	Skew	Kurt	Threshold
TiO_2	5517	0.13	3.56	1.27	1.30	0.33	0.11	0.26	-0.22	1.13	**1.9**
MnO	5517	0.01	2.25	0.17	0.11	0.19	0.04	1.10	3.41	17.70	**0.6**
Fe_2O_3	5517	0.35	26.69	3.89	3.43	2.02	4.07	0.52	2.59	14.25	**8**
Sc	5457	1.00	83.00	12.16	12.00	4.78	22.81	0.39	1.84	20.29	**22**
V	5496	1.00	229.00	39.58	35.00	22.39	501.50	0.57	1.83	6.48	**84**
Cr	5459	1.00	614.00	62.45	60.00	32.36	1047.34	0.52	4.26	44.91	**127**
Co	5454	1.00	767.00	10.41	10.00	14.42	207.99	1.39	49.29	2525.49	**39**
Ni	5517	6.00	339.00	27.46	24.00	15.51	240.63	0.56	15.51	62.03	**58**
Cu	5507	1.00	397.00	16.69	15.00	9.25	85.50	0.55	14.26	526.24	**35**
Zn	5517	10.00	731.00	37.18	35.00	16.34	267.08	0.44	19.40	719.19	**70**
As	4996	1.00	97.00	13.73	12.00	10.07	101.48	0.73	2.28	9.76	**34**
Rb	5517	21.00	147.00	72.54	75.00	15.29	233.87	0.21	-0.73	2.01	**103**
Sr	5517	18.00	508.00	52.66	50.00	23.04	530.91	0.44	7.46	91.71	**99**
Y	5517	4.00	44.00	24.42	25.00	5.67	32.19	0.23	-1.03	1.13	**36**
Zr	5517	69.00	3137.00	1101.45	1129.00	357.18	127576.32	0.32	-0.06	0.29	**1816**
Nb	5517	8.00	39.00	22.90	23.00	3.41	11.60	0.15	-0.55	0.37	**30**
Ba	5513	10.00	1604.00	363.59	368.00	118.47	14036.11	0.33	0.66	7.79	**601**
W	5481	1.00	71.00	9.97	10.00	2.70	7.28	0.27	6.40	111.86	**15**
Pb	3245	1.00	70.00	4.34	3.00	4.06	16.46	0.94	5.13	57.38	**12**
Th	5515	2.00	39.00	14.67	15.00	1.93	3.72	0.13	0.31	7.16	**19**
U	53	1.00	9.00	3.04	2.00	2.21	4.88	0.73	0.92	-0.16	**7**

Table 4.6-2: Correlation matrix of the elements on the 2723 Kuruman Sheet.

	TiO_2	MnO	Fe_2O_3	Sc	V	Cr	Co	Ni	Cu	Zn	As	Rb	Sr	Y	Zr	Nb	Ba
TiO_2	1																
MnO	0.14	1															
Fe_2O_3	0.14	0.27	1														
Sc	0.22	0.28	0.62	1													
V	-0.05	0.38	0.66	0.52	1												
Cr	0.22	0.25	0.57	0.48	0.58	1											
Co	-0.01	0.04	-0.02	0.3	0.22	0.21	1										
Ni	0.09	0.16	0.37	0.39	0.47	**0.72**	0.1	1									
Cu	-0.02	0.14	0.49	0.38	0.62	0.47	0.05	0.44	1								
Zn	-0.01	0.09	0.27	0.29	0.25	0.24	0.02	0.21	0.4	1							
As	-0.69	-0.09	-0.09	0.19	0.06	-0.13	0.02	0.02	0.07	0.07	1						
Rb	0.44	0.15	0.38	0.36	0.35	0.47	0.03	0.36	0.41	0.3	-0.31	1					
Sr	-0.17	-0.04	0.05	0.37	0.11	0.1	0.05	0.16	0.2	0.34	0.36	0.14	1				
Y	0.68	0.13	0.34	0.4	0.27	0.44	-0.01	0.34	0.33	0.22	-0.42	**0.82**	0.05	1			
Zr	**0.96**	0.09	0.03	0.16	-0.17	0.12	-0.06	0.02	-0.13	-0.06	-0.68	0.38	-0.13	0.64	1		
Nb	**0.94**	0.08	0.04	0.21	-0.12	0.19	-0.05	0.1	-0.04	-0.03	-0.62	0.52	-0.11	**0.76**	**0.95**	1	
Ba	0.57	0.6	0.5	0.48	0.52	0.49	0.11	0.32	0.33	0.22	-0.39	0.64	0.07	0.65	0.47	0.51	1
W	0.15	0.01	0.2	-0.04	0.07	0.21	0.01	0	0.01	-0.07	-0.09	0.05	-0.33	0.1	0.11	0.13	0.1
Pb	-0.18	0.08	0.03	0.35	0.12	0.16	0.06	0.21	0.18	0.48	0.31	0.27	0.36	0.12	-0.18	-0.1	0.08
Th	0.33	-0.14	-0.17	0.27	-0.17	0.03	-0.02	0.1	-0.04	-0.07	-0.01	0.3	0.21	0.46	0.38	0.48	0.09
U	-0.23	-0.04	-0.11	0.3	-0.05	-0.13	0.03	-0.05	-0.09	-0.06	0.41	-0.21	0.38	-0.22	-0.19	-0.2	-0.17

4.6.3 Statistical distribution

Fig. 4.6-1,show histograms fro manganese, iron, scandium, vanadium, chromium, cobalt, nickel, copper, zinc, strontium, tungsten and lead distributions all show asymmetrical, positively skewed, distribution patterns. Titanium, arsenic, rubidium yttrium, zirconium, niobium and barium have bimodal distributions. The populations of high concentration in Barium distribution reflect the lithologies of the Ghaap Group and the population of lower values on other lithological units of the area. Other elements outlined above that showed the bimodal distribution show that they are characterized by low values over mafic rocks and high values over the surface sand of the Kalahari Group. Higher iron values are located over the Asbestos Hill Group. Vanadium, copper and zinc are positively skewed with high values in calcrete or carbonate rock. Strontium, nickel and chromium had high values over the far east of the map area over the Allanridge Formation while low values are found over all lithological units.

Only thorium showed slightly normal or symmetrical and leptokurtic distribution patterns and uranium is not well distributed due to an outlier of high value.

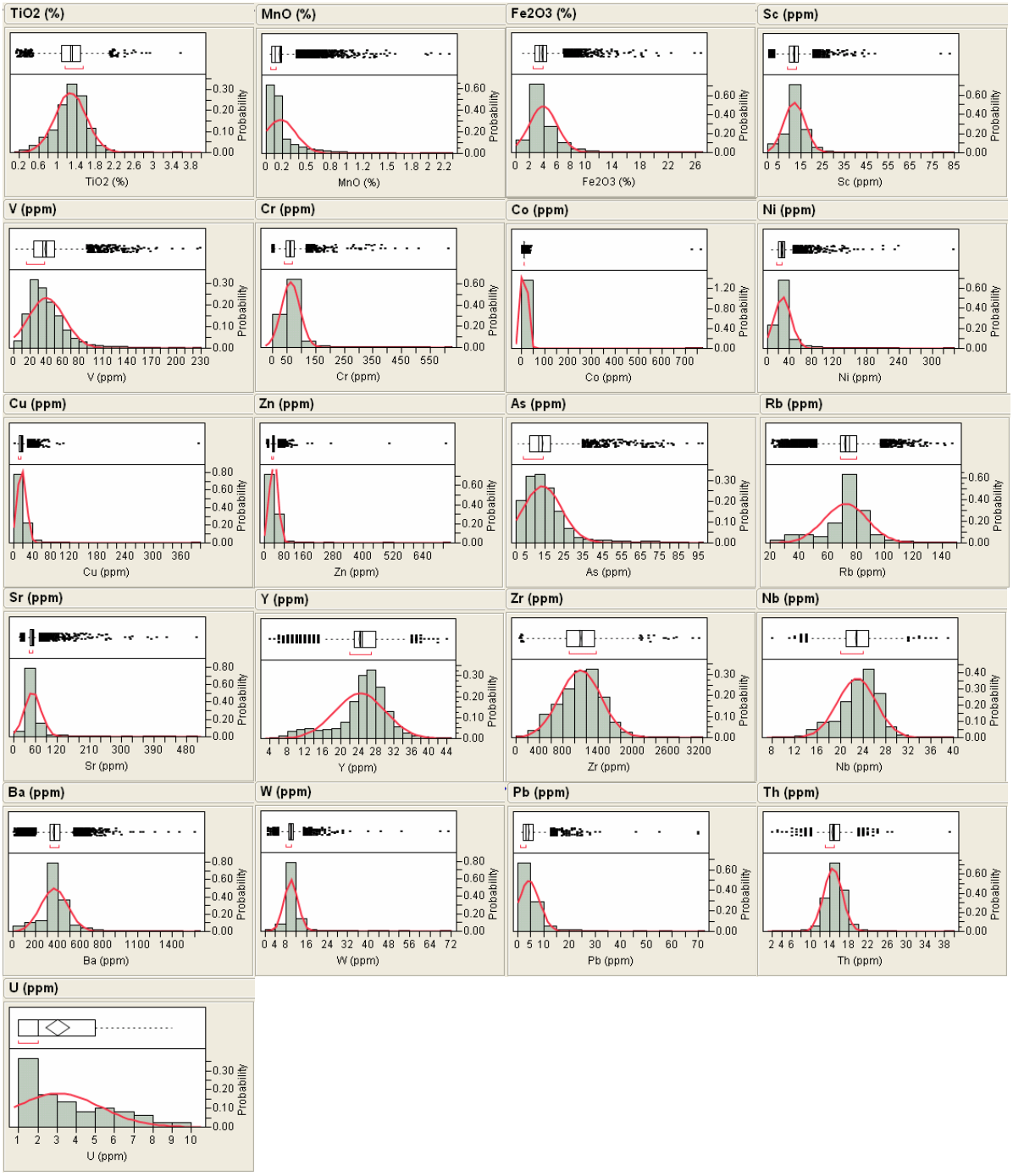

Figure 4.6-1: Histograms and box plots of the elements on the 2723 Kuruman Sheet.

4.6.4 Geochemical distribution

Chromium (Cr) and Nickel (Ni) Distribution

Both nickel and chromium show similar distribution patterns characterized by regional threshold values of (256-456 ppm for Cr and 60-140 ppm for nickel). The major anomalous area occurs in the north east part on the map area and extends up to the map margin (anomaly A). High chromium concentrations are consistent with mafic rocks Cr anomalies occupy the same area as iron and vanadium anomalies and all occur on andesitic and amygdaloidal lava, and agglomerate of the Allanridge Formation (Fig. 4.6-2, anomalous A). Nickel anomalies also to the west of Kuruman with most anomalous values occurring in the north-south trending Asbestos Hills Group. Chromium anomalies in this area are not as compares as nickel. Single point anomalies are mostly characterized by the regional threshold values.

Vanadium (V) and Copper (Cu) Distribution

Zones of vanadium and copper anomalies have north-south trends to the north-west of Kuruman. The anomalies are mostly dominated by the regional threshold values of between 83-166 ppm for vanadium and 35-70 ppm for copper. The major clustered of vanadium anomalies are found in the western part of the area with maximum values of 229 ppm (Fig. 4.6-3, anomaly A).

Anomalies B for both copper and vanadium are found over the andesitic lava, amygdaloidal lava and agglomerate of the Allanridge Formation

Iron (Fe) Distribution

Iron anomalies occur in a major cluster trending northwest to southeast (Fig. 4.6-4). Iron anomalies are scattered from north of Kuruman where they are characterized by the point values, to south east of Kuruman, where values become more clustered and form a concentric shape. The area of higher concentration for iron is located west of Kuruman on banded iron formation, jaspilite, and mudstone particularly in the vicinity of major faults. The anomalies

are believed to have been derived from hematite, magnetite and limonite which occur in the ferruginous jaspilite of the Danielskuil Formation of the Asbestos Hill Subgroup. Up to 16wt% of Fe is found over the Danielskuil Formation as compare to 12wt% iron over Kuruman Formation.

Arsenic (As) Distribution

Arsenic anomalies occur as a few clusters of points with regional threshold concentrations over calcrete and surface sand of tertiary age (Fig. 4.6-5, area A). A poorly developed north south arsenic trend, characterized by the widely dispersed point anomalies, is found over the dolomite and chert of the Ghaaplato Group. The trend extends from the Tsineng area where it is mostly represented by elevated values, south to Kuruman where the arsenic distribution pattern becomes scattered. East of the Kuruman area, arsenic shows an irregular distribution pattern (B) with few points forming clusters and with concentrations ranging between 60-98 ppm over the aeolian sand of Gordonia Formation.

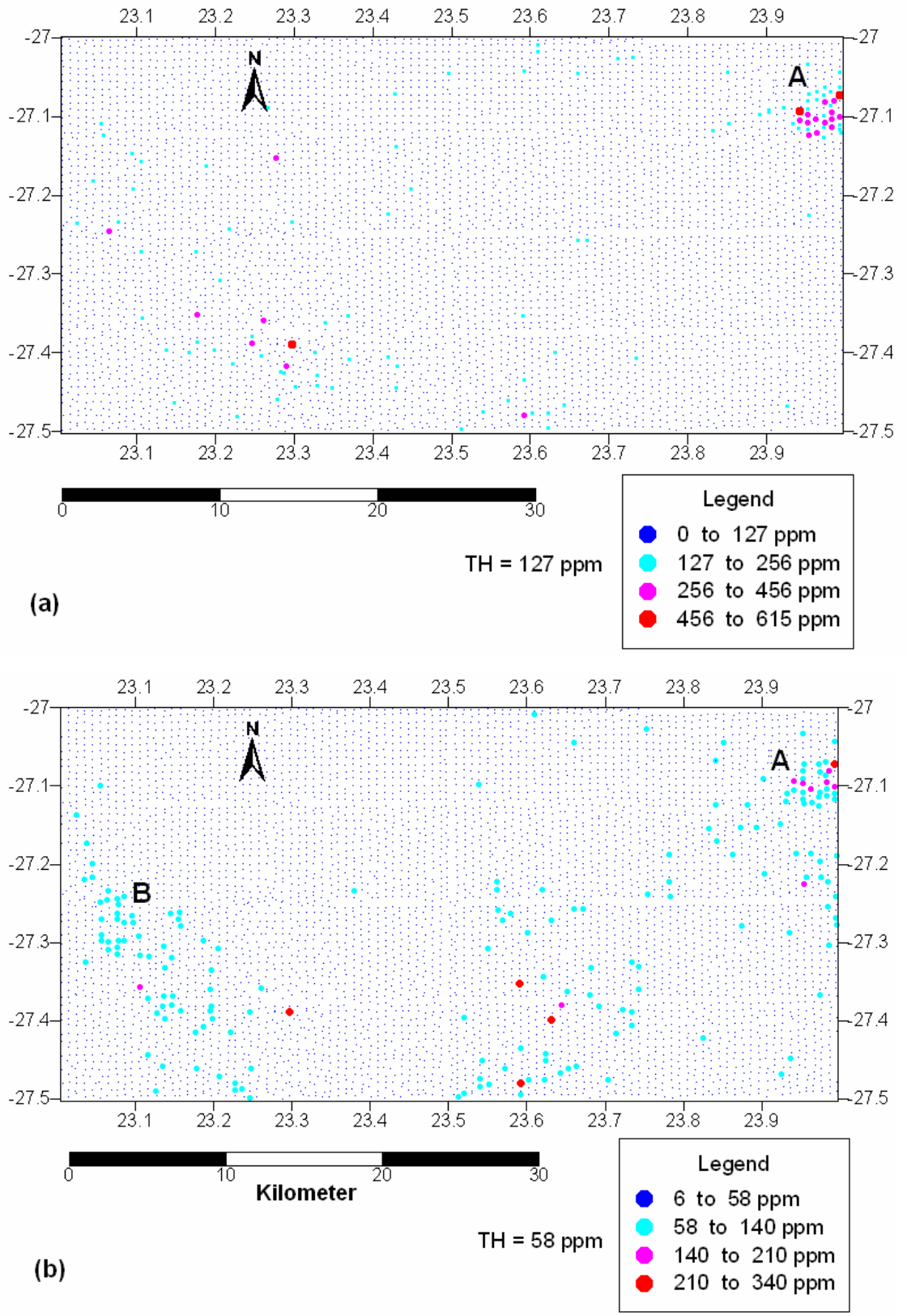

Figure 4.6-2: Distribution of chromium and nickel concentrations in the 2723 Kuruman Sheet; Cr (a) and Ni (b).

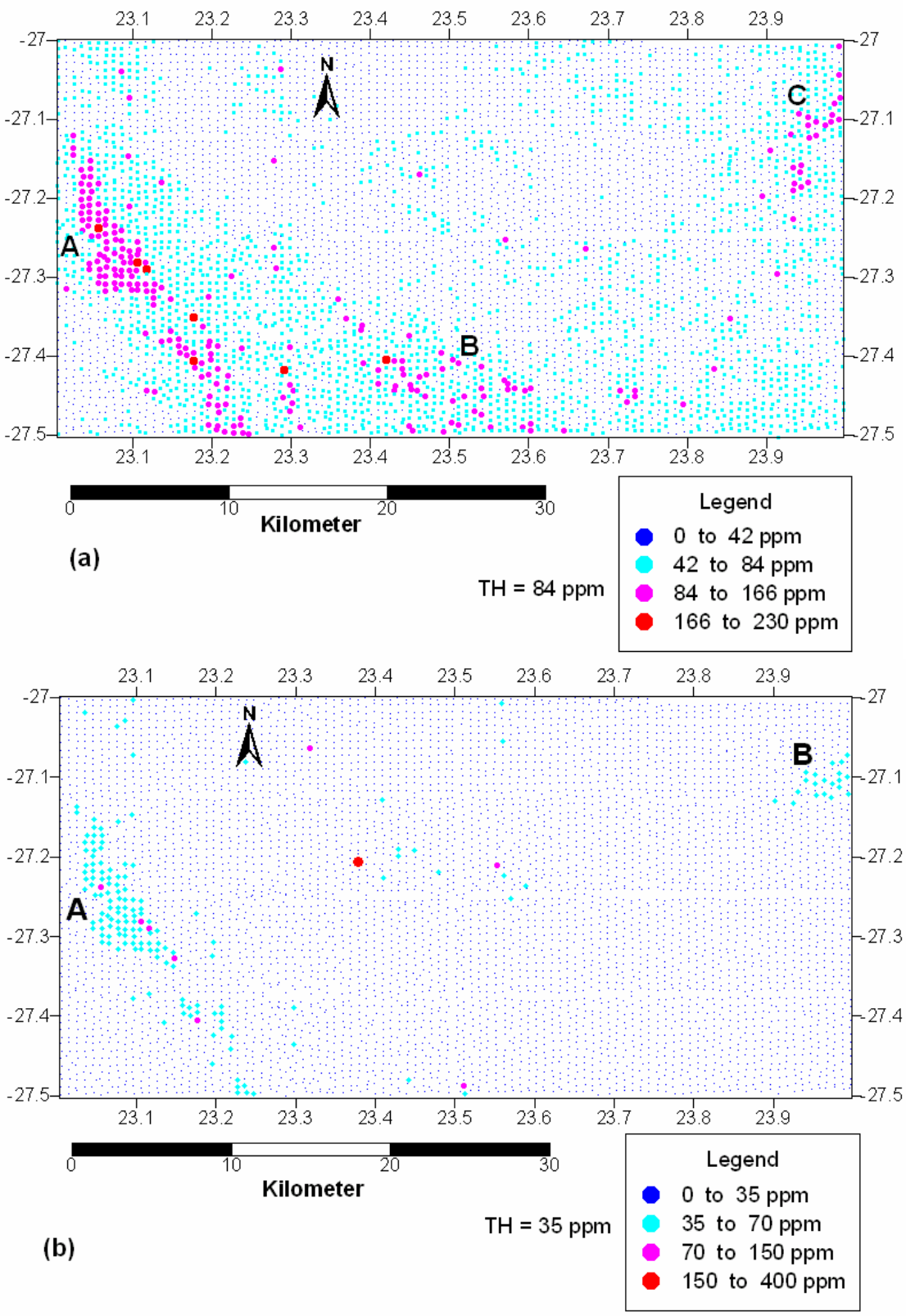

Figure 4.6-3: Distribution of vanadium (a) and copper (b) concentration in the 2723 Kuruman Sheet.

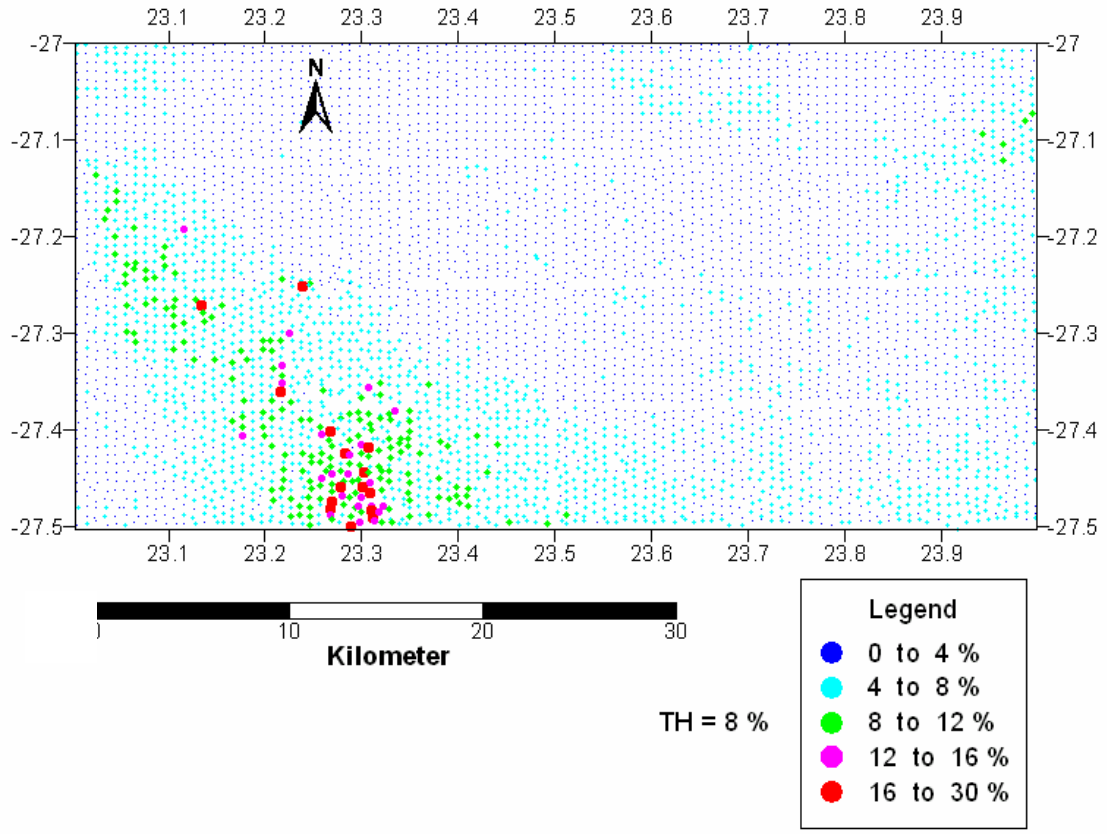

Figure 4.6-4: Distribution of iron concentration in the 2723 Kuruman Sheet.

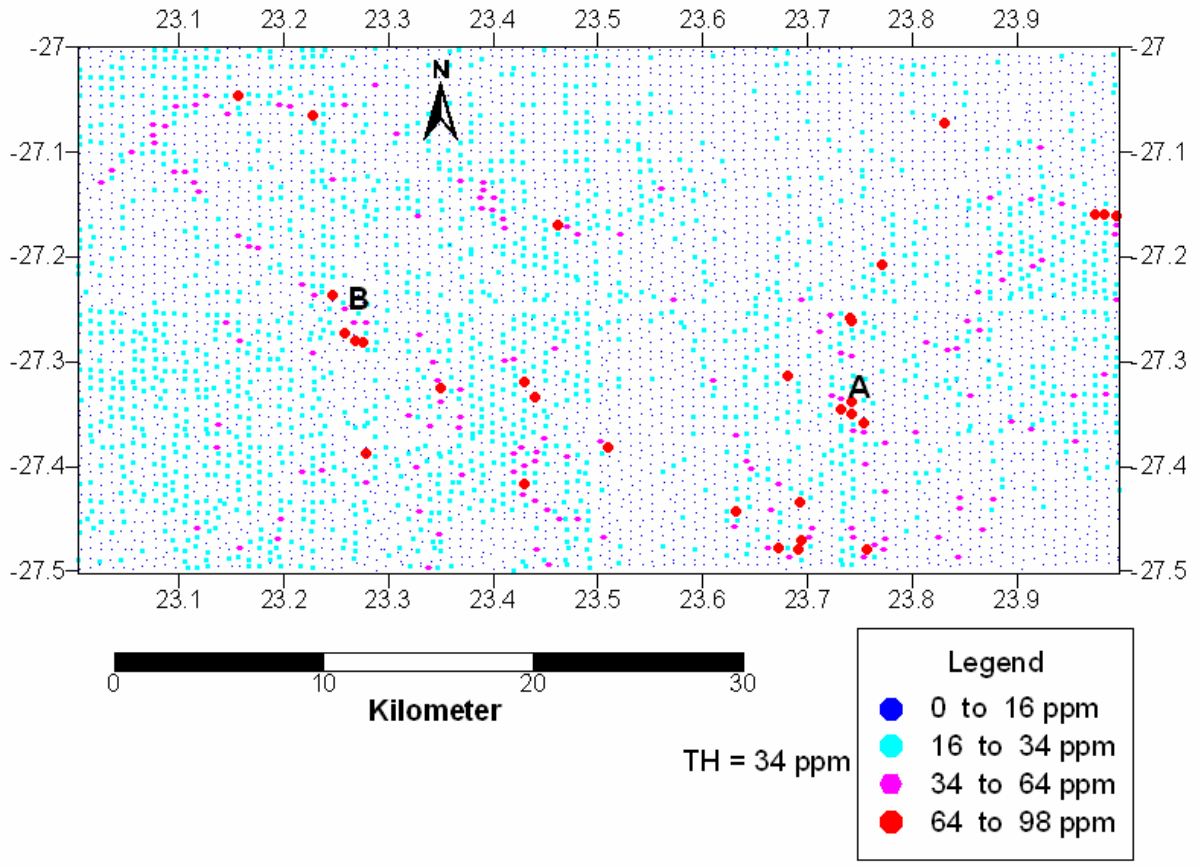

Figure 4.6-5: Classed post map of arsenic distribution in the 2723 Kuruman Sheet.

Barium (Ba) distributions

Fig. 4.6-6 shows a few major anomalies of barium in the Kuruman area. Anomalous A area contain scattered barium values over the dolomite and surface limestone of the Ghaap Group. This anomalous area is mostly dominated by the regional threshold values, with a highest value of 1605 ppm.

Anomaly B has more clustered barium values as compared to area A but the anomalous area covers only a few kilometers as compared to anomaly A. This anomaly is associated with the dolomite/limestone of the Ghaap Group.

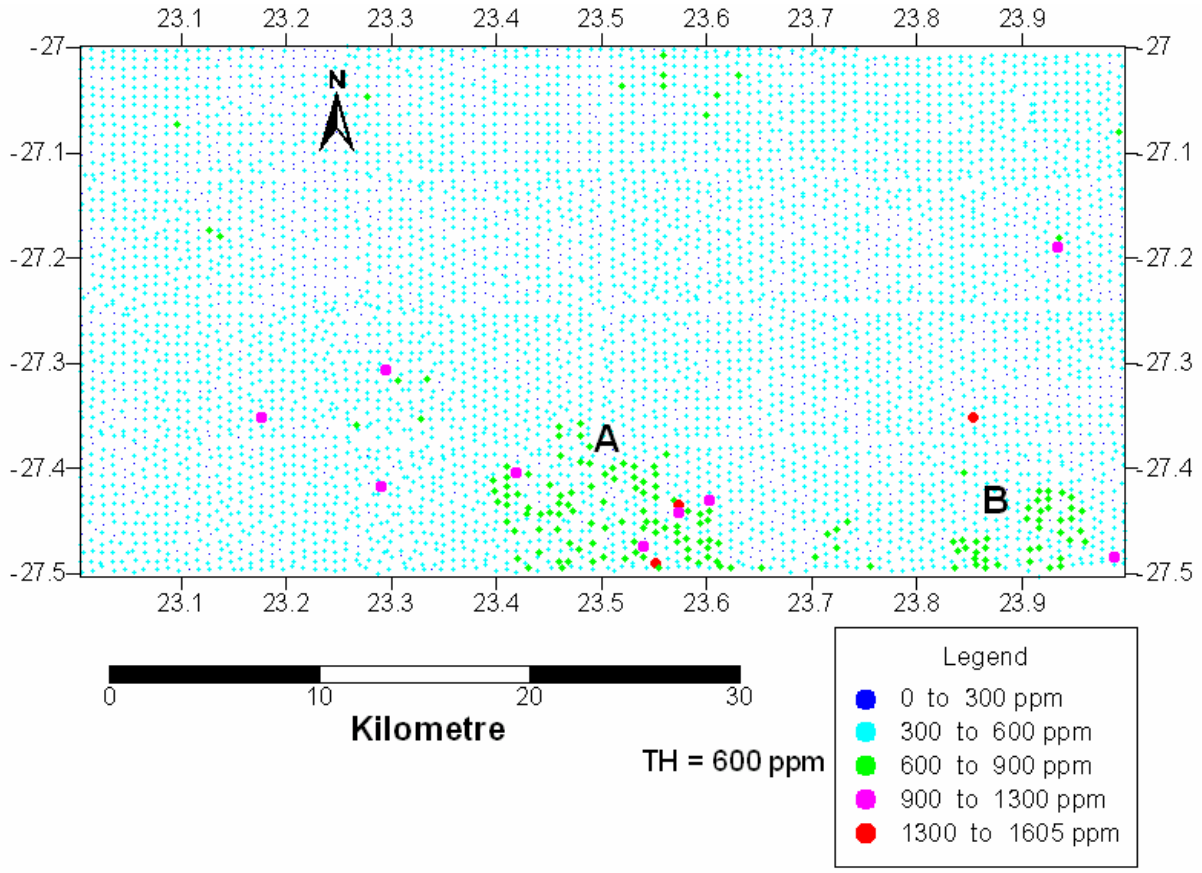

Figure 4.6-6: Distribution of barium concentration in the 2723 Kuruman Sheet.

Rubidium (Rb) Distribution

Rubidium shows regional background anomalies. Both anomalous area A and B in Fig. 4.6-7 cover fairly large areas with their concentrations ranging between 102 ppm and 140 ppm over Gordonia Formation. Anomalous area B, lying south of anomalous area A, trends west-east and reflects the position of the Clearwater Formation.

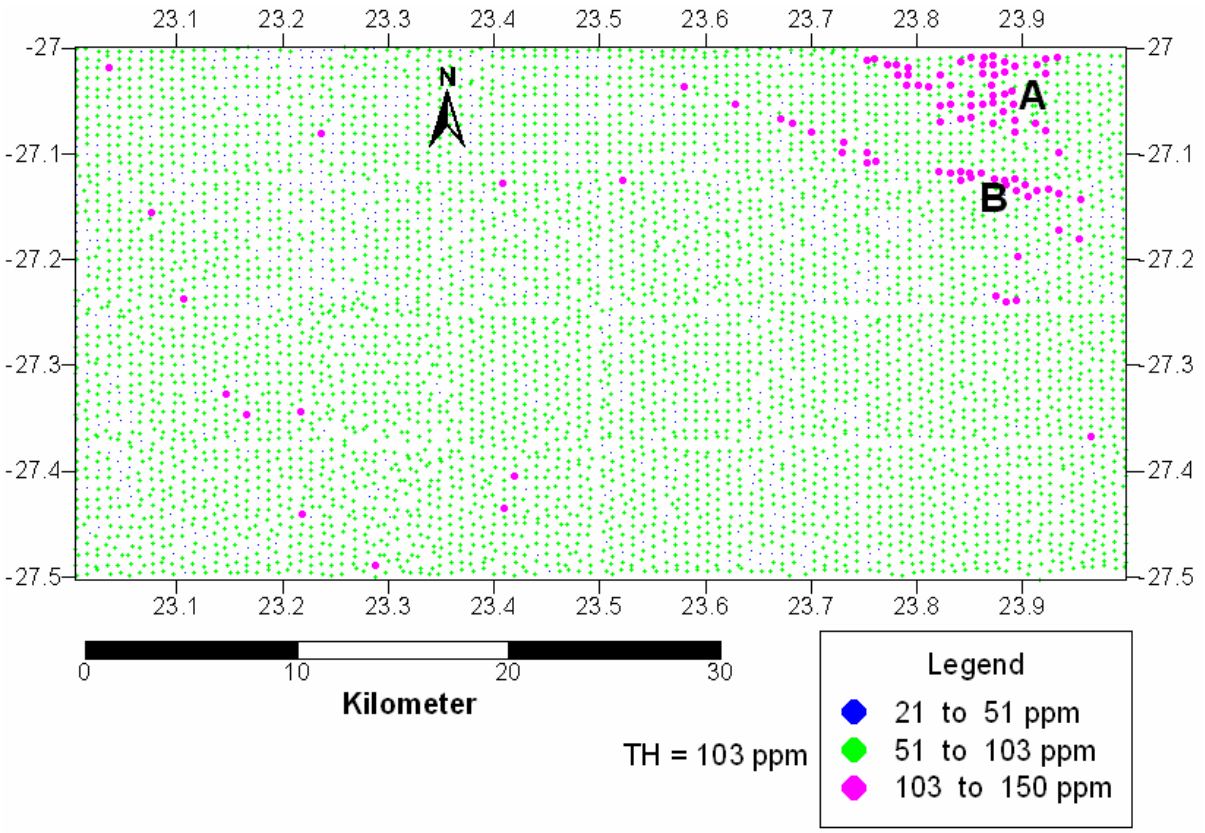

Figure 4.6-7: Distribution of rubidium concentration in the 2723 Kuruman Sheet.

Scandium (Sc) Distribution

Fig. 4.6-8 shows poorly developed distribution patterns of the scandium concentration over calcrete in the Kuruman area (anomaly A). More scandium values are scatted at the southern part of the map or around Kuruman area with the highest value up to 88 ppm. On anomaly B, scadium anomaly is hosted by the Asbestos Hill Formation where the lithologies include banded jaspilite, banded iron formation, riebekite, crocidolite, dolomite and limestone of the Ghaap group. The poorly developed anomalies or trends appear not well distributed (dispersed distribution pattern) with the regional concentrations on the dolomite/limestone of the Ghaap Group towards the south east of the map.

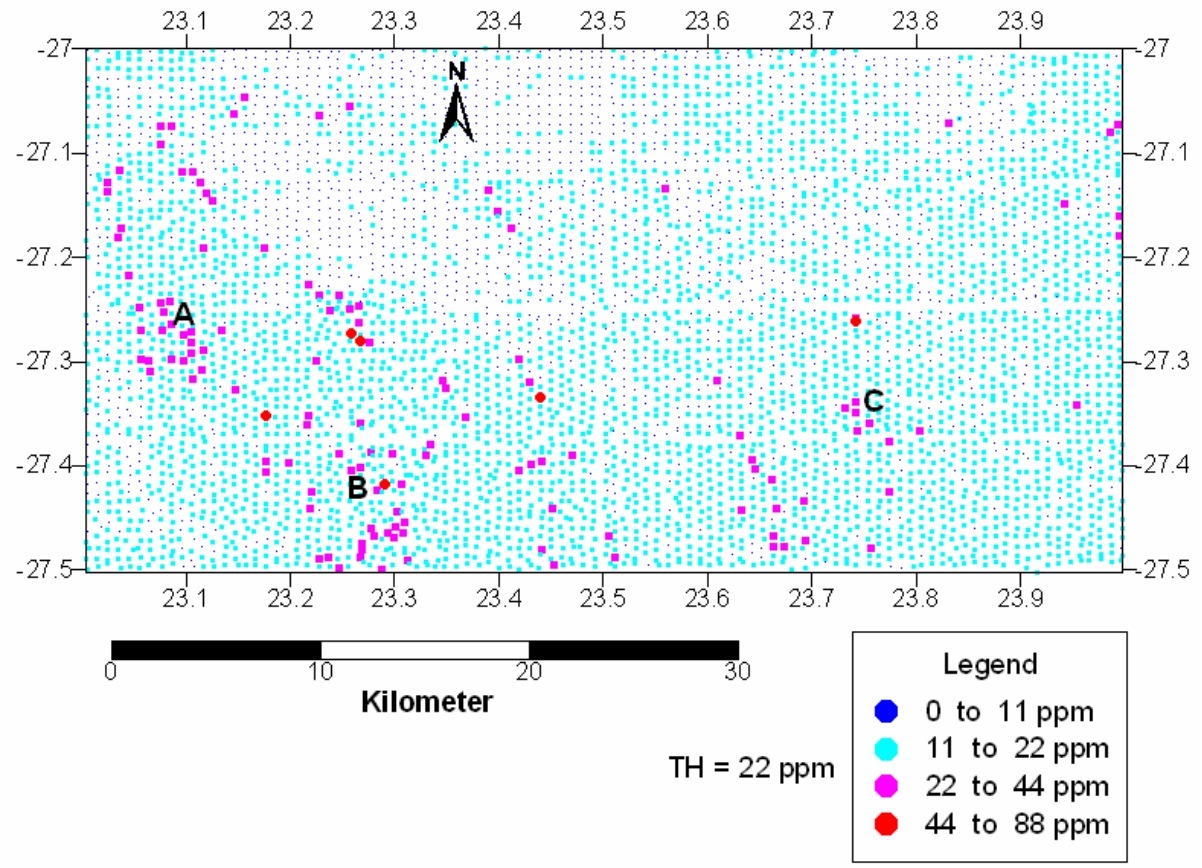

Figure 4.6-8: Distribution of scandium concentration in the 2723 Kuruman Sheet.

Strontium (Sr) and Thorium (Th) Distribution

Figure 4.6-10 shows strontium and thorium. Both thorium and strontium reflect the granitophile associations of these elements in anomaly A. The anomalies are characterized by the strontium values up to 380 ppm and thorium of 35 ppm which lie over the granitic rocks of the Swazian age. South west of the anomaly A the strontium distribution is characterized by the single point anomalies in which most of them are represented by the regional threshold values. Strontium shows a poorly developed belly like trend on the north-western part of the map which is characterized by the dispersed values over the calcrete, calcified padune and surface limestone with the maximum concentration of 508 ppm.

Fig. 4.5-10 (a) and (b), by comparing the strontium and thorium concentration find that both these elements are chalcophile. Thorium is more concentrated and clustered in the granitic

rocks at the northern part while strontium is more clustered towards the south where it forms a V-shape. It can be clearly seen that the granitic rocks of this area have various thorium and strontium concentrations, as the strontium concentration decreases northwards wile the thorium increases and vice-versa with thorium increasing northwards.

Distribution of other elements

The distribution of the following elements does not show any trend. Most of these are represented by the values which are below the regional threshold concentration. These elements include titanium, manganese, cobalt, lead, niobium, yttrium, tungsten, uranium and zinc.

Titanium and manganese show negative trends or anomalies which are characterized by concentrations below the regional threshold values of 2wt%. Negative manganese anomalies occur at the northern corner of the map extending to the map margin.

Cobalt shows two single point anomalies (Fig. 4.6-11) over the iron formation, jaspilite and crocidolite of the Danieslskuil Formation. Their concentration 730 ppm (upper anomalous) and 767 ppm (lower anomalous) and other lithologies have the background concentration values which range between 0 ppm and 80 ppm.

The lithologies on the western part of the map show zirconium concentration which does not show any trend or an anomaly Fig. 4.6-12. Up to 3140ppm of zirconium values are found over the aeolian sand, surface sand, calcrete and dolomite/limestone of the Ghaap Group with clustered zirconium values are found west of the map. The iron formation, jaspilite and crocidolite of the Asbestos Hill Group reflect the background concentration which range between 50 ppm to1300 ppm (Fig. 4.6-11).

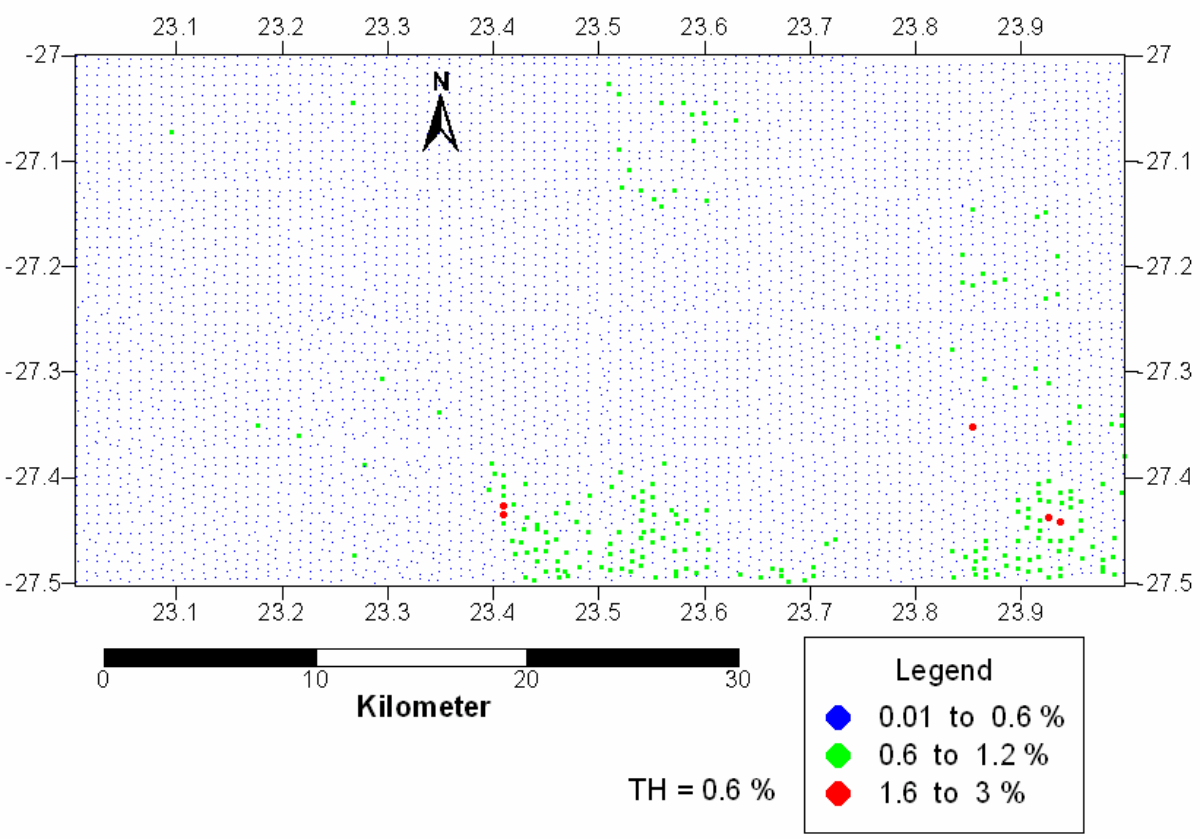

Figure 4.6-9: Distribution of the manganese concentration in the 2723 Kuruman Sheet.

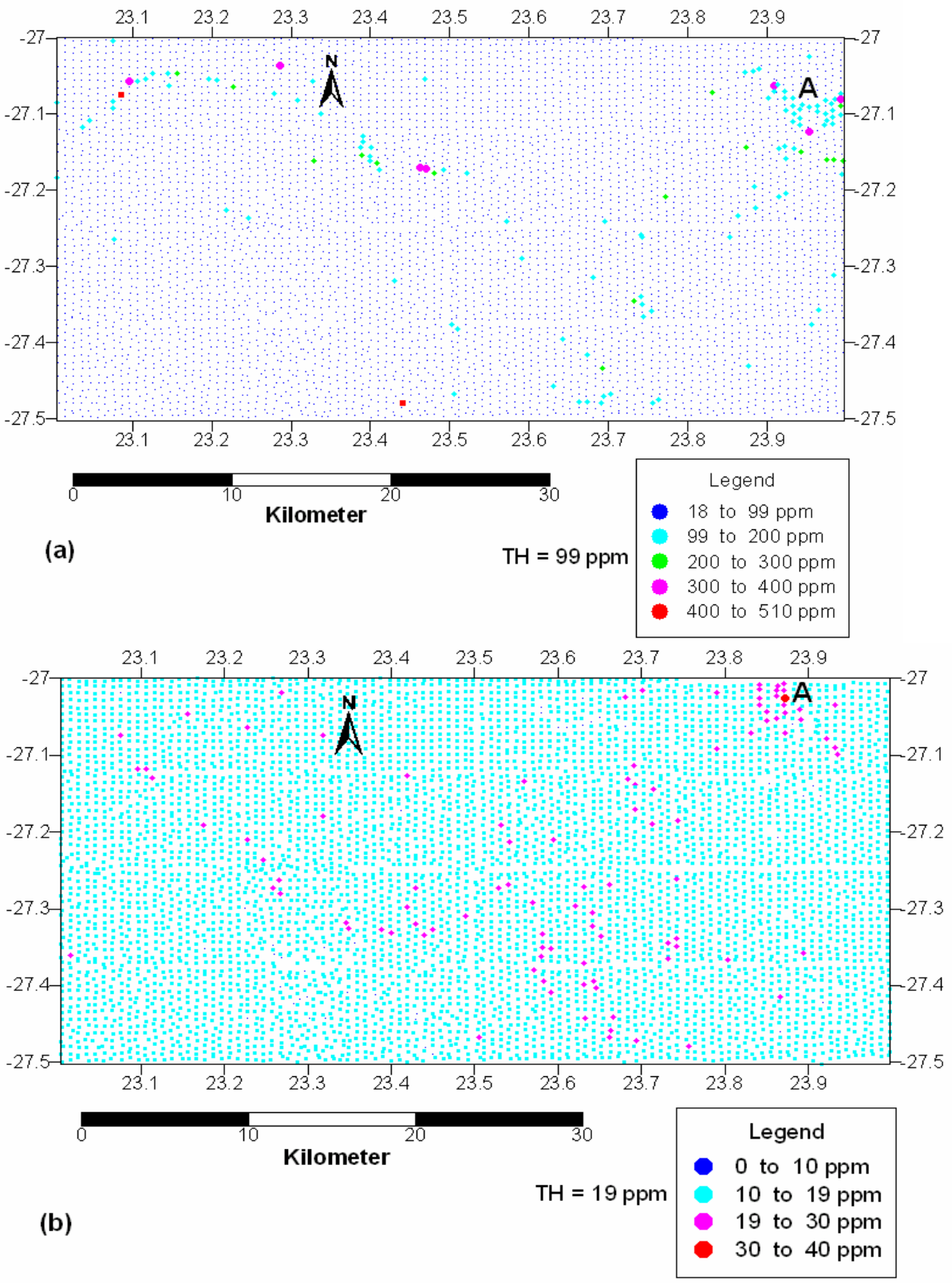

Figure 4.6-10: Distribution of strontium (a) and thorium (b) anomalies in the 2723 Kuruman Sheet.

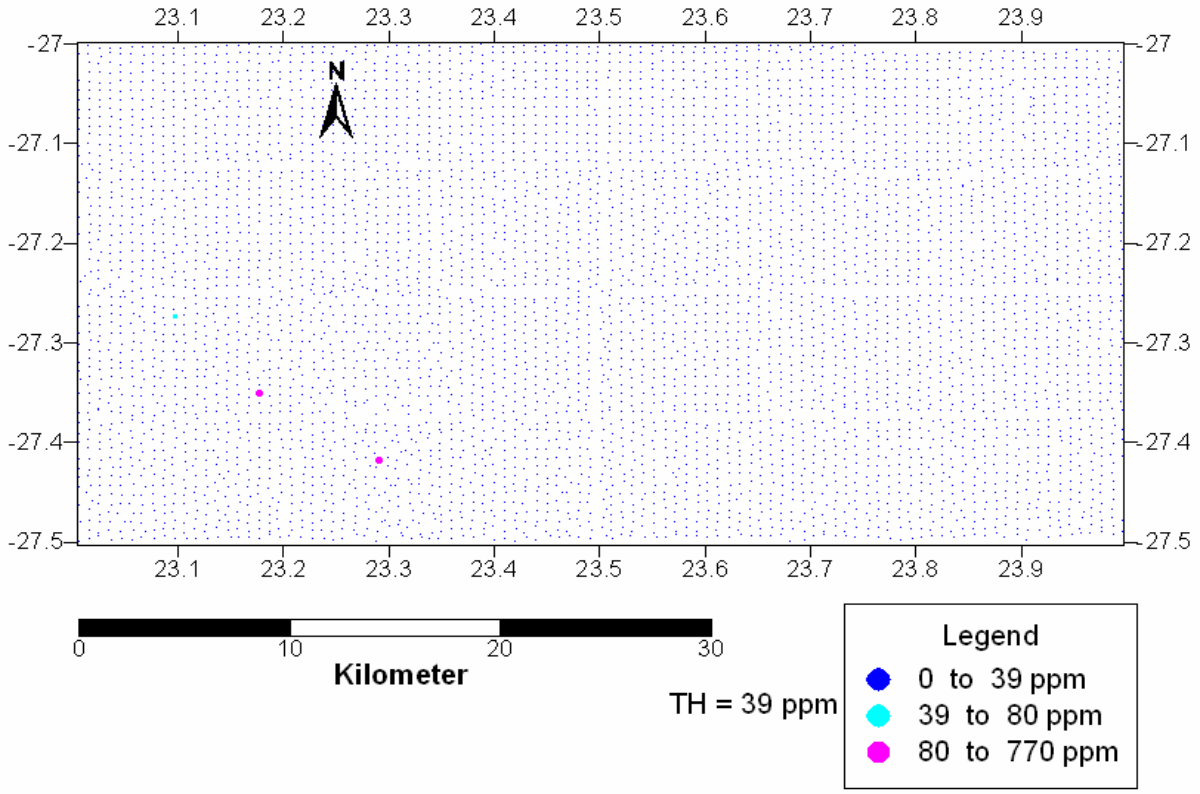

Figure 4.6-11: Distribution of the cobalt distribution in the 2723 Kuruman Sheet.

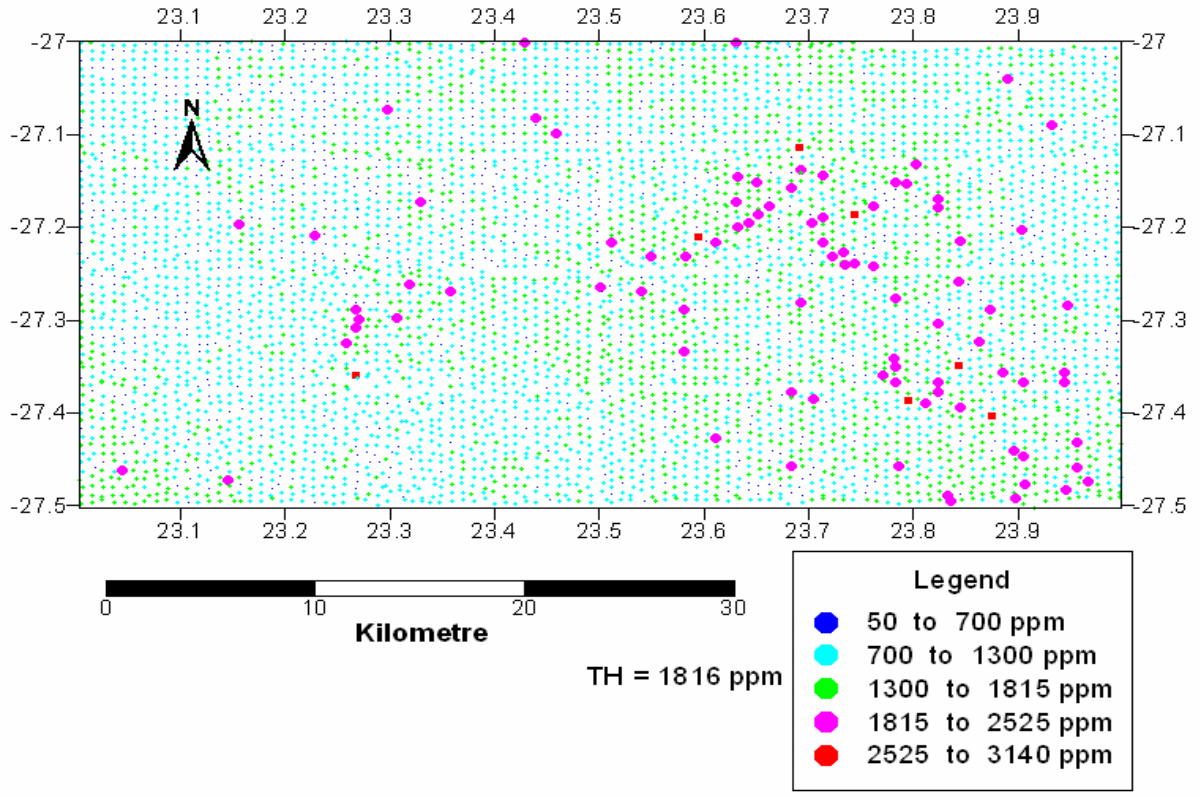

Figure 4.6-12: Distribution of zirconium concentration in the 2723 Kuruman Sheet.

Zinc also shows a single point anomaly which has a maximum concentration of 731 ppm over the calcrete, calcified padune and surface limestone of Tertiary age (Fig. 4.6-17). This single point anomaly at the same position as that of single point anomaly of copper in Fig. 4.6-3. (b)

Yttrium is widely dispersed by the elevated values between 36 ppm-40 ppm. The first poorly developed anomaly is found over the aeolian sand. The yttrium is represented by the single point's anomalies which are more dispersed to each other and are found over the surface sand in the northwestern part of the map. In the central part of the map the single points anomalies are widely dispersed to each other and few on these are found over the Asbestos Hill Group which trend north-south. The points are a few kilometers apart or are not connected to each other and have elevated concentrations of 40 ppm Fig. 4.6-13.

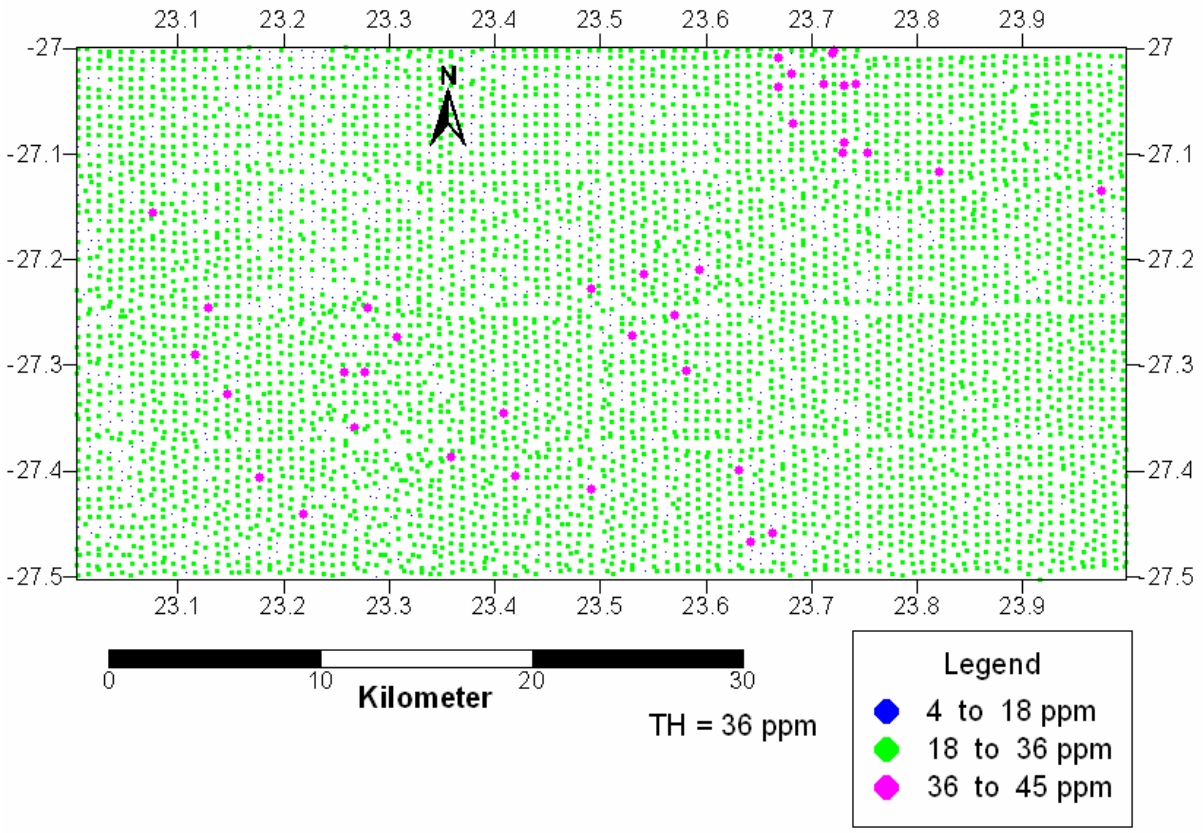

Figure 4.6-13: Distribution of yttrium concentration in the 2723 Kuruman Sheet.

Up to 74 ppm of tungsten concentrations are found over the banded iron formation, riebeckite-amphibolite, chert and crocidolite of the Kuruman Formation. Tungsten is mostly represented by the regional threshold values which are not clustered (Fig. 4.6-14).
Uranium does not show any trend and is also represented by the single point anomalies, which are elevated at the values of 6 ppm in Fig. 4.6-18.

The shales of the Clearwater Formation are characterized by the superjacent lead concentration, which is predominated by the threshold values. Lead is widely distributed in the Danielskuil and Kuruman Formation in the western part of the map, and does not show any trend and any potential area Fig. 4.6-15.

The lithologies of the Kuruman area show poor niobium concentration Fig. 4.6-16. Niobium does not show any values which represent an anomalous area, only few single point anomalies which are represented by the regional threshold values are found over the surface limestone.

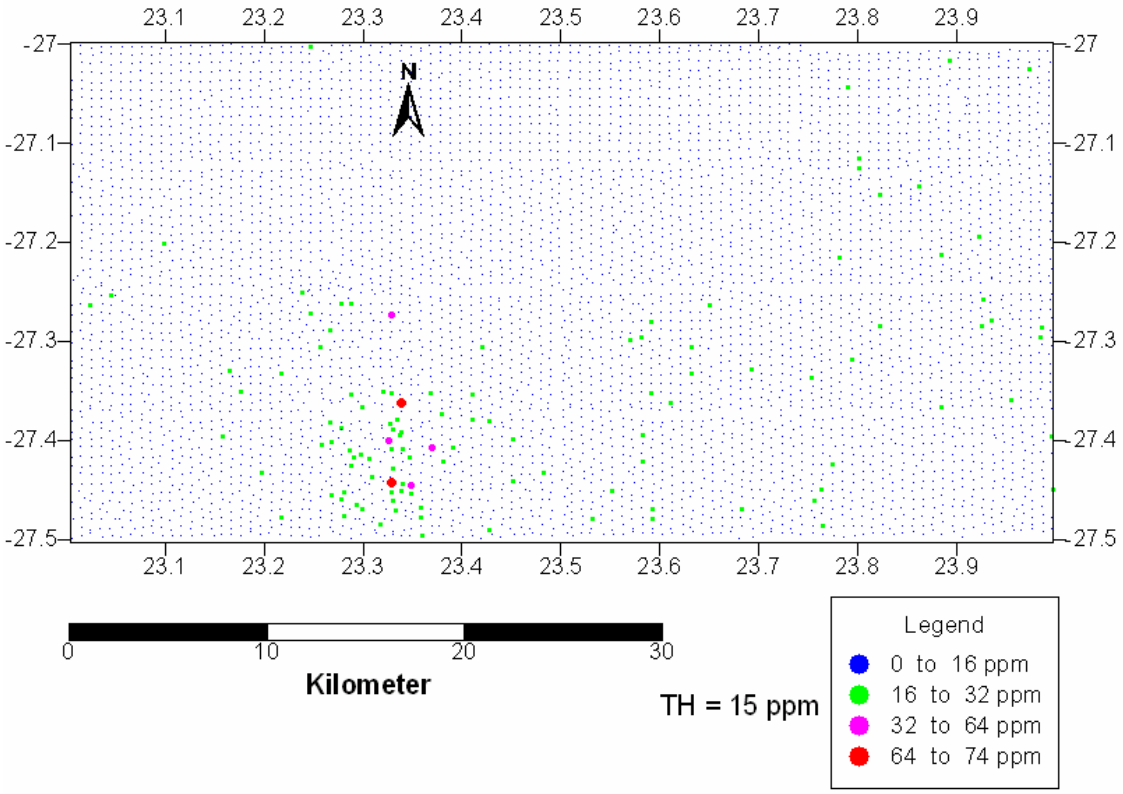

Figure 4.6-14: Distribution of tungsten concentration in the 2723 Kuruman Sheet.

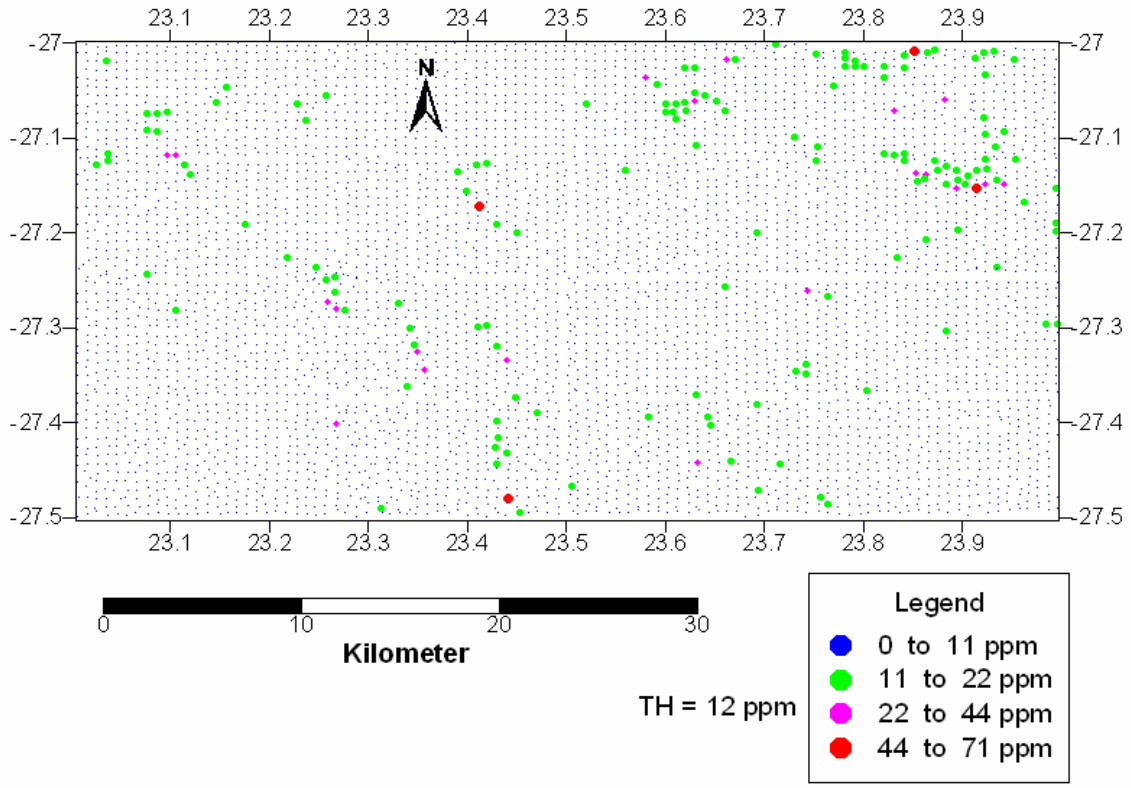

Figure 4.6-15: Distribution of lead concentration in the 2723 Kuruman Sheet.

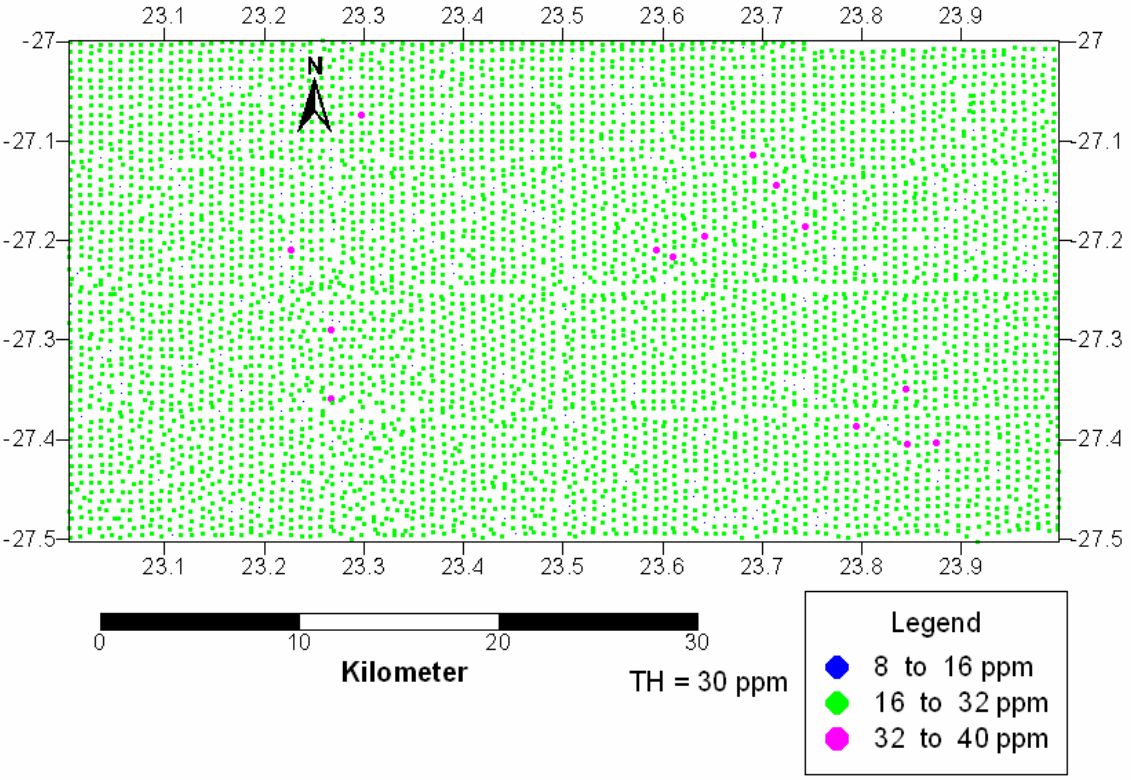

Figure 4.6-16: Distribution of niobium concentration in the 2723 Kuruman Sheet.

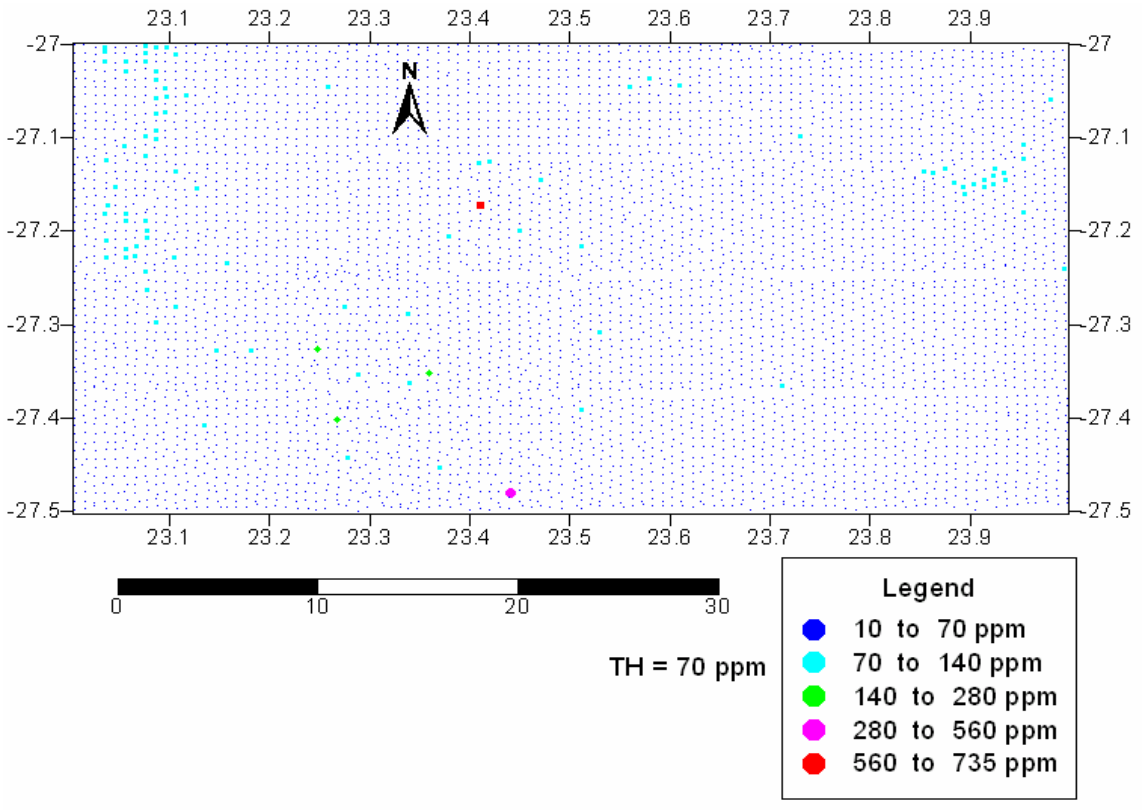

Figure 4.6-17: Distribution of zinc concentration in the 2723 Kuruman Sheet.

4.7 DISTRIBUTION OF ELEMENTS ON THE 2724 CHRISTIANA SHEET

4.7.1 Statistical analysis

A summary of the statistics on the 2724 Christiana Sheet data set (8505 samples) is presented in Table 4.6-1, with the values for threshold values (Thresh Values), minimum, maximum, standard deviation (Std. Dev), mean, range, variance kurtosis and skewness. The mean plus two standard deviation is displaced in the second column to show the general background of the complete data set across various lithological units Contouring intervals for the map were based on a 95% confidence interval (mean + 2 (Std Dev)) to show chemical variation in the different lithological Units. In general the values with concentrations higher than the average plus two times standard deviation (Threshold values) were considered anomalous. On a data set containing different lithological units, anomalous values were calculated separately for each element.

4.7.2 Correlation of elements

Table 4.7-2 shows the correlation matrix of elements in 2724 Christiana Sheets, where most of elements are not well correlated to each other and they had negative correlations. Some elements are correlated to one other and they are not strongly correlated. These elements include; Fe-V, Fe-Cu, Nb-Zr (their correlation matrix was 90%), Fe-Co, Fe-Ni, Ni-Co, Ni-cu, Cu-Co, Ti-Zr, Pb-Zn, V-Co, V-Ni, V-Cu and Ti-Nb, their coefficient of correlations ranging between 70-89%.

Table 4.7-1: Summary statistics on the complete data set for the 2724 Christina Sheet.

Element	N	Min	Max	Mean	Median	St. Dev	Var	CV	Skew	Kurt	Threshold
TiO_2	8205	0.15	4.18	1.18	1.17	0.26	0.07	0.22	1.02	5.57	**1.7**
MnO	8205	0.02	6.53	0.28	0.16	0.31	0.09	1.09	3.84	33.78	**0.9**
Fe_2O_3	8205	0.61	14.10	4.91	4.48	1.65	2.71	0.34	0.85	0.45	**8**
Sc	8204	1.00	49.00	14.48	14.00	3.52	12.39	0.24	0.81	3.62	**22**
V	8204	1.00	321.00	69.35	62.00	32.63	1064.64	0.47	0.88	1.27	**135**
Cr	8203	3.00	959.00	116.06	107.00	55.85	3119.27	0.48	4.03	35.23	**228**
Co	8203	2.00	41.00	14.02	12.00	6.00	35.95	0.43	1.30	1.38	**26**
Ni	8205	13.00	386.00	46.81	38.00	24.07	579.47	0.51	24.07	10.91	**95**
Cu	8203	1.00	157.00	32.31	27.00	16.40	269.00	0.51	1.47	2.37	**65**
Zn	8204	13.00	969.00	53.25	50.00	30.72	943.97	0.58	14.22	340.31	**115**
As	6148	1.00	97.00	11.56	9.00	9.21	84.74	0.80	1.86	5.89	**30**
Rb	8204	13.00	168.00	74.06	75.00	14.80	219.11	0.20	0.24	1.68	**104**
Sr	8203	22.00	640.00	101.39	69.00	79.92	6387.14	0.79	2.52	7.09	**261**
Y	8203	5.00	54.00	24.53	25.00	3.86	14.88	0.16	-0.12	2.58	**32**
Zr	8205	107.00	3705.00	897.69	858.00	322.27	103860.64	0.36	0.99	2.63	**1542**
Nb	8203	6.00	38.00	20.79	21.00	2.67	7.15	0.13	0.43	1.83	**26**
Ba	8205	33.00	1305.00	382.97	381.00	97.71	9546.66	0.26	0.98	5.33	**578**
W	8197	1.00	44.00	8.35	8.00	1.78	3.15	0.21	1.63	26.65	**12**
Pb	6791	1.00	231.00	6.40	5.00	8.56	73.22	1.34	10.16	171.93	**24**
Th	8181	1.00	24.00	13.37	13.00	1.70	2.87	0.13	-0.68	4.94	**17**
U	56	1.00	8.00	1.96	1.00	1.64	2.69	0.83	2.19	4.68	**5**

Table 4.7-2: Correlation matrix of the elements on the 2724 Christiana Sheet.

	TiO_2	MnO	Fe_2O_3	Sc	V	Cr	Co	Ni	Cu	Zn	As	Rb	Sr	Y	Zr	Nb	Ba	W	Pb	Th	U
TiO_2	1																				
MnO	-0.1	1																			
Fe_2O_3	0.11	-0.15	1																		
Sc	0.13	0	**0.72**	1																	
V	0.04	-0.14	**0.9**	0.7	1																
Cr	0	-0.08	0.37	0.3	0.46	1															
Co	-0.04	-0.32	**0.8**	0.61	**0.77**	0.29	1														
Ni	0	-0.25	**0.87**	0.6	**0.78**	0.41	**0.89**	1													
Cu	-0.02	-0.19	**0.91**	0.65	**0.83**	0.26	**0.85**	**0.86**	1												
Zn	-0.07	0.16	0.09	0.08	0.08	0.03	0.02	0.05	0.09	1											
As	-0.69	0.1	-0.27	0.05	-0.18	-0.06	-0.13	-0.2	-0.16	0.03	1										
Rb	0	0.25	-0.18	-0.23	-0.23	0.08	-0.44	-0.29	-0.3	-0.06	-0.03	1									
Sr	0.02	-0.25	0.6	0.44	0.56	0.06	0.69	0.68	0.65	0.03	-0.18	-0.54	1								
Y	0.49	-0.04	0.35	0.22	0.25	0.15	0.12	0.21	0.23	-0.12	-0.43	0.49	0.02	1							
Zr	**0.81**	0.03	-0.4	-0.25	-0.44	-0.17	-0.48	-0.43	-0.51	-0.12	-0.5	0.19	-0.31	0.3	1						
Nb	**0.79**	-0.03	-0.3	-0.19	-0.36	-0.09	-0.42	-0.36	-0.42	-0.26	-0.45	0.31	-0.36	0.5	**0.9**	1					
Ba	0.36	0.04	0.55	0.39	0.56	0.26	0.45	0.46	0.42	0.02	-0.4	0.06	0.35	0.51	0.06	0.09	1				
W	0.26	0.04	-0.1	-0.19	-0.08	0.09	-0.2	-0.13	-0.16	-0.13	-0.13	0.14	-0.19	0.18	0.28	0.32	0.09	1			
Pb	-0.1	0.25	-0.05	0	-0.07	-0.05	-0.12	-0.08	-0.07	**0.88**	0.07	0.06	-0.1	-0.13	-0.06	-0.22	-0.04	-0.14	1		
Th	0.24	-0.18	-0.16	0.11	-0.16	-0.06	-0.1	-0.13	-0.17	-0.32	0.06	-0.01	-0.08	0.23	0.29	0.48	-0.06	0.08	-0.35	1	
U	-0.14	-0.03	-0.06	0.19	-0.04	-0.08	0.04	-0.01	-0.03	-0.02	0.25	-0.15	0.14	-0.17	-0.1	-0.13	-0.09	-0.17	0.03	0.12	1

4.7.3 Statistical distributions

Titanium, yttrium, niobium, barium, tungsten and thorium show leptokurtic, normal distributions with occasional outliers. Rubidium is normally distributed, with a slight bimodal character. Chromium, scandium, nickel and zirconium have asymmetrical, positively skewed distribution where most of the high concentrations are on the andesitic lava of the Allanridge Formation and zirconium shows the opposite way and has a high concentration over the lithologies of the western part of the area.

Zinc and lead have similarly asymmetrical, positively skewed distribution. These two elements have high concentrations over the carbonate rocks of the Reivilo Formation, as compared to the entire areas or lithologies. Iron, vanadium and cobalt show bimodal positively skewed distributions. These elements have high concentrations over the lithologies of the eastern part of the map where the mafic rocks predominated, in the western part of the map they are fairly represented by a low concentration. Uranium shows any poor distribution (Fig. 4.7-1).

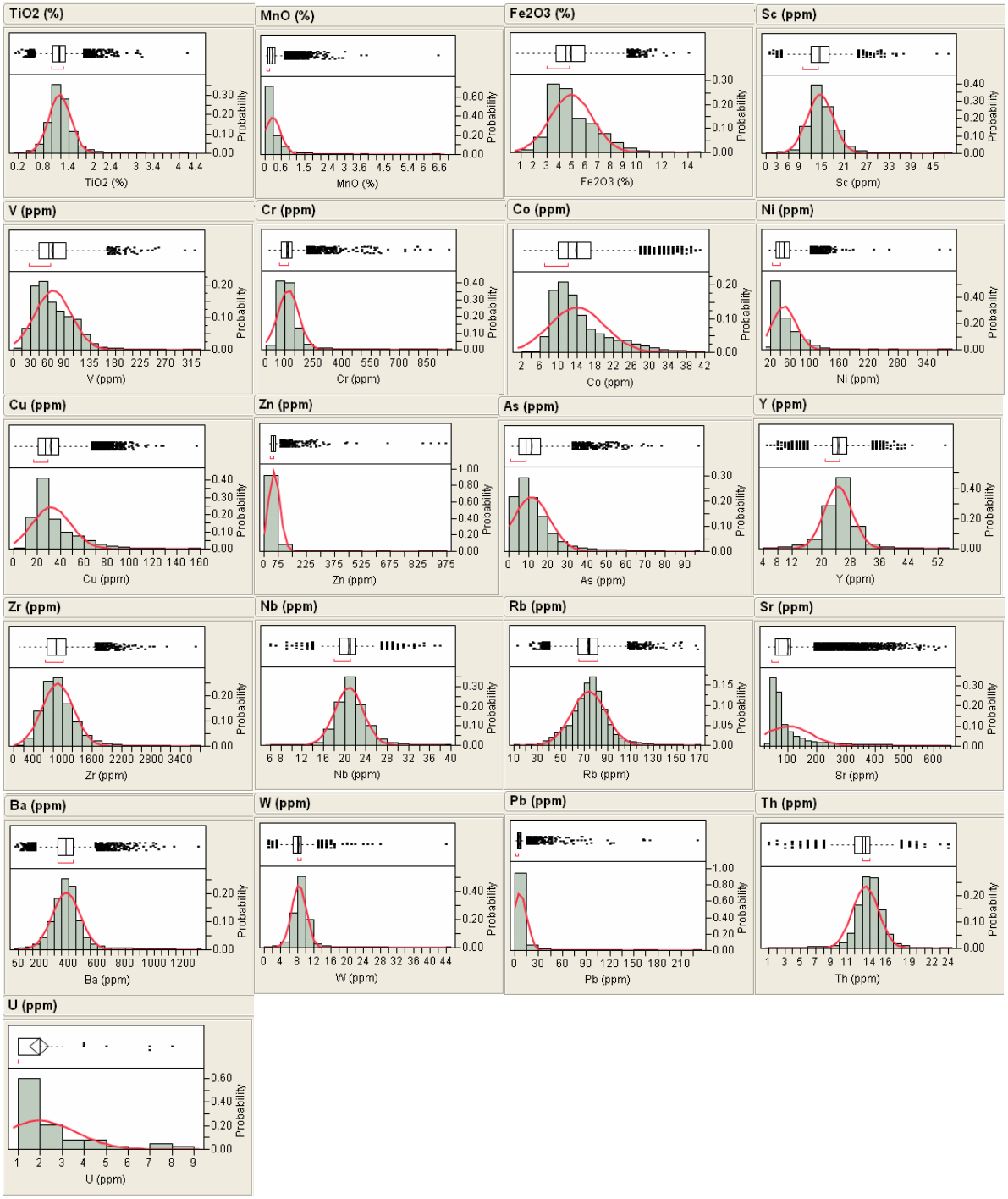

Figure 4.7-1: Histograms and box plot of the elements on the 2724 Christiana Sheet.

4.7.4 GEOCHEMICAL DISTRIBUTION

Chromium (Cr) Distribution

Fig. 4.7-2 shows chromium distribution in the Christiana area with anomaly A found over the Dwyka Tilite on the northern part of the map, as proceeding southwards of anomaly A. The chromium values are more clustered over the shale, siltstone with interbanded dolomite of the Boomplaas Formation.

Anomaly B is found over the diamictite, shale and mudstone of Dwyka Group. The anomaly is characterized by the widely clustered values dominated by the regional threshold values. Anomaly C (far western side of the map) mainly consists of elevated values (between 228 ppm to 400 ppm) and is characterized by a clustered distribution pattern extending west to east and reflecting the mafic rocks of the Allanridge Formation.

Nickel (Ni) and Iron (Fe) Distribution

The tholeiitic, calc alkali basalt and andesitic lava of the Allanridge Formation show north - south nickel and iron trends. Nickel is characterized by the regional threshold values of up to 370 ppm and iron 8-9wt% (Fig 4.6-3 and Fig. 4.7-4, anomaly A). On the eastern part of the map, nickel and iron are clustered and widely distributed. The anomalies cover a wide area, moving toward south on the map where the concentrations of both nickel and iron become scattered and narrower.

The second nickel anomaly is found over the tholeiitic basalt on the north-west of the map (Anomaly B).
A few scattered concentration of iron with maximum values of 14wt% (anomalous B) are found over the andesitic lava of Vryburg Formation.

Zinc (Zn) and Lead (Pb) Distribution

Zinc and Lead have elliptical anomalies over chert-poor dolomite of Reivilo Formation (Fig. 4.7-5 and Fig. 4.7-6). The zinc anomalies have a maximum value of 3442 ppm while lead has a maximum value of 911 ppm. Both zinc and lead values increase as moving towrds to the centre of the area A. These two elements are associated with sphalerite and galena in the dolomitic rocks. Both zinc and lead anomalies are reflect the known Mississippi Valley Type deposit.

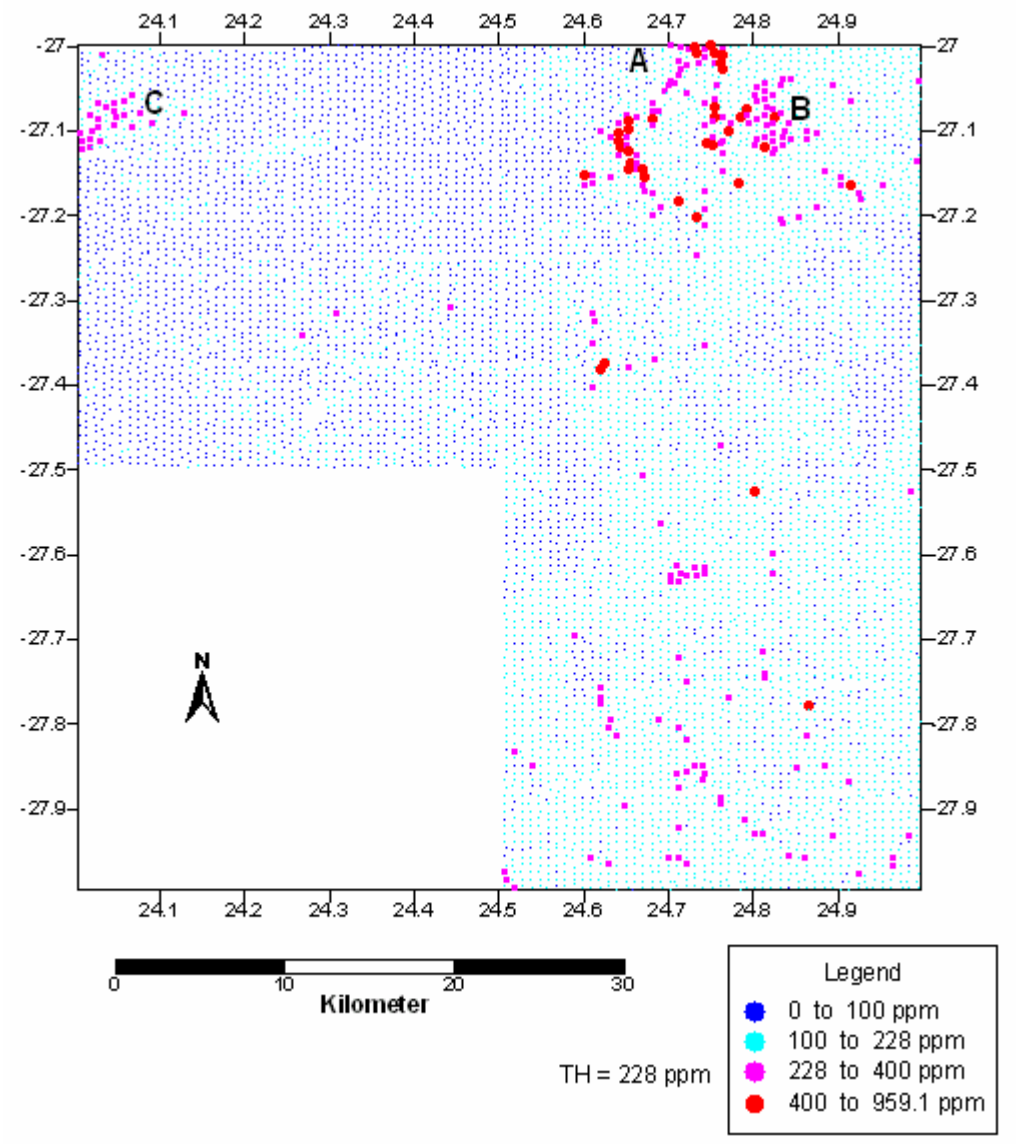

Figure 4.7-2: Classed post map of chromium anomalies in the 2724 Christiana Sheet.

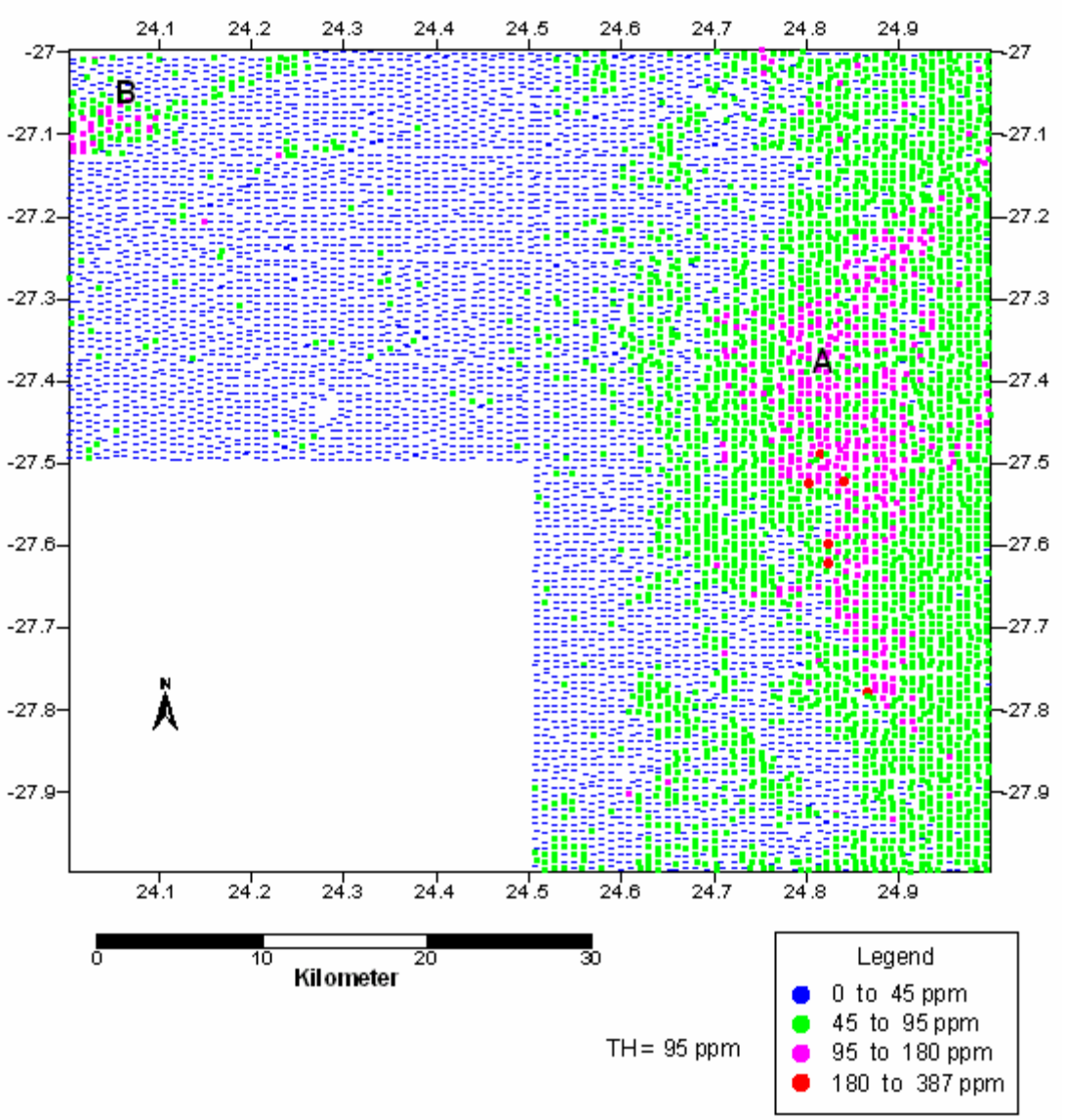

Figure 4.7-3: Classed post map of nickel distribution in the 2724 Christiana Sheet.

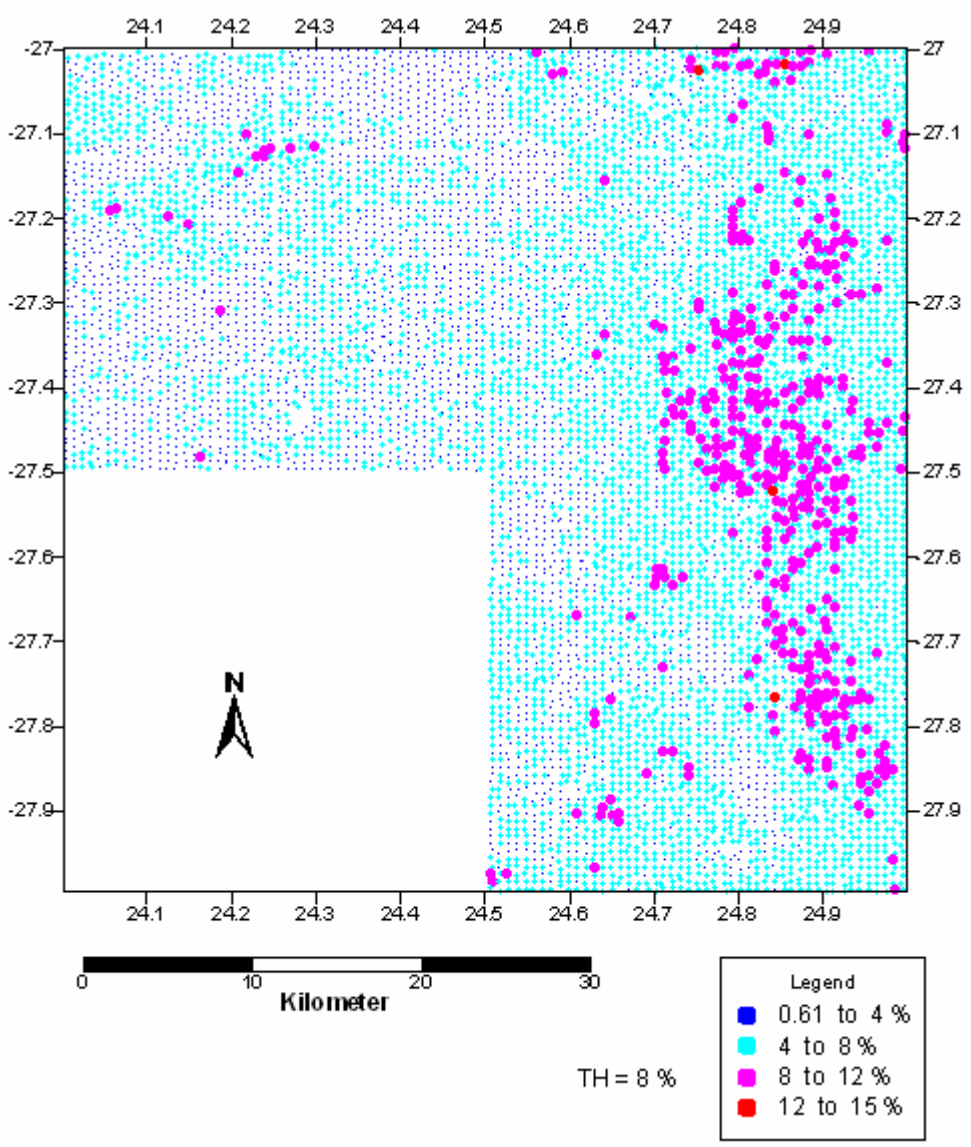

Figure 4.7-4: Classed post map of iron distribution in the 2724 Christiana Sheet.

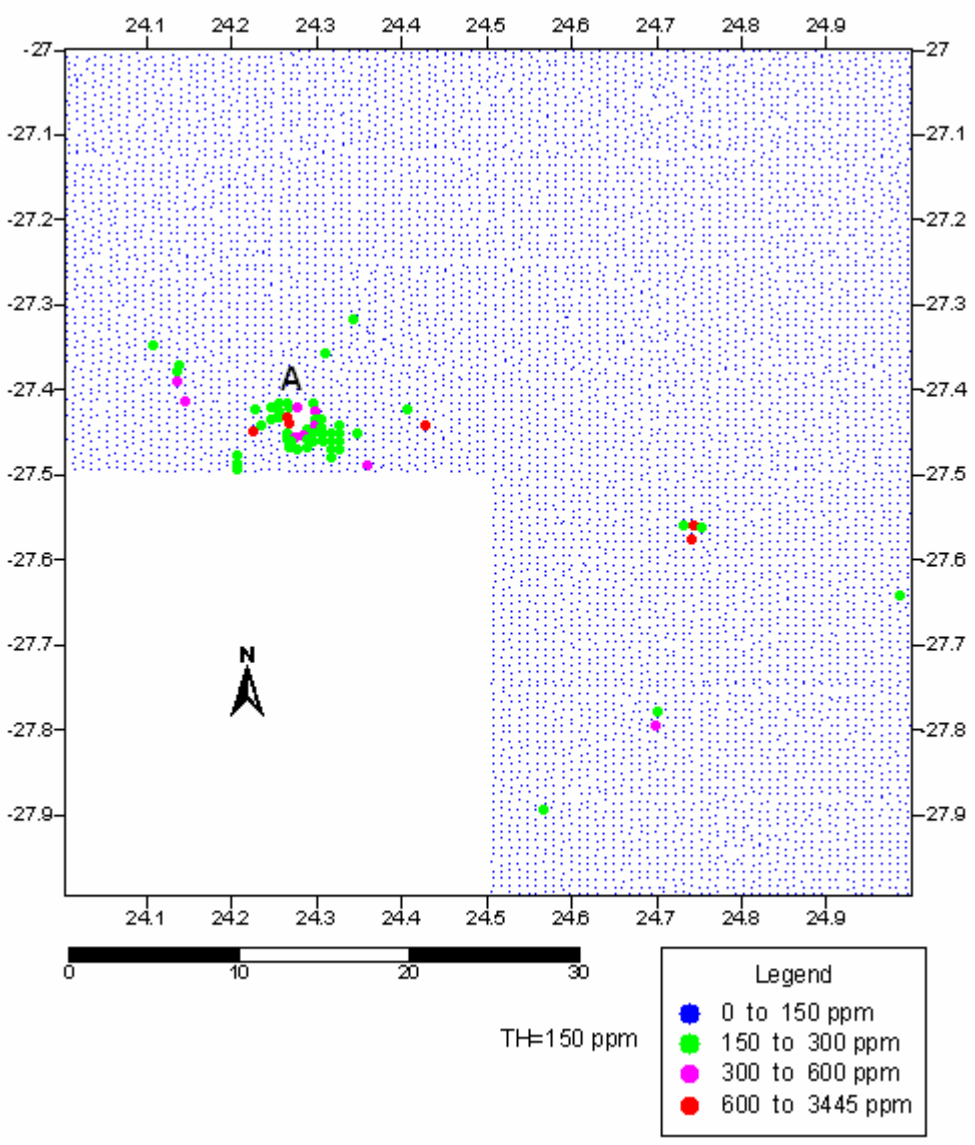

Figure 4.7-5: Classed post map of zinc anomaly in the 2724 Christiana Sheet.

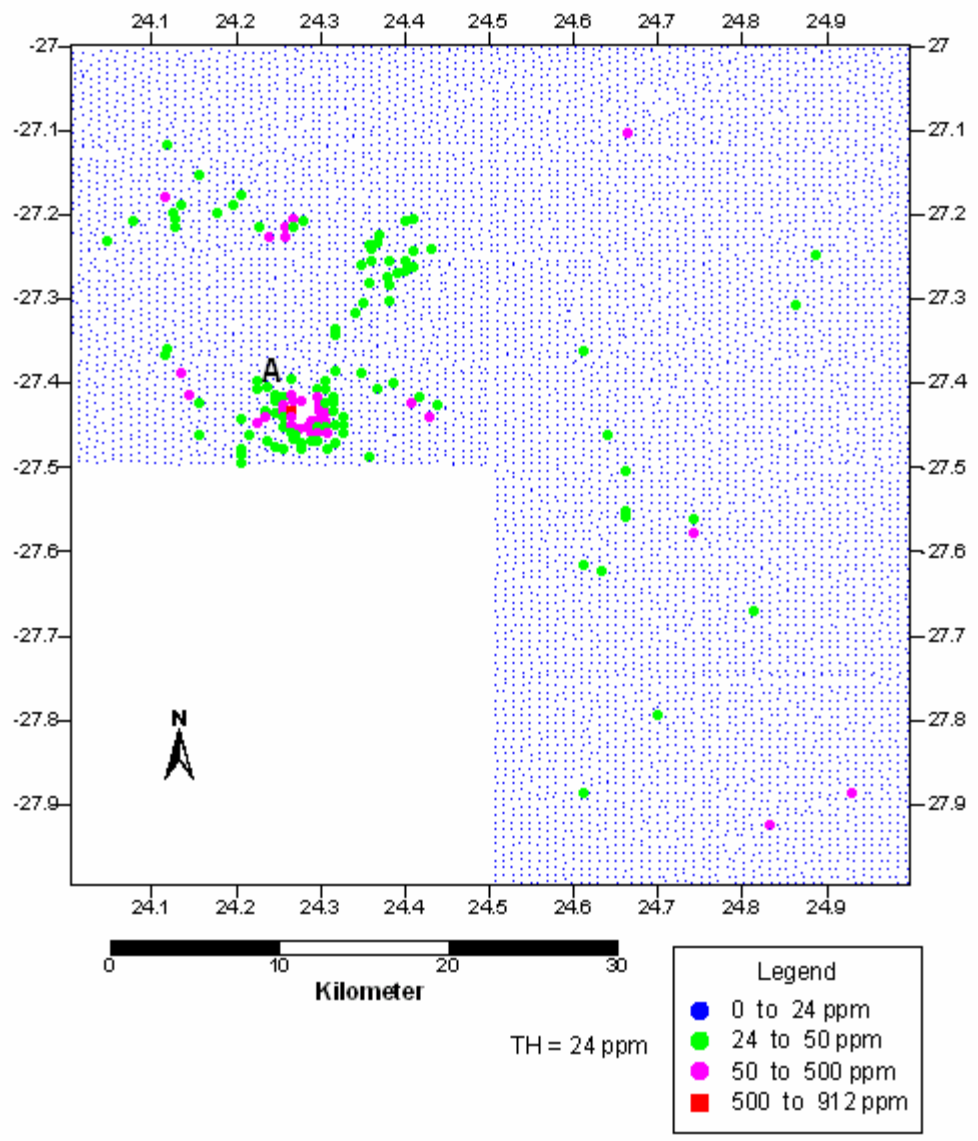

Figure 4.7-6: Classed post map of lead anomaly in 2724 Christiana Sheet.

Barium (Ba) distribution

Barium shows a north south trend A around the Hartwater area (Fig. 4.7-7), the trend is characterized by a clustered distribution and has a maximum concentration of 1306 ppm over the light green tholeiitic, calc alkali basalt and andesite .and carbonate rocks with chert layers conglomerate and tuffaceous sediments. The Barium in this area is associated with the carbonate rocks since it replaces the calcium based on their chemical behavior. As moving (north) of anomaly A, barium has scattered concentration dominated by the threshold values over the andesitic lava of Allanridge Formation and shale, conglomerates of the Kameeldoorns Formation.

Second barium anomaly B which shows a poorly developed elliptical shape and a scattered distribution pattern is found over the calcrete, calcified pandune and surface limestone.

Yttrium (Y) Distribution

The light green tholeiitic calc-alkali basalt and andesitic rocks of Rietgat Formation are characterized by the north-south trend of the yttrium superjacent anomaly (Fig. 4.7-8, anomaly A). Up to 54 ppm of Yttrium values are found south of the Hartswater area. Like barium, south of the Hartswater area the yttrium concentration become scattered and has elevated values.

The anomaly B of yttrium is found almost in the center of the map, and it is mostly represented by the threshold values which form circular scattered distribution over shale and minor dolomite of the Clearwater Formation and interbanded shale of the Monte Christo Formation. About 20 km north of anomaly B, yttrium is characterized by the elevated values forming clustered pattern (anomaly C) over andesitic lava of the Vryburg Formation.

Far west of Anomaly C around the Zwartfontein area, is characterized by the regional threshold and scattered distribution of yttrium concentration.

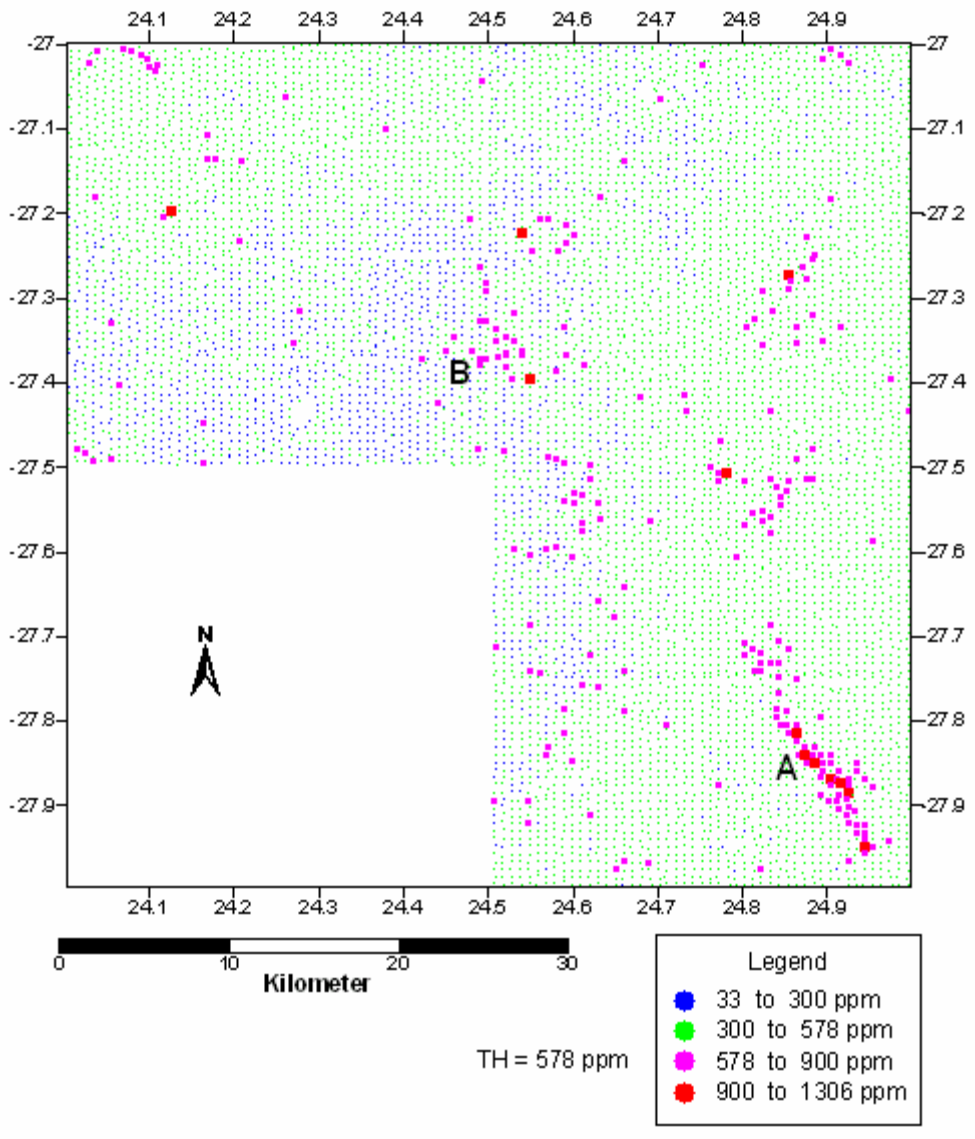

Figure 4.7-7: Classed post map of barium anomalies in the 2724 Christiana Sheet.

Strontium (Sr) Distribution

Strontium is characterized by the north-south trend over the tholeiitic basalt of the Allanridge Formation (Fig. 4.7-9). Up to 645 ppm of strontium element is found in this anomaly. The concentrations of strontium show a clustered distribution pattern of the regional threshold values over the Allanridge Formation. High Strontium concentrations or values are found over the light-coloured fine-medium fine granite and gneiss of the Swazian age.

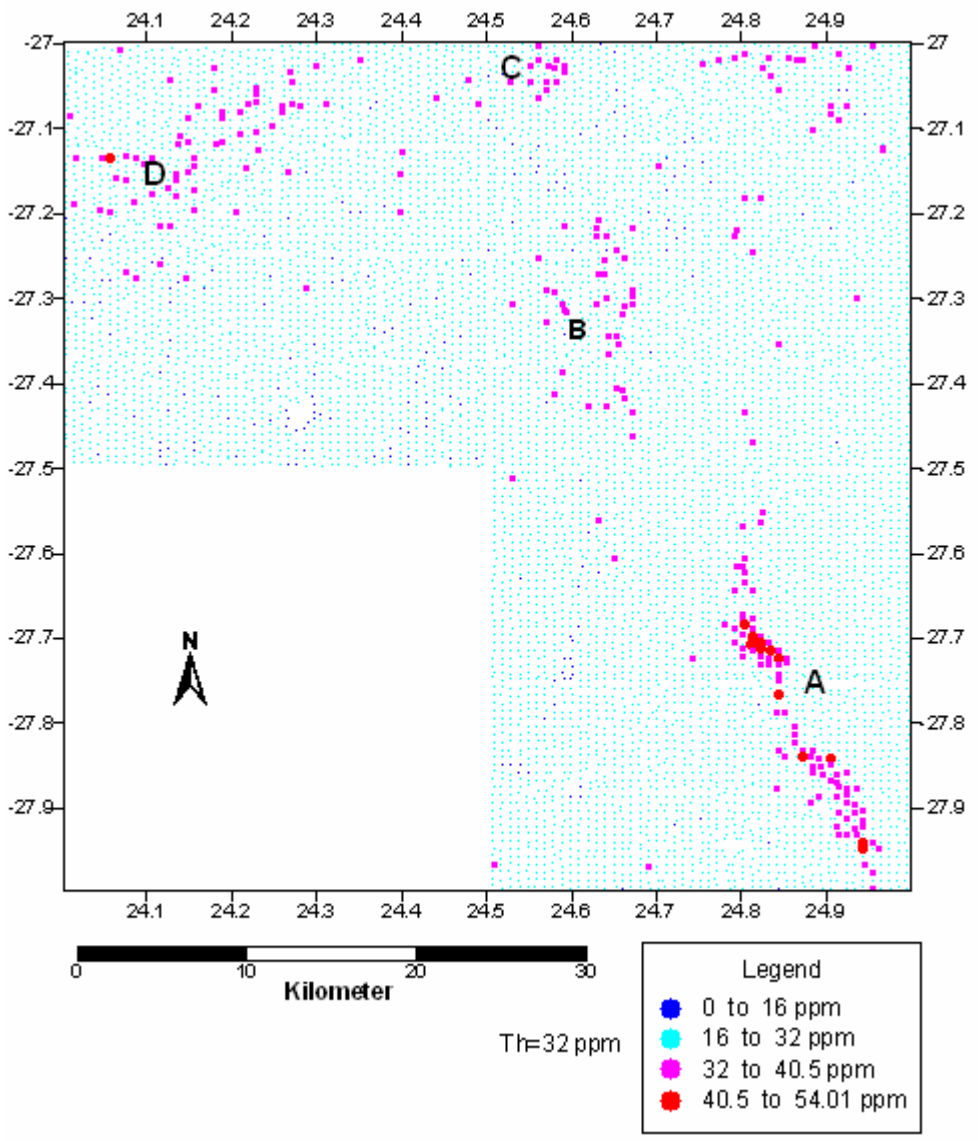

Figure 4.7-8: Classed post map of yttrium anomalies in the 2724 Christiana Sheet.

Copper (Cu) and Cobalt (Co) Distributions

Anomaly A of both copper and cobalt show the same trend as Strontium, iron and nickel distributions. In Fig. 4.7-10 and Fig. 4.7-11, both copper and cobalt anomalies are represented by the regional threshold concentration, where the copper anomaly is predominately concentration between 65 ppm to 105 ppm. Cobalt has maximum values of up to 160 ppm found over the tholeiitic basalt of Allanridge Formations and granitic rocks of the Swazian Age. Copper concentrations are very low (less than 65 ppm). The andesitic lava of

the Vryburg Formation is characterized by elongated shape and clustered values of copper concentration (Fig. 4.7-10, anomaly B), up to maximum values of 157 ppm of copper is found over this Formation.

The cobalt major anomaly is mostly represented by the background concentration between 26-45 ppm.

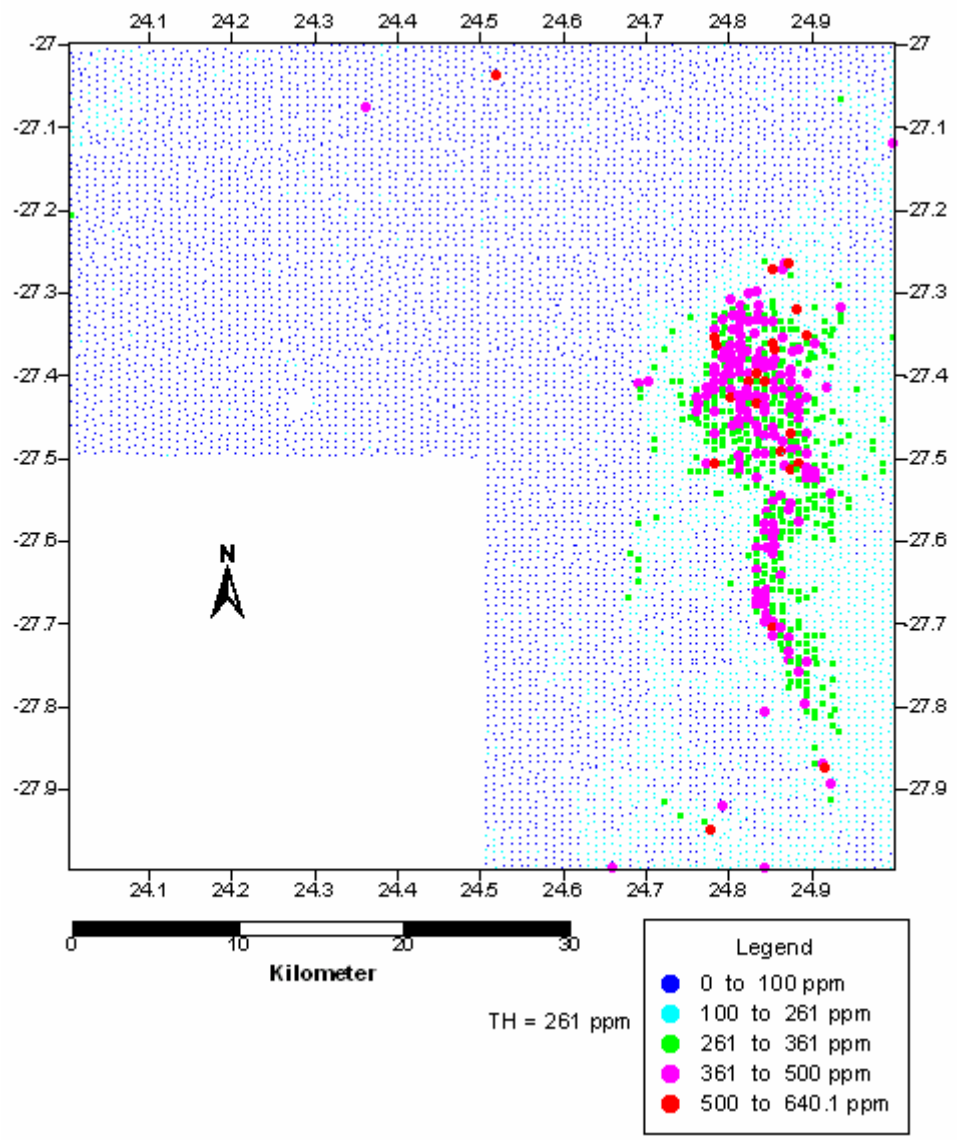

Figure 4.7-9: Classed post map of strontium distribution in the 2724 Christiana Sheet.

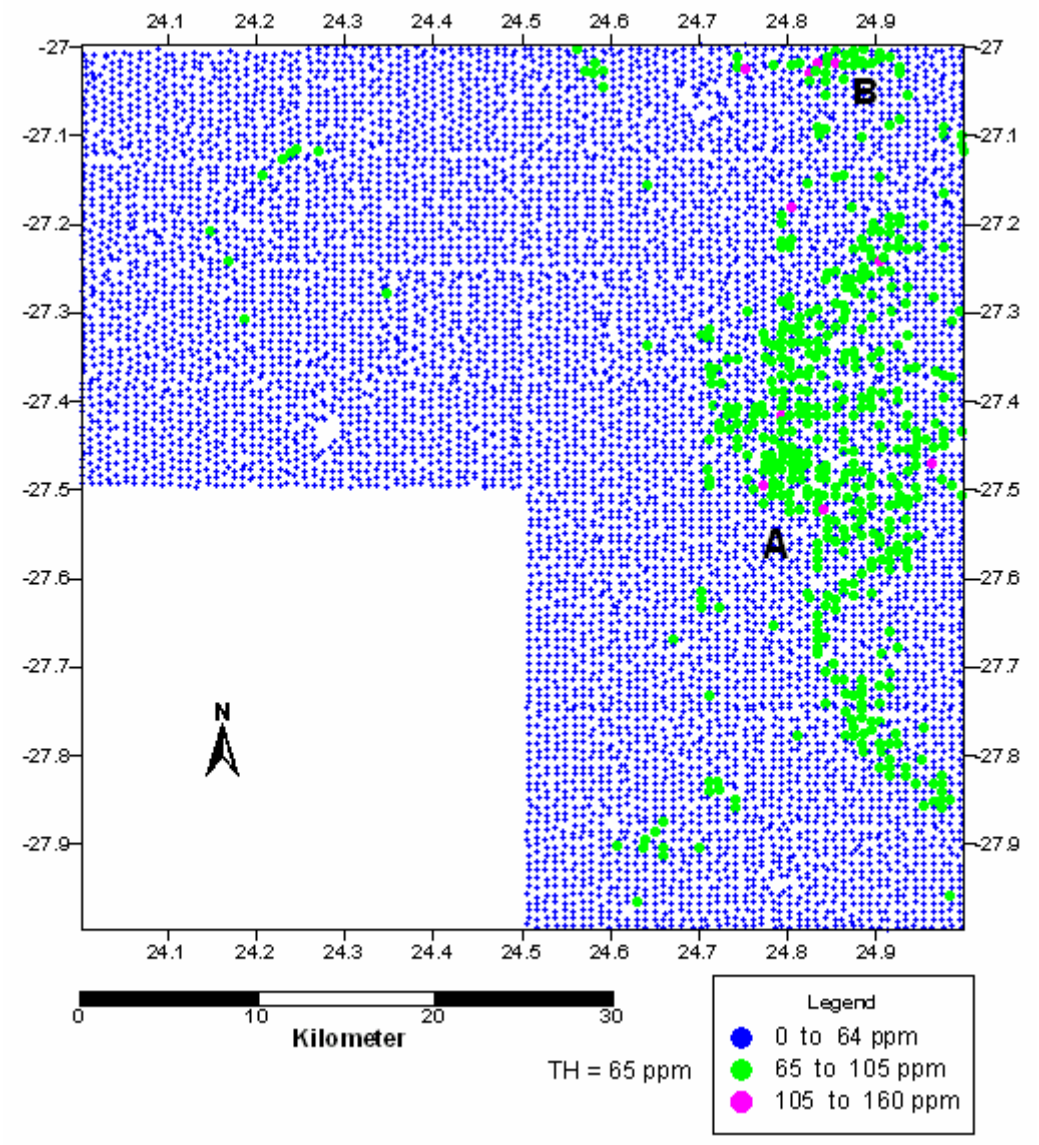

Figure 4.7-10: Classed post map of copper anomalies in the 2724 Christiana Sheet.

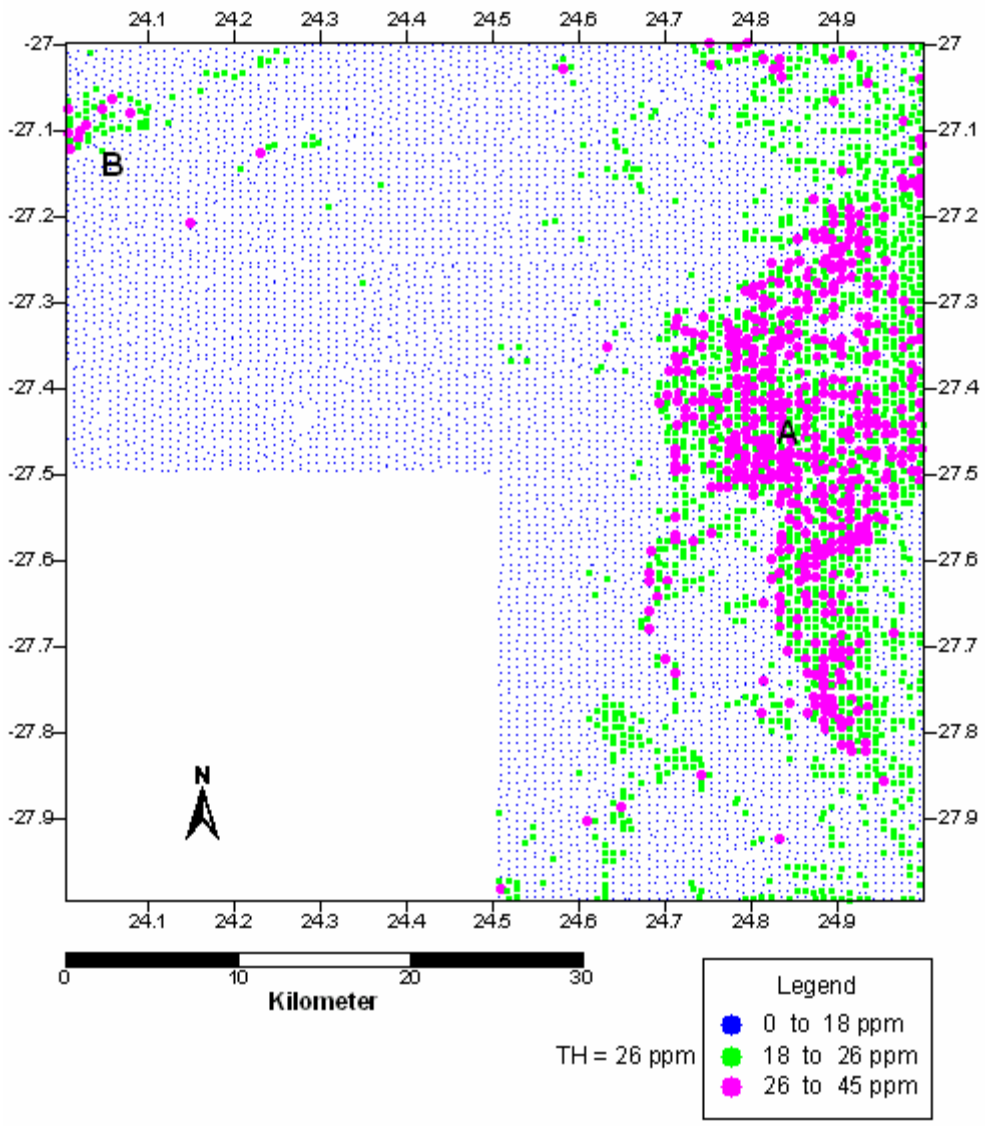

Figure 4.7-11: Classed post map of cobalt anomalies in the 2227 Christiana Sheet.

Zirconium (Zr) Distribution

Fig. 4.7-9 shows the distribution of zirconium concentration on the 2724 Christiana Sheet, with the major north to south trend (A), elongated in shape and covers a few kilometers with clustered distribution patterns with maximum values of 3705 ppm. Anomaly B is characterized or mainly consists of the regional threshold values which have a clustered pattern. Anomaly C shows scattered distribution patterns and is mostly dominated by

theelevated values. All zirconium anomalies in this area are found over the aeolian sand of the Gordonia Formation.

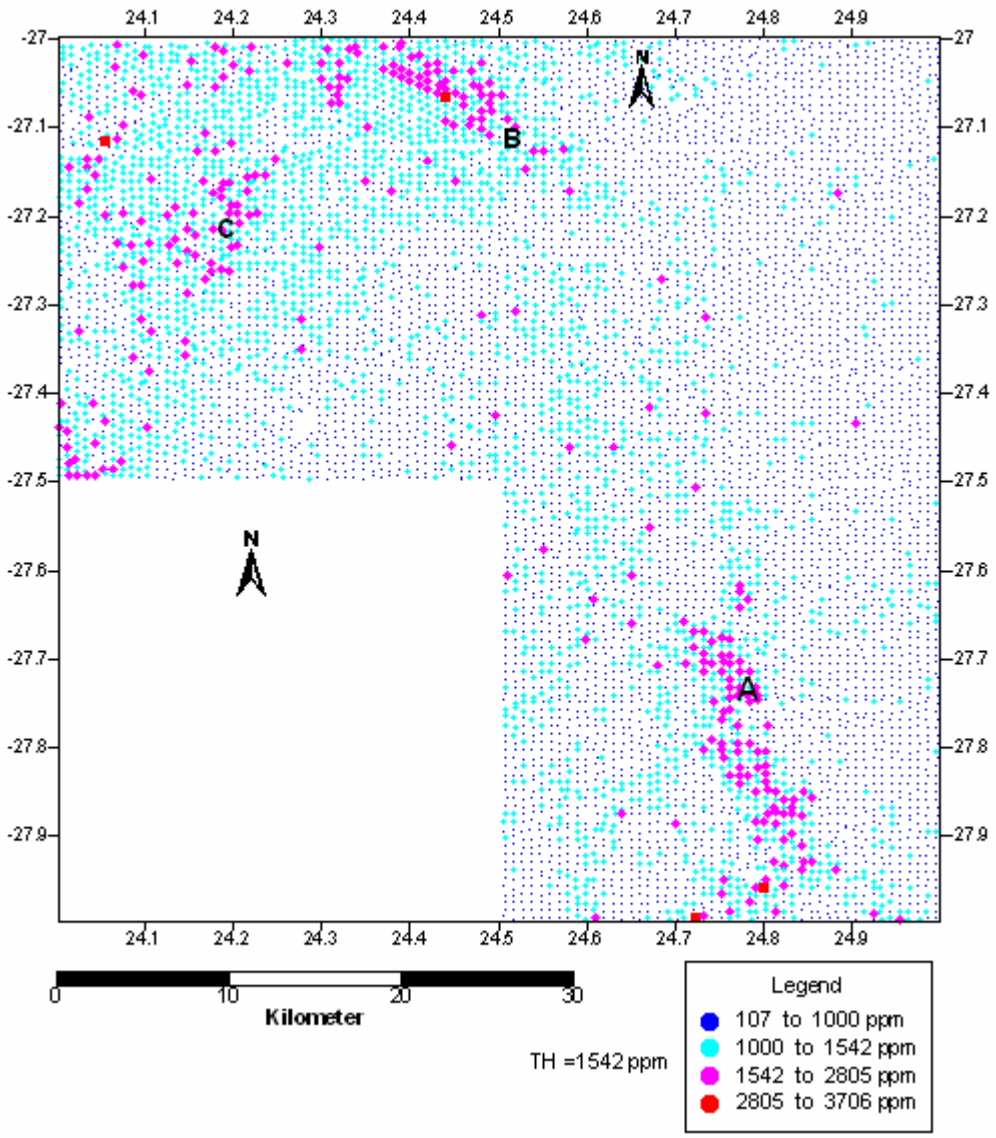

Figure 4.7-12: Classed post map of zirconium anomalies in the 2724 Christiana Sheet.

Rubidium (Rb) Distribution

Shale and dolomite of the Clearwater Formation show two rubidium anomalies (anomaly A and B) in Fig. 4.7-13. Anomaly A shows north to south trend which is characterized by clustered distribution of the Zr elevated values. This anomaly is found over the shale and dolomite of the Clearwater and Monte Christo Formations. Anomaly B resembles the shape of the lithologies in the area (east- west trend) and has a scattered distribution pattern. Over the tholeiitic basalt of Allanridge Formations and granitic rocks, where iron, nickel, strontium and vanadium are characterized by high values, rubidium has a negative anomaly area C.

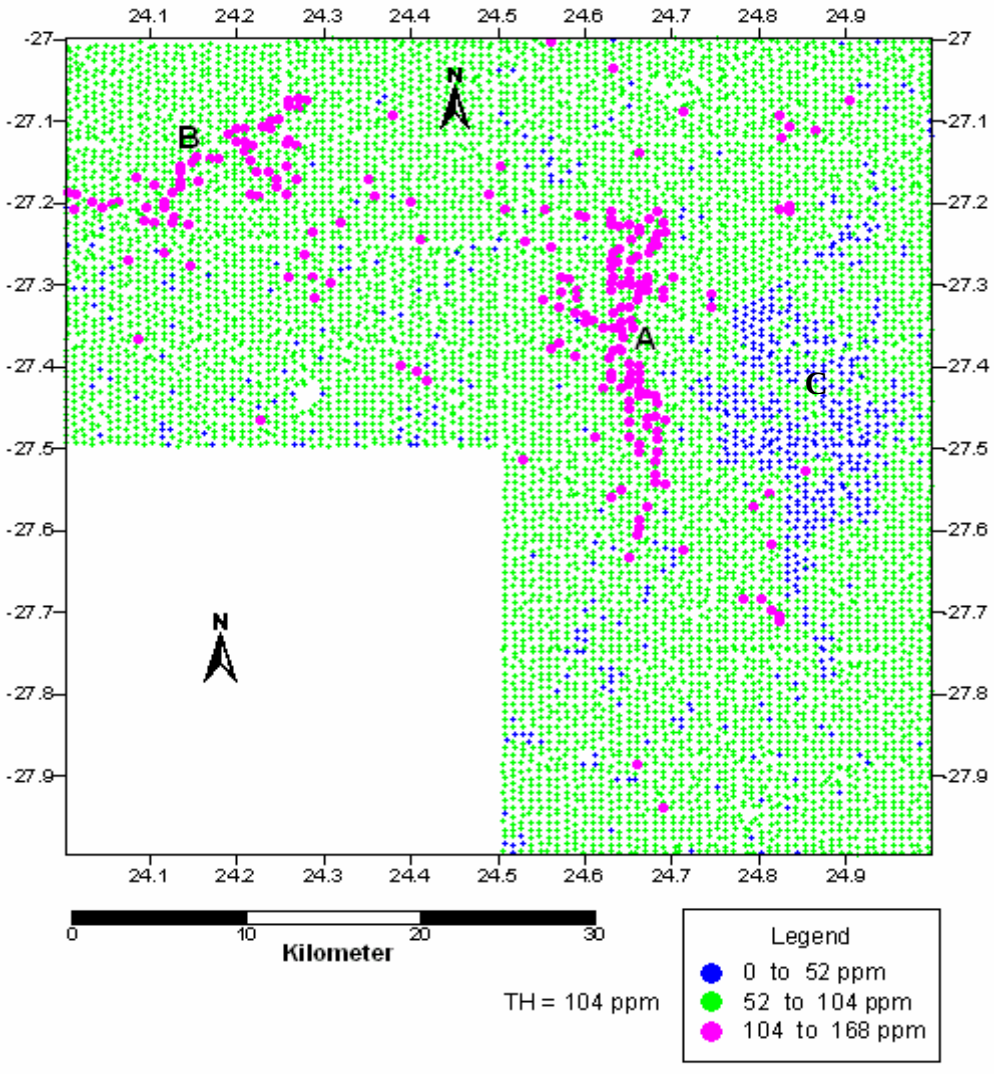

Figure 4.7-13: Classed post map of rubidium anomalies in the 2724 Christiana Sheet.

Vanadium (V) Distribution

Fig. 4.7-14 shows the geochemical distribution of vanadium in the Christiana area. In the western part of the map, over the surface sand and the carbonaceous rock of the Gordaonia and Reivilo Formations vanadium is mainly characterized by lower concentration (two times lower than the threshold values). Over the andesitic lava of Allanridge Formation (eastern part of the map) vanadium is mainly predominately by a threshold values. It shows the scattered distribution of the positive anomalies (A) over the diamictite of the Dwyka Group.

Distributions of other Elements in Christiana

These elements include Manganese, thorium, scandium, niobium tungsten titanium and uranium. Manganese in this area is mostly characterized by a lower concentration (below threshold value) and it only shows single point anomalies Fig. 4.6-15.

Uranium, titanium thorium, scandium and tungsten have a background concentration over the entire area. These elements do not show any trend within the study area. Niobium show background anomalies over the surface sand of the Gordonia formation (Fig. 4.7-16, to Fig. 4.7-20).

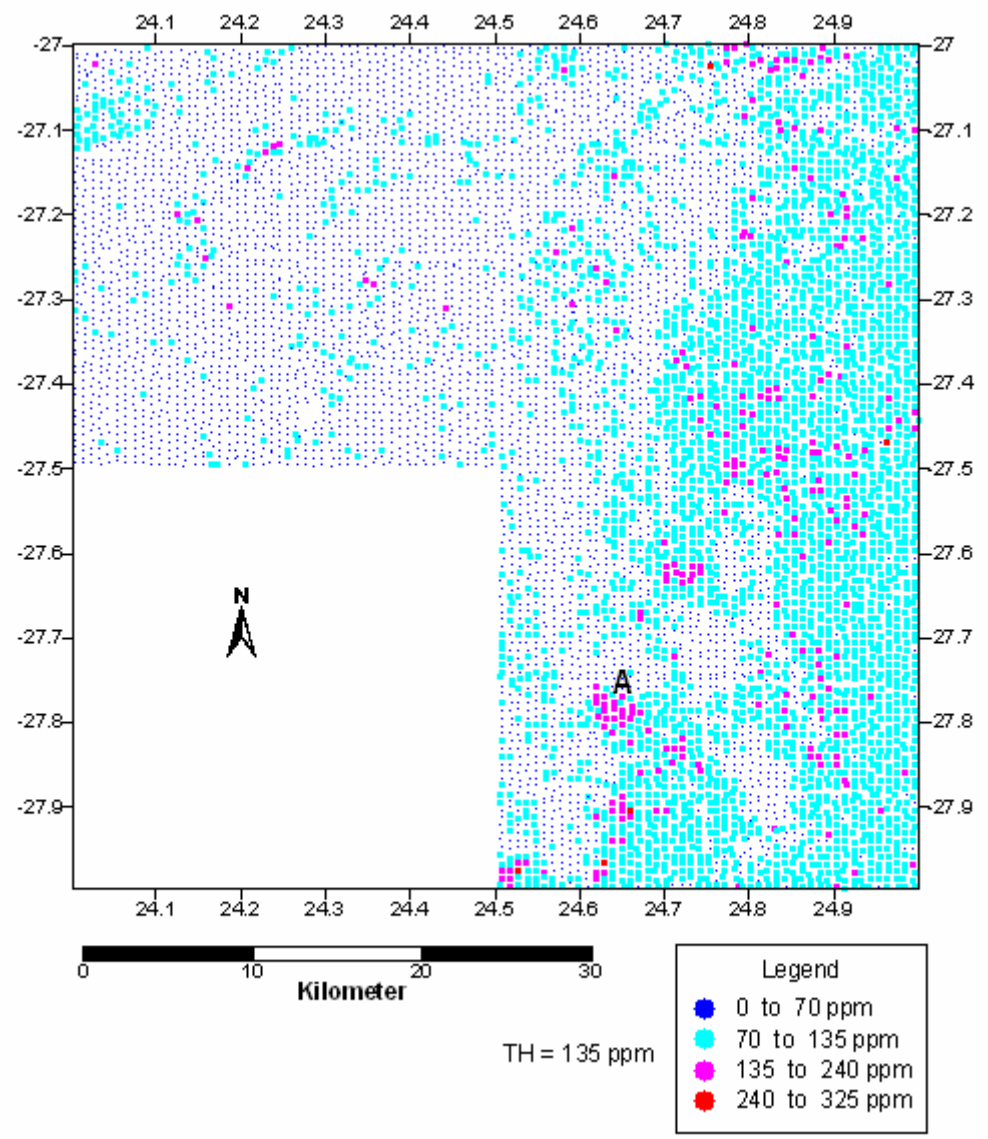

Figure 4.7-14: Classed post map of vanadium distribution in the 2724 Christiana Sheet.

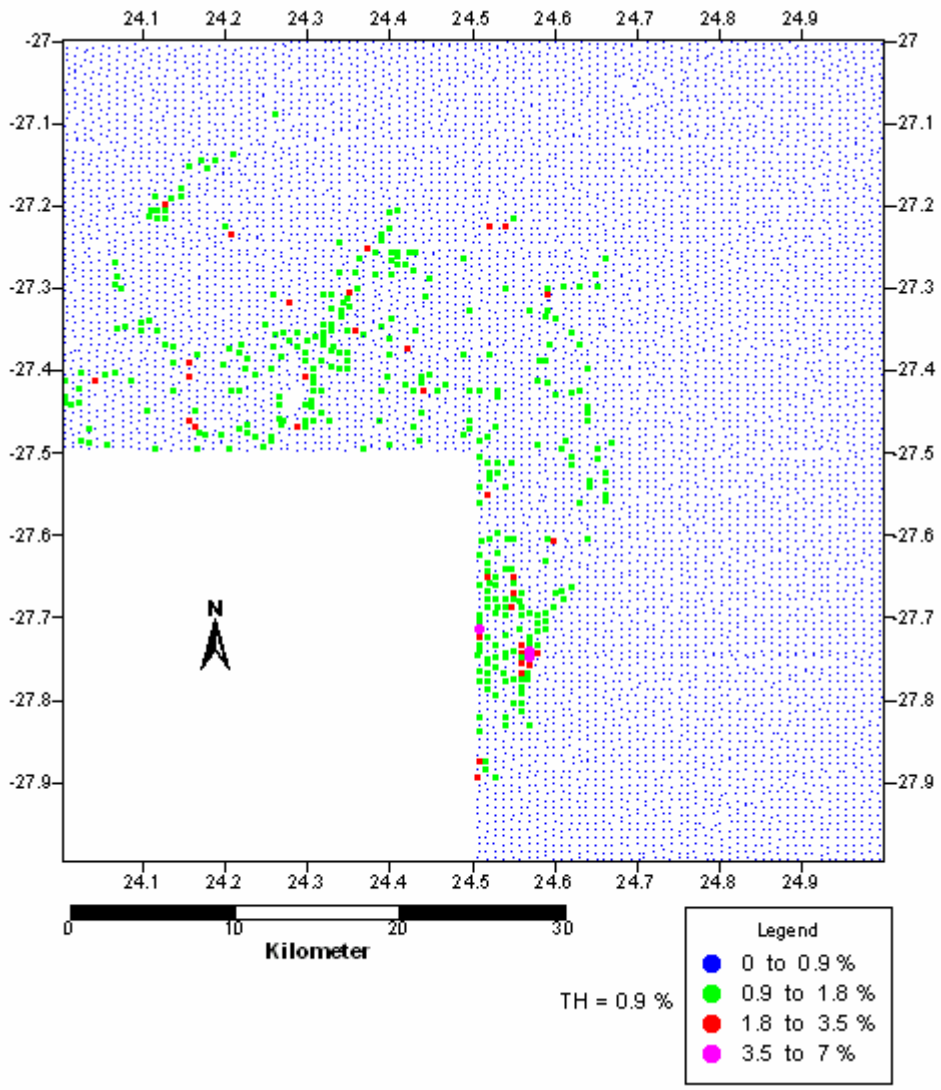

Figure 4.7-15: Classed post map of manganese distribution in the 2724 Christiana Sheet.

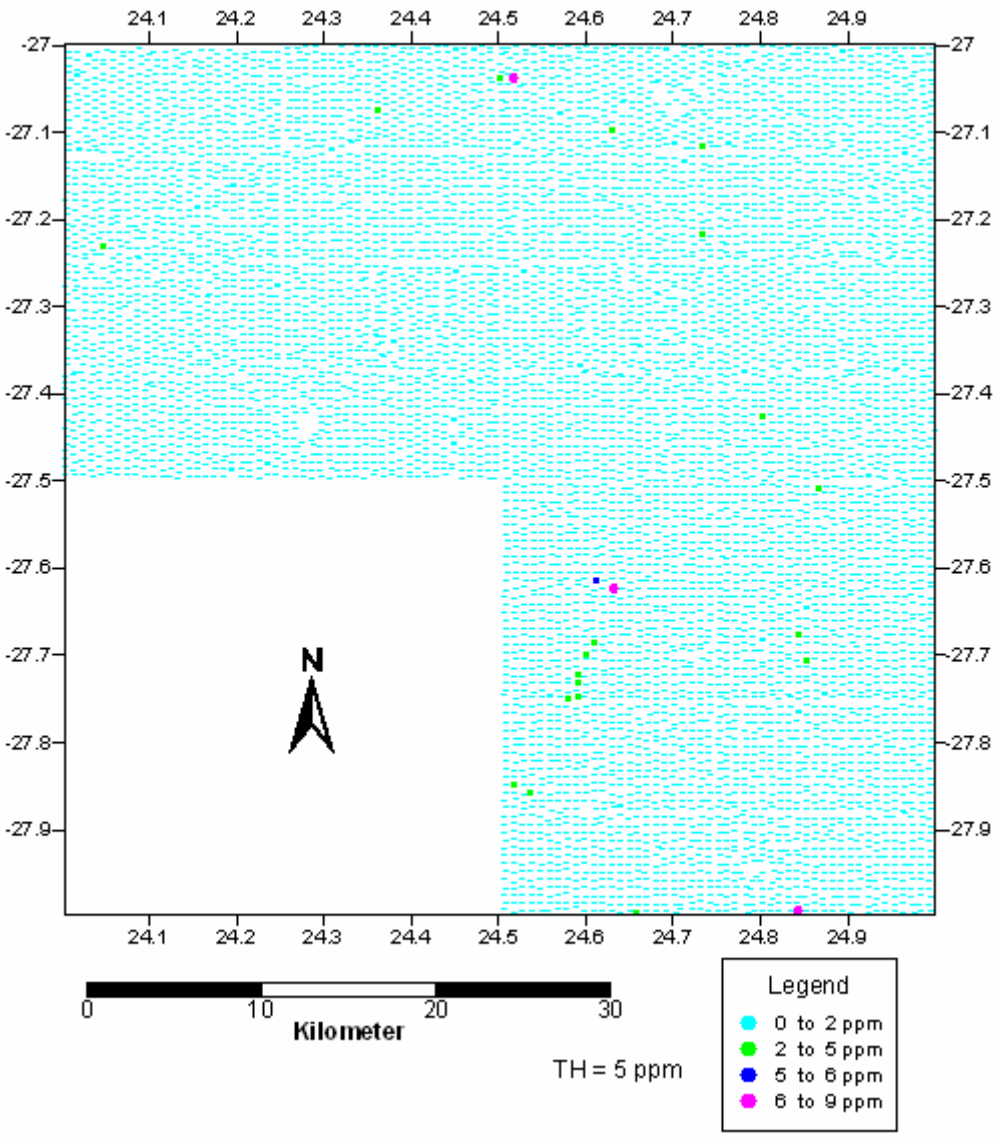

Figure 4.7-16: Classed post map of uranium distribution in the 2724Christiana Sheet.

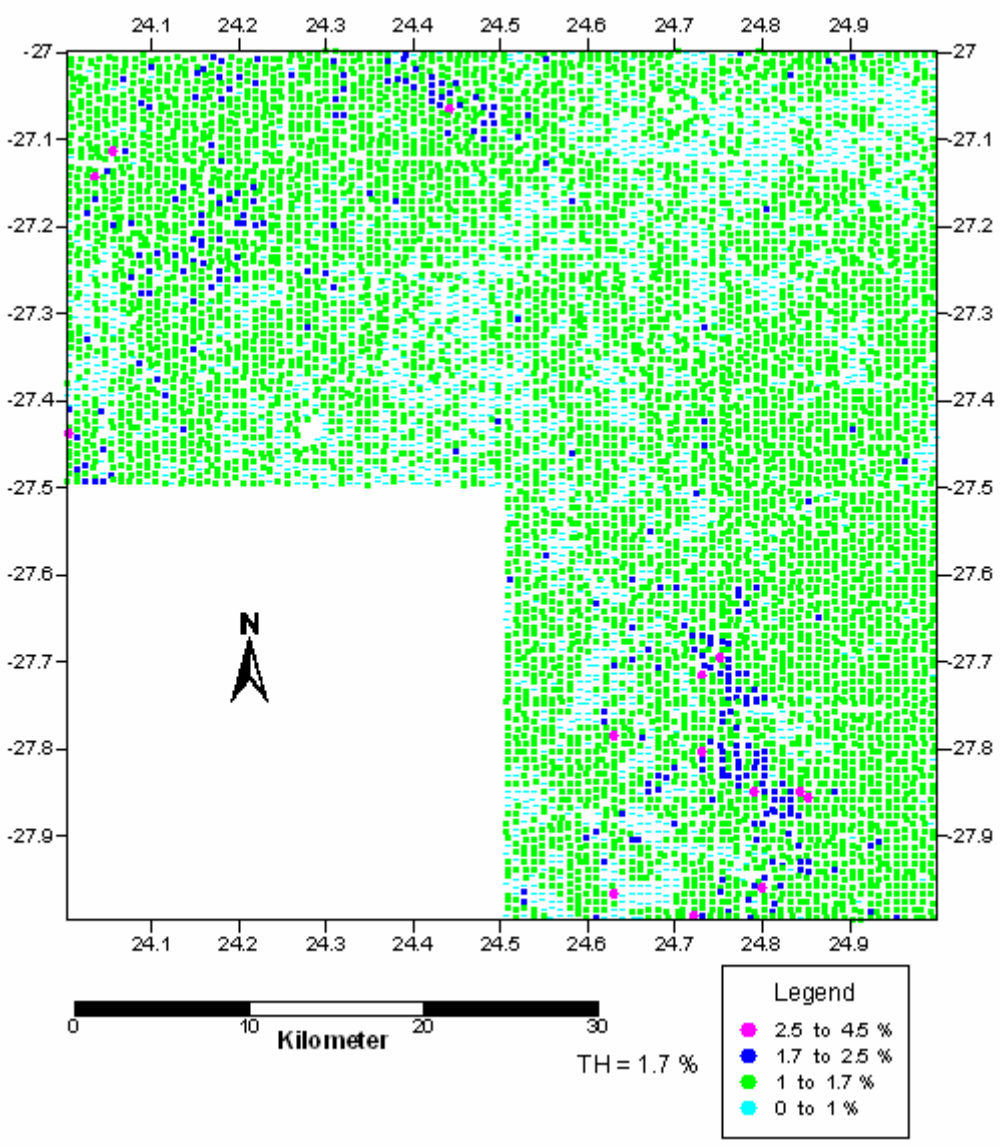

Figure 4.7-17: Classed post map of titanium distribution in the 2724 Christiana Sheet.

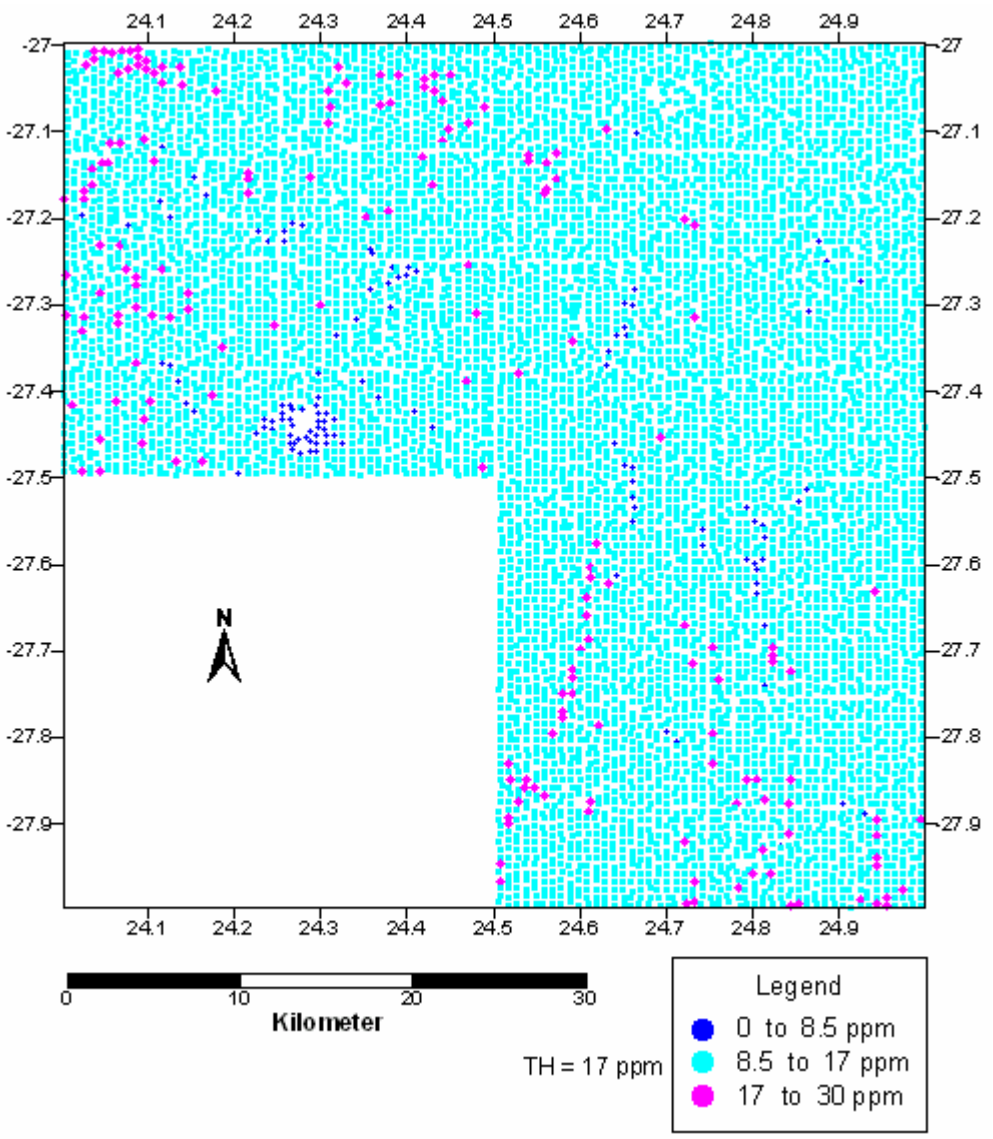

Figure 4.7-18: Classed post map of thorium distribution in the 2724 Christiana Sheet.

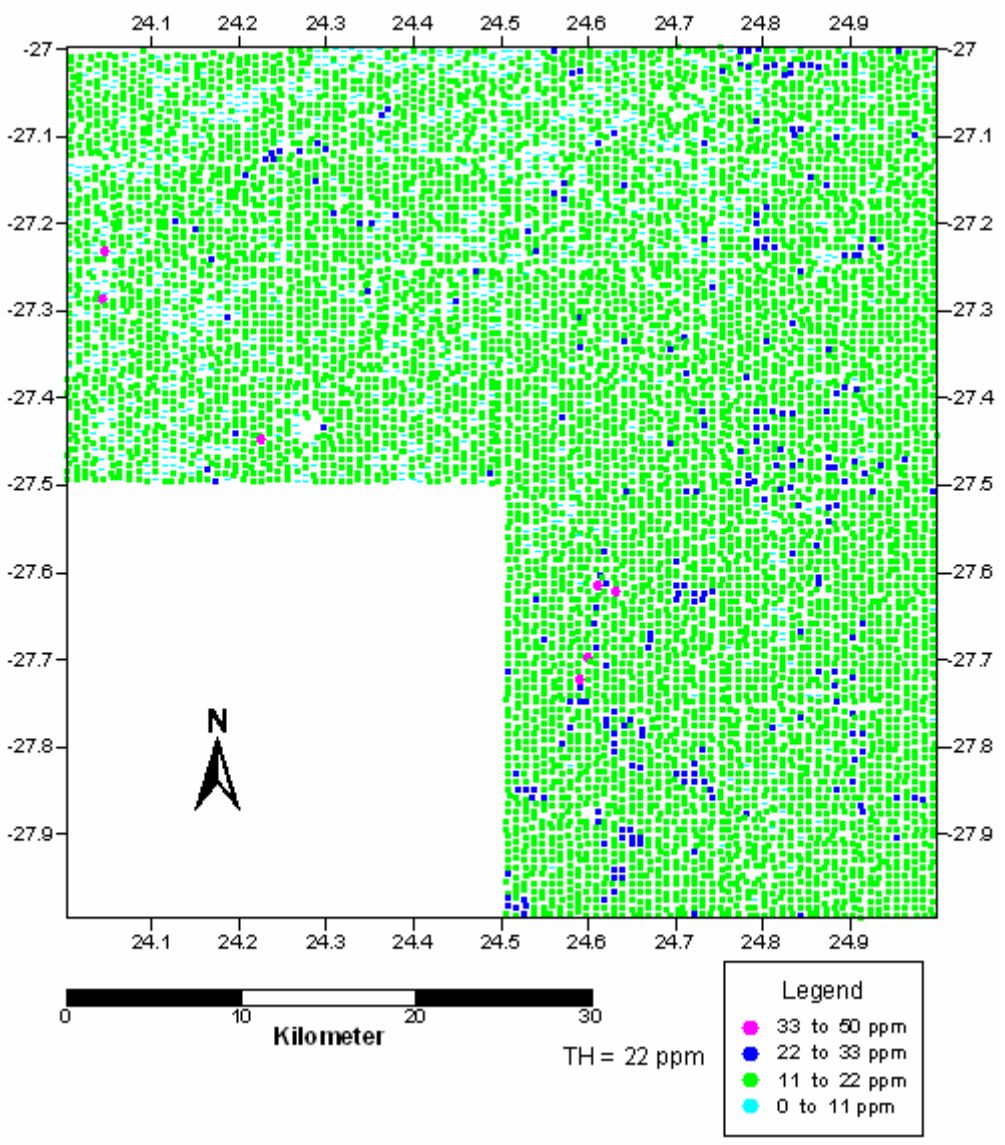

Figure 4.7-19: Classed post map of scandium distribution in the 2724 Christiana Sheet.

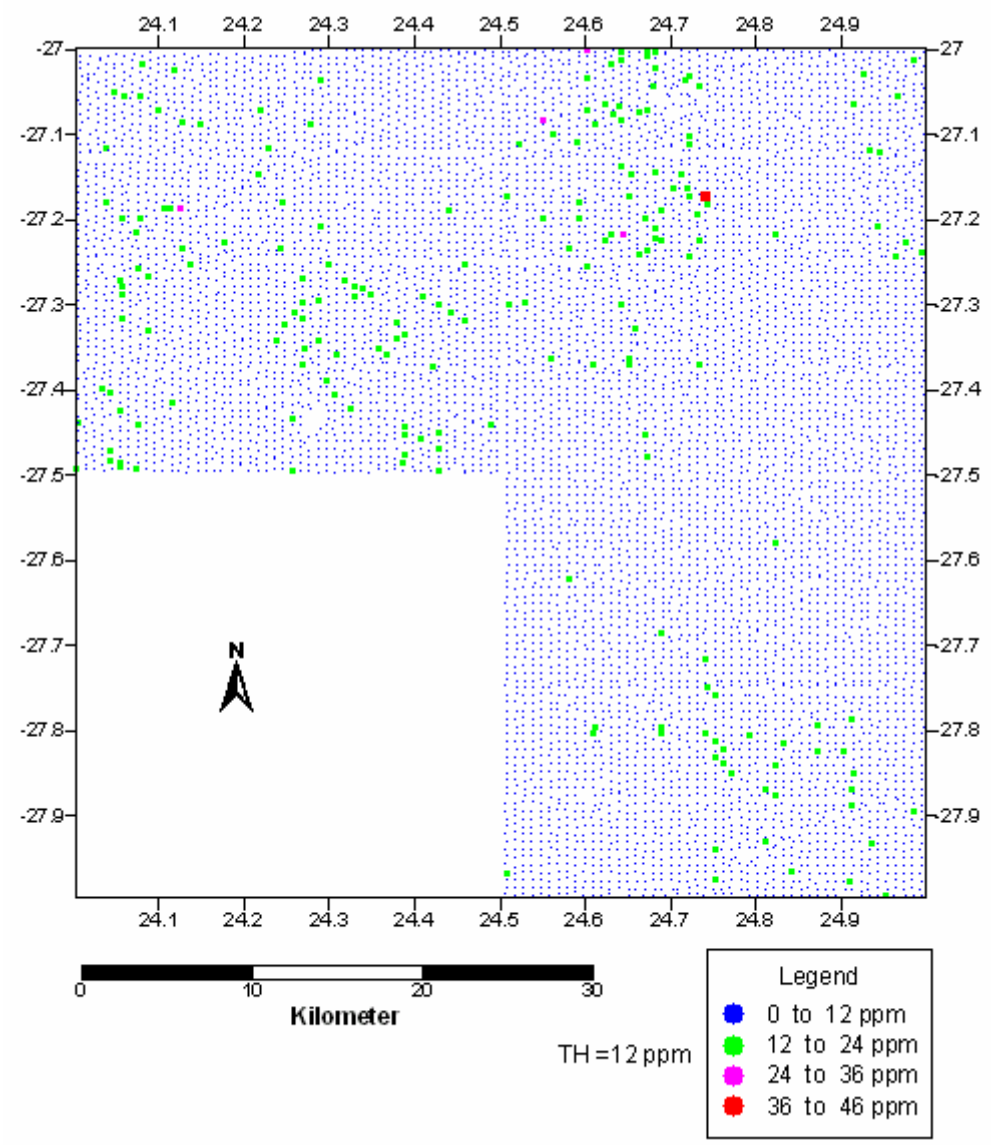

Figure 4.7-20: Classed post map of tungsten distribution in the 2724 Christiana Sheet.

CHAPTER FIVE

5 DISCUSSION AND TARGET GENERATION

5.1 DISCUSSION

The statistical analysis and geochemical element distribution of a number of elements show that various lithological units are characterized by different concentration of these elements Among the Mafikeng area has the strongest anomalies of chromium and nickel compared to the other areas (Vryburg, Christiana and Kuruman). The major strong/well developed (elliptical shape) anomalies for chromium and nickel in the Mafikeng area are located on the Gordonia Formation which is believed that the source is mafic rich rocks of the Lower Zone chromitite of the Bushveld Complex (SACS, 1980) and the north-south trend occurs over the andesitic lava and pyroclastic rock of the Hekpoort Formation (anomaly A and B in Figs. 4.4-2 and 4.4-3 in Chapter 4). Higher nickel and cromium anomalies were confirmed with the threshold of each lithological group associated with the identified anomalies for this particular element, by applying the threshold values of that litho groups on that areas.
Vanadium and iron in the same vicinity of the chromium and nickel anomalies in the Mafikeng area and show mainly concentrations above threshold. No other elements show significant anomalies in this area. It is believed that the anomalies (Fe, V, Cr (Critcal Zone), Cu and Ni (Critical Zone) in Area A are associated with the Bushveld Complex, which is believed to be overlain by the surface sand of the Gordonia Formation (SACS, 1980; Collins and Human, 1986; and Lourie, 2004).

The andesitic lava of the Allanridge Formation is characterized by a major trend of copper, iron, nickel, niobium and vanadium. The Formation is widely distributed over the entire study area but the area, which shows a major anomalous of the above outlined elements, outlined above, occurs in residual soil overlays andesitic lava of the Allanridge Formation which covers a large part of the Christiana area.

Lava of the Allanridge Formation in Christiana area has a potential target for the nickel, copper and cobalt which are associated with komatiitic basalts at the base of the Allanridge Formation.

The BIF of the Kuruman and Dunielskuil Formations of the Kuruman area have a strong iron anomaly occurring in areas of the major faulting area. The area has background magnetic anomalies of between -627 and 394 nT (refer to Fig. 2.3-2, Chapter 3). The Fe anomaly in Danielskuil Formation mostly shows high concentration of iron values along the fault areas and is associated with higher magnetic anomalies. It has been assumed that the higher concentration of iron resulted from the haematite and magnetite within the underlying BIF in the Transvaal Supergroup.

Iron also shows strong geochemical anomalies A and B in Fig. 4.4-8 which are parallel to each other over the lithologies of the Magaliesberg Formation (anomaly B) and Rooihoogte Formation (anomaly A). Chromium, nickel and vanadium also show strong anomalies in these area significant magnetic and bouguer anomalies are also present. The distribution of all these elements has the same trend direction and shape as the Magaliesberg and Rooihoogte Formations. The iron anomalies are believed to be resulted from the ferruginous quartzite and BIF of the Rooihoogte Formation. High nickel and chromium content are associated with the lavas of the Hekpoort Formation. It is believed that the iron, chromium and Ni anomalies in this area is associated with the xenoliths of the Bushveld complex which comprises recrystallized iron ere and hornfels in a large xenoliths of quartzite situated on the contact between the basic and the acidic phase of the Complex. This type of target is found in the form of speculate which occurs in the Silverton Formation

In Christiana and Vryburg area iron anomalies occur over the andesitic lava of the Allanridge Formation and the anomalies are mainly represented by the regional threshold values. Known iron mineralization (Kaaipan Group and Park Town Formation of the Hospital Hill Subgroup) are represented by single point anomalies.

The geochemical data does not show any high manganese anomalies within the selected study areas. Only on the Mafikeng area manganese is predominately by the regional threshold concentrations which form an elongated north-south trend over the dolomitic rock of the Malmani Subgroup. This tresnd were ploted from the the mapsheet, but when the date filted based on the lithoplogical groups it show poor manganese distribution. The manganese anomaly in Mafikeng area is from the soil which resulted from the weathering of the MN-rich dolomites and the subsequent accumulation of residual Mn-rich zone. The manganese in this area occurs as MnO_2 minerals nsutite, pyrolusite and psilomelane which are found over the Chuniespoort Group of the Transvaal Supergroup (Astrup and Tsikos, 2006). In Kuruman area it is believed that the geochemical anomalies of manganese would not be visible due to thick Kalahari sand.

The calcrete of Tertiary age in the Kuruman area is characterized by north south trend anomalies (A) of vanadium and copper Fig. 4.6-3. The anomaly is mainly consists of regional threshold concentrations. In the Mafikeng area vanadium has two parallel north south trends which have the same shape and are located over the lower volcanic units of the Hekpoort and Magaliesburg Formations.

The geochemical anomalies of zinc and lead in Christiana Area (Fig. 4.7-5 and Fig. 4.7-6 reflect the Pering Zn-Pb mineralization which is circular in shape, where the inner part of the anomalies has a gap as no sample collected from the abandoned open cast mine). The deposit was mined from 1984 to the end of November, 2002. Mineralization is centered on several sub-vertical breccia bodies that appear to merge at depth to one single body of only very poorly mineralized pyritic rock matrix breccias. Base metal sulphides, mostly sphalerite and galena, associated with only minor amounts of pyrite and chalcopyrite, are most abundant along the margin and roof zones of the breccia bodies, but also define stratabound zones of mineralization. Mineralization is associated with chemical wear brecciation and crackle brecciation (Wheatley et al., 1986).
Zinc and lead in the dolomitic rock are hosted by galena and sphalerite which predominate over galena.

In the Mafikeng Area, zinc and lead are represented by weakly developed geochemical anomalies over the carbonate rock of Eccles formation and Frisco formation (anomaly B and C, Fig. 4.5-6). These anomalies result from a very large stratabound zone of fluorite with only minor Zn-Pb sulfides and small base metal mineralized zones that are confined to crosscutting breccia bodies. Both deposit types are hosted by Neoarchaean, weakly metamorphosed and virtually undeformed stromatolitic carbonates of the Middle and Upper Frisco formations (2520 Ma) of the Malmani Subgroup of the Transvaal Supergroup. The fact that both, carbonaceous host rock and hydrothermal mineralization, have experienced a mild contact metamorphic overprint due to the intrusion of the Paleoproterozoic (2065 Ma) Bushveld Complex, is conclusive evidence for a Paleoproterozoic age of these deposits (Pötter, 2001). Carbonate host rock fragments are cemented by a very coarse-grained and massive assemblage of sparitic calcite or dolomite, fluorite and variable amounts of sphalerite and galena, together with minor pyrite, chalcopyrite and quartz. Among the sulfides, sphalerite usually dominates over galena.

Kanye Formation and leucogranite of the Gabrone Granite have positive geochemical anomalies of niobium, rubidium, yttrium, and uranium. All these elements are characterized by background concentrations and anomalies appear to be positively correlated with a strong magnetic anomaly of approximately 394 nT (Fig. 3.3-2). It is believed that the anomalies are related to the granitic rocks exposed at different erosion levels.

Yttrium also has a strong anomaly over the light green theolitic calc-alkali basalt of the Rietgat Formation in Christian region (Fig. 4.7-8). Uranium, niobium and rubidium show negative or background anomalies on other lithological groups.

Barium and manganese show the north south trends of weak anomalies over the chert-rich dolomite of the Malmani Subgroup in Mafikeng Area. Barium has a north south trend over the light green theolitic calc-alkali basalt of the Rietgat Formation in the same vicinity as yttrium in Christiana region see Fig. 4.7-7.

Other lithological units have lower concentrations of uranium, thorium and tungsten. All these elements are mostly characterized by background concentrations (below the threshold values) over the entire study area. The surface sand and the carbonaceous rocks especially in the Christiana area have local threshold concentrations of zirconium.

5.2 DELINEATED TARGETED AREAS FOR POSSIBLE MINERALIZATION

The identified areas of target areas for following up exploration were based on the following principle:

- The magnitude of the contrast between anomalous and background geochemical values;
- Shape and size or extent and of the area on anomalous values
- Geological, and other anomalies (geophysical) as well as historical information pertaining to the area;
- Mines and deposit occurances; and
- Integrated of all relevant information including aeromagnetic and geological maps

Based on the above approach the following areas (A-G) were delineated (Fig 5.2-1).

Area A

The area, located approximately 120 km north of the town of Mafikeng is found over outcropping Transvaal rocks and aeolian sand of the Gordonia Formation (Fig 5.2-2). The area is elliptical in shape and approximately 2 km wide and 4-9 km in lateral extent and characterized by significant chromium and nickel anomalies and regional local threshold concentrations of copper and vanadium. Other does not give rise to significant anomalies more details of this target are described in section 4.3.

The high levels of chromium and nickel in this area thought to be associated with chromitite of Critical Zone and marginal rocks, respectively, of the Bushveld Complex, which is overlain by the thick surface sands of the Gordonia Formation. Although PGM's were not analyzed, there is a close relationship between PGM's and chromium. The area is therefore also a target for PGM's although it is very limited due to lack of PGE's analysis.

Area B

Area B is located 3 km south of target A, about 16 km north-west of Zeerust. The area covers approximately 25 km in length and has two parallel north-south trending geochemical anomalies. These anomalies consist of the superjacent anomalies of chromium, nickel, vanadium, copper and iron lying on the Magaliesberg and Rooihoogte Formations of the Transavaal Supergroup (Fig.5.2-3). It is believed that the iron, chromium and Ni anomalies in this area is associated with the xenoliths of the Bushveld complex which comprises recrystallized iron ere and hornfels in a large xenoliths of quartzite situated on the contact between the basic and the acidic phase of the Complex. This area has a potential target for iron which could be in the form of speculate which occurs in the Silverton Formation. The previous studies outlined that the Clinton type ore iron deposits of the Pretoria Group has an extensive oolitic or pisolitic beds (2-6 m thick) of heamatite-maganetite-chamosite iron formation which can be traced intermittently from north of the Nietverdied Section of the Bushveld Complex to the Botswana border (Astrup *et al*, 2006).The presence of the nickel, vanadium chromium and iron in this area fall into the contact metamorphic aureole of the Bushveld Complex where the oolitic iron formation is completely recrystallised to a black lustrous rock essentially composed of specularite, magnetite, muscovite and roscoelite. Rare contact-metamorphic vanadium mica, counting for the vanadium anomalies in this area. Therefore this area has a pontential for iron and vanadium mineralization. Section 4.3 can be referred to for more details on the geochemical distribution of elements in this area.

Area C

This target area is located approximately 25 km northwest of Mafikeng and is triangular in shape. It is approximately 19 km from west to east and reflects the geology or lithologies of the Kanye Formation and Gaborone Granite (Fig. 5.2-4). The area is characterized by significant anomalies of niobium, rubidium, uranium and yttrium, which coincide with an east-west trending, positive magnetic anomaly of around 394-1420 nT of magnetic anomaly. The geochemical anomalies are associated with the Batsalano Ring Complex. The complex is dominated by orogenic felsic intrusive and extrusive rocks (Fig3.3-2), that have low concentration of CaO, MgO, Al_2O_3, Sr, P and Ti and are characterized by high concentrations of Rb, Zr, Nb, Y, Zn and Ga (Robb et al, 2006). This area has also a low potential target of

Rare Earth Elements pegmatite such as lithium, tin, niobium as well as beryllium (Richards, 1986). More details on the distribution of elements in this area are given in section 4.3.

Area D

The target area is located 33 km north of Christiana and covers a large area (approximately 40-50 km north-south and 9 km east-west), over the andesitic lavas of the Allanridge Formation (Fig. 5.2-5). This area is characterized by high magnetic intensity and geochemical anomalies above threshold of nickel, copper, iron, strontium and cobalt. It is assumed that the geochemical anomalies have resulted from the sulfides within komatiitic lava flows at the base of the Allanridge Formation of the Ventersdorp Supergroup, which may have been concentrated in lava channels by formed thermal erosion of the substrata by the komatiitic flow. The area constitutes a potential target for nickel, iron, copper and PGE mineralization. Examples of this type of mineralization include the Damba Sulphide Nickel Deposit in Zimbabwe (Killick, 1986) and Kambalda in Western Australia (Naldrett, 2004). More details of the distribution of the elements of interest are given in section 4.6.

Area E

This target area trends north to south, over a distance of approximately 15 km (Fig. 5.2-6). This area lies a few kilometers south of target D (Fig. 5.2-1) in the Christiana region. The area characterized by barium and yttrium anomalies which could indicate potential of barite occurrence in the area. Details in the geochemical distribution of the elements is given in Section 4.6

Area F and G

These two target areas lie approximately 6-20 km west of Kuruman (Fig. 5.2-1). Area F is defined by high iron geochemical anomalies and aeromagnetic anomalies resulting from haematite in the BIF of the Asbestos Hill Subgroup of the Transvaal Supergroup.

Area G is located approximately 20 km northwest of Kuruman and is defined by north-south trending (about 15 km) geochemical anomalies of vanadium and copper over calcrete of

Tertiary age (Fig. 5.2-7). The area might be useful for exploration for calcrete-hosted or surficial deposits of copper and vanadium could be warranted.

The presence of vanadium might be associated with the potassium-uranium vanadate minerals such as carnotite, that is mostly found in calcrete deposits, where the main composition of this carnotite uranium, potassium and vanadium which are derived from the granites (U and K) and possible mafic rocks. No (V) calcrete-hosted deposits of uranium are known in this area. Uranium is characterized by background values below the threshold concentration (i.e. of calcrete hosted uranium deposits includes Yeelirrie in Western Australia and Langer Heinrich in Namibia (Robb, 2005)). More details of the distribution of elements are given in section 4.5.

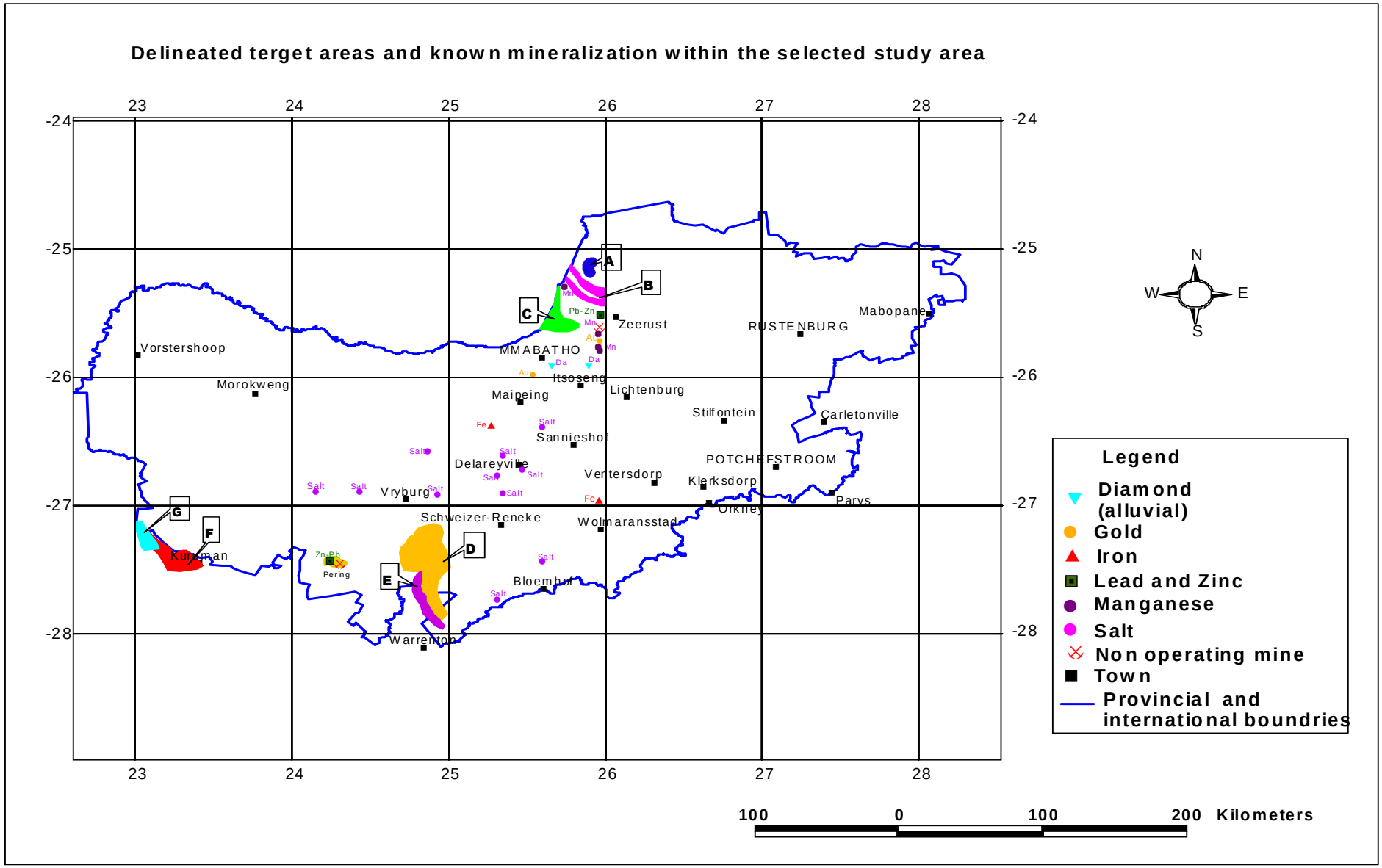

Figure 5.2-1: Delineated target areas for possible mineralization and known mineralization within the area surveyed.

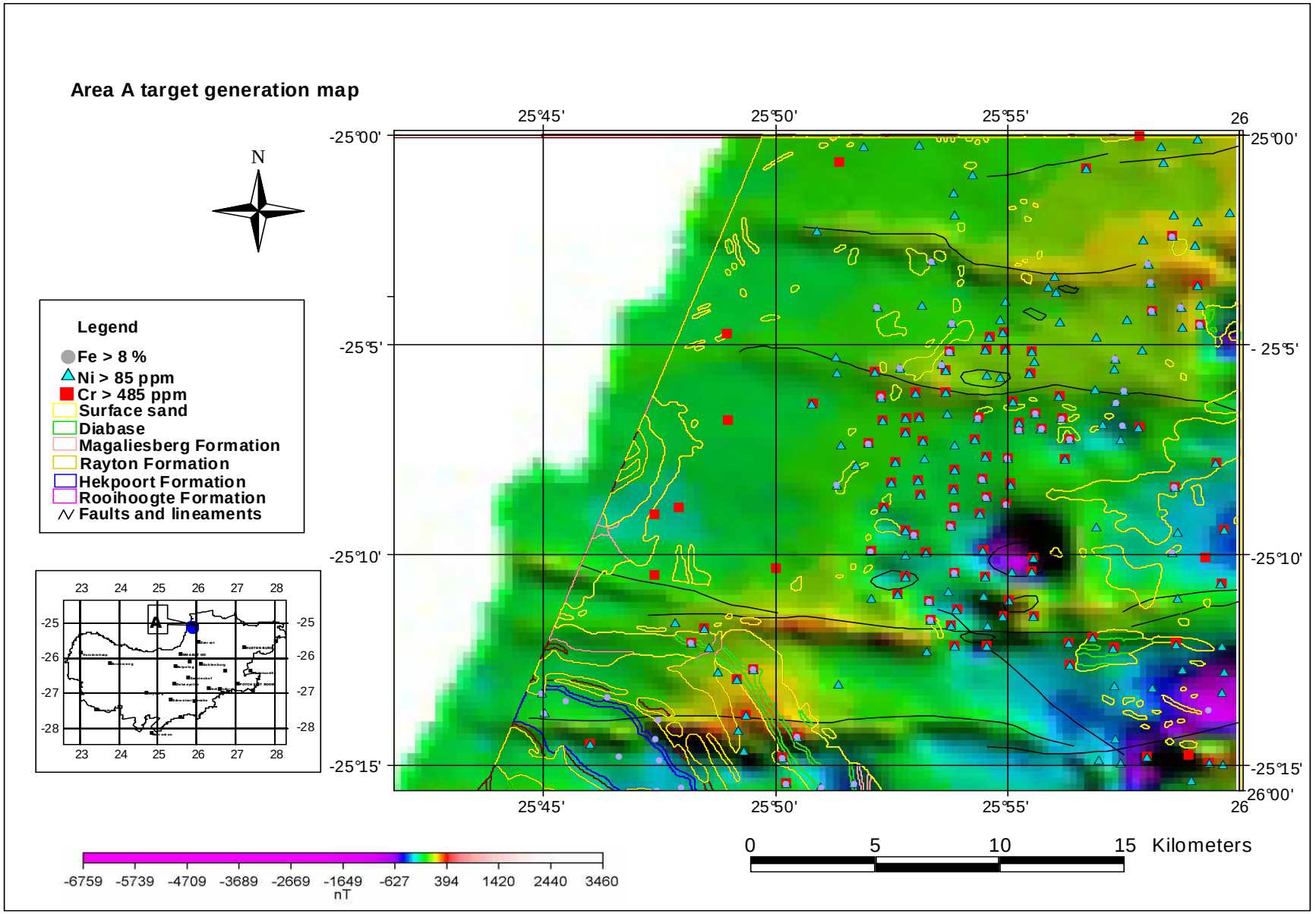

Figure 5.2-2: Integration of the geochemical, geology and geophysical interpretations for delineated target area A.

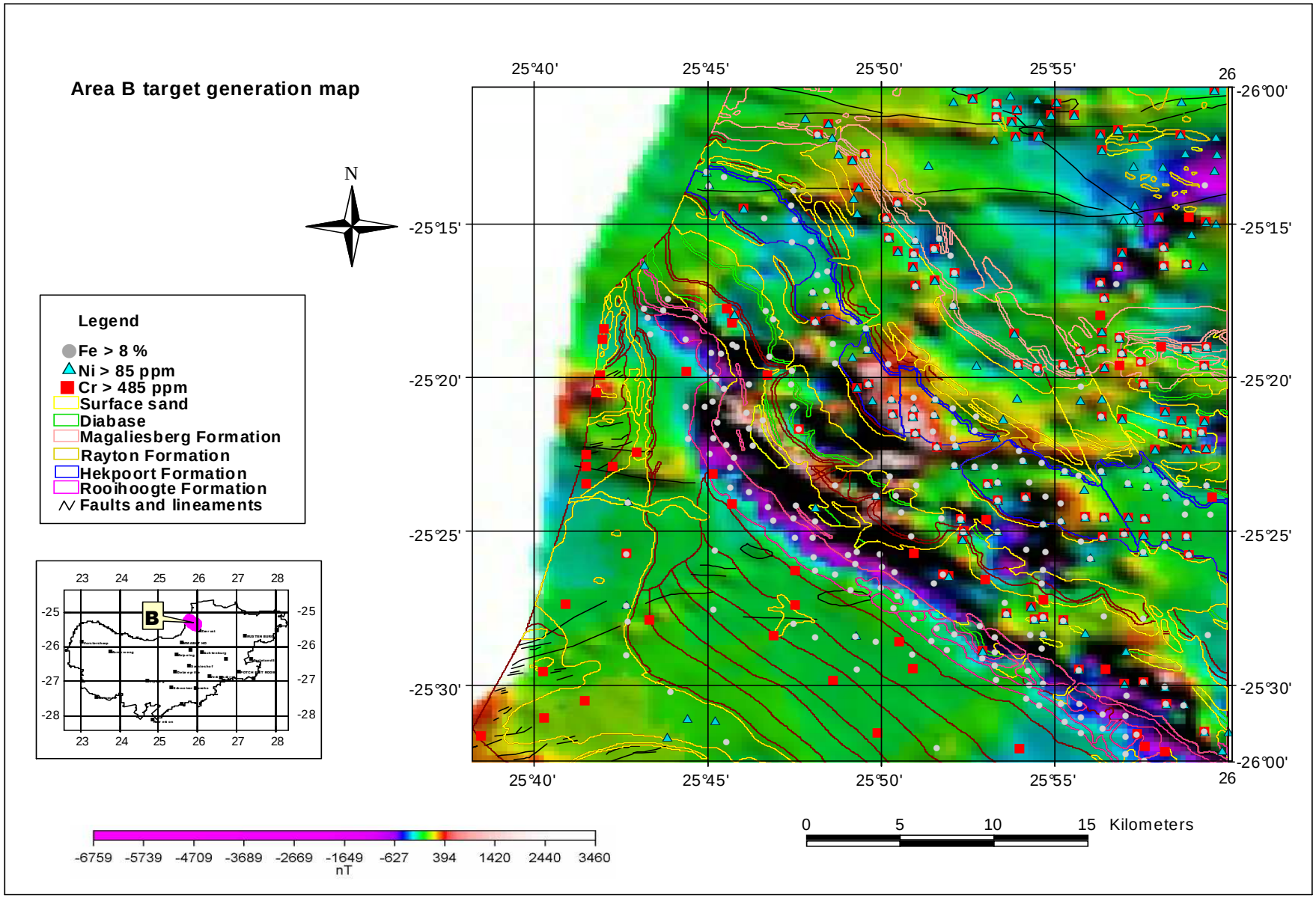

Figure 5.2-3: Integration of the geochemical, geology and geophysical interpretations for delineated target area B.

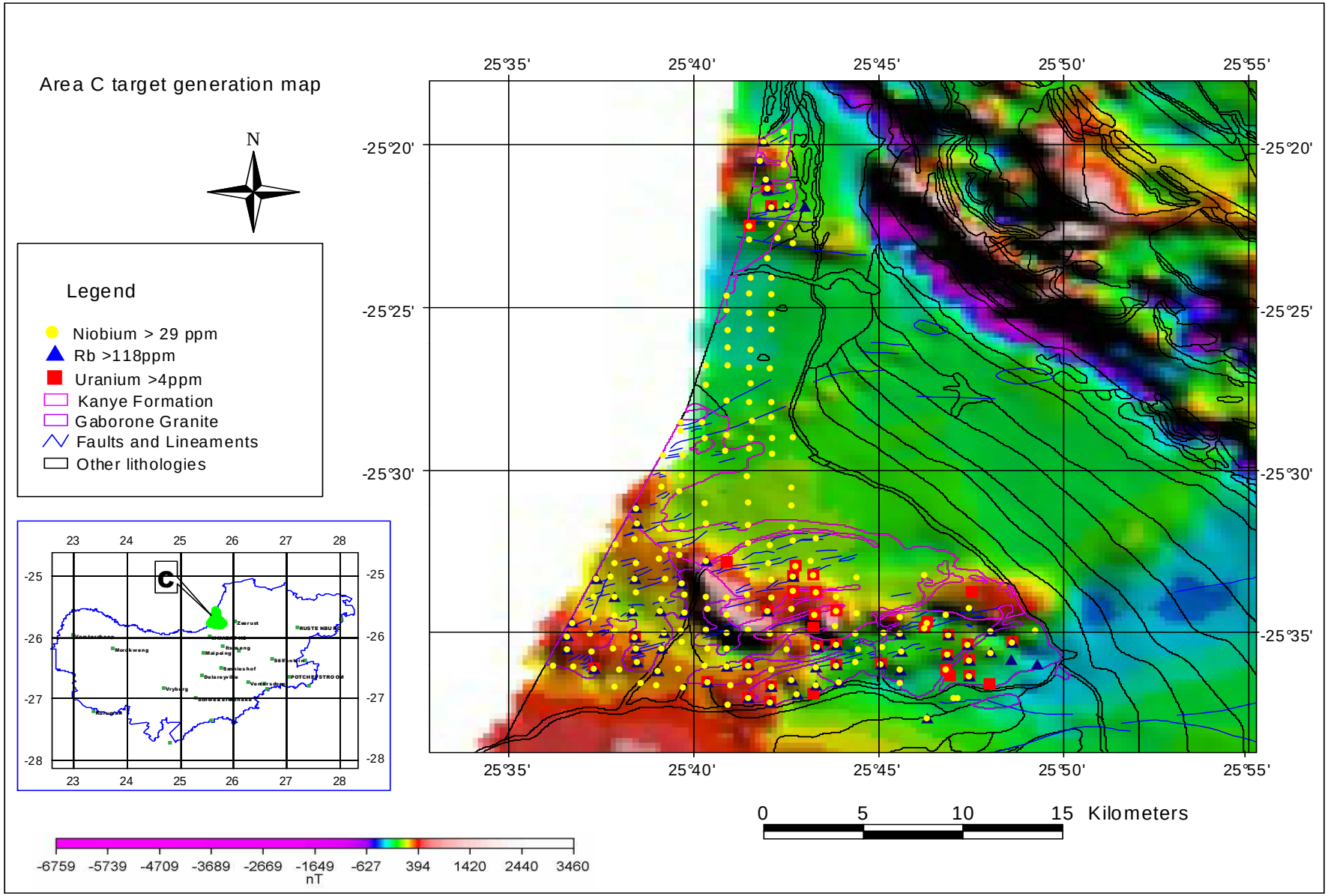

Figure 5.2-4: Integration of the geochemical, geology and geophysical interpretations for delineated target area C.

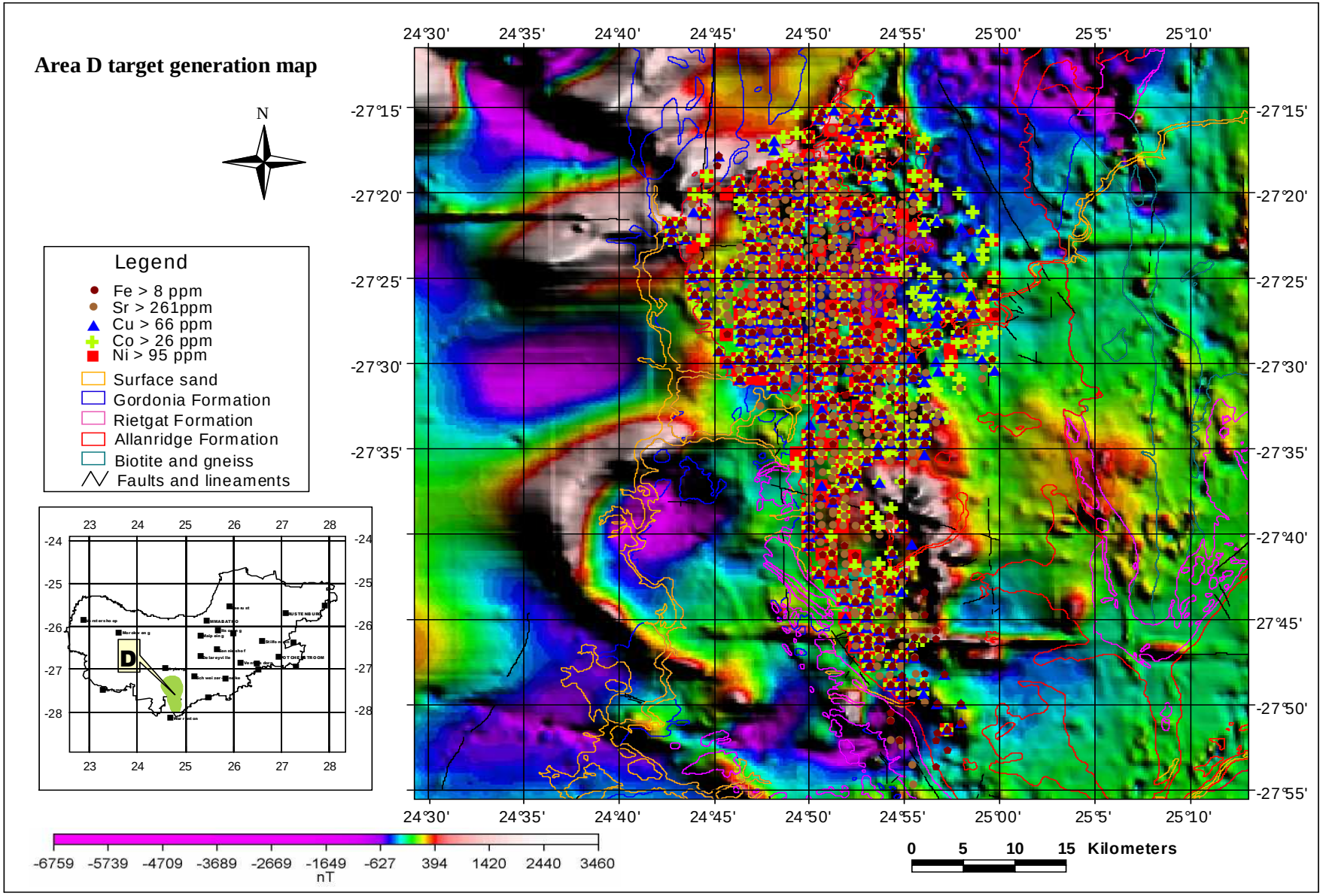

Figure 5.2-5: Integration of the geochemical, geology and geophysical interpretations for delineated target area D.

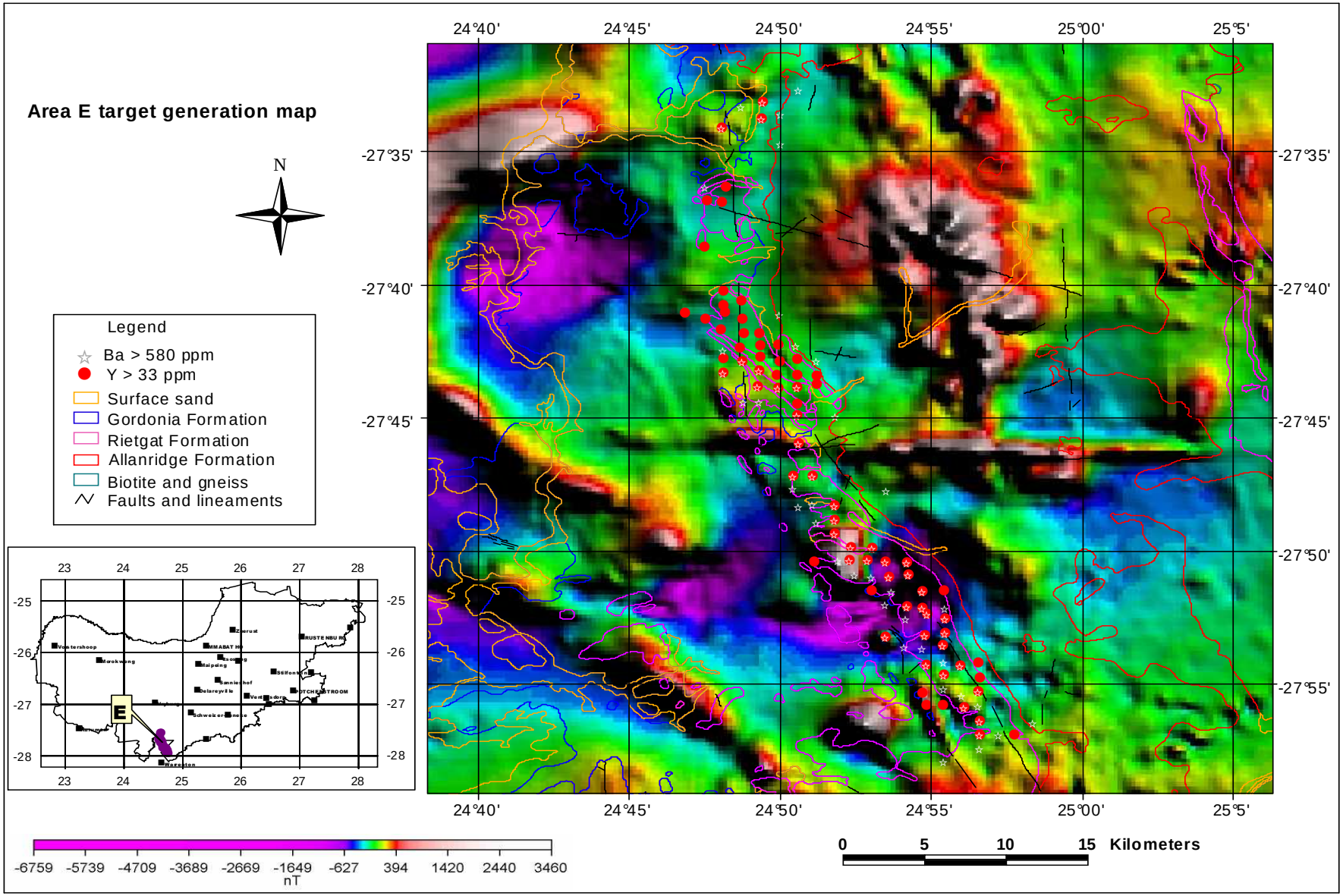

Figure 5.2-6: Integration of the geochemical, geology and geophysical interpretations for delineated target area E.

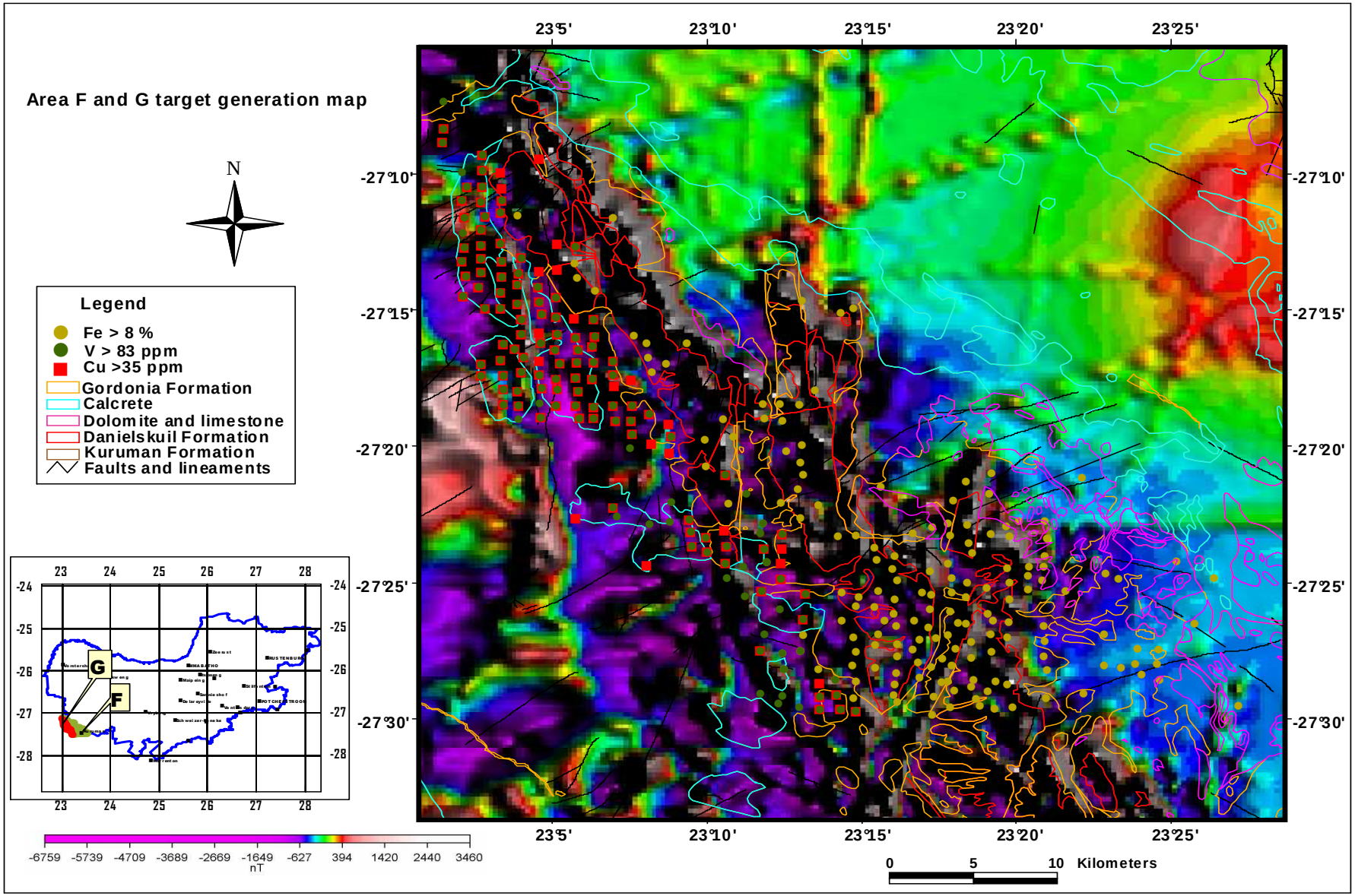

Figure 5.2-7: Integration of the geochemical, geology and geophysical interpretations for delineated target area F and G.

CHAPTER SIX

6 CONCLUSIONS AND RECOMENDATIONS

6.1 CONCLUSIONS

6.1.1 Overall conclusions

The integrated study of soil geochemical data, collected by the CGS, together with geologic and geophysical data, has provided a good basis for the delineation of target areas for following up exploration. Several target areas have been generated using this approach.

In the Mafikeng area the study has outlined a potential area for PGM, chromium and nickel mineralization thought to be associated with the Bushveld Complex. The area extends west towards the Botswana border. The basal komatiitic lavas of the Allanridge Formation of the Ventersdorp Supergroupcould have potential for nickel, copper and cobalt, of which a target area has been delineated. The granitic rocks of the Gaborone Granitic and Kanye Formation could have potential target for uranium and also possible target for feldspar, mica and beryl. It was evidenced from the calcrete of in Kuruman. A potential target for calcrete-hosted deposit of copper, vanadium and cobalt, as well as uranium in the calcrete of the Kuruman area. The BIF of the Asbestos Hill Subgroup of the Transvaal Supergroup has a potential for iron (possibly Manganese) mineralisation.

The integrated approach developed of this study can be extended to other areas where geochemical and geophysical data, produced by the Council for Geoscience available. No field work has been undertaken to verify the various targets delineated and further work is required to refine targets and commenced with exploration programmes.

This project has provided a good opportunity for the researcher to be trained in the skills of conducting geochemical sampling and analysis, data processing, interpretation and integration using geology, geophysics and geochemistry.

6.1.2 Target areas

Area A. The area located approximately 120 km north of the town of Mafikeng and characterized by significant chromium and nickel anomalies and regional local threshold concentrations of copper and vanadium. The area is therefore also a target for PGM's although it is very limited due to lack of PGE's analysis.

Area B. Area B is located 3 km south of target A, about 16 km north-west of Zeerust and consist of the superjacent anomalies of chromium, nickel, vanadium, copper and iron lying on the Magaliesberg and Rooihoogte Formations of the Transvaal Supergroup. This area has a low potential for iron and vanadium deposits.

Area C. This target area is located approximately 25 km northwest of Mafikeng and is triangular in shape. This area has also a low potential target of Rare Earth Elements pegmatite such as lithium, tin, niobium as well as beryllium.

Area D. This area is characterized by high magnetic intensity and geochemical anomalies above threshold of nickel, copper, iron, strontium and cobalt. The area constitutes a potential target for nickel, iron, copper and PGE mineralization.

Area E. This area lies a few kilometers south of target D (Fig. 5.2-1) in the Christiana region. The area characterized by barium and yttrium anomalies which could indicate potential of barite occurrence in the area.

Area F and G. These two target areas lie approximately 6-20 km west of Kuruman. The area might be useful for exploration for calcrete-hosted or surficial deposits of copper and vanadium could be warranted.

6.1.3 Problems highlight

The use of lithological groups threshold values were not very successful in this study, therefore the geological map sheet threshold values were used. The difficulties of using the litho group's threshold values arise when: 1. some litho groups were characterized by small data set with mostly extreme higher vales outliers which over estimate the threshold values; 2. Lack of spatial continuity, shape and size of the identified anomalies; 3. the visualization of the geochemical presentation results (maps). Some litho groups coves the lager areas which result in poor presentation of the geochemical anomalies as compared to the map sheet results.

The delineated targets areas are still large and the need to do infill sampling and analysis which involves field insight.

6.2 RECOMENDATIONS

The sampling density of 1 km^2 for geochemical sampling has proved to be effective for delineating a number of areas of potential interest for further exploration near-surface or buried deposits. The following strategies are recommended in order to verify and quantifying whether the target areas could be important for future exploration.

6.2.1 Revisiting delineated areas

Field checking of the delineated areas with a view to confirming the cause of the various anomalies and ascertaining whether any evidence for local enhancement or suppression of values emits, is recommended.

6.2.2 Reducing/minimizing the sampling density and infilling sampling

The sampling density of 1 km^2 per sample should be reduced to 500 m in specific target areas. This sampling scale should cover the non-sampled areas at a scale of 1 sample per square kilometer. This sampling density will also provide detailed information on the geochemical data of the identified anomalies. This should be only applied or done to the targeted areas as it will reduce the time, cost and labour involved.

6.2.3 Sampling depth

The initial sampling was based on sampling only the surface/top soil, and no study has been done to confirm where the anomalies originated from. It is recommend that the soil samples should be collected at a depth of 30 cm -2 m or more below the surface (in case where the overburden is more thicker i.e. surface sand of the Gordonia Formation in target area A). This will provide information on whether the anomalies are derived from in situ weathered rock or transported materials.

6.2.4 Chip sampling/ rock samples

The sampling of certain outcropping lithologies (litho-geochemistry) in the delineated target areas will provide more detailed information litho-geochemistry on the bedrock cause of the geochemical anomalies in soil or surficial material.

6.2.5 Borehole data

Borehole data should be laid out in future so that it will provide the detailed stratigraphy and the kind and extent of the mineralization. This will help in future exploration campaigns.

6.2.6 More applications for environmental assessment

6.2.7 More applications for agricukltural production assessments

REFERENCES

Aftabi, A. (1997). Geochemical aspects of sheared zones as an indication of porphyry Cu–Mo–Au–Ag mineralization at Derehamzeh, Jiroft, Kerman, Iran. Exploration and Mining Geololgy, Volume 6 (3), pp. 261–267.

Anhaeusser, C.R (1991). The Archaean Kraaipan Group volcano-sedimentary rocks and associated granites and gneisses of the southwestern Transvaal, northwestern Cape Province and Bopthuthatwana- Excursion guidebook. *Information Circular, Economic Geology Research Unit, University of Witwatersrand, Johannesburg, South Africa* 244, pp. 45.

Astrup, J., Hammerbeck, E.C.I. and van den Berg, H. (1998). Iron. In: Wilson, M.G.C. and Anhaeusser, C.R (Editors). *The Mineral Resources of Southern Africa:* Handbook. Council for Geoscience, Pretoria, pp. 402-415.

Astrup, J. and Tsikos, H. (1998). Manganese. In: Wilson, M.G.C. and Anhaeusser, C.R (Editors). *The Mineral Resources of Southern Africa:* Handbook. Council for Geoscience, Pretoria, pp. 450-460.

Atapour, H. and Aftabi, A. (2007). The geochemistry of gossans associated with Sarcheshmeh porphyry copper deposit, Rafsanjan, Kerman, Iran: Implications for exploration and the environment. *Journal of Geochemical Exploration.* Volume 93; pp. 47-65.

Atapour, H. (2000). Investigation on the distribution of gold, silver, molybdenum, copper and associated elements in gossans of Sarcheshmeh porphyry copper deposit, Proceedings of the 18th. *Symposium on Geoscience*, pp. 446–451.

Baker, P.M. and Waugh, R.S. (2005). The role of surface geochemistry in the discovery of the Babel and Nebo magmatic nickel-copper-PGE deposit. *Journal of Geochemical Exploration*. Volume 5 (3), pp. 195-200.

Beukes, N.J. (1987). Facies relations, depositional environments and diagenesis in a major early Proterozoic stromatolitic carbonate platform to basinal sequence, Campbellrand Subgroup, Transvaal Supergroup, Southern Africa. *Sedimentary Geology*, Volume 54 (1-2), pp.1-46.

Bless, C. and Kathura, R. (1993). *Fundamentals of Social Statistics, an African Perspective*. Juta and Co, Ltd; Cape Town.

Boyle R.W. (1974). The use of major elemental ratios in detailed geochemical prospecting utilizing primary halos. *Journal of Geochemical Exploration*. Volume 3 (4), pp. 345–369.

Bölviken, B., Bogen, J., Demetriades, A., De Vos, W., Ebbing, J., Hindel, R., Langedal, M., Locutura, J., O'Connor, P., Ottesen, R.T., Pulkkinen, E., Salminen, R., Schermann, O., Swennen, R., Van der Sluys, J. and VoldenRegional, T. (1996). Regional geochemical mapping of Western Europe towards the year 2000. *Journal of Geochemical Exploration*, Volume 56 (2), pp. 141-166.

Bølviken, B., Bogen, J., Jartun, M., Langedal, M., Ottesen, R.T. and Volden, T. (2004). Overbank sediments: a natural bed blending sampling medium for large—scale geochemical mapping. *Chemometrics and Intelligent Laboratory Systems*, Volume 74, pp. 183-199.

Brandl, G., Cloete, M. and Anhaeusser, C.R. (2006). Archaean Greenstone Belt. In: Johnson, M.R., Anhaeusser, C.R and Thomas, R.J. (Editors). *The Geology of South Africa*. Geological Society of South Africa, Johannesburg and Council for Geoscience, Pretoria, pp. 9-56

Canet, C., Alfonso, P., Melgarejo,C.J. and Belyatsky, B.V. (2004). Geochemical evidences of sedimentary-exhalative origin of the shale-hosted PGE–Ag–Au–Zn–Cu occurrences of the Prades Mountains (Catalonia, Spain): trace-element abundances and Sm–Nd isotopes. *Journal of Geochemical Exploration*, Volume 82 (1-3); pp. 17–33.

Cawthorn, R.G., Eales, H.V., Walraven, F., Uken, R. and Watkeys, M.K. (2006). The Bushveld Complex. In: Johnson, M.R., Anhaeusser, C.R and Thomas, R.J. (Editors). *The Geology of South Africa*. Geological Society of South Africa, Johannesburg and Council for Geoscience, Pretoria, pp. 261-281.

Chaffee, M.A. (1976). The zonal distribution of selected elements above the Kalamazoo porphyry copper deposit, San Manuel district, Pinal County, Arizona. *Journal of Geochemical Exploration,* Volume 5 (1-2), pp. 145-165.

Cheng, Q., Agterberg, F.P. and Ballantyne, S.B. (1994). The separation of geochemical anomalies from background by fractal methods. *Journal of Geochemical Exploration*. Volume 51 (2), pp. 109-130.

Cheng Q., 2007. Mapping singularities with stream sediment geochemical data for prediction of undiscovered mineral deposits in Gejiu, Yunnan Province, China Ore Geology Reviews. *Journal of Geochemical Exploration* ,Volume 32, pp. 314-324.

Chork, C.Y. and Mazzuchelli, R.H. (1989). Spatial filtering of exploration geochemical data using EDA and robust statistics. *Journal of Geochemical Exploration*, Volume 34 (3). pp 221-243.

Çiftçi, E., Kolayli, H. and Tokel, S. (2005). Lead-arsenic soil geochemical study as an exploration guide over the Killik volcanogenic massive sulfide deposit, Northeastern Turkey. *Journal of Geochemical Exploration*; Volume 86 (1): pp. 49–59.

Clay, A.N. (1986). The stratigraphy of the Malmani Dolomite Subgroup in the Carletonville Area, Transvaal: Genetic implications for lead-zinc mineralization. In: Anhaeusser, C.R and Maske, S. (Editors). *Mineral Deposits of Southern Africa*, Volume 1. Geological Society of South Africa, Johannesburg, pp.853-860.

Coope, A.J. (1973). Geochemical prospecting for porphyry copper-type mineralization- A review. *Journal of Geochemical Exploration*, Volume 2 (2), pp. 81-102.

Coetzee, L.L. (2001). *Genetic stratigraphy of the Paleoproterozoic Pretoria Group in the Western Transvaal.* M.Sc. thesis (unpublished) Rand Afrikaans University, Johannesburg, South Africa, pp. 220.

Collins, L.A. and Human, D.R. (1986). The Groot-Marico chromitite deposit, Western Transvaal. In: Anhaeusser, C.R and Maske, S. (Editors). *Mineral Deposits of Southern Africa*, Volume 2. Geological Society of South Africa, Johannesburg, pp.1229-1235.

Corner, B., Durrheim, R.J. and Nicolaysen, L.O. (1990). Relationship between the Vredefort structure and the Witwatersrand Basin within the tectonic framework of the Kaapvaal Craton as interpreted from regional gravity and aeromagnetic data. *Tectonophysics*, 171, pp.49–61.

Council for Geoscience (2000). *Gravity Map of the Republic of South Africa (1:1 000 000 Gravity map)*. Government Printer, Pretoria. South Africa (One sheet)

Council for Geoscience (2000). *Total Magnetic intensity map of the Republic of South Africa (1: 1 000 000 Magnetic map).* Government Printer, Pretoria. South Africa (One sheet).

Council for Geoscience (2006). *Current status of the national geochemical mapping programme of the Republic of South.* Government Printer, Pretoria. South Africa (One sheet).

Cox R. (1975). Geochemical soil surveys in exploration for nickel–copper sulfides at Pioneer, near Norseman, Western Australia. In: Elliott, I.L. and Fletcher, W.K. (Editors), *Fifth Geochemical Exploration 1994*, Vancouver Symposium, pp. 437–460.

Davis, J.C. (1973). *Statistical and Data Analysis in Geology*. New York: Wiley.

Davy, R., Pirajno, F., Sanders, A.J. and Morris, P.A. (1999). Regolith geochemical mapping as an adjunct to geological mapping and exploration; examples from three contiguous Proterozoic basins in Western Australia. *Journal of Geochemical Exploration*, Volume 66, pp. 37-50.

De Villers, B. and Mangold, S. (2002). The Biophysical Environment. *State of the Environment Report 2002 North West Province South Africa*. North West Province Department of Agriculture Conservation and Environment, Mmabatho.

http://www.nepg.org,za/soer/Fullrepot/toc.html.

De Wit, M., Roering, C., Hart, R.J., Amstrong, R.A., de Ronde, C.E., Green, R.W.E., Tredoux, M., Peberdy, E. and Hat, R.A. (1992). Formation of an Archean continent. *Nature* 357, pp. 553-562

Du Toit, A.L. (1905). Geological survey of portion of the Vryburg and Mafikeng: A. *Rep. geol. Surv.Comm*. Cape Good hope, pp. 205-258

Du Toit, A.L. (1926). *The geology of South Africa*. Oliver and Boyd, Edinburgh.

Elsenbroek J.H. (1995). Instrumentation and Analytical technique for the Analysis of Regional Geochemical samples used at the South African Council for Geoscence. *Analyst.* Volume 120, pp. 1532-1541.

Elsenbroek, J.H., Lombard, M., Szczesniak, H.L., & De Bruin, D. (2000a). Geochemical distribution of Scandium, Titanium, Vanadium, Chromium, Manganese, Iron (Fe2O3), Cobalt, Nickel, Copper, Zinc, Arsenic, Rubidium, Strontium, Yttrium, Zirconium,

Niobium, Molybdenum, Tin, Antimony, Barium, Tungsten, Lead, Thorium & Uranium. (1: 250 000, Geochemical map; 2328 Pietersburg). Council for Geoscience South Africa, (two sheets).

Elsenbroek, J.H., Lombard, M., Szczesniak, H.L., & De Bruin, D. (2000*b*). Geochemical distribution of Scandium, Titanium, Vanadium, Chromium, Manganese, Iron (Fe_2O_3), Cobalt, Nickel, Copper, Zinc, Arsenic, Rubidium, Strontium, Yttrium, Zirconium, Niobium, Molybdenum, Tin, Antimony, Barium, Tungsten, Lead, Thorium & Uranium (1: 250 000, 2426 Thabazimbi Geochemical map;). *Council for Geoscience South Africa*, (two sheets).

Eriksson, P.G., Altermann, W. and Hartzer, F.J. (2006). The Transvaal Supergroup and its Precursors. In Johnson, M.R., Anhaeusser, C.R and Thomas, R.J. (Editors). *The Geology of South Africa.* Geological Society of South Africa, Johannesburg, Pretoria, pp. 237-260.

Evans, A.M. (1995). *Introduction to Mineral Exploration*. Black Well Science Ltd, London, pp. 155-178.

Filippini-Alba, J.M., Crósta, A.P. and Barros De Oliveira, S.M. (2001). Interpretation of surface geochemical data and integration with geological maps and landsat-tm images for mineral exploration from a portion of the Precambrian of Uruguay. *Revista Brasileira de Geociências,* Volume. 31(2), pp. 123-130.

Fleming, A. W. and Neale, T. I. (1979). Geochemical exploration at yandera porphyry copper prospect, Papua New Guinea. *Journal of Geochemical Exploration*, Volume 11, pp. 33-5.

Fletcher, W.K, Hoffman, S.J., Mehttens M.B., Sandiland, A.J. and Tompson I. (1987). Exploration Geochemistry; design and interpretation of soil Survey. The Association of Exploration Geochemist. In: Robertson J.M. (Editor). *Economic Geology, Society of Economic Geologists*. Chelsea USA, Volume 3 pp. 180.

Garret, R.G. (1989). The role of computer in exploration geochemistry. In Garland, G. D (editor.), Proceedings of Exploration, 87, Spec. Volume 3, pp. 586–608. *Ontario, Geological Survey*. Toronto, Canada.

Gonclaves, M.A., Mateus, A. and Oliveria, V. (2001). Geochemical anomaly separation by multifractal modeling. *Journal of Geochemical Exploration*, Volume 72 (2), pp 91-114.

Govindanjaru, R. (1989). *Geostand*. Newsl. pp. 13-113.

Grobler, D.F. (Compiler), Van Eeden, O.R, (1934-35), De Wet, N.P., & Strauss C.A., 1938, Van Graan, S.J. (1946), Van Rooyen, L., Hodgson, F.D.I., & Van der Merwe, J, (1976), Liebenberg, ., (1977), Botha, P.J. (1985), Grobler, D.F. (1987). (Coordinator) Schutte, I.C. (Explanations) (1995). *The geology of Christina Area, 2724 (Christiana) (1: 250 000 Geological map)*. Government Printer; Pretoria. South Africa, (one Sheet).

Hugo, P.J. (1979). Salt in the Republic of South Africa: *mem. Geol. Opn. S.Afr*., 65, pp. 105.

Hugo, W.S. (1948). Verslag oor die geologie van blad 59 oos van Wolmaransstad: interne versl. *Geol.Opn. S. Afr.*, pp. 8.

Isaaks, Edward H. and. Srivastava, R.M. (1989). *Introduction to Applied Geostatistics*. Oxford University Press, New York.

Jekins, R. (1988). *X-ray Flourescence spectrometry*. John Wiley and Son. London.

Jones, I.M. and Anhaeusser, C.R. (1993). Accretionary lapilli associated with Archaean banded iron formation of the Kraaipan Group, Amalia greenstone belt, South Africa. *Journal of Precambrian Research,* Volume 61 (1-2), pp. 117-136.

Jordan, C., Zhang, C. and Higgins, A. (2007). Using GIS and statistics to study influences of geology on probability features of surface soil geochemistry in Northern Ireland. *Journal of Geochemical Exploration.* Volume 93, pp. 135-152.

Kauranne, K. (1992). *Regoloth Exploration Geochemistry in Arctic and Temperate terrain*. Elsevier Science Publisher B.V. Amsterdam.

Karger, M. and Sandomirsky, S. (2001). Multidimentional statistical technique fordtection of low contrast geochemical anomalies. *Journal of Geochemical Exploration*, Volume 72 (1-3), pp. 47-58.

Keyser N. (Compiler), Gribnitz, K.H., Schutte, I.C., Callow, M.J.W., Clubley-Armstrong, A.R., Du Plessis, C.P., Keyser, N., Labuschagne, L.S., Minnaar, C.L.J., Moen, H.F.G., De Wet, N.P., Van Zyl, C.Z., Prevost, X.M., Davies, G.R., (Coordinator) Keyser N and Du Plessis, C. P (Explanations) (1993). *The geology of Vryburg Area, 2624 (Vryburg) (1: 250 000 Geological map)*. Government Printer; Pretoria. South Africa, (one Sheet).

Keyser N and Du Plessis, C. P (1993). Explanations: Sheet *2624 (1: 250 000). The geology of Vryburg Area*. Government Printer; Pretoria. South Africa.

Killick, A.M. (1986). The Damba Nickel deposits, Zimbabwe. In: Anhaeusser, C.R and Maske, S. (Editors). *Mineral Deposits of Southern Africa*, Volume 1. Geological Society of South Africa, Johannesburg, pp. 263-273.

Klassen R. A. (2001). The interpretation of background variation in regional geochemical survey – an example from Nunavut, Canada. *Geochemistry*: *Exploration, Environment, Analysis,* Volume 1 (3), pp. 163-173.

Klop, A.A.C. (1978). The metamorphosed sediments of the Pretoria Group and associated rocksnoerhwest of Zeerust, Western Transvaal: *Unpublished M.Sc. Thesis*, Univ. Pretoria, pp. 87.

Kotzé, M. (1996*a*). Geophysical interpretation of the Vryburg (27624). *Unpublished Report. Council for Geoscience, South Africa, 1996-0286,* pp. 5-10.

Kotzé, M. (1996*b*). Geophysical interpretation of the Mafikeng (2524) 1:250 000 Sheet. *Unpublished Report. Council for Geoscience, South Africa,* 1996-00287, pp. 7-31.

Kotzé, M. and Stettler E.H. (1997).Geophysical interpretation of the 2724 Christiana 1:250 000 Sheet. *Unpublished Report, Council for Geoscience, South Africa*, 1997-00349, pp. 5-9.

Krige, D.G. (1985). The use of geostatistics in defining and reducing the uncertainty of grade estimate. *Transection Geological Society of South Africa,* Volume. 88, pp. 69-72.

Kürzl, H. (1989). Data analysis and geochemical mapping for the regional stream sediment survey of Austria. *Journal of Geochemical Exploration*, Volume 32 (1-3), pp. 349-351.

Levinson, A.A. (1974). *Introduction to exploration geochemistry, 2nd edition*. Applied Publishing Ltd. Wilmette.

Li, C., Ma, T. and Shi, J. (2003). Application of a fractal method relating concentrations and distances for separation of geochemical anomalies from background. *Journal of Geochemical Exploration*, Volume 77 (2-3), pp. 167-175.

Lourie, J. (2004). *South African Geology for mining, metallurgical, hydrological and civil engineering.* 9th edition. Lupon Publishing. Johannesburg, pp. 82-141.

Marka, G., Wildea, A., Oliverb, N.H.S., Williamsb, P.J. and Ryanc, C.G. (2005). Modeling outflow from the Ernest Henry Fe oxide Cu–Au deposit: implications for ore genesis and exploration. *Journal of Geochemical Exploration*. Volume 85 (1), pp. 31–46.

Marshall, T.R. (1987). The diamondiferous gravel deposit of the Bamboesspruit, Southwestern Transvaal: southwestern Transvaal, northwestern Cape Province and Bopthuthatwana- Excursion guidebook. *Information Circular, Economic Geology Research Unit, University of Witwatersrand, Johannesburg, South Africa*, 188, pp. 13.

McCount, S., Hillard, P. and Armstrong, R.A. (2000). SHRIMP U-PB Zircon geochronology of granitoids fron the western margin of the Kaapvaal Craton: implications for crustal evolution in the Neoarchaean. *Journal of African Earth Science*, 31 (1A), pp. 48.

Moen, H.F.G. (compiler), Van Zyl, C.Z., Stulting, D.B., Wilke, D.P., Smit, P.J., Malherbe, S.J., Engelbrecht, L.N.J., Drewes, E.F.R., & De Villiers, S.B. (Cordinator) (1977) *Geological Series of Kuruman Area, 2722 (Kuruman) (1:250 000 Geological Map)* Government Printer, Pretoria. South Africa, (one Sheet).

Moen, H.F.G. (2006). The Olifantshoek Supergroup. In Johnson, M.R., Anhaeusser, C.R and Thomas, R.J. (Editors). *The Geology of South Africa*. Geological Society of South Africa, Johannesburg and Council for Geoscience, Pretoria, pp. 319-324.

Mookherjee, A. (1992). Metallogeny- the search for a rationale behind space-time selectivity of ore deposit formation. *Current Science*. Volume 63 (4, 25), pp. 173.

Michaluk, E. and Keyser, N. (compiler), Klop, A.A.C., Kingsley, C.S., Michaluk, E., Gribnitz, K.H., Prevost, X.M., Davis, G.M., Smit, P.J., Schutte, I.C., Callow, M.J.W. Coordinator (1991), Michaluk, E. and Moen, H. F. G. (Explanation). *The Geology of Mafikeng Area, 2524 (Mafikeng) (1:250 000 Geological map*). Government Printer, Pretoria. South Africa, (One Sheet).

Michaluk, E. and Moen, H. F. G. (1991). Explanations: Sheet *2524 (1: 250 000).*). *The Geology of Mafikeng Area.*. Government Printer, Pretoria. South Africa.

Mulja, T., Collin, M., Wong, H.H., Rizal, R., Browm, T.and Zainuddin, M. (2003). An integrated mineral exploration programme in the Takengon tenement, Aceh magmatic arc, north Sumatra. *Geochemistry: Exploration, Environment, Analysis*, Volume 3 (4), pp. 321- 335.

Müller, R.O. (1972). *Spectrochemical analysis by X-ray fluorescence*. Adam Hilger, London.

Naldrett, A.J. (2004). Magmatic Sulfides Deposit, Geology; Geochemistry and Exploration. Springer, Canada, pp. 67-277.

Nezampour, M.H. and Mosazadeh, H. (2006). Using statistical method and geochemical mapping techniques in exploration of gold and base metals in Khuni area, Anarak. *Iran Geochimica et Cosmochimica Acta,* Volume 70 (18), pp. 443.

Nel, P., P. van Heerden, M. Momberg, C. Newbery, R. Newbery & T. de Wet. (1995). Report on the State of the Environment in the North West Province - *Preliminary Survey*. North West Province Environmental Conservation, pp. 48

Nisbet, E.G., Dietrich, C.J. and Esenwein A. (1979). *Fortschi mineral*, pp. 7-264.

(NWPSoER) North West Department of Agriculture, Conservation and Environment (RSA) (2002). *Report on the State of the Environment in the North West Province* - Preliminary Survey. Full report. Mmabatho: Department of Agriculture, Conservation and Environment. Available from: htt://www.nwpg.org.za/soer.

Ohta, A., Imai, N., Terashima, S. and Tachibana, Y. (2005). Influence of surface geology and mineral deposits on the spatial distributions of elemental concentrations in the stream sediments of Hokkaido, Japan. *Journal of Geochemical Exploration*. Volume 86 (2), pp. 86-103.

Pötter P. (2001): Origin and exploration potential of sediment-hosted Mississippi Valley-Type F-Zn-Pb deposits in the Neoarchean platform dolostones of the Transvaal Supergroup, Northwest Province, South Africa. *Unpublished Diploma Thesis*, Westfalische Wilhelms –Univesitat Munster, Germany, pp.193.

Potts, P.J. (1987). *A handbook of silicate rock analysis.* Blankie and Son, London.

Poujol, M. and Anhaeusser, C.R. (2001). The Johannesburg Dome, South Africa: new single zircon U-Pb isotopic evidence for early Archaean granite-greenstone development within the central Kaapvaal Craton. *Precambrian Research*, 108, pp.139–157.

Poujol, M., Robb, l.J., Anhaeusser, C.R. and Gericke, B. (2003). A review of the geochronological constraints on the evolution of the Kaapvaal Craton, South Africa. *Precabrian Research*: Volume 127 (1-3), pp. 181-213.

Prinsloo, J. (1998). Geophysical interpretation of the Kuruman (2722). *Unpublished Report. Council for Geoscience, South Africa,* 1998-0028, pp. 3-8.

Ranjbar, H., Honarmand, M. and Moezifar, Z. (2004). *Application of the Crosta technique for porphyry copper alteration mapping, using ETM+ data in the southern part of the Iranian volcanic sedimentary belt.* Journal of Asian Earth Sciences, Volume 24, pp. 237-243.

Richards, T.E. (1986). Geological characteristics of rare-metal pegmatites of the UIS type in the Damara Orogen, South west Africa/Namibia. In: Anhaeusser, C.R and Maske, S. (Editors). *Mineral Deposits of Southern Africa*, Volume 2. Geological Society of South Africa, Johannesburg, pp.1845-1862.

Robb, L., 2005. *Introduction to ore-forming processes*. Blackwell, United Kingdom. Pp. 235-238.

Robb, L.J., Brandl, G., Anhaeusser, C.R. and Pouljol, M. (2006). Archaean Granitoid intrusions. In: Johnson, M.R., Anhaeusser, C.R and Thomas, R.J. (Editors). *The Geology of South Africa*. Geological Society of South Africa, Johannesburg and Council for Geoscience, Pretoria, pp. 57-94.

Robertson I.D.M. (2001).Geochemical exploration around the Harmony gold deposit, Peak Hill Western Australia. *Geochemistry: Exploration, Environment, Analysis*, Volume 1 (3), pp. 277-288.

Rose, A.W., Hawkes, H.E. and Webb, J.S. (1979). *Geochemistry in Mineral Exploration.* 2nd edition. Academic Press INC, London.

SACS (South African Committee Stratigraphy) (1980) Stratigraphy of South Africa. Part 1. (Compiler L. E Kent) Lithostratigraphy of the Republic of South Africa, South West Africa/Namibia, and the Republic of Botswana, Transkei and Venda: *Handbook of the Geological Survey of South Africa*, 8, pp. 690.

Schaefer, M.O. (2002) Paleoproterozoic Mississippi Valley-type Pb-Zn deposits of the Ghaap Group, Transvaal Supergroup in Griqualand West, South Africa. *Unpublished Ph.D. thesis*, RAU, Johannesburg, 367 pp

Schanzlin, M.R (1928). Memorandum on the mineral occurrences of Kunana location No.1, District Lichtenburg). *Unpublished Report. Geological Survey, South Africa*

Schulze, R.E. (1997). *South African Atlas of Agrohydrology and -Climatology. Water Research Commission*, Pretoria, Report TT 82/96,

Schutte, I.C. (1994). De geologie van die Gebied Christiana (Toeligting: Blad 2724). *Unpublished Report. Council for Geoscience, South Africa.*

Segura, R., Arancibia, V., Zúñiga, M.C. and Pastén, P. (2006). Distribution of copper, zinc, lead and cadmium concentrations in stream sediments from the Mapocho River in Santiago, Chile. *Journal of Geochemical Exploration*, Volume 91 (1-3), pp. 71-80.

Shee, S.R., Bristow, J.W., Bell, D.R., Smith, C.B., Allsopp, H.L. and Shee P.B., 1989. Petrology of kimberlites, related rocks and associated mantle xenoliths from the Kuruman province, South Africa. In: Ross, J., Jaques, A.L., Ferguson, J., Green, D.H., O'Reilly, S.Y., Danchin, R.V., Janse, A.J.A. (Editors), *Proceedings of the Fourth International Kimberlite Conference, Kimberlites and Related Rocks*. Blackwell Carlton, 60-82.

Sinclair, A.J. and Blackwell, G.H. (2002). *Applied Mineral Inventory Estimation*. Cambridge University Press. United Kingdom.

Southwood, M.J. (1986). The mineralogy of the Pering zinc-lead deposit, Cape Province with special reference to supergene alteration. In: Anhaeusser, C.R and Maske, S. (Editors). *Mineral Deposits of Southern Africa*, Volume 1. Geological Society of South Africa, Johannesburg, pp.875-889.

Spadoni, M., Voltaggio, M. and Cavarretta, G. (2005). Recognition of areas of anomalous concentration of potentially hazardous elements by means of a subcatchment-based discriminant analysis of stream sediments. *Journal of Geochemical Exploration*, Volume 87 (3), pp. 83-91.

Stanley C.R., 2003 Statistical evaluation of anomaly recognition performance. *Journal of Geochemistry: Exploration, environment, Analysis*, Volume 3, pp. 3-12.

Stanley C.R. (2006a) Numerical transformation of geochemical data: 1. Maximizing geochemical contrast to facilitate information extraction and improve data presentation. *Journal of Geochemistry: Exploration, environment, Analysis*, Volume 6, pp. 69-78.

Stanley C.R. (2006*b)*. Numerical transformation of geochemical data: 2. Stabilization measurement error to facilitate data interpretation *Journal of Geochemistry: Exploration, environment, Analysis*, Volume 6, pp. 79-96.

Stanley C.R., and Ryan R.P. (2008). Qualitative assessment of the success of geochemical exploration techniques using minimum probability methods. *Journal of Geochemistry: Exploration, environment, Analysis*, Volume 6, pp. 115-127.

Swan, A.R.H., Sandilands, M. (1995). *Introduction to Geological Data Analysis*. Blackwell Science ltd, London.

Swennen, R. and Van der Sluys, J. (1998). Zn, Pb, Cu and As distribution patterns in overbank and medium-order stream sediment samples: their use in exploration and environmental geochemistry. *Journal of Geochemical Exploration*, Volume 65 (1), pp. 27-45.

Till R, 1974. *Statistical Methods for the Earth Scientist an introduction*. Macmillan Press Ltd, London.

Ujiie-Mikoshiba, M., Imai, N., Terashima, S., Tachibana, Y. and Okai, T. (2006). Geochemical mapping in northern Honshu, Japan. *Journal of Applied Geochemistry,* Volume 21 (2), pp. 492-514.

Van Eeden, O.R., De Wet, N.P. and Strauss, C.A. (1963). The geology of the area around Schweizer-Reneke. *Explanation Sheet 2724B (Pudimoe) and 2725A Schweizer-Reneke*, Geological Survey of South Africa, pp 76.

Van der Westhuizen, W.A, De Bruiyn, H. and Meintjes, P.G. (2006). The Ventersdorp Supergroup. In: Johnson, M.R., Anhaeusser, C.R and Thomas, R.J. (Editors). *The Geology of South Africa*. Geological Society of South Africa, Johannesburg and Council for Geoscience, Pretoria, pp.187-208.

Van Rooyen, R.C. (2001). Geochemical Distribution of the Scandium, Titanium, Vanadium, Chromium, Manganese, Iron (Fe2O3), Cobalt, Nickel, Copper, Zinc, Arsenic, Rubidium, Strontium, Yttrium, Zirconium, Niobium, Molybdenum, Tin, Antimony, Barium, Tungsten, Lead, Thorium & Uranium. (1: 250 000 3018 Loeriesfontein Geochemical map). Council for Geoscience South Africa, (two sheets)

Verwoed, W.J. (2006). In: Johnson, M.R., Anhaeusser, C.R and Thomas, R.J. (Editors). *The Geology of South Africa*. Geological Society of South Africa, Johannesburg and Council for Geoscience, Pretoria, pp. 381-393.

Vorster, C.J. (Producer) (2001). *Metallogenic Map of the Republic of South Africa and the Kingdoms of Lesotho and Swaziland, 1: 1 000 00.* Government Printer, Pretoria.

Wang, X. (2003). Delineation of geochemical blocks for undiscovered large ore deposits using deep-penetrating methods in alluvial terrains of eastern China. *Journal of Geochemical Exploration,* Volume 77 (1), pp.15–24.

Webster, R. and Oliver, M. A. (2001). *Geostatistics for Environmental Scientists*. John Wiley and Sons, LTD. Chichester, pp. 11-35.

Wheatley, C.J.V., Whitfield, G.G., Kenny, K.J., and Brich, A. (1986). The Pering carbonate-hosted Zinc-lead deposits, Griqualand West. In: Anhaeusser, C.R and Maske, S. (Editors). *Mineral Deposits of Southern Africa*, Volume 1. Geological Society of South Africa, Johannesburg, pp.867-874.

Zhang, C., Jordan, C. and Higgins, A. (2006). Using neighbourhood statistics and GIS to quantify and visualize spatial variation in geochemical variables: an example using Ni concentrations in the top soils of Northern Ireland. *Geoderma*, Volume 137 (3-4), pp. 466–476.

Zupan, N. and Pirc, S. (1999). Calcium distribution in soils and stream sediments in Istria (Croatia) and the Slovenian littoral. *Journal of Geochemical Exploration*, Volume 65 (3), pp. 205-218.

APPENDICES

APPENDIX 1: SUMMARY STATISTICS OF THE LITHOLOGICAL GROUPS

Table A- 1: Summary statistics of the Amphibolites Basement raw data set.

Element	N	Min	Max	Mean	Median	St. Dev	Var	CV	Skew	Kurt	Threshold
TiO_2	793	0.48	1.38	0.93	0.93	0.14	0.02	0.16	-0.10	-0.01	**1.2**
MnO	793	0.02	0.21	0.08	0.07	0.03	0.00	0.38	0.75	0.92	**0.1**
Fe_2O_3	793	1.34	9.48	4.23	4.09	1.33	1.78	0.32	0.39	-0.26	**7**
Sc	793	3.00	25.00	11.97	12.00	3.44	11.86	0.29	0.09	-0.32	**19**
V	793	18.00	184.00	66.32	63.00	23.66	559.57	0.36	0.73	1.06	**114**
Cr	792	19.00	630.00	109.45	101.00	57.16	3267.04	0.52	3.26	19.52	**224**
Co	792	8.00	33.00	15.50	15.00	4.25	18.08	0.27	0.78	0.59	**24**
Ni	792	14.00	250.00	48.27	45.00	22.73	516.48	0.47	22.73	11.74	**94**
Cu	793	10.00	72.00	27.05	25.00	9.73	94.64	0.36	1.03	1.58	**47**
Zn	793	20.00	139.00	43.80	42.00	13.60	184.99	0.31	1.24	4.62	**71**
As	788	1.00	164.00	13.67	12.00	9.86	97.14	0.72	8.43	110.79	**33**
Rb	793	43.00	150.00	84.75	84.00	16.66	277.50	0.20	0.44	0.60	**118**
Sr	793	26.00	360.00	78.90	70.00	34.31	1177.14	0.43	2.53	11.66	**148**
Y	793	3.00	102.00	25.22	25.00	5.16	26.64	0.20	4.11	61.93	**36**
Zr	792	236.00	1892.00	830.43	823.00	212.48	45147.39	0.26	0.42	1.29	**1255**
Nb	792	1.00	29.00	19.44	20.00	1.89	3.56	0.10	-1.67	13.17	**23**
Ba	793	102.00	1134.00	370.50	369.00	93.80	8797.73	0.25	1.56	9.10	**558**
W	793	2.00	16.00	9.79	10.00	2.41	5.79	0.25	0.10	-0.45	**15**
Pb	679	1.00	31.00	6.56	6.00	3.81	14.52	0.58	1.30	3.97	**14**
Th	790	3.00	26.00	14.72	15.00	2.16	4.66	0.15	-0.35	5.57	**19**
U	189	1.00	5.00	1.89	2.00	0.95	0.90	0.50	0.83	0.07	**4**

Table A- 2: Table Summary statistics of the Amphibolites Basement log-transformed data set.

Element	N	Min	Max	Mean	Median	St. Dev	Var	CV	Skew	Kurt	Log Threshold
TiO_2	793	-0.73	0.32	-0.09	-0.07	0.16	0.03	-1.83	-0.63	0.83	**1.3**
MnO	793	-3.91	-1.56	-2.66	-2.66	0.39	0.15	-0.15	-0.28	-0.15	**0.2**
Fe_2O_3	793	0.29	2.25	1.39	1.41	0.33	0.11	0.24	-0.34	-0.29	**8**
Sc	793	1.10	3.22	2.44	2.48	0.32	0.10	0.13	-0.75	0.73	**23**
V	793	2.89	5.21	4.13	4.14	0.37	0.13	0.09	-0.31	-0.05	**138**
Cr	792	2.94	6.45	4.59	4.62	0.44	0.19	0.10	0.14	1.41	**262**
Co	792	2.08	3.50	2.70	2.71	0.27	0.07	0.10	0.10	-0.39	**26**
Ni	792	2.64	5.52	3.78	3.81	0.43	0.18	0.11	0.09	0.13	**114**
Cu	793	2.30	4.28	3.24	3.22	0.35	0.12	0.11	0.06	-0.31	**54**
Zn	793	3.00	4.93	3.73	3.74	0.30	0.09	0.08	0.08	-0.14	**80**
As	788	0.00	5.10	2.48	2.48	0.53	0.29	0.22	-0.74	4.68	**40**
Rb	793	3.76	5.01	4.42	4.43	0.20	0.04	0.04	-0.22	0.26	**126**
Sr	793	3.26	5.89	4.30	4.25	0.36	0.13	0.08	0.69	0.90	**162**
Y	793	1.10	4.62	3.21	3.22	0.21	0.04	0.06	-2.10	24.06	**38**
Zr	793	5.46	7.55	6.69	6.71	0.27	0.07	0.04	-0.76	1.89	**1433**
Nb	792	0.00	3.37	2.96	3.00	0.14	0.02	0.05	-11.77	236.45	**26**
Ba	793	4.62	7.03	5.88	5.91	0.25	0.06	0.04	-0.37	2.66	**610**
W	793	0.69	2.77	2.25	2.30	0.26	0.07	0.12	-0.66	1.14	**17**
Pb	679	0.00	3.43	1.69	1.79	0.67	0.45	0.39	-0.79	0.52	**26**
Th	790	1.10	3.26	2.68	2.71	0.17	0.03	0.06	-3.32	25.92	**21**
U	189	0.00	1.61	0.52	0.69	0.49	0.24	0.95	0.22	-1.37	**5**

Table A- 3: Summary statistics of the Kraaipan Group raw data set.

Element	N	Min	Max	Mean	Median	St. Dev	Var	CV	Skew	Kurt	Threshold
TiO_2	51	0.79	1.73	1.05	0.99	0.21	0.04	0.20	1.75	3.28	**1.5**
MnO	51	0.04	0.15	0.09	0.08	0.03	0.00	0.35	0.42	-0.66	**0.1**
Fe_2O_3	51	2.25	16.50	6.21	5.64	3.06	9.35	0.49	1.50	2.50	**12**
Sc	51	7.00	28.00	15.25	14.00	5.16	26.63	0.34	0.69	-0.33	**26**
V	51	36.00	207.00	89.80	84.00	39.53	1562.68	0.44	0.91	0.56	**169**
Cr	51	19.00	814.00	201.48	157.50	165.88	27515.97	0.82	2.17	5.11	**533**
Co	51	2.00	32.00	17.14	17.00	6.00	36.00	0.35	0.39	0.57	**29**
Ni	51	20.00	278.00	72.78	59.00	51.86	2688.97	0.71	51.86	5.59	**176**
Cu	51	11.00	160.00	38.90	35.00	24.25	587.85	0.62	2.85	11.84	**87**
Zn	51	7.00	78.00	44.84	43.00	12.61	159.13	0.28	0.15	1.40	**70**
As	44	1.00	46.00	11.34	10.50	7.54	56.83	0.66	2.33	9.47	**26**
Rb	51	41.00	108.00	62.75	61.00	14.23	202.55	0.23	0.71	0.90	**91**
Sr	51	32.00	213.00	72.76	56.00	39.41	1552.82	0.54	2.30	5.67	**152**
Y	51	13.00	34.00	22.39	22.00	4.19	17.56	0.19	0.37	0.28	**31**
Zr	51	336.00	1524.00	777.45	772.00	228.37	52152.81	0.29	0.74	1.20	**1234**
Nb	51	13.00	22.00	18.10	19.00	2.28	5.21	0.13	-0.69	0.23	**23**
Ba	51	170.00	567.00	337.67	325.00	72.54	5261.87	0.21	0.77	1.67	**483**
W	51	6.00	18.00	12.75	13.00	3.02	9.11	0.24	-0.24	-0.49	**19**
Pb	19	1.00	11.00	3.21	2.00	2.72	7.40	0.85	1.90	3.46	**9**
Th	51	2.00	16.00	11.37	12.00	2.76	7.60	0.24	-1.00	1.63	**17**
U	2	1.00	1.00	1.00	1.00	0.00	0.00	0.00	0.00	0.00	**0**

Table A- 4: Summary statistics of the Kraaipan Group Log transformed data set.

Element	N	Min	Max	Mean	Median	St. Dev	Var	CV	Skew	Kurt	Log Threshold
TiO_2	51	-0.24	0.55	0.03	-0.01	0.18	0.03	5.91	1.24	1.55	**1.5**
MnO	51	-3.22	-1.90	-2.50	-2.53	0.36	0.13	-0.14	-0.20	-0.72	**0.2**
Fe_2O_3	51	0.81	2.80	1.73	1.73	0.44	0.20	0.26	0.37	-0.18	**15**
Sc	51	1.95	3.33	2.67	2.64	0.33	0.11	0.12	0.07	-0.61	**30**
V	51	3.58	5.33	4.41	4.43	0.43	0.19	0.10	0.08	-0.82	**214**
Cr	50	2.94	6.70	5.05	5.06	0.72	0.51	0.14	0.01	0.79	**847**
Co	51	0.69	3.47	2.77	2.83	0.44	0.19	0.16	-2.10	9.24	**42**
Ni	51	3.00	5.63	4.11	4.08	0.56	0.32	0.14	0.64	0.68	**220**
Cu	51	2.40	5.08	3.53	3.56	0.50	0.25	0.14	0.49	0.82	**105**
Zn	51	1.95	4.36	3.75	3.76	0.36	0.13	0.10	-2.56	12.49	**93**
As	44	0.00	3.83	2.22	2.35	0.71	0.51	0.32	-0.93	1.68	**49**
Rb	51	3.71	4.68	4.11	4.11	0.22	0.05	0.05	0.09	-0.29	**98**
Sr	51	3.47	5.36	4.19	4.03	0.42	0.18	0.10	1.11	1.13	**167**
Y	51	2.56	3.53	3.09	3.09	0.19	0.04	0.06	-0.21	0.30	**33**
Zr	51	5.82	7.33	6.61	6.65	0.30	0.09	0.04	-0.26	0.43	**1410**
Nb	51	2.56	3.09	2.89	2.94	0.13	0.02	0.05	-1.02	0.73	**24**
Ba	51	5.14	6.34	5.80	5.78	0.21	0.05	0.04	-0.22	1.58	**519**
W	51	1.79	2.89	2.51	2.56	0.26	0.07	0.10	-0.82	0.34	**21**
Pb	19	0.00	2.40	0.90	0.69	0.73	0.53	0.81	0.44	-0.36	**14**
Th	51	0.69	2.77	2.39	2.48	0.34	0.11	0.14	-2.89	12.26	**23**
U	2										

Table A- 5: Summary statistics of the Kanye Formation raw data set.

Element	N	Min	Max	Mean	Median	St. Dev	Var	CV	Skew	Kurt	Threshold
TiO_2	96	0.60	1.08	0.83	0.82	0.09	0.01	0.11	0.37	0.26	**1.01**
MnO	96	0.04	0.19	0.08	0.07	0.02	0.00	0.31	1.72	5.65	**0.12**
Fe_2O_3	96	2.13	6.44	3.62	3.50	0.83	0.69	0.23	1.29	2.15	**5**
Sc	96	4.00	16.00	7.93	8.00	2.39	5.73	0.30	1.31	2.43	**13**
V	96	10.00	74.00	34.66	32.00	13.14	172.75	0.38	0.75	0.26	**61**
Cr	96	50.00	144.00	80.29	79.00	17.70	313.45	0.22	0.94	1.74	**116**
Co	96	7.00	16.00	10.03	10.00	1.88	3.53	0.19	1.05	1.24	**14**
Ni	96	18.00	58.00	30.38	30.00	7.65	58.49	0.25	7.65	2.53	**46**
Cu	96	15.00	43.00	21.84	21.00	5.23	27.35	0.24	1.80	3.95	**32**
Zn	96	30.00	117.00	48.66	46.00	14.09	198.56	0.29	2.67	9.83	**77**
As	95	1.00	44.00	13.22	12.00	6.57	43.20	0.50	1.66	5.32	**26**
Rb	96	79.00	157.00	121.18	120.50	15.93	253.77	0.13	-0.36	-0.07	**153**
Sr	96	25.00	86.00	34.19	32.00	7.03	49.48	0.21	4.48	30.62	**48**
Y	96	32.00	69.00	47.88	46.50	7.71	59.39	0.16	0.39	-0.04	**63**
Zr	96	503.00	1116.00	826.93	828.50	105.30	11088.64	0.13	-0.23	0.57	**1038**
Nb	96	20.00	32.00	25.39	25.50	2.30	5.29	0.09	0.44	0.53	**30**
Ba	96	212.00	611.00	342.71	333.50	70.77	5008.63	0.21	1.13	1.94	**484**
W	96	6.00	11.00	8.72	9.00	0.79	0.63	0.09	-0.89	2.53	**10**
Pb	60	1.00	10.00	3.73	3.00	2.36	5.59	0.63	0.86	-0.24	**8**
Th	96	10.00	20.00	16.66	17.00	1.70	2.88	0.10	-1.18	2.64	**20**
U	77	1.00	5.00	2.26	2.00	1.15	1.33	0.51	0.69	-0.24	**5**

Table A- 6: Summary statistics of the Kanye Formation log-transformed data set.

Element	N	Min	Max	Mean	Median	St. Dev	Var	CV	Skew	Kurt	Log Threshold
TiO_2	96	-0.51	0.08	-0.19	-0.20	0.11	0.01	-0.56	0.03	0.22	**1.0**
MnO	96	-3.22	-1.66	-2.62	-2.66	0.29	0.08	-0.11	0.30	0.94	**0.1**
Fe_2O_3	96	0.76	1.86	1.26	1.25	0.21	0.05	0.17	0.52	0.77	**6**
Sc	96	1.39	2.77	2.03	2.08	0.28	0.08	0.14	0.24	0.67	**14**
V	96	2.30	4.30	3.47	3.47	0.39	0.15	0.11	-0.29	0.26	**75**
Cr	96	3.91	4.97	4.36	4.37	0.21	0.05	0.05	0.22	0.09	**123**
Co	96	1.95	2.77	2.29	2.30	0.18	0.03	0.08	0.49	0.40	**14**
Ni	96	2.89	4.06	3.39	3.40	0.23	0.05	0.07	0.57	0.59	**48**
Cu	96	2.71	3.76	3.06	3.04	0.21	0.04	0.07	1.07	1.38	**33**
Zn	96	3.40	4.76	3.85	3.83	0.24	0.06	0.06	1.33	3.30	**78**
As	95	0.00	3.78	2.46	2.48	0.55	0.30	0.22	-1.37	4.98	**41**
Rb	96	4.37	5.06	4.79	4.79	0.14	0.02	0.03	-0.74	0.51	**160**
Sr	96	3.22	4.45	3.52	3.47	0.16	0.03	0.05	2.29	10.80	**47**
Y	96	3.47	4.23	3.86	3.84	0.16	0.03	0.04	-0.02	-0.24	**66**
Zr	96	6.22	7.02	6.71	6.72	0.13	0.02	0.02	-0.74	1.34	**1078**
Nb	96	3.00	3.47	3.23	3.24	0.09	0.01	0.03	0.13	0.30	**30**
Ba	96	5.36	6.42	5.82	5.81	0.20	0.04	0.03	0.45	0.49	**507**
W	96	1.79	2.40	2.16	2.20	0.10	0.01	0.04	-1.41	3.82	**11**
Pb	60	0.00	2.30	1.11	1.10	0.67	0.44	0.60	-0.14	-0.83	**14**
Th	96	2.30	3.00	2.81	2.83	0.11	0.01	0.04	-1.77	5.21	**21**
U	77	0.00	1.61	0.68	0.69	0.53	0.28	0.77	-0.06	-1.22	**7**

Table A- 7: Summary statistics of the Gaborone Granite raw data set.

Element	N	Min	Max	Mean	Median	St. Dev	Var	CV	Skew	Kurt	Threshold
TiO_2	81	0.59	1.28	0.85	0.83	0.12	0.02	0.14	0.85	1.01	**1.1**
MnO	81	0.04	0.18	0.08	0.08	0.03	0.00	0.31	1.21	2.55	**0.1**
Fe_2O_3	81	1.28	7.45	3.73	3.49	1.11	1.24	0.30	1.20	1.99	**6**
Sc	81	3.00	20.00	8.49	8.00	2.95	8.73	0.35	1.35	3.03	**14**
V	81	16.00	107.00	41.77	36.00	17.04	290.26	0.41	1.47	2.39	**76**
Cr	81	45.00	469.00	89.73	84.00	47.06	2215.05	0.52	6.77	53.92	**184**
Co	81	7.00	24.00	11.00	10.00	2.71	7.35	0.25	2.02	6.08	**16**
Ni	81	17.00	127.00	33.20	30.00	13.56	183.76	0.41	13.56	28.68	**60**
Cu	81	12.00	60.00	23.15	21.00	7.72	59.58	0.33	2.13	6.30	**39**
Zn	81	20.00	136.00	43.36	41.00	16.07	258.23	0.37	3.09	14.29	**75**
As	76	2.00	19.00	10.25	10.00	4.15	17.23	0.40	-0.08	-0.45	**19**
Rb	81	87.00	176.00	135.89	137.00	17.37	301.65	0.13	0.03	0.03	**171**
Sr	81	23.00	71.00	35.28	34.00	7.15	51.06	0.20	1.79	6.63	**50**
Y	81	29.00	71.00	51.88	50.00	8.28	68.63	0.16	0.25	0.02	**68**
Zr	81	575.00	1531.00	956.15	920.00	188.87	35670.80	0.20	0.64	0.47	**1334**
Nb	81	19.00	37.00	28.41	29.00	3.53	12.44	0.12	-0.08	0.35	**35**
Ba	81	169.00	491.00	276.79	268.00	57.83	3344.22	0.21	0.95	1.57	**392**
W	81	6.00	11.00	8.68	9.00	1.07	1.15	0.12	-0.64	0.33	**11**
Pb	74	1.00	16.00	6.39	5.50	3.58	12.79	0.56	0.58	-0.44	**14**
Th	81	13.00	24.00	17.63	18.00	2.15	4.64	0.12	0.47	0.32	**22**
U	66	1.00	9.00	2.98	3.00	1.71	2.91	0.57	1.23	1.95	**6**

Table A- 8: Summary statistics of the Gaborone Granite log-transformed data set.

Element	N	Min	Max	Mean	Median	St. Dev	Var	CV	Skew	Kurt	Log Threshold
TiO_2	81	-0.53	0.25	-0.18	-0.19	0.14	0.02	-0.80	0.42	0.26	**1.1**
MnO	81	-3.22	-1.71	-2.57	-2.53	0.30	0.09	-0.12	0.15	0.21	**0.1**
Fe_2O_3	81	0.25	2.01	1.28	1.25	0.29	0.08	0.22	-0.06	1.83	**7**
Sc	81	1.10	3.00	2.08	2.08	0.33	0.11	0.16	-0.02	0.95	**17**
V	81	2.77	4.67	3.66	3.58	0.37	0.14	0.10	0.44	0.23	**87**
Cr	81	3.81	6.15	4.44	4.43	0.29	0.08	0.07	2.61	14.49	**158**
Co	81	1.95	3.18	2.37	2.30	0.22	0.05	0.09	1.11	1.77	**17**
Ni	81	2.83	4.84	3.45	3.40	0.28	0.08	0.08	1.91	7.04	**58**
Cu	81	2.48	4.09	3.10	3.04	0.28	0.08	0.09	1.02	1.51	**41**
Zn	81	3.00	4.91	3.72	3.71	0.29	0.09	0.08	1.09	3.21	**78**
As	76	0.69	2.94	2.22	2.30	0.52	0.28	0.24	-1.29	1.48	**30**
Rb	81	4.47	5.17	4.90	4.92	0.13	0.02	0.03	-0.40	0.59	**176**
Sr	81	3.14	4.26	3.55	3.53	0.19	0.03	0.05	0.77	1.63	**51**
Y	81	3.37	4.26	3.94	3.91	0.16	0.03	0.04	-0.30	0.84	**72**
Zr	81	6.35	7.33	6.84	6.82	0.19	0.04	0.03	0.07	0.05	**1411**
Nb	81	2.94	3.61	3.34	3.37	0.13	0.02	0.04	-0.52	0.75	**37**
Ba	81	5.13	6.20	5.60	5.59	0.20	0.04	0.04	0.25	0.33	**414**
W	81	1.79	2.40	2.15	2.20	0.13	0.02	0.06	-0.99	0.76	**11**
Pb	74	0.00	2.77	1.68	1.70	0.64	0.41	0.38	-0.53	-0.25	**24**
Th	81	2.56	3.18	2.86	2.89	0.12	0.01	0.04	0.12	0.00	**22**
U	66	0.00	2.20	0.94	1.10	0.58	0.33	0.62	-0.16	-0.58	**10**

Table A- 9: Summary statistics of the Dominion Group raw data set.

Element	N	Min	Max	Mean	Median	St. Dev	Var	CV	Skew	Kurt	Threshold
TiO_2	139	0.60	1.08	0.85	0.85	0.10	0.01	0.12	0.15	-0.29	**1.1**
MnO	139	0.03	0.15	0.06	0.06	0.02	0.00	0.32	1.35	2.37	**0.1**
Fe_2O_3	139	1.77	5.69	3.27	3.17	0.77	0.59	0.24	0.72	0.41	**5**
Sc	139	4.00	16.00	9.96	10.00	2.10	4.43	0.21	0.12	0.13	**14**
V	139	23.00	90.00	46.23	42.00	14.19	201.22	0.31	0.94	0.58	**75**
Cr	139	42.00	164.00	81.96	74.00	26.93	725.24	0.33	1.27	0.91	**136**
Co	139	8.00	22.00	11.54	11.00	2.82	7.95	0.24	1.13	1.13	**17**
Ni	139	14.00	75.00	27.95	24.00	11.38	129.40	0.41	11.38	3.66	**51**
Cu	139	11.00	58.00	20.36	19.00	6.38	40.74	0.31	2.00	8.01	**33**
Zn	139	27.00	236.00	44.52	42.00	19.06	363.18	0.43	7.57	74.44	**83**
As	139	6.00	30.00	14.17	14.00	4.80	22.99	0.34	0.59	0.40	**24**
Rb	139	50.00	103.00	72.71	73.00	10.03	100.67	0.14	0.23	0.45	**93**
Sr	139	34.00	132.00	46.06	44.00	9.44	89.16	0.21	5.62	49.33	**65**
Y	139	18.00	42.00	26.37	25.00	5.32	28.29	0.20	0.71	0.25	**37**
Zr	139	364.00	1389.00	831.22	851.00	199.37	39748.97	0.24	-0.18	-0.11	**1230**
Nb	139	17.00	26.00	21.34	21.00	1.98	3.92	0.09	0.37	-0.30	**25**
Ba	139	199.00	498.00	293.30	287.00	48.58	2359.78	0.17	0.64	1.20	**390**
W	139	7.00	31.00	12.06	12.00	2.38	5.67	0.20	3.59	28.15	**17**
Pb	103	1.00	22.00	4.24	3.00	3.49	12.15	0.82	2.28	7.24	**11**
Th	139	11.00	16.00	13.99	14.00	1.15	1.33	0.08	-0.23	-0.20	**16**
U	6	1.00	2.00	1.17	1.00	0.41	0.17	0.35	2.45	6.00	**2**

Table A- 10: Summary statistics of the Dominion Group log-transformed data set.

Element	N	Min	Max	Mean	Median	St. Dev	Var	CV	Skew	Kurt	Log Threshold	Threshold
TiO_2	139	-0.51	0.08	-0.17	-0.16	0.12	0.01	-0.70	-0.15	-0.14	**0.1**	**1.1**
MnO	139	-3.51	-1.90	-2.78	-2.81	0.29	0.09	-0.11	0.46	0.12	**-2.2**	**0.1**
Fe_2O_3	139	0.57	1.74	1.16	1.15	0.23	0.05	0.20	0.10	-0.17	**2**	**5**
Sc	139	1.39	2.77	2.28	2.30	0.22	0.05	0.10	-0.67	1.31	**3**	**15**
V	139	3.14	4.50	3.79	3.74	0.29	0.09	0.08	0.28	-0.44	**4**	**79**
Cr	139	3.74	5.10	4.36	4.30	0.30	0.09	0.07	0.71	-0.15	**5**	**141**
Co	139	2.08	3.09	2.42	2.40	0.23	0.05	0.09	0.61	-0.17	**3**	**18**
Ni	139	2.64	4.32	3.27	3.18	0.34	0.12	0.11	0.91	0.51	**4**	**52**
Cu	139	2.40	4.06	2.97	2.94	0.28	0.08	0.09	0.64	0.76	**4**	**34**
Zn	139	3.30	5.46	3.75	3.74	0.26	0.07	0.07	2.32	13.30	**4**	**71**
As	139	1.79	3.40	2.59	2.64	0.35	0.12	0.14	-0.31	-0.23	**3**	**27**
Rb	139	3.91	4.63	4.28	4.29	0.14	0.02	0.03	-0.23	0.18	**5**	**95**
Sr	139	3.53	4.88	3.82	3.78	0.16	0.02	0.04	2.40	14.36	**4**	**62**
Y	139	2.89	3.74	3.25	3.22	0.20	0.04	0.06	0.26	-0.46	**4**	**38**
Zr	139	5.90	7.24	6.69	6.75	0.26	0.07	0.04	-0.88	0.60	**7**	**1367**
Nb	139	2.83	3.26	3.06	3.04	0.09	0.01	0.03	0.16	-0.37	**3**	**26**
Ba	139	5.29	6.21	5.67	5.66	0.16	0.03	0.03	0.10	0.01	**6**	**401**
W	139	1.95	3.43	2.47	2.48	0.17	0.03	0.07	0.81	6.53	**3**	**17**
Pb	103	0.00	3.09	1.17	1.10	0.74	0.55	0.63	0.06	-0.43	**3**	**14**
Th	139	2.40	2.77	2.63	2.64	0.08	0.01	0.03	-0.46	0.10	**3**	**16**
U	6	0.00	0.69	0.12	0.00	0.28	0.08	2.45	2.45	6.00	**1**	**2**

Table A- 11: Summary statistics of the Hospital Hill Subgroup raw data set.

Element	N	Min	Max	Mean	Median	St. Dev	Var	CV	Skew	Kurt	Threshold
TiO_2	56	0.72	1.13	0.91	0.91	0.09	0.01	0.10	0.09	-0.28	**1.1**
MnO	56	0.03	0.10	0.06	0.06	0.01	0.00	0.24	0.51	0.69	**0.1**
Fe_2O_3	56	2.04	9.59	3.83	3.46	1.42	2.02	0.37	2.15	5.84	**7**
Sc	56	6.00	15.00	10.96	11.00	2.25	5.05	0.21	-0.15	-0.47	**15**
V	56	27.00	96.00	54.38	54.00	12.48	155.66	0.23	0.55	1.16	**79**
Cr	56	60.00	165.00	120.82	124.00	29.45	867.09	0.24	-0.45	-0.76	**180**
Co	56	3.00	20.00	11.88	12.00	3.20	10.22	0.27	0.18	1.22	**18**
Ni	56	18.00	54.00	33.61	32.50	8.68	75.33	0.26	8.68	-0.41	**51**
Cu	56	14.00	36.00	22.25	22.00	5.29	27.97	0.24	0.53	0.17	**33**
Zn	56	27.00	69.00	40.82	39.00	9.06	82.04	0.22	0.67	0.51	**59**
As	53	3.00	32.00	13.25	12.00	5.08	25.77	0.38	0.89	2.33	**23**
Rb	56	47.00	87.00	67.14	68.00	8.60	74.02	0.13	0.19	0.12	**84**
Sr	56	33.00	105.00	44.46	42.00	10.47	109.71	0.24	3.97	20.46	**65**
Y	56	19.00	35.00	24.66	24.00	3.59	12.88	0.15	0.73	0.59	**32**
Zr	56	597.00	1178.00	869.88	862.00	133.70	17875.42	0.15	0.04	-0.07	**1137**
Nb	56	17.00	26.00	20.61	20.00	1.58	2.50	0.08	0.74	2.13	**24**
Ba	56	170.00	365.00	273.88	273.50	37.50	1406.51	0.14	-0.01	0.48	**349**
W	56	9.00	29.00	12.93	13.00	2.69	7.23	0.21	3.90	23.21	**18**
Pb	28	1.00	16.00	3.50	2.00	3.44	11.81	0.98	2.34	6.03	**10**
Th	56	9.00	17.00	13.63	14.00	1.37	1.88	0.10	-0.56	1.77	**16**
U	1	2.00	2.00								

Table A- 12: Summary statistics of the Hospital Hill Subgroup log-transformed data set.

Element	N	Min	Max	Mean	Median	St. Dev	Var	CV	Skew	Kurt	Log Threshold
TiO_2	56	-0.33	0.12	-0.09	-0.09	0.10	0.01	-1.05	-0.16	-0.25	**1.1**
MnO	56	-3.51	-2.30	-2.84	-2.81	0.24	0.06	-0.09	-0.27	0.26	**0.1**
Fe_2O_3	56	0.71	2.26	1.29	1.24	0.31	0.10	0.24	0.96	1.43	**7**
Sc	56	1.79	2.71	2.37	2.40	0.22	0.05	0.09	-0.68	0.27	**17**
V	56	3.30	4.56	3.97	3.99	0.23	0.05	0.06	-0.29	0.55	**87**
Cr	56	4.09	5.11	4.76	4.82	0.27	0.07	0.06	-0.91	0.06	**209**
Co	56	1.10	3.00	2.43	2.48	0.31	0.10	0.13	-1.61	5.79	**22**
Ni	56	2.89	3.99	3.48	3.48	0.27	0.07	0.08	-0.29	-0.27	**57**
Cu	56	2.64	3.58	3.07	3.09	0.24	0.06	0.08	-0.05	-0.42	**36**
Zn	56	3.30	4.23	3.69	3.66	0.22	0.05	0.06	0.12	-0.43	**63**
As	53	1.10	3.47	2.51	2.48	0.42	0.17	0.17	-0.87	2.15	**31**
Rb	56	3.85	4.47	4.20	4.22	0.13	0.02	0.03	-0.20	0.22	**87**
Sr	56	3.50	4.65	3.78	3.74	0.18	0.03	0.05	2.56	9.92	**64**
Y	56	2.94	3.56	3.20	3.18	0.14	0.02	0.04	0.32	0.06	**33**
Zr	56	6.39	7.07	6.76	6.76	0.16	0.02	0.02	-0.40	0.06	**1193**
Nb	56	2.83	3.26	3.02	3.00	0.08	0.01	0.02	0.36	1.69	**24**
Ba	56	5.14	5.90	5.60	5.61	0.14	0.02	0.03	-0.56	1.30	**363**
W	56	2.20	3.37	2.54	2.56	0.17	0.03	0.07	1.76	9.63	**18**
Pb	28	0.00	2.77	0.93	0.69	0.78	0.60	0.84	0.63	-0.18	**16**
Th	56	2.20	2.83	2.61	2.64	0.11	0.01	0.04	-1.12	3.26	**17**
U	1										

Table A- 13: Summary statistics of the Klipriviersberg Group raw data set.

Element	N	Min	Max	Mean	Median	St. Dev	Var	CV	Skew	Kurt	Threshold
TiO_2	2191	0.34	1.46	0.91	0.91	0.10	0.01	0.11	-0.13	1.18	**1.1**
MnO	2191	0.02	0.96	0.09	0.09	0.03	0.00	0.33	10.19	271.78	**0.2**
Fe_2O_3	2191	0.95	8.87	4.66	4.63	1.01	1.03	0.22	0.29	0.58	**7**
Sc	2191	1.00	25.00	13.62	14.00	2.47	6.12	0.18	0.09	0.87	**19**
V	2191	22.00	156.00	75.06	74.00	15.70	246.46	0.21	0.55	1.55	**106**
Cr	2191	42.00	782.00	165.06	150.00	70.64	4990.16	0.43	2.47	11.08	**306**
Co	2191	7.00	36.00	17.27	17.00	3.86	14.87	0.22	0.57	0.57	**25**
Ni	2191	9.00	172.00	54.88	52.00	19.11	365.22	0.35	19.11	3.67	**93**
Cu	2191	8.00	72.00	29.11	29.00	6.80	46.29	0.23	0.85	2.47	**43**
Zn	2191	24.00	317.00	50.82	50.00	12.38	153.28	0.24	6.43	113.96	**76**
As	2188	1.00	45.00	13.85	13.00	4.62	21.33	0.33	0.70	2.11	**23**
Rb	2191	33.00	133.00	68.86	68.00	9.46	89.45	0.14	0.45	1.91	**88**
Sr	2191	19.00	145.00	50.97	49.00	12.55	157.40	0.25	1.50	5.44	**76**
Y	2191	11.00	58.00	23.54	23.00	3.35	11.25	0.14	0.98	5.67	**30**
Zr	2191	239.00	1824.00	784.98	781.00	163.87	26853.12	0.21	0.49	1.58	**1113**
Nb	2191	9.00	30.00	19.33	19.00	1.35	1.83	0.07	0.16	3.80	**22**
Ba	2191	10.00	479.00	262.09	259.00	46.88	2197.36	0.18	0.33	1.21	**356**
W	2191	2.00	56.00	11.70	12.00	2.31	5.34	0.20	4.20	69.79	**16**
Pb	1568	1.00	22.00	3.49	3.00	2.29	5.26	0.66	1.73	6.31	**8**
Th	2191	1.00	20.00	13.57	14.00	1.27	1.63	0.09	-0.68	5.62	**16**
U	15	1.00	3.00	1.20	1.00	0.56	0.31	0.47	2.92	8.39	**2**

Table A- 14: Summary statistics of the Klipriviersberg Group log-transformed data set.

Element	N	Min	Max	Mean	Median	St. Dev	Var	CV	Skew	Kurt	Log Threshold
TiO_2	2191	-1.08	0.38	-0.10	-0.09	0.11	0.01	-1.09	-0.76	3.29	**1.1**
MnO	2191	-3.91	-0.04	-2.40	-2.41	0.27	0.07	-0.11	0.04	3.10	**0.2**
Fe_2O_3	2191	-0.05	2.18	1.52	1.53	0.23	0.05	0.15	-0.65	1.91	**7**
Sc	2191	0.00	3.22	2.59	2.64	0.20	0.04	0.08	-1.65	15.57	**20**
V	2191	3.09	5.05	4.30	4.30	0.21	0.05	0.05	-0.51	2.10	**115**
Cr	2191	3.74	6.66	5.04	5.01	0.36	0.13	0.07	0.54	0.99	**339**
Co	2191	1.95	3.58	2.82	2.83	0.22	0.05	0.08	-0.09	0.00	**27**
Ni	2191	2.20	5.15	3.95	3.95	0.34	0.11	0.09	-0.09	0.74	**108**
Cu	2191	2.08	4.28	3.34	3.37	0.23	0.05	0.07	-0.21	1.08	**46**
Zn	2191	3.18	5.76	3.91	3.91	0.20	0.04	0.05	0.61	5.09	**76**
As	2188	0.00	3.81	2.57	2.56	0.36	0.13	0.14	-0.97	3.36	**29**
Rb	2191	3.50	4.89	4.22	4.22	0.14	0.02	0.03	-0.26	1.55	**91**
Sr	2191	2.94	4.98	3.90	3.89	0.23	0.05	0.06	0.34	0.90	**81**
Y	2191	2.40	4.06	3.15	3.14	0.14	0.02	0.04	0.08	1.72	**31**
Zr	2191	5.48	7.51	6.64	6.66	0.21	0.05	0.03	-0.48	1.55	**1205**
Nb	2191	2.20	3.40	2.96	2.94	0.07	0.00	0.02	-0.58	7.18	**22**
Ba	2191	2.30	6.17	5.55	5.56	0.19	0.04	0.03	-2.45	36.81	**386**
W	2191	0.69	4.03	2.44	2.48	0.19	0.03	0.08	-0.50	8.29	**17**
Pb	1568	0.00	3.09	1.04	1.10	0.66	0.43	0.63	-0.13	-0.73	**13**
Th	2191	0.00	3.00	2.60	2.64	0.11	0.01	0.04	-6.62	144.95	**17**
U	15	0.00	1.10	0.12	0.00	0.32	0.11	2.72	2.67	6.45	**2**

Table A- 15: Summary statistics of the Platberg Group raw data set.

Element	N	Min	Max	Mean	Median	St. Dev	Var	CV	Skew	Kurt	Threshold
TiO_2	628	0.50	3.01	1.11	1.07	0.23	0.05	0.20	1.55	8.89	**1.6**
MnO	628	0.02	0.31	0.09	0.09	0.03	0.00	0.37	1.10	4.45	**0.2**
Fe_2O_3	628	1.98	12.88	5.03	5.02	1.55	2.40	0.31	0.69	1.44	**8**
Sc	628	5.00	31.00	14.08	14.00	3.55	12.61	0.25	0.23	0.47	**21**
V	628	14.00	214.00	77.43	76.00	28.08	788.60	0.36	0.73	1.32	**134**
Cr	628	44.00	474.00	128.44	122.00	51.75	2678.10	0.40	1.37	4.03	**232**
Co	628	8.00	803.00	17.42	15.00	31.81	1012.16	1.83	24.09	595.61	**81**
Ni	628	16.00	386.00	53.45	51.00	27.60	761.70	0.52	27.60	41.89	**109**
Cu	628	12.00	127.00	31.51	30.00	12.55	157.57	0.40	2.00	8.38	**57**
Zn	628	25.00	195.00	50.52	49.00	15.50	240.26	0.31	2.69	16.23	**82**
As	558	1.00	50.00	12.54	13.00	6.63	43.92	0.53	0.75	2.17	**26**
Rb	628	35.00	118.00	71.36	71.00	11.60	134.64	0.16	0.19	0.77	**95**
Sr	628	29.00	640.00	94.40	70.00	68.59	4704.24	0.73	3.34	16.73	**232**
Y	628	13.00	54.00	26.24	26.00	4.77	22.73	0.18	0.97	2.41	**36**
Zr	628	262.00	2673.00	850.26	825.00	238.81	57031.21	0.28	1.25	6.30	**1328**
Nb	628	12.00	33.00	20.42	20.00	2.00	3.99	0.10	0.29	4.05	**24**
Ba	628	115.00	1134.00	388.57	350.50	147.50	21755.29	0.38	1.89	4.54	**684**
W	628	2.00	34.00	10.61	10.00	2.44	5.98	0.23	1.61	14.17	**16**
Pb	468	1.00	74.00	5.06	4.00	5.74	32.95	1.13	6.06	56.52	**17**
Th	627	1.00	24.00	13.64	14.00	1.80	3.23	0.13	-1.12	7.91	**17**
U	12	1.00	2.00	1.25	1.00	0.45	0.20	0.36	1.33	-0.33	**2**

Table A- 16: Summary statistics of the Platberg Group log-log-transformed data set.

Element	N	Min	Max	Mean	Median	St. Dev	Var	CV	Skew	Kurt	Log Threshold	Threshold
TiO_2	628	-0.69	1.10	0.08	0.07	0.19	0.04	2.37	0.17	1.70	**0.47**	**1.6**
MnO	628	-3.91	-1.17	-2.49	-2.41	0.38	0.14	-0.15	-0.46	0.37	**-1.73**	**0.2**
Fe_2O_3	628	0.68	2.56	1.57	1.61	0.31	0.10	0.20	-0.24	-0.31	**2**	**9**
Sc	628	1.61	3.43	2.61	2.64	0.27	0.07	0.10	-0.57	0.35	**3**	**23**
V	628	2.64	5.37	4.28	4.33	0.38	0.14	0.09	-0.45	0.35	**5**	**155**
Cr	628	3.78	6.16	4.78	4.80	0.39	0.15	0.08	-0.02	-0.06	**6**	**259**
Co	628	2.08	6.69	2.74	2.71	0.34	0.12	0.12	2.61	27.75	**3**	**31**
Ni	628	2.77	5.96	3.89	3.93	0.42	0.17	0.11	0.24	1.42	**5**	**112**
Cu	628	2.48	4.84	3.38	3.40	0.36	0.13	0.11	0.12	0.60	**4**	**61**
Zn	628	3.22	5.27	3.88	3.89	0.27	0.07	0.07	0.62	1.71	**4**	**83**
As	558	0.00	3.91	2.34	2.56	0.69	0.48	0.30	-1.27	1.74	**4**	**42**
Rb	628	3.56	4.77	4.25	4.26	0.17	0.03	0.04	-0.51	1.21	**5**	**98**
Sr	628	3.37	6.46	4.38	4.25	0.53	0.28	0.12	0.85	0.67	**5**	**232**
Y	628	2.56	3.99	3.25	3.26	0.18	0.03	0.05	0.19	0.92	**4**	**37**
Zr	628	5.57	7.89	6.71	6.72	0.28	0.08	0.04	-0.42	1.75	**7**	**1437**
Nb	628	2.48	3.50	3.01	3.00	0.10	0.01	0.03	-0.50	3.48	**3**	**25**
Ba	628	4.74	7.03	5.90	5.86	0.33	0.11	0.06	0.58	1.23	**7**	**708**
W	628	0.69	3.53	2.34	2.30	0.23	0.05	0.10	-0.89	5.99	**3**	**17**
Pb	468	0.00	4.30	1.30	1.39	0.77	0.60	0.60	0.19	0.28	**3**	**17**
Th	627	0.00	3.18	2.60	2.64	0.18	0.03	0.07	-6.35	80.75	**3**	**19**
U	12	0.00	0.69	0.17	0.00	0.31	0.10	1.81	1.33	-0.33	**1**	**2**

Table A- 17: Summary statistics of the Allanridge Formation raw data set.

Element	N	Min	Max	Mean	Median	St. Dev	Var	CV	Skew	Kurt	Threshold
TiO_2	4695	0.17	2.96	1.09	1.08	0.17	0.03	0.16	0.81	6.84	**1.4**
MnO	4695	0.02	0.21	0.10	0.09	0.02	0.00	0.26	0.47	0.67	**0.1**
Fe_2O_3	4695	0.87	11.51	5.89	5.82	1.50	2.26	0.26	0.22	-0.07	**9**
Sc	4695	2.00	46.00	15.42	15.00	3.06	9.36	0.20	0.11	3.22	**22**
V	4695	3.00	303.00	88.18	87.00	23.18	537.17	0.26	0.32	1.43	**135**
Cr	4695	23.00	518.00	112.11	106.00	37.17	1381.37	0.33	2.73	16.05	**186**
Co	4695	8.00	42.00	20.74	20.00	5.24	27.46	0.25	0.40	0.13	**31**
Ni	4695	16.00	364.00	65.45	62.00	22.83	521.13	0.35	22.83	7.82	**111**
Cu	4694	6.00	122.00	43.01	40.00	15.29	233.79	0.36	0.79	0.66	**74**
Zn	4695	13.00	469.00	51.44	50.00	13.65	186.45	0.27	9.86	253.27	**79**
As	3975	1.00	68.00	11.66	12.00	5.86	34.32	0.50	0.84	4.50	**23**
Rb	4695	18.00	128.00	68.97	70.00	12.07	145.67	0.18	-0.33	0.43	**93**
Sr	4695	32.00	621.00	131.82	103.00	89.34	7981.73	0.68	1.85	3.59	**311**
Y	4695	7.00	42.00	25.38	25.00	3.42	11.66	0.13	-0.22	1.70	**32**
Zr	4695	88.00	2870.00	744.00	736.00	201.57	40632.38	0.27	1.20	6.64	**1147**
Nb	4695	9.00	35.00	19.58	20.00	1.64	2.69	0.08	0.40	4.84	**23**
Ba	4695	62.00	1029.00	369.32	368.00	78.98	6237.79	0.21	0.65	3.61	**527**
W	4693	2.00	28.00	9.61	9.00	2.28	5.21	0.24	0.48	0.94	**14**
Pb	3796	1.00	45.00	4.26	4.00	2.88	8.28	0.67	2.68	20.11	**10**
Th	4695	3.00	25.00	13.52	14.00	1.27	1.62	0.09	-0.36	4.41	**16**
U	108	1.00	11.00	1.58	1.00	1.28	1.63	0.81	4.73	29.84	**4**

Table A- 18: Summary statistics of the Allanridge Formation log-transformed data set.

Element	N	Min	Max	Mean	Median	St. Dev	Var	CV	Skew	Kurt	Log Threshold
TiO_2	4695	-1.77	1.09	0.07	0.08	0.16	0.03	2.27	-0.91	8.03	**1.5**
MnO	4695	-3.91	-1.56	-2.38	-2.41	0.27	0.07	-0.11	-0.54	1.12	**0.2**
Fe_2O_3	4695	-0.14	2.44	1.74	1.76	0.27	0.07	0.16	-0.64	1.12	**10**
Sc	4695	0.69	3.83	2.71	2.71	0.22	0.05	0.08	-1.31	5.61	**24**
V	4695	1.10	5.71	4.44	4.47	0.29	0.08	0.06	-1.15	6.37	**157**
Cr	4694	3.14	6.25	4.68	4.66	0.29	0.08	0.06	0.46	2.21	**199**
Co	4695	2.08	3.74	3.00	3.00	0.26	0.07	0.09	-0.30	-0.09	**35**
Ni	4695	2.77	5.90	4.12	4.13	0.34	0.12	0.08	-0.12	0.31	**129**
Cu	4694	1.79	4.80	3.70	3.69	0.36	0.13	0.10	-0.24	0.21	**88**
Zn	4695	2.56	6.15	3.92	3.91	0.21	0.05	0.05	0.42	6.27	**79**
As	3975	0.00	4.22	2.29	2.48	0.67	0.45	0.29	-1.44	2.38	**47**
Rb	4695	2.89	4.85	4.22	4.25	0.19	0.04	0.04	-1.02	1.81	**101**
Sr	4695	3.47	6.43	4.71	4.63	0.57	0.32	0.12	0.57	-0.30	**405**
Y	4695	1.95	3.74	3.22	3.22	0.14	0.02	0.04	-1.22	5.61	**34**
Zr	4695	4.48	7.96	6.58	6.60	0.27	0.07	0.04	-0.45	2.08	**1285**
Nb	4695	2.20	3.56	2.97	3.00	0.08	0.01	0.03	-0.34	4.02	**23**
Ba	4695	4.13	6.94	5.89	5.91	0.22	0.05	0.04	-0.83	4.24	**577**
W	4693	0.69	3.33	2.23	2.20	0.24	0.06	0.11	-0.31	0.49	**16**
Pb	3796	0.00	3.81	1.24	1.39	0.67	0.45	0.54	-0.30	-0.41	**17**
Th	4695	1.10	3.22	2.60	2.64	0.10	0.01	0.04	-1.94	19.92	**17**
U	108	0.00	2.40	0.31	0.00	0.48	0.23	1.57	1.65	3.03	**4**

Table A- 19: Summary statistics of the Black Reef Formation raw data set.

Element	N	Min	Max	Mean	Median	St. Dev	Var	CV	Skew	Kurt	Threshold
TiO_2	43	0.75	1.38	0.96	0.95	0.15	0.02	0.15	1.02	1.46	**1.3**
MnO	43	0.07	0.82	0.18	0.12	0.17	0.03	0.93	3.06	9.17	**0.5**
Fe_2O_3	43	3.16	9.24	5.58	5.63	1.17	1.38	0.21	0.79	1.85	**8**
Sc	43	6.00	23.00	14.91	15.00	3.09	9.56	0.21	-0.26	1.64	**21**
V	43	36.00	153.00	90.12	91.00	24.60	605.30	0.27	0.35	0.92	**139**
Cr	43	80.00	192.00	146.30	147.00	26.89	722.83	0.18	-0.23	-0.45	**200**
Co	43	7.00	29.00	16.02	15.00	4.95	24.55	0.31	0.66	0.17	**26**
Ni	43	27.00	87.00	55.95	55.00	12.78	163.43	0.23	12.78	0.42	**82**
Cu	43	18.00	83.00	37.88	35.00	13.00	168.96	0.34	1.88	5.10	**64**
Zn	43	31.00	95.00	53.86	55.00	13.85	191.88	0.26	0.74	0.90	**82**
As	43	5.00	27.00	16.12	17.00	5.09	25.91	0.32	-0.05	-0.09	**26**
Rb	43	65.00	117.00	88.74	89.00	13.75	189.00	0.15	0.03	-0.94	**116**
Sr	43	26.00	68.00	39.93	40.00	8.75	76.54	0.22	1.05	2.77	**57**
Y	43	19.00	43.00	28.72	29.00	5.23	27.35	0.18	0.64	0.34	**39**
Zr	43	400.00	1154.00	714.58	713.00	154.07	23737.06	0.22	0.30	0.85	**1023**
Nb	43	17.00	25.00	19.95	20.00	1.66	2.76	0.08	0.31	1.34	**23**
Ba	43	136.00	470.00	301.30	278.00	77.13	5948.93	0.26	0.59	0.05	**456**
W	43	6.00	15.00	10.53	11.00	2.19	4.78	0.21	-0.20	-0.71	**15**
Pb	34	1.00	29.00	5.00	4.00	4.81	23.15	0.96	3.95	19.35	**15**
Th	43	8.00	17.00	13.07	13.00	1.71	2.92	0.13	-0.59	1.27	**16**

Table A- 20: Summary statistics of the Black Reef Formation log-transformed data set.

Element	N	Min	Max	Mean	Median	St. Dev	Var	CV	Skew	Kurt	Log Threshold
TiO_2	43	-0.29	0.32	-0.05	-0.05	0.15	0.02	-3.06	0.53	0.56	**1.3**
MnO	43	-2.66	-0.20	-1.93	-2.12	0.56	0.32	-0.29	1.77	3.14	**0.5**
Fe_2O_3	43	1.15	2.22	1.70	1.73	0.21	0.04	0.12	-0.08	0.88	**8**
Sc	43	1.79	3.14	2.68	2.71	0.23	0.06	0.09	-1.50	4.48	**24**
V	43	3.58	5.03	4.46	4.51	0.29	0.09	0.07	-0.83	1.68	**163**
Cr	43	4.38	5.26	4.97	4.99	0.19	0.04	0.04	-0.72	0.55	**216**
Co	43	1.95	3.37	2.73	2.71	0.31	0.10	0.11	-0.14	0.01	**30**
Ni	43	3.30	4.47	4.00	4.01	0.24	0.06	0.06	-0.58	0.95	**90**
Cu	43	2.89	4.42	3.59	3.56	0.31	0.09	0.09	0.45	1.57	**70**
Zn	43	3.43	4.55	3.95	4.01	0.25	0.06	0.06	0.00	-0.08	**90**
As	43	1.61	3.30	2.72	2.83	0.37	0.13	0.13	-1.07	1.36	**34**
Rb	43	4.17	4.76	4.47	4.49	0.16	0.02	0.04	-0.21	-0.96	**122**
Sr	43	3.26	4.22	3.66	3.69	0.21	0.04	0.06	0.13	0.79	**61**
Y	43	2.94	3.76	3.34	3.37	0.18	0.03	0.05	0.17	-0.17	**41**
Zr	43	5.99	7.05	6.55	6.57	0.22	0.05	0.03	-0.51	0.77	**1119**
Nb	43	2.83	3.22	2.99	3.00	0.08	0.01	0.03	-0.05	0.84	**24**
Ba	43	4.91	6.15	5.68	5.63	0.26	0.07	0.05	-0.19	0.69	**504**
W	43	1.79	2.71	2.33	2.40	0.22	0.05	0.09	-0.60	-0.36	**16**
Pb	34	0.00	3.37	1.35	1.39	0.70	0.50	0.52	0.18	1.10	**20**
Th	43	2.08	2.83	2.56	2.56	0.14	0.02	0.05	-1.20	2.78	**17**
U	0										

Table A- 21: Summary statistics of the Vryburg Formation raw data set.

Element	N	Min	Max	Mean	Median	St. Dev	Var	CV	Skew	Kurt	Threshold
TiO_2	535	0.27	2.42	1.24	1.24	0.26	0.07	0.21	0.14	1.19	**1.7**
MnO	535	0.02	0.49	0.11	0.10	0.07	0.00	0.57	2.18	7.15	**0.2**
Fe_2O_3	535	0.94	14.10	4.79	4.51	1.90	3.62	0.40	0.93	1.20	**9**
Sc	534	4.00	31.00	13.66	13.00	4.08	16.65	0.30	1.08	1.63	**22**
V	535	2.00	246.00	64.18	57.00	34.76	1208.32	0.54	1.22	2.16	**134**
Cr	534	16.00	782.00	131.97	110.00	88.07	7756.27	0.67	3.12	14.54	**308**
Co	535	7.00	37.00	13.38	12.00	4.53	20.54	0.34	1.25	1.85	**22**
Ni	535	13.00	129.00	44.36	41.00	19.45	378.17	0.44	19.45	0.30	**83**
Cu	535	8.00	157.00	32.68	27.00	20.91	437.33	0.64	1.68	3.93	**75**
Zn	535	16.00	74.00	39.68	36.00	11.75	137.99	0.30	0.76	-0.30	**63**
As	407	1.00	78.00	9.98	8.00	8.12	66.01	0.81	2.95	17.52	**26**
Rb	535	35.00	142.00	78.30	78.00	11.62	135.14	0.15	0.47	2.58	**102**
Sr	535	31.00	256.00	61.61	55.00	22.92	525.31	0.37	4.03	24.30	**107**
Y	535	9.00	41.00	26.67	27.00	4.39	19.30	0.16	-0.19	0.92	**35**
Zr	535	187.00	2478.00	950.99	907.00	340.74	116104.41	0.36	0.42	0.11	**1632**
Nb	535	11.00	33.00	21.81	21.00	2.66	7.07	0.12	0.13	0.76	**27**
Ba	535	122.00	811.00	377.86	369.00	69.79	4870.03	0.18	1.17	5.61	**517**
W	533	1.00	16.00	8.46	8.00	1.54	2.37	0.18	0.45	2.57	**12**
Pb	379	1.00	97.00	4.20	3.00	5.87	34.45	1.40	11.22	168.06	**16**
Th	534	7.00	22.00	13.62	14.00	1.44	2.08	0.11	0.28	3.05	**17**
U	3	3.00	5.00	4.00	4.00	1.00	1.00	0.25	0.00	0.00	**6**

Table A- 22: Summary statistics of the Vryburg Formation log-transformed data set.

Element	N	Min	Max	Mean	Median	St. Dev	Var	CV	Skew	Kurt	Log Threshold
TiO_2	535	-1.31	0.88	0.19	0.22	0.22	0.05	1.19	-1.23	5.63	**1.9**
MnO	535	-3.91	-0.71	-2.29	-2.30	0.50	0.25	-0.22	0.15	0.32	**0.3**
Fe_2O_3	535	-0.06	2.65	1.49	1.51	0.40	0.16	0.27	-0.15	-0.06	**11**
Sc	534	1.39	3.43	2.57	2.56	0.29	0.08	0.11	0.14	0.38	**24**
V	535	0.69	5.51	4.02	4.04	0.56	0.31	0.14	-0.51	1.75	**198**
Cr	534	2.77	6.66	4.73	4.70	0.52	0.28	0.11	0.41	0.96	**372**
Co	535	1.95	3.61	2.54	2.48	0.31	0.10	0.12	0.50	-0.35	**25**
Ni	535	2.56	4.86	3.70	3.71	0.43	0.19	0.12	0.09	-0.88	**105**
Cu	535	2.08	5.06	3.31	3.30	0.58	0.33	0.17	0.34	-0.70	**103**
Zn	535	2.77	4.30	3.64	3.58	0.28	0.08	0.08	0.28	-0.72	**70**
As	407	0.00	4.36	2.00	2.08	0.83	0.70	0.42	-0.53	0.08	**55**
Rb	535	3.56	4.96	4.35	4.36	0.15	0.02	0.03	-0.58	3.81	**106**
Sr	535	3.43	5.55	4.08	4.01	0.27	0.07	0.07	1.68	4.85	**106**
Y	535	2.20	3.71	3.27	3.30	0.18	0.03	0.05	-1.21	4.61	**38**
Zr	535	5.23	7.82	6.79	6.81	0.39	0.15	0.06	-0.54	0.24	**2068**
Nb	535	2.40	3.50	3.07	3.04	0.12	0.02	0.04	-0.46	1.90	**28**
Ba	535	4.80	6.70	5.92	5.91	0.18	0.03	0.03	-0.52	5.42	**546**
W	533	0.00	2.77	2.12	2.08	0.20	0.04	0.09	-2.31	23.94	**13**
Pb	379	0.00	4.57	1.13	1.10	0.73	0.53	0.64	0.35	0.82	**17**
Th	534	1.95	3.09	2.61	2.64	0.11	0.01	0.04	-0.53	3.81	**17**
U	3										

Table A- 23: Summary statistics of the Malmani Dolomite Subgroup raw data set.

Element	N	Min	Max	Mean	Median	St. Dev	Var	CV	Skew	Kurt	Threshold
TiO_2	590	0.21	1.24	0.66	0.66	0.15	0.02	0.23	0.22	0.23	**1.0**
MnO	590	0.10	5.35	0.83	0.65	0.61	0.38	0.74	2.16	7.65	**2.1**
Fe_2O_3	590	1.94	16.71	5.33	4.95	1.83	3.35	0.34	1.92	6.34	**9**
Sc	590	1.00	32.00	10.45	10.00	4.28	18.35	0.41	0.98	1.81	**19**
V	590	19.00	203.00	70.23	66.00	20.43	417.29	0.29	1.34	4.56	**111**
Cr	590	21.00	651.00	132.84	126.00	47.72	2277.08	0.36	3.86	30.24	**228**
Co	581	1.00	35.00	10.25	10.00	3.48	12.10	0.34	1.36	6.50	**17**
Ni	590	20.00	134.00	42.48	40.00	12.63	159.53	0.30	12.63	12.49	**68**
Cu	590	9.00	141.00	25.09	23.00	10.62	112.72	0.42	4.40	31.99	**46**
Zn	589	17.00	207.00	34.01	30.00	16.99	288.63	0.50	4.84	35.37	**68**
As	589	3.00	73.00	18.09	17.00	7.58	57.51	0.42	2.68	13.29	**33**
Rb	590	18.00	137.00	54.63	52.00	18.92	358.08	0.35	0.80	0.92	**92**
Sr	589	8.00	72.00	25.03	24.00	6.40	41.00	0.26	1.70	7.37	**38**
Y	589	1.00	46.00	19.28	19.00	6.02	36.25	0.31	0.54	1.01	**31**
Zr	590	108.00	1092.00	508.75	505.00	146.71	21522.69	0.29	0.23	-0.23	**802**
Nb	590	4.00	35.00	16.41	16.00	2.54	6.43	0.15	0.03	6.21	**21**
Ba	590	48.00	1819.00	361.78	341.00	172.15	29636.48	0.48	1.73	9.65	**706**
W	590	1.00	17.00	8.67	9.00	1.71	2.92	0.20	1.39	6.42	**12**
Pb	91	1.00	122.00	9.58	4.00	19.48	379.40	2.03	4.19	19.05	**49**
Th	578	1.00	19.00	12.10	13.00	2.57	6.61	0.21	-1.34	2.96	**17**
U	15	1.00	5.00	1.67	1.00	1.05	1.10	0.63	2.51	7.69	**4**

Table A- 24: Summary statistics of the Malmani Dolomite Subgroup log-transformed data set.

Element	N	Min	Max	Mean	Median	St. Dev	Var	CV	Skew	Kurt	Log Threshold
TiO_2	590	-1.56	0.22	-0.45	-0.42	0.24	0.06	-0.53	-0.53	0.63	**1.1**
MnO	590	-2.30	1.68	-0.41	-0.43	0.66	0.44	-1.60	0.10	-0.18	**3.1**
Fe_2O_3	590	0.66	2.82	1.62	1.60	0.30	0.09	0.19	0.54	0.87	**10**
Sc	590	0.00	3.47	2.26	2.30	0.43	0.19	0.19	-0.69	2.31	**25**
V	590	2.94	5.31	4.21	4.19	0.28	0.08	0.07	-0.10	1.54	**123**
Cr	590	3.04	6.48	4.84	4.84	0.30	0.09	0.06	0.18	4.85	**242**
Co	581	0.00	3.56	2.27	2.30	0.36	0.13	0.16	-1.22	5.95	**21**
Ni	590	3.00	4.90	3.72	3.69	0.25	0.06	0.07	1.05	2.73	**70**
Cu	590	2.20	4.95	3.17	3.14	0.31	0.09	0.10	1.39	4.42	**46**
Zn	589	2.83	5.33	3.46	3.40	0.34	0.11	0.10	1.57	4.63	**66**
As	589	1.10	4.29	2.82	2.83	0.38	0.15	0.14	-0.38	3.41	**39**
Rb	590	2.89	4.92	3.94	3.95	0.35	0.12	0.09	-0.21	-0.09	**110**
Sr	590	2.08	4.28	3.19	3.18	0.24	0.06	0.08	0.18	1.86	**40**
Y	589	0.00	3.83	2.91	2.94	0.35	0.12	0.12	-1.50	8.94	**39**
Zr	590	4.68	7.00	6.19	6.22	0.31	0.10	0.05	-0.62	0.76	**946**
Nb	590	1.39	3.56	2.78	2.77	0.17	0.03	0.06	-2.04	12.86	**23**
Ba	590	3.87	7.51	5.78	5.83	0.50	0.25	0.09	-0.70	1.10	**1001**
W	590	0.00	2.83	2.14	2.20	0.20	0.04	0.10	-1.94	22.68	**13**
Pb	91	0.00	4.80	1.35	1.39	1.22	1.50	0.91	0.74	0.04	**95**
Th	578	0.00	2.94	2.46	2.56	0.32	0.10	0.13	-4.09	24.80	**23**
U	15	0.00	1.61	0.38	0.00	0.48	0.23	1.25	1.15	1.27	**4**

Table A- 25: Summary statistics of the Ghaap Group Dolomites raw data set.

Element	N	Min	Max	Mean	Median	St. Dev	Var	CV	Skew	Kurt	Threshold
TiO_2	2818	0.30	2.35	1.11	1.10	0.22	0.05	0.20	0.38	1.57	**1.6**
MnO	2818	0.04	6.53	0.51	0.42	0.40	0.16	0.78	3.17	25.43	**1.3**
Fe_2O_3	2818	1.18	11.09	4.07	3.96	0.97	0.93	0.24	1.08	3.60	**6**
Sc	2816	2.00	37.00	13.10	13.00	2.94	8.62	0.22	1.02	6.62	**19**
V	2818	5.00	198.00	50.39	47.00	19.56	382.47	0.39	1.41	4.20	**90**
Cr	2818	7.00	959.00	100.81	93.00	47.95	2298.92	0.48	5.74	71.68	**197**
Co	2816	2.00	36.00	9.94	10.00	2.44	5.97	0.25	1.97	11.52	**15**
Ni	2818	10.00	120.00	32.93	31.00	9.70	94.11	0.29	9.70	7.52	**52**
Cu	2817	6.00	92.00	24.35	24.00	6.87	47.20	0.28	2.49	16.54	**38**
Zn	2817	15.00	969.00	56.80	50.00	43.71	1910.63	0.77	10.86	185.09	**144**
As	2451	1.00	71.00	12.66	11.00	9.07	82.31	0.72	1.60	4.02	**31**
Rb	2817	13.00	168.00	79.80	79.00	14.63	213.93	0.18	0.61	3.53	**109**
Sr	2816	22.00	195.00	60.39	58.00	14.13	199.61	0.23	3.29	20.72	**89**
Y	2816	5.00	39.00	23.86	24.00	4.12	16.97	0.17	-0.35	1.21	**32**
Zr	2818	208.00	2162.00	919.53	900.50	261.93	68608.36	0.28	0.62	1.35	**1443**
Nb	2816	6.00	30.00	20.90	21.00	2.44	5.97	0.12	-0.36	3.00	**26**
Ba	2818	51.00	935.00	333.96	328.00	91.45	8363.17	0.27	1.03	4.18	**517**
W	2813	1.00	28.00	8.51	9.00	1.84	3.37	0.22	0.95	10.34	**12**
Pb	2594	1.00	231.00	9.10	7.00	12.14	147.33	1.33	8.20	100.14	**33**
Th	2797	2.00	23.00	13.12	13.00	1.87	3.48	0.14	-1.04	4.15	**17**
U	12	1.00	4.00	1.67	1.00	1.23	1.52	0.74	1.47	0.37	**4**

Table A- 26: Summary statistics of the Ghaap Group Dolomites log-transformed data set.

Element	N	Min	Max	Mean	Median	St. Dev	Var	CV	Skew	Kurt	Log Th
TiO_2	2818	-1.20	0.85	0.09	0.10	0.21	0.04	2.46	-0.68	2.17	**1.7**
MnO	2818	-3.22	1.88	-0.94	-0.87	0.73	0.54	-0.78	-0.22	-0.07	**2.2**
Fe_2O_3	2818	0.17	2.41	1.38	1.38	0.23	0.05	0.17	-0.26	2.18	**7**
Sc	2816	0.69	3.61	2.54	2.56	0.24	0.06	0.09	-1.47	9.27	**21**
V	2818	1.61	5.29	3.85	3.85	0.37	0.14	0.10	-0.13	1.01	**106**
Cr	2818	1.95	6.87	4.54	4.53	0.38	0.15	0.08	-0.12	4.42	**216**
Co	2816	0.69	3.58	2.27	2.30	0.23	0.05	0.10	0.12	3.70	**16**
Ni	2818	2.30	4.79	3.46	3.43	0.26	0.07	0.08	0.63	1.37	**55**
Cu	2817	1.79	4.52	3.16	3.18	0.26	0.07	0.08	0.11	2.46	**41**
Zn	2817	2.71	6.88	3.93	3.91	0.40	0.16	0.10	1.44	5.51	**124**
As	2451	0.00	4.26	2.26	2.40	0.81	0.66	0.36	-0.74	0.57	**67**
Rb	2817	2.56	5.12	4.36	4.37	0.19	0.04	0.04	-0.91	5.70	**117**
Sr	2817	3.09	5.27	4.08	4.06	0.20	0.04	0.05	0.86	5.62	**90**
Y	2816	1.61	3.66	3.16	3.18	0.19	0.04	0.06	-1.44	4.99	**35**
Zr	2818	5.34	7.68	6.78	6.80	0.30	0.09	0.04	-0.57	1.26	**1670**
Nb	2816	1.79	3.40	3.03	3.04	0.13	0.02	0.04	-1.80	12.92	**27**
Ba	2818	3.93	6.84	5.77	5.79	0.28	0.08	0.05	-0.78	3.57	**589**
W	2813	0.00	3.33	2.12	2.20	0.24	0.06	0.11	-1.77	11.13	**14**
Pb	2594	0.00	5.44	1.85	1.95	0.82	0.67	0.44	-0.01	0.92	**46**
Th	2797	0.69	3.14	2.56	2.56	0.17	0.03	0.07	-3.25	23.35	**19**
U	10	0.00	1.39	0.28	0.00	0.59	0.34	2.11	1.78	1.41	**5**

Table A- 27: Summary statistics of the Asbestos Hill Subgroup raw data set.

Element	N	Min	Max	Mean	Median	St. Dev	Var	CV	Skew	Kurt	Threshold
TiO_2	328	0.46	1.70	1.12	1.11	0.20	0.04	0.18	-0.02	0.69	**1.5**
MnO	328	0.04	0.80	0.13	0.11	0.09	0.01	0.64	4.50	27.03	**0.3**
Fe_2O_3	328	2.80	25.77	7.66	6.84	3.08	9.46	0.40	2.04	6.16	**14**
Sc	328	2.00	83.00	15.66	15.00	6.48	41.93	0.41	6.51	62.89	**29**
V	328	19.00	226.00	53.02	51.00	17.85	318.57	0.34	5.00	43.26	**89**
Cr	328	12.00	377.00	78.70	73.00	30.03	902.10	0.38	4.85	40.09	**139**
Co	277	1.00	767.00	12.01	7.00	63.00	3968.94	5.25	11.68	135.81	**138**
Ni	328	11.00	91.00	28.29	26.00	9.78	95.65	0.35	9.78	9.49	**48**
Cu	328	5.00	51.00	20.67	20.00	5.16	26.59	0.25	1.27	5.36	**31**
Zn	328	19.00	268.00	43.78	40.50	16.79	281.97	0.38	7.74	97.46	**77**
As	298	1.00	67.00	16.21	15.00	9.27	85.96	0.57	1.24	3.30	**35**
Rb	328	36.00	110.00	74.34	76.00	10.13	102.62	0.14	-0.68	1.87	**95**
Sr	328	26.00	87.00	53.83	54.00	8.17	66.78	0.15	-0.20	1.84	**70**
Y	328	9.00	39.00	24.17	24.00	4.62	21.34	0.19	-0.54	1.14	**33**
Zr	328	208.00	1655.00	907.48	894.00	214.16	45865.60	0.24	0.09	0.78	**1336**
Nb	328	13.00	26.00	20.74	21.00	2.10	4.40	0.10	-0.80	1.92	**25**
Ba	328	122.00	959.00	376.68	374.00	70.71	5000.52	0.19	2.44	23.86	**518**
W	328	3.00	71.00	11.51	10.00	5.67	32.12	0.49	5.20	42.61	**23**
Pb	125	1.00	22.00	2.46	2.00	2.44	5.94	0.99	4.74	33.43	**7**
Th	328	2.00	17.00	13.43	14.00	1.77	3.12	0.13	-1.42	6.59	**17**

Table A- 28: Summary statistics of the Asbestos Hill Subgroup log-transformed data set.

Element	N	Min	Max	Mean	Median	St. Dev	Var	CV	Skew	Kurt	Log Threshold
TiO_2	328	-0.78	0.53	0.09	0.10	0.19	0.04	2.03	-0.94	2.71	**1.6**
MnO	328	-3.22	-0.22	-2.12	-2.21	0.42	0.18	-0.20	1.16	3.26	**0.3**
Fe_2O_3	328	1.03	3.25	1.97	1.92	0.35	0.12	0.18	0.61	0.93	**15**
Sc	328	0.69	4.42	2.70	2.71	0.31	0.09	0.11	-0.20	11.59	**29**
V	328	2.94	5.42	3.93	3.93	0.26	0.07	0.07	0.78	5.52	**89**
Cr	328	2.48	5.93	4.32	4.29	0.31	0.10	0.07	-0.29	9.15	**146**
Co	277	0.00	6.64	1.81	1.95	0.68	0.46	0.37	1.76	17.71	**30**
Ni	328	2.40	4.51	3.30	3.26	0.29	0.08	0.09	1.01	2.11	**50**
Cu	328	1.61	3.93	3.00	3.00	0.25	0.06	0.08	-0.70	4.95	**34**
Zn	328	2.94	5.59	3.74	3.70	0.26	0.07	0.07	1.33	7.56	**74**
As	298	0.00	4.20	2.60	2.71	0.66	0.44	0.26	-0.97	1.61	**63**
Rb	328	3.58	4.70	4.30	4.33	0.15	0.02	0.03	-1.50	4.32	**100**
Sr	328	3.26	4.47	3.97	3.99	0.16	0.03	0.04	-1.13	3.42	**75**
Y	328	2.20	3.66	3.16	3.18	0.22	0.05	0.07	-1.59	4.24	**38**
Zr	328	5.34	7.41	6.78	6.80	0.26	0.07	0.04	-1.33	4.67	**1541**
Nb	328	2.56	3.26	3.03	3.04	0.11	0.01	0.04	-1.36	3.61	**26**
Ba	328	4.80	6.87	5.91	5.92	0.19	0.04	0.03	-1.49	12.59	**553**
W	328	1.10	4.26	2.37	2.30	0.34	0.12	0.14	1.12	5.19	**23**
Pb	125	0.00	3.09	0.64	0.69	0.67	0.45	1.05	0.75	0.15	**9**
Th	328	0.69	2.83	2.59	2.64	0.17	0.03	0.07	-5.07	48.55	**19**
U	0										

Table A- 29: Summary statistics of the Pretoria Group Quartzite raw data set.

Element	N	Min	Max	Mean	Median	St. Dev	Var	CV	Skew	Kurt	Threshold
TiO_2	86	0.44	2.24	0.88	0.80	0.32	0.10	0.37	2.18	5.99	**1.5**
MnO	86	0.02	0.19	0.09	0.08	0.05	0.00	0.55	0.54	-0.82	**0.2**
Fe_2O_3	86	0.97	25.41	6.22	5.10	3.55	12.64	0.57	2.24	8.96	**13**
Sc	86	1.00	30.00	13.57	11.50	7.28	53.02	0.54	0.58	-0.65	**28**
V	86	12.00	333.00	96.58	76.00	59.04	3485.40	0.61	1.24	2.05	**215**
Cr	86	67.00	2614.00	390.98	221.50	468.56	219547.51	1.20	2.99	9.71	**1328**
Co	86	6.00	59.00	18.65	15.00	12.19	148.49	0.65	1.77	2.90	**43**
Ni	86	19.00	474.00	78.01	48.00	80.36	6457.00	1.03	80.36	8.63	**239**
Cu	86	9.00	134.00	39.97	35.00	22.87	522.88	0.57	1.85	4.25	**86**
Zn	86	17.00	145.00	43.58	39.00	23.41	548.18	0.54	1.97	5.72	**90**
As	76	2.00	54.00	18.26	16.50	10.82	116.97	0.59	0.89	0.85	**40**
Rb	86	23.00	141.00	61.81	57.00	22.61	511.07	0.37	1.00	1.37	**107**
Sr	86	16.00	152.00	34.44	29.00	18.37	337.50	0.53	3.57	19.33	**71**
Y	86	10.00	53.00	25.10	23.00	7.92	62.75	0.32	0.83	0.79	**41**
Zr	86	186.00	1911.00	543.37	488.00	285.71	81629.88	0.53	2.04	6.33	**1115**
Nb	86	11.00	35.00	17.65	17.00	3.86	14.89	0.22	1.57	4.94	**25**
Ba	86	20.00	665.00	263.92	237.50	128.81	16591.06	0.49	0.73	0.32	**522**
W	86	4.00	15.00	8.63	9.00	2.00	4.00	0.23	0.02	0.56	**13**
Pb	24	1.00	20.00	7.50	6.00	5.41	29.22	0.72	0.92	0.06	**18**
Th	86	3.00	24.00	13.97	14.00	3.22	10.34	0.23	-0.59	2.00	**20**
U	9	1.00	5.00	1.78	1.00	1.39	1.94	0.78	1.92	3.38	**5**

Table A- 30: Summary statistics of the Pretoria Group Quartzite log-transformed data set.

Element	N	Min	Max	Mean	Median	St. Dev	Var	CV	Skew	Kurt	Log Threshold
TiO_2	86	-0.82	0.81	-0.18	-0.22	0.31	0.09	-1.70	0.90	1.64	**1.61**
MnO	86	-3.91	-1.66	-2.61	-2.59	0.61	0.37	-0.23	-0.33	-0.75	**0.30**
Fe_2O_3	86	-0.03	3.24	1.69	1.63	0.52	0.27	0.31	-0.13	1.04	**18**
Sc	86	0.00	3.40	2.44	2.44	0.63	0.40	0.26	-0.95	1.81	**50**
V	86	2.48	5.81	4.39	4.33	0.63	0.39	0.14	-0.29	0.07	**344**
Cr	86	4.20	7.87	5.58	5.40	0.79	0.62	0.14	1.01	0.80	**1753**
Co	86	1.79	4.08	2.76	2.71	0.55	0.30	0.20	0.60	-0.27	**55**
Ni	86	2.94	6.16	4.05	3.87	0.71	0.51	0.18	1.00	0.63	**306**
Cu	86	2.20	4.90	3.55	3.55	0.52	0.27	0.15	0.08	0.37	**113**
Zn	86	2.83	4.98	3.66	3.66	0.47	0.22	0.13	0.39	-0.09	**111**
As	76	0.69	3.99	2.70	2.80	0.72	0.52	0.27	-0.90	0.67	**81**
Rb	86	3.14	4.95	4.06	4.04	0.36	0.13	0.09	-0.15	0.30	**128**
Sr	86	2.77	5.02	3.45	3.37	0.40	0.16	0.12	0.92	2.08	**76**
Y	86	2.30	3.97	3.18	3.14	0.31	0.10	0.10	0.02	-0.16	**47**
Zr	86	5.23	7.56	6.19	6.19	0.46	0.21	0.07	0.30	0.18	**1366**
Nb	86	2.40	3.56	2.85	2.83	0.20	0.04	0.07	0.52	1.44	**26**
Ba	86	3.00	6.50	5.44	5.47	0.56	0.32	0.10	-1.08	3.10	**832**
W	86	1.39	2.71	2.13	2.20	0.25	0.06	0.12	-0.80	0.85	**14**
Pb	24	0.00	3.00	1.73	1.79	0.83	0.69	0.48	-0.49	-0.27	**42**
Th	86	1.10	3.18	2.60	2.64	0.29	0.08	0.11	-2.28	8.49	**25**
U	9	0.00	1.61	0.38	0.00	0.61	0.37	1.62	1.37	0.60	**6**

Table A- 31: Summary statistics of the Pretoria Group shale and slate raw data set.

Element	N	Min	Max	Mean	Median	St. Dev	Var	CV	Skew	Kurt	Threshold
TiO_2	123	0.54	1.91	0.88	0.86	0.23	0.05	0.26	1.66	4.09	**1.3**
MnO	123	0.02	0.67	0.10	0.08	0.08	0.01	0.87	4.58	27.56	**0.3**
Fe_2O_3	123	0.68	14.38	6.38	6.08	2.71	7.37	0.43	0.53	-0.14	**12**
Sc	123	2.00	79.00	14.80	13.00	8.44	71.31	0.57	3.82	26.39	**32**
V	123	21.00	382.00	95.15	85.00	50.87	2587.85	0.53	2.06	8.20	**197**
Cr	111	47.00	830.00	239.87	190.00	163.84	26842.40	0.68	1.70	3.06	**568**
Co	123	5.00	619.00	26.85	19.00	55.51	3081.72	2.07	10.12	108.41	**138**
Ni	122	19.00	881.00	97.90	61.50	118.47	14034.59	1.21	118.47	18.46	**335**
Cu	123	12.00	234.00	39.24	35.00	26.32	692.79	0.67	4.29	26.96	**92**
Zn	123	19.00	231.00	49.83	45.00	24.80	614.95	0.50	3.53	22.57	**99**
As	115	2.00	79.00	20.04	17.00	12.65	160.04	0.63	2.13	7.19	**45**
Rb	123	18.00	196.00	80.72	77.00	28.47	810.68	0.35	0.72	1.62	**138**
Sr	123	16.00	290.00	49.75	40.00	36.39	1324.09	0.73	3.49	16.82	**123**
Y	123	14.00	46.00	25.37	25.00	6.08	36.91	0.24	0.81	0.70	**38**
Zr	123	150.00	1191.00	512.24	454.00	230.41	53087.02	0.45	0.84	0.26	**973**
Nb	123	6.00	30.00	18.05	18.00	3.27	10.69	0.18	0.48	3.20	**25**
Ba	123	121.00	910.00	357.82	335.00	128.67	16555.13	0.36	1.48	3.97	**615**
W	123	4.00	12.00	8.54	9.00	1.98	3.91	0.23	-0.20	-0.57	**12**
Pb	43	1.00	38.00	6.09	5.00	6.47	41.90	1.06	3.39	14.45	**19**
Th	121	3.00	23.00	14.42	14.00	3.12	9.76	0.22	-0.18	1.17	**21**
U	16	1.00	4.00	1.88	2.00	0.96	0.92	0.51	0.80	-0.23	**4**

Table A- 32: Summary statistics of the Pretoria Group shale and Slate log-transformed data set.

Element	N	Min	Max	Mean	Median	St. Dev	Var	CV	Skew	Kurt	Log Threshold
TiO_2	121	-0.62	0.65	-0.15	-0.16	0.23	0.05	-1.50	0.72	1.18	**1.4**
MnO	123	-3.91	-0.40	-2.54	-2.53	0.58	0.34	-0.23	0.65	1.33	**0.3**
Fe_2O_3	123	-0.39	2.67	1.75	1.81	0.48	0.23	0.27	-0.91	2.21	**17**
Sc	123	0.69	4.37	2.58	2.56	0.48	0.23	0.19	-0.10	2.11	**39**
V	123	3.04	5.95	4.43	4.44	0.50	0.25	0.11	-0.12	0.33	**261**
Cr	111	3.85	6.72	5.28	5.25	0.62	0.39	0.12	0.10	-0.07	**835**
Co	123	1.61	6.43	2.97	2.94	0.61	0.37	0.21	1.68	7.52	**80**
Ni	122	2.94	6.78	4.23	4.12	0.74	0.55	0.18	1.05	1.08	**403**
Cu	123	2.48	5.46	3.54	3.56	0.48	0.23	0.14	0.63	1.64	**102**
Zn	123	2.94	5.44	3.82	3.81	0.40	0.16	0.11	0.46	1.17	**111**
As	115	0.69	4.37	2.82	2.83	0.62	0.38	0.22	-0.53	1.47	**70**
Rb	123	2.89	5.28	4.32	4.34	0.38	0.14	0.09	-0.78	1.64	**174**
Sr	123	2.77	5.67	3.75	3.69	0.51	0.26	0.14	1.06	1.57	**134**
Y	123	2.64	3.83	3.21	3.22	0.23	0.05	0.07	0.13	0.00	**40**
Zr	123	5.01	7.08	6.14	6.12	0.45	0.20	0.07	-0.09	-0.52	**1268**
Nb	123	1.79	3.40	2.88	2.89	0.19	0.04	0.07	-1.34	8.32	**27**
Ba	123	4.80	6.81	5.82	5.81	0.34	0.12	0.06	0.01	0.90	**707**
W	123	1.39	2.48	2.11	2.20	0.25	0.06	0.12	-0.81	0.56	**14**
Pb	39	0.69	3.64	1.61	1.61	0.72	0.51	0.45	0.58	0.45	**27**
Th	121	1.10	3.14	2.64	2.64	0.25	0.06	0.10	-2.10	10.61	**24**
U	9	0.69	1.39	0.91	0.69	0.27	0.07	0.29	0.72	-0.97	**4**

Table A- 33: Summary statistics of the Hekpoort Formation raw data set.

Element	N	Min	Max	Mean	Median	St. Dev	Var	CV	Skew	Kurt	Threshold
TiO_2	89	0.63	3.09	1.04	0.92	0.39	0.15	0.38	3.61	16.05	**1.8**
MnO	89	0.03	0.20	0.13	0.13	0.03	0.00	0.25	-0.23	0.12	**0.2**
Fe_2O_3	89	3.03	17.75	8.72	8.64	2.09	4.37	0.24	1.46	5.57	**13**
Sc	89	6.00	30.00	19.58	20.00	3.91	15.29	0.20	-0.49	1.08	**27**
V	89	41.00	226.00	130.29	134.00	30.88	953.39	0.24	-0.06	1.01	**192**
Cr	89	188.00	702.00	351.94	292.00	133.37	17786.39	0.38	1.03	0.02	**619**
Co	89	8.00	49.00	29.36	28.00	8.17	66.73	0.28	-0.01	-0.21	**46**
Ni	89	43.00	190.00	100.44	91.00	34.02	1157.59	0.34	34.02	-0.35	**168**
Cu	89	26.00	98.00	54.33	52.00	14.28	204.04	0.26	0.68	1.22	**83**
Zn	89	23.00	123.00	46.97	45.00	12.62	159.37	0.27	2.72	14.53	**72**
As	78	2.00	47.00	14.36	12.00	9.41	88.54	0.66	1.55	3.01	**33**
Rb	89	28.00	98.00	63.83	65.00	15.14	229.30	0.24	-0.26	-0.15	**94**
Sr	89	19.00	98.00	30.91	29.00	10.98	120.61	0.36	3.55	17.27	**53**
Y	89	14.00	34.00	21.62	21.00	4.13	17.06	0.19	0.55	0.01	**30**
Zr	89	208.00	1157.00	406.67	353.00	184.19	33925.97	0.45	2.28	6.18	**775**
Nb	89	12.00	27.00	17.98	18.00	2.82	7.98	0.16	0.98	2.00	**24**
Ba	89	183.00	482.00	287.40	280.00	56.57	3199.68	0.20	0.73	0.89	**401**
W	89	5.00	12.00	7.82	8.00	1.44	2.08	0.18	0.25	-0.36	**11**
Pb	45	1.00	12.00	5.09	4.00	2.91	8.49	0.57	0.68	-0.32	**11**
Th	89	4.00	19.00	13.47	14.00	2.68	7.21	0.20	-1.23	2.56	**19**
U	0										

Table A- 34: Summary statistics of the Hekpoort Formation log-transformed data set.

Element	N	Min	Max	Mean	Median	St. Dev	Var	CV	Skew	Kurt	Log Threshold
TiO_2	89	-0.46	1.13	-0.01	-0.08	0.27	0.08	-26.77	1.93	5.71	**1.8**
MnO	89	-3.51	-1.61	-2.07	-2.04	0.29	0.08	-0.14	-1.66	5.92	**0.2**
Fe_2O_3	89	1.11	2.88	2.14	2.16	0.24	0.06	0.11	-0.46	4.72	**14**
Sc	89	1.79	3.40	2.95	3.00	0.23	0.05	0.08	-1.80	6.54	**31**
V	89	3.71	5.42	4.84	4.90	0.27	0.07	0.06	-1.27	3.28	**223**
Cr	89	5.24	6.55	5.80	5.68	0.35	0.12	0.06	0.58	-0.79	**703**
Co	89	2.08	3.89	3.34	3.33	0.31	0.10	0.09	-1.09	2.26	**55**
Ni	89	3.76	5.25	4.55	4.51	0.33	0.11	0.07	0.07	-0.51	**196**
Cu	89	3.26	4.58	3.96	3.95	0.27	0.07	0.07	-0.29	0.54	**93**
Zn	89	3.14	4.81	3.82	3.81	0.24	0.06	0.06	0.56	3.50	**75**
As	78	0.69	3.85	2.46	2.48	0.66	0.44	0.27	-0.31	0.11	**55**
Rb	89	3.33	4.58	4.12	4.17	0.26	0.07	0.06	-0.95	0.78	**109**
Sr	89	2.94	4.58	3.39	3.37	0.27	0.07	0.08	1.72	4.90	**52**
Y	89	2.64	3.53	3.06	3.04	0.19	0.04	0.06	0.11	-0.44	**32**
Zr	89	5.34	7.05	5.93	5.87	0.36	0.13	0.06	1.05	1.21	**833**
Nb	89	2.48	3.30	2.88	2.89	0.15	0.02	0.05	0.31	1.19	**24**
Ba	89	5.21	6.18	5.64	5.63	0.19	0.04	0.03	0.13	0.11	**422**
W	89	1.61	2.48	2.04	2.08	0.19	0.03	0.09	-0.16	-0.47	**11**
Pb	45	0.00	2.48	1.45	1.39	0.65	0.42	0.45	-0.51	-0.20	**19**
Th	89	1.39	2.94	2.57	2.64	0.26	0.07	0.10	-2.50	8.21	**23**
U	0										

Table A- 35: Summary statistics of the calcrete and surface limestone raw data set.

Element	N	Min	Max	Mean	Median	St. Dev	Var	CV	Skew	Kurt	Threshold
TiO_2	2430	0.13	2.92	1.03	1.02	0.29	0.09	0.28	0.69	2.22	**1.6**
MnO	2430	0.02	1.48	0.19	0.12	0.18	0.03	0.94	2.46	8.18	**0.5**
Fe_2O_3	2430	0.51	10.83	4.07	3.91	1.35	1.82	0.33	0.74	1.55	**7**
Sc	2428	1.00	49.00	13.44	13.00	4.47	19.99	0.33	1.68	9.96	**22**
V	2423	1.00	194.00	54.45	51.00	26.58	706.73	0.49	1.09	1.95	**108**
Cr	2408	1.00	575.00	95.07	93.00	46.57	2169.02	0.49	1.48	7.66	**188**
Co	2430	3.00	51.00	13.32	13.00	3.48	12.12	0.26	2.12	10.62	**20**
Ni	2430	8.00	157.00	38.14	35.00	16.39	268.48	0.43	16.39	4.21	**71**
Cu	2423	1.00	97.00	25.56	24.00	10.39	107.98	0.41	1.24	4.19	**46**
Zn	2430	10.00	731.00	49.01	48.00	22.09	487.88	0.45	15.65	425.66	**93**
As	2277	1.00	89.00	17.42	16.00	10.89	118.59	0.63	1.90	6.35	**39**
Rb	2430	21.00	132.00	72.75	74.00	16.18	261.71	0.22	-0.12	0.89	**105**
Sr	2430	20.00	1115.00	72.10	61.00	48.59	2360.52	0.67	7.75	111.27	**169**
Y	2430	4.00	42.00	23.16	24.00	4.79	22.96	0.21	-0.64	1.15	**33**
Zr	2430	69.00	3137.00	845.35	818.00	310.25	96254.94	0.37	0.89	2.35	**1466**
Nb	2430	11.00	39.00	20.33	20.00	2.86	8.20	0.14	0.47	1.50	**26**
Ba	2429	17.00	883.00	343.97	345.00	106.01	11239.03	0.31	0.45	1.96	**556**
W	2412	1.00	36.00	8.96	9.00	2.47	6.08	0.28	0.70	7.08	**14**
Pb	1966	1.00	70.00	5.31	4.00	4.09	16.74	0.77	3.61	37.02	**13**
Th	2429	3.00	24.00	14.06	14.00	1.75	3.06	0.12	0.57	3.25	**18**
U	128	1.00	10.00	2.35	2.00	1.89	3.58	0.81	1.90	3.50	**6**

Table A- 36: Summary statistics of the calcrete and surface limestone log-transformed data set.

Element	N	Min	Max	Mean	Median	St. Dev	Var	CV	Skew	Kurt	Log Threshold
TiO_2	2430	-2.04	1.07	-0.01	0.02	0.31	0.09	-33.90	-1.07	4.66	**1.9**
MnO	2430	-3.91	0.39	-1.96	-2.12	0.73	0.54	-0.37	0.61	-0.14	**0.8**
Fe_2O_3	2430	-0.67	2.38	1.34	1.36	0.36	0.13	0.27	-0.95	3.12	**8**
Sc	2428	0.00	3.89	2.54	2.56	0.39	0.15	0.15	-2.40	13.15	**30**
V	2423	0.00	5.27	3.87	3.93	0.53	0.28	0.14	-0.90	3.12	**160**
Cr	2408	0.00	6.35	4.42	4.53	0.58	0.34	0.13	-1.60	6.24	**314**
Co	2430	1.10	3.93	2.56	2.56	0.23	0.05	0.09	0.59	1.95	**21**
Ni	2430	2.08	5.06	3.55	3.56	0.43	0.18	0.12	-0.25	0.39	**90**
Cu	2423	0.00	4.57	3.16	3.18	0.42	0.18	0.13	-0.80	3.42	**60**
Zn	2430	2.30	6.59	3.84	3.87	0.30	0.09	0.08	0.10	6.21	**90**
As	2277	0.00	4.49	2.66	2.77	0.69	0.48	0.26	-1.05	2.34	**72**
Rb	2430	3.04	4.88	4.26	4.30	0.25	0.06	0.06	-1.17	2.37	**120**
Sr	2430	3.00	7.02	4.18	4.11	0.40	0.16	0.10	1.35	4.55	**158**
Y	2430	1.39	3.74	3.12	3.18	0.25	0.06	0.08	-1.83	5.48	**38**
Zr	2430	4.23	8.05	6.67	6.71	0.39	0.15	0.06	-0.84	2.88	**1863**
Nb	2430	2.40	3.66	3.00	3.00	0.14	0.02	0.05	-0.16	0.94	**27**
Ba	2429	2.83	6.78	5.78	5.84	0.36	0.13	0.06	-1.71	7.22	**716**
W	2412	0.00	3.58	2.15	2.20	0.32	0.10	0.15	-1.78	8.09	**17**
Pb	1966	0.00	4.25	1.42	1.39	0.73	0.54	0.52	-0.27	-0.26	**23**
Th	2429	1.10	3.18	2.64	2.64	0.13	0.02	0.05	-0.78	10.66	**18**
U	128	0.00	2.30	0.62	0.69	0.66	0.43	1.07	0.71	-0.54	**9**

Table A- 37: Summary statistics of the Gordonia Formation raw data set.

Element	N	Min	Max	Mean	Median	St. Dev	Var	CV	Skew	Kurt	Threshold
TiO_2	10347	0.15	4.18	1.23	1.21	0.28	0.08	0.23	0.62	3.62	**1.8**
MnO	10347	0.01	2.77	0.09	0.06	0.10	0.01	1.11	6.88	97.22	**0.3**
Fe_2O_3	10346	0.35	18.72	3.63	3.36	1.40	1.95	0.38	1.59	5.31	**6**
Sc	10295	1.00	44.00	11.86	12.00	3.43	11.75	0.29	0.46	4.17	**19**
V	10331	1.00	305.00	49.35	45.00	25.42	646.02	0.52	1.46	4.09	**100**
Cr	10310	1.00	761.00	78.51	68.00	47.57	2262.60	0.61	4.15	34.94	**174**
Co	10341	1.00	36.00	11.71	11.00	3.56	12.65	0.30	1.93	5.69	**19**
Ni	10347	5.00	298.00	32.55	28.00	18.43	339.72	0.57	18.43	32.75	**69**
Cu	10343	3.00	397.00	19.62	17.00	11.32	128.05	0.58	5.72	127.41	**42**
Zn	10346	2.00	894.00	34.27	33.00	20.53	421.62	0.60	16.88	624.03	**75**
As	8485	1.00	97.00	10.13	9.00	7.38	54.41	0.73	2.29	12.09	**25**
Rb	10346	22.00	154.00	72.88	74.00	13.23	175.08	0.18	-0.30	2.03	**99**
Sr	10347	18.00	582.00	60.69	51.00	32.21	1037.28	0.53	4.20	35.07	**125**
Y	10347	6.00	60.00	26.42	26.00	5.67	32.18	0.21	0.01	2.00	**38**
Zr	10347	45.00	4196.00	1154.13	1163.00	364.80	133080.72	0.32	0.38	1.93	**1884**
Nb	10347	12.00	47.00	22.62	23.00	3.03	9.19	0.13	-0.03	1.06	**29**
Ba	10340	10.00	1305.00	336.44	338.00	84.54	7146.70	0.25	0.22	5.35	**506**
W	10335	1.00	53.00	10.89	11.00	2.60	6.74	0.24	1.23	14.60	**16**
Pb	6650	1.00	72.00	4.24	4.00	3.58	12.84	0.84	5.42	67.44	**11**
Th	10344	1.00	39.00	14.52	14.00	1.88	3.54	0.13	0.10	5.42	**18**
U	484	1.00	8.00	1.56	1.00	0.86	0.75	0.55	3.10	16.63	**3**

Table A- 38: Summary statistics of the Gordonia Formation log-transformed data set.

Element	N	Min	Max	Mean	Median	St. Dev	Var	CV	Skew	Kurt	Log Threshold
TiO_2	10347	-1.90	1.43	0.18	0.19	0.24	0.06	1.31	-0.95	4.72	**2.0**
MnO	10347	-4.61	1.02	-2.68	-2.81	0.67	0.44	-0.25	0.90	1.03	**0.3**
Fe_2O_3	10346	-1.05	2.93	1.22	1.21	0.37	0.14	0.30	-0.18	1.51	**8**
Sc	10295	0.00	3.78	2.42	2.48	0.37	0.13	0.15	-2.51	11.97	**25**
V	10331	0.00	5.72	3.77	3.81	0.54	0.29	0.14	-0.86	3.33	**148**
Cr	10310	0.00	6.63	4.23	4.22	0.54	0.29	0.13	-1.00	7.38	**231**
Co	10341	0.00	3.58	2.42	2.40	0.27	0.07	0.11	0.47	2.90	**20**
Ni	10347	1.61	5.70	3.38	3.33	0.44	0.19	0.13	0.54	1.48	**77**
Cu	10343	1.10	5.98	2.87	2.83	0.44	0.20	0.15	0.64	1.04	**47**
Zn	10346	0.69	6.80	3.43	3.50	0.46	0.21	0.13	-0.19	1.09	**85**
As	8485	0.00	4.57	2.05	2.20	0.80	0.64	0.39	-0.71	0.41	**53**
Rb	10346	3.09	5.04	4.27	4.30	0.20	0.04	0.05	-1.51	4.60	**110**
Sr	10347	2.89	6.37	4.02	3.93	0.39	0.15	0.10	1.07	2.19	**130**
Y	10347	1.79	4.09	3.25	3.26	0.24	0.06	0.07	-1.51	5.12	**43**
Zr	10347	3.81	8.34	6.99	7.06	0.36	0.13	0.05	-1.13	2.73	**2383**
Nb	10347	2.48	3.85	3.11	3.14	0.14	0.02	0.04	-0.57	0.81	**30**
Ba	10340	2.30	7.17	5.78	5.82	0.32	0.10	0.06	-2.79	15.61	**643**
W	10335	0.00	3.97	2.36	2.40	0.25	0.06	0.10	-0.85	4.47	**18**
Pb	6650	0.00	4.28	1.19	1.39	0.72	0.52	0.61	-0.09	-0.40	**18**
Th	10344	0.00	3.66	2.67	2.64	0.14	0.02	0.05	-2.99	42.04	**19**
U	484	0.00	2.48	0.34	0.00	0.44	0.19	1.28	1.08	1.19	**4**

Table A- 39: Summary statistics of the undifferentiated aeolian sand raw data set.

Element	N	Min	Max	Mean	Median	St. Dev	Var	CV	Skew	Kurt	Threshold
TiO_2	5008	0.13	2.92	0.94	0.92	0.23	0.05	0.24	1.33	5.96	**1.4**
MnO	5008	0.01	1.48	0.10	0.09	0.06	0.00	0.64	6.21	90.32	**0.2**
Fe_2O_3	5008	0.50	21.79	4.65	4.43	1.85	3.42	0.40	1.30	4.89	**8**
Sc	5005	1.00	49.00	12.81	13.00	4.34	18.82	0.34	0.94	4.29	**21**
V	5001	1.00	321.00	66.83	63.00	30.83	950.22	0.46	0.96	2.50	**128**
Cr	4986	1.00	2676.00	148.73	111.00	173.40	30067.71	1.17	6.19	53.96	**496**
Co	5006	2.00	79.00	15.98	15.00	6.46	41.72	0.40	2.86	15.05	**29**
Ni	5006	8.00	706.00	54.29	46.00	43.73	1912.40	0.81	43.73	46.53	**142**
Cu	5002	1.00	177.00	28.92	27.00	13.06	170.62	0.45	1.69	8.26	**55**
Zn	5008	10.00	731.00	46.58	44.00	22.24	494.52	0.48	14.90	398.08	**91**
As	4874	1.00	144.00	15.68	14.00	9.27	85.93	0.59	3.48	26.71	**34**
Rb	5008	21.00	171.00	79.54	79.00	19.95	397.87	0.25	0.28	0.77	**119**
Sr	5006	9.00	710.00	61.95	54.00	41.49	1721.11	0.67	4.44	37.25	**145**
Y	5006	4.00	80.00	25.57	25.00	6.10	37.19	0.24	1.21	6.38	**38**
Zr	5008	69.00	3137.00	759.04	746.00	293.69	86252.71	0.39	1.06	3.73	**1346**
Nb	5007	3.00	101.00	19.67	20.00	2.96	8.73	0.15	4.37	116.15	**26**
Ba	5007	10.00	1651.00	330.87	331.00	97.96	9595.61	0.30	1.03	9.57	**527**
W	4989	1.00	36.00	9.67	9.00	2.78	7.73	0.29	0.66	2.71	**15**
Pb	3821	1.00	177.00	5.53	5.00	6.19	38.28	1.12	13.44	300.51	**18**
Th	4990	1.00	30.00	14.42	14.00	2.18	4.75	0.15	-0.28	4.34	**19**
U	601	1.00	13.00	1.72	1.00	1.21	1.47	0.71	3.50	19.65	**4**

Table A- 40: Summary statistics of the undifferentiated aeolian sand log-transformed data set.

Element	N	Min	Max	Mean	Median	St. Dev	Var	CV	Skew	Kurt	Log Threshold
TiO_2	5008	-2.04	1.07	-0.09	-0.08	0.24	0.06	-2.68	-0.73	6.41	**1.5**
MnO	5008	-4.61	0.39	-2.43	-2.41	0.50	0.25	-0.21	0.12	0.86	**0.3**
Fe_2O_3	5008	-0.69	3.08	1.46	1.49	0.40	0.16	0.28	-0.48	1.30	**10**
Sc	5005	0.00	3.89	2.49	2.56	0.38	0.15	0.15	-1.61	7.45	**28**
V	5001	0.00	5.77	4.09	4.14	0.51	0.26	0.13	-0.93	2.74	**189**
Cr	4986	0.00	7.89	4.72	4.71	0.70	0.49	0.15	0.17	3.30	**581**
Co	5006	0.69	4.37	2.71	2.71	0.34	0.11	0.12	0.58	2.12	**31**
Ni	5006	2.08	6.56	3.82	3.83	0.56	0.31	0.15	0.45	1.38	**162**
Cu	5002	0.00	5.18	3.27	3.30	0.44	0.20	0.14	-0.32	1.13	**70**
Zn	5008	2.30	6.59	3.79	3.78	0.31	0.10	0.08	0.48	4.91	**87**
As	4874	0.00	4.97	2.60	2.64	0.58	0.34	0.22	-1.01	3.51	**51**
Rb	5008	3.04	5.14	4.34	4.37	0.27	0.07	0.06	-0.79	1.52	**137**
Sr	5008	2.20	6.57	3.99	3.99	0.50	0.25	0.13	0.49	0.98	**167**
Y	5006	1.39	4.38	3.21	3.22	0.25	0.06	0.08	-0.95	5.85	**42**
Zr	5008	4.23	8.05	6.56	6.61	0.41	0.16	0.06	-0.60	1.18	**1719**
Nb	5007	1.10	4.62	2.97	3.00	0.15	0.02	0.05	-1.27	18.26	**26**
Ba	5007	2.30	7.41	5.75	5.80	0.33	0.11	0.06	-1.61	8.13	**649**
W	4989	0.00	3.58	2.23	2.20	0.30	0.09	0.14	-0.74	3.10	**18**
Pb	3821	0.00	5.18	1.44	1.61	0.74	0.55	0.52	-0.16	0.24	**24**
Th	4990	0.00	3.40	2.65	2.64	0.18	0.03	0.07	-3.36	31.63	**21**
U	601	0.00	2.56	0.39	0.00	0.50	0.25	1.28	1.09	0.72	**5**

Table A- 41: Abundance of elements in average crustal rocks (source: Rose *et al.*, 1979; Mookherjee, 1992).

Element	Abundance (ppm)
As	5
Ba	580
Co	25
Cr	200
Cu	50
Fe	50000
Mn	1000
Nb	20
Ni	80
Pb	13
Rb	150
Sc	13
Sr	300
Th	12
Ti	4400
U	2.5
V	150
W	69
Y	70
Zn	80
Zr	150

APPENDIX 2: CORRELATION MATRIX OF THE ELEMENTS IN THE LITHOLOGICAL GROUPS

Table A- 42: Correlation matrix of the elements on the Amphibolites Basement.

	TiO_2	MnO	Fe_2O_3	Sc	V	Cr	Co	Ni	Cu	Zn	As	Rb	Sr	Y	Zr	Nb	Ba	W	Pb	Th	U
TiO_2	1.00																				
MnO	0.27	1.00																			
Fe_2O_3	0.42	0.79	1.00																		
Sc	**0.50**	**0.74**	**0.90**	1.00																	
V	0.36	**0.75**	**0.93**	**0.85**	1.00																
Cr	0.10	**0.53**	**0.59**	**0.55**	**0.55**	1.00															
Co	0.36	**0.84**	**0.82**	**0.78**	**0.78**	**0.62**	1.00														
Ni	0.20	**0.64**	**0.75**	**0.68**	**0.66**	**0.86**	**0.78**	1.00													
Cu	0.28	**0.72**	**0.90**	**0.80**	**0.86**	**0.51**	**0.78**	**0.69**	1.00												
Zn	0.20	**0.63**	**0.63**	**0.62**	**0.53**	0.29	**0.51**	**0.43**	**0.58**	1.00											
As	-0.20	0.29	0.28	0.27	0.32	0.38	0.32	0.40	0.31	0.24	1.00										
Rb	-0.06	-0.13	-0.03	-0.13	-0.12	-0.20	-0.15	-0.09	-0.06	-0.05	-0.16	1.00									
Sr	-0.20	-0.17	-0.11	-0.13	-0.15	-0.16	-0.12	-0.10	-0.05	-0.07	-0.17	0.35	1.00								
Y	0.44	0.37	0.47	0.41	0.39	0.04	0.31	0.20	0.37	0.32	-0.22	0.30	0.00	1.00							
Zr	0.47	-0.41	-0.40	-0.23	-0.39	-0.24	-0.37	-0.37	-0.44	-0.39	-0.46	-0.05	-0.02	0.02	1.00						
Nb	**0.67**	-0.06	0.00	0.11	-0.08	-0.23	-0.08	-0.17	-0.14	0.01	-0.55	0.11	-0.17	0.48	**0.60**	1.00					
Ba	0.01	-0.12	-0.04	-0.10	-0.10	-0.18	-0.07	-0.09	-0.03	-0.09	-0.20	**0.66**	**0.69**	0.27	0.08	0.07	1.00				
W	0.20	-0.08	-0.15	-0.08	-0.10	-0.18	-0.09	-0.20	-0.20	0.05	0.03	-0.38	-0.39	-0.07	0.10	0.26	-0.35	1.00			
Pb	-0.17	-0.05	-0.02	0.01	-0.06	-0.11	-0.04	-0.07	-0.04	0.13	0.07	**0.57**	0.33	0.10	-0.12	-0.12	0.45	-0.24	1.00		
Th	0.07	-0.31	-0.22	-0.18	-0.31	-0.36	-0.29	-0.27	-0.25	-0.21	-0.33	0.54	0.27	0.19	0.25	0.40	0.47	-0.17	0.39	1.00	
U	-0.19	-0.31	-0.30	-0.31	-0.30	-0.30	-0.32	-0.27	-0.27	-0.15	-0.19	0.30	0.32	-0.13	0.12	-0.04	0.26	-0.12	0.08	0.23	1.00

Table A- 43: Correlation matrix of the elements on the Kraaipan Group.

	TiO_2	MnO	Fe_2O_3	Sc	V	Cr	Co	Ni	Cu	Zn	As	Rb	Sr	Y	Zr	Nb	Ba	W	Pb	Th
TiO_2	1.00																			
MnO	0.33	1.00																		
Fe_2O_3	0.35	**0.75**	1.00																	
Sc	0.45	**0.86**	**0.85**	1.00																
V	0.38	**0.83**	**0.67**	**0.89**	1.00															
Cr	0.18	0.46	**0.64**	**0.52**	0.29	1.00														
Co	0.09	**0.65**	0.30	**0.61**	**0.63**	0.42	1.00													
Ni	0.01	**0.62**	**0.68**	**0.60**	0.44	**0.87**	**0.62**	1.00												
Cu	0.17	**0.70**	**0.55**	**0.73**	**0.75**	0.29	**0.73**	**0.55**	1.00											
Zn	0.13	0.39	**0.53**	**0.54**	0.41	**0.51**	0.48	**0.58**	**0.51**	1.00										
As	-0.44	-0.12	-0.40	-0.15	0.05	-0.61	0.14	-0.29	0.16	-0.08	1.00									
Rb	-0.41	-0.28	-0.40	-0.39	-0.27	-0.37	-0.13	-0.26	-0.23	0.00	0.33	1.00								
Sr	0.02	0.24	0.04	0.21	0.20	-0.04	0.36	0.09	0.43	0.23	0.24	0.04	1.00							
Y	0.22	0.32	-0.01	0.27	0.39	-0.17	0.32	-0.07	0.28	0.06	0.25	0.38	0.17	1.00						
Zr	0.39	-0.45	-0.42	-0.39	-0.40	-0.21	-0.41	-0.51	-0.45	-0.41	-0.29	0.11	0.01	0.05	1.00					
Nb	0.15	-0.48	-0.68	-0.52	-0.44	-0.45	-0.25	-0.59	-0.49	-0.45	0.05	0.37	-0.13	0.41	**0.68**	1.00				
Ba	0.33	0.41	0.32	0.39	0.36	0.06	0.18	0.12	0.24	0.24	-0.01	0.30	0.50	0.41	0.04	-0.06	1.00			
W	0.34	-0.13	0.07	-0.06	0.00	0.05	-0.23	-0.07	-0.24	-0.07	-0.24	-0.33	-0.51	-0.29	0.09	0.07	-0.29	1.00		
Pb	-0.02	0.00	-0.24	-0.06	0.09	-0.02	-0.02	-0.23	-0.39	-0.50	-0.17	0.01	-0.20	0.15	0.32	0.35	-0.06	0.05	1.00	
Th	-0.28	-0.22	-0.68	-0.29	-0.09	-0.49	0.26	-0.39	-0.01	-0.25	**0.59**	0.53	0.29	**0.58**	0.16	**0.58**	0.11	-0.46	0.29	1.00

Table A- 44: Correlation matrix of the elements on Kanye Formation.

	TiO_2	MnO	Fe_2O_3	Sc	V	Cr	Co	Ni	Cu	Zn	As	Rb	Sr	Y	Zr	Nb	Ba	W	Pb	Th	U
TiO_2	1.00																				
MnO	0.12	1.00																			
Fe_2O_3	0.47	**0.59**	1.00																		
Sc	**0.52**	**0.50**	**0.88**	1.00																	
V	**0.56**	**0.45**	**0.74**	**0.73**	1.00																
Cr	0.45	0.49	**0.66**	**0.69**	**0.81**	1.00															
Co	0.46	**0.69**	**0.73**	**0.69**	**0.77**	**0.68**	1.00														
Ni	0.48	**0.53**	**0.71**	**0.77**	**0.85**	**0.88**	**0.76**	1.00													
Cu	0.39	0.48	**0.67**	**0.76**	**0.73**	**0.64**	**0.71**	**0.81**	1.00												
Zn	0.00	0.36	0.46	0.44	0.11	0.05	0.25	0.21	**0.53**	1.00											
As	-0.21	0.13	0.05	0.21	0.10	0.05	0.20	0.18	0.38	0.35	1.00										
Rb	0.34	0.19	**0.59**	**0.54**	0.20	0.17	0.30	0.26	0.27	0.39	-0.11	1.00									
Sr	0.01	0.04	0.17	0.15	-0.09	-0.09	-0.05	-0.04	0.20	0.28	-0.02	0.21	1.00								
Y	0.18	-0.09	0.20	0.19	-0.15	-0.18	0.03	-0.07	0.02	0.29	-0.13	**0.73**	0.22	1.00							
Zr	0.25	-0.37	-0.48	-0.40	-0.27	-0.19	-0.31	-0.35	-0.48	-0.49	-0.43	-0.33	-0.07	-0.04	1.00						
Nb	0.16	-0.30	-0.05	-0.03	-0.23	-0.19	-0.17	-0.23	-0.30	-0.15	-0.21	0.49	0.19	0.67	0.27	1.00					
Ba	0.04	0.29	0.40	0.29	-0.14	-0.16	0.10	-0.08	0.08	0.47	-0.07	**0.61**	**0.51**	**0.57**	-0.30	0.21	1.00				
W	-0.06	-0.25	-0.32	-0.22	-0.27	-0.34	-0.23	-0.35	-0.29	-0.19	0.20	-0.15	-0.13	0.12	0.17	0.18	0.04	1.00			
Pb	0.21	0.15	0.17	0.13	-0.04	0.01	0.14	0.02	0.12	0.28	-0.31	0.29	0.23	0.38	0.13	0.08	0.39	-0.08	1.00		
Th	0.10	-0.16	-0.11	-0.01	-0.13	0.04	-0.18	-0.02	-0.23	-0.31	-0.30	0.27	0.14	0.32	0.21	**0.60**	0.06	0.13	-0.01	1.00	
U	-0.18	-0.38	-0.31	-0.33	-0.49	-0.39	-0.41	-0.37	-0.44	-0.12	-0.33	0.16	0.12	0.31	0.17	0.33	0.19	0.04	0.06	**0.50**	1.00

Table A- 45: Correlation matrix of the elements on the Gaborone Granite.

	TiO_2	MnO	Fe_2O_3	Sc	V	Cr	Co	Ni	Cu	Zn	As	Rb	Sr	Y	Zr	Nb	Ba	W	Pb	Th	U
TiO_2	1.00																				
MnO	0.14	1.00																			
Fe_2O_3	**0.59**	**0.68**	1.00																		
Sc	**0.51**	**0.67**	**0.90**	1.00																	
V	0.49	**0.53**	**0.77**	**0.76**	1.00																
Cr	0.12	**0.53**	**0.59**	**0.66**	**0.65**	1.00															
Co	0.38	**0.74**	**0.78**	**0.77**	**0.81**	**0.72**	1.00														
Ni	0.22	**0.67**	**0.72**	**0.77**	**0.78**	**0.94**	**0.84**	1.00													
Cu	0.47	**0.65**	**0.82**	**0.82**	**0.83**	**0.56**	**0.84**	**0.74**	1.00												
Zn	0.30	0.26	0.42	0.41	0.24	0.18	0.30	0.22	0.38	1.00											
As	-0.34	0.27	0.00	0.22	0.17	0.31	0.23	0.37	0.26	-0.16	1.00										
Rb	-0.06	-0.42	-0.28	-0.34	-0.32	-0.40	-0.41	-0.42	-0.33	-0.04	-0.27	1.00									
Sr	0.35	0.24	0.37	0.42	0.41	0.23	0.47	0.30	**0.52**	**0.62**	-0.03	-0.16	1.00								
Y	-0.28	-0.16	-0.25	-0.24	-0.41	-0.35	-0.43	-0.36	-0.31	0.11	-0.12	**0.54**	-0.18	1.00							
Zr	0.09	-0.53	-0.42	-0.33	-0.40	-0.33	-0.52	-0.49	-0.51	0.01	-0.52	0.25	-0.20	0.28	1.00						
Nb	-0.14	-0.55	-0.51	-0.51	-0.49	-0.42	-0.63	-0.54	-0.61	-0.17	-0.32	0.72	-0.37	**0.61**	**0.62**	1.00					
Ba	**0.58**	**0.50**	**0.71**	**0.62**	0.33	0.22	0.47	0.33	**0.53**	0.43	-0.13	-0.20	0.44	-0.19	-0.33	-0.51	1.00				
W	-0.38	-0.36	-0.49	-0.44	-0.58	-0.31	-0.56	-0.40	-0.49	-0.24	0.16	0.00	-0.43	0.29	0.23	0.25	-0.32	1.00			
Pb	-0.26	0.08	-0.13	-0.09	-0.23	-0.08	-0.13	-0.12	-0.20	0.34	-0.14	0.26	0.11	0.36	0.05	0.27	-0.01	0.01	1.00		
Th	-0.45	-0.32	-0.45	-0.41	-0.39	-0.19	-0.43	-0.26	-0.39	-0.32	0.25	0.32	-0.33	**0.54**	0.04	**0.56**	-0.52	0.48	0.07	1.00	
U	-0.42	-0.53	-0.59	-0.58	-0.54	-0.43	-0.54	-0.52	-0.49	-0.37	-0.06	0.46	-0.30	0.44	0.27	**0.57**	-0.58	0.31	-0.07	**0.70**	1.00

Table A- 46: Correlation matrix of the elements on the Dominion Group.

	TiO_2	MnO	Fe_2O_3	Sc	V	Cr	Co	Ni	Cu	Zn	As	Rb	Sr	Y	Zr	Nb	Ba	W	Pb	Th
TiO_2	1.00																			
MnO	-0.08	1.00																		
Fe_2O_3	-0.16	**0.69**	1.00																	
Sc	0.14	**0.64**	**0.85**	1.00																
V	-0.23	**0.65**	**0.88**	0.74	1.00															
Cr	-0.02	**0.57**	**0.78**	**0.74**	**0.77**	1.00														
Co	-0.07	**0.75**	**0.75**	**0.70**	**0.81**	**0.72**	1.00													
Ni	-0.13	**0.65**	**0.85**	**0.79**	**0.80**	**0.86**	**0.81**	1.00												
Cu	-0.13	**0.65**	**0.89**	**0.78**	**0.87**	**0.76**	**0.83**	**0.87**	1.00											
Zn	-0.04	0.37	0.37	0.33	0.25	0.25	0.31	0.29	0.38	1.00										
As	-0.28	0.46	0.40	0.48	0.39	0.32	0.36	0.35	0.40	0.28	1.00									
Rb	-0.10	0.24	0.36	0.27	0.11	0.05	0.01	0.12	0.22	0.20	0.06	1.00								
Sr	-0.14	0.42	0.42	0.37	0.37	0.35	0.45	0.43	**0.50**	**0.83**	0.26	0.16	1.00							
Y	0.03	0.05	0.08	0.08	-0.16	-0.12	-0.20	-0.10	-0.05	0.17	-0.07	**0.67**	0.10	1.00						
Zr	**0.68**	-0.54	-0.64	-0.40	-0.68	-0.43	-0.53	-0.52	-0.60	-0.26	-0.61	-0.19	-0.31	0.15	1.00					
Nb	**0.54**	-0.31	-0.37	-0.18	-0.58	-0.38	-0.50	-0.43	-0.42	-0.02	-0.28	0.31	-0.16	**0.67**	**0.69**	1.00				
Ba	0.17	0.24	0.16	0.18	-0.07	-0.07	0.04	0.02	0.08	0.39	0.01	**0.65**	0.37	**0.61**	0.04	0.42	1.00			
W	0.38	-0.20	-0.26	-0.03	-0.27	-0.11	-0.25	-0.15	-0.21	-0.16	0.02	-0.17	-0.19	0.00	0.42	0.34	0.08	1.00		
Pb	-0.06	0.36	0.28	0.25	0.16	0.09	0.20	0.17	0.23	**0.60**	0.31	0.19	0.48	0.13	-0.32	-0.05	0.39	-0.10	1.00	
Th	0.34	-0.05	-0.06	0.08	-0.19	-0.11	-0.27	-0.15	-0.16	-0.18	0.02	0.31	-0.21	0.42	0.24	0.53	0.25	0.26	-0.12	1.00

Table A- 47: Correlation matrix of the elements on the Hospital Hill Subgroup.

	TiO_2	MnO	Fe_2O_3	Sc	V	Cr	Co	Ni	Cu	Zn	As	Rb	Sr	Y	Zr	Nb	Ba	W	Pb	Th	U
TiO_2	1.00																				
MnO	0.22	1.00																			
Fe_2O_3	0.15	**0.56**	1.00																		
Sc	0.49	**0.60**	**0.71**	1.00																	
V	0.16	**0.53**	0.46	**0.59**	1.00																
Cr	0.12	0.12	0.25	0.40	0.34	1.00															
Co	0.19	0.35	-0.23	0.12	0.49	0.07	1.00														
Ni	0.16	0.43	0.24	**0.54**	**0.63**	**0.66**	**0.59**	1.00													
Cu	0.25	0.35	0.08	0.45	**0.69**	0.35	**0.73**	**0.78**	1.00												
Zn	0.24	0.33	0.12	0.40	**0.50**	0.03	0.49	0.47	**0.52**	1.00											
As	-0.20	-0.16	-0.55	-0.11	-0.11	0.07	0.23	0.17	0.23	0.12	1.00										
Rb	0.35	-0.05	-0.28	0.12	0.26	0.16	**0.51**	0.40	**0.53**	0.45	0.21	1.00									
Sr	0.10	0.43	0.10	0.36	0.47	-0.09	0.44	0.32	0.48	0.33	0.00	0.04	1.00								
Y	**0.50**	0.05	-0.20	0.25	0.16	0.13	0.36	0.27	0.37	0.50	0.19	**0.63**	0.06	1.00							
Zr	**0.69**	-0.08	0.00	0.06	-0.37	-0.15	-0.20	-0.35	-0.28	-0.22	-0.37	-0.06	-0.12	0.14	1.00						
Nb	**0.57**	-0.29	-0.45	-0.03	-0.32	-0.10	0.03	-0.14	-0.05	0.22	0.27	0.40	-0.15	**0.70**	**0.51**	1.00					
Ba	**0.59**	**0.53**	0.37	**0.65**	**0.55**	0.07	0.29	0.35	0.44	0.38	-0.13	0.44	0.38	0.39	0.13	0.17	1.00				
W	0.11	-0.10	-0.03	0.12	-0.21	-0.03	-0.25	-0.19	-0.19	-0.28	0.39	-0.20	-0.24	-0.13	0.18	0.20	0.13	1.00			
Pb	0.04	0.22	-0.06	0.34	0.20	-0.10	0.25	0.18	0.21	0.32	0.29	0.15	**0.50**	0.23	-0.11	0.12	0.22	0.06	1.00		
Th	0.35	-0.29	-0.50	0.01	-0.29	-0.09	0.13	-0.01	0.11	0.15	**0.52**	0.38	-0.08	**0.57**	0.24	**0.76**	0.00	0.24	0.25	1.00	
U	-0.25	-0.19	-0.17	-0.30	-0.22	-0.25	-0.08	-0.24	-0.19	-0.19	0.03	-0.11	-0.08	-0.06	-0.03	0.03	-0.27	-0.10	0.15	0.14	1.00

Table A- 48: Correlation matrix of the elements on the Klipperiviersberg Group.

	TiO_2	MnO	Fe_2O_3	Sc	V	Cr	Co	Ni	Cu	Zn	As	Rb	Sr	Y	Zr	Nb	Ba	W	Pb	Th	U
TiO_2	1.00																				
MnO	-0.02	1.00																			
Fe_2O_3	0.07	**0.51**	1.00																		
Sc	0.23	0.43	**0.88**	1.00																	
V	0.10	0.44	**0.83**	**0.72**	1.00																
Cr	-0.13	0.21	**0.57**	**0.56**	0.36	1.00															
Co	0.18	**0.57**	**0.60**	**0.58**	**0.52**	0.42	1.00														
Ni	-0.06	0.43	**0.84**	**0.79**	**0.64**	**0.81**	**0.69**	1.00													
Cu	0.05	0.40	**0.92**	**0.81**	**0.77**	0.46	**0.57**	**0.76**	1.00												
Zn	-0.12	0.53	**0.51**	0.41	0.35	0.18	0.16	0.32	0.47	1.00											
As	-0.37	0.14	0.19	0.19	0.16	0.08	-0.08	0.10	0.23	0.30	1.00										
Rb	0.36	0.27	**0.64**	**0.54**	**0.53**	0.14	0.34	0.37	**0.60**	0.35	0.06	1.00									
Sr	-0.05	-0.12	0.14	0.21	0.13	0.18	0.10	0.21	0.28	-0.03	0.11	0.00	1.00								
Y	**0.56**	0.34	0.39	0.36	0.38	-0.05	0.40	0.18	0.34	0.19	-0.07	**0.63**	-0.23	1.00							
Zr	**0.62**	-0.31	-0.53	-0.30	-0.44	-0.31	-0.22	-0.42	-0.56	-0.42	-0.52	-0.28	-0.15	0.06	1.00						
Nb	**0.80**	-0.25	-0.26	-0.06	-0.20	-0.26	-0.11	-0.32	-0.28	-0.28	-0.27	0.18	-0.18	0.44	**0.71**	1.00					
Ba	**0.52**	0.17	0.33	0.38	0.35	0.07	0.38	0.23	0.38	0.06	-0.02	**0.50**	0.37	0.39	0.01	0.29	1.00				
W	0.19	-0.20	-0.35	-0.22	-0.26	-0.22	-0.13	-0.27	-0.34	-0.32	0.01	-0.28	-0.17	-0.04	0.41	0.31	-0.07	1.00			
Pb	0.19	0.17	0.15	0.19	0.11	-0.03	0.14	0.02	0.17	0.26	0.28	0.30	0.02	0.33	-0.13	0.22	0.25	-0.07	1.00		
Th	**0.53**	-0.20	-0.12	0.04	-0.09	-0.15	0.00	-0.15	-0.11	-0.26	-0.06	0.21	-0.14	0.39	0.37	**0.72**	0.21	0.26	0.27	1.00	
U	-0.02	-0.04	-0.02	-0.06	-0.05	-0.02	-0.06	-0.02	0.02	-0.07	0.02	0.11	0.00	0.13	0.02	0.12	-0.01	-0.04	0.00	0.13	1.00

Table A- 49: Correlation matrix of the elements on the Platberg Group.

	TiO_2	MnO	Fe_2O_3	Sc	V	Cr	Co	Ni	Cu	Zn	As	Rb	Sr	Y	Zr	Nb	Ba	W	Pb	Th	U
TiO_2	1.00																				
MnO	0.13	1.00																			
Fe_2O_3	0.37	**0.70**	1.00																		
Sc	**0.51**	**0.62**	**0.92**	1.00																	
V	0.35	**0.62**	**0.92**	**0.88**	1.00																
Cr	0.28	0.49	**0.61**	**0.62**	**0.62**	1.00															
Co	0.00	0.03	0.04	0.04	0.03	0.00	1.00														
Ni	0.16	**0.52**	**0.72**	**0.62**	**0.58**	**0.65**	0.07	1.00													
Cu	0.13	**0.60**	**0.83**	**0.71**	**0.71**	0.46	0.07	**0.81**	1.00												
Zn	0.05	0.45	**0.58**	**0.52**	0.47	0.30	0.04	0.45	**0.54**	1.00											
As	-0.70	-0.11	-0.24	-0.26	-0.25	-0.13	-0.01	-0.10	-0.10	0.11	1.00										
Rb	-0.19	0.13	0.01	-0.01	-0.11	0.10	-0.05	-0.05	-0.05	0.06	0.26	1.00									
Sr	0.43	0.28	**0.56**	**0.53**	**0.53**	0.22	0.03	0.39	**0.52**	0.35	-0.38	-0.36	1.00								
Y	0.36	0.41	0.45	0.45	0.37	0.27	-0.01	0.14	0.14	0.25	-0.12	0.36	0.11	1.00							
Zr	**0.55**	-0.36	-0.43	-0.22	-0.42	-0.21	0.00	-0.35	-0.46	-0.41	-0.46	-0.16	-0.12	-0.11	1.00						
Nb	**0.63**	-0.21	-0.19	-0.03	-0.22	-0.06	-0.04	-0.26	-0.36	-0.30	-0.39	0.08	-0.14	0.40	**0.73**	1.00					
Ba	**0.61**	0.33	**0.63**	**0.62**	**0.63**	0.35	0.00	0.30	0.34	0.37	-0.44	-0.11	**0.65**	**0.53**	-0.12	0.13	1.00				
W	-0.14	-0.43	-0.51	-0.36	-0.39	-0.28	0.00	-0.37	-0.52	-0.39	0.26	-0.10	-0.41	-0.19	0.31	0.23	-0.37	1.00			
Pb	-0.02	0.19	0.27	0.24	0.20	0.13	0.02	0.21	0.27	0.43	0.05	0.18	0.07	0.09	-0.19	-0.27	0.15	-0.22	1.00		
Th	0.16	-0.10	-0.14	-0.02	-0.13	-0.04	-0.03	-0.19	-0.23	-0.28	-0.01	0.13	-0.21	0.27	0.25	0.60	-0.12	0.22	-0.38	1.00	
U	-0.16	-0.01	-0.11	-0.16	-0.16	-0.09	-0.02	-0.06	-0.01	0.04	0.16	0.12	0.01	0.06	-0.05	0.02	-0.06	-0.12	-0.05	0.13	1.00

Table A- 50: Correlation matrix of the elements on the Allanridge Formation.

	TiO_2	MnO	Fe_2O_3	Sc	V	Cr	Co	Ni	Cu	Zn	As	Rb	Sr	Y	Zr	Nb	Ba	W	Pb	Th	U
TiO_2	1.00																				
MnO	0.27	1.00																			
Fe_2O_3	0.42	**0.68**	1.00																		
Sc	0.46	**0.64**	**0.88**	1.00																	
V	0.35	**0.66**	**0.94**	0.82	1.00																
Cr	0.10	0.29	0.37	0.41	0.37	1.00															
Co	0.24	**0.76**	**0.76**	**0.68**	**0.73**	0.24	1.00														
Ni	0.30	**0.63**	**0.87**	**0.77**	**0.80**	**0.52**	**0.75**	1.00													
Cu	0.33	**0.63**	**0.92**	**0.78**	**0.87**	0.21	**0.73**	**0.81**	1.00												
Zn	0.06	0.41	0.44	0.40	0.37	0.13	0.31	0.36	0.43	1.00											
As	-0.67	-0.16	-0.30	-0.17	-0.27	-0.04	-0.16	-0.24	-0.28	0.05	1.00										
Rb	-0.16	-0.02	-0.19	-0.09	-0.24	0.17	-0.19	-0.26	-0.31	0.07	0.38	1.00									
Sr	0.38	0.31	**0.54**	0.42	**0.51**	0.02	0.38	**0.54**	**0.59**	0.16	-0.54	-0.61	1.00								
Y	0.36	0.43	0.37	0.45	0.33	0.18	0.40	0.26	0.25	0.24	-0.01	0.46	-0.07	1.00							
Zr	**0.50**	-0.33	-0.45	-0.27	-0.47	-0.11	-0.41	-0.44	-0.51	-0.27	-0.33	0.11	-0.17	0.11	1.00						
Nb	**0.60**	-0.14	-0.21	-0.02	-0.27	0.00	-0.23	-0.28	-0.33	-0.15	-0.17	0.35	-0.31	0.43	**0.81**	1.00					
Ba	**0.57**	0.47	**0.62**	**0.56**	**0.56**	0.18	0.44	**0.55**	**0.58**	0.22	-0.51	-0.12	**0.56**	0.23	-0.07	0.01	1.00				
W	-0.29	-0.42	-0.60	-0.50	-0.52	-0.22	-0.36	-0.54	-0.57	-0.30	0.34	0.16	-0.49	-0.09	0.33	0.21	-0.53	1.00			
Pb	-0.09	0.21	0.08	0.18	0.04	0.07	0.18	0.07	0.04	0.30	0.26	0.33	-0.12	0.29	-0.12	0.02	0.08	-0.09	1.00		
Th	0.18	-0.06	-0.07	0.12	-0.08	0.10	-0.09	-0.11	-0.17	-0.14	0.14	0.30	-0.23	0.36	0.27	**0.53**	-0.07	0.08	0.13	1.00	
U	-0.11	0.02	0.03	0.16	0.02	-0.01	0.06	0.07	0.06	-0.04	0.14	-0.10	0.09	-0.08	-0.12	-0.13	-0.05	-0.17	0.07	0.17	1.00

Table A- 51: Correlation matrix of the elements on the Black Reef Formation.

	TiO_2	MnO	Fe_2O_3	Sc	V	Cr	Co	Ni	Cu	Zn	As	Rb	Sr	Y	Zr	Nb	Ba	W	Pb	Th
TiO_2	1.00																			
MnO	-0.17	1.00																		
Fe_2O_3	0.42	0.23	1.00																	
Sc	0.36	-0.02	**0.83**	1.00																
V	0.42	-0.14	**0.83**	**0.80**	1.00															
Cr	-0.01	0.17	**0.54**	0.37	**0.53**	1.00														
Co	0.55	-0.08	0.44	0.38	0.41	-0.11	1.00													
Ni	0.30	-0.03	**0.76**	**0.73**	**0.84**	**0.62**	0.48	1.00												
Cu	**0.52**	-0.14	**0.79**	**0.70**	**0.77**	0.25	**0.75**	**0.75**	1.00											
Zn	-0.03	-0.36	0.16	0.25	0.26	0.24	-0.23	0.00	0.00	1.00										
As	-0.39	-0.10	-0.05	0.27	0.06	0.00	-0.20	0.08	-0.09	0.23	1.00									
Rb	-0.05	0.36	0.35	0.16	0.30	**0.62**	-0.37	0.38	0.01	0.05	0.12	1.00								
Sr	-0.15	-0.34	0.03	0.27	0.11	0.00	0.27	0.13	0.23	0.25	0.32	-0.45	1.00							
Y	0.06	0.38	0.03	-0.24	-0.07	0.11	-0.03	0.07	0.01	-0.50	-0.29	0.44	-0.45	1.00						
Zr	0.34	-0.17	-0.52	-0.56	-0.41	-0.46	-0.11	-0.55	-0.41	-0.23	-0.45	-0.32	-0.45	0.08	1.00					
Nb	0.11	0.10	-0.37	-0.57	-0.39	-0.04	-0.38	-0.37	-0.41	-0.36	-0.31	0.26	-0.58	**0.58**	**0.62**	1.00				
Ba	0.42	**0.52**	0.59	0.29	0.34	0.17	**0.60**	0.38	0.46	-0.25	-0.38	0.15	-0.07	0.33	-0.16	-0.09	1.00			
W	0.07	-0.48	-0.31	-0.02	0.02	0.02	-0.21	-0.04	-0.24	0.23	0.24	-0.15	0.34	-0.35	0.19	-0.02	-0.37	1.00		
Pb	-0.11	0.11	-0.29	-0.54	-0.40	-0.29	-0.01	-0.32	-0.21	-0.22	-0.34	0.04	-0.33	0.40	0.18	0.37	0.11	-0.39	1.00	
Th	-0.23	0.18	-0.29	-0.24	-0.27	0.14	-0.42	-0.14	-0.41	-0.40	0.14	0.21	-0.23	0.36	0.26	**0.55**	-0.22	0.04	-0.24	1.00

Table A- 52: Correlation matrix of the elements on the Vryburg Formation.

	TiO_2	MnO	Fe_2O_3	Sc	V	Cr	Co	Ni	Cu	Zn	As	Rb	Sr	Y	Zr	Nb	Ba	W	Pb	Th	U
TiO_2	1.00																				
MnO	-0.15	1.00																			
Fe_2O_3	-0.05	0.44	1.00																		
Sc	0.02	0.34	**0.90**	1.00																	
V	-0.13	0.32	**0.94**	**0.87**	1.00																
Cr	-0.34	0.21	0.45	0.38	0.48	1.00															
Co	-0.18	0.24	**0.78**	**0.77**	**0.85**	**0.50**	1.00														
Ni	-0.28	0.27	**0.84**	**0.77**	**0.86**	**0.70**	**0.86**	1.00													
Cu	-0.03	0.21	**0.91**	**0.86**	**0.92**	0.32	**0.81**	**0.78**	1.00												
Zn	-0.24	0.23	**0.74**	**0.72**	**0.76**	0.41	**0.73**	**0.75**	**0.73**	1.00											
As	-0.69	-0.01	0.00	0.23	0.10	0.12	0.20	0.17	0.06	0.27	1.00										
Rb	-0.07	0.25	0.15	0.05	0.08	0.10	0.02	0.20	0.03	0.10	-0.18	1.00									
Sr	-0.38	-0.03	0.26	0.38	0.34	0.14	0.43	0.32	0.35	0.37	**0.55**	-0.33	1.00								
Y	**0.54**	0.05	0.24	0.25	0.16	-0.10	0.09	0.09	0.24	0.01	-0.44	0.43	-0.33	1.00							
Zr	**0.75**	-0.23	-0.61	-0.52	-0.67	-0.47	-0.65	-0.71	-0.62	-0.63	-0.55	-0.08	-0.50	0.26	1.00						
Nb	**0.80**	-0.20	-0.46	-0.36	-0.52	-0.35	-0.51	-0.53	-0.49	-0.46	-0.54	0.01	-0.54	0.43	**0.93**	1.00					
Ba	0.41	0.46	0.49	0.45	0.47	0.09	0.43	0.34	0.46	0.26	-0.35	0.35	-0.11	0.51	0.01	0.13	1.00				
W	0.15	-0.02	-0.15	-0.18	-0.15	-0.05	-0.21	-0.18	-0.18	-0.25	-0.10	0.03	-0.24	0.10	0.18	0.20	0.08	1.00			
Pb	-0.07	0.04	0.02	0.02	0.00	-0.02	-0.03	0.01	-0.02	-0.01	0.02	0.10	-0.07	-0.06	-0.03	-0.18	-0.03	-0.10	1.00		
Th	0.29	-0.16	-0.22	-0.04	-0.25	-0.20	-0.22	-0.20	-0.21	-0.12	-0.03	0.12	-0.16	0.32	0.36	0.48	0.00	-0.02	-0.10	1.00	
U	-0.26	-0.93	-0.79	-0.81	**0.93**	1.00	-0.72	-0.87	-0.28	1.00	-0.35	-0.06	**0.98**	-0.24	0.24	0.00	-0.42	0.00	-0.80	-0.72	1.00

Table A- 53: Correlation matrix of the elements on the Malmani Dolomite Subgroup.

	TiO_2	MnO	Fe_2O_3	Sc	V	Cr	Co	Ni	Cu	Zn	As	Rb	Sr	Y	Zr	Nb	Ba	W	Pb	Th	U
TiO_2	1.00																				
MnO	0.27	1.00																			
Fe_2O_3	0.45	**0.54**	1.00																		
Sc	**0.63**	**0.55**	**0.81**	1.00																	
V	**0.54**	0.38	**0.54**	**0.58**	1.00																
Cr	**0.59**	0.30	**0.53**	**0.60**	**0.56**	1.00															
Co	0.20	-0.39	-0.21	0.00	0.37	0.25	1.00														
Ni	**0.53**	0.37	**0.68**	**0.69**	**0.58**	**0.75**	0.28	1.00													
Cu	**0.53**	0.16	**0.53**	**0.56**	0.48	**0.50**	0.27	**0.53**	1.00												
Zn	0.15	0.16	0.26	0.30	0.10	0.28	-0.03	0.28	0.28	1.00											
As	-0.18	0.00	0.10	0.23	-0.17	-0.06	-0.05	0.15	0.08	0.17	1.00										
Rb	**0.68**	0.16	0.23	0.45	0.24	0.38	0.13	0.36	0.34	0.12	0.00	1.00									
Sr	0.45	0.46	0.19	**0.52**	0.18	0.34	-0.07	0.25	0.17	0.17	0.09	**0.60**	1.00								
Y	**0.79**	0.15	0.27	0.52	0.43	0.39	0.26	0.41	0.36	0.05	-0.06	**0.84**	**0.53**	1.00							
Zr	**0.72**	0.06	-0.03	0.17	0.19	0.20	0.10	0.05	0.04	-0.07	-0.31	**0.50**	0.40	**0.64**	1.00						
Nb	**0.69**	0.07	0.04	0.30	0.19	0.27	0.20	0.22	0.17	-0.18	-0.09	**0.69**	0.48	**0.83**	**0.71**	1.00					
Ba	0.46	**0.56**	0.41	**0.51**	**0.69**	0.40	0.25	0.49	0.25	0.05	-0.15	0.37	0.40	0.43	0.28	0.26	1.00				
W	0.28	-0.12	0.00	0.03	0.27	0.00	0.24	-0.03	0.00	-0.12	-0.14	0.00	-0.11	0.25	0.42	0.25	0.13	1.00			
Pb	-0.03	-0.06	-0.07	-0.02	-0.06	0.00	0.00	-0.02	-0.03	**0.55**	-0.02	-0.02	-0.02	-0.13	-0.06	-0.32	-0.06	-0.18	1.00		
Th	0.29	-0.12	-0.32	0.00	0.08	0.05	0.27	-0.13	-0.05	-0.39	-0.31	0.38	0.32	0.49	0.41	**0.64**	0.12	0.11	-0.34	1.00	
U	-0.05	-0.07	-0.14	0.14	-0.22	-0.08	-0.03	-0.11	-0.08	0.00	0.19	0.07	0.32	0.02	-0.01	0.06	-0.04	-0.23	0.07	0.20	1.00

Table A- 54: Correlation matrix of the elements on the Ghaap Group Dolomite.

	TiO_2	MnO	Fe_2O_3	Sc	V	Cr	Co	Ni	Cu	Zn	As	Rb	Sr	Y	Zr	Nb	Ba	W	Pb	Th	U
TiO_2	1.00																				
MnO	0.10	1.00																			
Fe_2O_3	0.26	0.29	1.00																		
Sc	0.15	0.40	**0.52**	1.00																	
V	0.11	0.43	**0.74**	0.47	1.00																
Cr	0.02	0.10	0.46	0.25	**0.55**	1.00															
Co	-0.21	-0.03	0.30	0.35	0.47	0.41	1.00														
Ni	0.06	0.14	**0.70**	0.40	**0.71**	**0.65**	**0.67**	1.00													
Cu	-0.03	0.20	**0.68**	0.41	**0.65**	0.41	0.47	**0.70**	1.00												
Zn	-0.11	0.23	0.04	0.14	0.01	-0.01	-0.07	-0.05	0.09	1.00											
As	-0.72	-0.09	-0.27	0.25	-0.19	-0.13	0.22	-0.11	-0.07	0.06	1.00										
Rb	0.32	0.05	**0.52**	0.13	0.38	0.28	0.09	**0.56**	0.49	-0.07	-0.39	1.00									
Sr	-0.23	0.28	-0.01	0.41	0.13	0.06	0.29	0.10	0.13	0.03	0.33	-0.09	1.00								
Y	**0.59**	0.05	**0.54**	0.26	0.37	0.23	0.10	0.48	0.43	-0.21	-0.47	**0.81**	-0.09	1.00							
Zr	**0.93**	0.01	0.04	0.03	-0.07	-0.10	-0.30	-0.13	-0.28	-0.15	-0.66	0.16	-0.22	0.44	1.00						
Nb	**0.84**	-0.10	0.10	0.06	-0.06	-0.02	-0.22	-0.02	-0.12	-0.39	-0.54	0.33	-0.24	**0.64**	**0.84**	1.00					
Ba	**0.53**	0.43	**0.56**	0.32	**0.58**	0.26	0.32	0.49	0.30	-0.06	-0.45	0.44	0.04	**0.54**	0.41	0.37	1.00				
W	0.24	0.01	0.08	-0.14	0.06	0.06	-0.13	0.06	0.01	-0.20	-0.17	0.07	-0.29	0.16	0.21	0.27	0.16	1.00			
Pb	-0.08	0.22	0.06	0.15	0.04	-0.01	-0.09	-0.02	0.03	**0.82**	0.03	-0.01	-0.01	-0.23	-0.12	-0.45	0.00	-0.20	1.00		
Th	0.15	-0.18	-0.20	0.18	-0.21	-0.08	-0.02	-0.15	-0.13	-0.38	0.18	-0.10	0.06	0.16	0.18	0.41	-0.11	0.01	-0.54	1.00	
U	-0.37	-0.36	-0.30	0.28	-0.48	0.00	0.26	-0.31	0.00	-0.27	0.27	-0.34	-0.02	-0.46	-0.48	-0.23	-0.17	-0.17	0.46	0.32	1.00

Table A- 55: Correlation matrix of the elements on the Asbestos Hill Subgroup.

	TiO_2	MnO	Fe_2O_3	Sc	V	Cr	Co	Ni	Cu	Zn	As	Rb	Sr	Y	Zr	Nb	Ba	W	Pb	Th
TiO_2	1.00																			
MnO	-0.12	1.00																		
Fe_2O_3	-0.13	0.40	1.00																	
Sc	0.07	**0.71**	0.48	1.00																
V	-0.03	0.44	0.03	**0.66**	1.00															
Cr	0.13	0.48	0.35	**0.81**	**0.71**	1.00														
Co	0.06	0.49	-0.11	**0.77**	**0.73**	**0.67**	1.00													
Ni	0.06	0.12	0.01	0.19	0.20	0.30	0.10	1.00												
Cu	0.06	-0.09	-0.13	-0.17	0.26	0.01	-0.20	0.26	1.00											
Zn	0.02	-0.04	0.00	-0.08	0.14	0.00	-0.09	0.01	0.34	1.00										
As	-0.50	-0.02	-0.16	-0.10	-0.10	-0.07	-0.11	0.20	0.06	-0.17	1.00									
Rb	0.30	0.03	-0.20	-0.07	0.25	0.04	-0.03	0.27	**0.63**	0.23	-0.17	1.00								
Sr	-0.12	0.05	0.02	-0.09	-0.10	-0.11	-0.17	0.08	0.41	0.10	0.19	0.42	1.00							
Y	0.33	-0.08	-0.13	-0.12	0.12	-0.04	-0.20	0.27	**0.62**	0.07	-0.03	**0.70**	0.34	1.00						
Zr	**0.90**	-0.24	-0.07	-0.12	-0.33	-0.10	-0.20	0.00	-0.04	-0.02	-0.39	0.16	-0.03	0.28	1.00					
Nb	**0.84**	-0.22	-0.15	-0.13	-0.21	-0.01	-0.19	0.13	0.17	-0.06	-0.22	0.44	0.11	**0.54**	**0.86**	1.00				
Ba	0.44	**0.50**	0.12	**0.66**	**0.66**	**0.61**	**0.62**	0.20	0.19	0.11	-0.37	0.45	0.16	0.34	0.18	0.25	1.00			
W	0.11	0.04	0.19	0.25	0.15	0.50	0.11	0.05	-0.04	0.00	0.16	-0.18	-0.22	-0.13	0.06	0.13	0.08	1.00		
Pb	-0.13	0.11	0.15	0.13	0.23	0.29	0.04	0.09	0.18	**0.62**	0.11	0.12	0.05	-0.01	-0.19	-0.09	0.10	0.36	1.00	
Th	0.21	-0.20	-0.25	-0.25	-0.13	-0.09	-0.25	0.21	0.38	-0.20	0.25	0.47	0.31	**0.64**	0.23	**0.56**	-0.02	0.06	-0.03	1.00

Table A- 56: Correlation matrix of the elements on the Pretoria quartzite Group.

	TiO_2	MnO	Fe_2O_3	Sc	V	Cr	Co	Ni	Cu	Zn	As	Rb	Sr	Y	Zr	Nb	Ba	W	Pb	Th	U
TiO_2	1.00																				
MnO	0.09	1.00																			
Fe_2O_3	**0.52**	0.54	1.00																		
Sc	0.39	**0.75**	**0.88**	1.00																	
V	0.43	**0.57**	**0.82**	**0.85**	1.00																
Cr	0.00	**0.59**	0.44	**0.62**	0.45	1.00															
Co	0.02	**0.81**	0.49	**0.73**	**0.54**	0.83	1.00														
Ni	-0.01	**0.69**	**0.52**	**0.72**	**0.52**	**0.93**	**0.91**	1.00													
Cu	0.26	**0.59**	0.45	**0.66**	**0.73**	0.28	0.49	0.39	1.00												
Zn	-0.10	**0.69**	0.26	0.43	0.27	0.33	0.49	0.43	0.40	1.00											
As	-0.22	-0.14	-0.17	-0.09	-0.09	-0.17	-0.19	-0.15	0.02	-0.01	1.00										
Rb	0.22	0.13	-0.11	0.00	-0.23	-0.21	0.01	-0.11	0.04	0.28	-0.06	1.00									
Sr	-0.11	0.39	0.05	0.15	-0.04	0.14	0.24	0.20	0.12	**0.53**	0.10	0.41	1.00								
Y	0.33	-0.03	-0.07	-0.03	0.02	-0.27	-0.12	-0.25	0.12	-0.07	-0.31	0.33	-0.05	1.00							
Zr	0.46	-0.33	-0.23	-0.27	-0.15	-0.23	-0.39	-0.36	-0.15	-0.25	-0.22	0.11	-0.15	**0.53**	1.00						
Nb	**0.63**	-0.18	-0.13	-0.16	-0.29	-0.17	-0.22	-0.23	-0.18	-0.23	-0.11	**0.52**	0.02	0.34	**0.51**	1.00					
Ba	0.48	0.36	0.29	0.33	0.14	0.03	0.23	0.13	0.23	0.40	-0.18	**0.72**	**0.52**	0.34	0.14	0.40	1.00				
W	0.29	-0.35	-0.06	-0.20	-0.12	-0.43	-0.44	-0.48	-0.22	-0.42	0.04	-0.04	-0.25	0.32	0.28	0.32	-0.06	1.00			
Pb	0.26	0.08	0.24	0.21	0.03	-0.08	0.17	0.20	0.17	0.20	0.17	0.31	-0.02	-0.05	-0.16	-0.02	0.20	-0.20	1.00		
Th	-0.08	-0.24	-0.42	-0.42	-0.48	-0.24	-0.27	-0.27	-0.31	-0.19	-0.46	0.31	0.08	0.45	0.21	0.46	0.13	0.28	-0.61	1.00	
U	0.25	-0.31	-0.17	-0.20	-0.27	-0.29	-0.24	-0.25	-0.24	-0.26	-0.28	0.14	-0.05	**0.62**	**0.52**	**0.60**	-0.11	0.45	1.00	**0.75**	1.00

Table A- 57: Correlation matrix of the elements on the Pretoria Shale and slate Group.

	TiO_2	MnO	Fe_2O_3	Sc	V	Cr	Co	Ni	Cu	Zn	As	Rb	Sr	Y	Zr	Nb	Ba	W	Pb	Th	U
TiO_2	1.00																				
MnO	0.15	1.00																			
Fe_2O_3	0.04	0.22	1.00																		
Sc	0.33	**0.62**	**0.51**	1.00																	
V	0.22	**0.52**	**0.62**	**0.87**	1.00																
Cr	0.00	0.24	**0.51**	**0.57**	**0.51**	1.00															
Co	0.39	**0.61**	-0.04	**0.80**	**0.61**	**0.53**	1.00														
Ni	-0.11	0.28	**0.54**	0.47	0.40	**0.70**	0.21	1.00													
Cu	0.15	0.25	**0.50**	0.46	0.55	0.27	0.16	0.39	1.00												
Zn	0.01	0.16	0.29	0.19	0.19	0.16	0.04	0.21	0.20	1.00											
As	-0.08	-0.04	0.01	0.01	0.14	0.05	-0.02	-0.11	0.00	-0.08	1.00										
Rb	0.03	-0.35	-0.18	-0.30	-0.29	-0.23	-0.21	-0.27	-0.25	0.17	-0.09	1.00									
Sr	-0.25	-0.14	-0.23	-0.14	-0.04	-0.13	-0.08	-0.04	-0.05	-0.04	0.15	-0.04	1.00								
Y	0.30	-0.23	-0.05	-0.05	-0.05	-0.12	-0.09	-0.18	0.22	-0.01	-0.07	0.37	-0.16	1.00							
Zr	0.34	-0.24	-0.47	-0.38	-0.47	-0.32	-0.17	-0.36	-0.30	-0.30	-0.15	-0.06	0.13	0.21	1.00						
Nb	**0.63**	-0.18	-0.29	-0.18	-0.42	-0.24	-0.06	-0.24	-0.11	-0.14	-0.30	0.22	-0.20	**0.50**	**0.57**	1.00					
Ba	0.25	0.18	-0.08	0.25	0.23	-0.02	0.34	-0.09	0.04	0.22	0.03	0.48	0.22	0.33	-0.07	0.07	1.00				
W	0.20	-0.34	-0.25	-0.45	-0.30	-0.24	-0.31	-0.47	-0.25	-0.22	0.32	0.07	-0.18	0.32	0.31	0.23	-0.14	1.00			
Pb	0.24	-0.07	0.02	-0.02	-0.02	-0.15	-0.06	-0.08	0.01	0.10	-0.09	0.47	0.16	0.14	0.10	0.18	**0.53**	-0.10	1.00		
Th	-0.03	-0.31	-0.20	-0.18	-0.21	-0.12	-0.15	-0.14	-0.06	-0.08	-0.30	0.41	0.00	**0.57**	-0.01	0.41	0.21	0.19	-0.05	1.00	
U	0.24	-0.45	-0.06	0.02	-0.29	0.08	-0.23	-0.21	-0.01	-0.28	0.41	0.36	0.00	0.61	0.02	0.43	0.54	0.42	0.45	**0.63**	1.00

Table A- 58: Correlation matrix of the elements on the Hekpoort Formation.

	TiO_2	MnO	Fe_2O_3	Sc	V	Cr	Co	Ni	Cu	Zn	As	Rb	Sr	Y	Zr	Nb	Ba	W	Pb	Th
TiO_2	1.00																			
MnO	0.09	1.00																		
Fe_2O_3	**0.64**	0.45	1.00																	
Sc	0.28	**0.64**	**0.79**	1.00																
V	-0.11	0.34	**0.53**	**0.75**	1.00															
Cr	0.14	0.44	0.34	0.39	0.17	1.00														
Co	-0.35	**0.76**	0.02	0.43	0.31	**0.53**	1.00													
Ni	-0.04	0.60	0.36	**0.57**	0.39	**0.91**	**0.74**	1.00												
Cu	-0.13	0.42	0.33	**0.59**	**0.55**	-0.03	0.35	0.21	1.00											
Zn	-0.13	0.49	0.26	0.34	0.18	0.28	0.29	0.37	0.40	1.00										
As	-0.45	-0.21	-0.33	-0.08	0.26	-0.16	0.14	-0.05	0.06	-0.15	1.00									
Rb	-0.52	0.29	-0.20	0.16	0.23	-0.22	0.46	0.00	0.47	0.21	0.34	1.00								
Sr	-0.20	-0.08	-0.15	-0.16	-0.03	0.07	-0.02	0.06	0.06	0.28	0.00	-0.03	1.00							
Y	0.07	0.24	0.11	0.36	0.28	-0.12	0.23	-0.01	0.36	-0.01	0.04	**0.59**	-0.17	1.00						
Zr	0.41	-0.24	-0.04	-0.14	-0.23	-0.22	-0.34	-0.37	-0.22	-0.31	-0.14	-0.13	-0.20	0.41	1.00					
Nb	**0.77**	0.05	0.24	0.08	-0.32	0.04	-0.23	-0.11	-0.17	-0.20	-0.55	-0.36	-0.21	0.30	**0.55**	1.00				
Ba	0.30	0.39	0.53	0.49	0.35	0.10	0.14	0.15	0.44	0.34	0.02	0.34	0.22	0.42	0.04	0.06	1.00			
W	0.43	-0.41	-0.05	-0.36	-0.37	-0.38	-0.57	-0.57	-0.30	-0.46	0.05	-0.28	-0.19	-0.02	0.48	0.36	-0.05	1.00		
Pb	-0.25	0.39	0.09	0.37	0.36	-0.07	0.40	0.13	0.45	0.08	-0.06	0.46	-0.09	0.35	-0.32	-0.11	0.07	-0.31	1.00	
Th	-0.24	0.21	-0.24	0.00	-0.09	0.01	0.30	0.10	0.09	0.00	-0.38	0.31	-0.04	0.34	-0.14	0.26	-0.18	-0.25	**0.50**	1.00

Table A- 59: Correlation matrix of the elements on the Calcrete and surface limestone.

	TiO_2	MnO	Fe_2O_3	Sc	V	Cr	Co	Ni	Cu	Zn	As	Rb	Sr	Y	Zr	Nb	Ba	W	Pb	Th	U
TiO_2	1.00																				
MnO	0.13	1.00																			
Fe_2O_3	0.14	0.16	1.00																		
Sc	-0.05	0.16	0.37	1.00																	
V	-0.02	0.18	**0.82**	0.35	1.00																
Cr	0.04	0.23	**0.60**	0.20	**0.59**	1.00															
Co	-0.18	0.06	**0.62**	0.47	**0.66**	0.35	1.00														
Ni	-0.13	0.05	**0.76**	0.29	**0.65**	**0.65**	**0.65**	1.00													
Cu	-0.10	0.14	**0.87**	0.29	**0.77**	**0.55**	**0.70**	**0.78**	1.00												
Zn	-0.06	0.18	0.33	0.18	0.23	0.26	0.21	0.25	0.36	1.00											
As	-0.69	-0.15	-0.20	0.42	-0.10	-0.22	0.15	0.01	-0.05	0.00	1.00										
Rb	0.27	0.25	**0.61**	0.07	0.33	0.43	0.13	0.44	0.47	0.25	-0.31	1.00									
Sr	-0.22	-0.06	-0.05	0.27	0.12	-0.07	0.25	0.08	0.09	0.06	0.32	-0.23	1.00								
Y	**0.61**	0.19	**0.58**	0.09	0.34	0.30	0.21	0.34	0.41	0.15	-0.51	**0.75**	-0.23	1.00							
Zr	**0.90**	0.04	-0.12	-0.15	-0.24	-0.09	-0.35	-0.27	-0.33	-0.16	-0.65	0.12	-0.22	0.46	1.00						
Nb	**0.93**	0.04	0.05	-0.09	-0.16	-0.05	-0.27	-0.17	-0.19	-0.12	-0.61	0.32	-0.28	**0.65**	**0.91**	1.00					
Ba	**0.54**	**0.57**	0.41	0.11	0.34	0.27	0.20	0.16	0.29	0.17	-0.46	**0.51**	-0.04	**0.63**	0.37	0.46	1.00				
W	0.27	-0.13	-0.02	-0.43	0.01	-0.01	-0.17	-0.09	-0.08	-0.16	-0.38	-0.01	-0.35	0.21	0.35	0.30	0.06	1.00			
Pb	-0.21	0.33	0.10	**0.54**	0.06	0.05	0.22	0.10	0.11	0.43	0.36	0.14	0.14	0.04	-0.28	-0.21	0.11	-0.34	1.00		
Th	0.16	-0.16	-0.17	0.43	-0.28	-0.26	-0.06	-0.19	-0.25	-0.20	0.26	-0.08	0.04	0.14	0.19	0.32	-0.08	-0.17	0.22	1.00	
U	-0.33	-0.10	-0.18	0.39	-0.07	-0.16	0.11	-0.04	-0.12	-0.09	0.47	-0.24	**0.53**	-0.33	-0.26	-0.31	-0.24	-0.38	0.23	0.30	1.00

Table A- 60: Correlation matrix of the elements on the undifferentiated aeolian sand.

	TiO_2	MnO	Fe_2O_3	Sc	V	Cr	Co	Ni	Cu	Zn	As	Rb	Sr	Y	Zr	Nb	Ba	W	Pb	Th	U
TiO_2	1.00																				
MnO	0.08	1.00																			
Fe_2O_3	0.01	0.45	1.00																		
Sc	0.11	0.42	**0.70**	1.00																	
V	-0.06	0.40	**0.83**	**0.63**	1.00																
Cr	-0.20	0.16	**0.50**	0.34	0.43	1.00															
Co	-0.13	0.29	**0.61**	**0.54**	**0.63**	**0.71**	1.00														
Ni	-0.19	0.21	**0.59**	0.44	**0.52**	**0.87**	**0.81**	1.00													
Cu	-0.05	0.33	**0.78**	**0.57**	**0.80**	0.37	**0.66**	**0.55**	1.00												
Zn	0.01	0.37	0.31	0.31	0.30	0.08	0.18	0.15	0.34	1.00											
As	-0.45	0.08	0.04	0.30	0.07	0.03	0.04	0.06	0.09	0.07	1.00										
Rb	0.03	-0.01	0.13	-0.03	0.08	-0.08	-0.06	-0.02	0.13	0.13	-0.13	1.00									
Sr	-0.03	-0.04	-0.08	0.13	0.02	-0.17	0.02	-0.07	0.08	0.11	0.03	-0.03	1.00								
Y	0.30	0.16	0.22	0.09	0.17	-0.03	0.08	0.02	0.23	0.11	-0.24	**0.57**	-0.21	1.00							
Zr	**0.73**	-0.14	-0.43	-0.25	-0.47	-0.33	-0.41	-0.38	-0.48	-0.18	-0.47	-0.02	-0.04	0.19	1.00						
Nb	**0.70**	-0.04	-0.21	-0.08	-0.30	-0.23	-0.26	-0.25	-0.25	-0.10	-0.41	0.23	-0.07	**0.55**	**0.70**	1.00					
Ba	0.29	0.14	0.08	0.04	0.08	-0.14	0.00	-0.08	0.08	0.13	-0.29	0.49	0.40	0.18	0.17	0.15	1.00				
W	0.28	-0.16	-0.27	-0.29	-0.20	-0.23	-0.25	-0.28	-0.31	-0.17	-0.26	-0.06	-0.18	-0.01	0.41	0.19	0.04	1.00			
Pb	-0.11	0.05	-0.07	0.07	-0.03	-0.07	-0.01	-0.07	-0.05	0.35	0.03	0.20	0.15	-0.01	-0.07	-0.15	0.24	-0.05	1.00		
Th	0.08	-0.16	-0.22	-0.03	-0.25	-0.08	-0.13	-0.12	-0.20	-0.24	-0.13	0.25	-0.04	0.34	0.17	0.45	0.02	-0.12	-0.03	1.00	
U	-0.19	-0.14	-0.17	0.00	-0.15	-0.07	-0.09	-0.07	-0.12	-0.11	0.12	0.02	0.30	-0.02	0.02	0.05	-0.05	-0.25	0.05	0.27	1.00

Table A- 61: Correlation matrix of the elements on the Gordonia Formation.

	TiO_2	MnO	Fe_2O_3	Sc	V	Cr	Co	Ni	Cu	Zn	As	Rb	Sr	Y	Zr	Nb	Ba	W	Pb	Th	U
TiO_2	1.00																				
MnO	0.11	1.00																			
Fe_2O_3	0.05	0.39	1.00																		
Sc	0.32	0.32	**0.77**	1.00																	
V	-0.21	0.22	**0.81**	**0.61**	1.00																
Cr	-0.02	0.19	**0.63**	**0.52**	**0.65**	1.00															
Co	-0.24	0.05	**0.56**	0.45	**0.67**	**0.55**	1.00														
Ni	-0.15	0.16	**0.69**	**0.53**	**0.68**	**0.80**	**0.76**	1.00													
Cu	-0.16	0.21	**0.77**	**0.58**	**0.79**	**0.58**	**0.72**	**0.72**	1.00												
Zn	-0.01	0.27	0.44	0.35	0.37	0.37	0.37	0.40	0.47	1.00											
As	-0.57	0.03	0.08	0.06	0.15	0.02	0.18	0.13	0.15	0.11	1.00										
Rb	0.10	0.24	0.39	0.35	0.25	0.24	0.13	0.22	0.24	0.20	-0.04	1.00									
Sr	-0.17	0.07	0.36	0.31	0.36	0.32	0.48	0.42	0.45	0.39	0.11	0.12	1.00								
Y	**0.50**	-0.01	0.16	0.38	0.11	0.08	0.01	0.04	0.05	-0.14	-0.38	0.41	-0.16	1.00							
Zr	**0.85**	-0.09	-0.30	0.06	-0.44	-0.24	-0.42	-0.38	-0.43	-0.25	-0.62	-0.03	-0.32	**0.54**	1.00						
Nb	**0.89**	0.00	-0.18	0.17	-0.39	-0.20	-0.40	-0.32	-0.36	-0.21	-0.54	0.14	-0.34	**0.62**	**0.91**	1.00					
Ba	0.35	0.42	**0.53**	0.49	0.31	0.32	0.30	0.32	0.36	0.38	-0.16	**0.62**	0.45	0.25	0.07	0.18	1.00				
W	-0.03	-0.30	-0.24	-0.22	-0.13	-0.15	-0.13	-0.15	-0.21	-0.27	-0.09	-0.10	-0.23	0.14	0.17	0.07	-0.20	1.00			
Pb	-0.14	0.28	0.20	0.22	0.17	0.15	0.19	0.20	0.21	0.43	0.17	0.43	0.21	0.03	-0.21	-0.16	0.31	-0.14	1.00		
Th	0.42	-0.17	-0.24	0.11	-0.30	-0.18	-0.21	-0.23	-0.28	-0.24	-0.14	0.16	-0.22	**0.51**	**0.51**	**0.62**	0.03	-0.02	0.03	1.00	
U	-0.06	-0.08	-0.13	0.00	-0.06	-0.04	0.04	-0.02	-0.05	-0.04	0.06	-0.12	0.02	0.03	0.07	0.01	-0.11	-0.15	0.08	0.27	1.00

APPENDIX 3: HISTOGRAMS AND BOX BLOTS OF LITHOLOGICAL GROUPS

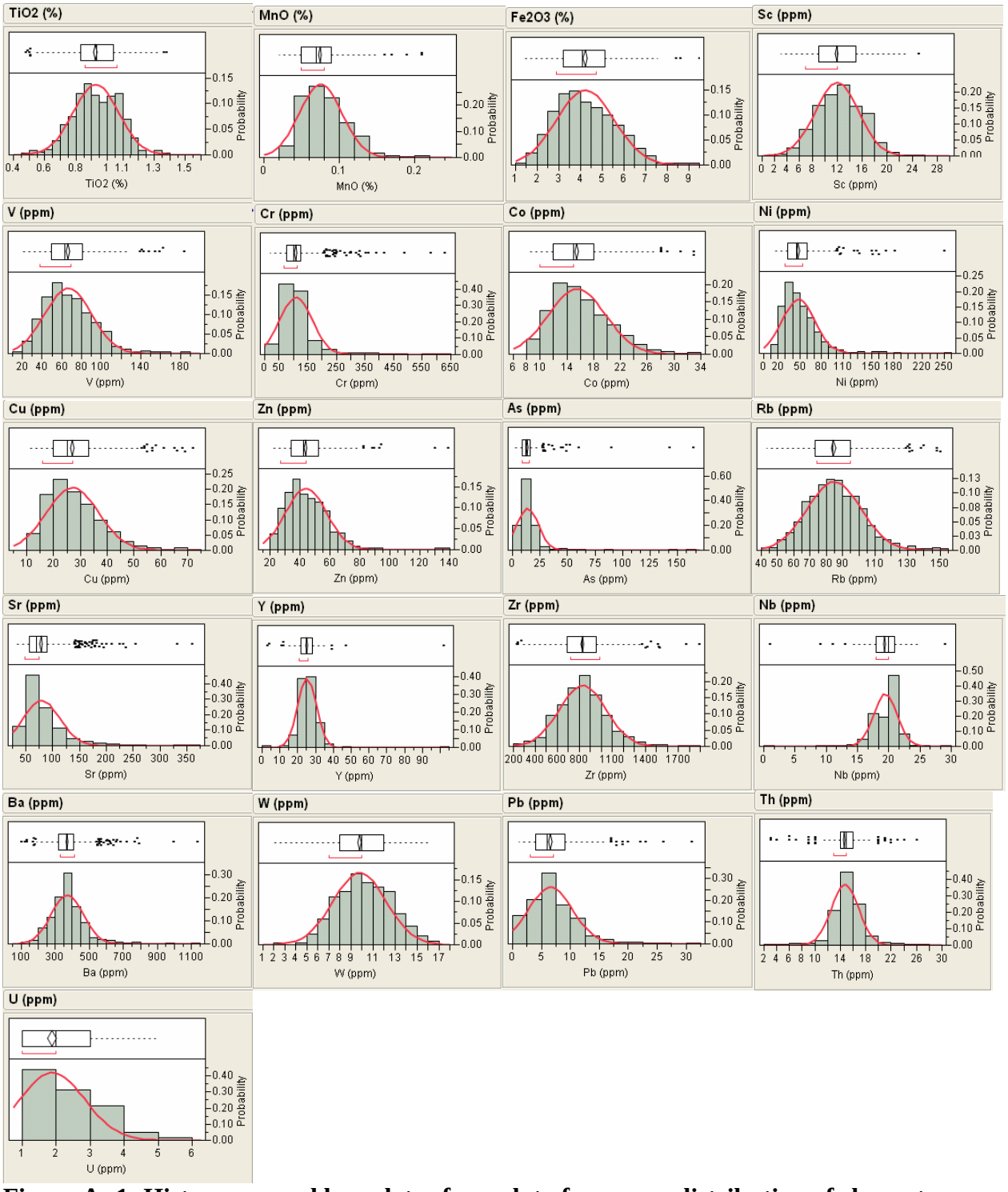

Figure A- 1: Histograms and box plots of raw data frequency distribution of elements in Amphibolites basement complex.

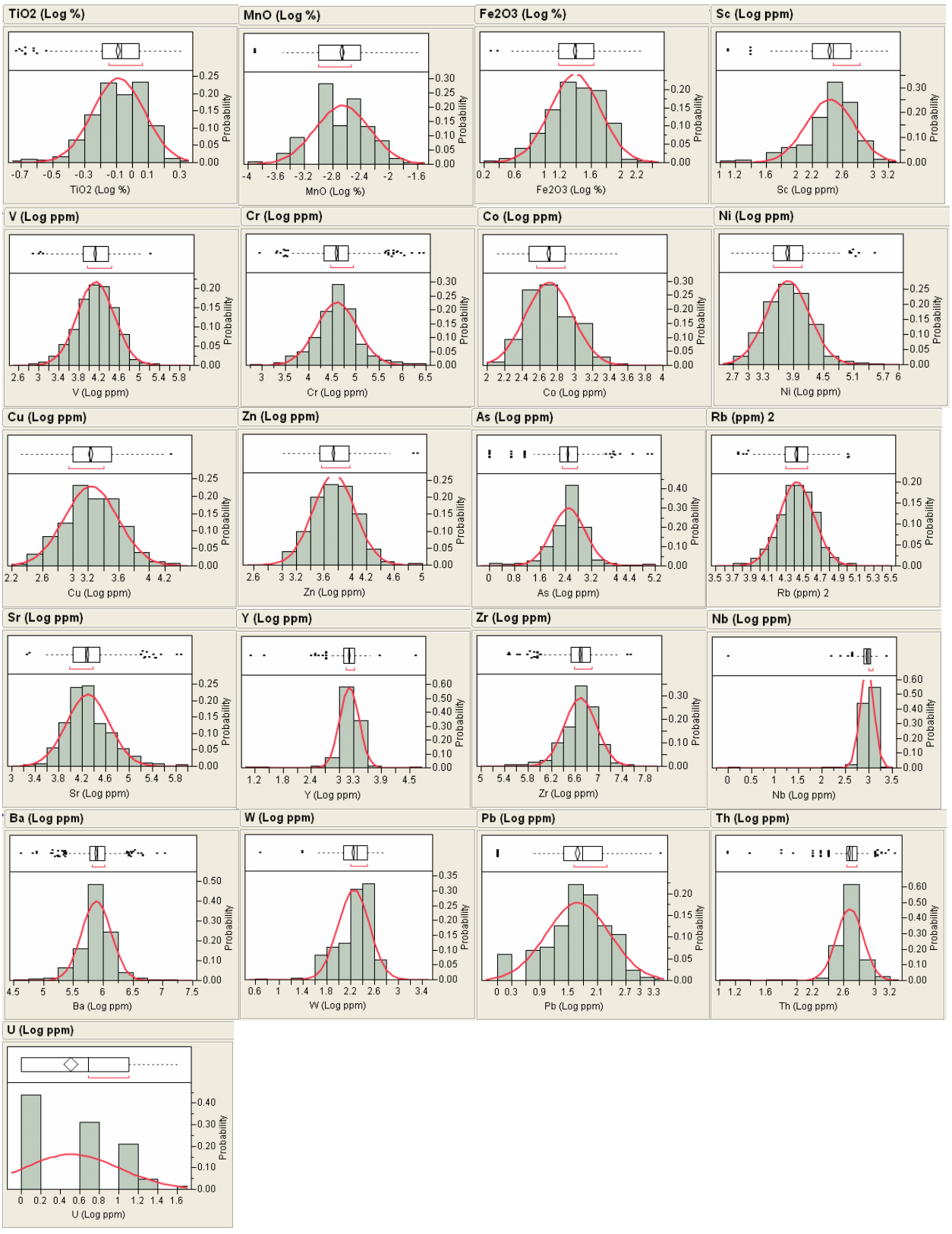

Figure A- 2: Histograms and box plots of log-normal frequency distribution of elements in Amphibolites basement complex.

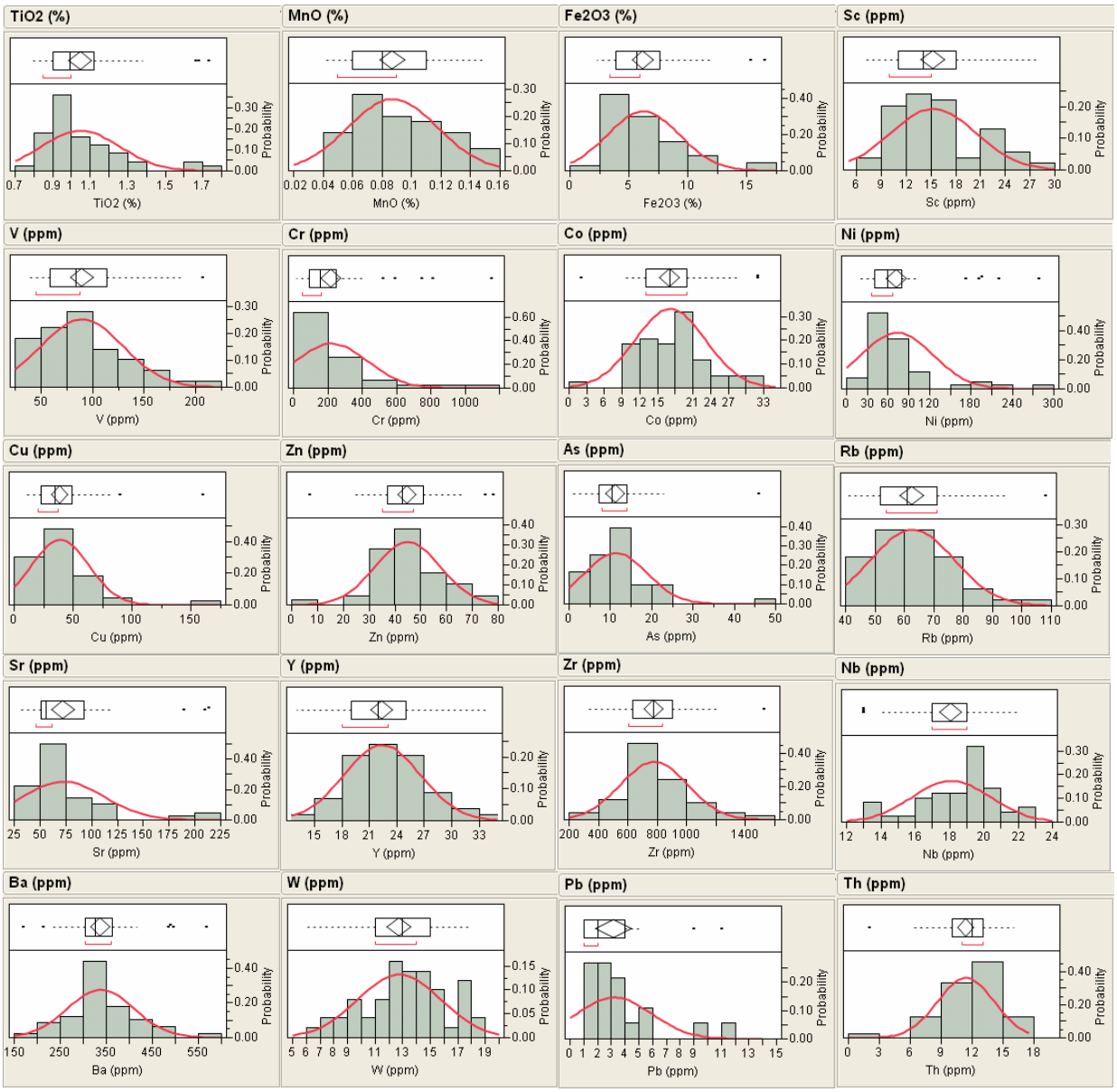

Figure A- 3: Histograms and box plots of raw data frequency distribution of elements in Kraaipan Group.

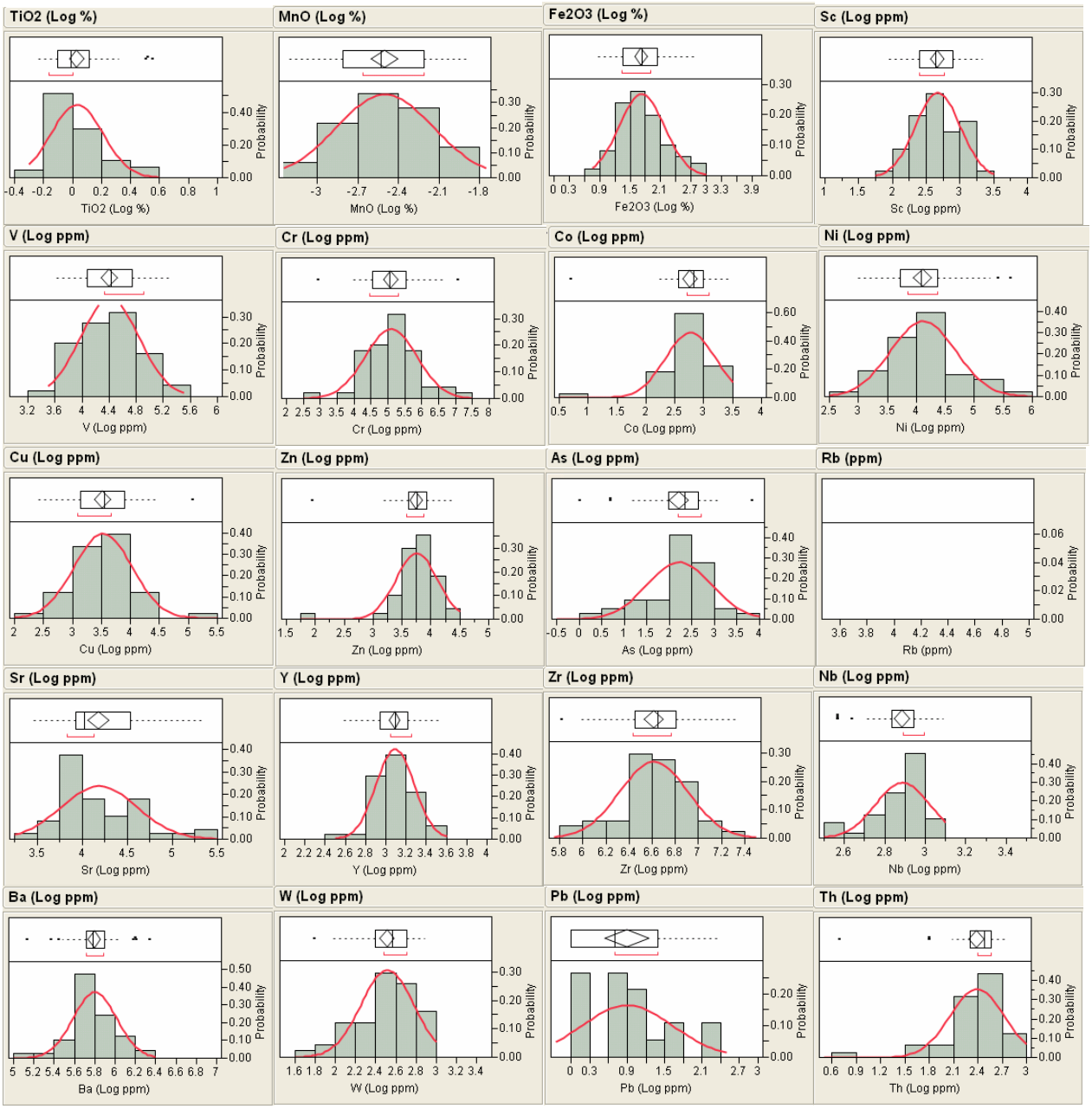

Figure A- 4: Histograms and box plots of log-normal frequency distribution of elements in Kraaipan Group.

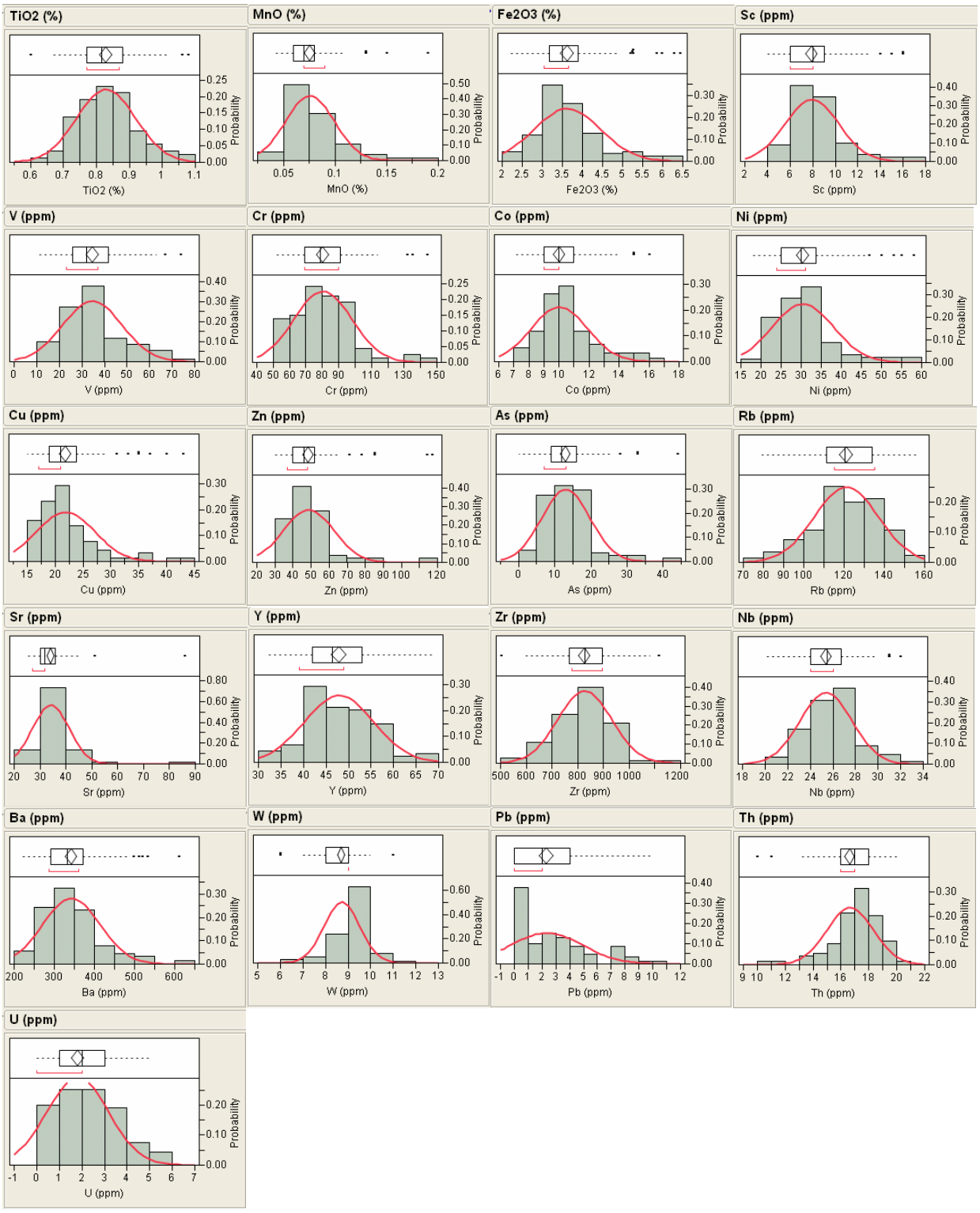

Figure A- 5: Histograms and box plots of raw data frequency distribution of elements in Kanye Formation.

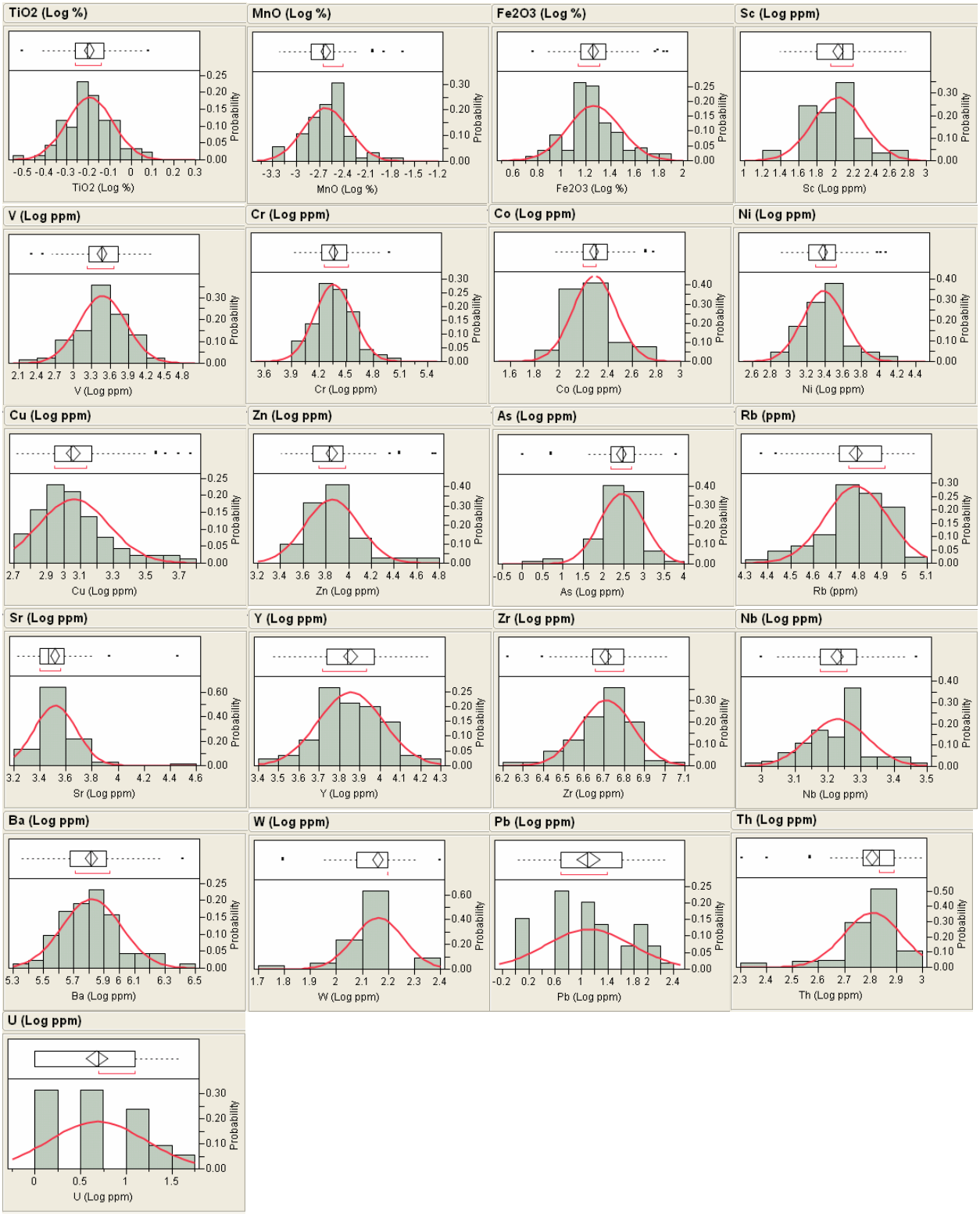

Figure A- 6: Histograms and box plots of log-normal frequency distribution of elements in Kanye Formation.

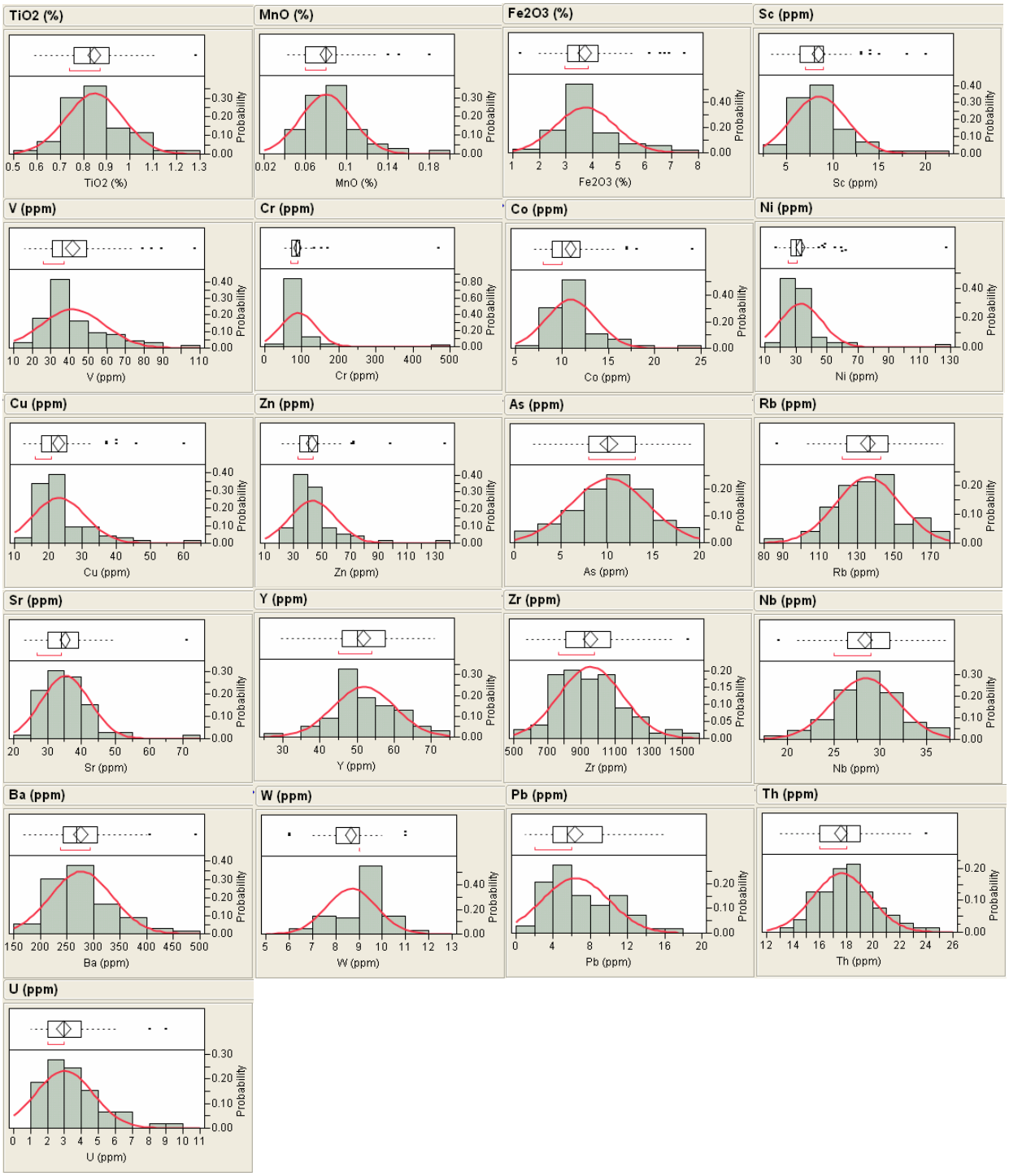

Figure A- 7: Histograms and box plots of raw data frequency distribution of elements in Gaborone Granite.

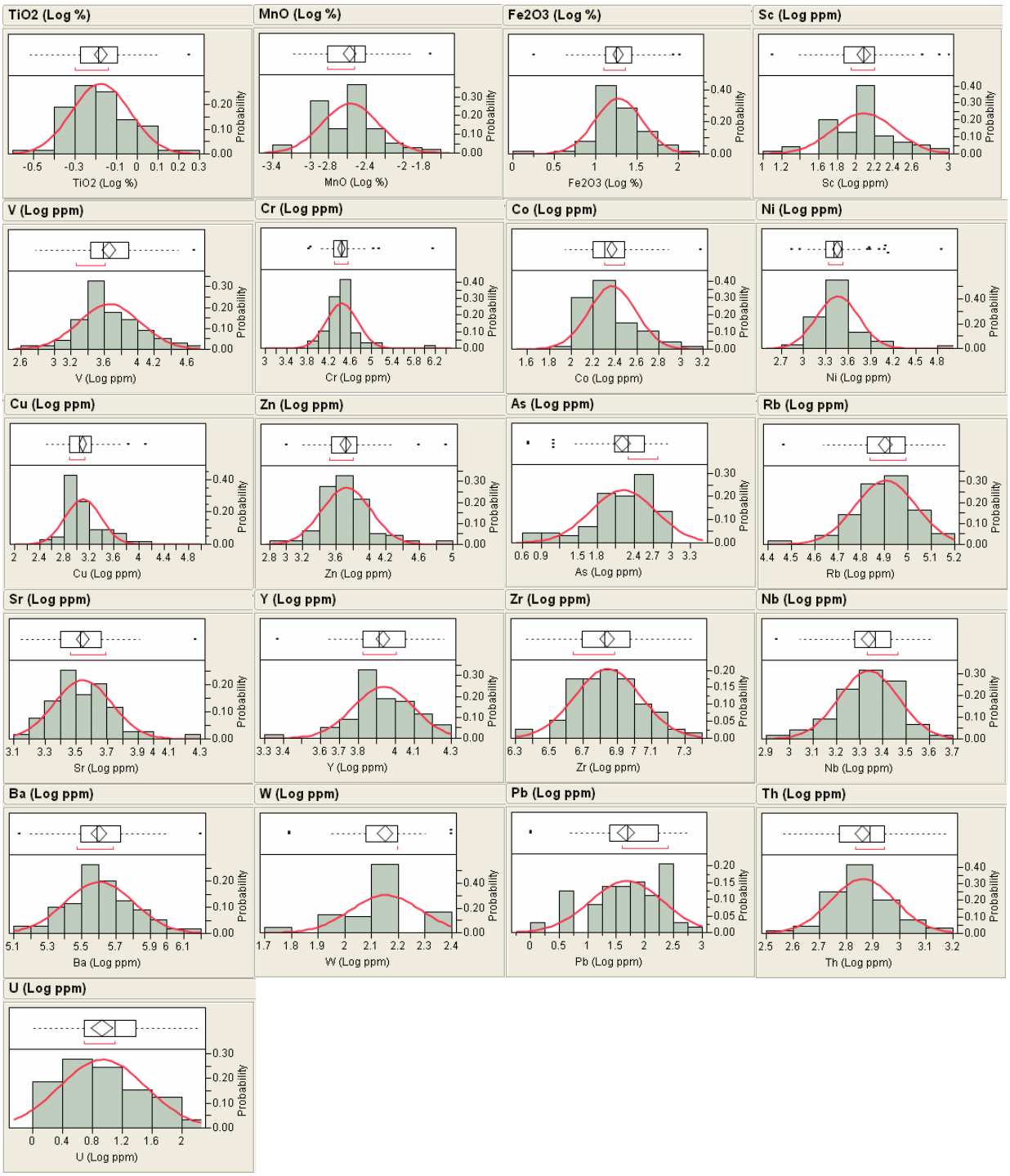

Figure A- 8: Histograms and box plots of log-normal frequency distribution of elements in Gaborone Granite.

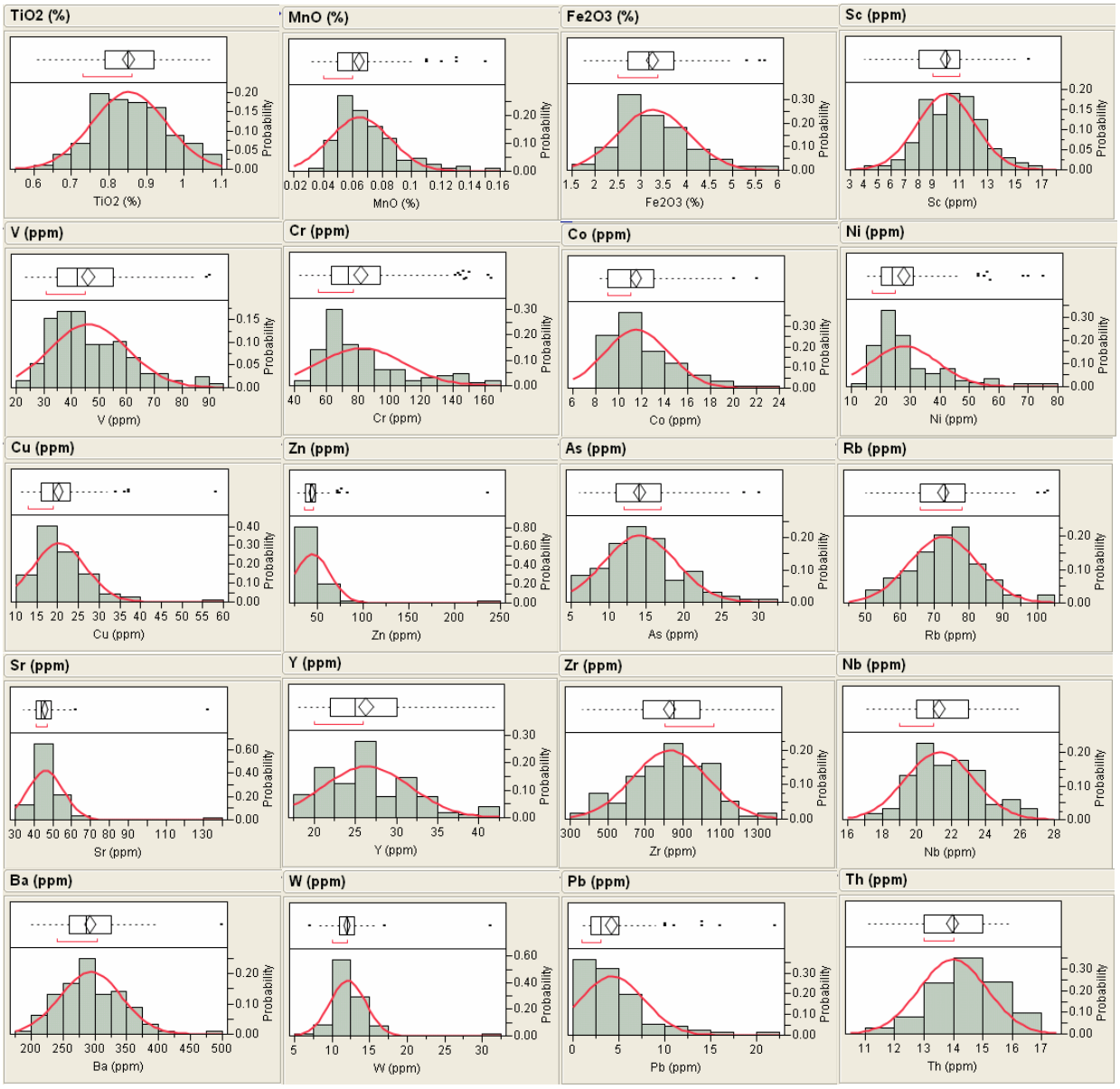

Figure A- 9: Histograms and box plots of raw data frequency distribution of elements in Dominion Group.

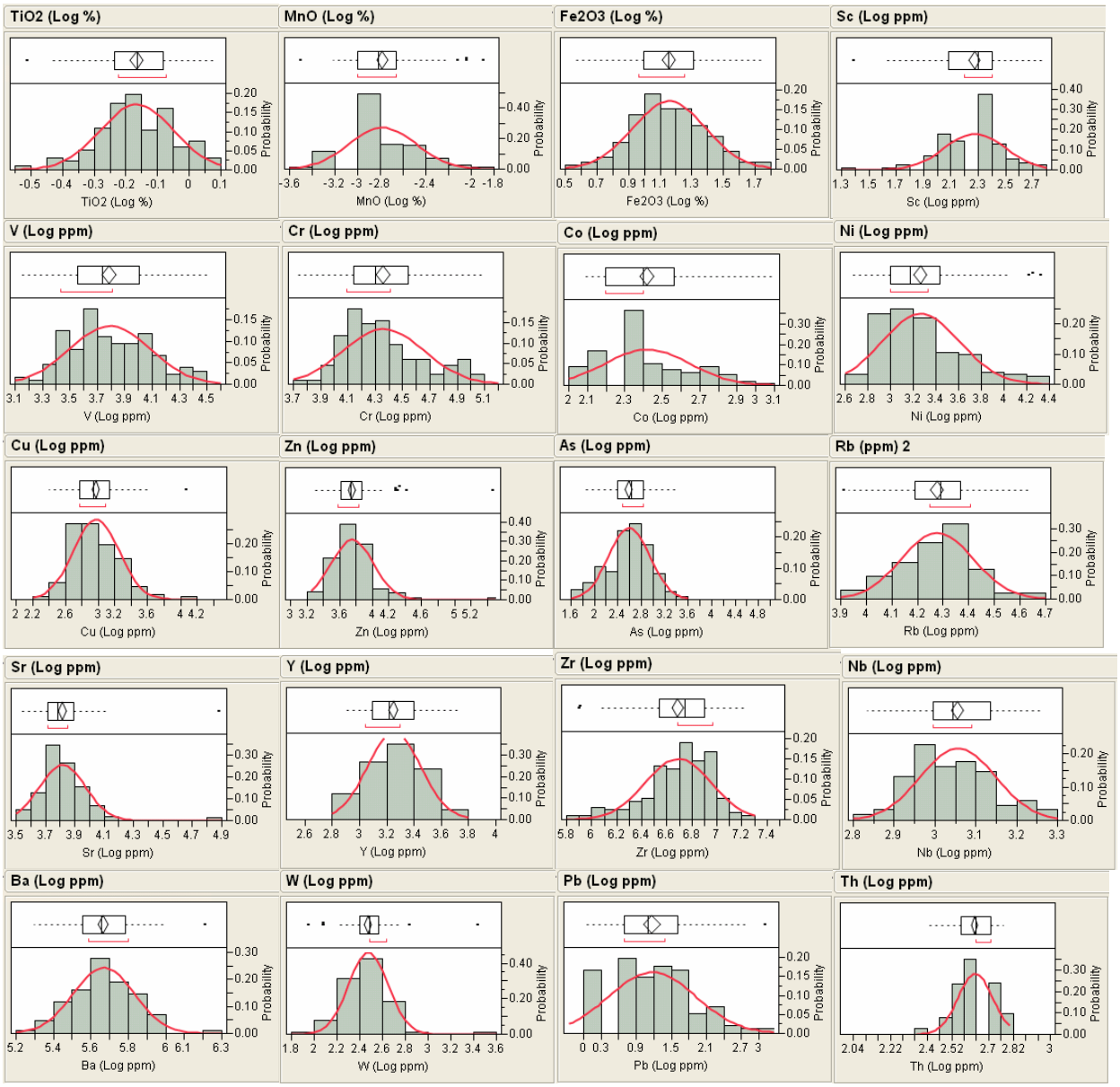

Figure A- 10: Histograms and box plots of log-normal frequency distribution of elements in Dominion Group.

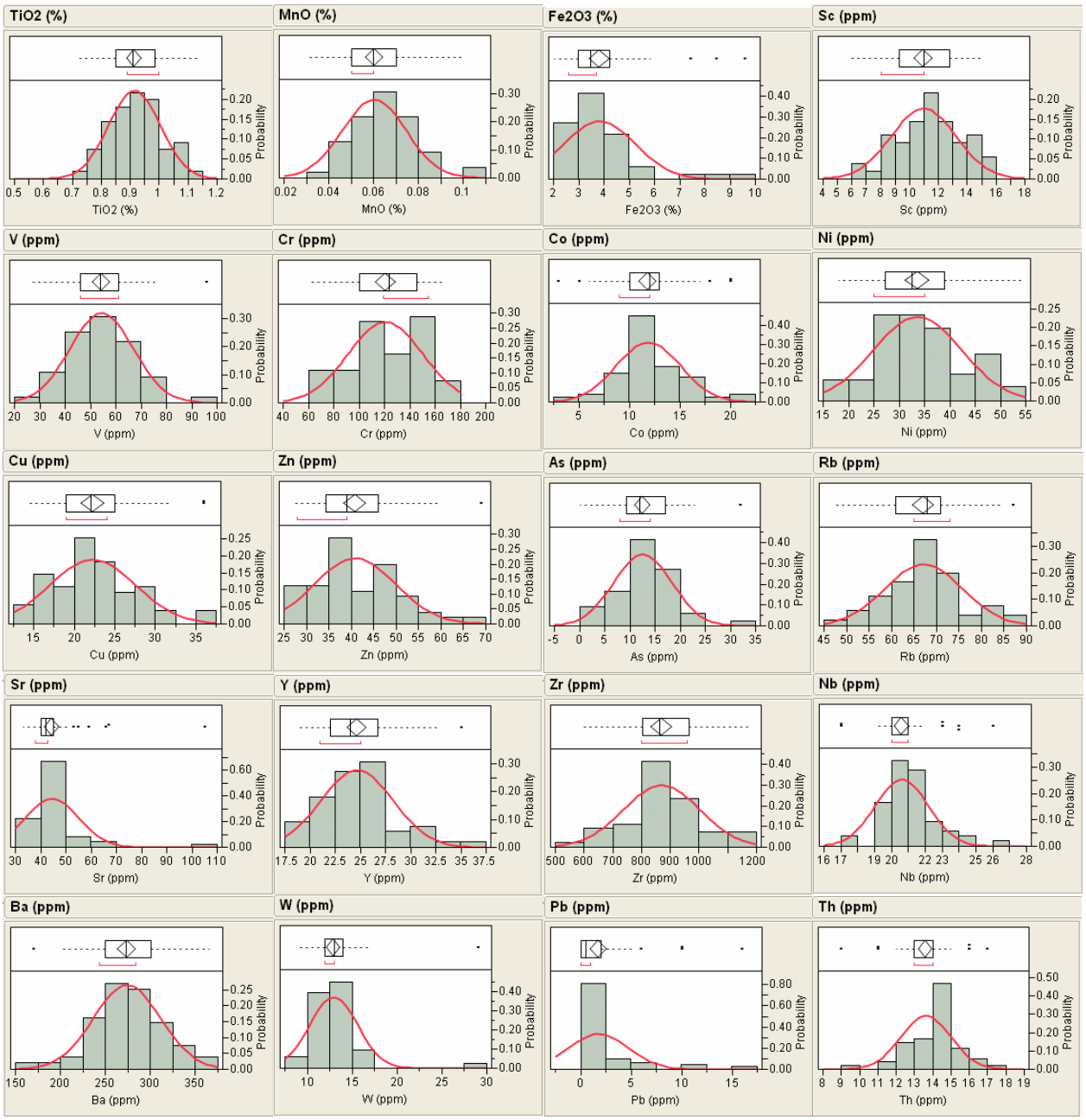

Figure A- 11: Histograms and box plots of raw data frequency distribution of elements in Hospital Hill Subgroup.

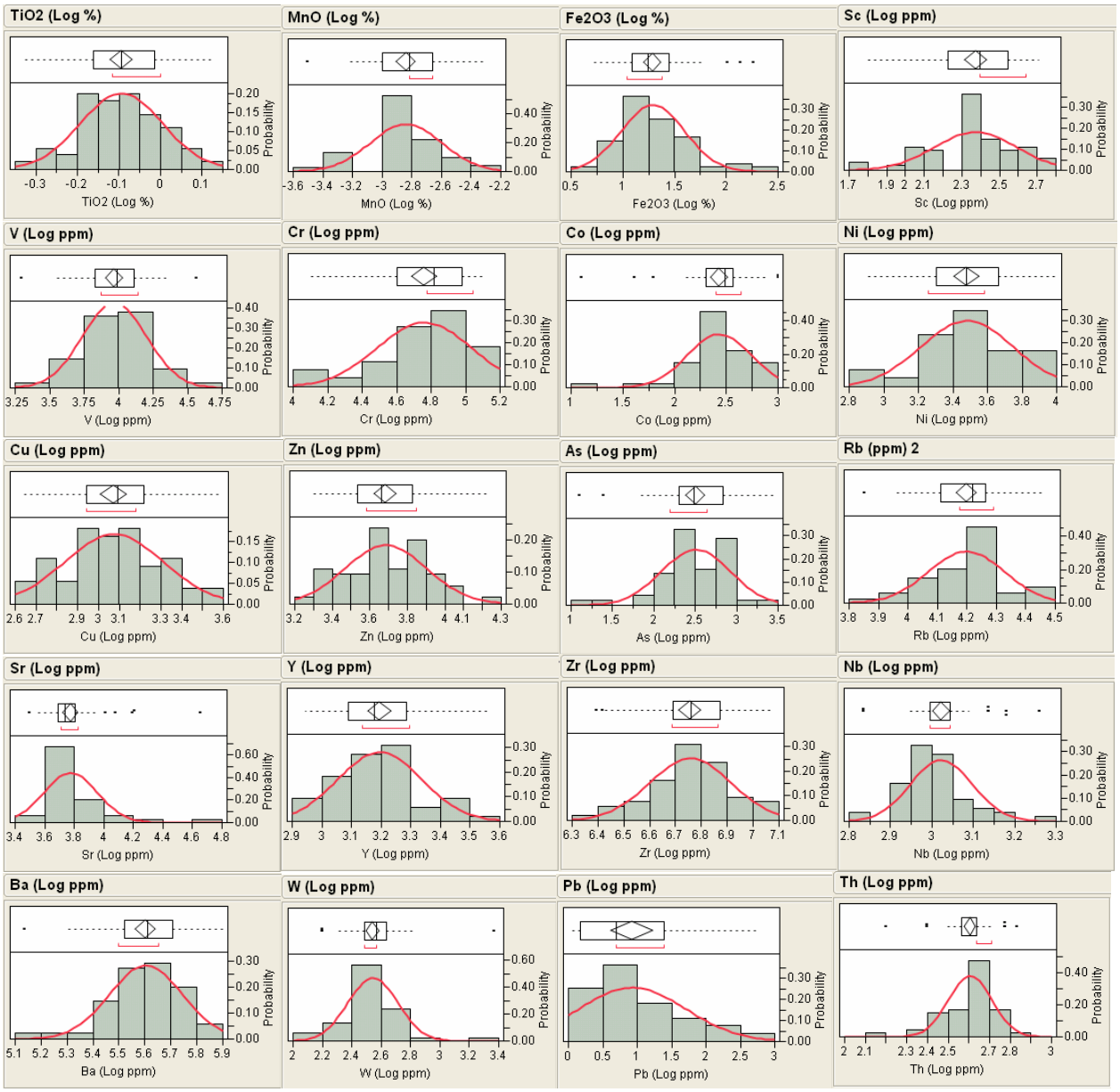

Figure A- 12: Histograms and box plots of log-normal frequency distribution of elements in Hospital Hill Subgroup.

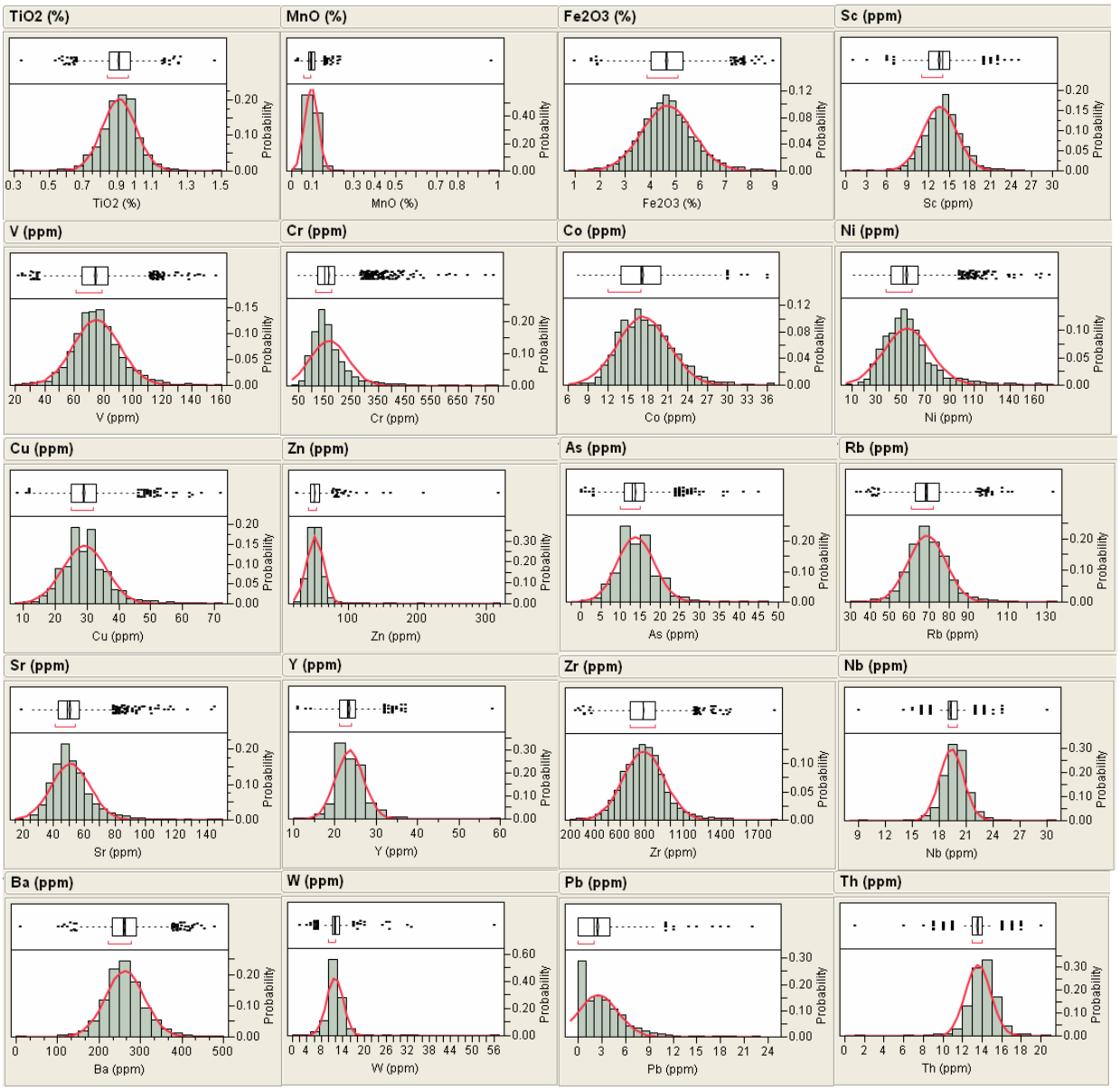

Figure A- 13: Histograms and box plots of raw data frequency distribution of elements in Klipriviersberg Group.

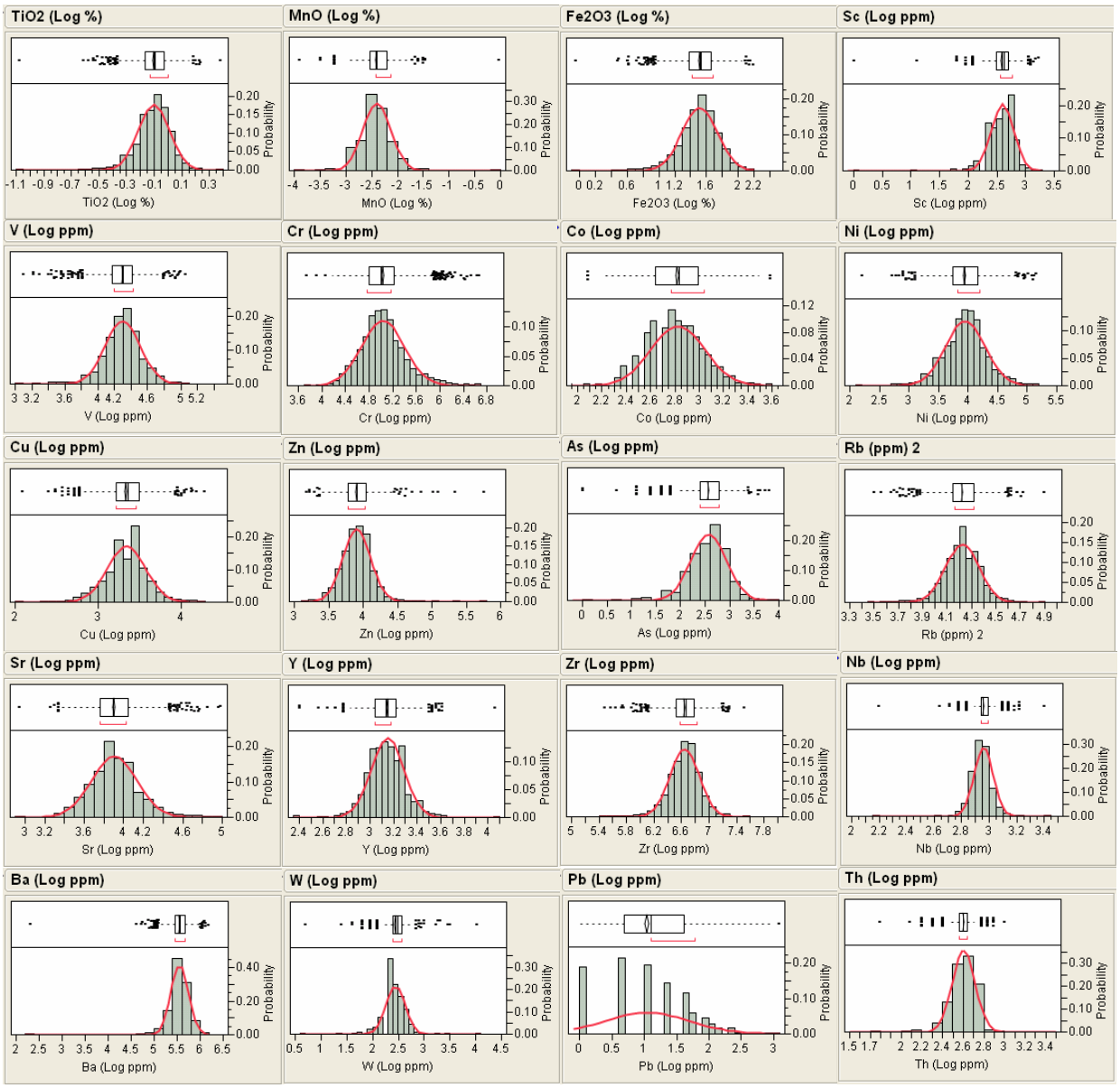

Figure A- 14: Histograms and box plots of log-normal frequency distribution of elements in Klipriviersberg Group.

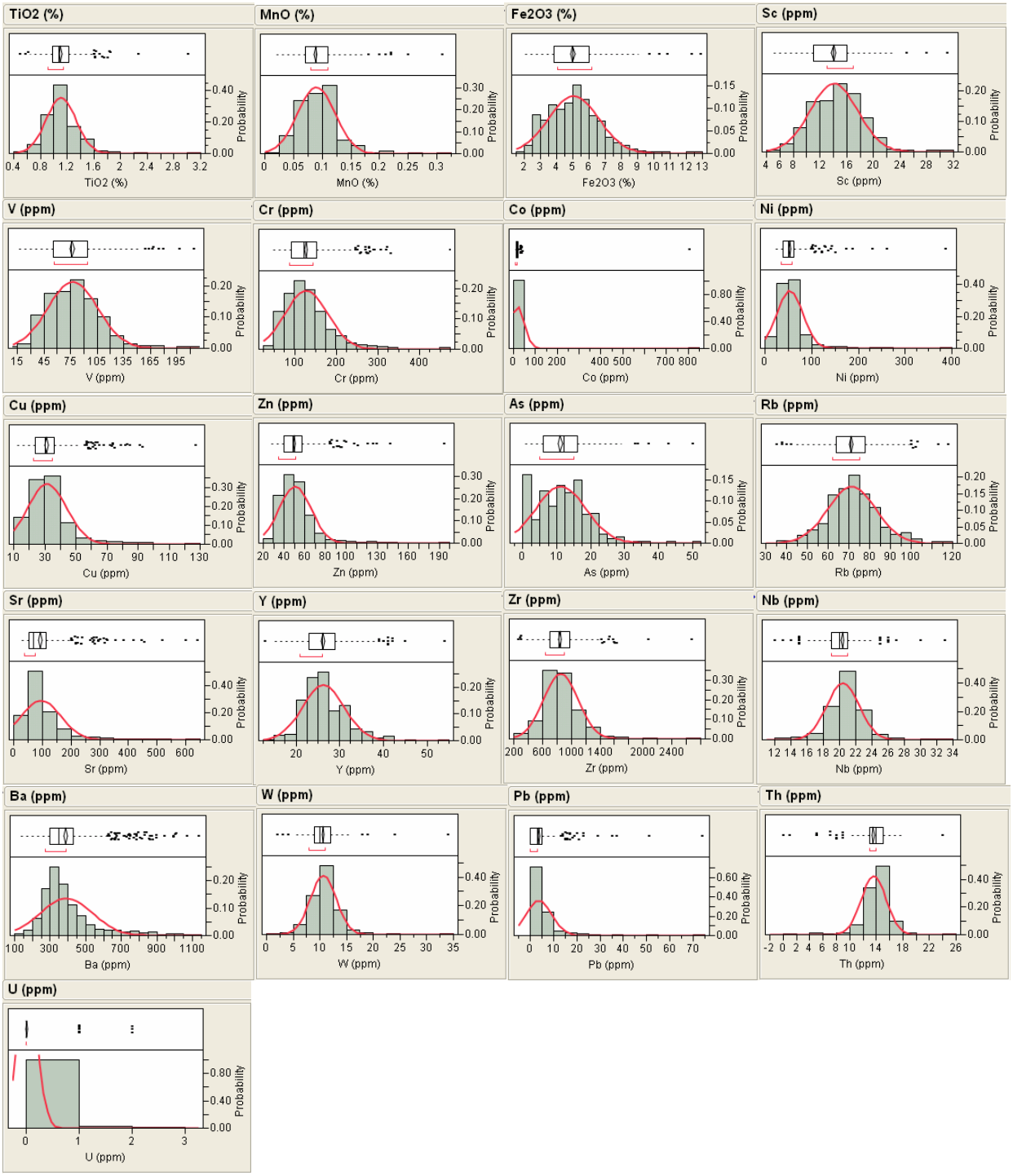

Figure A- 15: Histograms and box plots of raw data frequency distribution of elements in Platberg Group.

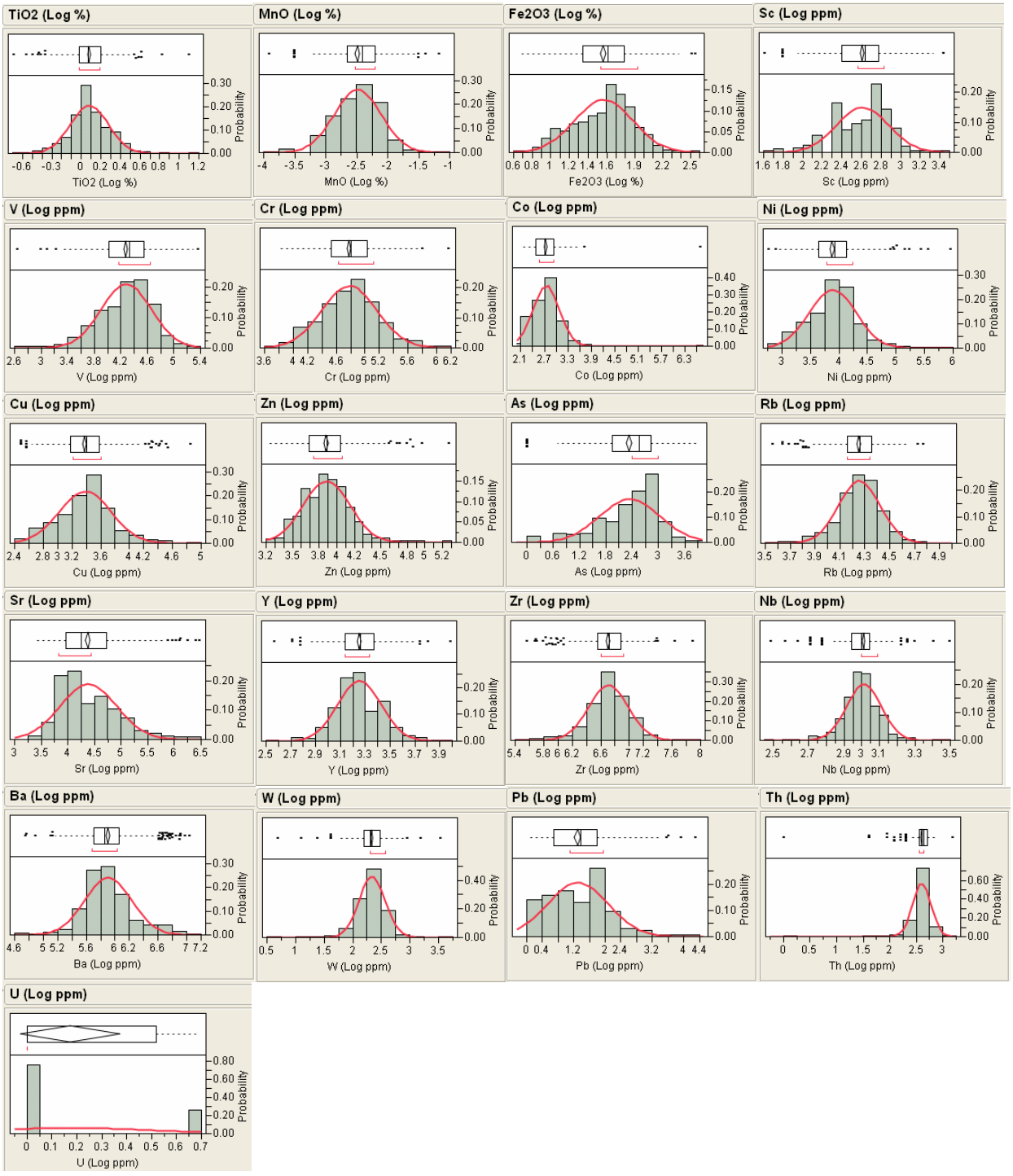

Figure A- 16: Histograms and box plots of log-normal frequency distribution of elements in Platberg Group.

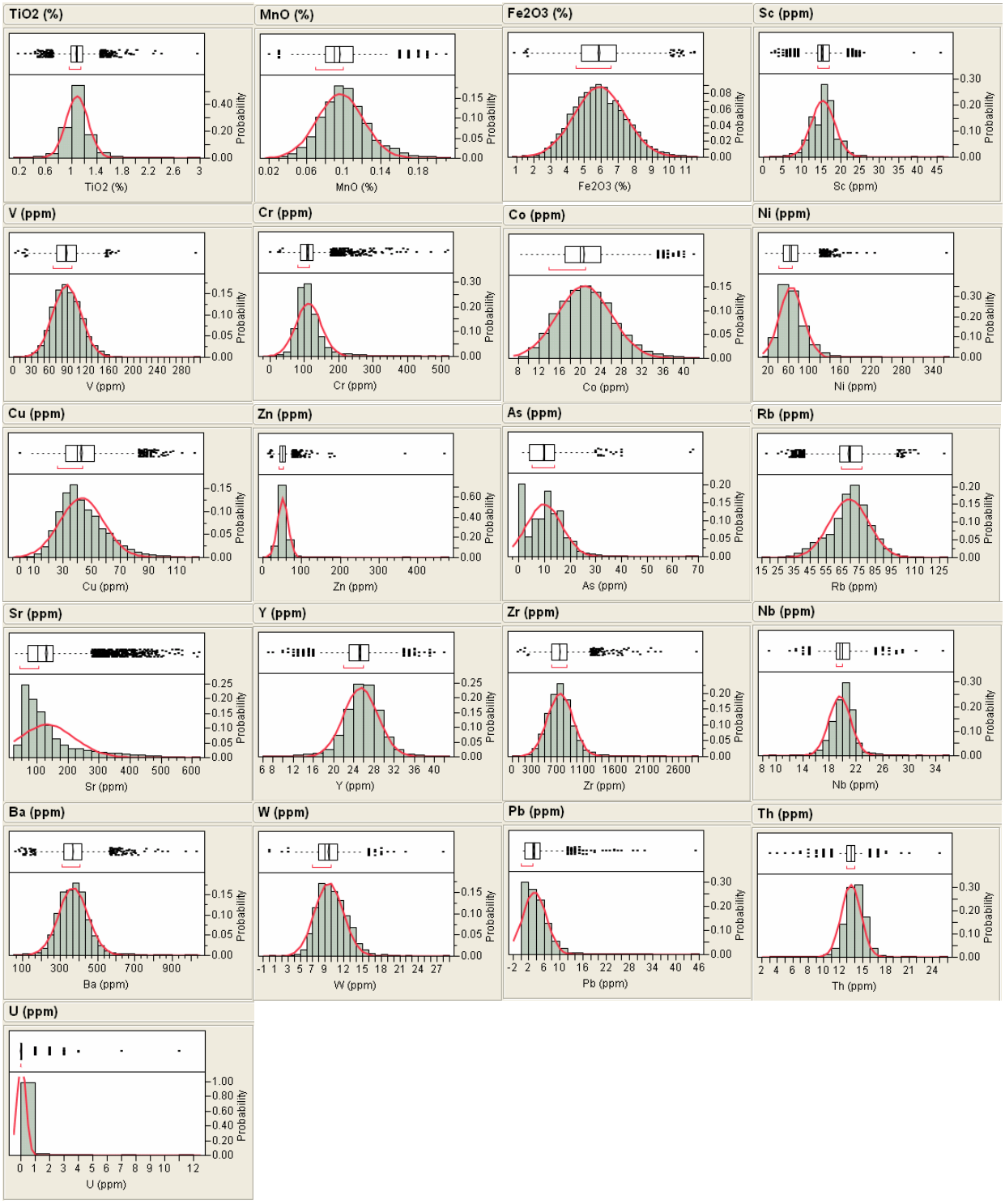

Figure A- 17: Histograms and box plots of raw data frequency distribution of elements in Allanridge Formation.

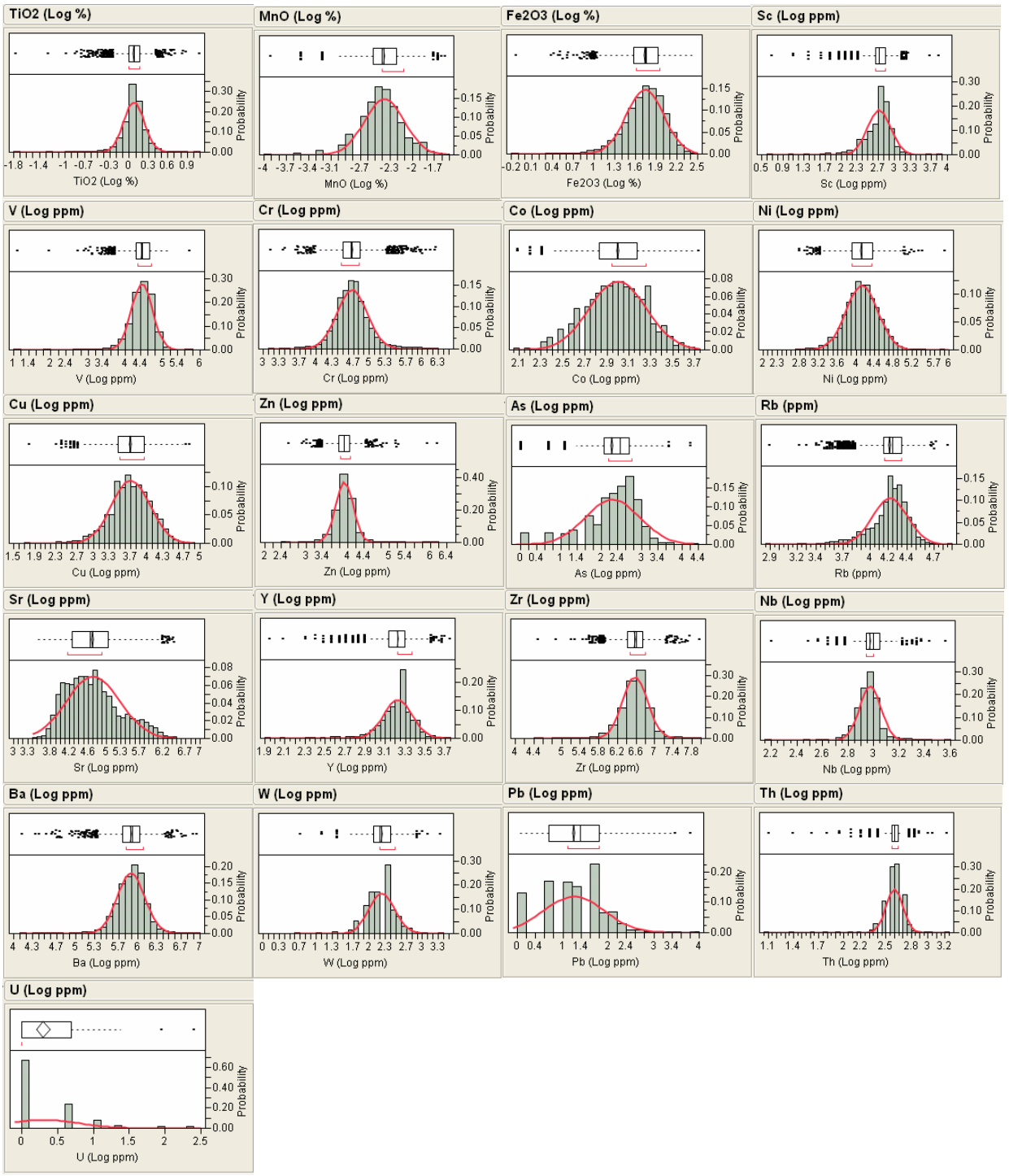

Figure A- 18: Histograms and box plots of log-normal frequency distribution of elements in Allanridge Formation.

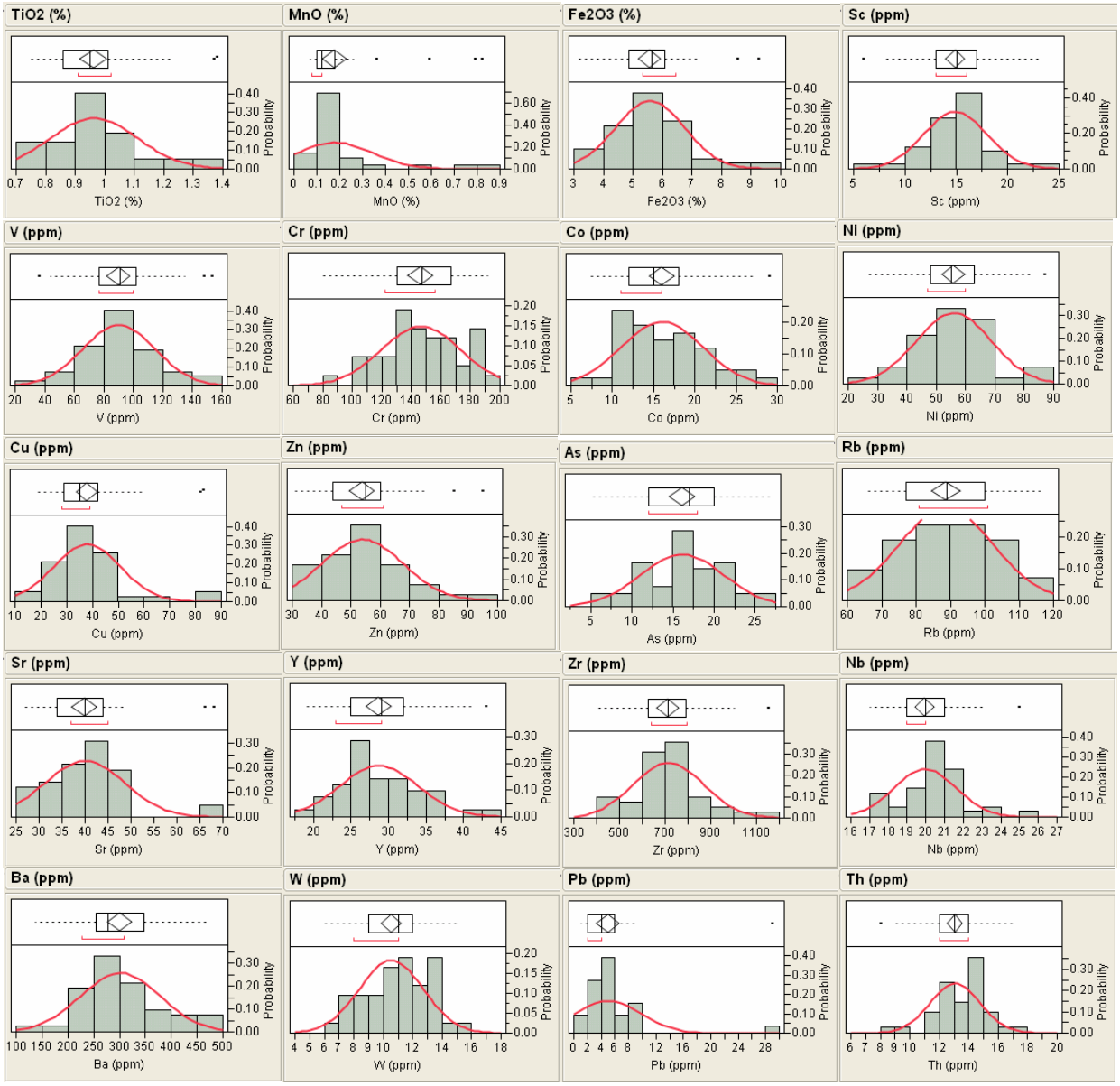

Figure A- 19: Histograms and box plots of raw data frequency distribution of elements in Black Reef Formation.

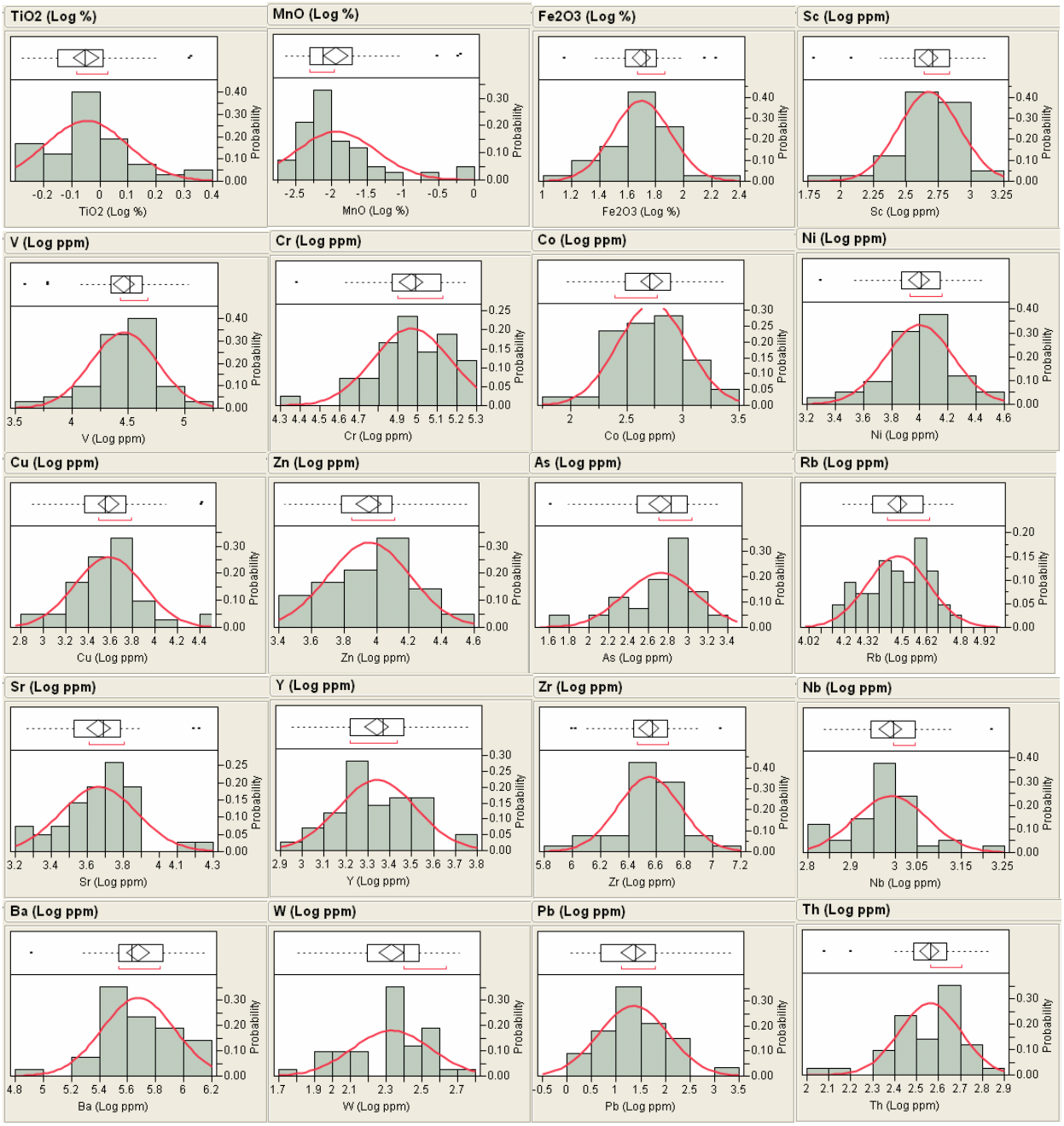

Figure A- 20: Histograms and box plots of log-normal frequency distribution of elements in Black Reef Formation.

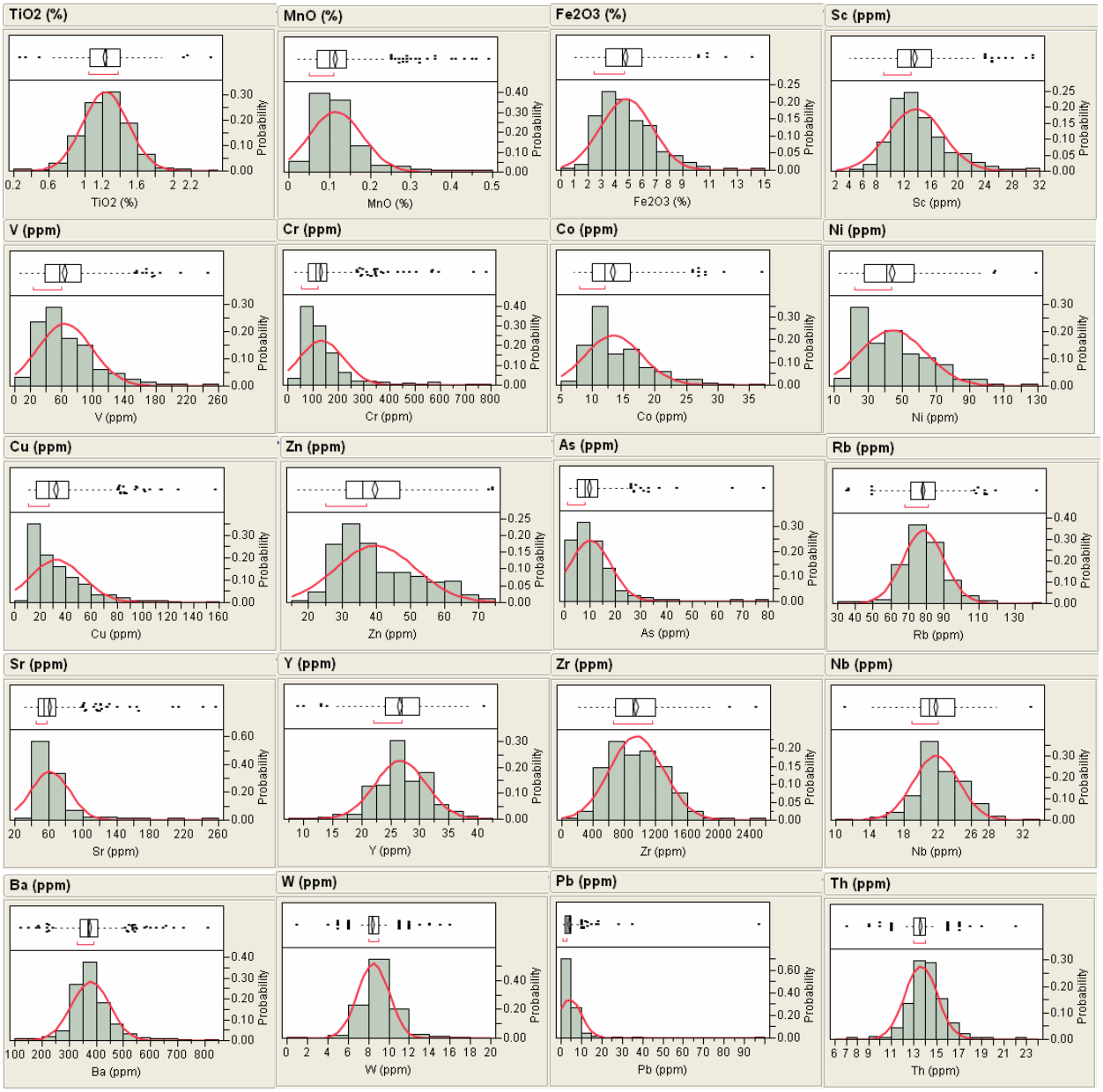

Figure A- 21: Histograms and box plots of raw data frequency distribution of elements in Vryburg Formation.

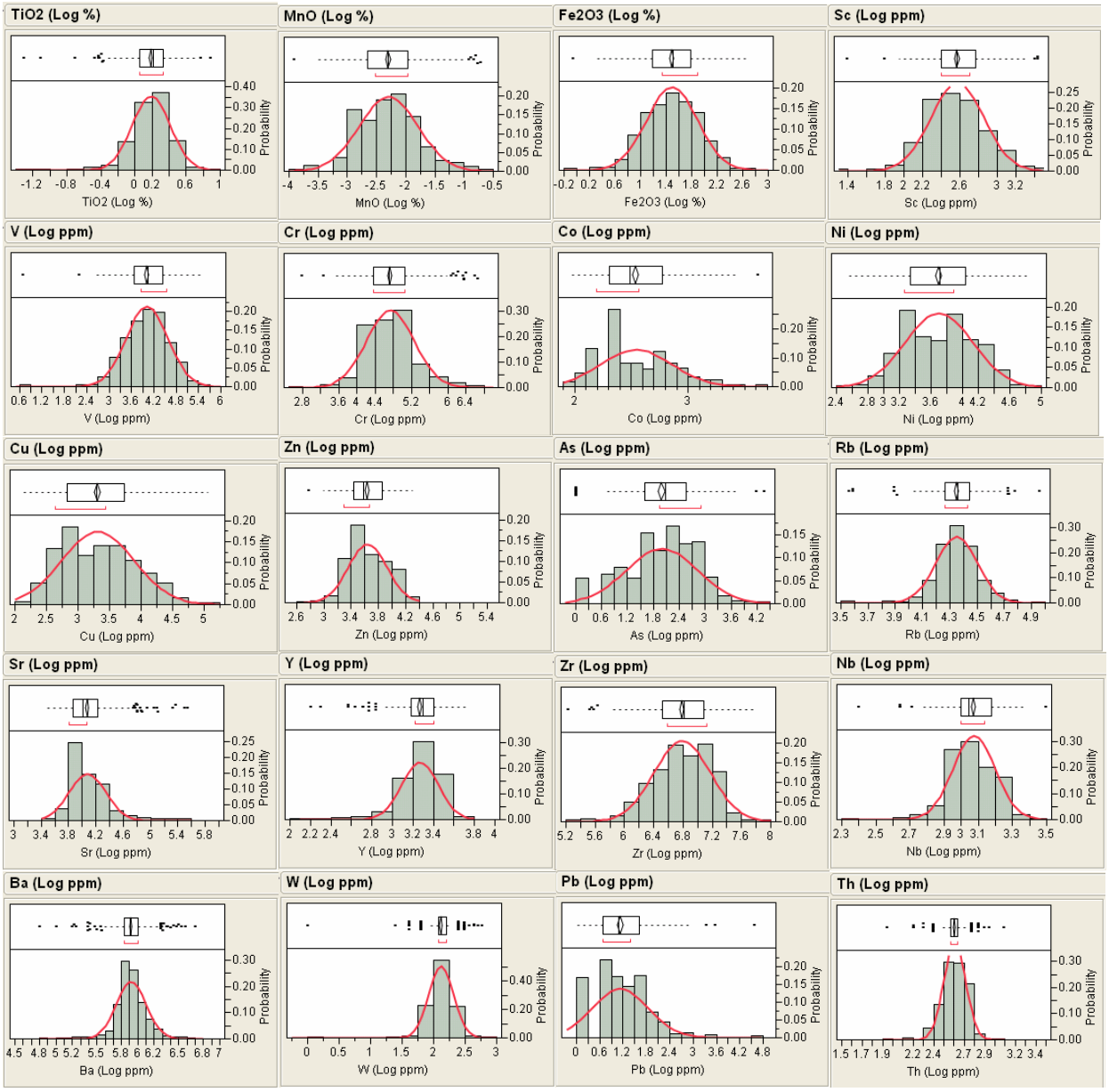

Figure A- 22: Histograms and box plots of log-normal frequency distribution of elements in Vryburg Formation.

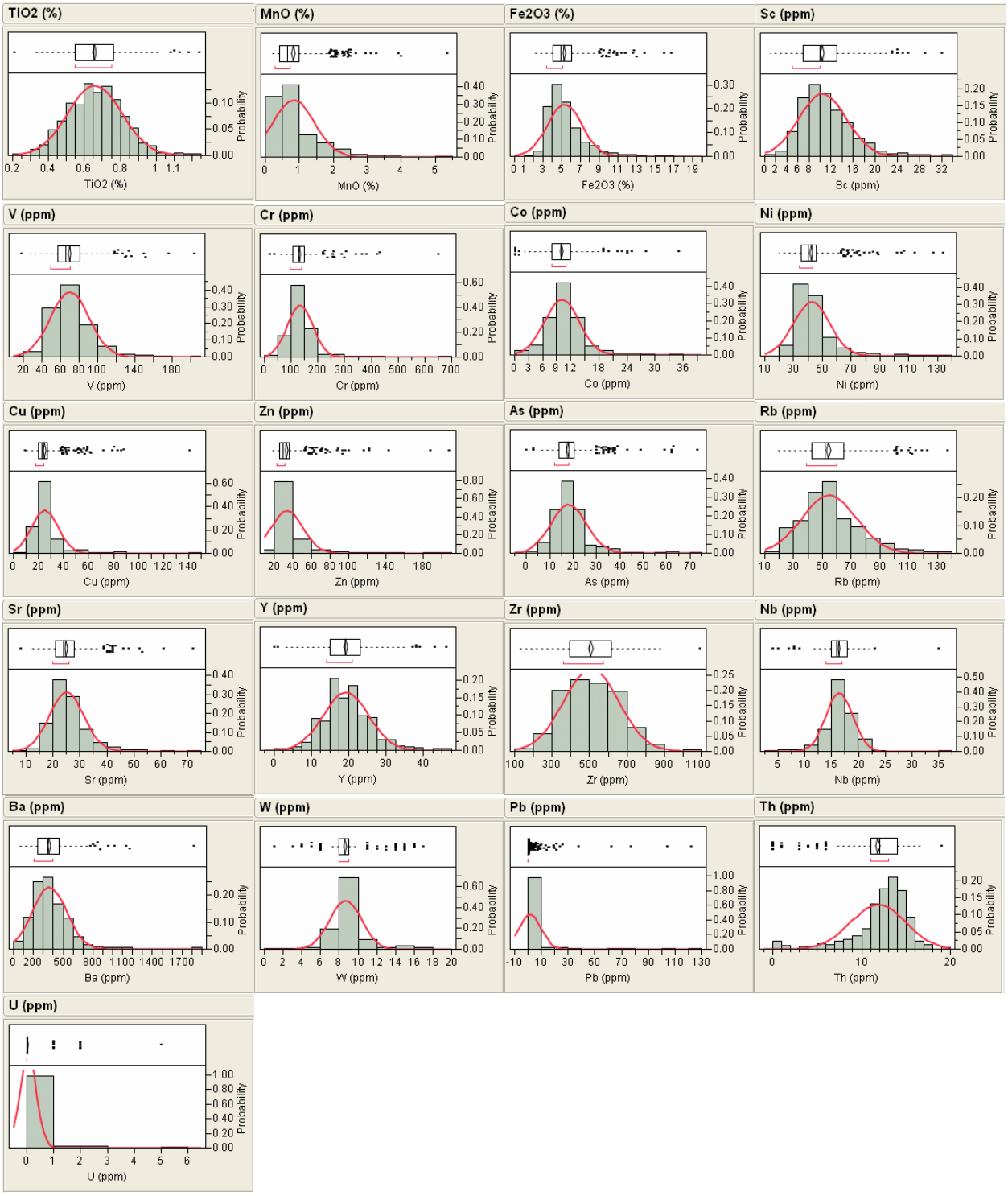

Figure A- 23: Histograms and box plots of raw data frequency distribution of elements in Malmani Subgroup dolomites.

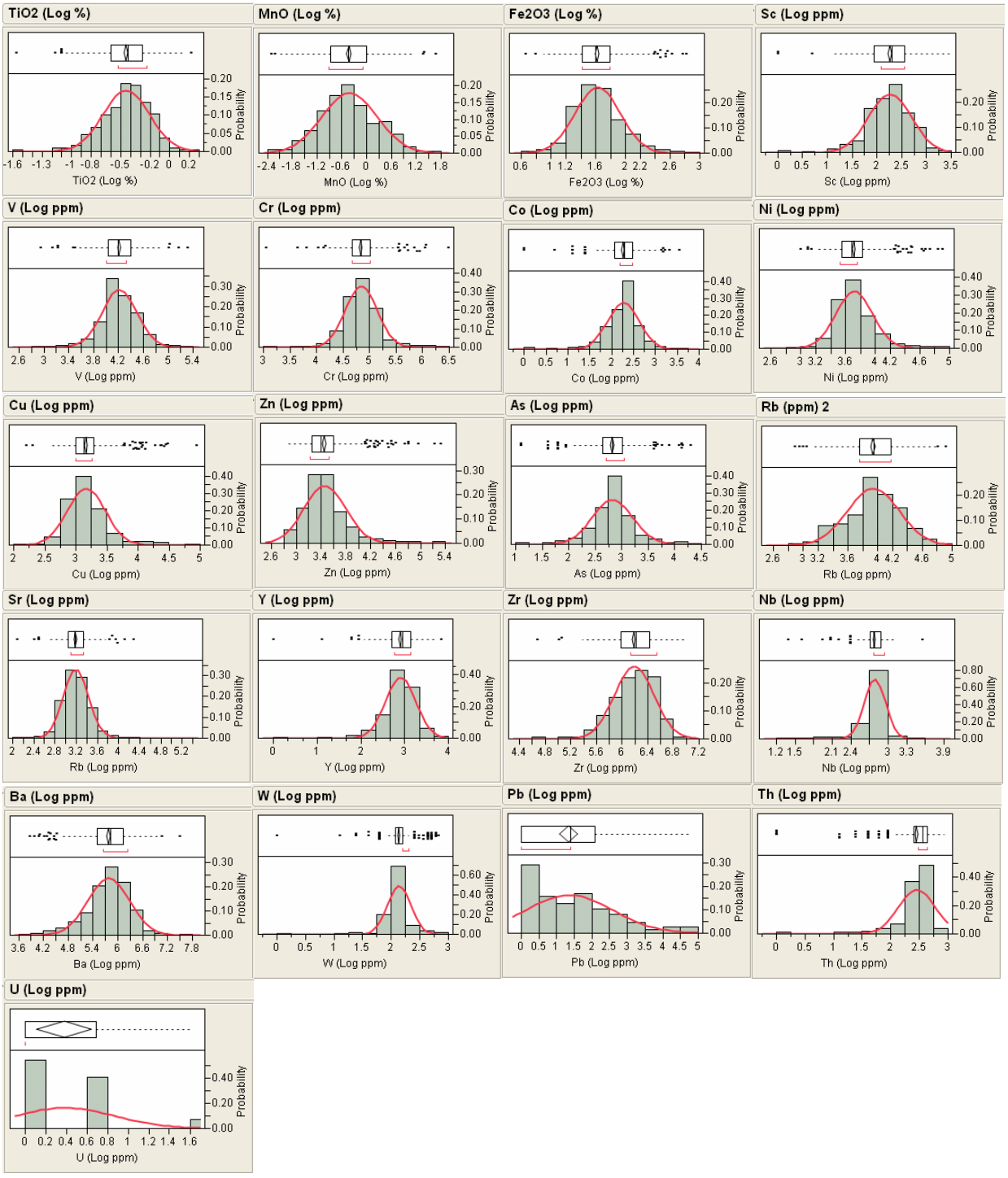

Figure A- 24: Histograms and box plots of log-normal frequency distribution of elements in Malmani Subgroup dolomites.

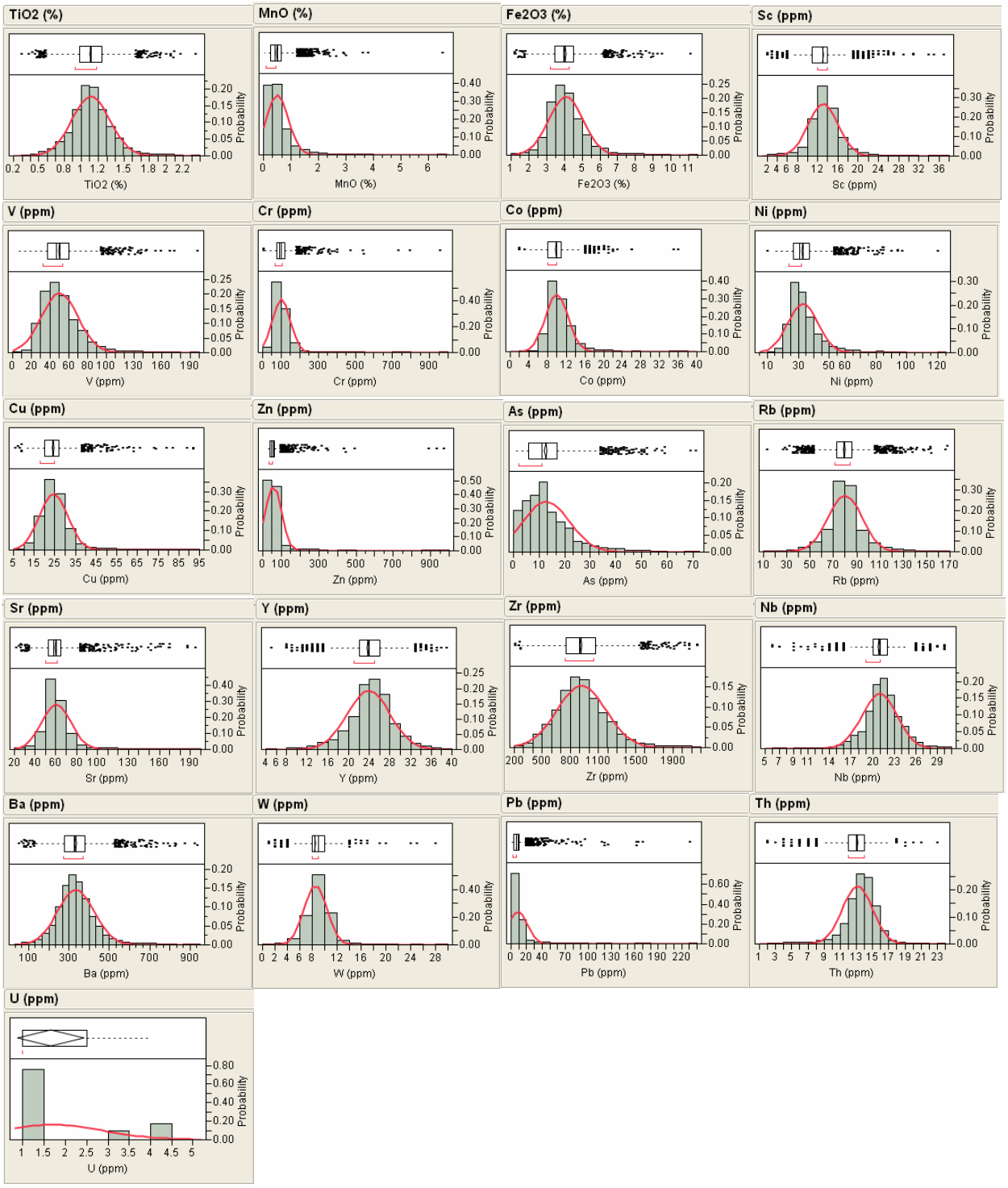

Figure A- 25: Histograms and box plots of raw data frequency distribution of elements in Ghaap Group dolomitic series.

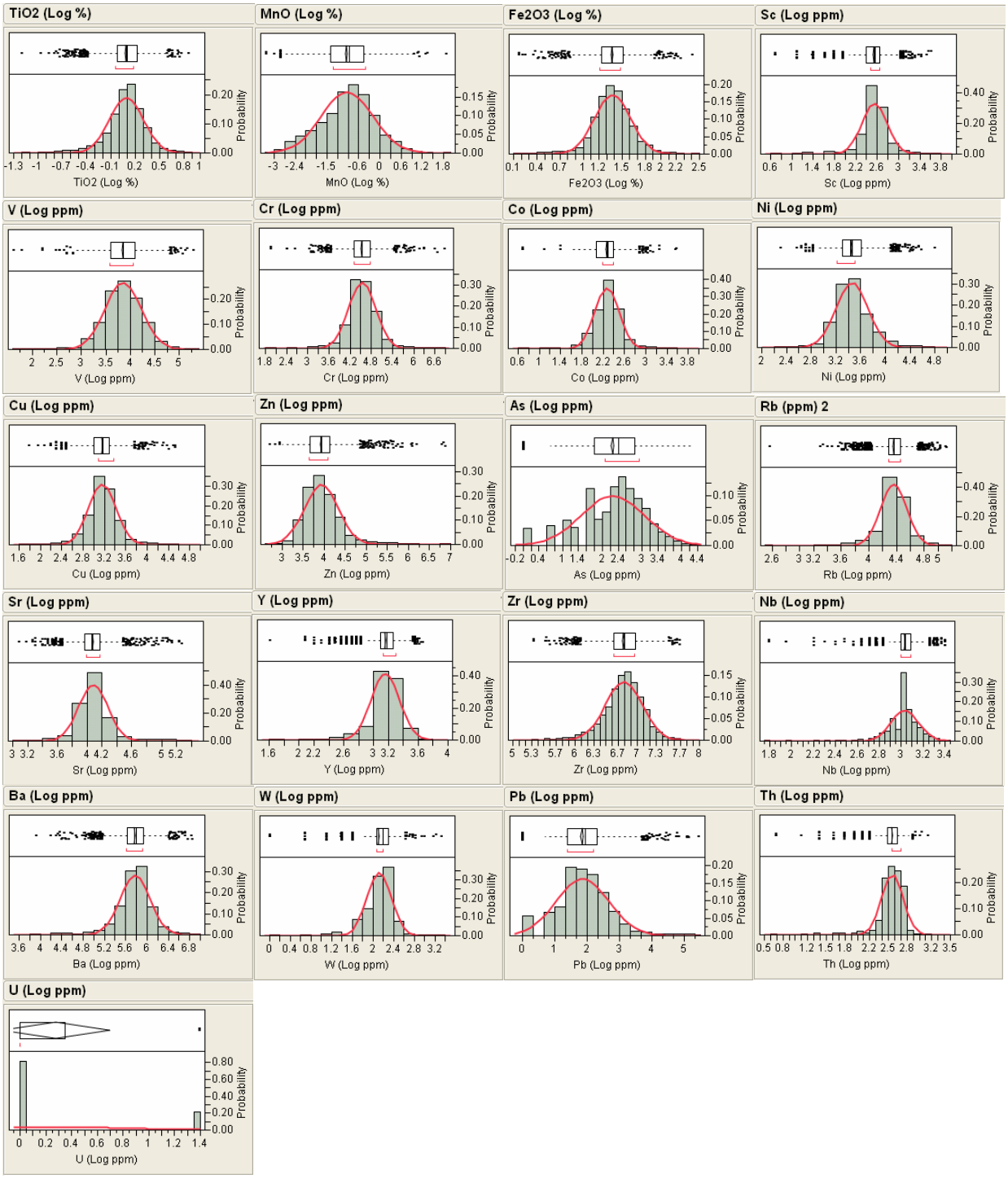

Figure A- 26: Histograms and box plots of log-normal frequency distribution of elements in Ghaap Group dolomitic series.

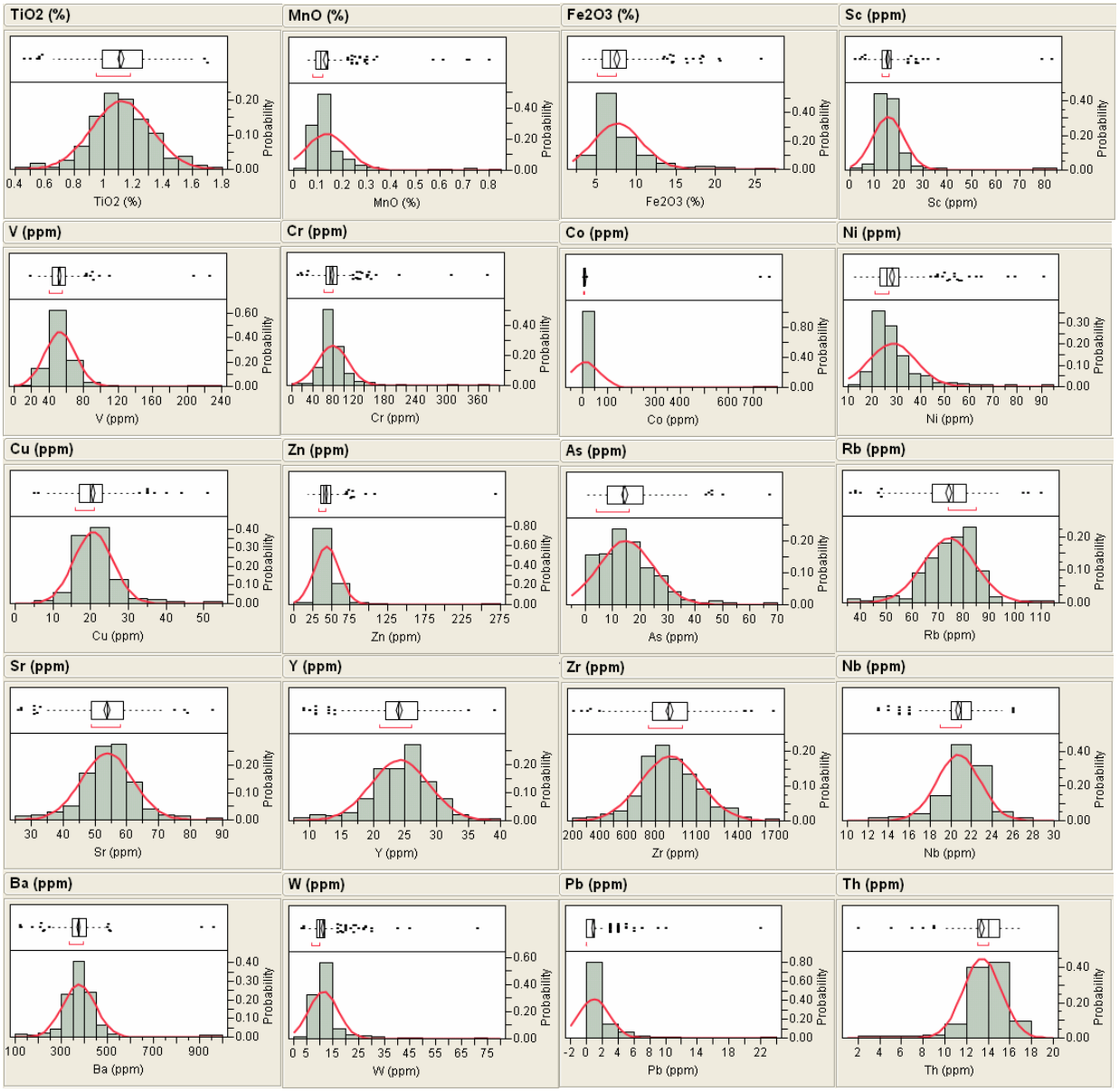

Figure A- 27: Histograms and box plots of raw data frequency distribution of elements in Asbestos Hill Subgroup.

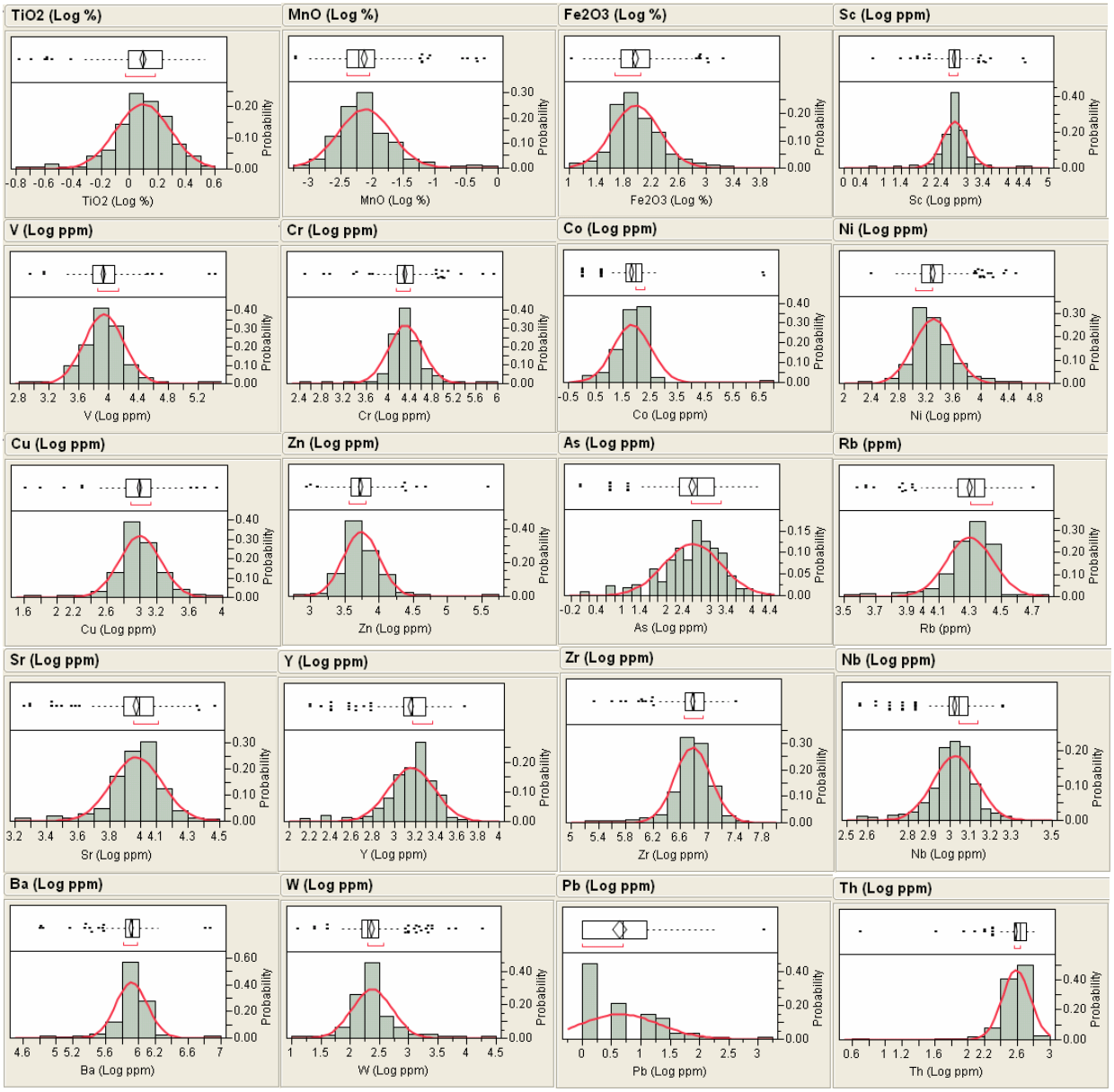

Figure A- 28: Histograms and box plots of log-normal frequency distribution of elements in Asbestos Hill Subgroup.

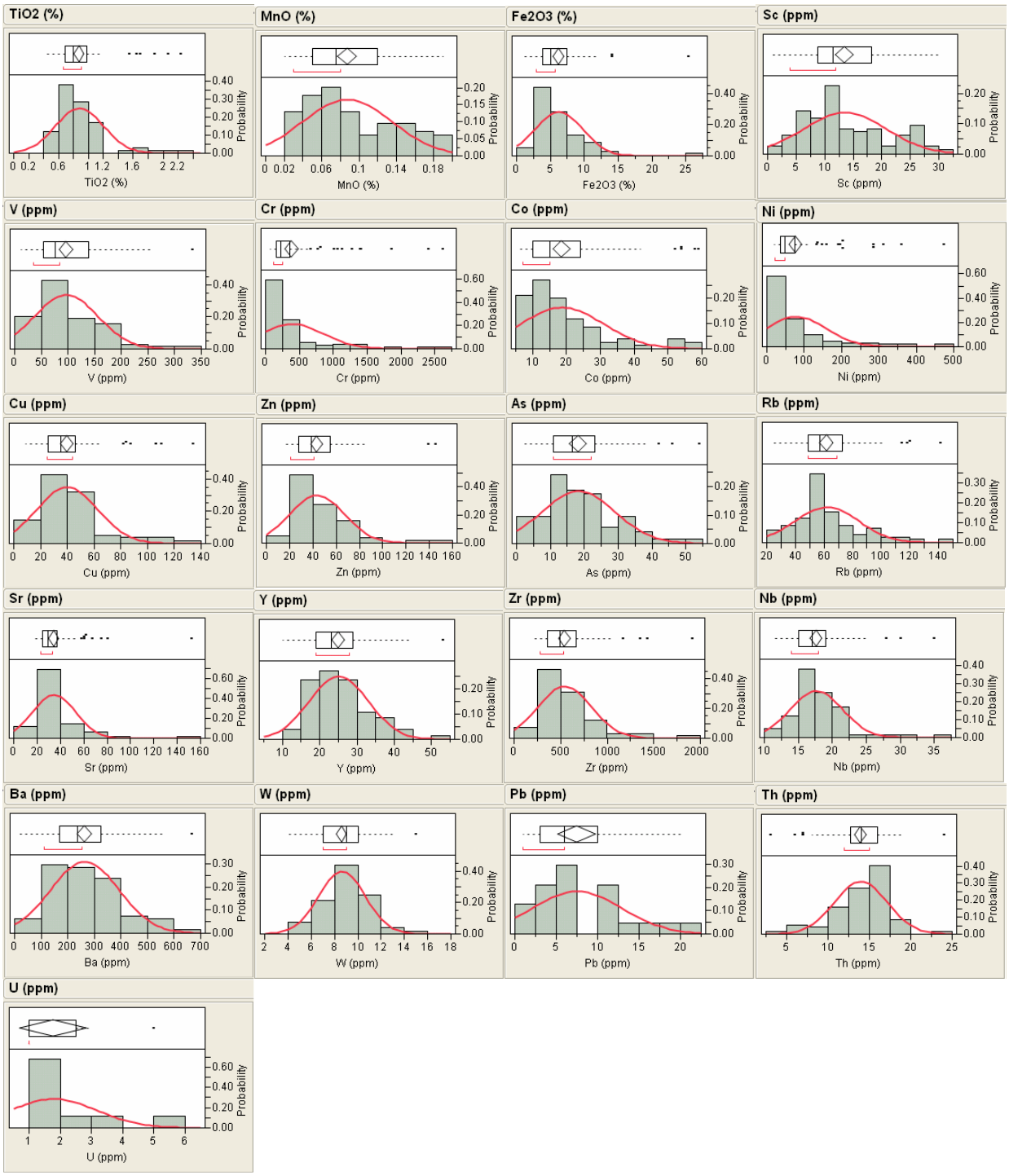

Figure A- 29: Histograms and box plots of raw data frequency distribution of elements in Pretoria Group quartzite.

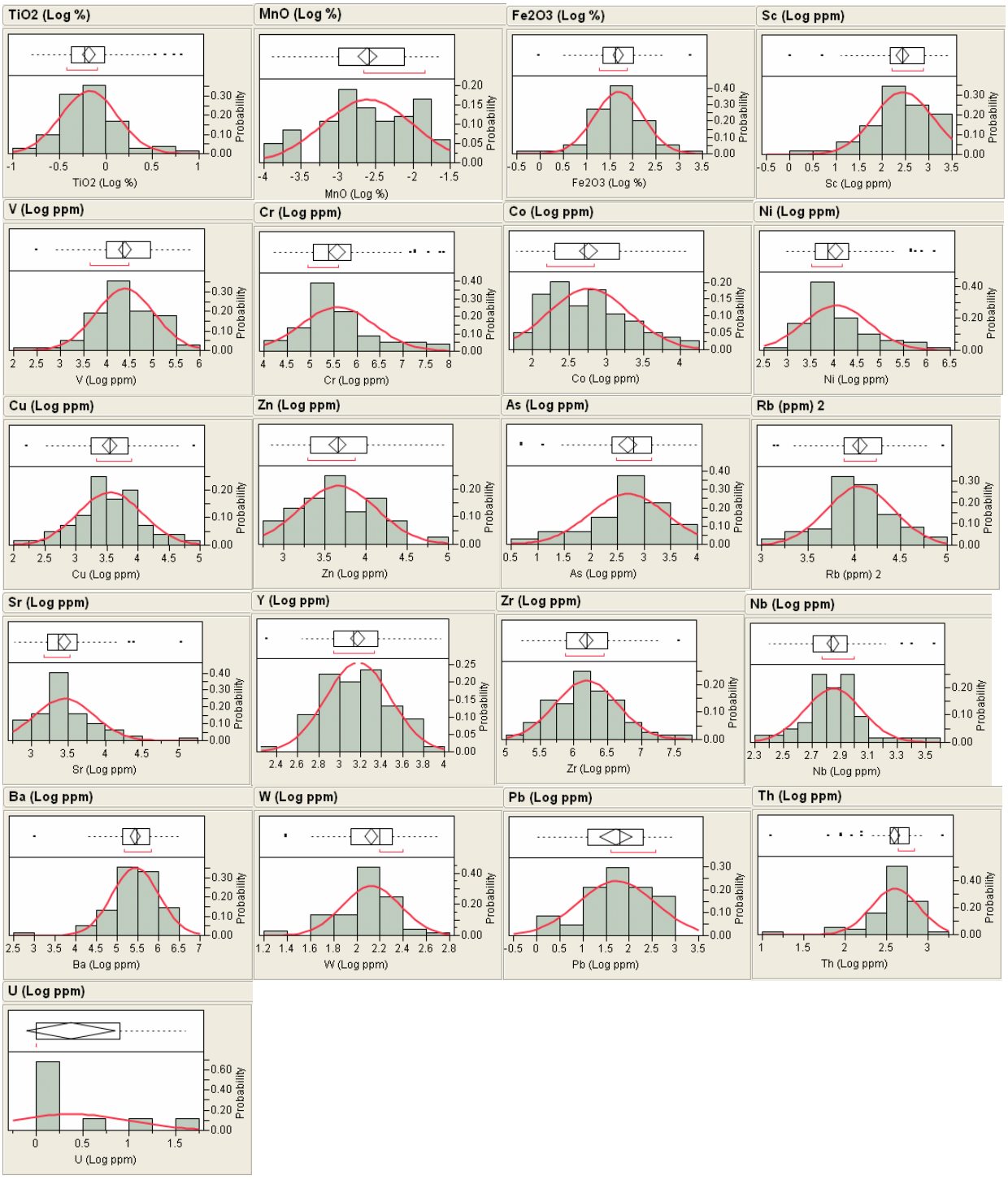

Figure A- 30: Histograms and box plots of log-normal frequency distribution of elements in Pretoria Group quartzite.

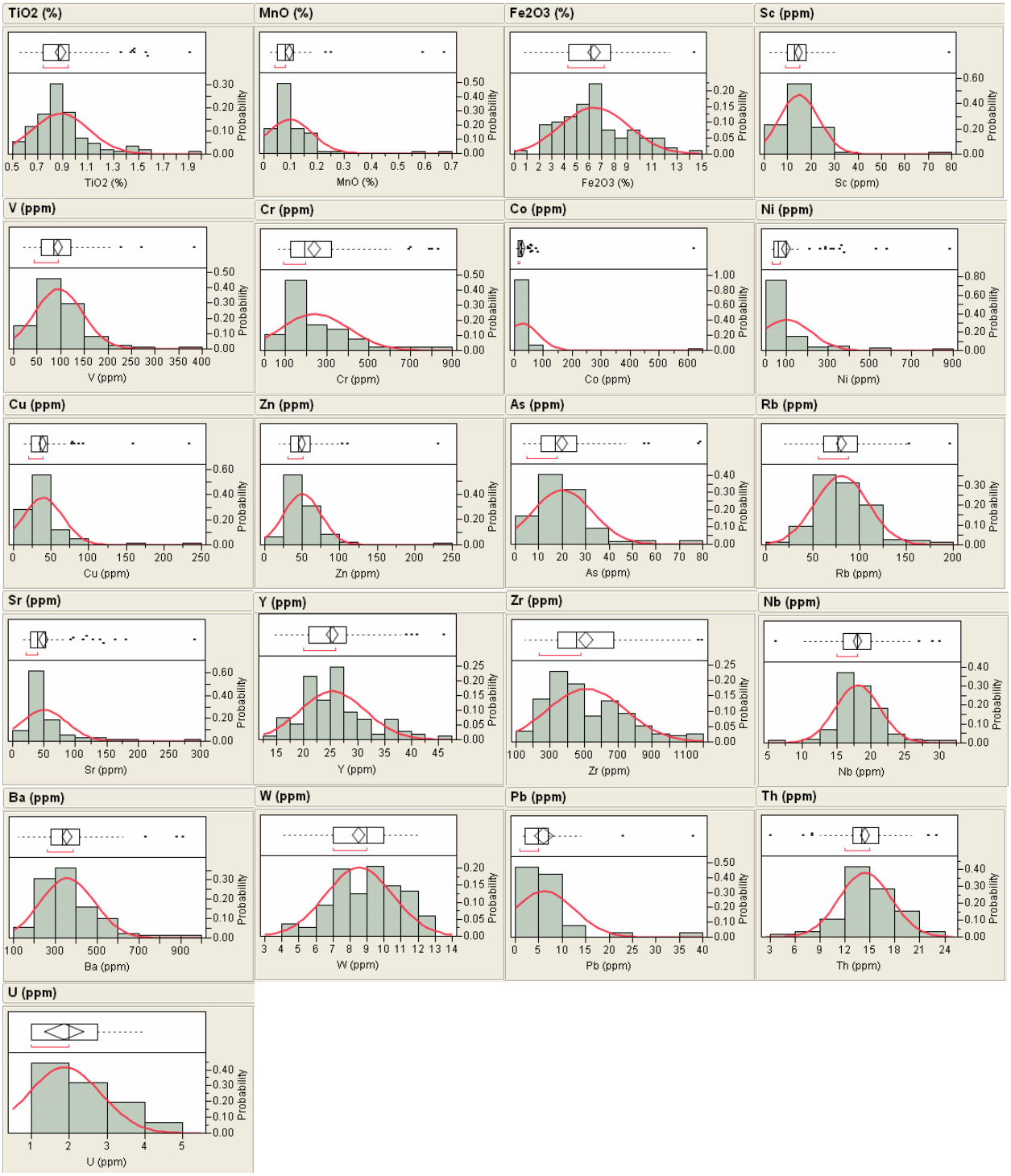

Figure A- 31: Histograms and box plots of raw data frequency distribution of elements in Pretoria Group shale and slate.

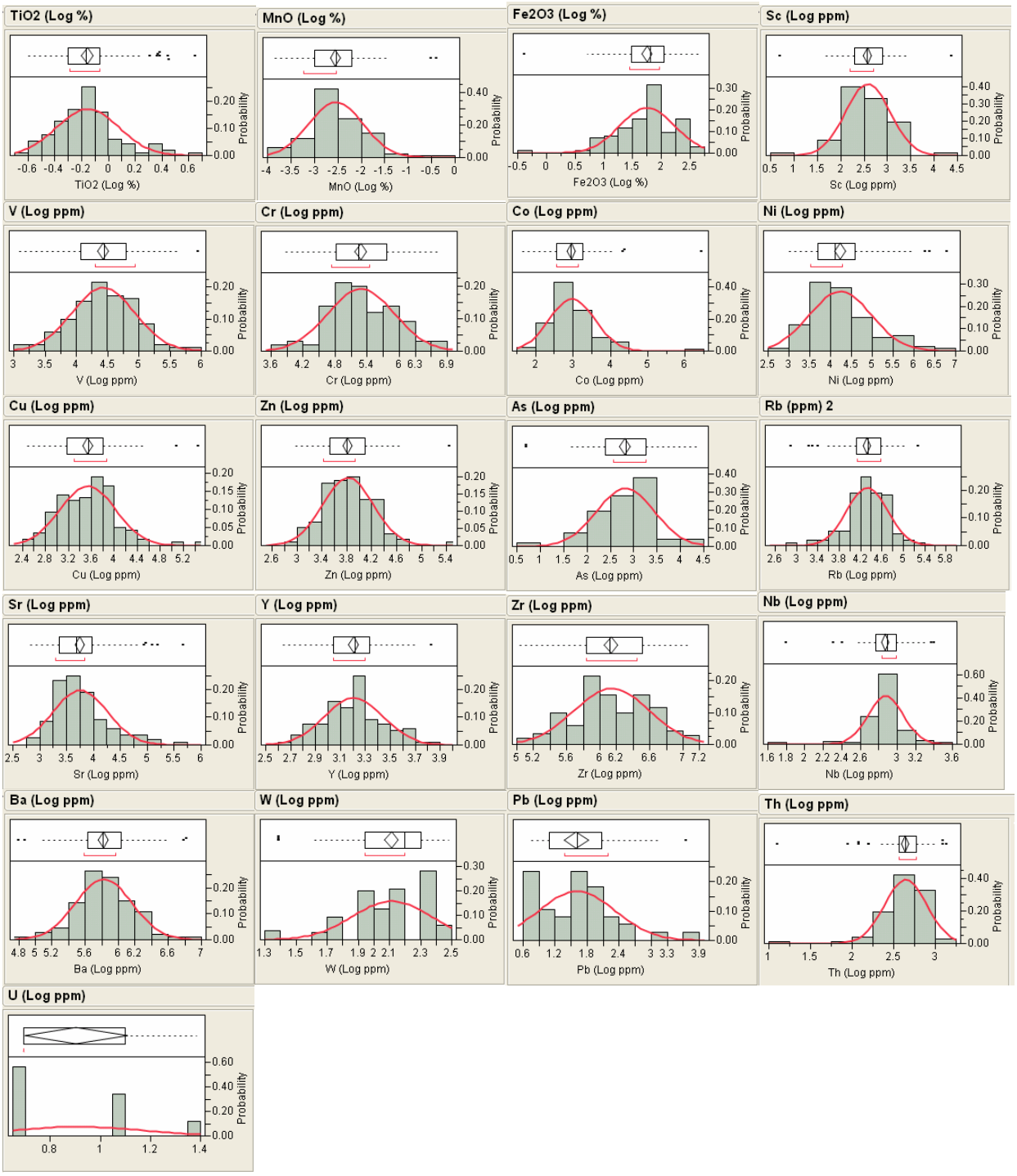

Figure A- 32: Histograms and box plots of log-normal frequency distribution of elements in Pretoria Group shale and slate.

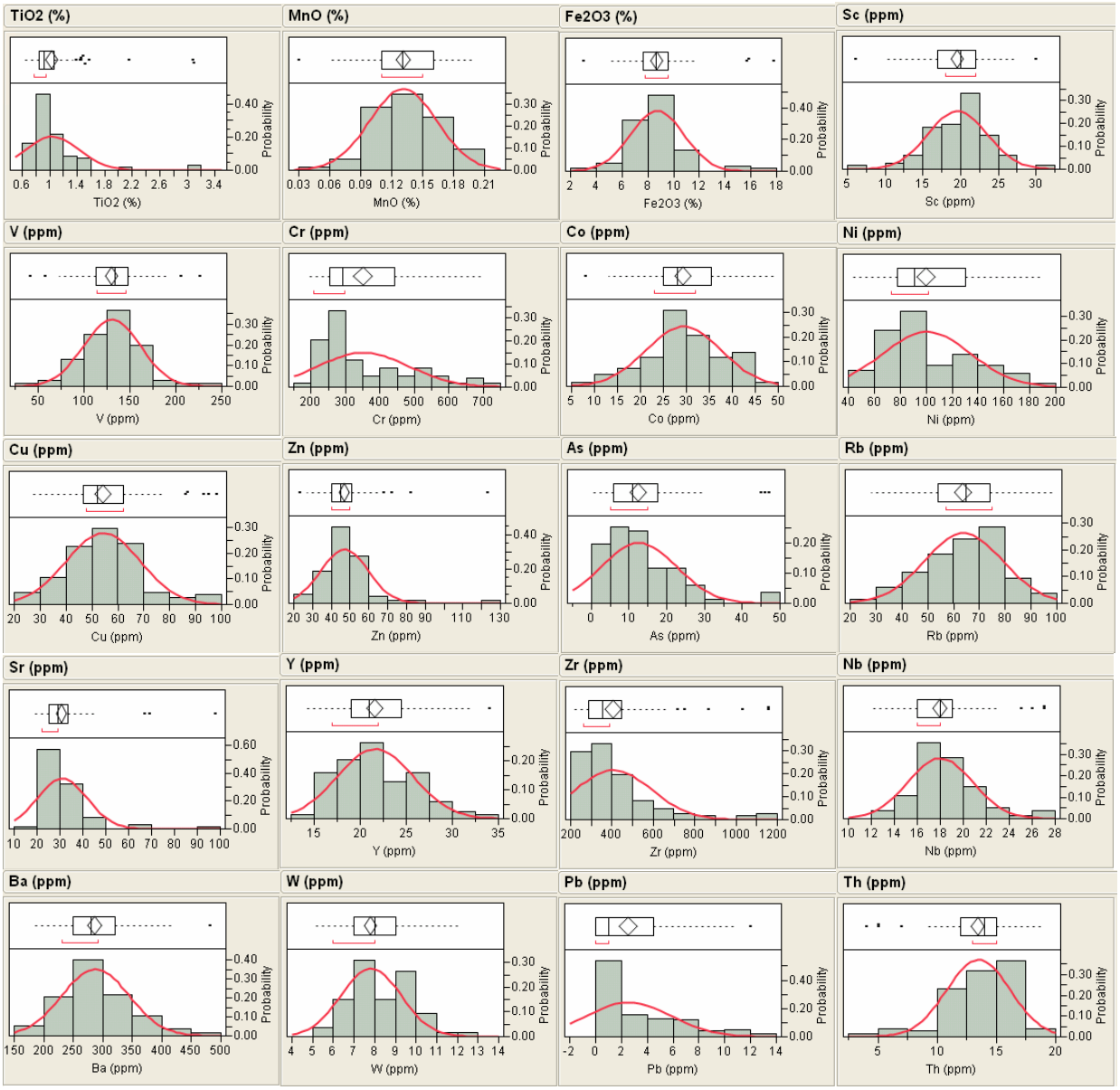

Figure A- 33: Histograms and box plots of raw data frequency distribution of elements in Hekpoort Formation.

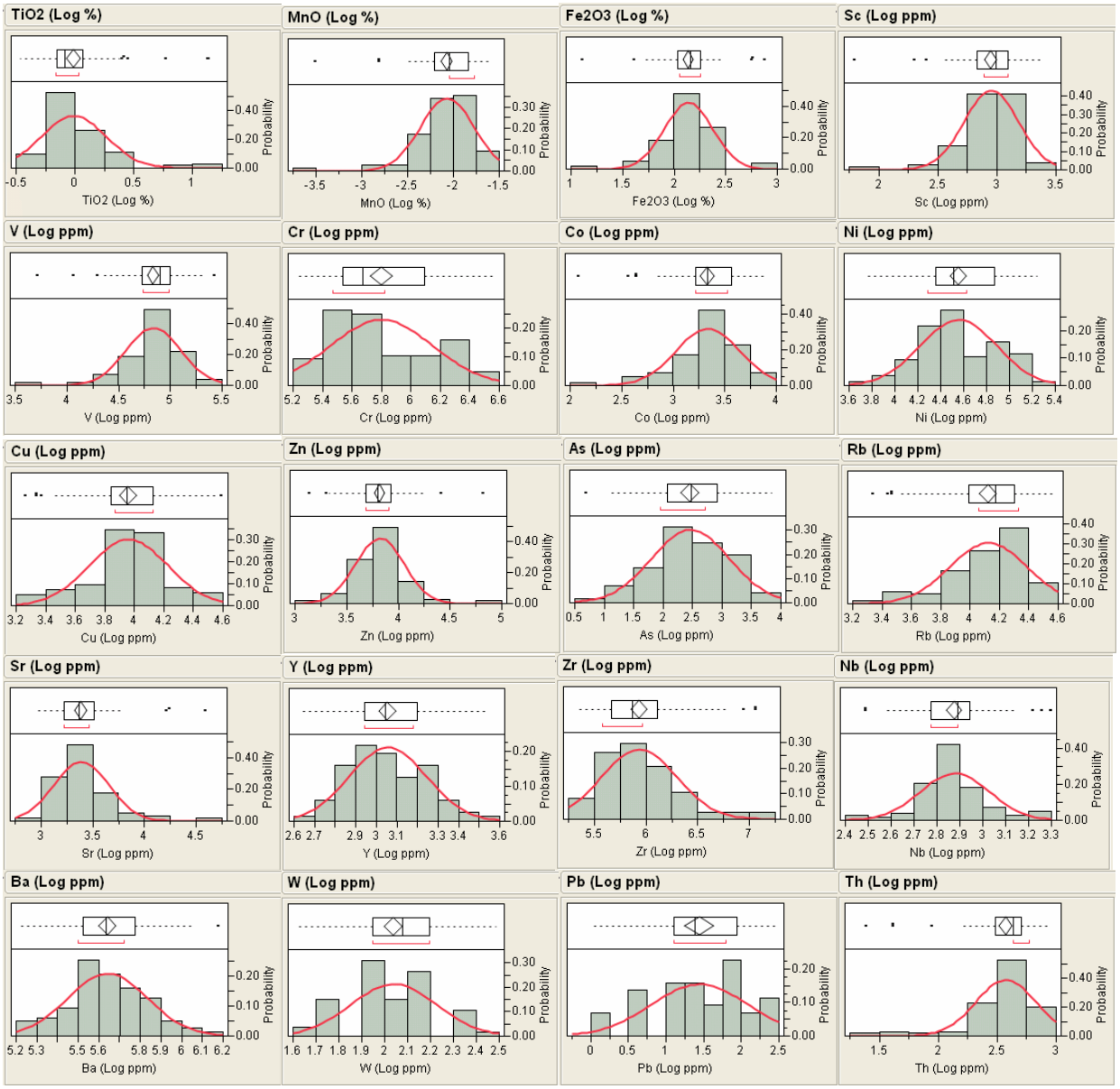

Figure A- 34: Histograms and box plots of log-normal frequency distribution of elements in Hekpoort Formation.

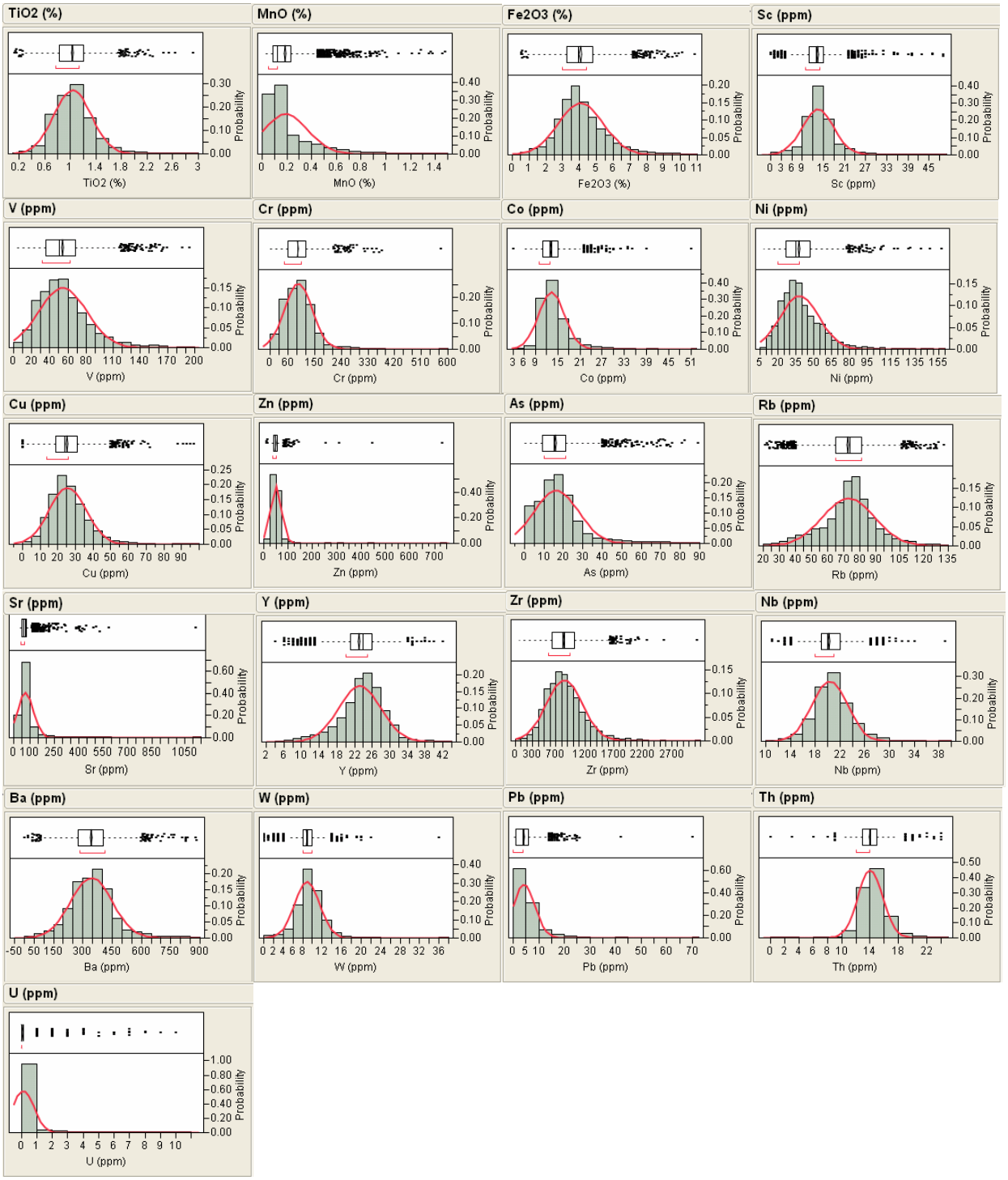

Figure A- 35: Histograms and box plots of raw data frequency distribution of elements in calcrete and surface limestone.

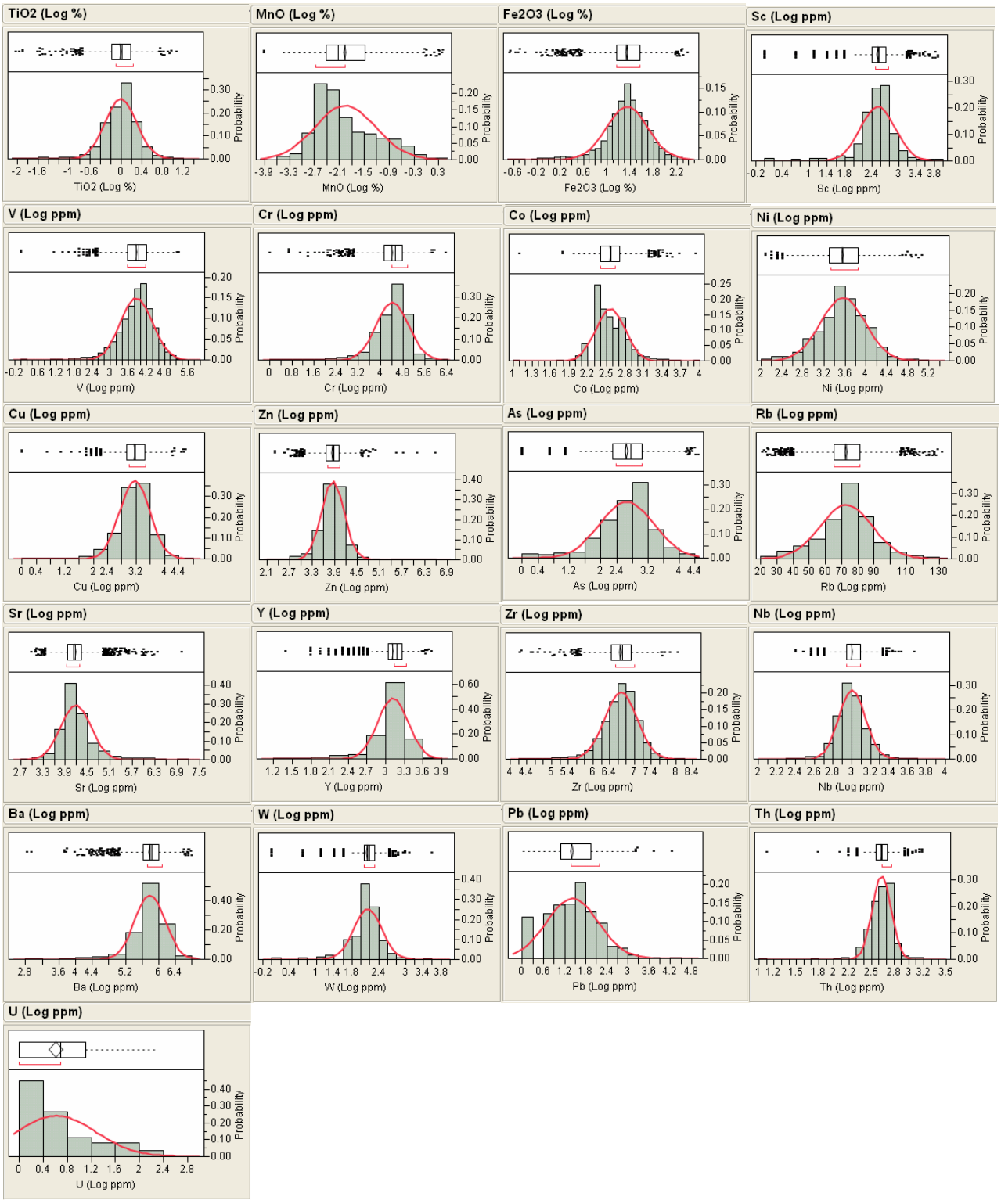

Figure A- 36: Histograms and box plots of log-normal frequency distribution of elements in calcrete and surface limestone.

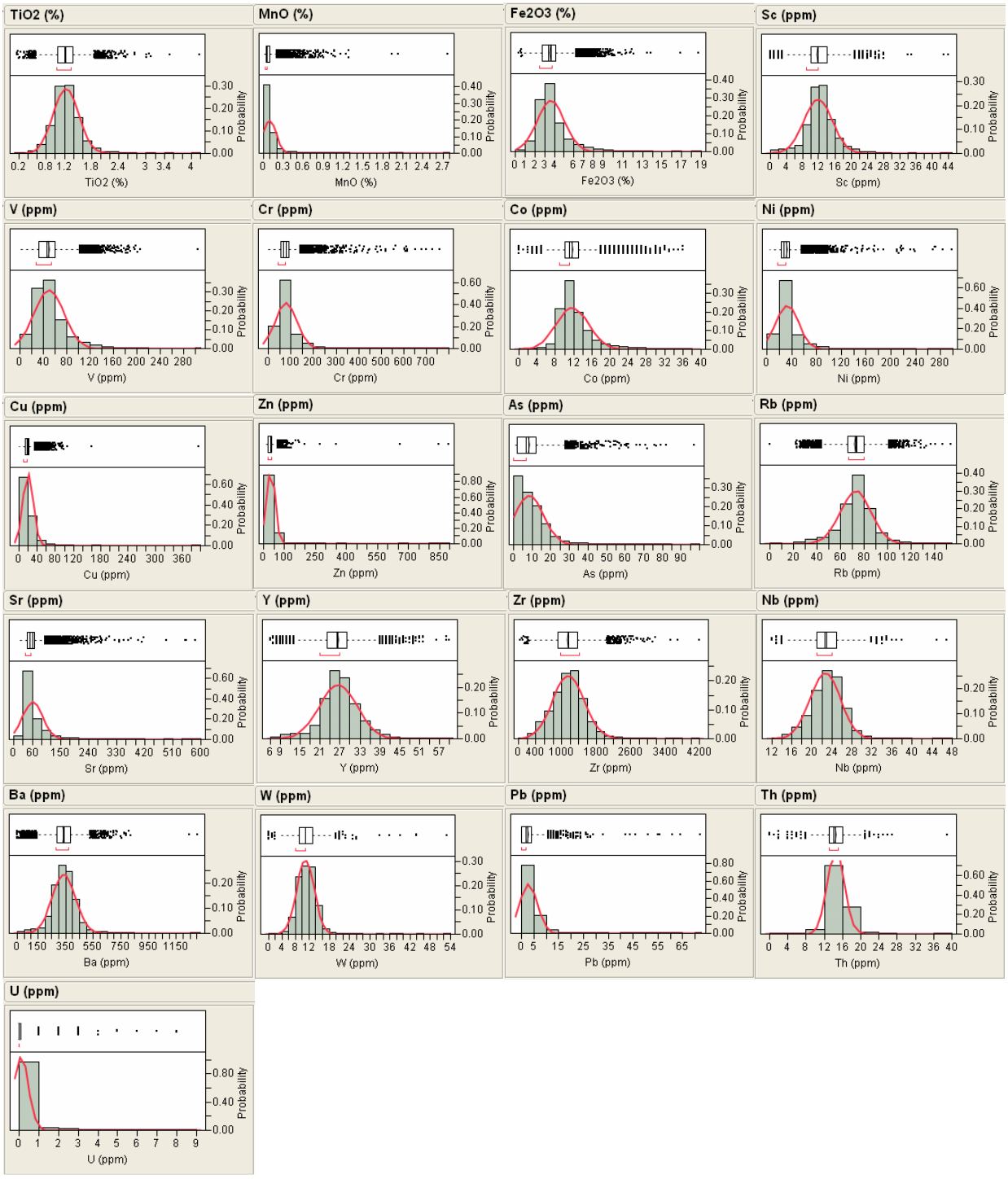

Figure A- 37: Histograms and box plots of raw data frequency distribution of elements in Gordonia Formation.

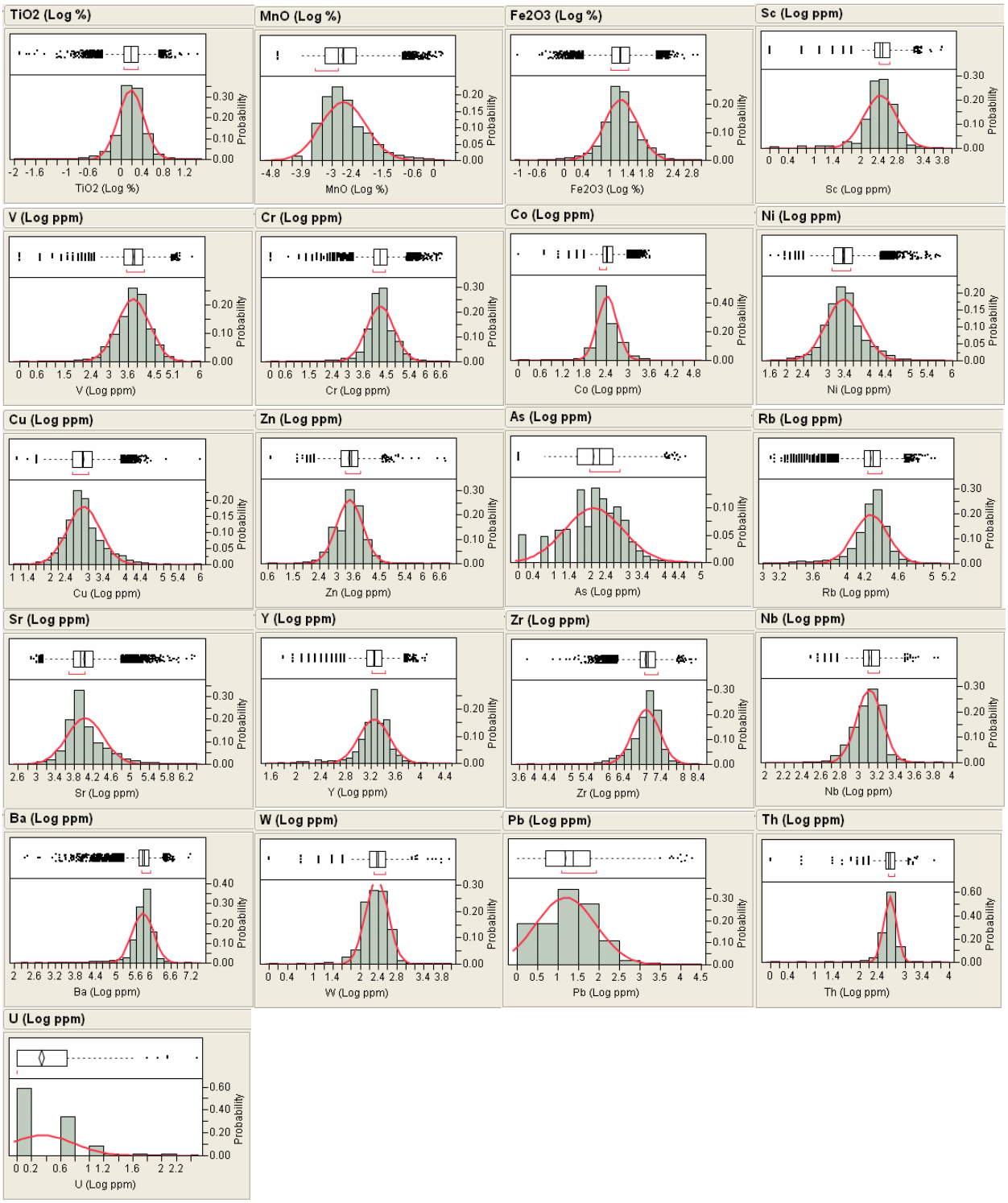

Figure A- 38: Histograms and box plots of log-normal frequency distribution of elements in Gordonia Formation.

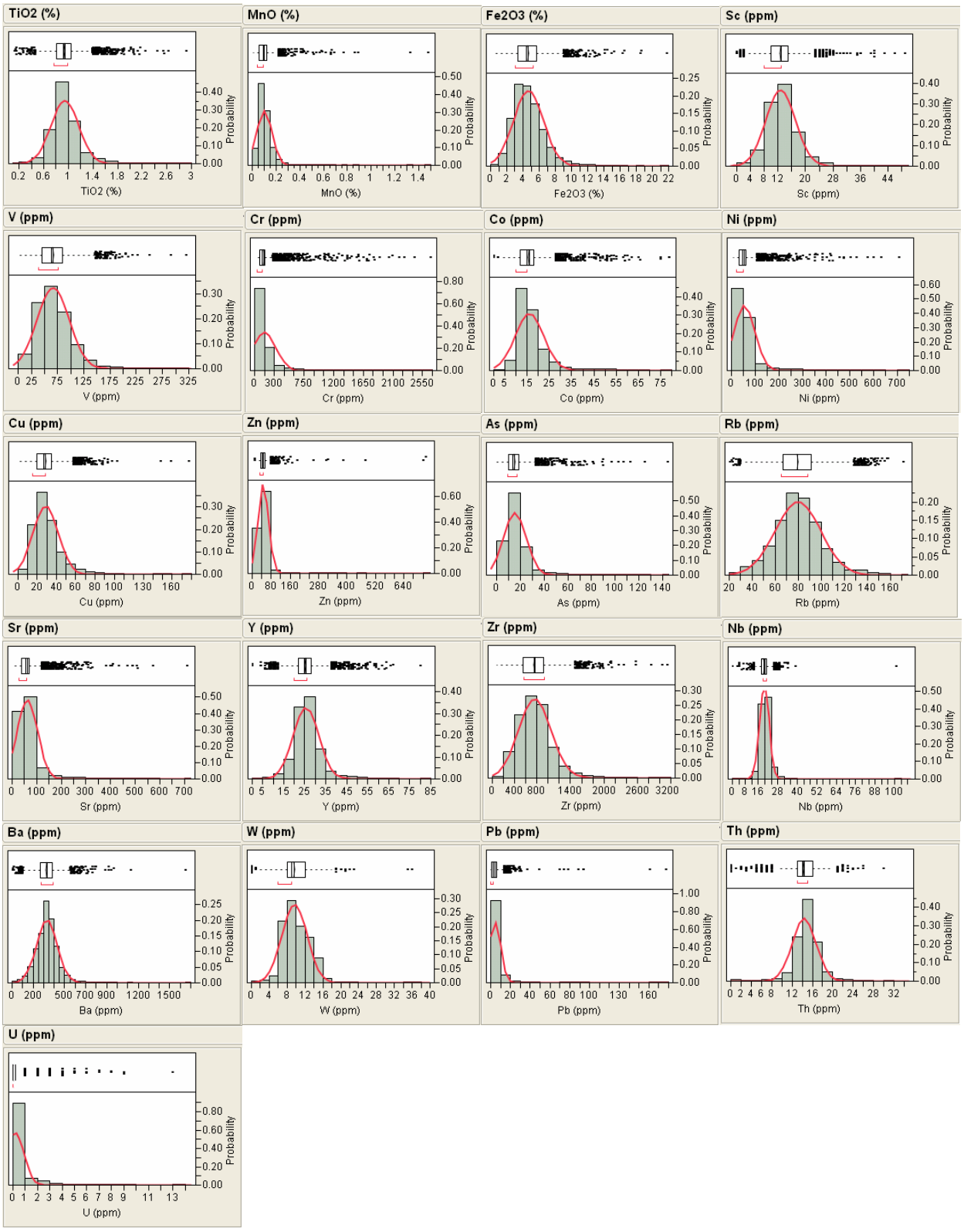

Figure A- 39: Histograms and box plots of raw data frequency distribution of elements in surface sand.

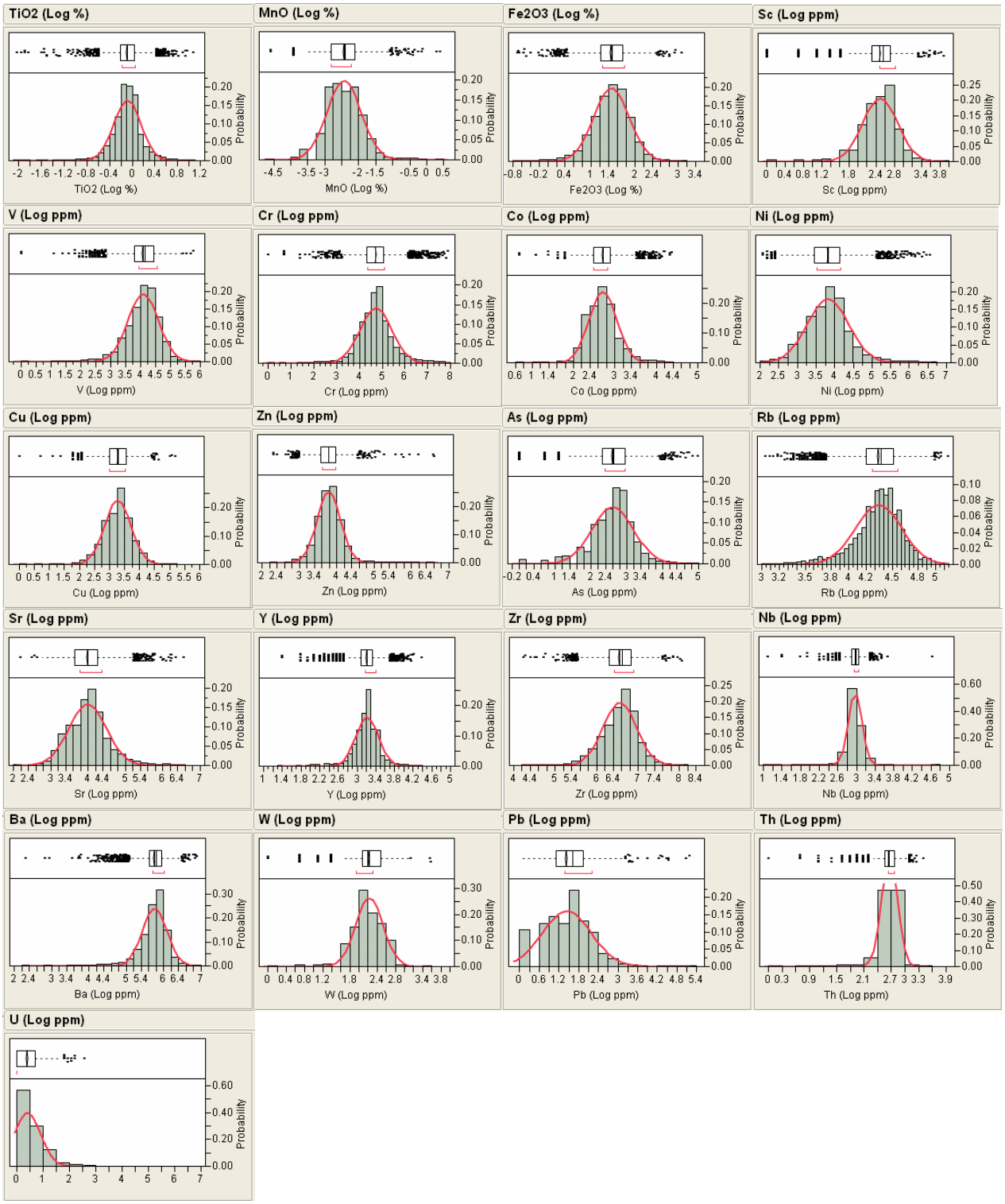

Figure A- 40: Histograms and box plots of log-normal frequency distribution of elements in surface sand.